NO STRAIN NO GAIN; FROM CONSTRUCTING CONTINENTAL CRUST TO BUILDING DIVERSITY IN THE GEOSCIENCES

By

ANYA LAWRENCE

A thesis submitted to

The University of Birmingham

for the degree of

DOCTOR OF PHILOSOPHY

School of Geography, Earth and Environmental Sciences
College of Life and Environmental Sciences
University of Birmingham
May 2022

UNIVERSITY OF
BIRMINGHAM

University of Birmingham Research Archive

e-theses repository

This unpublished thesis/dissertation is copyright of the author and/or third parties. The intellectual property rights of the author or third parties in respect of this work are as defined by The Copyright Designs and Patents Act 1988 or as modified by any successor legislation.

Any use made of information contained in this thesis/dissertation must be in accordance with that legislation and must be properly acknowledged. Further distribution or reproduction in any format is prohibited without the permission of the copyright holder.

ABSTRACT

Granite petrogenesis is a fundamental Earth process that underpins the construction and evolution of the continental crust. Understanding how granites are generated and structurally emplaced is key to answering the question of how the continental crust has grown throughout geological time and can also provide insights on tectonic and geodynamic processes; styles of mineralisation; and the interaction between the Earth's mantle and crust.

The study of granite petrogenesis is also deeply influenced by the experience of the researchers that engage in this field. For researchers from minoritized backgrounds, pursuing scholarly studies in the Geosciences, a disciplinary area with a documented lack of diversity in the context of UK higher education, can be experienced as particularly challenging.

This thesis presents a dual approach which examines both the fundamental Earth process of granite petrogenesis as well as documenting and reflecting on the perspective of the author as a researcher from a diverse, intersectional background. A variety of research designs are employed including: rock magnetics to provide novel structural data to link granite petrogenesis to tectonics; geochemistry to investigate the sources of granitic magmas and their evolution in the continental crust; review of the literature to examine equity, diversity and inclusion in the Geosciences; and finally, autoethnography to document and provide reflection on individual experiences and challenges and proposed solutions to the persistent inequities in the wider field.

The findings of this thesis suggest that parallels can be drawn between constructing the continental crust and building diversity in the Geosciences. Just as granite petrogenesis and emplacement is often pulsatory and incremental in nature, efforts to address structural inequalities, systemic discrimination and exclusionary cultures within academic Geoscience are shown to be equally episodic and prolonged by institutional inaction, departmental unaccountability and personal biases deeper-seated than the continental crust itself.

In order to improve our understanding of granite petrogenesis and enhance equity, diversity and inclusion it is paramount that intersectional approaches are applied in future work, both in terms of research methodologies and the frameworks by which we acknowledge individual's different experiences and identities within the academic Geosciences.

ACKNOWLEDGMENTS

By convention, a doctoral thesis begins with an acknowledgements section in which the author names, shames and invariably forgets those who have been an integral part of their project.

But, as will hopefully become clear in the writing that follows, this thesis was destined to defy convention from the outset.

So I’m not going to waste ink or bytes on reciting names in a rambling list devoid of any meaning, personality and humanity. Instead, to open this thesis, I offer the first of many glimpses into my autistic world. I show you in a melange of shape, colour and form, just some of the charismatic cast of characters who have helped me along the way in my academic endeavours so far.



LIST OF PUBLICATIONS AND PRESENTATIONS

During the course of my postgraduate studies with the School of Geography, Earth and Environmental Sciences, the University of Birmingham, the following publications, presentations/ workshops and media appearances arose from my research.

Publications

Lawrence, A., Maffione, M. & Stevenson, C.T.E. 2022. Mush ado about the Ratagain Complex, NW Scotland: Insights on Caledonian granitic magmatism and emplacement from magnetic fabric analyses. *The Scottish Journal of Geology*, **58**(1), sjg2021-018.

Lawrence, A. & Dowey, N. 2021. Six Simple Steps to making GEES fieldwork more accessible and inclusive. *Area*, **54**(1), 52-59.

Lawrence A. (2021, August 25) How Zoom helped the neurotypical world hear my autistic voice. *Nature*, Available from: https://doi.org/10.1038/d41586-021-02325-9

Lawrence, A. 2021. Defining equality. *Physics World*, **34**(11), 27-28.

Lawrence, A., 2021. Beware of the 'alliars' when it comes to diversity in science. *Physics World*, **34**(7),17-17.

Lawrence, A. 2021. Between a Rock and a Workplace. *Nature Geoscience*, **14**, 454–455.

Dowey, N., Barclay, J., Fernando, B., Giles, S., Houghton, J., Jackson, C., Khatwa, A., **Lawrence, A.**, Mills, K., Newton, A., Rogers, R. and Williams, R. 2021. A UK perspective on tackling the geoscience racial diversity crisis in the Global North. *Nature Geoscience*, **14**, 256–259.

Presentations

Disability in Geoscience workshop, Universität Bern. Online March 2022 (Workshop)

Lawrence, A. Hidden disabilities in the field

(Re)defining fieldwork: a virtual workshop. Online February 2022 (Oral presentation)

Lawrence, A. & Dowey, N. Six simple steps towards making GEES fieldwork more accessible and inclusive

University Geoscience UK, Equality Diversity and Inclusivity Workshop Series. Online January 2022 (Workshop and panel discussion)

Lawrence, A., Dowey, N., Greene, S., Houghton, J. & Williams, R. Workshop 1: Designing Inclusive Fieldwork

11th Enhancing Fieldwork Learning Showcase. Online September 2021 (Oral presentation and panel discussion)

Lawrence, A. & Dowey, N. Six simple steps towards making GEES fieldwork more accessible and inclusive

Lawrence, A., Askew, E., Jackson, C., Pan, Y. Rewhorn, E. & Viseur, S. “Diversity and inclusion in fieldwork”

Goldschmidt Virtual 2021. Online July 2021 (Oral presentation and panel discussion)

Lawrence, A. Six Simple Steps towards making fieldwork more accessible and inclusive

Lawrence, A., Biswakarma, J., Conley, D.J., Gómez-Arias, A., Jackson, J., Piccoli, F., Sun, Q. “Diversity and inclusion in geosciences”

Royal Society of Chemistry Identifying Barriers in STEM Seminar Series. Online May 2021 (Oral presentation)

Lawrence, A. Autistic *and* Academic? The perks and pitfalls of being a neurodiverse researcher

Metamorphic Studies Group Research in Progress Meeting. Online March 2021 (Panel discussion)

Lawrence, A., Bidgood, A., Murphy, K., Stokes, A., Storey, C., Tual, L. & Warren, C. “How to be inclusive- Big change or small steps?”

University of Birmingham Human Geography Brown Bag Seminar Series. Online March 2021 (Oral presentation)

Lawrence, A. A perspective on Equality, Diversity and Inclusivity in Geoscience Fieldwork

University of Cambridge Sedgwick Club talks. Online February 2021 (Oral presentation)

Lawrence, A. & Fernando, B. Improving EDI in academic and field settings

The EDIG Conference. Online December 2020 (Oral presentation and panel discussion)

Lawrence, A. Six simple steps to make fieldwork more accessible and inclusive

Lawrence, A., Christakou, D., Crane, L., Fernando, B. & Mapani, B. Equality, Diversity and Inclusivity in Geoscience Session 3: Where are we going?

University of Birmingham Earth Science Seminar Series. Online October 2020 (Oral presentation)

Lawrence, A. & Atterby, J. Fixing fieldwork: How can we make geological fieldwork more inclusive and accessible?

Volcanic and Magmatic Studies Group Conference. Plymouth, UK January 2020 (Poster)

Lawrence, A., Hastie, A.R., Stevenson, C.T.E. & Fowler, M.F. Petrogenesis and emplacement of the Ratagain Granite Complex, Western Scotland

Open University Geological Society 47th Annual Symposium. Milton Keynes, UK August 2019 (Poster)

Lawrence, A., Hastie, A.R., Stevenson, C.T.E., Fowler, M.F. & Storey, C. Petrogenesis and emplacement of the Ratagain Granite Complex, Western Scotland

Winner, Best poster by popular vote

The University of Birmingham GEES Doctoral Research Conference. Birmingham, UK May 2019 (Poster)

Lawrence, A., Hastie, A.R., Stevenson, C.T.E., Fowler, M.F. & Storey, C. Petrogenesis and emplacement of the Ratagain Granite Complex, Western Scotland

Winner, Best poster

Press releases/ media appearances

University of Birmingham Press Office (2021, June 10) Institutional environments trap disabled geoscientists between a rock and a workplace

Quays News (2021, May 27) Feature Report: Highlighting the 'diversity crisis' in Geoscience

University of Birmingham Press Office (2021, April 30) Geoscientists Call for Action on Tackling Racial Inequity

CONTENTS LISTING

Abstract

Acknowledgements

List of Publications and Presentations

Table of Contents

List of Figures

List of Tables

List of Abbreviations

TABLE OF CONTENTS

Chapter 1 Introduction 1

Perspective and overview 2

Thesis structure 5

List of references 5

Chapter 2 Mush ado about the Ratagain Complex, NW Scotland: Insights on Caledonian granitic magmatism and emplacement from magnetic fabric analyses 9

Abstract 10

Introduction 10

Geological background 11

Methods 18

Discussion 36

Conclusions 42

Acknowledgements 43

List of references 44

Chapter 3 Slab-failure or Slab-success? Examining the contributions of crust and mantle to post-subduction magmatism in the Ratagain Complex, NW Scotland 53

Abstract 54

Introduction 54

Geological background 55

Sampling and analytical methods 60

Results 61

Discussion 71

Conclusions 78

Acknowledgements 78

List of references 79

Chapter 4 A UK perspective on tackling the geoscience racial diversity crisis in the Global North 86

Abstract 88

Introduction 88

Factors involved in racial inequity in UK geoscience 89

What can we do about it? 91

Acknowledgements 94

Additional information 94
List of references 94

Chapter 5 Between a rock and a workplace 97
Introduction 98
Exclusion from the outset 98
Falling flat when fitting in 98
Ableist academic systems 99
Gaining ground 99
List of references 100

Chapter 6 Six simple steps towards making GEES fieldwork more accessible and inclusive 102
Abstract 103
Introduction 103
The Six Steps 104
Summary 110
Acknowledgements 110
List of references 111

Chapter 7 Muddy Glee at the crossroads: How can we consider intersectionality more holistically in fieldwork? 115
Abstract 116
Introduction 116
Intersectionality in action 116
Gatekeepers to the field 117
Personal accounts and framing 117
Conclusion 118
Acknowledgments 119
List of references 119

Chapter 8 Conclusions and outlook 122
Introduction 123
Summary 123
Concluding remarks 125
List of references 126

Appendices **127**

Appendix 1: Supplementary materials for Chapter 2 ..... **128**

Table S1 Summary of anisotropy of magnetic susceptibility data from the Ratagain Complex 129-130

Table S2 Summary of anhysteretic remanent magnetization data from the Ratagain Complex 131

Table S3 Summary thin-section microstructural analyses from the Ratagain Complex 132

Table S4 Summary of isothermal remanent magnetization component analysis for representative samples 133

Thermomagnetic results for sample AL002 134

Thermomagnetic results for sample AL009 135

Thermomagnetic results for sample AL011 136

Thermomagnetic results for sample AL017 137

Thermomagnetic results for sample AL031 138

Thermomagnetic results for sample AL038 139

Thermomagnetic results for sample AL045 140

Thermomagnetic results for sample AL048 141

Thermomagnetic results for sample AL054 142

Thermomagnetic results for sample AL062 143

Thermomagnetic results for sample AL067 144

Thermomagnetic results for sample AL079 145

Thermomagnetic results for sample AL081 146

Thermomagnetic results for sample AL094 147

Thermomagnetic results for sample AL096 148

Thermomagnetic results for sample AL100 149

Appendix 2: Supplementary materials for Chapter 3 ..... **150**

Table SA1 XRF standards 151

Table SA2 XRF data for the Ratagain Complex 152-153

Table SA3 LOI data for the Ratagain Complex 154-155

Table SA4 XRF data for the Northern Highlands Granite Suite 156-157

Table SA5 XRF data for representative lamphrophyres of the Northern Highlands Minette Suite 158

Table SB1 RbSr isotope analyses and recalculated values for the Ratagain Complex 159

Table SB2 SmNd isotope analyses and recalculated values for the Ratagain Complex 160

Table SC1 SEM standards 161-162

Table SC2 SEM data for sample AL013 163
Table SC3 SEM data for sample AL059 164
Table SC4 SEM data for sample AL063 165
Table SC5 SEM data for sample AL074 166
Table SC6 SEM data for sample AL092 167
Table SD1 Crystal-liquid separation models for the Ratagain Complex 168
Table SD2 PCA results for the Ratagain Complex 169
PCA scree plot for samples from the Ratagain Complex 170
PCA score plot for samples from the Ratagain Complex 171
PCA loading plot for samples from the Ratagain Complex 172

Appendix 3: Supplementary materials for Chapter 4 173
Full Reading List 174

List of figures

Figure 2.1 Overview map of the Late Caledonian Silurian-Devonian granitoids in Great Britain and Ireland 12

Figure 2.2 Simplified geological map of the Ratagain Complex 14

Figure 2.3 Mesoscopic features of the Ratagain Complex 16

Figure 2.4 Microstructural features of Pl, Bt and Qz in the Ratagain Complex 17

Figure 2.5 Map of the Ratagain Complex showing the sampling locations and the AMS stereograms at each site. 21

Figure 2.6 Equal area lower hemisphere stereoplots of AMS axes for all sample points in the Ratagain Complex 23

Figure 2.7 Plot of magnetic susceptibility anisotropy against the mean susceptibility for the Ratagain Complex 24

Figure 2.8 Maps showing various magnetic parameters interpolated across the Ratagain Complex 24

Figure 2.9 AMS and anisotropy of AARM results from 16 representative sites of the Ratagain Complex. 25-26

Figure 2.10 Thermal variation of low-field magnetic susceptibility from representative samples. 28-29

Figure 2.11 Normalized pARM coercivity spectra for representative samples 30

Figure 2.12 Representative photomicrographs of magnetite in the Ratagain Complex 32

Figure 2.13 EDX spectra, data and BSE images of magnetite grains 33

Figure 2.14 IRM acquisition curves and coercivity unmixing analysis of IRM acquisition curves for representative samples 34

Figure 2.15 Interpretations of the magnetic fabric pattern of the Ratagain Complex 38

Figure 2.16 Maps showing the magnetic lineation, foliation and overall fabric pattern of the Ratagain Complex 39

Figure 2.17 Schematic 3D cut-away model of the Ratagain Complex 42

Figure 3.1 Overview map of the Late Caledonian Silurian-Devonian granitoids of Great Britain and Ireland 57

Figure 3.2 Simplified geological map of the Ratagain Complex 59

Figure 3.3 QAP rock classification diagram showing the rocks of the Ratagain Complex 64

Figure 3.4 Representative hand specimen photographs of the Ratagain Complex 65

Figure 3.5 Representative photomicrographs of the Ratagain Complex 66

Figure 3.6 Geochemical characteristics of the Ratagain Complex 67

Figure 3.7 Variation diagrams for major element oxides plotted against SiO_2 for the Ratagain Complex and NHG suite 68

Figure 3.8 Variation diagrams for selected trace elements plotted against SiO_2 for the Ratagain Complex, NHM and NHG suite 69

Figure 3.9 Chondrite-normalized REE diagrams and primitive-mantle-normalized trace-element spider diagrams for samples from the Ratagain Complex 70

Figure 3.10 Initial Nd vs initial Sr isotope plot for samples from the Ratagain Complex 71

Figure 3.11 Tectonomagmatic discrimination diagrams showing slab-failure, arc and A-type fields for the Ratagain Complex and NHG suite 72

Figure 3.12 Tectonomagmatic discrimination diagrams plotting samples from the Ratagain Complex and NHG suite 73

Figure 3.13 Principal component analysis biplot of PC1 vs. PC2 scores for samples from the Ratagain Complex 75

Figure 4.1 Representation of BAME students in geology, environmental science and physical geography. 90

Figure 6.1 Example problems in the field and outcomes 106

Figure 6.2 Different destinations, same aims. 109

Figure 6.3 Representation of BAME students in the geology, environmental science and physical geography. 110

List of tables

Table 2.1 AMS and AARM data from representative sites from the Ratagain Complex 22

Table 2.2 Results of IRM component analysis for the representative samples. 35

Table 3.1 Representative whole-rock geochemical analyses for the range of rock compositions present in the Ratagain Complex 62-63

Table 3.2 Representative whole-rock radiogenic isotope data for samples from the Ratagain Complex 70

Table 3.3 Summary least-squares mixing models of crystal fractionation in the Ratagain Complex 74

List of abbreviations

AARM - Anisotropy of anhysteretic remanent magnetization

AF - Alternating field

Afs - Alkali feldspar

AMS - Anisotropy of magnetic susceptibility

Ap - Apatite

ARM - Anhysteretic remanent magnetization

ASI - Alumina saturation index

BAME - Black, Asian and minority ethnic

BSE - Back-scattered electrons

Bt - Biotite

Chl - Chlorite

Cpx - Clinopyroxene

DP - Dispersion parameters

EDI - Equity, Diversity and Inclusivity

EDX - Energy dispersive X-Ray analysis

ERA - Enabling remote activity

GEES - Geography, Earth and Environmental Sciences

GIS - Geographical Information Systems

Hbl - Hornblende

HE - Higher education

HEI - Higher education institute

HESA - Higher Education Statistics Agency

HFSE - High field strength elements

HREE - Heavy rare earth elements

IRM - Isothermal remanent magnetisation

LA-ICP-MS - Laser ablation inductively coupled plasma mass spectrometry

LGBTQ+ - Lesbian, gay, bisexual, transgender, queer and other sexual identities

LILE - Large ion lithophile elements

LOI - Loss on ignition

LREE - Light rare earth elements

MALI - Modified alkali-lime index

MD - Multidomain

MME - Mafic microgranular enclave

MRes - Master of Research

NHG - Northern Highland granite

NHM - Northern Highland minette

pARM - Partial anhysteretic remanent magnetisation

PC - Principal component

PCA - Principal component analysis

PGR - Postgraduate research

PhD - Doctorate of Philosophy

Plg - Plagioclase

PPL - Plane-polarised light

PSD - Pseudo-single-domain

Qz - Quartz

REE - Rare earth elements

SCLM - Subcontinental lithospheric mantle

SD - Single-domain

SEM - Scanning electron microscope

Ser - Sericite

SIRM - Saturation isothermal remanent magnetization

STEM - Science, Technology, Engineering and Mathematics

TIMS - Thermal ionization mass spectrometer

Ttn - Titanite

UGR - Undergraduate

XPL - Crossed-polarised light

XRF - X-ray fluorescence

XRD - X-ray diffraction

Zrn - Zircon

Zo - Zoisite

Chapter 1

Introduction

Perspective and overview

When one thinks of Geoscience, one often thinks of rocks. And when one thinks of rocks, one may also think of granites.

As the primary component of the upper continental crust, granites are amongst the most abundant and important rock types on Earth. They have been extensively studied in order to investigate: tectonic and geodynamic processes; styles of mineralisation; and the interaction between the Earth's mantle and crust (Kemp et al., 2007; Bonin, 2007; Sial et al., 2011; Gao et al., 2016a). Understanding how granites are generated and structurally emplaced is key to answering the question of how Earth's continental crust has grown throughout geological time; an enigma that has puzzled geoscientists since Read (1948) directed attention towards a so-called 'room problem' in his landmark talk 'Granites and granites'.

The 'room problem' is concerned with how space could be created in pre-existing continental crust to accommodate large volumes of granitic magmas and polarised views in the Geoscience community at the time (Kemp, 2005). Some researchers asserted that granitoids arose from non-magmatic, solid-state alteration, which circumvented the 'room problem' as existing country rocks were simply replaced (or transformed) into granitic plutons through 'granitisation' (Read, 1948). On the other hand, magmatist factions argued that plutons formed via a melt-dominated mechanism, crystallizing from magmas (Coleman et al., 2016).

The pioneering experimental melting studies of Tuttle and Bowen (1958) provided firm support for the magmatic origin of granite, as they concluded that partial melting and fractional crystallisation offered "a mechanism for producing large batholithic masses of granite" (Tuttle & Bowen 1958, p. 2).

Yet finding 'room' for granites still remained problematic as following their genesis in the uppermost mantle or lower crustal source regions, granitic magmas must ascend to higher structural levels (Nédélec & Bouchez, 2015), effectively displacing existing crustal rocks, to reach their ultimate position (Anderson et al., 2018). Precisely how such vertical transport of melt and emplacement of large intrusive bodies in the rigid upper continental crust takes place can be difficult to pinpoint (Petford et al., 2000; Kemp, 2005) as this is essentially a hidden, sub-surface phenomenon.

It follows that over the years many, often conflicting, hypotheses have been forwarded for how space is made for newly incoming magma in the upper continental crust (Petford et al., 2000). A range of emplacement mechanisms have been proposed, from the now-discounted diapirism that dominated twentieth-century thought (Grout, 1945; Ramberg, 1967; Fyfe, 1973; Marsh, 1982; England, 1990); to its successor ballooning/ inflation (Holder, 1979, Molyneux & Hutton, 2000; Stevenson, 2004; Gill, 2010; McCarthy et al., 2015); to stoping and cauldron subsidence (Žák et al., 2006; Burchardt et al., 2012; Burchardt et al.,2016; Mattsson et al., 2019).

The most recent paradigm is that intrusions are constructed incrementally from small, discrete batches of magma, which are fed to the growing intrusive body via dike and sill complexes (e.g., Petford et al., 2000; Glazner et al., 2004; Gudmundsson, 2011; Coleman et al, 2016). Space is provided for intruding magmas in the crust by the development or reactivation of major tectonic structures, such as strike-slip faults, and pre-existing structures including fault stepovers, pull-aparts, releasing bends, thrusts, high-angle reverse faults may act as dilatant sites (Hutton, 1996; Stevenson, 2004). Subsequent combinations of inflation and roof lifting or small-scale, localised stoping can also progressively accommodate the incoming magma (Kemp, 2005). This mechanism of emplacement and assembly is

supported by numerical modelling (e.g Annen, 2009), U-Pb geochronology (e.g., Matzel et al., 2006; Miller, 2008; Barbaroni et al., 2015) and the 3D subsurface geometry of many investigated intrusions (e.g., Annen et al., 2015). Structural investigations utilising rock magnetic techniques further support incremental emplacement through sheet accretion, as mineral fabrics representing temporally distinct magma pulses have been identified within intrusive bodies (Clemens & Benn, 2010; Sheibi et al., 2012; Anderson et al., 2018).

However, there still remains a lack of consensus regarding the exact type and spatio-temporal extent of the processes controlling granitic magma ascent, emplacement and crystallisation (Hines et al., 2018) and debate also surrounds the linkages between the growth of granitic intrusions and local or regional tectonic processes. Further investigation of the links between magmatism and tectonism is needed to aid understanding of the controls that tectonic processes have on the dynamics of magma transfer and storage within different tectonic systems and the resultant geometry and evolution of granitic intrusions (Zellmer & Annen, 2008).

Therefore, this thesis explores the links between tectonics, granitic magmatism and emplacement through a case study of the Late Caledonian Ratagain Granite Complex, Scotland, UK, to inform our understanding of how the continental crust is constructed.

My studies of the Ratagain Complex involved four field sessions in the remote northwest highlands of Scotland, wherein I had to undertake physically demanding fieldwork on challenging terrain. Through my determination and perseverance, I was able to collect over 100 block samples of rock which represents the largest geochemical sample haul for a Late Caledonian intrusion to date. This research led to several co-authored manuscripts, which are presented in Chapter 2 and Chapter 3 of this thesis.

However, whilst I bore witness to great compositional heterogeneity in the rocks of the Ratagain Complex in the field, this was not mirrored by the diversity of the Geoscience community in the academy. Since its rise to prominence as a discipline in Western academia during the 18th century (Stafford, 1984; Sangwan, 1993) knowledge production in the Geosciences has been firmly set within a frame of white, able, cisgender, heterosexual affluence. Those whose voices didn't conform to the status quo, by virtue of class, ethnicity, gender or (dis)ability were historically excluded and this legacy continues; to this day the Geosciences remains one of the least diverse branches of the science, technology, engineering and mathematics (STEM) tree (e.g. Stokes et al., 2015; Bernard & Cooperdock, 2018; Núñez et al., 2020;). Indeed Morris (2021) postulates that Geoscience culture, is defined by who it excludes, as opposed to who it includes.

Over the course of my PhD, I became more interested in equity, diversity and inclusivity (EDI), in the Geosciences, particularly with the onset of the COVID-19 pandemic, which brought matters of social inequality into the wider public conscience. The pandemic also heightened my awareness of my own intersectionality; as a mixed ethnicity, autistic and LGBTQ+ individual, I sit at the intersection between various marginalized groups, with these different aspects of my identity facing prejudice both separately and simultaneously.

For the first time I began to understand that the complex ways in which my disability, ethnicity, sexuality and gender interacted and affected my individual experience of academic Geoscience and had served to increase the marginalization and discrimination that I had faced throughout my education and continued to face in my PhD studies. Crenshaw (2016) articulates experiencing such challenges and dilemmas as a consequence of one's intersectionality as 'discrimination squared'. It was with this heightened awareness of the diversity of my lived experience and a determination to help others like myself in academic

Geoscience, who were encountering similar barriers, that I began to undertake considerable EDI advocacy work. I became an active member of my School's EDI Committee making worthwhile contributions, which included both voicing concerns and offering potential solutions, in my discussions with other faculty and student members.

Although my committee work greatly improved my confidence in social situation, the slow pace of change and reluctance of some colleagues to implement EDI measures, was a constant source of frustration for me. Ever determined to maintain progress, I decided to leap forwards into EDI-related research. To integrate social science methods into my existing skill set, I took it upon myself to seek out training alongside my committee work and PhD project, learning about qualitative lines of inquiry, mixed methods research design and researching aspects of marginalization such as disability. What resonated with me most of all was the power of autoethnography as genre of research and inquiry. Like so many other academics in STEM disciplines I was imbibed in positivist epistemology; accepting without question that quantitative, observable evidence that conformed to established research methods, were the fundamental constituents of science.

Yet paradoxically it was during the pandemic, when lockdowns and travel restrictions had prevented me from conducting scientific research, that I was given the unique and unexpected opportunity to consider my own reflexivity and voice in this research. I came to realize that I was naïve to consider a researcher a separate entity from the scientific research process and wrong to assume that the researcher's own rhetoric, internal prejudices and experiences had no effect on the research outcomes (Wall, 2006). As my intersectionality affected my entire experience of the world, it followed that it affected every aspect of my research too. From the way I experienced the myriad of stimuli in the field environments I worked in through to the way I formed interpretations of mineral textures and deformational microstructures in petrographical thin sections- all of my work was influenced through my identity.

Moreover, I came to see the value in these personal experiences; as suggested by Adams et al. (2017) those who have directly experienced institutional oppressions, racism, sexism and ableism, can talk about these issues in ways different from others who have no lived experiences of such prejudice.

It was with this understanding that I could use the nuance of my lived experience to articulate new, valuable knowledge that I went on to publish articles concerned with EDI in Geoscience, STEM disciplines and academia as a whole. These articles form Chapters 4, 5, 6 and 7 of this thesis. Whilst the EDI issues discussed were far-ranging- from the systemic exclusion and barriers to progression that marginalized researchers face to the benefits of using virtual communication with neurodiverse individuals- a common aspect of all the writing was its grounding in autoethnography. These publications featured in internationally-renowned journals, including *Nature* titles, and attracted interest not only from the academic community but gained attention from the media, private enterprises and public sector organisations too.

Thus, it can be seen that this thesis seeks to dually address perhaps some of Geoscience's most classic and contemporary questions; how do granites construct the continental crust and how do we build diversity in the Geosciences?

Thesis structure

This thesis consists of a compilation of published and unpublished research carried out over the course of this PhD project. The chapters of this thesis (with the exception of the introduction) are self-contained manuscripts with separate introductions, detailed methodologies and conclusions as they have either been published or submitted for publication as independent papers. Each chapter is prefaced by a brief synopsis of what stage the manuscript is at in the publication process, as well as a statement of all author contributions.

List of references

Adams, T. E., C. Ellis, & S. H. Jones. 2017. “Autoethnography.” In The International Encyclopedia of Communication Research Methods, edited by J. Matthes, 1–11. Wiley-Blackwell. Available from: https://doi:10.1002/9781118901731.iecrm0011

Anderson, P.E., Stevenson, C.T., Cooper, M.R., Meighan, I.G., Reavy, R.J., Hurley, C.T., Inman, J. & Ellam R.M. 2018. Refined model of incremental emplacement based on structural evidence from the granodioritic Newry igneous complex, Northern Ireland. *Geological Society of America Bulletin*, **130**(5-6) ,740-756. Available from: https://doi.org/10.1130/B31756.1

Annen, C. 2009. From plutons to magma chambers: Thermal constraints on the accumulation of eruptible silicic magma in the upper crust. *Earth and Planetary Science Letters*, **284**(3-4), 409-416. Available from: https://doi.org/10.1016/j.epsl.2009.05.006

Barboni M., Annen C. & Schoene B. 2015. Evaluating the construction and evolution of upper crustal magma reservoirs with coupled U/Pb zircon geochronology and thermal modelling: a case study from the Mt. Capanne pluton (Elba, Italy). *Earth and Planetary Science Letters*, **432**, 436–448. Available from: https://doi.org/10.1016/j.epsl.2015.09.043

Bernard, R. E. & Cooperdock, E. H. G. 2018. No progress on diversity in 40 years. *Nature Geoscience*, **11**, 292–295. Available from: http://doi:10.1038/s41561-018-0116-6

Bonin, B. 2007. A-type granites and related rocks: Evolution of a concept, problems and prospects. *Lithos*, **97**(1-2), 1-29. Available from: https://doi.org/10.1016/j.lithos.2006.12.007

Burchardt, S., Tanner, D. & Krumbholz, M. 2012. The Slaufrudalur Pluton, Southeast Iceland — an example of shallow magma emplacement by coupled cauldron subsidence and magmatic stoping. *Geological Society of America Bulletin*. **124**(1-2). 213-227. Available from: https://doi.org/10.1130/B30430.1

Burchardt, S., Troll, V., Schmeling, H., Koyi, H. & Blythe, L. 2016. Erupted frothy xenoliths may explain lack of country-rock fragments in plutons. *Scientific Reports*, **6**, 34566. Available from: https://doi.org/10.1038/srep34566

Clemens, J.D. & Benn, K. 2010. Anatomy, emplacement and evolution of a shallow-level, post-tectonic laccolith: the Mt Disappointment pluton, SE Australia. *Journal of the Geological Society*, **167**(5), 915-941. Available from: https://doi.org/10.1144/0016-76492009-120

Coleman, D.S., Mills, R.D. & Zimmerer, M.J. 2016. The Pace of Plutonism. *Elements*, **12** (2), 97-102. Available from: https://doi.org/10.2113/gselements.12.2.97

Crenshaw, K. W. 2016. The urgency of intersectionality. [Video]. Available from: http://www.ted.com/talks/kimberle_crenshaw_the_urgency_of_intersectionality#t-556746. Accessed: 06/07/2021.

England, R.W. 1990. The identification of granite diapirs. *Journal of the Geological Society*, **147**(6), 931-933. Available from: https://doi.org/10.1144/gsjgs.147.6.0931

Fyfe, W.S. 1973. The generation of batholiths. *Tectonophysics*, **17**(3) 273-283. Available from: https://doi.org/10.1016/0040-1951(73)90007-3

Gao, P., Zheng, Y.F. & Zhao, Z.F. 2016. Experimental melts from crustal rocks: a lithochemical constraint on granite petrogenesis. *Lithos*, **266-267**,133-157. Available from: https://doi.org/10.1016/j.lithos.2016.10.005

Gill, R. 2010. *Igneous Rocks and Processes: A Practical Guide*. Wiley-Blackwell.

Glazner, A.F., Bartley, J.M., Coleman, D.S., Gray, W. & Taylor, R.Z. 2004. Are plutons assembled over millions of years by amalgamation from small magma chambers? *GSA Today*, **14**(4), 4-11. Available at: http://www.geosociety.org/gsatoday/archive/14/4/pdf/gt0404-05.pdf

Grout, F.S. 1945. Scale models of structures related to batholiths. *American Journal of Science*, **243**, 260-284.

Gudmundsson, A. 2011. Deflection of dykes into sills at discontinuities and magma-chamber formation. *Tectonophysics*, **500**(1-4), 50-64. Available from: https://doi.org/10.1016/j.tecto.2009.10.015

Holder, M.A. 1979. An emplacement mechanism for post tectonic granites and its implications for the geochemical features. In Atherton, M.P.& Tarney, J. (Eds) *Origin of Granite Batholiths Geochemical Evidence* (pp.117–126). Shiva

Hines, R., Paterson, S.R., Memeti, V. & Chambers, J.A. 2018. Nested incremental growth of zoned upper crustal plutons in the Southern Uplands Terrane, UK: fractionating, mixing, and contaminated magma fingers. *Journal of Petrology*, **59**(3), 483–516. Available from: https://doi.org/10.1093/petrology/egy034

Hutton, D.H.W. 1996. The ‘space problem’ in the emplacement of granite. *Episodes*, **19**(4), 114-119.

Kemp, A.I.S. 2005. Granite. In Selley, R.C., Robin, L., Cocks, M. & Plimer, I.R. (Eds.) *Encyclopaedia of Geology* (pp.233-247). Elsevier Academic. Available from: https://doi.org/10.1016/B0-12-369396-9/00301-4

Kemp, A.I.S., Hawkesworth, C. J., Foster, G. L., Paterson, B. A., Woodhead, J. D., Hergt, J. M., Gray, C. M. & Whitehouse, M. J. 2007. Magmatic and Crustal Differentiation History of Granitic Rocks from Hf-O Isotopes in Zircon. *Science*, **315**(5814), 980-983. Available from: http://science.sciencemag.org/content/315/5814/980

Marsh, B.D. 1982. On the mechanics of igneous diapirism, stoping and zone melting. *American Journal of Science*, **282**(6) 808-855. Available from: https://doi.org/10.2475/ajs.282.6.808

Mattsson, T., Burchardt, S., Mair, K. and Place, J. 2019. Host-rock deformation during the emplacement of the Mourne Mountains granite pluton: Insights from the regional fracture pattern. *Geosphere*, **16**(1), 182–209. Available from: https://doi.org/10.1130/GES02148.1

Matzel, J. E., Bowring, S. A., & Miller, R. B. 2006. Time scales of pluton construction at differing crustal levels: Examples from the Mount Stuart and Tenpeak intrusions, North Cascades, Washington. *Geological Society of America Bulletin*, **118**(11-12), 1412-1430. Available from: https://doi.org/10.1130/B25923.1

McCarthy, Petronis, W., M. S., Reavy, R. J. & Stevenson, C. T. 2015. Distinguishing diapirs from inflated plutons: an integrated rock magnetic fabric and structural study on the Roundstone Pluton, western Ireland. *Journal of the Geological Society*, **172**(5), 550-565. Available from: https://doi.org/10.1144/jgs2014-067

Miller, J. S. 2008. Assembling a pluton… one increment at a time. Geology, **36**(6), 511-512. Available from: https://doi.org/10.1130/focus062008.1

Molyneux, S.J. & Hutton, D.H.W. 2000. Evidence for significant granite space creation by the ballooning mechanism: The example of the Ardara pluton, Ireland. *Geological Society of America Bulletin*,**112**(10), 1543-1558. Available from: https://doi.org/10.1130/0016-7606(2000)112<1543:EFSGSC>2.0.CO;2

Morris, V.R. 2021. Combating Racism in the Geosciences: Reflections From a Black Professor. AGU Advances, 2e2020AV000358. Available from: Available from: https://doi.org/10.1029/2020AV000358

Nédélec, A. & Bouchez, J-L. 2015. *Granites: Petrology, Structure, Geological Setting, and Metallogeny*. Oxford University Press.

Núñez, A. M., Rivera, J., & Hallmark, T. 2020. Applying an intersectionality lens to expand equity in the geosciences. Journal of Geoscience Education, **68**(2), 97–114. Available from: https://doi.org/10.1080/10899995.2019.1675131

Petford, N., Cruden, A.R., McCaffrey, K.J.W. & Vigneresse, J.L. 2000. Granite magma formation, transport and emplacement in the Earth's crust. *Nature*, **408**, 669–673. Available from: https://doi.org/10.1038/35047000

Ramberg, H. 1967. *Gravity, Deformation and the Earth's Crust as studied by Centrifuged Models*. Academic Press.

Read, H.H. 1948. Granites and granites. *Memoirs of the Geological Society of America*, **28**, 1–19.

Sangwan, S. 1993. Reordering the Earth: The emergence of geology as a scientific discipline in colonial India. *Earth Sciences History*, **12**(2), 224–233. Available from: http://www.jstor.org/stable/24138610

Sheibi, M., Bouchez, J. L., Esmaeily, D., and Siqueira, R. 2012. The Shir-Kuh pluton (Central Iran): magnetic fabric evidences for the coalescence of magma batches during emplacement. *Journal of Asian Earth Sciences*, **46**, 39-51. Available from: https://doi.org/10.1016/j.jseaes.2011.10.006

Sial, A.N., Bettencourt, J. S., De Campos, C. P. & Ferreira, V.P. (Eds.) 2011. Granite-Related Ore Deposits [Special issue], *Geological Society, London, Special Publications*, **350**,1-5. Available from: https://doi.org/10.1144/SP350.1

Stafford, R.A. (1984) Geological Surveys, Mineral Discoveries, and British Expansion, 1835–71. *Journal of Imperial and Commonwealth History*, **12**(3), 5–32. Available from: https://doi.org/10.1080/03086538408582669

Stevenson, C. T. E. 2004. *Magma Flow and Granite emplacement in Contrasting Tectonic Environments using Anisotropy of Magnetic Susceptibility* [Unpublished PhD dissertation]. University of Birmingham, United Kingdom.

Stokes, P.J., Levine, R., & Flessa, K.W. 2015. Choosing the geoscience major: important factors, race/ethnicity, and gender. *Journal of Geoscience Education,* **63**(3), 250–263. Available from: https://doi.org/10.5408/14-038.1

Tuttle, O. F. & Bowen, N. L. 1958. *Origin of granite in the light of experimental studies in the system $NaAlSi_3O_8$-$KAlSi_3O_8$-SiO_2-H_2O*. *Geological Society of America Memoirs*, **74**.

Wall S. 2006. An Autoethnography on Learning About Autoethnography. *International Journal of Qualitative Methods*, **5**(2), 146-160. Available from: https://doi.org/10.1177/160940690600500205

Žák, J., Holub, F. & Kachlík, V. 2006. Magmatic stoping as an important emplacement mechanism of Variscan plutons: evidence from roof pendants in the Central Bohemian Plutonic Complex (Bohemian Massif). *International Journal of Earth Sciences*, **95**, 771-78. Available from: https://doi.org/10.1007/s00531-006-0076-8

Zellmer G.F. & Annen C. 2008. An introduction to magma dynamics. *Geological Society, London, Special Publications*, **304**, 1-13. Available from: https://doi.org/10.1144/SP304.1

Chapter 2

Mush ado about the Ratagain Complex, NW Scotland: Insights on Caledonian granitic magmatism and emplacement from magnetic fabric analyses

Published paper

Lawrence, A. [1], Maffione, M.[1] and Stevenson, C.T.E.[1]

The Scottish Journal of Geology, 2022. 58, sjg2021-018. https://doi.org/10.1144/sjg2021-018

I collected, managed, analysed and presented all the field, structural and petrographic data that informed this publication. I also conceptualised and wrote the majority of the manuscript, with input on the IRM modelling from Marco Maffione and Carl Stevenson assisting with the AMS analyses, magnetic fabric interpretation and design of the final emplacement model for the Ratagain Complex.

[1]School of Geography, Earth and Environmental Sciences, University of Birmingham, Birmingham, UK

Abstract

The anisotropy of magnetic susceptibility (AMS) is used to reveal subtle mineral alignment fabrics in apparently isotropic crystalline lithologies, including granites. Such petrofabrics can be produced by emplacement-related magma flow or post-emplacement tectonic strain. However, discriminating between flow-related and tectonic fabrics using field observations alone may be challenging and is usually a broad and arbitrary interpretation. In this contribution, we employ a range of magnetic analyses to characterize the origin of the petrofabric in the c. 425 Ma Ratagain Complex, NW Scotland, a composite Late Caledonian granitic intrusion. Our detailed magnetic analyses reveal that whilst all intrusive units carry an ambient tectonic overprint, critically, this has not developed into an obvious tectonic fabric and contains a horizontal shortening component indicative of transpression. This appears at odds with the well-defined Silurian (Scandian phase) regional transtensional tectonic regime from c. 420–415 Ma onwards. Accordingly, we suggest that either the complex is younger than previously thought or that it existed as a crystal-mush close to the magmatic solidus for a protracted period after its initial emplacement. This study lays the foundations for much-needed further investigations into the detailed emplacement mechanisms, timescales and petrogenesis of individual granitic intrusions, to aid understanding of Late Caledonian tectonics.

Introduction

The anisotropy of magnetic susceptibility (AMS) is an important tool used for reconstructing petrofabrics (i.e. preferred orientations and distributions of minerals) in granitic rocks where visible flow markers are often weak or completely absent (Tarling & Hrouda, 1993; Bouchez,1997). For over six decades it has been documented that the patterns of magnetic foliation and lineation in a granitic intrusion (i.e. the magnetic fabric) can be coaxial with the petrofabric of the intrusion (e.g. King, 1966; Heller, 1973; Tarling & Hrouda, 1993; Borradaile & Henry, 1997; Nédélec & Bouchez 2015; Temporim et al., 2020). Socalled ‘normal’ magnetic fabrics have a maximum susceptibility axis (K_1) that is parallel to the petrofabric lineation, whilst the minimum susceptibility axis (K_3) is generally found perpendicular to the petrofabric foliation. In magnetite-series granites (Ishihara, 1977) normal fabrics are characterized by multidomain (MD – great than 0.1 μm diameter) ferromagnetic minerals including magnetite, maghemite and other related cubic iron oxides (Rochette et al., 1992).

However, the interpretation of AMS data can be complicated by the presence of single-domain (SD – smaller than 0.1 μm diameter) ferromagnetic grains, which can result in an inverse magnetic fabric where K_1 and K_3 are swapped, hence showing K_3 parallel to the lineation and K_1 perpendicular to the foliation (Rochette, 1988). In granites containing mixed populations of MD and SD magnetite particles, the AMS ellipsoid is unlikely to accurately describe the petrofabric (Potter, 2004). It has even been suggested that in granites containing similarly aligned MD and stable SD particles the competing anisotropy signals could cancel each other out, resulting in very low anisotropy despite the rock being strongly magnetic (Potter & Stephenson, 1988).

Furthermore, if a granite comprises magnetic mineralogical species formed at different stages in the emplacement history, then several magnetic fabrics may be recorded by the same intrusive body and can often overprint one another (Benn, 2010). For example, secondary alteration products may yield a magnetic fabric that is geometrically unrelated to that acquired during emplacement of the granite (Martín-Hernández & Ferré, 2007). Therefore, determination of the primary magnetic fabric, which can serve as a proxy for the petrofabric of the intrusion, cannot be achieved solely through AMS analyses (Bouchez, 1997; Potter, 2004; Stevenson, 2004). Instead, an accurate and reliable fabric analysis requires the separation of the different

contributions of the paramagnetic–diamagnetic and ferromagnetic minerals to the magnetic fabric, and the reconstruction of the nature, shape and concentration of the magnetic carriers. Employing such a multifaceted approach to distinguish between primary and secondary fabrics, can also help to verify whether an entire intrusive body was affected by regional strain during its emplacement (Silva & Raposo, 2020).

When the magnetic fabric has been tested with various magnetic techniques, the interpretation of what the fabric records requires detailed petrological observations (e.g. Anderson et al., 2018). Even then, there may be uncertainty about the forces that created the fabric in terms of emplacement-related magma body forces ('magma flow' e.g. Stevenson et al., 2007), or post-emplacement ambient tectonic strain (Burton-Johnson et al., 2019) or a combination of the two (e.g. Petronis et al., 2012).

In this contribution we present the results of a detailed analyses of the Ratagain Granite Complex, which includes AMS, anisotropy of anhysteretic remanent magnetization (AARM), thermomagnetic experiments, isothermal remanent magnetization (IRM) acquisition and coercivity unmixing, partial anhysteretic remanent magnetization (pARM) acquisition, optical microscopy and scanning electron microscope (SEM) observations. The results allow us to reconstruct the nature, main orientation, evolution and precise timing of the magnetic fabric recorded in the Ratagain Complex and contributes to our understanding of both the different mineral sources that confer AMS and the interplays between magmatic and tectonic processes in granitic fabric development (e.g. Burton-Johnson et al., 2019). Our integrated rock magnetic characterization of the Ratagain Complex thus provides an important case study that can be applied in investigations of other composite, granitic intrusions worldwide.

Geological background

The lower Paleozoic Caledonian Orogen of Scotland and Ireland resulted from the oblique continental convergence of Laurentia, Avalonia and Baltica and associated closure of the Iapetus Ocean (e.g. Dewey, 1969; Lambert & McKerrow, 1976; Pickering et al,. 1988; Soper et al., 1992; Dewey & Strachan 2003; Corfu et al., 2014). Whilst the orogenic cycle comprised various episodes, the three major events of relevance to the Scottish Caledonides are the Grampian (c. 490–460 Ma), the Scandian (c. 435–425 Ma;) and the Acadian (c. 400–380 Ma).

The Grampian Event involved collision of an intra-oceanic island arc with Laurentia (e.g. Chew & Strachan 2014; Johnson et al., 2017) and the deformation and metamorphism of Neoproterozoic–Cambrian (Dalradian) sediments deposited on the Laurentian continental margin (Mark et al., 2020), culminating in the development of major NW-directed fold and nappe complexes. Syn-collisional magmatic activity took place in the Grampian Event, with the intrusion of two-mica S-type granites ('Older Granites' – Read, 1961; Oliver et al., 2008) and associated gabbroic rocks.

The collision of Laurentia and Baltica in the Scandian Event caused considerable regional thrusting and folding of Neoproterozoic (Moine) sedimentary rocks and associated basement inliers north of the Great Glen Fault (GGF; see Figure 2.1), but such deformational effects are difficult to trace southwards (Dallmeyer et al., 2001; Kinny et al., 2003).

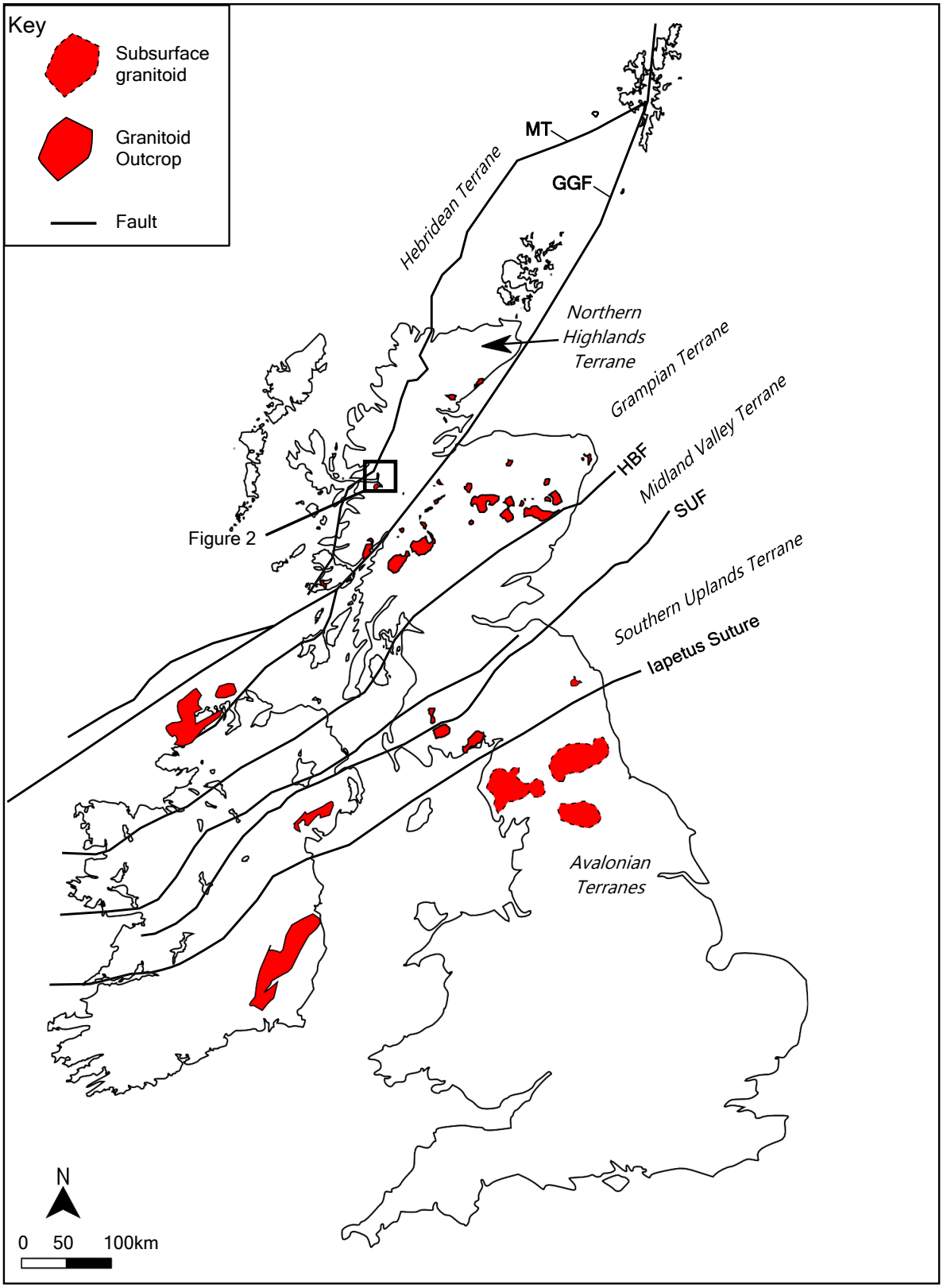


Figure 2.1 Overview map of the Late Caledonian Silurian–Devonian granitoids in Great Britain and Ireland adapted from Brown et al. (2008). The box labelled Figure 2 highlights the location of the Ratagain Complex. GGF, Great Glen Fault; HBF, Highland Boundary Fault; MT, Moine Thrust; SUF, Southern Uplands Fault.

Following the end of Iapetus subduction, the latest stages of the Scandian saw the onset of intrusion and emplacement of the Late Caledonian suite, a set of relatively undeformed granitic

(sensu lato) bodies and coeval lamprophyre and hornblende-rich dykes (i.e. ‘appinites’) that intrude much of the lower Paleozoic Caledonian Orogen of Scotland and Ireland (Figure 2.1; Archibald & Murphy, 2021). It is widely held that the emplacement of many Late Caledonian intrusions was modulated by the Scandian sinistral stress regime, with crustal-scale thrusts and shear zones within transtensional basins serving as intrusive conduits for the upwelling magma (Hutton, 1988; Hutton & Reavy, 1992; Stevenson et al., 2008; Miles et al., 2016; Strachan et al., 2020; Archibald & Murphy, 2021).

Acadian transpression is ascribed to the collision of Iberia/Armorica with Avalonia and closure of the Rheic Ocean at c.400–390 Ma (Woodcock et al., 2007). In Scotland, the Acadian is bracketed at 404–394 Ma (Miles et al., 2016; Woodcock et al., 2019) and was characterized by northward-directed, orthogonal contractional and sinistral strike-slip movements along major tectonic structures, including the Southern Upland, Highland Boundary and Great Glen faults (e.g. Phillips et al., 1995; Jones et al., 1997; Mendum & Noble, 2010; see also Figure 2.1). The intensity and effects of deformation were focused along the aforementioned fault zones and decreased with distance away from them (Mendum, 2012).

The Ratagain Complex is a granitic Late Caledonian intrusion located along the shores of Loch Duich in the western Highlands of Scotland (Figure 2.2; Nicholls, 1951; Hutton et al., 1993). The complex was emplaced into the metamorphic rocks of the Neoproterozoic Morar Group and the Archean–Paleoproterozoic Lewisian Gneiss basement of the Eastern Glenelg inlier (Krabbendam et al., 2018) in the hanging wall of the Moine Thrust. The complex is adjacent to the Strathconon Fault, one of many Silurian–Devonian NE–SW sinistral strike-slip structures associated with the GGF (Watson, 1984; Law & Johnson, 2010; Krabbendam et al., 2018).

With a composition transitional between the alkaline syenites of NW Scotland and the more commonplace metaluminous calc-alkaline granites found in central and eastern areas (Fowler et al. 2008; Bruand et al., 2014), and geochemical characteristics typical of high Ba–Sr granitic magmatism (Fowler & Henney, 1996; Fowler & Rollinson, 2012; Searle, 2022), the origin of the Ratagain Complex has been attributed to slab break-off processes based on regional geological syntheses (Atherton & Ghani, 2002; Fowler et al., 2008; Neilson et al., 2009; Fowler & Rollinson, 2012; Miles et al., 2016; Archibald & Murphy, 2021).

Petrography

A range of intrusives, including granite (Figure 2.3a, e), quartz monzonite (Figure 2.3b, c, d and h), quartz monzodiorite (Figure 2.3f, g), monzonite, monzodiorite, granodiorite and syenite occur within the postulated boundaries of the complex. All the above lithologies are characterized by quartz, plagioclase and alkali feldspars as the main felsic minerals and biotite, amphibole and relict clinopyroxene as the main mafic minerals.

The complex also varies in texture from fine-grained and equigranular, to coarse-grained and porphyritic. Coeval mafic microgranular enclaves (MMEs) occur in all intrusive units (Figure 2.3d, f) ranging from a few centimetres up to 5 m in diameter; such features are suggestive of magma mingling and possible mixing processes involving juvenile mafic to ultramafic material (Fowler et al., 2008).

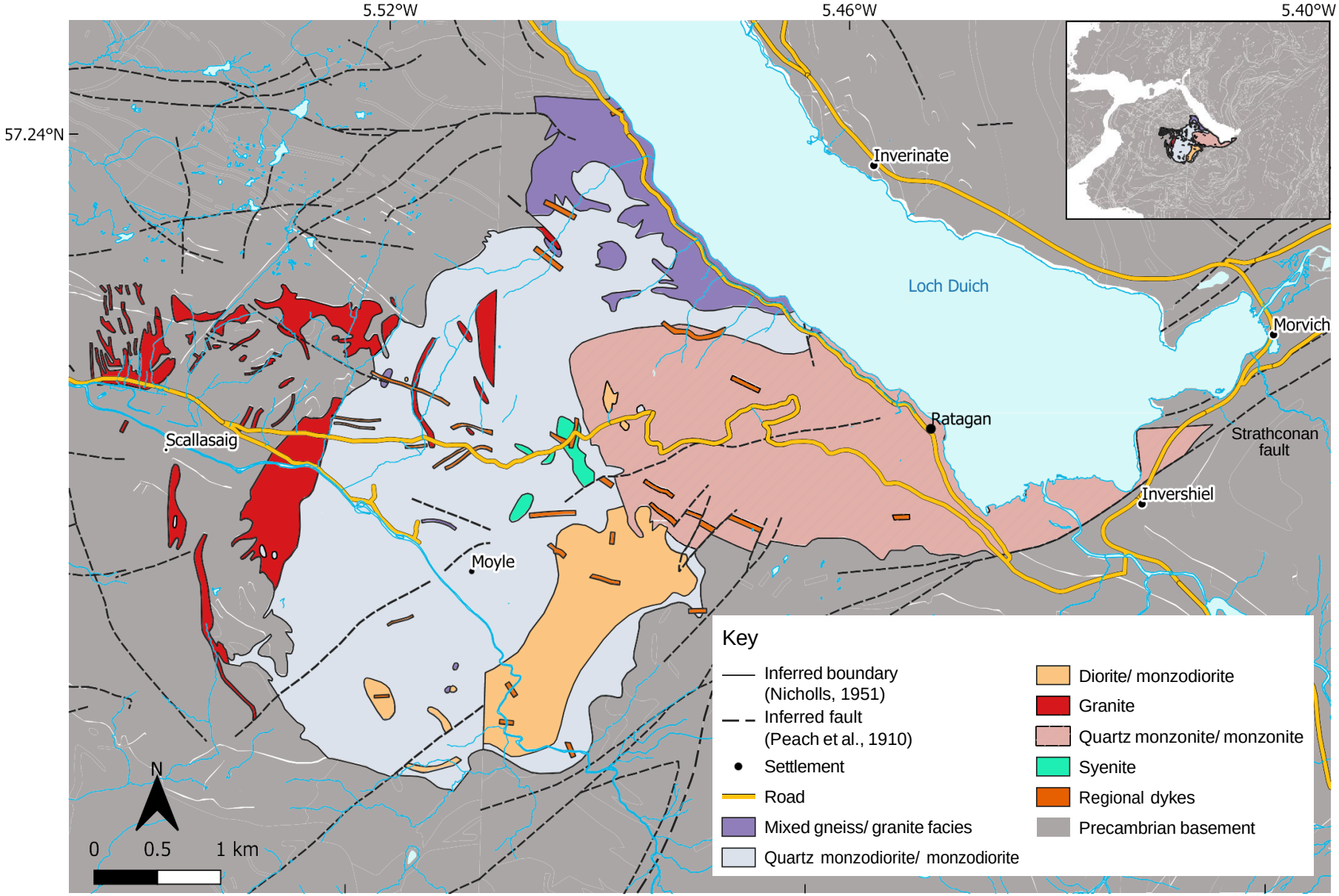


Figure 2.2 Simplified geological map of the Ratagain Complex, redrawn after Peach et al. (1910), Nicholls (1951) and Hutton et al. (1993).

Microstructures

In all the intrusive units of the Ratagain Complex, magmatic microtextures (Vernon, 2004) can be observed in thin section. The magmatic microtextures are typified by compositionally zoned euhedral to subhedral plagioclase phenocrysts (Figure 2.4a), euhedral to subhedral biotite (Figure 2.4e), subhedral to anhedral K-feldspar and anhedral quartz, which exhibits no or rare undulatory extinction (Figure 2.4i). With the exception of one locality (57° 13′ 22.86″ N, 5° 29′ 12.91″W, Figure 2.4e; see also Figure 2.3c), the biotite and quartz grains are randomly oriented and do not define a magmatic flow foliation.

In samples from the northeastern edge of the complex (Figure 2.2, see also Figure 2.3g, h), coexisting magmatic microtextures and low-temperature (T < 400°C) solid-state microstructures are evident. The low-temperature microstructures comprise highly altered plagioclase, with phenocrysts displaying partial to complete sericitization (Figure 2.4d), broken or folded grains of biotite (Figure 2.4h), and quartz showing bulging recrystallization or sutured grain boundaries (Figure 2.4k).

By contrast, shear-related medium- (400°C < T < 500°C) and high-temperature (T > 650°C) solid-state microstructures are weakly developed and only discernible in a few thin sections. The medium-temperature microstructures feature occasional myrmekite (Figure 2.4c), kinked plagioclase twins, cleavage traces in biotite (Figure 2.4g) and quartz subgrains (Figure 2.4i). The high-temperature deformation microstructures display deformation twinning in plagioclase (Figure 2.4b), chessboard extinction in quartz (Figure 2.4j) and bent biotite.

Internal structures

Hutton and McErlean (1991) mapped visible, steeply dipping foliations consisting of aligned plagioclase feldspar throughout the Ratagain Complex. The authors interpreted these as pre-full crystallization (PFC) fabrics and attributed them to mid-Silurian deformation (Hutton & McErlean, 1991; Hutton et al., 1993; McErlean, 1993) and they interpreted the mapped fabric pattern to show two NW–SE-trending sinistral shear zones. The authors attributed these PFC fabrics to mid-Silurian deformation. However, the mesoscopic fabrics described by these workers are typically weak (Figure 2.3b) and difficult to identify in the field.

Small-scale cataclasite-breccia zones (Figure 2.3g) within the intrusion have been taken as evidence of Early Devonian post-emplacement, low-temperature, solid-state deformation (Hutton & McErlean, 1991). These minor shear zones are restricted to the NE of the intrusion, in close proximity to Loch Duich, and are cut by numerous quartz–fluorite–calcite veins (Figure 2.3h).



Figure 2.3 Mesoscopic features of the Ratagain Complex. (a) Highly irregular boundary between country rocks and the Ratagain monzonite (57° 14′ 28.15″ N, 5° 29′ 41.89″ W). (b) A rare pre-full crystallization fabric in the Ratagain quartz monzodiorite aligned parallel to the scale (57° 13′ 16.73″ N, 5° 29′ 22.20″ W). (c) Magmatic flow structure in the quartz monzonite (57° 13′ 22.86″ N, 5° 29′ 12.91″ W). (d) Dark ellipsoidal and circular mafic microgranular enclaves embedded within the Ratagain quartz monzonite (57° 13′ 22.21″ N, 5° 29′ 14.28″ W). (e) Sharp contact between the Ratagain granite and Lewisian gneiss country rock (57° 12′ 6.37″ N, 5° 29′ 15.37″ W). (f) Subangular mafic microgranular enclaves enclosed by the Ratagain quartz monzodiorite (57° 13′ 16.61″ N, 5° 29′ 22.82″ W). (g) Zones of high intensity fracturing and jointing within the Ratagain quartz monzonite (57° 13′ 23.41″ N, 5° 24′ 49.63″ W). (h) Secondary quartz veins cross-cutting highly oxidized Ratagain quartz monzonite (57° 13′ 12.10″ N, 5° 27′ 2.74″ W). LG, Lewisian gneiss; MMEs, mafic microgranular enclaves; Qz, quartz; RG, Ratagain granite; RQmd, Ratagain quartz monzodiorite; RQmz, Ratagain quartz monzodiorite.

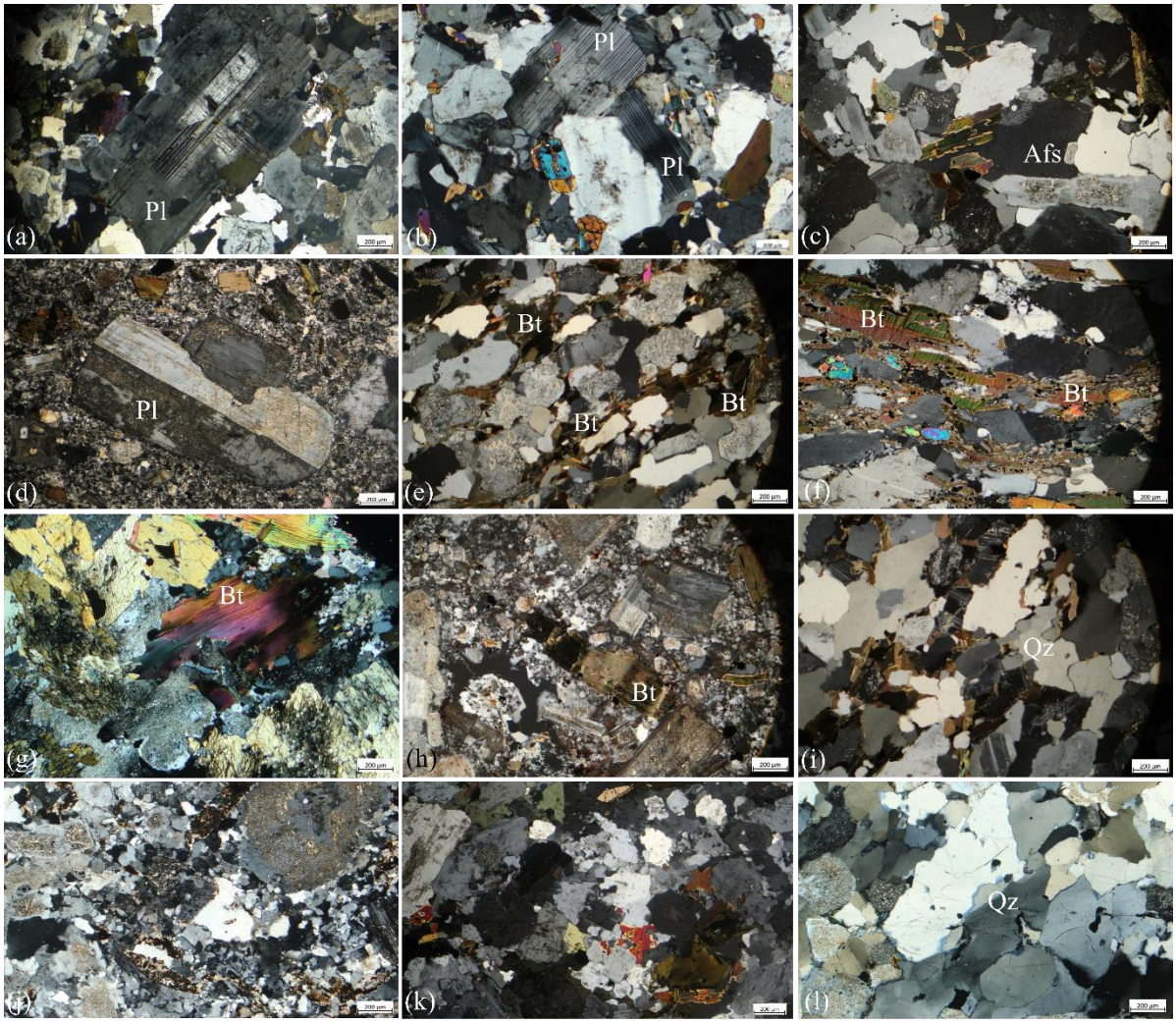


Figure 2.4 Microstructural features of Pl, Bt and Qz in the Ratagain Complex: (a) twinned magmatic Pl phenocryst; (b) deformation twinning in Pl; (c) lobes of myrmekite advancing into Pl; (d) Pl phenocryst partially replaced by sericite with remnant growth twinning; (e) magmatic flow fabric with aligned Bt grains; (f) high-temperature solid-state fabric with Bt parallel to thin bands of recrystallized (mylonitic) Qz; (g) low-temperature fabric with kinked cleavage in Bt; (h) kinked and folded cleavage in Bt; (i) magmatic Qz with slight undulatory extinction; (j) chessboard extinction and dynamic recrystallization of Qz aggregates; (k) Qz subgrains bordering larger Qz grains; (l) sutured grain boundaries in Qz. All photomicrographs taken in cross-polarized light; all scale bars measure 200 μm. Mineral abbreviations after Whitney and Evans (2010).

Contact relationships

The shape of the Ratagain Complex has not been discussed in detail, but McErlean (1993) depicted a steep-sided body with a gently dipping roof. McErlean (1993) recorded gently SE-dipping contacts with host rocks (albeit irregular) in the NW. These appear to be approximately parallel to the presumed roof of the intrusion close to the Strathconan Fault and suggest that the intrusion may exhibit an overall gently dipping, roughly tabular geometry, with a floor cropping out in the NW and a roof in the SE.

Furthermore, with the exception of sharp contacts in the SE (Figure 2.3e) the boundaries observed between the Lewisian country rocks and the Ratagain Complex have a highly irregular

and diffuse or gradational nature (Figure 2.3a), with no obvious deflection or shouldering of the country rocks and no thermal aureole.

Geochronology

A range of ages are reported for the Ratagain Complex. A Devonian U–Pb zircon age of c. 365 Ma was yielded by Pidgeon and Aftalion (1978) in a monzonite, although the authors considered this to be anomalously young for a Late Caledonian intrusion, invoking Pb loss from the zircons as an explanation. Turnell (1985) yielded biotite–whole-rock and biotite–feldspar–whole-rock ages ranging between 408 and 416.8 Ma, yielding a mean age of 415 ± 5 Ma for the complex, which Thirlwall (1988) readjusted to 419 ± 3 Ma. U–Pb baddeleyite dating undertaken by Rogers and Dunning (1991) suggests that crystallization of the Ratagain Complex occurred in the Silurian at 425 ± 3 Ma.

All in all, the Ratagain Complex provides the opportunity to investigate magnetic mineral fabrics across a visually isotropic intrusion of small areal extent (17 km^2) but remarkably varied composition (Stephenson et al., 1999) where rock magnetic techniques have not been applied previously.

Methods

Overview

In total, 100 oriented block samples were obtained from exposures across the Ratagain Complex, including one syenite sample, six samples of granite, three granodiorite samples, seven samples of monzodiorite, 12 monzonite samples, 38 samples of the quartz monzodiorite, 32 quartz monzonite samples, and one quartz-rich granitoid sample. Oriented block samples were cored (21.5 mm diameter) in the laboratory. The number of cores per block sample varied from 3 to 10, being conditional on the state of weathering; in one sample (AL025) the internal jointing and disintegration due to weathering was such that no cores could be obtained. The cores were then cut into 22 mm-long sub-specimens; in total between 5 and 18 sub-specimens were yielded per block sample.

Rock powders were obtained by cutting a rectangular fragment c. 100 × 50 mm in dimensions from each block sample and removing any visibly weathered surfaces. Coarse crushing of the fragments was achieved using a jaw crusher, whilst further crushing to yield fine powders (200 mesh) was undertaken on a TEMA T750k laboratory disc mill.

The AMS of the subsamples was measured at the University of Birmingham Palaeomagnetic Unit and Magnetic Anisotropy (PUMA) laboratory using a KLY4S Kappabridge operating at 875 Hz. Measurements were made at room temperature at 300 Am^{-1}. Statistical analysis of the data was carried out using ANISOFT 4.2 and 5 software (Chadima & Jelinek 2009), whilst the programme ‘Stereonet 11.3.0 64-bit version’ (Allmendinger et al., 2012; Cardozo & Allmendinger, 2013) facilitated statistical interpretation. Interpolations of the three main parameters used to further characterize the AMS fabric (namely K_m, P_j and T) were made using QGIS, an open-source geographic information system (GIS) application that supports the visualization and analysis of geospatial data (QGIS.org, 2021).

To test the efficacy of our AMS analyses of the Ratagain Complex, gain further insights into the magnetic mineralogy and verify whether the entire intrusive body was affected by regional strain during its emplacement, we employed magnetic approaches that are widely used in sedimentary K_m and palaeomagnetic studies (e.g. Martín-Hernández et al., 2004) but less commonplace in investigations of granitic intrusions (e.g. Raposo & Gastal, 2009; Silva & Raposo, 2020).

Complementary thermomagnetic, rock magnetic (pARM and IRM), and magnetic fabric analyses (AARM) were undertaken on 16 representative sites. In addition, based on a comparison between AMS and AARM results, we selected three samples, representative of domains with distinct AMS fabrics, for further study of the magnetic carriers through SEM, optical microscopy, IRM experiments and pARM acquisition.

Anisotropy of magnetic susceptibility (AMS)

All materials, rocks included, produce a magnetization at temperatures above absolute zero (0 K) when in an applied magnetic field (Tarling & Hrouda, 1993). How magnetisable a material is, or its magnetic susceptibility, relates to the strength of the induced magnetization and the strength of the applied field, as follows:

$M = KH$

where M is the induced magnetization or, in more precise terms, the magnetic dipole moment per unit volume (in A/m); H is the magnetic field (in A/m); and *K* is the (volumetric) susceptibility (dimensionless).

The AMS records the bulk magnetic fabric of the rock that results from the preferred orientation and magnetic behaviour of its constituent minerals (Rochette et al., 1992; Hrouda, 2007). The different forms of magnetic behaviour exhibited by rock-forming minerals can be broadly classified as diamagnetic, paramagnetic, ferromagnetic, ferrimagnetic and antiferrimagnetic (Tarling & Hrouda, 1993). In most cases, the rock magnetic fabric is dominated by the contribution from the distribution and shape-preferred orientation of Fe-bearing minerals (chiefly magnetite and biotite) and can be used as a proxy for the rock fabric (e.g., Tarling & Hrouda, 1993; Dunlop & Özdemir, 1997; Bouchez, 1997).

AMS is measured by applying a weak magnetic field to symmetrical drill-core samples, which have been drilled in the laboratory from oriented blocks or directly oriented in the field (Tarling & Hrouda, 1993). If the magnetization induced in a core sample is constant in strength, regardless of the orientation of the sample within the applied field, then it is said to be magnetically isotropic. However, the majority of rock samples are magnetically anisotropic; the strength of the induced magnetization varies depending on the direction in which the field is applied (Tarling & Hrouda, 1993; Bouchez, 1997).

AMS is graphically represented by an ellipsoid of magnetic susceptibility (Rochette et al., 1992), which has the three principal axes represented by the maximum (K_1), intermediate (K_2), and minimum (K_3) susceptibility axis, where $K_1 > K_2 > K_3$.

A standardized way of presenting AMS data utilises the following parameters of the ellipsoid:

$K_m = (K_1 + K_2 + K_3)/3$, the mean susceptibility

$L = K_1/K_2$, the lineation parameter

$F = K_2/K_3$, the foliation parameter

The AMS ellipsoid is further characterised by the corrected degree of anisotropy (P_j), and the shape factor (T), which are given in the following equations (Jelinek, 1981):

$$P_j = exp\sqrt{\{2[(\eta_1 - \eta_m)^2 + (\eta_2 - \eta_m)^2 + (\eta_3 - \eta_m)^2]\}}$$

$$T = [(2\eta_2 - \eta_1 - \eta_3)/(\eta_1 - \eta_3) - 1\,]$$

where $\eta_1$is lnK_1, η_2 is lnK_2, η_3 is lnK_3 and η_m is $(\eta_1 + \eta_2 + \eta_3)/3$. *T* varies between -1 and 1, where a value greater than 0 tends toward oblateness and a value below 0 is in the prolateness field. *T* of 1 is oblate and *T* of -1 is prolate, *T* of 0 is triaxial.

AMS results

The complete results from the AMS study are presented in Supplementary Table S1 and are stereographically projected in Figure 2.5. Summary stereograms showing poles to the AMS foliation throughout the complex is also shown in Figure 2.6. Susceptibility values have an average of 19.22 x 10^{-3} SI. The average P_j value is 1.17 reflecting an anisotropy of around 17% (Figure 2.7). The shape of the AMS ellipsoid is extremely skewed towards oblateness with a small minority of samples showing negative *T* values (Figure 2.7). There is no systematic spatial variation of these parameters across the Ratagain Complex (Figure 2.8).

AARM

The interpretation of AMS as a direct proxy of the rock fabric is not straightforward in granites with composite fabrics wherein several magnetic minerals are present (e.g. Bouchez, 1997; Stevenson, 2004). Analysis of such mixed magnetic fabrics, necessitates separating the respective subfabrics. A range of methods, which essentially involving measuring samples at varying temperatures or field strengths, have been devised to isolate the different magnetic components and quantify their contribution to the bulk susceptibility (see Owens & Bamford, 1976; Rochette et al., 1992; Richter & van der Pluijm, 1994).

AARM analysis involves measuring the anisotropy of the anhysteretic remanent magnetization (ARM) imparted over a specific pattern of directions in a rock sample. Unlike AMS, which represents the susceptibility contributions of all minerals in the rock, including those exhibiting ferromagnetic, diamagnetic, and paramagnetic behaviour (e.g., Borradaile & Gauthier, 2001), AARM is provided solely by remanence-bearing minerals (e.g., Potter, 2004; Silva & Raposo, 2020) and therefore distinguishes the contributions of ferromagnetic minerals.

ARM is acquired by simultaneously exposing the sample to a decaying alternating field (AF) and a weak direct current (DC field) (e.g., Borradaile & Jackson, 2010). As with AMS, the AARM provides an ellipsoid with the principal axes $AARM_{max} > AARM_{int} > AARM_{min}$, in which $AARM_{max}$ is parallel to the magnetic lineation and $AARM_{min}$ is the pole to the magnetic foliation (e.g., Jackson, 1991).

AARM measurements were carried out with an AGICO JR5A spinner magnetometer at the University of Birmingham. ARM was imparted over six directions parallel to the *X*, *Y*, and *Z* (and opposite) axes of the specimen using an ASC D2000 magnetizer, and adopting an AF of 100 mT and a DC field of 0.05 mT. Between each ARM acquisition the sample was fully demagnetized with a tumbling system at 100 mT AF using an AGICO LDA5 demagnetizer. Results from the AARM study are presented in Table 2.1, together with representative AMS results for comparison.

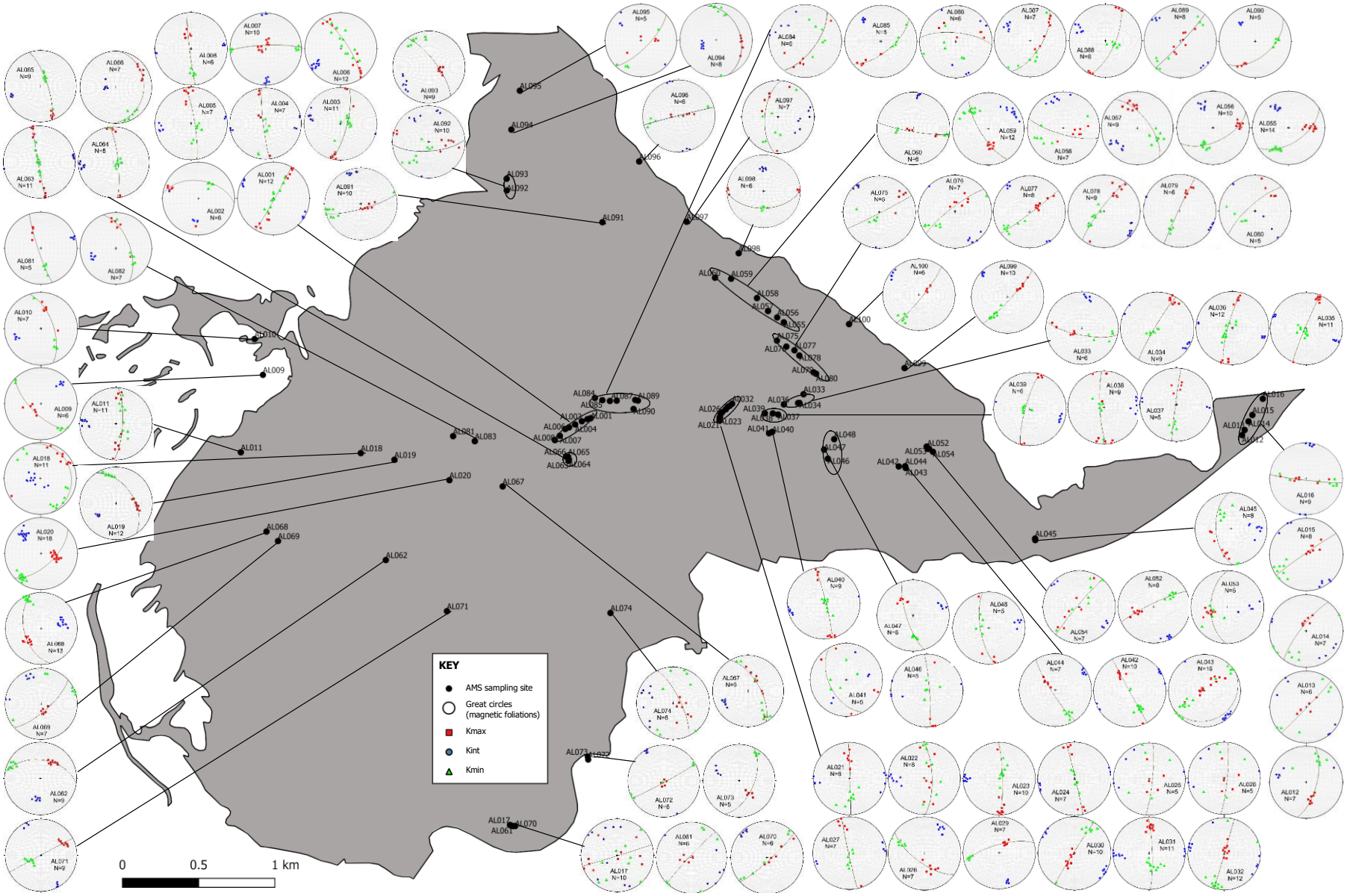


Figure 2.5 Map of the Ratagain Complex showing the sampling locations and the AMS stereograms at each site. Stereograms are lower-hemisphere equal area projections showing the magnetic lineation (red squares), foliation (great circles) and the principal axis normal to foliation (blue circles) for each location.

Table 2.1 Anisotropy of magnetic susceptibility (AMS) and anisotropy of anhysteretic remanent magnetization (AARM) data from representative sites from the Ratagain Complex

		AMS							AARM						
Site	*N*	K_m $(10^{-3}$ SI)	K_1		*L*	*F*	P_j	*T*	R_m $(10^{-3}$ A/m)	$AARM_{max}$		*L*	*F*	P_j	*T*
			D	*I*						*D*	*I*				
AL002	6	21.2	292.8	16.6	1.078	1.147	1.240	0.293	3.574	203.7	4.2	1.323	1.505	1.999	0.189
AL009	6	6.1	241.9	66.2	1.010	1.041	1.055	0.608	2.869	142.3	33.7	1.078	1.064	1.150	-0.151
AL011	11	22.1	179.9	12.2	1.011	1.170	1.206	0.875	5.748	174.5	13.7	1.137	1.283	1.469	0.327
AL017	10	55.1	073.9	37.6	1.003	1.009	1.013	0.502	13.46	109.6	39.7	1.050	1.106	1.169	0.320
AL031	10	26.5	001.8	26.1	1.026	1.114	1.153	0.612	3.284	355.0	16.8	1.105	1.161	1.294	0.162
AL038	9	14.2	177.6	5.1	1.027	1.126	1.167	0.631	2.919	174.9	7.5	1.129	1.214	1.378	0.230
AL045	8	0.4	208.3	37.3	1.017	1.030	1.048	0.272	377.7	197.2	52.6	1.044	1.081	1.132	0.222
AL048	5	20.6	174.5	11.8	1.039	1.222	1.293	0.680	4.605	161.1	7.6	1.218	1.366	1.671	0.227
AL054	7	2.4	225.3	51.2	1.017	1.056	1.078	0.534	1.129	222.4	31.6	1.010	1.04	1.113	-0.112
AL062	9	17.3	037.9	43.4	1.061	1.171	1.252	0.452	3.332	026.6	44.7	1.170	1.520	1.821	0.467
AL067	9	2.8	035.0	60.7	1.055	1.238	1.343	0.599	1.409	109.8	23.9	1.120	1.088	1.226	-0.098
AL079	6	19.4	022.9	42.3	1.053	1.202	1.282	0.563	5.267	026.8	27.9	1.144	1.404	1.631	0.438
AL081	5	12.8	334.9	45.5	1.045	1.283	1.373	0.698	2.502	334.5	41.2	1.250	1.564	1.982	0.350
AL094	7	56.8	104.4	27.6	1.068	1.222	1.321	0.505	9.256	116.2	23.3	1.160	1.656	1.989	0.584
AL096	6	34.8	068.0	81.4	1.052	1.278	1.373	0.657	6.098	070.1	68.0	1.216	1.467	1.814	0.352
AL100	6	7.8	058.3	66.9	1.062	1.080	1.147	0.122	1.799	056.1	64.4	1.148	1.181	1.368	0.087

N is the number of samples taken per site; K_m is the mean magnetic susceptibility (in SI units); R_m is the mean magnitude of AARM (measured in A m^{-1}); $AARM_{max}$ is the mean maximum remanent magnetization axis; *D* is declination; *I* is inclination; *L* is the lineation parameter; *F* is the foliation parameter; P_j is the degree of anisotropy; and T is the shape parameter (Jelínek, 1981).

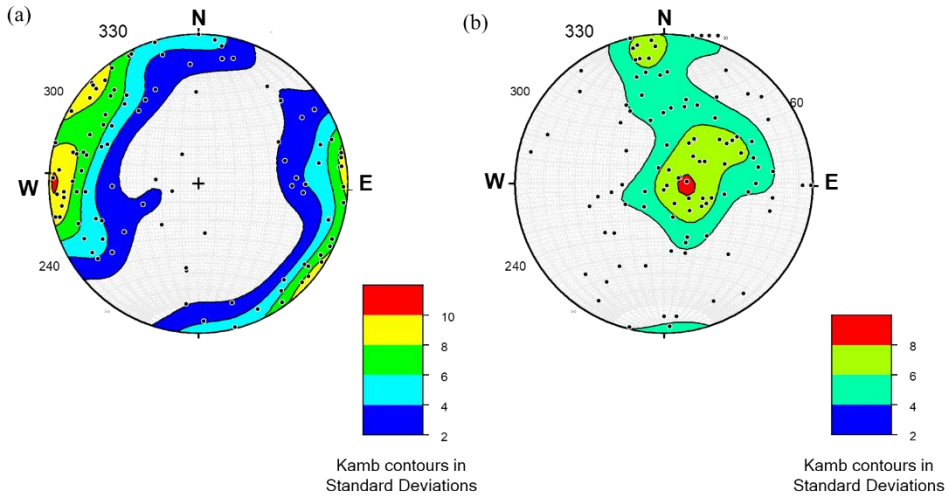


Figure 2.6 Equal-area lower-hemisphere stereoplots of AMS axes for all sample points in the Ratagain Complex with density of data distribution contoured with *K*amb intervals indicated: (a) K_3 axes; (b) K_1 axes.

AARM results

Almost all AMS and AARM tensors are coaxial (Figure 2.9), as the K_1, K_2, and K_3 susceptibility axes are sub-parallel to the $AARM_{max}$, $AARM_{int}$, and $AARM_{min}$ axes, respectively. A discrepancy between the AMS and AARM tensors is however observed at sites AL002 and AL009, where the $AARM_{max}$ axis is parallel to the K_1 and K_2 axes, respectively. At site AL002, a susceptibility carried by SD to pseudo-single-domain (PSD) magnetite grains could account for the observed inverse fabric (Rochette, 1988). The non-coaxiality between the AMS and AARM tensor observed at site AL009 (Figure 2.9) may be explained by the low degree of anisotropy (see Table 2.1) characterizing these sites, which may have affected the calculation of the AMS and AARM tensors. Another possible explanation for the abnormal fabric at site AL009 is that there are coexisting normal and inverse anisotropies, due to the presence of MD and SD grains, hence producing a possible "intermediate fabric" (Rochette et al., 1992).

We can therefore conclude that AARM tensors yield a normal magnetic fabric. Furthermore, the coaxiality of the AMS and the other 14 sites showing coaxiality between the AMS and AARM tensors suggests that the ferromagnetic and paramagnetic matrix-forming grains may have the same preferred orientation. It is therefore likely that the ferromagnetic mineral assemblages and matrix-forming minerals were aligned under the same magmatic or tectonic episode, implying that the ferromagnetic minerals are primary and magmatic in origin as opposed to secondary and hydrothermal.

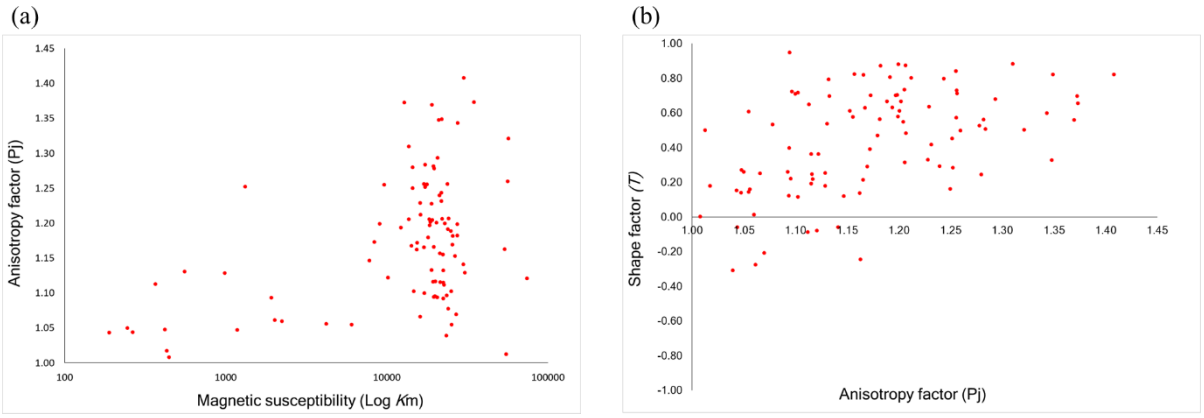


Figure 2.7 (a) Plot of magnetic susceptibility anisotropy, P_j, against the mean susceptibility, K_m, for the Ratagain Complex. (b) Plot of shape of magnetic susceptibility anisotropy, T, against the anisotropy, P_j, of the Ratagain Complex.

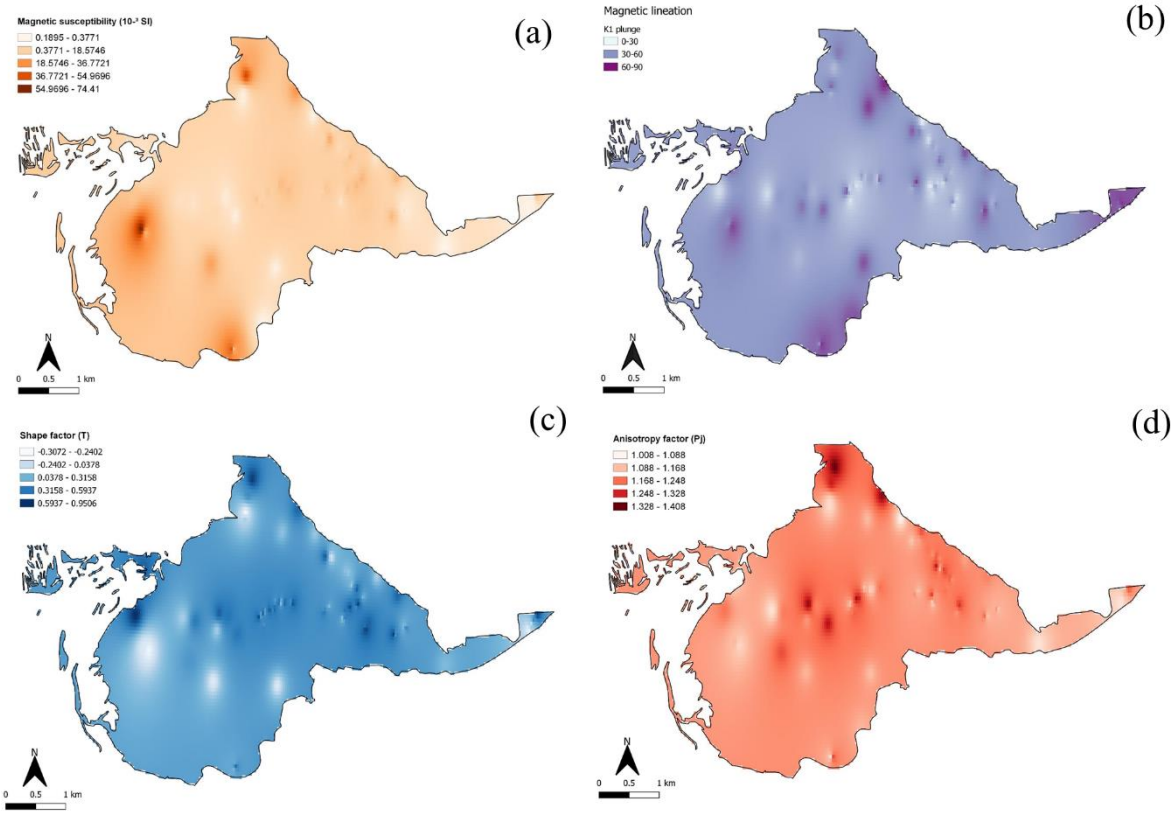


Figure 2.8 Maps showing various parameters interpolated across the Ratagain Granite Complex: (a) magnetic susceptibility; (b) plunge of the magnetic lineation; (c) shape parameter, T; (d) anisotropy factor, P_j.

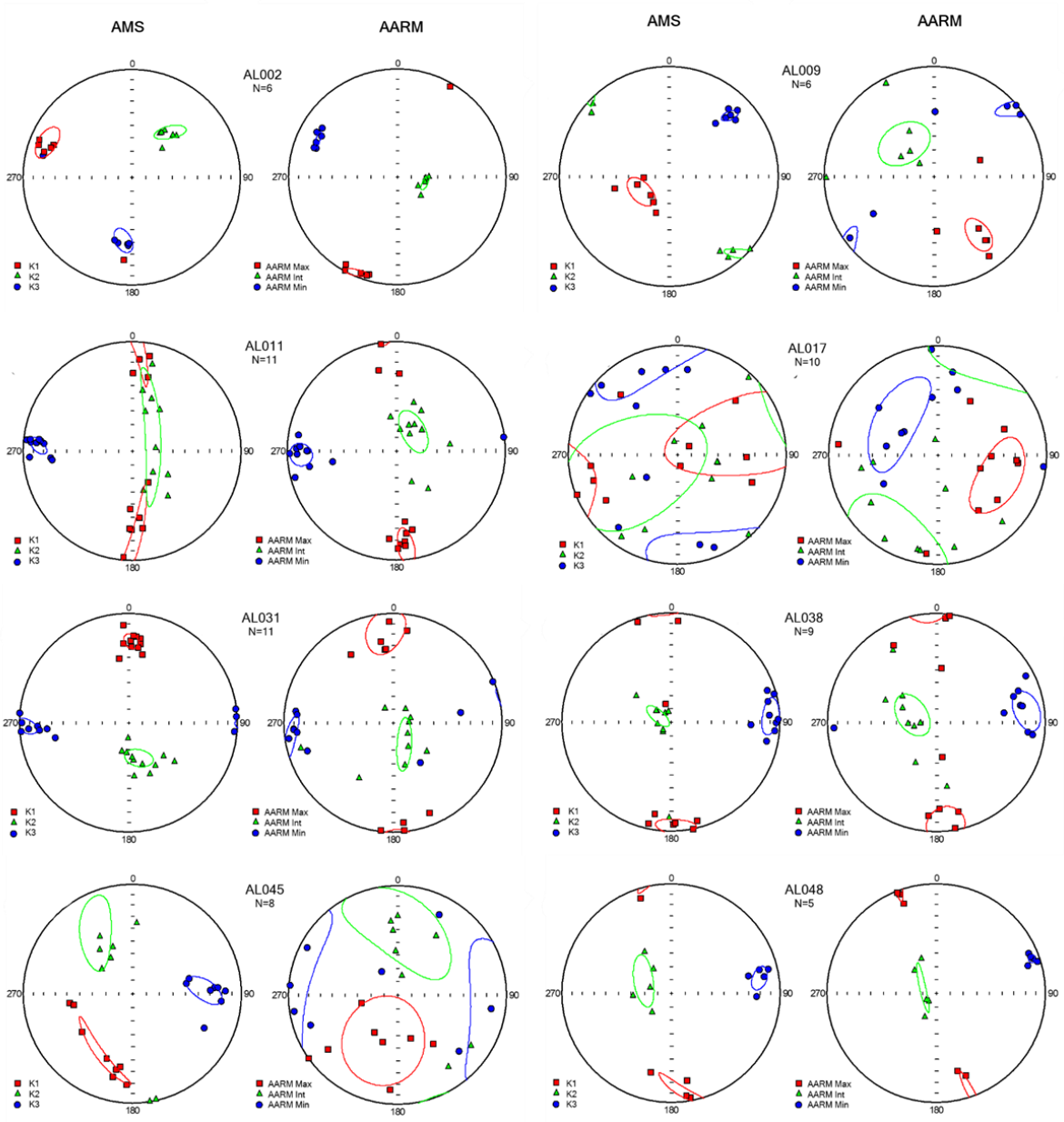


Figure 2.9 Anisotropy of magnetic susceptibility (AMS) and anisotropy of anhysteretic remanent magnetization (AARM) results from 16 representative sites of the Ratagain Complex. Red squares are maximum susceptibility (K_1) and maximum remanence ($AARM_{max}$); green triangles are intermediate susceptibility (K_2) and intermediate remanence ($AARM_{int}$) and blue circles are minimum susceptibility (K_3) and minimum remanence ($AARM_{min}$). Data are plotted in the lower-hemisphere stereograms wherein the red, green and blue ellipses are the 95% confidence ellipses.

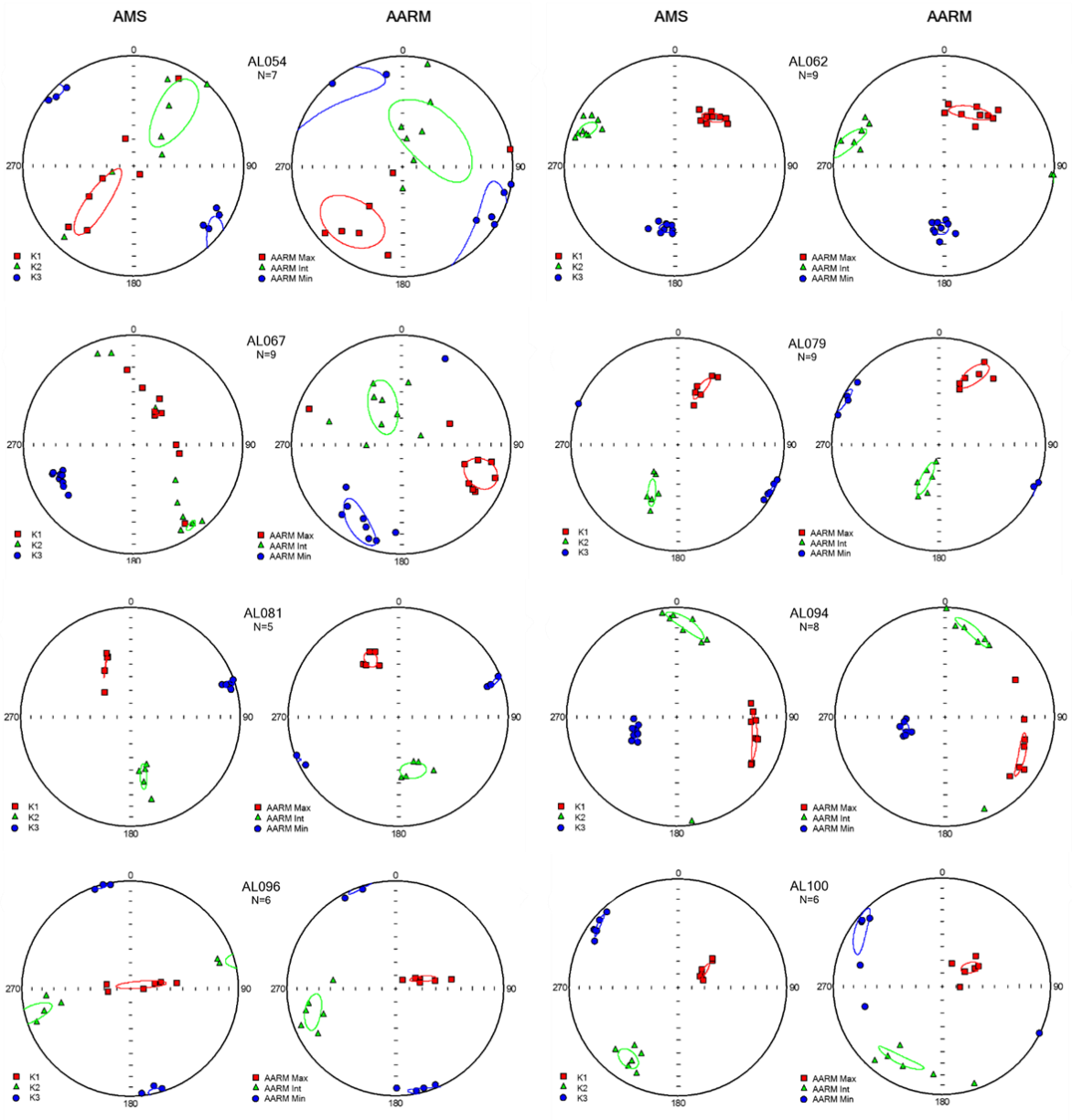


Figure 2.9 Continued

Thermomagnetic curves

The variation of magnetic susceptibility with temperature can provide insights into the magnetic mineralogy of rocks (Orlický, 1990). High-temperature thermomagnetic analyses were performed in an Argon-controlled atmosphere using an AGICO KLY-4S Kappabridge coupled with a CS-3 apparatus. Powdered samples from the 16 representative sites were subjected to a heating-cooling cycle from room temperature to 700°C. Curie temperatures were calculated using the graphical method of Petrovský & Kapička (2006).

Thermomagnetic results

All sites record a significant fall of magnetic susceptibility at temperatures between 580 and 650°C (Figure 2.10), which corresponds to the Curie temperature (T_c) of both magnetite and maghemite (Dunlop & Özdemir, 1997). These T_c values preclude the presence of titanomagnetite, iron sulphides, and hematite as potential contributors to the AMS and AARM fabrics (Orlický, 1990; Dunlop & Özdemir, 1997). Most of the samples show similar non-reversible heating curves that exhibit a broad peak at temperatures above 300°C, which can be taken as further evidence of maghemite. Sites AL067 and AL081 show a T_c of 580 and 590°C, respectively, indicating the occurrence of pure, or slightly oxidized magnetite (Dunlop & Özdemir, 1997). The remaining 14 sites show T_c ranging between 605 and 650°C, which indicate the occurrence of partially to heavily oxidized (i.e. maghemitized) magnetite.

The lack of significant Hopkinson peaks (Hopkinson, 1889) in most thermomagnetic curves suggests that MD magnetic particles dominate over SD particles, which are thought to be responsible for this peak (Dunlop, 1974). The predominantly gentle or negligible rise in susceptibility with temperature is consistent with relatively large MD magnetite grains being the dominant carrier (e.g., Liss et al., 2004; Burton-Johnson et al., 2019). The form of the Hopkinson peak is controlled by the magnetic blocking temperature and the Curie temperature where the increased susceptibility with temperature is enhanced between these two temperatures. The presence of a relatively narrow Hopkinson peak in the heating curves of AL038 and AL054 (Figure 2.10) indicates a greater contribution from PSD or SD magnetite grains. In addition, the cooling curves of these samples display a marked increase in susceptibility in the vicinity of 600℃ and much higher susceptibilities than the heating curve, suggesting the likely creation of secondary magnetite at high temperatures (Hrouda,1994). In samples AL002 and AL011, the cooling curve exhibits a narrow Hopkinson peak suggesting that some secondary SD magnetite has been generated during heating. The absence of a clear Hopkinson peak at site AL002 is surprising, as its inverse AMS tensor would indicate the occurrence of SD magnetite.

Partial anhysteretic remanent magnetization (pARM) acquisition

As natural rock samples can be dominated by a single magnetic phase, such as magnetite, with a wide range of grain sizes (Liu et al., 2005), estimating the relative distributions of SD, PSD and MD grains will in turn help to characterize the contributions of these different fractions to the bulk magnetic fabric. Partial ARM (pARM) measurements can be used to examine the distribution of grain size fractions by virtue of their coercivity – the resistance of individual magnetic grains to an opposing magnetic field (Butler 1992, p. 35) – as coercivity is strongly related to grain size (Jackson et al., 1988).

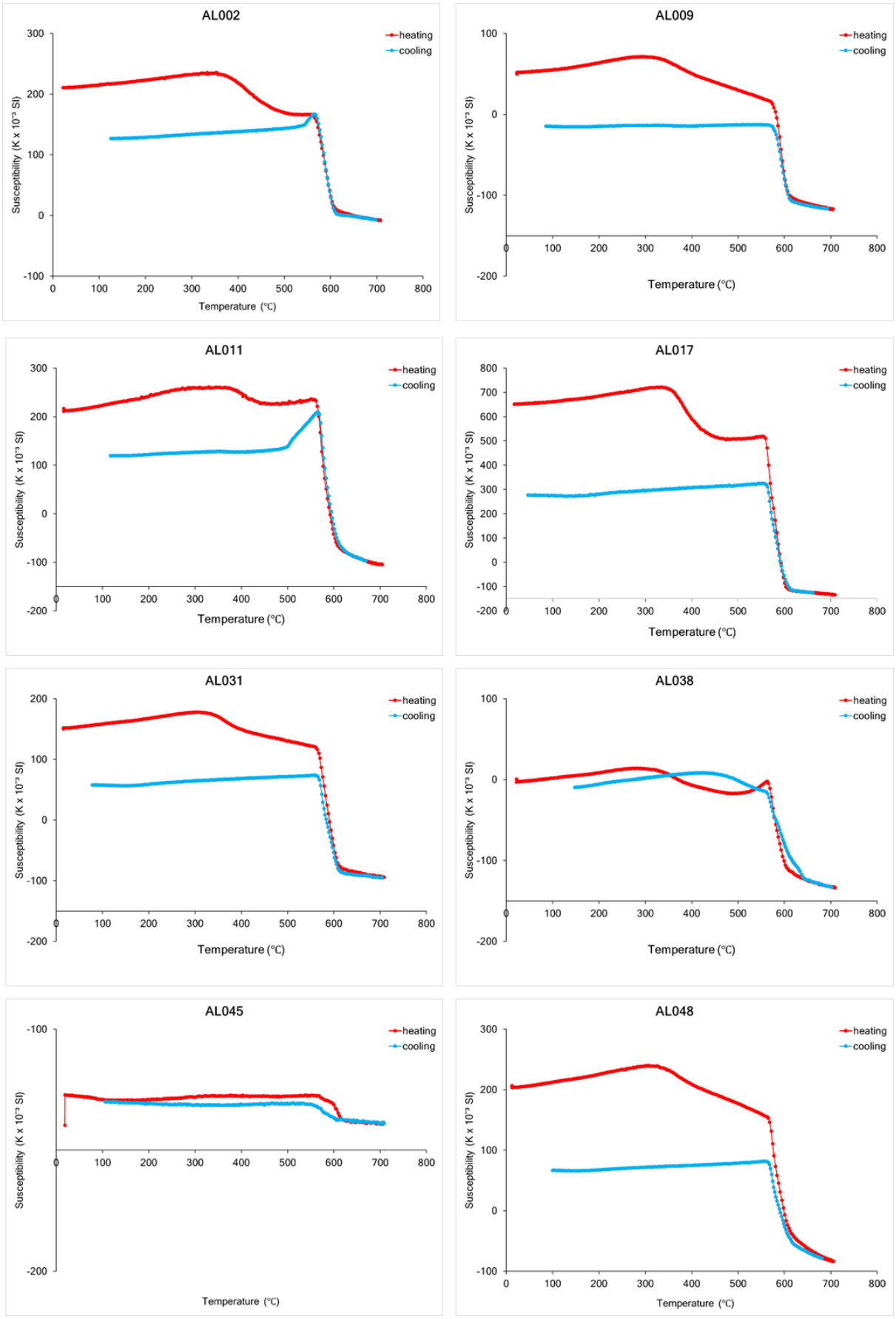


Figure 2.10 Thermal variation of the low-field magnetic susceptibility (*K*) from representative samples. Heating curves are red, cooling curves are blue.

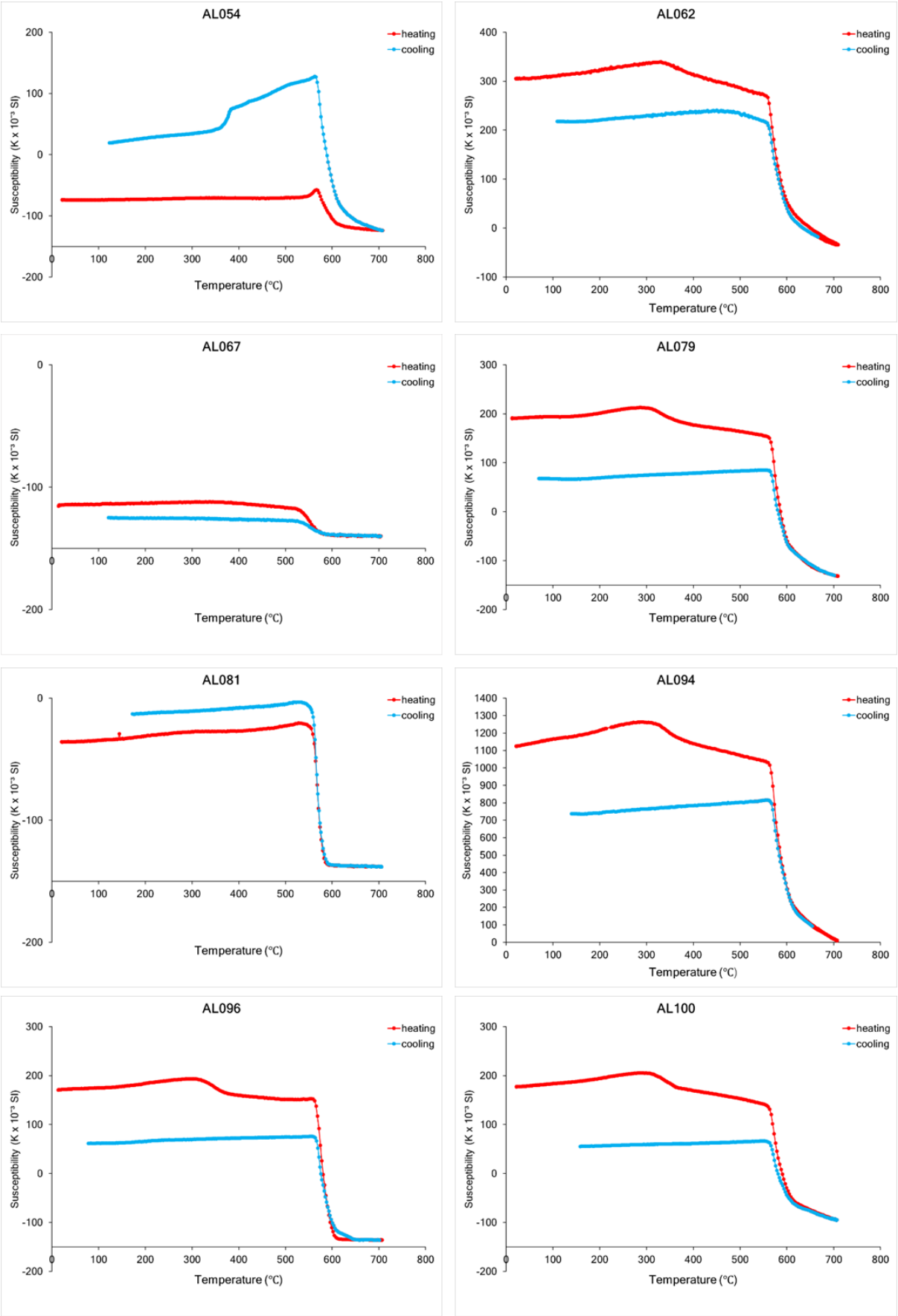


Figure 2.10 Continued

A stepwise pARM was imparted on three specimens from representative sites (AL002, AL009 and AL048) using a D2000 magnetizer, and the remanence was then measured with a JR5A magnetometer. Similar to the methodologies of Trindade et al. (2001) and Bolle et al. (2003), following AF tumbling demagnetization of the specimens at 100 mT, pARM was imparted at 15 AF steps with windows 5 mT in width from 5 to 50 mT, and 10 mT in width from 50 to 100 mT. A full demagnetization at 100 mT was performed before each pARM step.

pARM results

The pARM spectra for all three samples show a well-defined peak at 5 mT (Figure 2.11). According to Jackson et al. (1988), a pARM peak at 5 mT corresponds to >25 *μ*m grains, hence MD grains. The pARM curve from site AL009 displays an additional peak between 50 and 80 Mt, corresponding to PSD-MD grains in the range of 0.1–0.7 *μ*m (Jackson et al., 1988). For site AL002 this further evidence for MD grains is, once again, at odds with its inverse AMS fabric, which would require the occurrence of SD grains. Conversely, the normal magnetic fabric displayed by site AL048 is consistent with the occurrence of MD magnetite revealed by pARM analysis. The occurrence of both PSD–SD and MD grains at site AL009 is consistent with our hypothesis of a dual (i.e. normal and inverse) magnetic fabric being responsible for the 'intermediate' fabric.

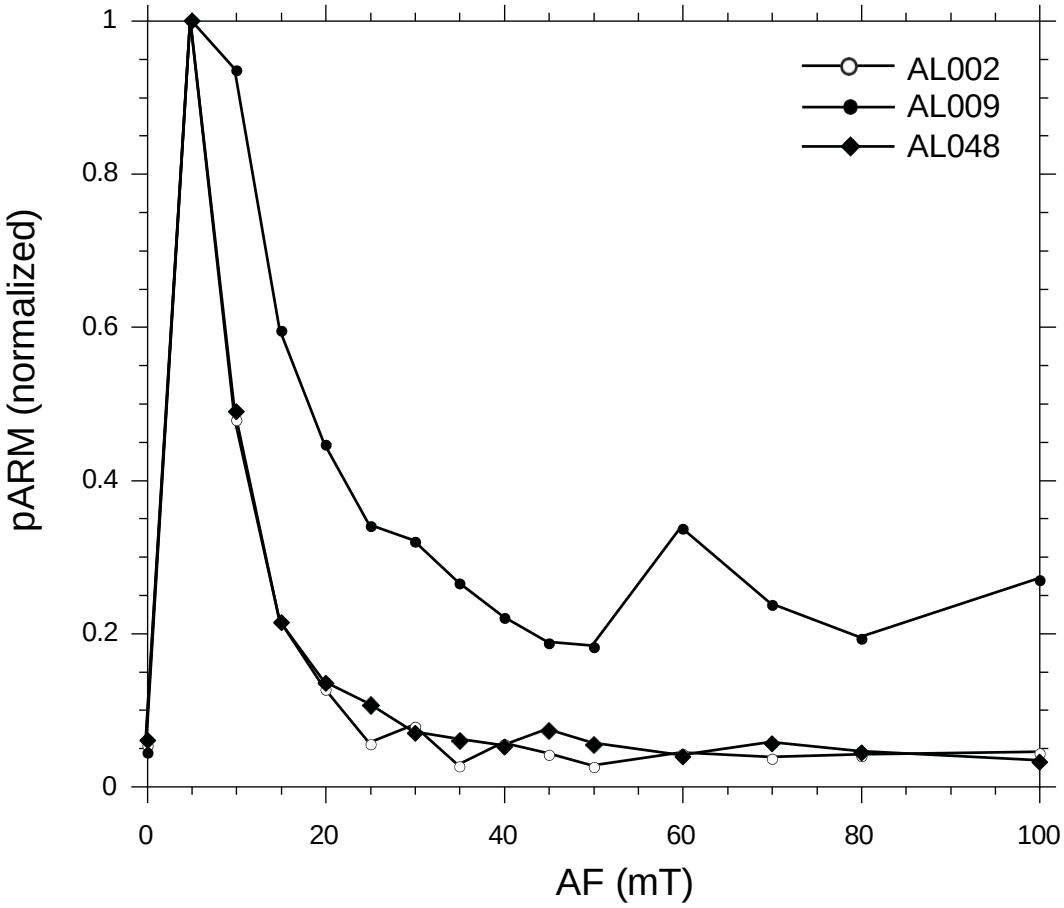


Figure 2.11 Normalized partial anhysteretic remanent magnetization (pARM) coercivity spectra for representative samples AL002, AL009 and AL048.

Optical and scanning electron microscopy

Optical and scanning electron microscopy (SEM) can characterise opaque magnetic minerals and, when the latter is combined with an energy-dispersive X-ray (EDX) detector, further insights on the distribution and concentration of elements within these minerals may be provided. Optical microscopy studies were carried out at the University of Birmingham using a stereomicroscope Zeiss Axioplan 2 Imaging microscope with a Canon EOS 550D Digital SLR Camera. The EDX analyses and SEM images were obtained using a Hitachi TM3000 instrument coupled with Quantax 70 software at the University of Liverpool, UK.

Photomicrographs show that the magnetite of the Ratagain Complex occurs as highly dispersed accessory crystals (Figure 2.12). Although volumetrically variable and differing in grain size, the magnetite is ubiquitous across all rock types constituting the intrusion from quartz monzodiorites (Figure 2.12a) to syenites (Figure 2.12f).

Back-scattered electron (BSE) images (Figure 2.13) show three different size fractions of magnetite were present in all samples, which can be broadly categorised as MD, PSD and SD (Day et al., 1977). MD magnetite occurs as large, individual, 20-100 µm subhedral grains (Figure 2.13a) and accounts for 75% of the magnetite observed in thin section. Approximately 15% of the magnetite comprises PSD grains of 5-20 μm size (Figure 2.13b), which also appear as individual microphenocrysts. The SD fraction, accounting for only 5% or so of all the observed magnetite, consists of elongated grains less than 1µm wide and equant grains >0.05 μm wide (Figure 2.13c), which typically occur as inclusions inside the feldspars.

EDX analyses of selected magnetite grains from each of the grain size fractions (Figure 2.13) indicate that the magnetite is nearly pure, with a marked absence of titanium or other elements. This could be accounted for by the exceptional amount of titanite in these rocks (Figure 2.12c, e), into which titanium may have partitioned preferentially prior to the crystallisation of magnetite. A high oxygen fugacity (fO_2) would also favour the crystallisation of pure magnetite (Ishihara, 2004; dos Santos Dias, 2019), but a detailed discussion of the magmatic redox conditions and evolution is beyond the scope of this paper.

Isothermal remanent magnetization (IRM) acquisition

The exposure of a rock containing ferromagnetic minerals to a strong magnetic impulse at room temperature produces an isothermal remanent magnetization (IRM) (Dunlop & Özdemir, 1997). Stepwise acquisition of an IRM in a rock sample up to its saturation isothermal remanent magnetization (SIRM) and the coercivity unmixing methods that use these curves (Kruiver et al., 2001; Heslop et al., 2002; Maxbauer et al., 2016) have frequently been used to determine the nature and relative concentration of the magnetic carriers. In particular, the unmixing methods help separate the contributions of magnetic minerals with known coercivities (Dunlop, 1972; Sant'Ovaia et al., 2015; Maxbauer et al., 2016).

IRM experiments were performed on the same three representative samples from sites AL002, AL009, and AL048 used for the pARM experiments and SEM observations. IRM was imparted with an ASC Scientific IM 10-30 impulse magnetizer by applying 39 increasing peak fields from 10 to 1000 mT. The remanence after each IRM step was measured with a JR5A spinner magnetometer.

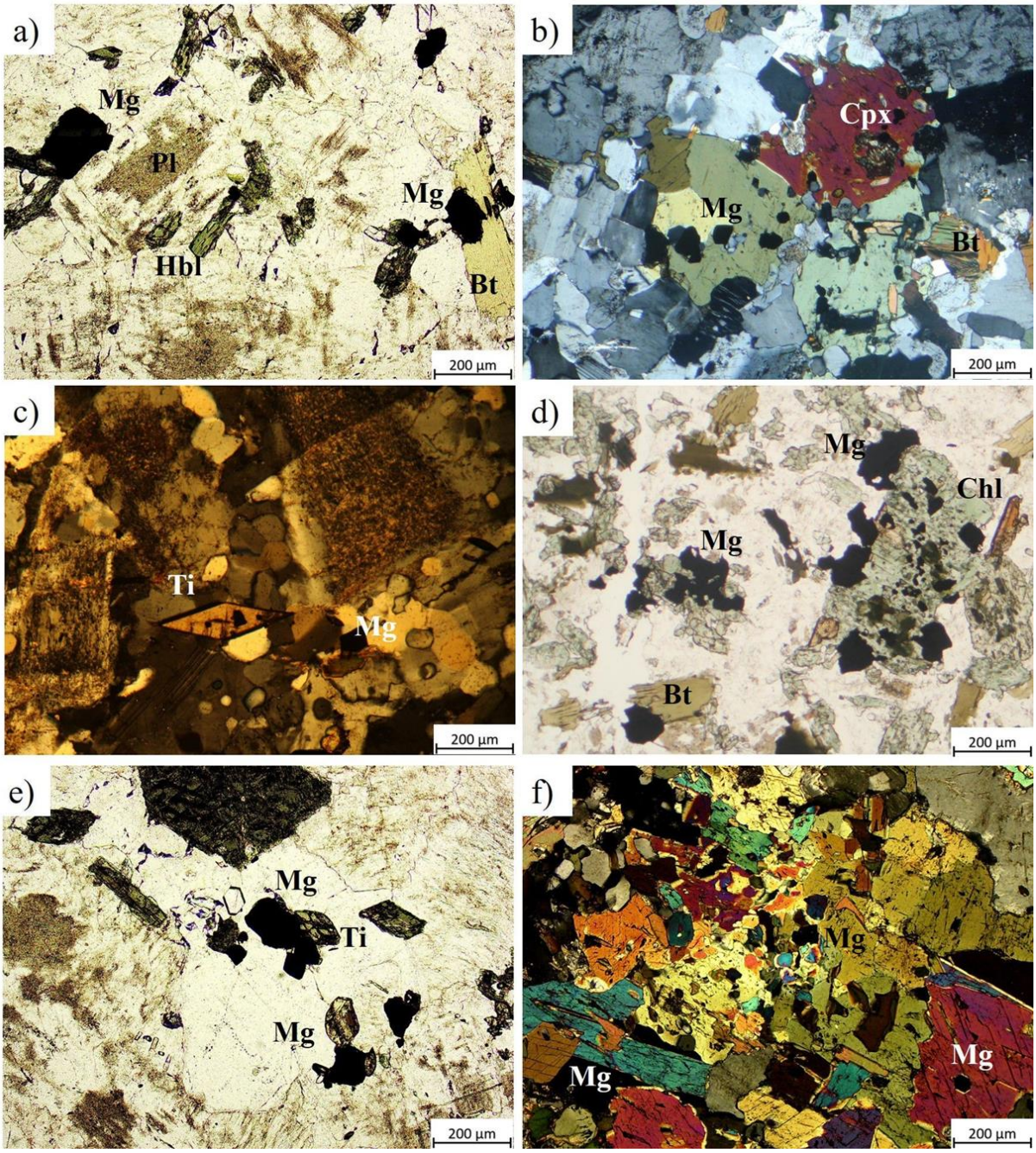


Figure 2.12 Representative photomicrographs of magnetite in the Ratagain Complex. (a) Plane polarized light (PPL) image of quartz monzodiorite with large, blocky magnetite grains set in a groundmass of quartz, alkali feldspar and sericitized plagioclase with minor hornblende and biotite. (b) Crosspolarized light (XPL) image of quartz monzodiorite showing magnetite overgrowths on clinopyroxene. (c) XPL image of monzodiorite showing a large, euhedral titanite crystal alongside a smaller magnetite grain. (d) PPL image of quartz monzonite containing magnetite, chlorite and biotite. (e) PPL image of quartz monzodiorite with blocky magnetite and titanite. (f) XPL image of syenite consisting of abundant ferromagnesian phases hosting magnetite inclusions. Mineral abbreviations after Whitney and Evans (2010).

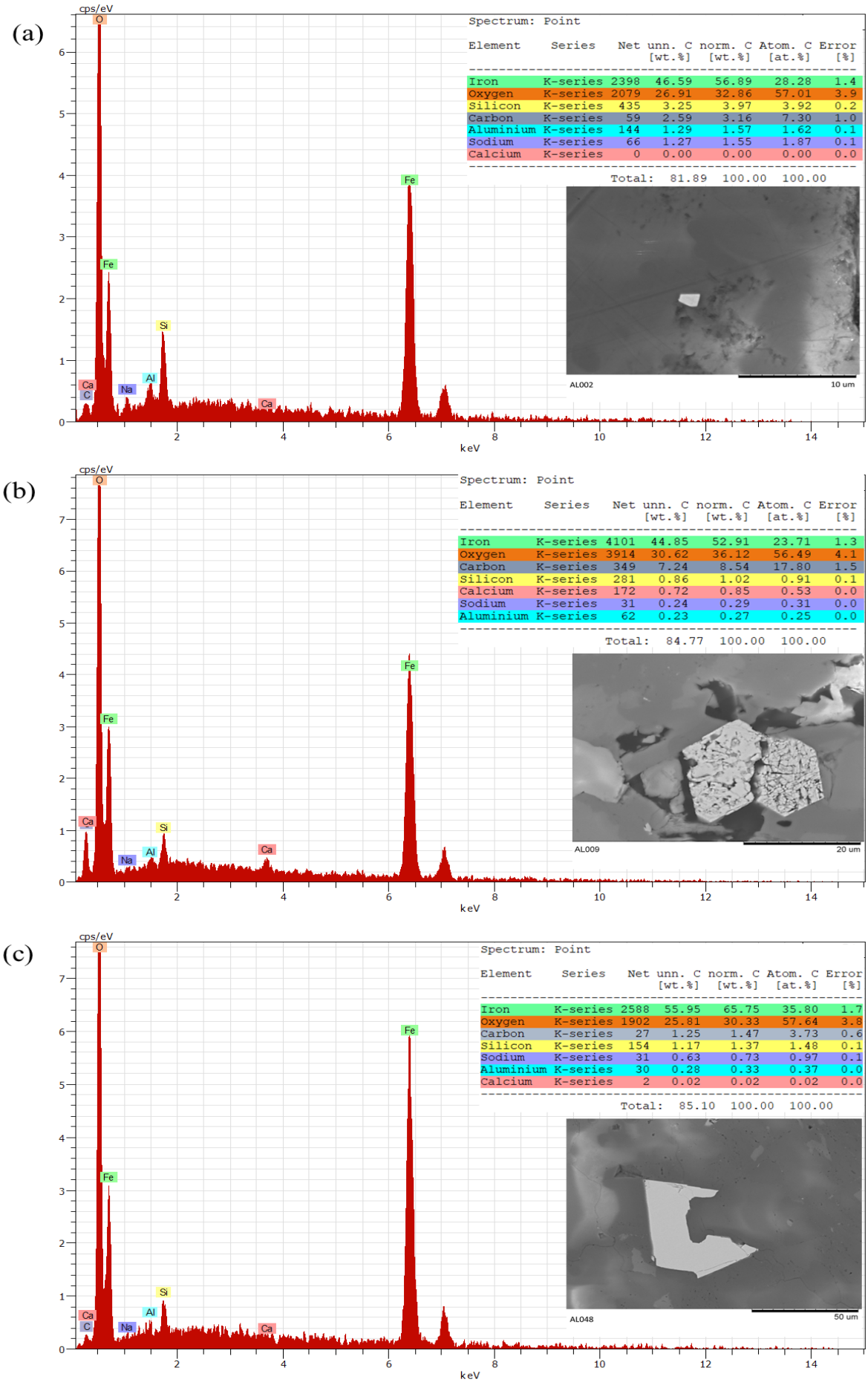


Figure 2.13 EDX spectra, data and BSE images of magnetite grains in specimens (a) AL002, (b) AL009 and (c) AL048.

IRM results

IRM curves show that all representative samples yield steep acquisition between 10 and 150-200 mT (Figure 2.14a). For samples AL002 and AL048, the acquisition curves flatten thereafter, indicating complete saturation and the dominance of low-coercivity (or soft) magnetic fractions. Sample AL009 however does not reach saturation at the maximum applied field of 1T, which indicates the occurrence of high-coercivity (or hard) fractions. To characterize the nature and relative contribution of the various magnetic fractions in these samples we unmixed the coercivities using the Max UnMix online software (Maxbauer et al., 2016).

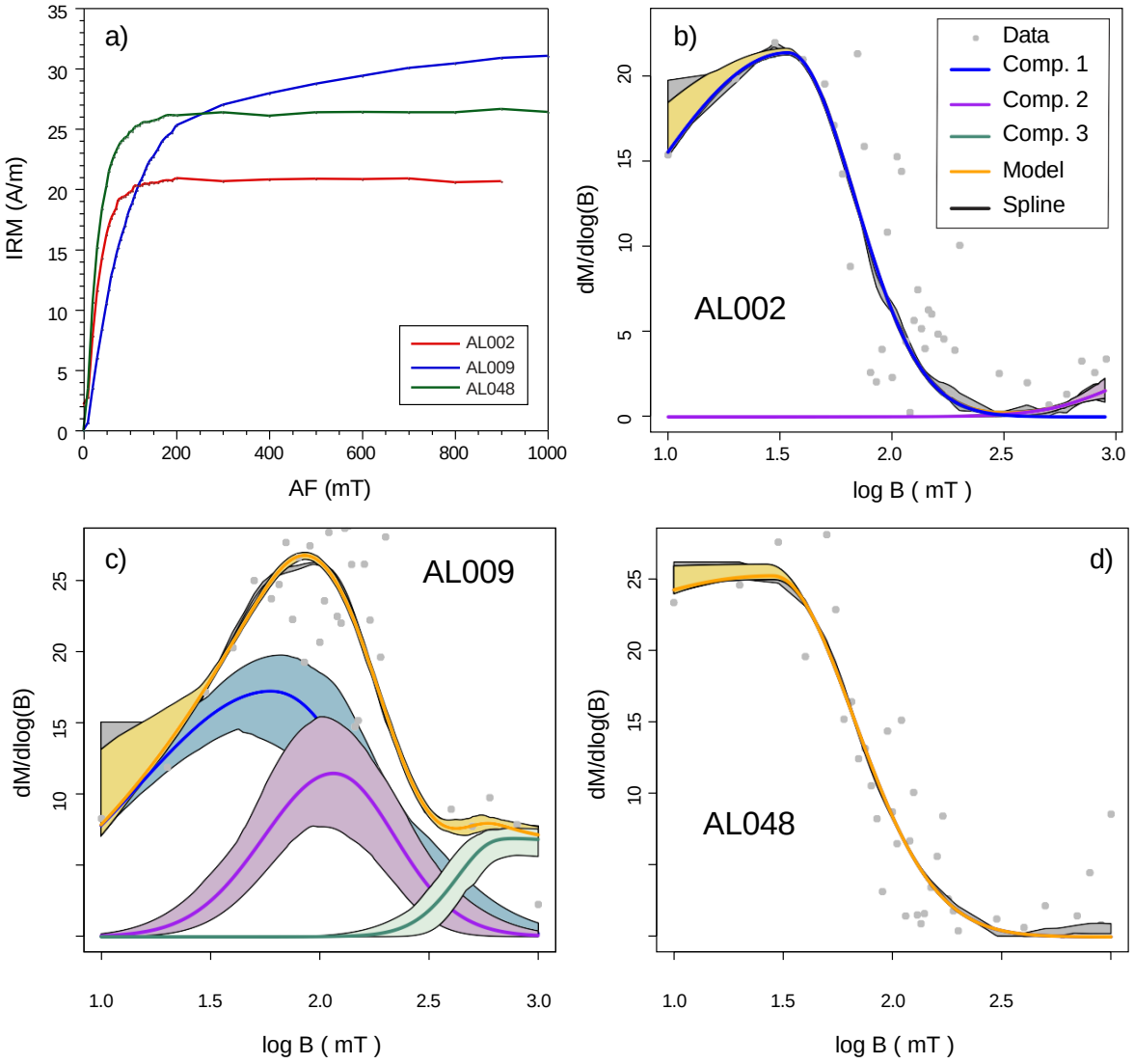


Figure 2.14 (a) Isothermal remanent magnetization (IRM) acquisition curves for representative samples. The red, blue and green lines represent AL002, AL009 and AL048, respectively. (b–d) Coercivity unmixing analysis of IRM acquisition curves for the representative samples. Grey circles are the IRM data and the grey shaded area represents error envelopes of 95% confidence intervals. The contribution from all magnetic components is represented by the gold line and shaded area. The blue, purple and green lines and corresponding shaded areas represent the first, second and third component, respectively.

Table 2.2 Results of isothermal remanent magnetization (IRM) component analysis for the representative samples. Bh is the mean coercivity; DP is the dispersion parameter; S is the skewness and EC is the extrapolated contribution associated to each component.

	Component 1					Component 2					Component 3				
Site no.	B_h (mT)	B_h ($\log_{10}$ units)	DP	S	EC (%)	B_h (mT)	B_h ($\log_{10}$ units)	DP	S	EC (%)	B_h (mT)	B_h ($\log_{10}$ units)	DP	S	EC (%)
AL002	16.81	1.23	0.51	0.66	0.95	2922.1	3.47	0.36	0.89	0.05	-	-	-	-	-
AL009	39.66	1.60	0.52	0.78	0.52	107.89	2.03	0.30	0.94	0.21	3885.42	3.59	0.75	2.40	0.28
AL048	2.05	0.31	1.19	0.57	1.00	-	-	-	-	-	-	-	-	-	-

Our modelling (Figure 2.14b-d; Table 2.2) indicates that a soft coercivity fraction (component 1) is present in all samples, with variable coercivity (Bh) between 2.05 and 39.66 mT (0.31-1.60 mT in log_{10} units) and dispersion parameters (DP) between 0.51 and 1.19; an intermediate coercivity fraction is present in samples AL002 and AL009 in variable proportions lower than 20%, and is characterized by higher Bh values of 107.89 and 2922.10 mT (2.03 and 3.47 mT in Log_{10} units) and DP of 0.30 and 0.36; a hard fraction is present in site AL009 only, and is characterized by a Bh of 3885.42 mT (3.59 mT in Log_{10} units) and a DP of 0.75.

Considering these coercivity spectra together with the SEM observations and the thermomagnetic analyses, we infer that the soft fractions correspond to pure magnetite of variable grain size, with site AL048 showing the coarsest magnetite (indicated by its exceptionally low coercivity). The intermediate fraction is likely represented by partially maghematized magnetite and the hard fractions may be represented by magnetite with a higher degree of maghemitization.

Discussion

Interpretation of the magnetic fabric

Overall, our rock magnetic analyses and microscopy indicate that the intrusive units of the Ratagain Complex contain ferromagnetic minerals of variable grain size from SD to MD, but mainly MD. Mean magnetic susceptibilities of around 20×10^{-3} SI confirms that magnetite is the dominant ferromagnetic mineral (Ishihara, 1977). Thermomagnetic analyses (Figure 2.10) further reveal that the magnetite is Ti-poor and that, locally, the magnetite grains have been oxidized, and partially maghemitized, most probably due to weathering. However, our optical microscope and SEM observations of well-defined, subhedral to euhedral magnetite grains indicate that the magnetite of the Ratagain Complex is mostly primary and magmatic in origin; any hydrothermal alteration following intrusion and emplacement of the granite is not pervasive enough to have compromised the original magnetic mineralogy.

Out of the 16 representative sites selected to test the magnetic fabric using high field measurements, only one (AL002) shows an inverse fabric, in which the K_1 and K_3 axes are swapped. This is typically caused by the occurrence of SD magnetic grains (Rochette, 1988); however, both pARM and IRM experiments on this sample exclude the presence of a significant proportion of SD grains, suggesting that the inverse fabric in this case may be yielded by PSD grains. The sole intermediate AMS fabric (site AL009) can be interpreted either in terms of a low degree of anisotropy or an inverse fabric carried by SD magnetite grains partly camouflaging the normal fabric yielded by the MD magnetite (Borradaile & Gauthier, 2001). Such samples are rare in the entire dataset. Therefore, the bulk magnetic fabric of the Ratagain Complex revealed by our AMS measurements can thus be taken as representative of the shape preferred alignment of magnetite grains and likely parallel to the the main silicate petrofabric i.e. the foliation and lineation defined by mineral shape alignment (e.g. Bouchez, 1997; O'Driscoll et al., 2007; Archanjo et al., 2012).

A possible emplacement mechanism for the Ratagain Complex

The AMS ellipsoids determined in this study are predominantly oblate and the fabric orientations are consistent with a steeply dipping foliation (where K_3 is gently plunging) (Figure 2.5), indicating that there was a flattening ambient strain field as this magma crystallized.

Plotting all K_1 axes confirms the preponderance of a steeply subvertical orientation of the magnetic lineation and thus vertical stretching (Figure 2.6a). Plotting all K_3 shows a general NE–SW strike (Figure 2.15b), although with a bimodal north–south and NE–SW spread owing to the sigmoidal trace of the fabric. Following the reasoning of Burton-Johnson et al., (2019) and Di Chiara et al., (2020), the ambient tectonic strain field operating during the emplacement of the Ratagain Complex is NW–SE shortening. Modelling by Tikoff and Greene (1997) showed that transpression may produce vertical stretching lineations which may be relevant in terms of Caledonian tectonic events involving transpression.

Because the *T* values are predominantly positive, we place more confidence in the magnetic foliation. From Figure 2.16 we can see that the magnetic fabric is consistent with the weak visible fabric described by McErlean (1993); the magnetic lineation, although much weaker, is mainly subvertical (Figure 2.16). Combining the magnetic and visible fabrics reveals a markedly sigmoidal pattern (Figure 2.15a). The sigmoidal combined fabric trace may represent two opposing magmatic lobes (Figure 2.15b) (e.g. Stevenson et al., 2008). However, the fabric cross-cuts internal boundaries inferred by previous workers (Nicholls, 1951; Hutton et al., 1993). This would suggest that the fabric was imposed at the latter stages or at the end of emplacement and it follows that the mainly oblate shape of the AMS records a flattening ambient strain field. We find it more likely that the sigmoidal pattern records a sinistral magmatic shear zone (Figure 2.15c) much like the interpretation of McErlean (1993), who proposed that sinistral slip on the Strathconan Fault and a parallel shear zone to the NW linked by faults acted to permit space for magma intrusion during sinistral transpression and thus controlled the emplacement of the Ratagain Complex.

Post-emplacement fabric development

With the exception of one field locality (57° 13′ 23.41″ N, 5°24′ 49.63″ W; see also Figure 2.3g), the rocks of the Ratagain Complex do not evidence solid-state deformation in thinsection, hand-specimen or field exposures and also lack visible fabrics. The magmatic texture preserved in the majority of studied thin sections (see Figure 2.4) and the undeformed appearance of the MMEs (Figure 2.3f) provide strong evidence against deformation in the magmatic-flow stage as well as extensive solid-state grain-shape modification after full crystallization of the intrusion. This is further supported by the occurrence of flow structures in some outcrops, which are decoupled from tectonic structures in the metamorphic country rocks (Figure 2.3c).

The field observations outlined above suggest that the timing of fabric acquisition for the Ratagain Complex was restricted to a brief window post or at the end of its emplacement, when the granite was near the magmatic solidus but still contained substantial interstitial melt to accommodate most of the tectonic stress and shield crystallizing grains from substantial deformation (e.g. Liu et al., 2018). This is further corroborated by our microstructural observations, which clearly evidence that whilst the petrofabric of the Ratagain Complex records a deformational overprint, critically, this overprint has not developed into a solid-state tectonic fabric.

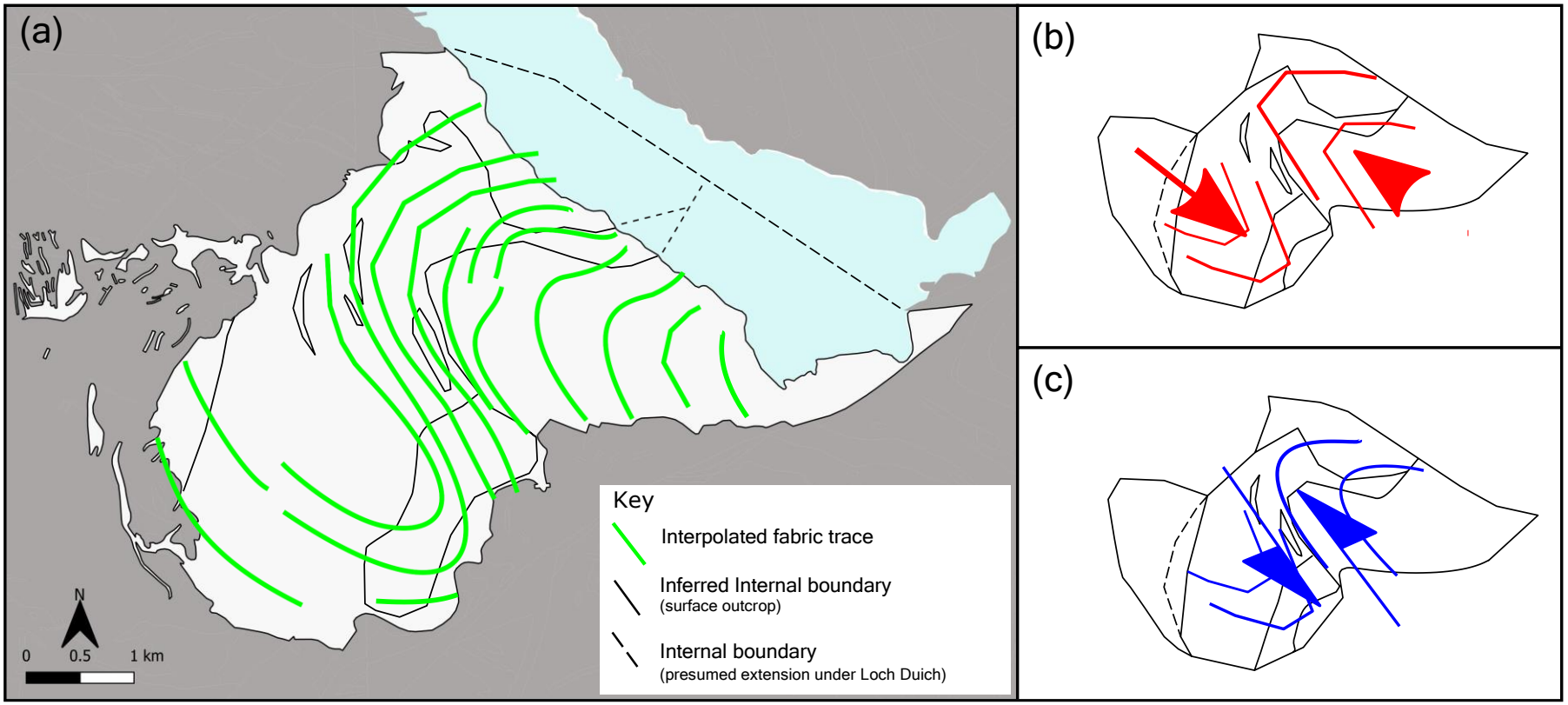


Figure 2.15 (a) Interpolated fabric trace for the Ratagain Complex. The base map is simplified from Figure 2 and fabric traces are based on magnetic fabrics from this study, combined with weak visible fabrics described by McErlean (1993). (b) Interpretation of the fabric pattern in (a) considering the emplacement of opposing lobes of magma similar to Stevenson et al. (2008). (c) Interpretation of the fabric pattern in (a) considering the strain recorded by a sinistral shear zone under a generally horizontal shortening or flattening strain field.

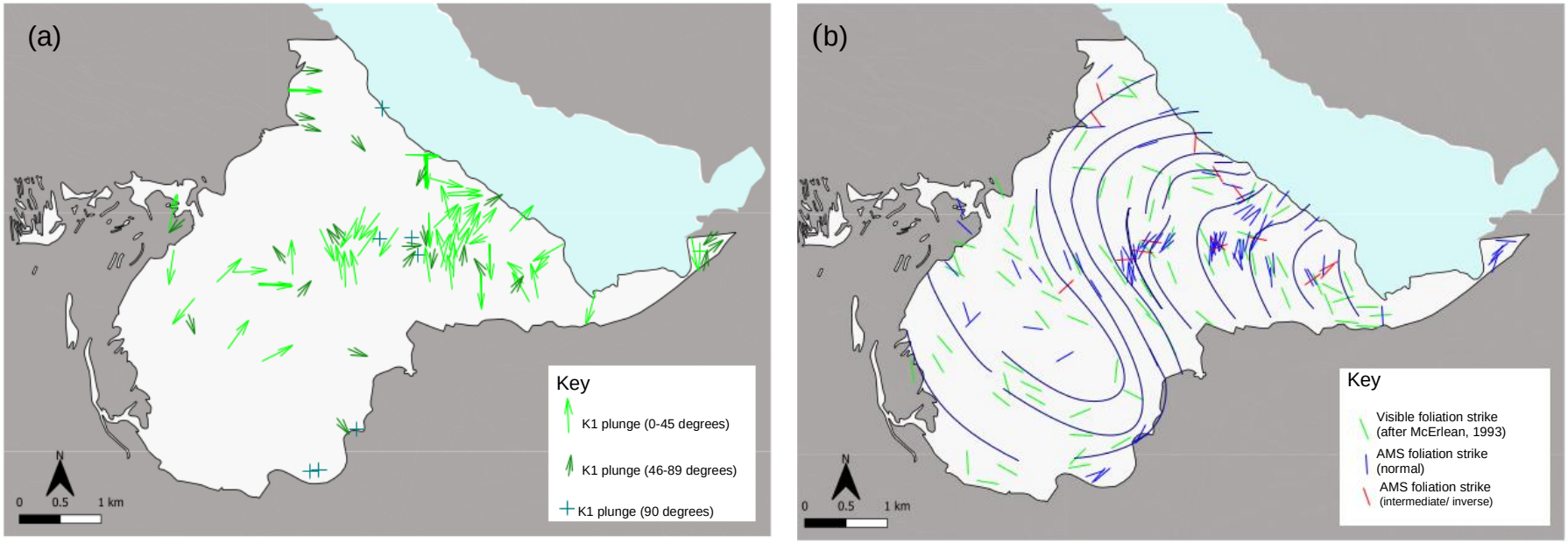


Figure 2.16 (a) Map showing the direction and plunge of the magnetic lineation (K_1). Light green arrows are a K_1 lineation plunging 0–45°; dark green arrows are a K_1 lineation plunging 46–89°; and green crosses are a vertical K_1 lineation. (b) Map showing the strike of the visible foliation, magnetic foliation and our overall interpretation of the fabric pattern. Light green lines are visible foliations mapped by McErlean (1993); light blue lines are normal magnetic foliations; red lines are intermediate or inverse magnetic lineations; dark blue continuous lines are interpolations between the foliation data points.

Timing of emplacement

The petrofabric of the Ratagain Complex carries an ambient tectonic overprint, which is most likely to have developed post or at the end of emplacement. Our data provide insights on the regional kinematics and timing of deformation relative to granite emplacement as the significant horizontal shortening component of the overprint can be ascribed to NW–SE shortening and is consistent with transpression.

The Late Caledonian suite of Britain and Ireland was emplaced in a complicated and varied tectonic setting that included alternating transtensional and transpressional strike-slip deformations (Jacques & Reavy, 1994; Miles et al., 2016). The major deformation phases that could potentially have produced the observed overprint are Iapetan (Scandian) transpression between c. 425 and 420 Ma, and Acadian transpression from 404 to 394 Ma (Miles et al., 2016).

Whilst the favoured age of crystallization (425 ± 3 Ma, Rogers & Dunning, 1991) and interpretation of the Ratagain Complex as a late Silurian intrusion (Hutton & McErlean, 1991; Hutton et al., 1993; McErlean, 1993) may seem consistent with emplacement during the Iapetus transpression, this hypothesis presents several significant problems.

(1) Both previous (Fowler et al., 2008; Fowler & Rollinson, 2012) and contemporary geochemical studies, the latter of which will be presented in a companion paper, evidence that the Ratagain Complex bears the characteristic elemental and isotopic signatures of post-collisional, slab breakoff magmatism (see Moyen et al., 2017; Hildebrand et al., 2018), precluding intrusion and emplacement during active Iapetan subduction.

(2) As Iapetus subduction was followed by orogen-wide transtension and thereafter a return to transpression in the Acadian, it follows that if the Ratagain Complex was emplaced during the late Silurian, the intrusion would reflect these respective kinematic events in the form of multiple tectonic fabrics (see Benn, 2010). Even if Iapetus transpression is backdated to c. 430 Ma, as postulated by some authors (Archibald et al., 2022), the Ratagain Complex would nonetheless record multiple tectonic fabrics, as opposed to a single, moderate tectonic overprint, if it was emplaced and crystallized at c. 425 Ma.

(3) The late Silurian to early Devonian in the Scottish Caledonides is understood to have been a period of brittle, upper crustal thrusting and strike-slip faulting along the GGF and related structures (Strachan et al., 2020; Searle, 2022). Given the proximity of the Ratagain Complex to the Strathconan fault, an offset of the GGF, one would expect the primary magmatic fabric to be reworked or obliterated by a well-developed, solid-state fabric imparted by the regionwide strike-slip faulting. Our thin-section petrographical analyses and field observations, do not show this and instead demonstrate that in the majority of the Ratagain Complex the primary magmatic-state fabric has been preserved.

For these reasons, we find it difficult to unequivocally place the final emplacement and crystallization of the majority of the Ratagain Complex at c. 425 Ma during Iapetus transpression. We instead suggest two hypotheses to satisfy the field, petrological and rock magnetic evidence.

a. The Ratagain Complex is younger than previously reported and could be a syn-Acadian intrusion. Although zircon age spectra for the Late Caledonian suite compiled by Miles et al. (2016) suggest that volumes of granitic emplacement were suppressed during the Acadian, emplacement within transpressional settings can be facilitated by transtensional sites formed at releasing bends (e.g. Glazner, 1991), as has recently been suggested for the Late Caledonian Shap, Skiddaw and Weardale granites, Lake District (Miles &

Woodcock, 2018; Woodcock et al., 2019). In our specific case, we postulate that a fault splay from the Strathconan Fault, subjacent to the Ratagain Complex emplacement site, may have interacted with the Strathconan Fault to create a local transtensional jog or opening, in an otherwise transpressional setting, to facilitate magma ascent from a deeper-seated mid- or lower-crustal source region. We envisage that the magma was sufficiently crystallized to accommodate ambient strain during the Acadian but, owing to both the presence of interstitial melt and the relatively short duration of the Acadian Event, the development of a significant solid-state deformational fabric was unable to take place before the cessation of the transpression at c. 394 Ma.

b. The Ratagain Complex was emplaced incrementally with crystallization of different magma batches over a protracted period. Rather than dating the final crystallization of the complex, Rogers and Dunning's (1991), 25 ± 3 Ma U–Pb baddeleyite age for the complex could instead record pre-emplacement magmatic activity in a deeper part of the transcrustal crystal-mush system (see Cashman et al., 2017; Jackson et al., 2018; Sparks et al., 2019). The intrusion of new magma pulses into partially crystallized magma mush could have accommodated most of the ambient tectonic strain (Liu et al., 2018) during the period of Silurian strike-slip faulting and offers a plausible explanation as to why the Ratagain Complex bears no obvious solid-state fabric, has no thermal aureole and is decoupled from tectonic structures in the host Precambrian rock (Figure 2.2a, e). Whilst direct evidence for multiple injections of magma, especially internal contact boundaries, may be lacking in the field, this is resolved by a model in which the remelting and/or recrystallization of successive magma pulses resulted in the contacts becoming diffuse (Miller et al., 2011; Liu et al., 2018). On the other hand, indicative features of new injections of magma, such as the MMEs and complex zoning patterns in feldspar phenocrysts identified in this study (Figures 2.2d, f and 2.3a), were preserved.

A tentative model of emplacement

Summing up, our field, microstructural and magnetic data would support emplacement of the Ratagain Complex in a compressive (likely transpressive) system. As the steeply dipping magnetic fabric pattern of the complex cross-cuts any internal boundaries, and there are also no apparent pulses in the fabric (cf. Stevenson et al., 2007), we interpret this fabric pattern as recording an ambient strain field operating post or at the very end of emplacement. The mostly irregular contact boundaries – such as that of the western granite, which has not been discussed in great detail by previous workers – could also be taken as representative of sheeting linked to wedging and sill-like intrusions with broken bridges (Schofield et al., 2012; Eide et al., 2017), similar to those recorded at the eastern contact of the Ross of Mull Granite (Petronis et al., 2012). We therefore tentatively suggest that the juxtaposition of the considerable compositional heterogeneity with diffuse or indistinguishable internal boundaries observed in the Ratagain Complex reflects incremental emplacement of a sheeted intrusive complex (Figure 2.17).

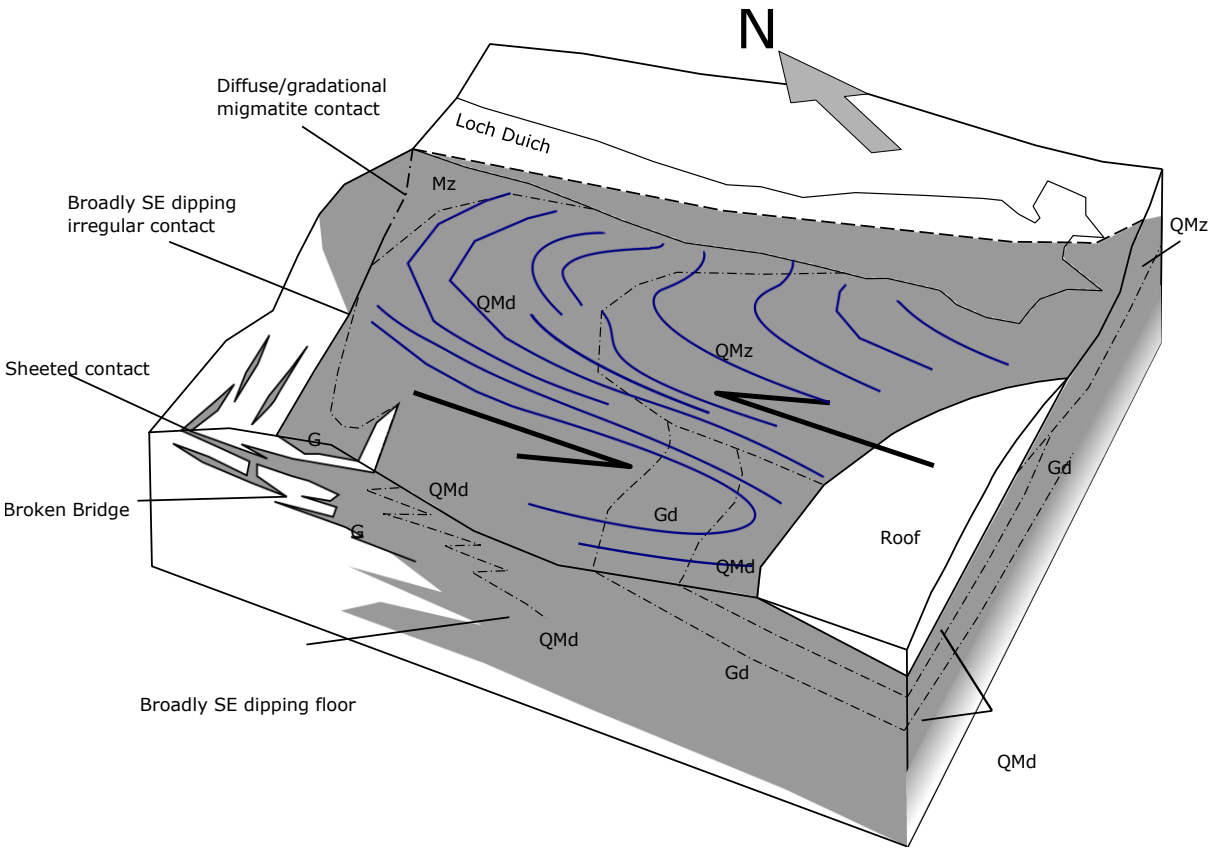


Figure 2.17 Schematic 3D cut-away model showing the suggested roughly tabular shape of the Ratagain Complex and sheeted or diffuse/gradational contacts. Blue curved lines represent the interpreted fabric trace. Dashed lines represent postulated internal boundaries based on Figure 2.1. G, granite; Gd, granodiorite; M, mixed granite and gneiss facies; Mz, monzonite; QMd, quartz monzodiorite; QMz, quartz monzonite.

Conclusions

(i) Strong agreement with visible fabrics (Hutton & McErlean 1991) and our detailed rock magnetic analyses confirming that MD ferromagnetic minerals are the main contributors to the magnetic fabric, allows us to interpret our AMS data as normal fabrics where the K_3 axis represents the pole to the magnetic foliation and the K_1 axis the magnetic lineation. The magnetic fabric of the Ratagain Complex as revealed by AMS can thus be considered a valid proxy for the petrofabric.

(ii) Further evidence for the predominant occurrence of a 'normal' magnetic fabric in the Ratagain Complex is provided by the coaxiality of AARM and AMS tensors; only two sites out of 16 showed an inverse (AL002) and intermediate (AL009) fabric, where the ARM_{max} axis coincides with the K_3 and K_2 susceptibility axis, respectively.

(iii) Thermomagnetic, IRM and pARM acquisition experiments, together with optical and scanning electron microscopy indicate that MD magnetite and minor maghemite (or partially maghemitized magnetite) are the main contributors to the magnetic susceptibility, and hence to the magnetic fabric.

(iv) Thin-section petrological investigations evidence predominantly magmatic textures with a tectonic overprint, but critically there is no obvious solidstate fabric. Together with the observation that the magnetite of the Ratagain Complex is magmatic (as indicated by the coaxiality between the AMS and AARM data and our microscopy studies) we propose that the magnetic fabric of the Ratagain Complex was formed post-emplacement, when the granite was near solidus temperature and in a crystal-rich but rheologically magmatic state. Sinistral transpressive strain imparted a tectonic overprint but did not persist long enough to form a solid-state fabric.

(v) Previous emplacement models for the Ratagain Complex do not fully correlate with all the field, petrographic and magnetic observations presented in this study, leading us to propose two hypotheses for its emplacement and relationship to regional kinematics. We suggest that either the Ratagain Complex is younger than previously suggested and records only Acadian transpression, or that it was intruded and emplaced incrementally over a protracted time period, whereby incremental remobilization by successive magma pulses accommodated most of the ambient tectonic strain, enabling the preservation of the primary magmatic fabric whilst simultaneously preventing the full development of a solid-state tectonic fabric.

(vi) Our work demonstrates that using a suite of rock magnetic analyses can provide insights on the detailed emplacement history of a granitic complex, particularly its relationship to regional tectonic strain, and allows us to infer temporal relations between different kinematic events that have taken place.

Acknowledgements

We thank Mike Fowler and Craig Storey for their initial suggestion to investigate the Ratagain Complex and all their advice since. Thanks go to Paul Hands for producing excellent thin sections for petrological analysis, Joshua Hicks for his kindness and assistance in the SEM studies, Bethan Hughes for facilitating the optical microscopy work and Filip Tomek for his advice on specialized stereographic software. AL would also like to thank Jon Oldfield for his encouragement and support. Reviewers Rob Strachan and Robin Shail are thanked for their great knowledge and insight into all things Caledonian, which substantially improved this manuscript! Finally, AL extends thanks to parent carers Paul and Mannpreet Lawrence for providing transport and social support in all research visits associated with the project.

All field sampling was carried out in accordance with the Geologists' Association code of conduct for field work.

Funding

AL acknowledges generous field support from the Open University Ian Gass Bursary and the Edinburgh Geological Society Fieldwork Grant. All field sampling was carried out in accordance with the Geologists' Association code of conduct for field work.

List of references

Allmendinger, R. W., Cardozo, N. & Fisher, D. 2012. *Structural geology algorithms: Vectors and tensors in structural geology*. Cambridge: Cambridge University Press.

Anderson, P.E., Stevenson, C.T., Cooper, M.R., Meighan, I.G., Reavy, R.J., Hurley, C.T., Inman, J. & Ellam R.M. 2018. Refined model of incremental emplacement based on structural evidence from the granodioritic Newry igneous complex, Northern Ireland. *Geological Society of America Bulletin*, **130**(5-6), 740-756. Available from: https://doi.org/10.1130/B31756.1

Archanjo, C.J., Campanha, G.A.C., Salazar, C.A. & Launeau, P. 2012. Using AMS combined with mineral shape preferred orientation analysis to understand the emplacement fabrics of the Apiaí gabbro-norite (Ribeira Belt, SE Brazil). *International Journal of Earth Sciences*, **101**, 731–745. Available from: https://doi.org/10.1007/s00531-011-0659-x

Archibald, D.B. & Murphy, J.B. 2021. A slab failure origin for the Donegal composite batholith, Ireland as indicated by trace-element geochemistry. *Geological Society, London, Special Publications*, **503**, 347-370. Available from: https://doi.org/10.1144/SP503-2020-6

Archibald, D.B., Murphy, J.B., Fowler, M., Strachan, R.A. & Hildebrand, R.S. 2022. Testing petrogenetic models for contemporaneous mafic and felsic to intermediate magmatism within the "Newer Granite" suite of the Scottish and Irish Caledonides. In Kuiper, Y.D., Murphy, J.B., Nance, R.D., Strachan, R.A. & Thompson, M.D. (Eds.), New Developments in the Appalachian-Caledonian- Variscan Orogen, *Geological Society of America Special Paper*, **554** (p. 1–XXX). Available from: https://doi.org/10.1130/2021.2554(15)

Atherton, M.P. & Ghani, A.A. 2002. Slab breakoff: a model for Caledonian, Late Granite syn-collisional magmatism in the orthotectonic (metamorphic) zone of Scotland and Donegal, Ireland. *Lithos*, **62**(3-4), 65-85. Available from: https://doi.org/10.1016/S0024-4937(02)00111-1

Benn, K. 2010. Anisotropy of magnetic susceptibility fabrics in syntectonic plutons as tectonic strain markers: The example of the Canso pluton, Meguma Terrane, Nova Scotia. *Transactions of the Royal Society of Edinburgh: Earth and Environmental Science*, **100**(1-2), 147–158. Available from: https://doi.org/10.1017/S1755691009016028

Bolle, O., Diot, H. & Trindade, R.I.F. 2003. Magnetic fabrics in the Holum granite (Vest-Agder, southernmost Norway): implications for the late evolution of the Sveconorwegian (Grenvillian) orogen of SW Scandinavia. *Precambrian Research*, **121**(3-4), 221-249. Available from: https://doi.org/10.1016/S0301-9268(03)00013-5

Borradaile, G.J. & Henry, B. 1997. Tectonic applications of magnetic susceptibility and its anisotropy. *Earth-Science Reviews*, **42**(1-2), 49-93. Available from: https://doi.org/10.1016/S0012-8252(96)00044-X

Borradaile, G.J. & Gauthier, D. 2001. AMS-detection of inverse fabrics without AARM, in ophiolite dikes. *Solid Earth*, **28**(18), 3517-3520. Available from: https://doi.org/10.1029/2001GL012976

Borradaile, G.J. & Jackson M. 2010. Structural geology, petrofabrics and magnetic fabrics (AMS, AARM, AIRM). *Journal of Structural Geology*, **32**(10), 1519-1551. Available from: https://doi.org/10.1016/j.jsg.2009.09.006

Bouchez J.L. 1997. Granite is never isotropic: an introduction to AMS studies of granitic rocks. In Bouchez J.L., Hutton, D.H.W. and Stephens, W.E. (Eds.) *Granite: from segregation of melt to emplacement fabrics* (pp.95–112). Dordrecht: Kluwer Academic Publishers.

Brown, P. E. & Ryan, P. D. and Soper, N. J. and Woodcock, N. H. 2008. The Newer Granite problem revisited: a transtensional origin for the Early Devonian Trans-Suture Suite. *Geological Magazine*, **145**(2), 235-256. Available from: https://doi:10.1017/S0016756807004219

Bruand, E., Storey, C. & Fowler, M. 2014. Accessory mineral chemistry of high Ba-Sr granites from Northern Scotland: Constraints on petrogenesis and records of whole-rock Signature. *Journal of Petrology*, **55**(8), 1619-1651. Available from: https://doi.org/10.1093/petrology/egu037

Burton-Johnson, A., Macpherson, C.G., Muraszko, J. R., Harrison, R. J. & Jordan, T.A. 2019. Tectonic strain recorded by magnetic fabrics (AMS) in plutons, including Mt Kinabalu, Borneo: A tool to explore past tectonic regimes and syn-magmatic deformation. *Journal of Structural Geology*, **119**, 50-60. Available from: https://doi.org/10.1016/j.jsg.2018.11.014

Butler, R.F. 1992. *Paleomagnetism: magnetic domains to geologic terranes*. Oxford: Blackwell Scientific Publications.

Cardozo, N. & Allmendinger, R.W. 2013. Spherical projections with OSXStereonet. *Computers & Geosciences*, **51**, 193-205. Available from: https://doi.org/10.1016/j.cageo.2012.07.021

Cashman, K. V., Sparks, R. S. J. & Blundy, J. D. 2017. Vertically extensive and unstable magmatic systems: A unified view of igneous processes. *Science*, **355** (6331). Available from: https://doi.org/10.1126/science.aag3055

Chadima, M. & Jelinek, V. 2009. Anisoft 4.2: Anisotropy Data Browser for Windows, Agico, Inc., Brno, Czech Republic.

Chambers, M., Memeti, V., Eddy, M. P. & Schoene, B. 2020. Half a million years of magmatic history recorded in a K-feldspar megacryst of the Tuolumne Intrusive Complex, California, USA. *Geology*, **48**. Available from: https://doi.org/10.1130/G46873.1

Chew D.M. & Strachan R.A. 2014. The Laurentian Caledonides of Scotland and Ireland. *Geological Society, London, Special Publications*, **390**, 45–91. Available from: https://doi.org/10.1144/SP390.16

Corfu, F., Gasser, D. & Chew, D.M. 2014. New Perspectives on the Caledonides of Scandinavia and Related Areas. *Geological Society, London, Special Publications,* **390**, 1-8. Available from: https://doi.org/10.1144/SP390.28

Cruden, A.R. & Weinberg, R.F. 2018. Mechanisms of Magma Transport and Storage in the Lower and Middle Crust—Magma Segregation, Ascent and Emplacement, in Burchardt, S. (Eds.) *Volcanic and Igneous Plumbing Systems* (pp.13-53). Amsterdam: Elsevier.

Dallmeyer, R.D., Strachan, R.A., Rogers, G., Watt, G.R. & Friend, C.R.L. 2001. Dating deformation and cooling in the Caledonian thrust nappes of north Sutherland, Scotland: insights from 40Ar/39Ar and Rb–Sr chronology. *Journal of the Geological Society, London,* **158**(3), 501–12. Available from: https://doi.org/10.1144/jgs.158.3.501

Day, R., Fuller, M.D. & Schmidt, V.A. 1977. Hysteresis properties of titanomagnetites: grain size and composition dependence. *Physics of the Earth and Planetary Interiors*, **13**(4), 260-266. Available from: https://doi.org/10.1016/0031-9201(77)90108-X

Dewey, J. 1969. Evolution of the Appalachian/Caledonian Orogen. *Nature*, **222**, 124–129 Available from: https://doi.org/10.1038/222124a0

Dewey, J.F. & Strachan, R.A. 2003. Changing Silurian–Devonian relative plate motion in the Caledonides: sinistral transpression to sinistral transtension. *Journal of the Geological Society, London*, **160**(2), 219-229. Available from: https://doi.org/10.1144/0016-764902-085

Di Chiara, A., Morris, A., Anderson, M.W., Menegon, L. & Tremblay, A. 2020. Magnetic anisotropy reveals Acadian transpressional fabrics in an Appalachian ophiolite (Thetford Mines, Canada). *Geophysical Journal International*, **222**(2), 1034–1045, Available from: https://doi.org/10.1093/gji/ggaa173

dos Santos Dias, J.C., Gonçalves, L. & Gonçalves, C.C. 2019. Contrasting oxygen fugacity of I- and S-type granites from the Araçuaí orogen, SE Brazil: an approach based on opaque mineral assemblages. *Mineralogy and Petrology*, **113**, 667–686. Available from: https://doi.org/10.1007/s00710-019-00670-2

Dunlop, D.J. 1972. Magnetic Mineralogy of Unheated and Heated Red Sediments by Coercivity Spectrum Analysis. *Geophysical Journal International*, **27**, 37–55. Available from: https://doi.org/10.1111/j.1365-246X.1972.tb02346.x

Dunlop, D.J. 1974. Thermal Enhancement of Magnetic Susceptibility. *Journal of Geophysics*, **40**, 439-51.

Dunlop, D.J. & Özdemir, O.1997. *Rock Magnetism: Fundamentals and Frontiers*., Cambridge: Cambridge University Press.

Eide, C.H., Schofield, N., Jerram, D.A. & Howell, J.A. 2017. Basin-scale architecture of deeply emplaced sill complexes: Jameson Land, East Greenland. *Journal of the Geological Society, London*, **174**(1), 23-40. Available from: https://doi.org/10.1144/jgs2016-018

Fowler, M. & Henney, P. 1996. Mixed Caledonian appinite magmas: implications for lamprophyre fractionation and high Ba-Sr granite genesis. *Contributions to Mineralogy and Petrology*, **126**, 199–215. Available from: https://doi.org/10.1007/s004100050244

Fowler, M.B., Kocks, H., Darbyshire, D.P.F. & Greenwood, P.B. 2008. Petrogenesis of high Ba-Sr plutons from the Northern Highlands Terrane of the British Caledonian Province. *Lithos*, **105**(1-2), 129-148. Available from: https://doi.org/10.1016/j.lithos.2008.03.003

Fowler, M. & Rollinson H. 2012. Phanerozoic sanukitoids from Caledonian Scotland: Implications for Archean subduction. *Geology*, **40**(12), 1079-1082. Available from: https://doi.org/10.1130/G33371.1

Glazner, A.F.1991. Plutonism, oblique subduction, and continental growth: An example from the Mesozoic of California. *Geology*, **19**(8), 784-786. Available from: https://doi.org/10.1130/0091-7613(1991)019<0784:POSACG>2.3.CO;2

Heller, F. 1973. Magnetic anisotropy of granitic rocks of the Bergell massif (Switzerland). *Earth and Planetary Science Letters*, **20**(2), 180–188. Available from: https://doi.org/10.1016/0012-821X(73)90156-8

Heslop, D. Dekkers,M. J., Kruiver, P. P. & Van Oorschot, I. H. M. 2002. Analysis of isothermal remanent magnetization acquisition curves using the expectation-maximization algorithm. *Geophysical Journal International*, **148**(1), 58–64. Available from: https://doi.org/10.1046/j.0956-540x.2001.01558.x

Hildebrand R.S., Whalen J.B., & Bowring S.A. 2018. Resolving the crustal composition paradox by 3.8 billion years of slab failure magmatism and collisional recycling of continental crust. *Tectonophysics*, **734–735**, 69–88. Available from: https://doi.org/10.1016/j.tecto.2018.04.001

Hopkinson, J. 1889. Magnetic and other physical properties of iron at a high temperature. *Philosophical Transactions of the Royal Society of London Series A, Mathematical and Physical Sciences*, **180**, 443-446. Available from: https://doi.org/10.1098/rsta.1889.0014

Hrouda, F. 1994. A technique for the measurement of thermal changes of magnetic susceptibility of weakly magnetic rocks by the CS-2 apparatus and KLY-2 Kappabridge. *Geophysical Journal International*, **118**(3), 604–612. Available from: https://doi.org/10.1111/j.1365-246X.1994.tb03987.x

Hrouda, F. 2007. Magnetic susceptibility, anisotropy. In D. Gubbins & E. Herrero-Bervera (Eds.), *Encyclopedia of Geomagnetism and Paleomagnetism* (pp. 546-560). Dordrecht: Springer.

Hutton, D. 1988. Granite emplacement mechanisms and tectonic controls: Inferences from deformation studies. *Earth and Environmental Science Transactions of the Royal Society of Edinburgh*, **79**(2-3), 245-255. Available from: https://doi:10.1017/S0263593300014255

Hutton, D.H.W. & McErlean, M. 1991. Silurian and early Devonian sinistral deformation of the Ratagain granite, Scotland: constraints on the age of Caledonian movements on the Great Glen fault system. *Journal of the Geological Society, London*, **148**(1), 1-4. Available from: https://doi.org/10.1144/gsjgs.148.1.0001

Hutton, D. H. W. & Reavy, R. J., 1992. Strike-slip tectonics and granite petrogenesis. *Tectonics*, **11**(5), 960-967. Available from: https://doi.org/10.1029/92TC00336

Hutton, D. H. W. Stephens, W. E., Yardley, B., McErlean, M. & Halliday, A. N., 1993. Ratagain Plutonic complex. In May, F., Peacock, J. D., Smith, D. I. and Barber, A. J. (Eds.), *Geology of the Kintail district* (pp.52-56). Memoir of the British Geological Survey, London: HMSO.

Ishihara, S. 1977. The Magnetite-series and Ilmenite-series Granitic Rocks. *Mining Geology*, **27**(145), 293-305. Available from: https://doi.org/10.11456/shigenchishitsu1951.27.293

Ishihara, S. 2004. The redox state of granitoids relative to tectonic setting and earth history: the magnetite-ilmenite series 30 years later. *Transactions of the Royal Society of Edinburgh: Earth Sciences*, **95**(1-2), 23–33. Available from: https://doi.org/10.1017/S0263593300000894

Jackson M. 1991. Anisotropy of magnetic remanence: A brief review of mineralogical sources, physical origins, and geological applications, and comparison with susceptibility anisotropy. *Pure and Applied Geophysics*, **136**, 1-28. Available from: https://doi.org/10.1007/BF00878885

Jackson, M., Gruber, W., Marvin, J., & Banerjee, S. K. (1988). Partial anhysteretic remanence and its anisotropy: Applications and grain size-dependence. *Geophysical Research Letters*, **15**(5), 440–443. Available from: https://doi.org/10.1029/GL015i005p00440

Jackson, M.D., Blundy, J. & Sparks, R.S.J. 2018. Chemical differentiation, cold storage and remobilization of magma in the Earth's crust. *Nature*, **564**, 405–409. Available from: https://doi.org/10.1038/s41586-018-0746-2

Jacques, J.M. & Reavy, R.J. 1994. Caledonian plutonism and major lineaments in the SW Scottish Highlands. *Journal of the Geological Society, London*, **151**(6), 955-969. Available from: https://doi.org/10.1144/gsjgs.151.6.0955

Jelínek, V. 1981. Characterization of the magnetic fabrics of rocks. *Tectonophysics*, **79**(3-4), T63-T67. Available from: https://doi.org/10.1016/0040-1951(81)90110-4

Johnson, T.E., Kirkland, C.L., Viete, D.R., Fischer, S., Reddy, S.M., Evans, N.J. & McDonald, B.J. 2017. Zircon geochronology reveals polyphase magmatism and crustal anatexis in the Buchan

Block, NE Scotland: implications for the Grampian Orogeny. *Geoscience Frontiers*, **8**(6),1469–1478. Available from: https://doi.org/10.1016/j.gsf.2017.02.002

Jones, R.R., Holdsworth, R.E. & Bailey, W. 1997. Lateral extrusion in transpression zones: the importance of boundary conditions. *Journal of Structural Geology*, **19**(9), 1201–1217. Available from: https://doi.org/10.1016/S0191-8141(97)00034-5

King, R. F. 1966. The magnetic fabric of some Irish granites. *Geological Journal*, **5**(1), 43–46. Available from: https://doi.org/10.1002/gj.3350050106

Kinny, P., Strachan, R., Friend, C., Kocks, H., Rogers, G. & Paterson, B. 2003. U -Pb geochronology of deformed metagranites in central Sutherland, Scotland: evidence for widespread late Silurian metamorphism and ductile deformation of the Moine Supergroup during the Caledonian orogeny. *Journal of the Geological Society*, **160**(2), 259–269, Available from: https://doi.org/10.1144/0016-764901-087

Krabbendam, M., Ramsay, J.G., Leslie, A.G., Tanner, P.W.G., Dietrich, D. & Goodenough, K.M. 2018. Caledonian and Knoydartian overprinting of a Grenvillian inlier and the enclosing Morar Group rocks: structural evolution of the Precambrian Proto-Moine Nappe, Glenelg, NW Scotland. *Scottish Journal of Geology*, **54**(1), 13–35. Available from: https://doi.org/10.1144/sjg2017-006

Kruiver, P.P., Dekkers, M.J. & Heslop, D. 2001. Quantification of magnetic coercivity components by the analysis of acquisition curves of isothermal remanent magnetisation. *Earth and Planetary Science Letters*, **189**(3-4), 269–276. Available from: https://doi.org/10.1016/S0012-821X(01)00367-3

Lambert, R.S.J. & McKerrow, W. S. 1976. The Grampian Orogeny. *Scottish Journal of Geology*, **12**(4), 271-292. Available from: https://doi.org/10.1144/sjg12040271

Law, R. D. & Johnson, M. R. W. 2010. Microstructures and crystal fabrics of the Moine Thrust zone and Moine Nappe: history of research and changing tectonic interpretations. *Geological Society, London, Special Publications*, **335**, 443-503. Available from: https://doi.org/10.1144/SP335.21

Liss, D., Owens, W.H. & Hutton, H.W. 2004. New palaeomagnetic results from the Whin Sill complex: evidence for a multiple intrusion event and revised virtual geomagnetic poles for the late Carboniferous for the British Isles. *Journal of the Geological Society, London*, **161**(6), 927–938. Available from: https://doi.org/10.1144/0016-764903-156

Liu, H., Martelet, G., Wang, B., Erdmann, S., Chen, Y., Faure, M., Huang, F.F., Scaillet, B., Breton, N., Shu, L.S., Wang, R.C. & Zhu, J.C. 2018. Incremental emplacement of the late Jurassic Midcrustal, Lopolith-Like Qitianling Pluton, South China, revealed by AMS and Bouguer Gravity Data. *Journal of Geophysical Research: Solid Earth*, **123**(10), 9249-9268. Available from: https://doi/10.1029/2018JB015761

Liu, Q., Yu, Y., Pan, Y., Zhu, R. & Zhao, X. 2005. Partial anhysteretic remanent magnetization (pARM) of synthetic single- and multidomain magnetites and its paleoenvironmental significance. *Chinese Science Bulletin*, **50**, 2381–2384. Available from: https://doi.org/10.1007/BF03183751

Mark, D., Rice, C., Hole, M., & Condon, D. 2020. Multi-chronometer dating of the Souter Head complex: Rapid exhumation terminates the Grampian Event of the Caledonian Orogeny. *Earth and Environmental Science Transactions of the Royal Society of Edinburgh*, **111**(2), 95-108. Available from: https://doi.org/10.1017/S1755691020000043

Martín-Hernández, F., Lüneburg, C.M., Aubourg, C. & Jackson, M. 2004. Magnetic fabric: methods and applications—an introduction. *Geological Society, London, Special Publications*, **238**,1-7. Available from: http://dx.doi.org/10.1144/GSL.SP.2004.238.01.28

Martín-Hernández, F. & Ferré, E.C. 2007. Separation of paramagnetic and ferrimagnetic anisotropies: A review. *Journal of Geophysical Research: Solid Earth*, **112**, B03105. Available from: https://doi.org/10.1029/2006JB004340

Maxbauer, D.P., Feinberg, J.M. & Fox, D.L. 2016. MAX UnMix: a web application for unmixing magnetic coercivity distributions. *Computers & Geosciences*, **95**, 140-145. Available from: https://doi.org/10.1016/j.cageo.2016.07.009

McErlean, M.A. 1993. *Granitoid emplacement and deformation: a case study of the thorr pluton, Ireland, with contrasting examples from Scotland*. Unpublished PhD thesis, Durham University

Mendum, J.R. 2012. Late Caledonian (Scandian) and Proto-Variscan (Acadian) orogenic events in Scotland. *OUGS Journal*, **33**, 37–51.

Mendum, J.R. & Noble, S.R. 2010. Mid-Devonian sinistral transpressional movements on the Great Glen Fault: the rise of the Rosemarkie Inlier and the Acadian Event in Scotland. *Geological Society, London, Special Publications*, **335**, 161–187. Available from: https://doi.org/10.1144/SP335.8

Miles, A.J. & Woodcock, N.H. 2018. A combined geochronological approach to investigating long lived granite magmatism, the Shap granite, UK. *Lithos*, **304–307**, 245-257. Available from: https://doi.org/10.1016/j.lithos.2018.02.012

Miles, A. J., Woodcock, N. & Hawkesworth, C. 2016. Tectonic controls on postsubduction granite genesis and emplacement: The late Caledonian suite of Britain and Ireland. *Gondwana Research*, **39**, 250-260. Available from: https://doi.org/10.1016/j.gr.2016.02.006

Miller, C.F., Furbish, D.J., Walker, B.A., Claiborne, L.L., Koteas, G.C., Bleick, H.A. & Miller, J.S. 2011. Growth of plutons by incremental emplacement of sheets in crystal-rich host: Evidence from Miocene intrusions of the Colorado River region, Nevada, USA. *Tectonophysics*, **500**(1-4), 65–77. Available from: http://doi.org/10.1016/j.tecto.2009.07.011

Moyen, J.-F., Laurent, O., Chelle-Michou, C., Couzinié, S., Vanderhaeghe, O., Zeh, A., Villaros, A. & Gardien V., 2017. Collision vs. subduction-related magmatism: two contrasting ways of granite formation and implications for crustal growth. *Lithos*, **277**, 154–177. Available from; https://doi.org/10.1016/j.lithos.2016.09.018

Nédélec, A. & Bouchez, J.-L., 2015. *Granites: Petrology, Structure, Geological Setting and Metallogeny*. Oxford: Oxford University Press.

Neilson J.C., Kokelaar B.P. & Crowley Q.G. 2009. Timing, relations and cause of plutonic and volcanic activity of the Siluro-Devonian post-collision magmatic episode in the Grampian Terrane, Scotland. *Journal of the Geological Society*, **166**(3), 545–561. https://doi.org/10.1144/0016-76492008-069

Nicholls, G.D. 1951. The Glenelg-Ratagain igneous complex. *Quarterly Journal of the Geological Society*, **106**(1-4), 309-344.

O'Driscoll, B, Hargraves, R.B., Emeleus, C.H., Troll, V.R., Donaldson, C.H. & Reavy, R.J. 2007. Magmatic lineations inferred from anisotropy of magnetic susceptibility fabrics in Units 8, 9, and 10 of the Rum Eastern Layered Series, Scotland. *Lithos*, **98**(1-4), 27- 44. Available from: https://doi.org/10.1016/j.lithos.2007.01.009

Oliver, G.J., Wilde, S.A. & Wan, Y. 2008. Geochronology and geodynamics of Scottish granitoids from the late Neoproterozoic break-up of Rodinia to Palaeozoic collision. *Journal of the Geological Society*, **165**(3), 661–674. Available from: https://doi.org/10.1144/0016-76492007-105

Orlický, O. 1990. Detection of magnetic carriers in rocks: results of susceptibility changes in powdered rock samples induced by temperature. *Physics of the Earth and Planetary Interiors*, **63**(1-2), 66-70. Available from: https://doi.org/10.1016/0031-9201(90)90060-B

Owens, W.H., & Bamford, D. 1976. Discussion on natural strain and geological structure - Magnetic, seismic, and other anisotropic properties of rock fabrics. *Philosophical Transactions of the Royal Society of London. Series A, Mathematical and Physical Sciences*, **283**(1312), 55–68. Available from: http://doi.org/10.1098/rsta.1976.0069

Peach, B. N., Horne, J., Woodward, H. B., Clough, C. T., Harker, A. & Wedd, C. B. 1910. *The geology of Glenelg, Lochalsh and south-east part of Skye (Explanation of one-inch map 71)*. Edinburgh: HMSO (Memoirs of the Geological Survey of Great Britain [Scotland])

Petronis, M. S., O'Driscoll, B., Stevenson, C. T. E., & Reavy, R. J. 2012. Controls on emplacement of the Caledonian Ross of Mull Granite, NW Scotland: Anisotropy of magnetic susceptibility and magmatic and regional structures. *Geological Society of America Bulletin*, **124**(5-6), 906-927. Available from: https://doi.org/10.1130/B30362.1

Petrovský, E., & Kapička, A. 2006. On determination of the Curie point from thermomagnetic curves. *Journal of Geophysical Research*, **111**, B12S27. Available from: https://doi.org/10.1029/2006JB004507

Phillips, E.R., Barnes, R.P., Boland, M.P., Fortey, N.J. & McMillan, A.A. 1995. The Moniaive Shear Zone: a major zone of sinistral strike-slip in the Southern Uplands of Scotland. *Scottish Journal of Geology*, **31**(2),139-149. Available from: https://doi.org/10.1144/sjg31020139

Pickering, K., Bassett, M., & Siveter, D. (1988). Late Ordovician–early Silurian destruction of the Iapetus Ocean: Newfoundland, British Isles and Scandinavia—a discussion. *Transactions of the Royal Society of Edinburgh: Earth Sciences*, **79**(4), 361-382. Available from: https://doi.org/10.1017/S0263593300014358

Pidgeon, R. T. & Aftalion, M. 1978. Cogenetic and inherited zircon U-Pb systems in Palaeozoic granites from Scotland and England. In Bowls, D. R. & Leake, B.E. (Eds.), *Crustal evolution in northwestern Britain and adjacent regions* (pp.183-220). Liverpool: Seal House Press.

Potter, D.K. 2004. A comparison of anisotropy of magnetic remanence methods — a user's guide for application to palaeomagnetism and magnetic fabric studies. *Geological Society, London, Special Publications*, **238**, 21-35. Available from: https://doi.org/10.1144/GSL.SP.2004.238.01.03

Potter, D.K. & Stephenson, A. 1988. Single-domain particles in rocks and magnetic fabric analysis. *Geophysical Research Letters*, **15**(10), 1097-1100. Available from: https://doi.org/10.1029/GL015i010p01097

QGIS.org, 2021. QGIS Geographic Information System. QGIS Association. http://www.qgis.org

Raposo, M.I.B. & Gastal, M.C.P. 2009. Emplacement mechanism of the main granite pluton of the Lavras do Sul intrusive complex, South Brazil, determined by magnetic anisotropies. *Tectonophysics*, **466**(1-2), 18-31. Available from: https://doi.org/10.1016/j.tecto.2008.10.015

Read, H.H. 1961. Aspects of Caledonian magmatism in Britain. *Geological Journal*, **2**(4), 653–683. Available from: https://doi.org/10.1002/gj.3350020408

Richter, C. & van der Pluijm, B. A. 1994. Separation of paramagnetic and ferrimagnetic susceptibilities using low temperature magnetic susceptibilities and comparison with high field methods. *Physics of The Earth and Planetary Interiors*, **82**(2), 113-123. Available from: https://doi.org/10.1016/0031-9201(94)90084-1

Rochette, P. 1988. Inverse magnetic fabric in carbonate-bearing rocks. *Earth and Planetary Science Letters*, **90**(2), 229-237. Available from: https://doi.org/10.1016/0012-821X(88)90103-3

Rochette, P., Jackson, M. & Aubourg, C. 1992. Rock magnetism and the interpretation of anisotropy of magnetic susceptibility. *Reviews of Geophysics*, **30**(3), 209-266. Available from: https://doi.org/10.1029/92RG00733

Rogers, G. & Dunning, G. R. 1991. Geochronology of appinitic and related granitic magmatism in the W Highlands of Scotland: constraints on the timing of transcurrent fault movement. *Journal of the Geological Society, London*, **148**(1),17-27. Available from: https://doi.org/10.1144/gsjgs.148.1.0017

Sant'Ovaia, H., Nogueria, P.,Lopes, J.,Gomes, C., Ribiero, M., Martins, H., DÓria, A., Cruz, C., Lopes, L., Sardinha, R.,Rocha, A. & Noronha, F. 2015. Building up of a nested granite intrusion: Magnetic fabric, gravity modelling and fluid inclusion planes studies in Santa Eulália Plutonic Complex (Ossa Morena Zone, Portugal). *Geological Magazine*, **152**(4), 648-667. Available from: https://doi:10.1017/S0016756814000569

Schofield, N.J., Brown, D.J., Magee, C. & Stevenson, C.T. 2012. Sill morphology and comparison of brittle and non-brittle emplacement mechanisms. *Journal of the Geological Society, London*, **169**(2), 127–141. Available from: https://doi.org/10.1144/0016-76492011-078

Searle, M.P. 2022. Tectonic evolution of the Caledonian orogeny in Scotland: a review based on the timing of magmatism, metamorphism and deformation. *Geological Magazine*, **159**(1), 124–152. Available from: https://doi.org/10.1017/S0016756821000947

Silva, O. B. D., & Raposo, M. I. B. 2020. Emplacement of the Anta Granite from Rio de Janeiro State (SE, Brazil); determined by magnetic fabrics. *Brazilian Journal of Geology*, **50**(4). Available from: https://doi.org/10.1590/2317-4889202020200007

Soper, N. J., Strachan, R. A., Holdsworth, R. E., Gayer, R. A., & Greiling, R. O. 1992. Sinistral transpression and the Silurian closure of Iapetus. Journal of the Geological Society, London, **149**(6), 871-880. Available from: https://doi.org/10.1144/gsjgs.149.6.0871

Sparks, R.S.J, Annen, C., Blundy, J.D., Cashman, K.V., Rust, A.C. & Jackson, M.D. 2019. Formation and dynamics of magma reservoirs. *Philosophical Transactions of the Royal society Series A, Mathematical and Physical Sciences*, **377**, 20180019. Available from: http://dx.doi.org/10.1098/rsta.2018.0019

Stephenson, D., Bevins, R.E., Millward, D., Stone, P., Parsons, I., Highton, A.J. & Wadsworth, W.J. (1999) *Caledonian Igneous Rocks of Great Britain*. Peterborough: JNCC.

Stevenson, C. T. E. 2004. *Magma Flow and Granite emplacement in Contrasting Tectonic Environments using Anisotropy of Magnetic Susceptibility*. Unpublished PhD Thesis, University of Birmingham.

Stevenson, C.T.E., Owens, W.H., Hutton, D.H., Hood, D.N. & Meighan, I.G. 2007. Laccolithic, as opposed to cauldron subsidence, emplacement of the Eastern Mourne pluton, N. Ireland: evidence from anisotropy of magnetic susceptibility. *Journal of the Geological Society, London*, **164**(1), 99–110. Available from: https://doi.org/10.1144/0016076492006-008

Stevenson, C.T.E., Owens, W.H. & Hutton, D.H.W. 2008. Flow lobes in granite: The determination of magma flow direction in the Trawenagh Bay Granite, northwestern Ireland, using anisotropy of magnetic susceptibility. *Geological Society of America Bulletin*, **119**(11-12),1368–1386. Available from: https://doi.org/10.1130/B25970.1

Strachan, R.A., Alsop, G.I., Ramezani, J., Frazer, R.E., Burns, I.M. & Holdsworth, R.E. 2020. Patterns of Silurian deformation and magmatism during sinistral oblique convergence, northern Scottish Caledonides. *Journal of the Geological Society, London*, **177**(5), 893–910. Available from: https://doi.org/10.1144/jgs2020-039

Tarling, D. H. & Hrouda, F. 1993. *The Magnetic Anisotropy of Rocks*. London: Chapman and Hall.

Temporim, F. A., Trindade, R. I. F.,Tohver, E., Soares, C. C., Gouvêa, L. P.,Egydio-Silva, M., Amaral, C. A. D. & Souza, G. F. Jr. 2020. Magnetic fabric and geochronology of a Cambrian "isotropic" pluton in the Neoproterozoic Araçuaí Orogen. *Tectonics*, **39**(6), e2019TC005877. Available from: https://doi.org/10.1029/2019TC005877

Thirlwall, M. F. 1988. Geochronology of late Caledonian magmatism in northern Britain. *Journal of the Geological Society, London*, **145**(6), 951-967. Available from: https://doi.org/10.1144/gsjgs.145.6.0951

Tikoff, B. & Greene, D. 1997. Stretching lineations in transpressional shear zones: an example from the Sierra Nevada Batholith, California. *Journal of Structural Geology*, **19**(1), 29-39. Available from: https://doi.org/10.1016/S0191-8141(96)00056-9

Trindade, R.I.F., Bouchez, J.L., Bolle, O., Nédélec, A., Peschler, A. & Poitrasson, F. 2001. Secondary fabrics revealed by remanence anisotropy: methodological analysis and examples from plutonic rocks. *Geophysical Journal International*, **147**(2), 310–318. Available from: https://doi.org/10.1046/j.0956-540x.2001.01529.x

Turnell, H. B. 1985. Palaeomagnetism and Rb-Sr ages of the Ratagan and Comrie intrusions. *Geophysical Journal International*, **83**(2), 363–378. Available from: https://doi.org/10.1111/j.1365-246X.1985.tb06492.x

Vernon, R.H. 2004. *A Practical guide to rock microstructure*. Cambridge: Cambridge University Press.

Watson, J.V. 1984. The ending of the Caledonian orogeny in Scotland. *Journal of the Geological Society*, *London*, **141**(2), 193–214. Available from: https://doi.org/10.1144/gsjgs.141.2.0193

Whitney, D. L., & Evans, B. W. 2010. Abbreviations for names of rock-forming minerals. *American Mineralogist*, **95**(1), 185–187. Available from: https://doi.org/10.2138/am.2010.3371 4

Woodcock, N.H., Soper, N.J. & Strachan, R.A. 2007. A Rheic cause for the Acadian deformation in Europe. *Journal of the Geological Society, London*, **164**(5), 1023–1036. Available from: https://doi.org/10.1144/0016-76492006-129

Woodcock, N.H., Soper, N.J. & Miles, A.J. 2019. Age of the Acadian deformation and Devonian granites in northern England: a review. *Proceedings of the Yorkshire Geological Society*, **62**(4), 238–253. Available from: https://doi.org/10.1144/pygs2018-009

Chapter 3

Slab failure or slab success? Examining the contributions of crust and mantle to post-subduction magmatism in the Ratagain Complex, NW Scotland.

Paper in submission

Lawrence, A.[1], Fowler, M. [2], Kingsbury, C. [3], Knott, T. [4], Mark, D.[5] and Stevenson, C.T.E.[1]

Lithos

My role involved conducting all fieldwork at the Ratagain Complex, approximately half of the XRF and LAICPMS analytical preparations and all thin section petrographical studies. I was also responsible for collating the geochemical data, conceptualising the manuscript, writing the manuscript and coordinating inputs from multiple authors. Development of a plan for the manuscript and fractionation modelling was undertaken by Mike Fowler. Assistance with plotting geochemical discrimination diagrams was received from Cole Kingsbury. SEM compositional analyses were performed by Tom Knott. Isotopic analyses were coordinated and overseen by Darren Mark. Assistance with writing the manuscript, particularly discussions of regional tectonics and the wider implications of the study, was given by Carl Stevenson.

[1]School of Geography, Earth and Environmental Sciences, University of Birmingham, Birmingham, UK, B15 2TT

[2]School of the Environment, Geography and Geosciences, University of Portsmouth, Burnaby Road, Portsmouth, UK, PO1 3QL

[3]Faculty of Geology and Geography, National Research Tomsk State University, Lenin Avenue, 36, Tomsk, Tomsk Oblast, Russian Federation, 634050

[4]SciMed, Unit B4, The Embankment Business Park, Vale Road, Heaton Mersey, UK, SK4 3GN

[5]Scottish Universities Environmental Research Centre, Rankine Avenue, East Kilbride, UK, G75 0QF

Abstract

The Ratagain Complex is an enigmatic Late Caledonian granitic intrusion and a member of the high Ba-Sr Northern Highlands granite (NHG) suite that has been related to slab failure. Slab failure magmatism explains varying contributions of mafic and felsic magmas in post-collision orogenic settings. It is therefore of major importance in understanding crustal accretion. However, the source and nature of any mantle derived contribution is poorly understood. This study reveals that Ratagain is not only transitional in nature between the high Ba-Sr calc-alkaline granites and syenite intrusions of the Northern Highlands Terrane, but overlaps with the entire compositional range of the NHG suite. New lithogeochemical data from Ratagain confirm remarkably high Sr (>1600 ppm) and Ba (>2200 ppm) contents, high LREEs, notable depletions in Nb, U, P and Ti, low HREEs and negligible Eu anomalies, associated with high initial $^{87}Sr/^{86}Sr$ (0.7055 to 0.7062) and low εNd (− 11.8 to − 13.3). Although mafic parts of the complex have strong elemental and isotopic similarities with broadly coeval lamprophyres, signalling derivation from enriched mantle sources, details of the isotope array with respect to local crustal reservoirs indicate a significant Lewisian component. Such geochemical characteristics, combined with tectonic and petrological evidence, may be attributable to long-lived, incremental emplacement of successive magma batches originating from the same enriched mantle but differing in age and extent of assimilation-fractionation crystallisation. We therefore propose that some of the age dates for the Late Caledonian intrusions, particularly those obtained from older geochronology studies, are in need of review as they may record early crystallisation in the deep crust and not be a valid proxy for granite emplacement.

Keywords:

Granite, High Ba-Sr, Slab break-off, Caledonian, Crystal mush, Crustal contamination

Introduction

Granites are the primary component of the upper continental crust. Therefore, understanding how granitic magmas are generated is key to understanding how the Earth's continental crust has grown throughout geological time. Whilst traditional arguments centre on arc-derived magmatism to account for the presence of granites and related rocks with compositions greater than 60% SiO_2 in the continental crust (Rudnick, 1995; Lee et al., 2007; Hawkesworth et al., 2009), the more recent and increasingly popular paradigm is that intermediate-felsic magma is formed during the closing stages of continental collision and ensuing rupture and separation of subducting plates during such collisions (Atherton & Ghani, 2002; Macera et al., 2008; Hildebrand et al., 2018).

Late Caledonian intrusive complexes in Scotland have offered a long-standing opportunity to study the growth of continental crust by the emplacement of granitic bodies. These granites (sensu lato) were generated during the late stages of the Caledonian Orogeny, a major crust-forming episode which took place between the Cambrian (c.500 Ma) and early Devonian (c. 360 Ma) (MacDonald & Fettes, 2006) and involved the convergence of the three palaeocontinents of Laurentia, Baltica and Avalonia (Stephenson et al., 1999).

The Late Caledonian granites are interpreted to have formed in the Silurian and Devonian, following the subduction of the Iapetus oceanic crust beneath Laurentia. However, as a result of intensive research over many decades, the detailed petrogenesis and structural emplacement of the granitoids has been the subject of much debate. This is partly because the rocks have several subduction-related characteristics (Thompson & Fowler, 1986; Pidgeon & Aftalion, 1978; Harmon

et al.,1984) yet their spatial distribution, age and geochemistry cannot be ascribed to active subduction of Iapetus Oceanic crust (Atherton & Ghani, 2002; Miles et al, 2016).

Research in the past few decades has largely focused on investigating the precise origin for the Late Caledonian granites (Conliffe et al., 2010). Atherton and Ghani (2002) were the first to link post-subduction Late Caledonian magmatism to a 'slab break-off' event, suggesting that oblique continental convergence following the subduction of the Iapetus oceanic crust caused the subducted plate to weaken, rupture and detach near the oceanic-continental crust interface, leaving a 'gap' at the base of the mantle lithosphere.

The rise of hot, dry asthenosphere to fill this gap initiated partial melting in the overlying subcontinental lithospheric mantle (SCLM) and underplated lamprophyric magma was formed. Some of this early, mafic magma was emplaced at high crustal levels as lamprophyre-appinite dykes in the middle-Silurian (c.430 Ma) (Atherton & Ghani, 2002; Neilson et al. 2009).Continued asthenospheric upwelling, replacement and sustained high temperatures at the base of the mantle lithosphere as the detached slab sank away subsequently caused partial melting of the early lamprophyric underplate, generating magmas with unusual trace elements-signatures (high Ba, Sr and LREE contents) characteristic of the Late Caledonian granites (Atherton & Ghani, 2002). Subsequent magmatic differentiation was achieved through assimilation-fractional crystallisation (AFC) processes involving different crustal reservoirs (Fowler et al., 2008; Fowler & Rollinson, 2012).

Since Atherton and Ghani (2002), the slab break-off model has been refined step-by-step by various authors to account for the elemental peculiarities and considerable volumes of granitic magmas emplaced post-collision in the British Caledonian (Oliver et al., 2008; Nielsen et al., 2009; Dewey et al., 2015; Miles et al., 2016; Archibald & Murphy, 2021). Archibald et al (2022) provide further confirmation of the hypothesis, by comparison of compiled elemental data with the slab failure discrimination diagrams of Hildebrand et al (2018) and Whalen and Hildebrand (2019).

This study presents new field, petrographical and geochemical data for the Ratagain Complex, an under-studied granitic intrusion in north west Scotland, whose petrogenesis has been ascribed to slab break-off processes based on regional synthesis of the Late Caledonian suite (Fowler et al., 2008; Fowler & Rollison, 2012; Miles et al., 2016, Archibald et al, 2022). Our sizeable geochemical dataset (>100 samples from a single pluton) provides further constraints on potential source regions for Late Caledonian high Ba-Sr intrusions, mechanisms of magmatic evolution and the relative importance of mantle and crustal components in the wider context of slab failure and post-collision mafic magmatism.

Geological Background

Caledonian Orogeny

Caledonian granites, such as those that make up the Ratagain Complex, were generated during the Caledonian Orogeny, the crust-forming episode that is largely responsible for the present-day configuration of terranes and terrane-bounding faults in the British Isles (McKerrow et al., 2000; Searle, 2022). The orogeny resulted from the closure of the Iapetus Ocean and the subsequent convergence of Laurentia (which is represented today largely by the Precambrian basement rocks of North America, Greenland, north of Ireland and Scotland), Baltica (Scandinavia and Russia) and Avalonia (the basement of southern Ireland, Wales and England) (e.g. Kinny et al., 2003; Goodenough et al., 2011: Strachan et al. 2020; Searle, 2022). As well as causing considerable deformation and crustal thickening, the Caledonian Orogeny was accompanied by an extended

period of magmatism in the British Isles and the Caledonian igneous rocks have a variety of compositions and modes of emplacement (Stephenson et al, 1999).

Caledonian magmatism

Caledonian magmatism in Britain and Ireland mainly occurred in two episodes. The first was the Mid-Ordovician Grampian event (c. 470–460Ma), a phase of arc–continent collisions along the southern margin of Laurentia (e.g. Oliver, 2001; Oliver et al., 2008; Johnson et al., 2017). The later magmatic episode took place during the Late Silurian–Early Devonian (c.447–383 Ma) as the Iapetus Ocean finally closed (Dewey et al., 2015). In Scotland, this magmatism was marked by volcanic activity in the Midland Valley and Southern Uplands, regional dyke swarms, and the emplacement of granitic intrusions across large areas of the country, especially the Grampian and Northern Highlands.

Read (1961) first categorised the Caledonian granitic intrusions as the 'Older Granites' and 'Newer Granites'. The Older Granites are two-mica S-type granites (Oliver et al., 2008) which, together with an associated suite of gabbroic rocks (the Newer Gabbros), are representative of syn-collisonal magmatic activity that took place in the Mid-Ordovician Grampian event (Brown et al. 2008).The Newer Granites (hereafter Late Caledonian granites) are a much larger group of over one hundred intrusions, including sheets, veins and plutons varying in areal extent from 1 to 380 km², with mostly I-type but also some S-type affinities (Figure 3.1; MacDonald & Fettes, 2006). The Late Caledonian granites are typically associated with mantle-derived lamprophyres and appinites (Rock et al., 1988) and yield Rb-Sr and U-Pb ages between c.435–390 Ma (Soper, 1986). This period encompasses the closure of the Iapetus Ocean (c. 435–425Ma), the Scandian collision of Laurentia and Baltica, the collision of Laurentia and Eastern Avalonia and Acadian regional sinistral shear deformation (Rogers & Dunning, 1991; Lancaster et al., 2017; Archibald & Murphy, 2021).

The Late Caledonian granites

On the basis of isotope and geochemical characteristics, Stephens and Halliday (1984) categorised the Late Caledonian granites into the Argyll, Cairngorm and South of Scotland suites, the latter of which was later divided into the South of Scotland and Galloway subgroups by Highton (1999). However, Brown et al. (2008) recognised that the Galloway subgroup had compositional similarities to granites in northern England, the Isle of Man and western Ireland and thus they amalgamated all of these granitoid intrusions into a single group named the Trans-Suture Suite.

The Argyll and Northern Highlands Suite consists of hornblende-granodiorite, biotite-granodiorite and syenite plutons with dioritic and monzo-granitic components (MacDonald & Fettes, 2006) together with spatially and temporally associated appinites. The rocks of this suite are characterised by relatively high Ba-Sr concentrations (Fowler et al, 2008), which are discussed below.

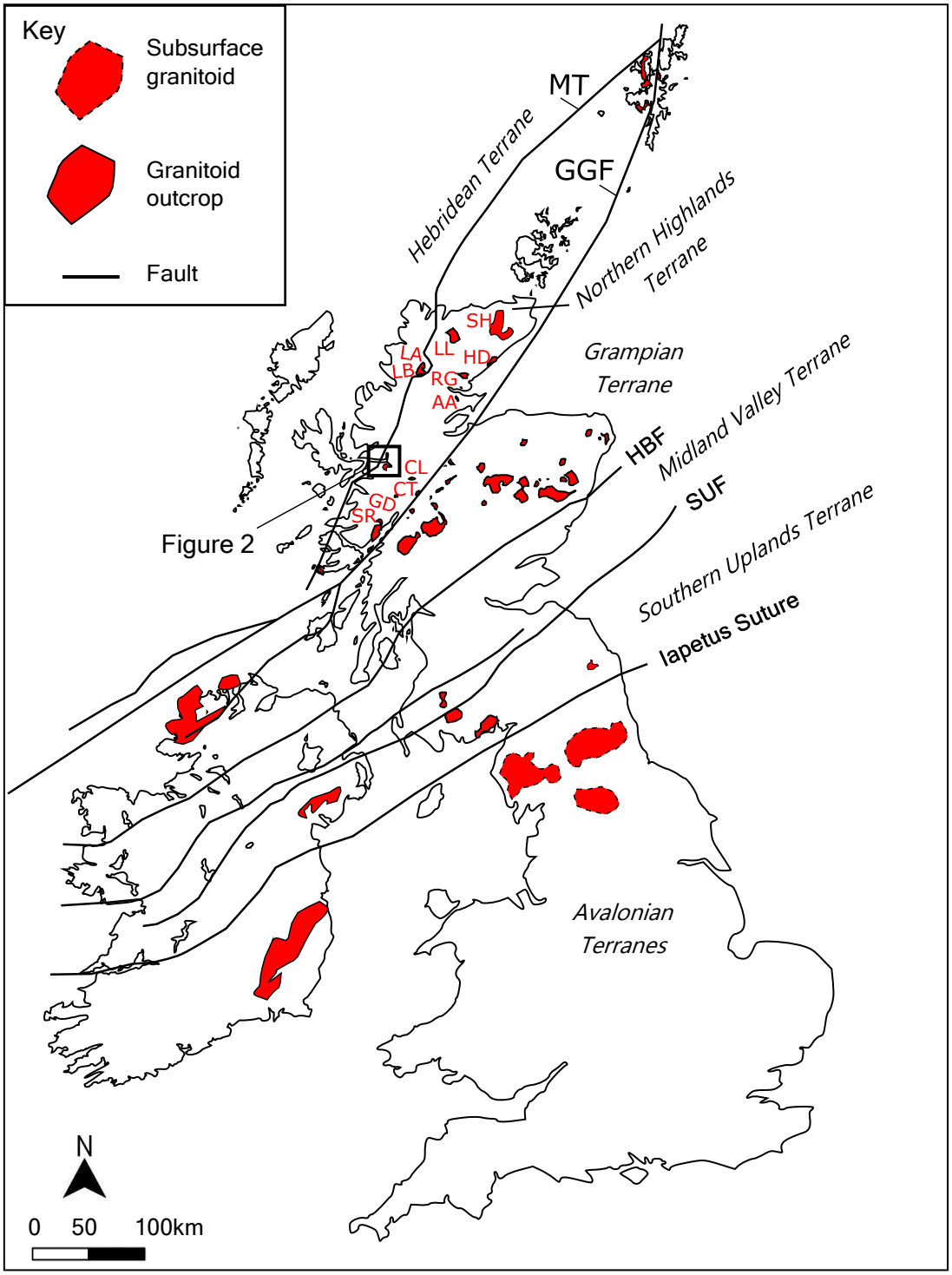


Figure 3.1 Overview map of the Late Caledonian Silurian-Devonian granitoids of Great Britain and Ireland adapted from Brown et al., (2008) and Fowler et al., (2008). The box Figure 2 highlights the location of the Ratagain Complex. High Ba-Sr intrusions mentioned in the text are labelled in red. Key to abbreviations: AA is Ach'Uaine Appinites; CL is Cluanie; CT is Clunes tonalite; GD is Glen Dessary; GGF is Great Glen Fault; HBF is Highland Boundary Fault; HD is Helmsdale; LA is Loch Ailsh; LB is Loch Borralan; LL is Loch Loyal; MT is Moine Thrust; SH is Strath Halladale; SR is Strontian; SUF is Southern Uplands Fault; RG is Rogart.

The Cairngorm Suite is dominated by biotite-monzogranite plutons (Stephens & Halliday,1984) and when compared to the granitoids of the Argyll and Northern Highlands Suite, they have lower Ba and Sr abundances and intermediate and appinitic rocks are scarce. The South of Scotland and Trans-Suture suites comprise composite granodiorite and pyroxene diorite plutons, which are richer in K and Th than the other suites (MacDonald & Fettes, 2006). Nevertheless, similar to the Cairngorm Suite, they have relatively low Ba-Sr contents.

High Ba-Sr granites

First recognised by Tarney and Jones (1994), high Ba-Sr granites are characterised by extreme enrichment in barium (Ba) and strontium (Sr). In addition to high Ba and Sr (>1000 ppm) Mg#, Cr, V and Ni contents, high Ba-Sr granites can also be distinguished from traditional I-, S- and A-types (Fowler et al., 2001) owing to their absent or small negative Eu anomalies, LREE (light rare earth elements) and LILE (large ion lithophile elements) enrichment, and relatively low HFSE (high field strength elements) contents (Tarney & Jones, 1994).

Whilst high Ba-Sr granites have been described in other locations in the world, such as the Tibetan Plateau (Ye et al., 2008) and central Brazil (Leite et al., 2021), the Northern Highlands of Scotland are a type locality for this group. The Late Caledonian high Ba-Sr suites of the Northern Highlands (hereafter 'NHG suite') can be divided, on the basis of petrographic and geochemical criteria, into two subgroups: (1) alkaline syenitic plutons that crop out in the west and (2) calc-alkaline granitic plutons in central and eastern areas (Figure 3.1; Bruand et al., 2014).

The Ratagain Complex

The Ratagain Complex is a Late Caledonian granitic intrusion which crops out along the shores of Loch Duich in the western Highlands of Scotland (Hutton et al., 1993; Figure 3.2). The intrusion is hosted by metasedimentary rocks of the Neoproterozoic Morar Group and the Archean-Paleoproterozoic Lewisian Gneiss basement of the Eastern Glenelg inlier (Krabbendam et al., 2018). Biotite- and feldspar-whole-rock ages of 415±5 Ma (Turnell, 1985) and 419±3Ma (Thirlwall, 1988) are reported for the complex, whilst U-Pb zircon and baddeleyite dating places the emplacement at 425 ± 3 Ma (Rogers & Dunning, 1991).

Although loosely termed 'granitic', the Ratagain Complex is composed of a variety of intrusive units besides granite, such as syenite, monzonite, monzodiorite (Hutton & McErlean, 1991) and can thus be considered as compositionally transitional between the aforementioned Late Caledonian alkaline syenites and the more common metaluminous calc-alkaline granites (Fowler et al., 2008). According to Fowler et al. (2008), the calc-alkaline granites of the NHG suite evolved by amphibole and plagioclase-dominated fractionation involving contamination with Moine metasedimentary rocks, whilst the syenites resulted from biotite-pyroxene-dominated fractionation accompanied by assimilation of Lewisian granulite-facies gneisses.

Ratagain also exhibits elemental characteristics typical of high Ba-Sr intrusives, notably: extreme enrichment in Ba, Sr and the light REEs (Stevenson et al., 1999); enrichment in the alkalis, especially Na and K (Alderton, 1988); and relatively low HFSEs including distinct negative Nb-Ta anomalies (Fowler et al., 2008).

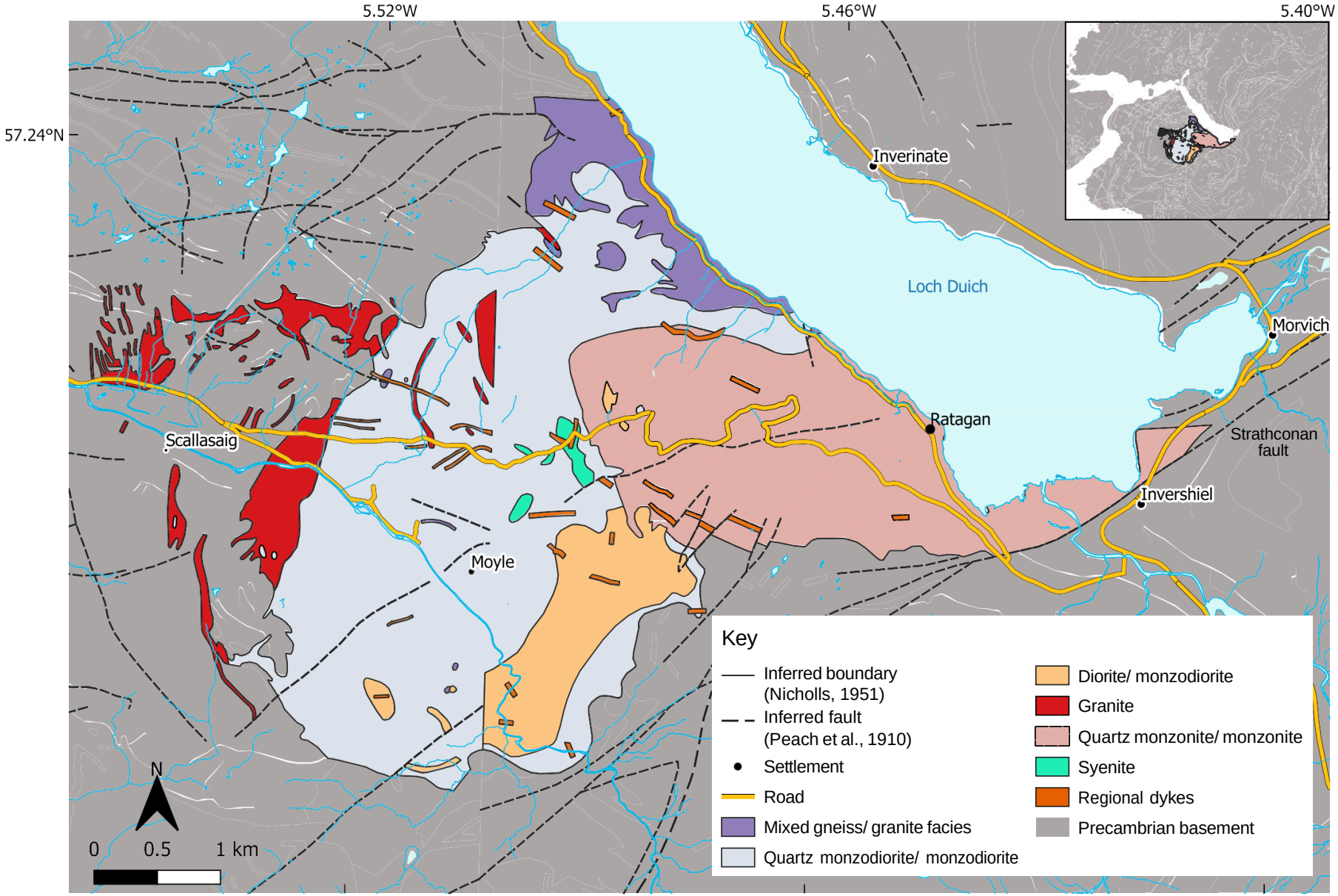


Figure 3.2 Simplified geological map of the Ratagain Complex reproduced from Lawrence et al. (2022). Locational information for all 112 sampling sites is provided in Supplementary Table SA2.

Whilst the Ratagain Complex has already been the subject of a comprehensive rock magnetic study (Lawrence et al., 2022), chemical and isotopic data for the intrusion are somewhat lacking in the literature (Thompson & Fowler 1986; Fowler et al., 2008). Therefore, although the Ratagain Complex's distinctive abundance of mafic-intermediate compositions and transitional nature could likely inform the Late Caledonian tectonic regime (e.g. Hutton et al., 1993; Stephenson et al., 1999; Macdonald & Fettes, 2006; Fowler et al., 2008), a more robust geochemical dataset is required to better understanding of the intrusion's petrogenetic and tectonic implications in the context of the British Caledonides.

Sampling and analytical methods

112 block samples, ranging from 1-5 kg in weight, were collected and prepared for geochemical analysis at the University of Birmingham. Preparations included removing all visibly weathered surfaces from the block samples and cutting a rectangular fragment, approximately 100mm x 50mm in dimensions, from each block sample. Coarse crushing of the fragments was achieved using a jawcrusher, whilst further crushing to yield fine powders (200 mesh) was undertaken on a tungsten-carbide TEMA T750k laboratory disc mill.

Petrographic classification of all samples was made on the basis of thin section observations and X-ray fluorescence (XRF) major and minor elemental analyses. XRF analyses were undertaken at the University of Portsmouth using pressed powder pellets. Pressed powder pellets were prepared by combining 5 g of powdered rock sample and 1 g of CEREOX® binder and then placing the sample in a tungsten carbide die. The die was compressed for 30 seconds under a manual press with 21 tons of applied pressure. Estimates for loss on ignition (LOI) were made after heating 1 g of sample in an oven at 1000 ◦C for 1.5 h, cooling and reweighing.

Ten major element oxides (SiO_2, TiO_2, Al_2O_3, Fe_2O_3, MnO, MgO, CaO, Na_2O, K_2O and P_2O_5) and nineteen trace element compositions (Sc, V, Cr, Ni, Cu, Zn, Ga, Rb, Sr, Y, Zr, Nb, Ba, Pb, La, Ce,Th, U and Sn) were analysed using a Rigaku Primus ZSX II WDXRF spectrometer with instrumental lower limits of detection of ca. <10 ppm. Precision and accuracy were monitored using the standards JB-1A and JG-1A and are estimated at ca. <2% for major elements and ca. <5% for trace elements. The rare earth element (REE) compositions of 40 samples were analysed through inductively coupled plasma mass spectrometry (ICP-MS, Analytic Jena PQ Elite) following fusion dissolution with a lithium metaborate flux, also at the University of Portsmouth. Accuracy and precision were analysed routinely with the same CRMs, estimated to be ca <5%. For full major and trace element XRF data see Supplementary table SA2; for LOI estimates see Supplementary table SA3.

5 samples were also analysed for Sr and Nd radiogenic isotope compositions at the Scottish Universities Environmental Research Centre (SUERC), East Kilbride, Scotland on a VG Sector 54–30 thermal ionization mass spectrometer (TIMS). $^{87}Sr/^{86}Sr$ was corrected for mass fractionation using $^{86}Sr/^{88}Sr = 0.1194$. Repeat analysis of the NIST SRM-987 Sr standard gave 0.710257 ± 17 (2 sd, $n = 10$) for the duration of this study (see Troll et al., 2019 for full analytical details). The decay constant used was (σ) 1.42×10^{-11} (Steiger & Jäger, 1977) to determine the initial Sr isotope ratios (see Supplementary Table SB1).

$^{143}Nd/^{144}Nd$ was corrected for mass fractionation using $^{146}Nd/^{144}Nd = 0.7219$. During the course of this study, the SUERC internal Nd laboratory standard (JM), which is calibrated against the La Jolla Nd solution and the JNdi-1 standard, gave $^{143}Nd/^{144}Nd = 0.511511 \pm 8$ (2 sd, $n = 8$). To estimate initial isotope ratios the decay constant used was (σ) 6.54×10^{-12} (Lugmair & Marti, 1978). Chondritic Uniform Reservoir (CHUR) modelling (DePaolo, 1988) was used to compare the initial isotopic compositions of the Ratagain Complex samples with that of primitive mantle at

the time of their generation. The assumed present-day values for CHUR were $^{147}Sm/^{144}Nd$ = 0.1967 and $^{143}Nd/^{144}Nd$ = 0.512638 (Jacobsen & Wasserburg, 1980; see also Supplementary Table SB2).

Finally, single crystal major element data for 5 representative samples were obtained using a Zeiss SIGMA 300VP Scanning Electron Microscope (SEM), at the University of Leicester, equipped with two Bruker XFlash 6|60 energy-dispersive X-ray detectors (EDX) with 126-eV energy resolution. A high-resolution back-scattered electron (BSE) contrast image was collected at each site of interest in order to accurately locate analytical points (typically cores and rims in selected mineral phases). Quantitative analyses were performed using a 15 kV beam acceleration and a 60 µm aperture providing a 10 nA beam current. Dwell time at each analytical point was fixed at 20 seconds, generating a spectra with >1,000,000 counts for accurate deconvolution. Quantification utilised a Phi-Rho-Z correction routine and resultant element concentrations are reported as normalised weight percent (wt.%). Simultaneous analyses of MAC reference minerals (Albite, Orthoclase, Hornblende) indicate that precision for the observed data range over the period of analytical work was typically better than 3% (1σ – RSD) whilst accuracy was typically better than 5% (see Supplementary table SC1).

Results

Geology and petrography

For a detailed account on key field relationships and features of the Ratagain Complex, the reader is referred to Lawrence et al. (2022). The new whole-rock geochemical data (Table 3.1) presented in this study confirm that the Ratagain Complex is markedly heterogeneous in composition. The lithological names assigned to the rock compositions we analysed are based on their CIPW normative mineralogy (Figure 3.3). It can thus be seen that the Ratagain complex is dominated by quartz monzonite and quartz monzodiorite, but granite, monzonite, monzodiorite, granodiorite and syenite facies also crop out within the mapped boundaries of the intrusion.

Igneous textures vary from fine-grained and equigranular (Figure 3.4D) to medium-grained (Figure 3.4A, C, E) to coarse-grained and porphyritic (Figure 3.4F). Mafic microgranular enclaves (MMEs) ranging from a few cm up to 5m in size (Figure 3.4B, C) occur in all facies of the Ratagain Complex; such features are suggestive of magma mixing and mingling processes involving juvenile mafic to ultramafic material (Fowler et al, 2008).

The typical felsic mineralogy of the granite, granodiorite, quartz monzonite, monzonite, quartz monzodiorite and monzodiorite is characterised by quartz, plagioclase and alkali feldspars in variable proportions. Plagioclase occurs in high abundances as elongate, euhedral crystals often showing multiple twinning, perthitic textures and zoning, whilst alkali feldspar occurs in lower abundances as tabular crystals showing simple twinning (Figure 3.5C, D). Both are intergrown with ubiquitous irregular, anhedral crystals of quartz (Figure 3.5A, B). Sericitization of the feldspars occurs to varying degrees across all samples (Figure 3.5A-D). Mafic minerals, which may include biotite, hornblende and relict clinopyroxene (Figure 3.5E, F), occur in lesser proportions and usually show partial or complete alteration to chlorite.

Table 3.1 Representative whole-rock geochemical analyses for the range of rock compositions present in the Ratagain Complex. Key to abbreviations: G is granite; Grd is granodiorite; Md is monzodiorite; Mz is monzonite; Sy is syenite; QzG is quartz-rich granitoid; Qmd is quartz monzodiorite; Qmz is quartz monzonite

Sample	Sy	Mz			Md		Grd	QzG	G				Qmz			Qmd			
	AL 071	AL 017	AL 059	AL 067	AL 031	AL 062	AL 054	AL 011	AL 013	AL 038	AL 072	AL 100	AL 063	AL 079	AL 081	AL 002	AL 009	AL 045	AL 096
Major oxides (wt. %)																			
SiO_2	45.72	56.16	62.77	54.84	64.39	57.00	65.69	81.92	71.88	70.31	65.20	69.74	68.21	65.97	59.87	67.54	67.98	69.75	62.53
TiO_2	1.62	0.68	0.43	1.74	0.39	0.84	0.46	0.37	0.17	0.36	1.25	0.43	0.36	0.49	0.93	0.46	0.40	0.43	0.74
Al_2O_3	11.36	14.05	18.05	11.57	18.27	16.42	17.06	9.04	14.71	15.78	14.23	13.98	15.76	16.22	14.24	16.58	16.70	16.07	15.48
Fe_2O_3	6.88	6.46	2.89	8.42	2.51	5.33	3.29	2.10	0.91	1.86	2.84	2.33	2.21	3.21	5.14	2.75	2.74	1.97	6.23
MnO	0.11	0.10	0.04	0.13	0.03	0.08	0.01	0.03	0.02	0.01	0.11	bdl	0.03	0.04	0.08	0.04	0.04	0.07	bdl
MgO	9.50	3.12	0.59	7.24	0.74	3.69	0.55	0.35	0.22	0.44	1.66	2.56	0.95	1.96	4.11	1.22	1.13	0.29	3.03
CaO	9.74	6.60	1.66	7.95	1.47	4.57	1.20	0.48	0.97	0.70	2.54	1.26	1.77	1.27	4.77	2.10	1.23	1.47	3.74
Na_2O	2.20	3.95	5.52	2.80	6.55	5.60	5.09	2.26	5.22	5.22	2.45	4.26	5.33	4.89	3.75	5.67	5.78	5.82	3.81
K_2O	5.98	5.19	5.25	4.84	4.95	3.48	3.90	2.58	4.60	4.88	4.88	4.83	4.07	5.53	5.29	3.72	4.04	3.93	3.56
P_2O_5	2.47	0.90	0.18	1.52	0.19	0.63	0.27	0.05	0.03	0.18	0.34	0.28	0.18	0.29	0.88	0.22	0.20	0.24	0.33
LOI	0.56	0.37	0.52	0.59	0.44	0.51	1.81	1.00	1.26	0.87	0.96	0.82	0.31	0.71	0.59	0.89	1.35	1.63	0.98
Total	96.14	97.57	97.90	101.65	99.94	98.14	99.32	100.17	99.97	100.62	96.45	100.49	99.18	100.58	99.65	101.19	101.58	101.66	100.43

Table 3.1 Continued

Sample	Sy	Mz			Md		Grd	QzG	G				Qmz			Qmd			
	AL 071	AL 017	AL 059	AL 067	AL 031	AL 062	AL 054	AL 011	AL 013	AL 038	AL 072	AL 100	AL 063	AL 079	AL 081	AL 002	AL 009	AL 045	AL 096
Trace elements (ppm)																			
Ba	3778	2371	5812	2139	2720	2620	2491	1026	1570	1802	786	1880	2693	1533	1816	1842	1657	1859	1181
Rb	97	91	47	85	39	45	65	47	75	75	98	75	70	59	99	62	68	74	42
Sr	2228	2724	4101	1825	2017	2427	1258	283	610	1337	416	1588	1579	1464	1437	1443	1223	1214	815
Nb	16	21	54	14	11	9	14	6	8	12	12	14	13	15	15	9	12	15	7
Zr	257	301	814	227	236	202	239	146	122	152	310	183	179	196	257	164	194	184	138
Y	32	26	34	28	14	19	19	9	12	13	30	16	14	13	22	14	15	16	14
Th	12	37	45	13	4	5	8	11	13	7	9	11	8	15	22	6	14	12	6
Cr	407	47	37	343	31	163	84	139	71	56	98	40	70	45	193	131	64	112	180
Ni	304	209	131	317	136	193	178	433	292	161	137	114	96	142	277	161	253	103	219
V	160	116	61	116	39	117	59	42	9	51	129	47	45	43	105	55	48	53	105
Cu	23	7	7	1	bdl	35	3	7	14	23	34	7	1	1	bdl	1	1	8	19
Zn	98	68	39	99	33	71	41	bdl	bdl	1	46	39	42	32	71	16	40	17	51
La	97.7	191	87.5	72.9	74.9	65.1	120	35.7	43.7	85.5	42.1	61.3	56.1	63.9	104	51.9	109	85.4	18.6
Ce	196	396	191	148	151	133	259	75.4	85.7	141	86.4	95.8	111	129	203	112	214	147	39.4
Pr	21.7	49.2	23.4	17	16.9	15.1	25.9	7.6	9.1	13.8	10.2	8.8	11.9	12.1	23.1	12.6	24.6	16.2	4.2
Nd	73.6	165.7	86.3	61.9	59.3	56.1	92.8	23.6	28.1	45.9	38.5	28.7	42.1	41.8	84.6	40.8	78.3	55.7	16.5
Sm	12.3	24.3	14.6	10.9	8.1	9.3	14.9	3.3	3.9	5.6	7.1	3.6	6.7	6.7	14.6	5.7	10.8	9	2.9
Eu	3.3	6.4	3.7	2.1	2.5	2.3	4.1	1	1.4	1.5	1.4	0.8	1.8	1.6	3.2	1.8	3.3	2.4	0.7
Tm	bdl	0.39	bdl	bdl	bdl	bdl	bdl	0.06	0.11	bdl	bdl	bdl	bdl	bdl	bdl	0.1	0.18	bdl	bdl
Yb	1.42	2.2	1.36	0.81	0.84	0.70	1.08	0.37	0.69	0.42	3.00	0.50	0.62	0.63	1.16	0.6	1.08	0.86	0.70
Lu	bdl	0.35	bdl	bdl	bdl	bdl	bdl	0.08	0.11	bdl	bdl	bdl	bdl	bdl	bdl	0.09	0.17	bdl	bdl

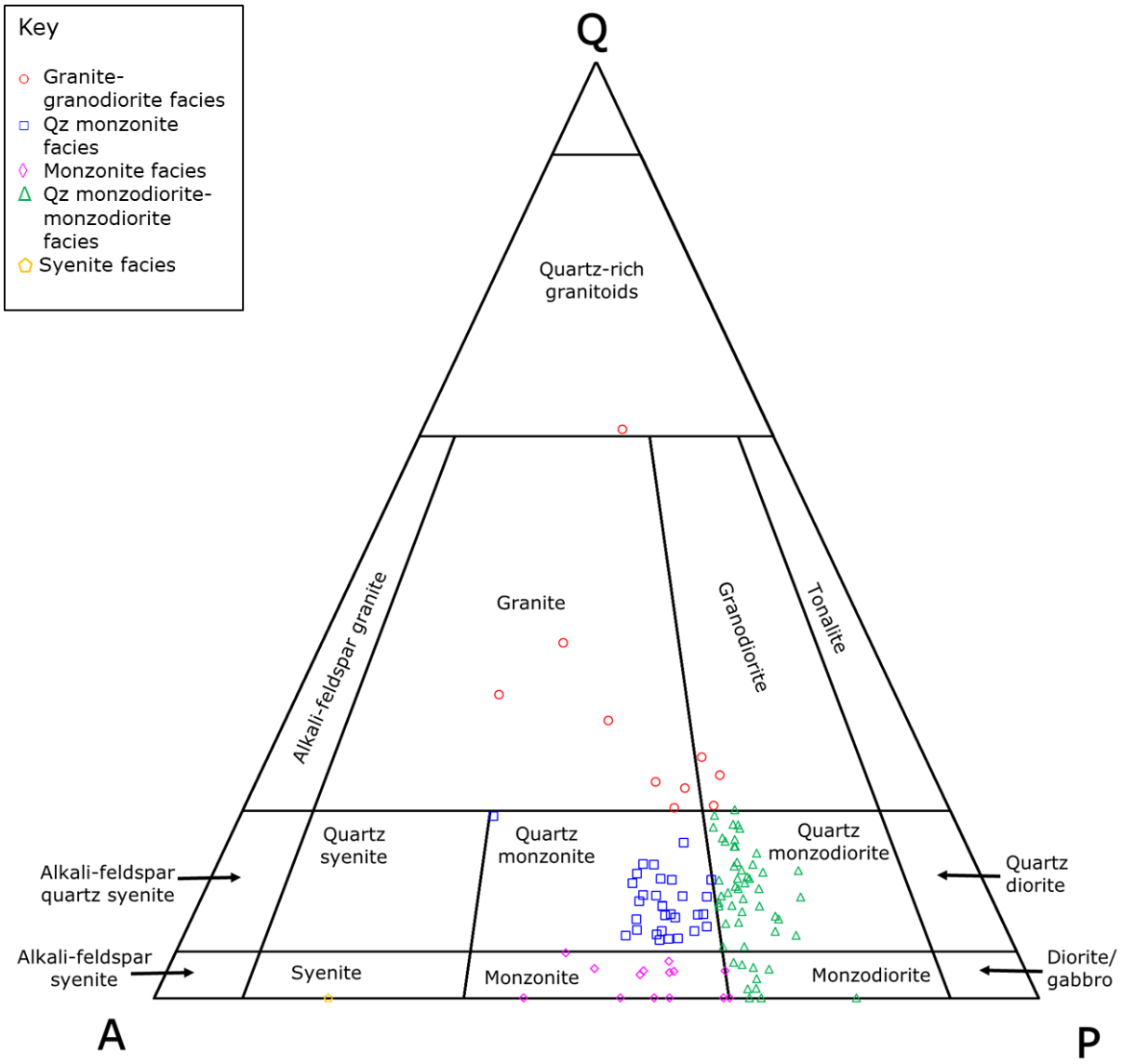


Figure 3.3 QAP rock classification diagram (Streckeisen, 1976) showing the rocks of the Ratagain Complex sampled in this study using the CIPW normative mineralogy (Irvine & Baragar, 1971) calculated from lithogeochemical analysis and plotted in TERNPLOT (Marshall, 1996). Key to abbreviations: Q is quartz; A is alkali-feldspar; P is plagioclase.

In the Ratagain syenite however, mafic phases dominate the mineralogy and appear markedly fresher and less affected by alteration than in the other facies (Figure 3.5G, H). Biotite occurs as elongate lamellae or plates, with some crystals hosting opaque inclusions and dark pleochroic zircon haloes. Clinopyroxene is present as equidimensional crystals, the latter of which typically show prominent cleavage intersections at 90° and simple twinning in some cases. Hornblende occurs as prismatic or lozenge-shaped euhedral crystals which display prominent 120° cleavage intersections and/or zoning.

The accessory mineralogy of all facies is characterised by mixtures of titanite, apatite, zircon, zoisite and/or opaque minerals (Fe-Ti oxides), which are interpreted as primary owing to their partial to complete encompassment by the main mafic minerals. Apatite occurs as small, high-relief, euhedral crystals or inclusions within biotite, hornblende and the feldspars. Crystals have a cloudy interior and dark rim. Titanite is present as small, rectangular lozenges and less common

diamond-shaped crystals (Figure 3.5A, B). Rare bladed and acicular crystals of zoisite, distinguished by their high-relief, are evident in some studied samples.

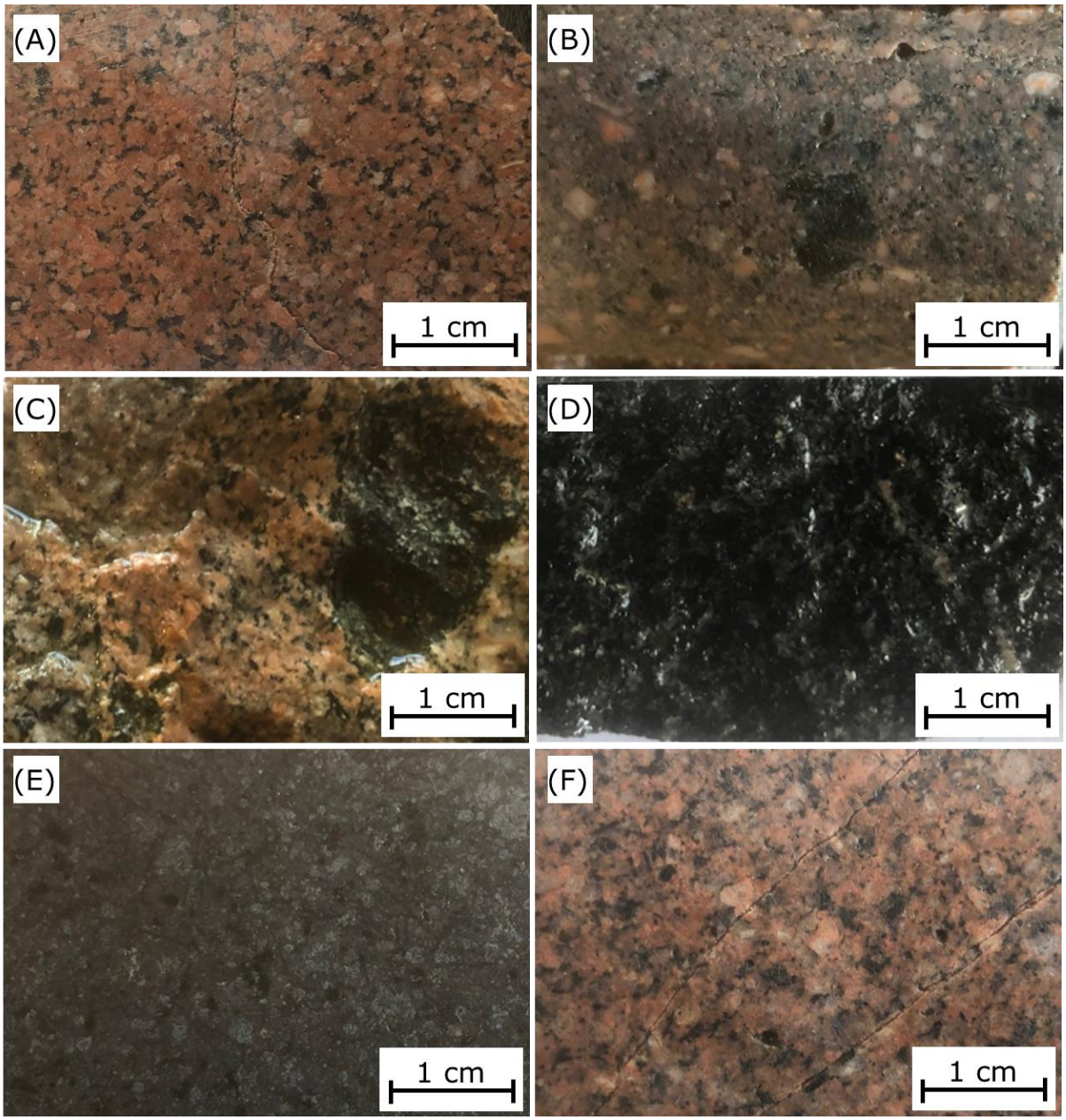


Figure 3.4 Representative hand specimen photographs of the various facies of the Ratagain Complex. (A) Quartz monzonite showing a medium-grained porphyritic texture (B) Porphyritic monzodiorite sample in which pinkish alkali feldspar phenocrysts stand out from a dark fine-grained matrix of quartz, plagioclase feldspar and biotite (C) Medium-grained granite hosting a dark mafic microgranular enclave (D) Close view of a large mafic microgranular enclave (E) Medium-grained granodiorite (F) Monzonite sample with a coarse-grained porphyritic texture

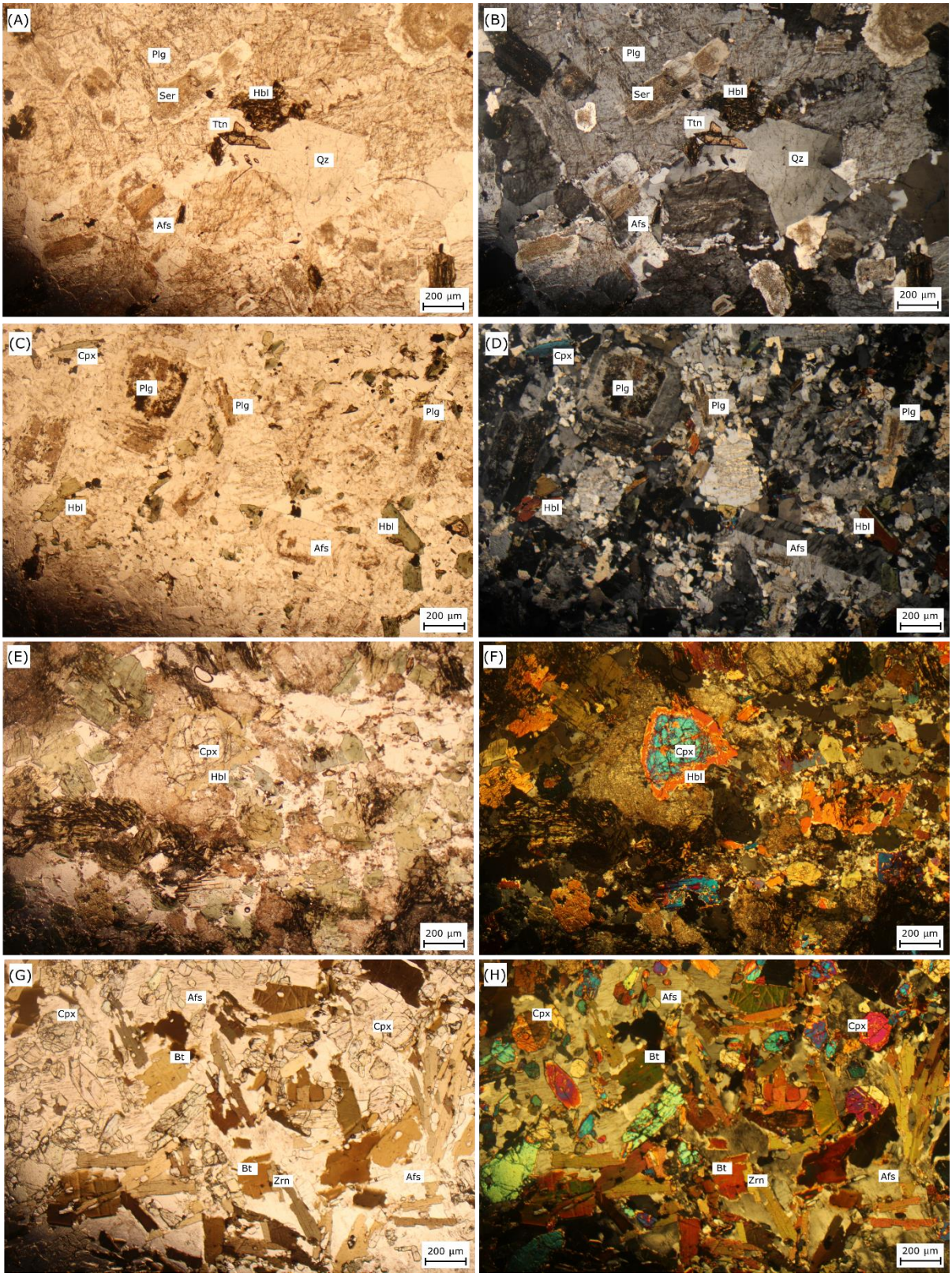


Figure 3.5. Representative photomicrographs of the various facies of the Ratagain Complex (A) PPL image of granodiorite with euhedral titanite and hornblende set in a groundmass of quartz, alkali feldspar and sericitized plagioclase (B) XPL image of granodiorite (C) PPL image of quartz monzonite showing plagioclase phenocrysts with relict compositional zoning, alkali feldspar with simple twinning and minor hornblende and clinopyroxene (D) XPL image of quartz monzonite (E) PPL image of quartz monzodiorite with large, equidimensional clinopyroxene crystals surrounded by a hornblende alteration rim (F) XPL image of quartz monzodiorite (G) PPL image of syenite consisting of abundant ferromagnesian phases,

including twinned clinopyroxene and biotite with pleochroic haloes around enclosed zircon (H) XPL image of syenite. Mineral abbreviations after Whitney & Evans (2010).

Major and trace element data

XRF major and trace elemental data for all 112 samples are reported in the Supplementary Material (Supplementary table SA2). Representative whole-rock major and trace element data for the Ratagain Complex are presented in Table 3.1.

The alumina saturation index of Maniar and Piccoli (1989) demonstrates that the facies are mostly metaluminous in nature, with only a small number of the granitic-granodiorite and quartz monzodiorite-monzodiorite facies showing a slightly peraluminous affinity. All the studied intrusives mainly plot in the magnesian series (Figure 3.6C) of Frost et al. (2001) and can be classified as non-tholeiitic according to Irvine and Baragar's (1971) AFM diagram (Figure 3.6B). The MALI (Modified Alkali-Lime index) versus SiO_2 diagram of Frost et al. (2001) (Figure 3.6D), indicates that both the quartz monzodiorite-monzodiorite facies and quartz monzonite facies mostly fall within the alkalic domain, whilst the monzonite and granite-granodiorite facies mainly plot across the alkalic and alkali-calcic fields.

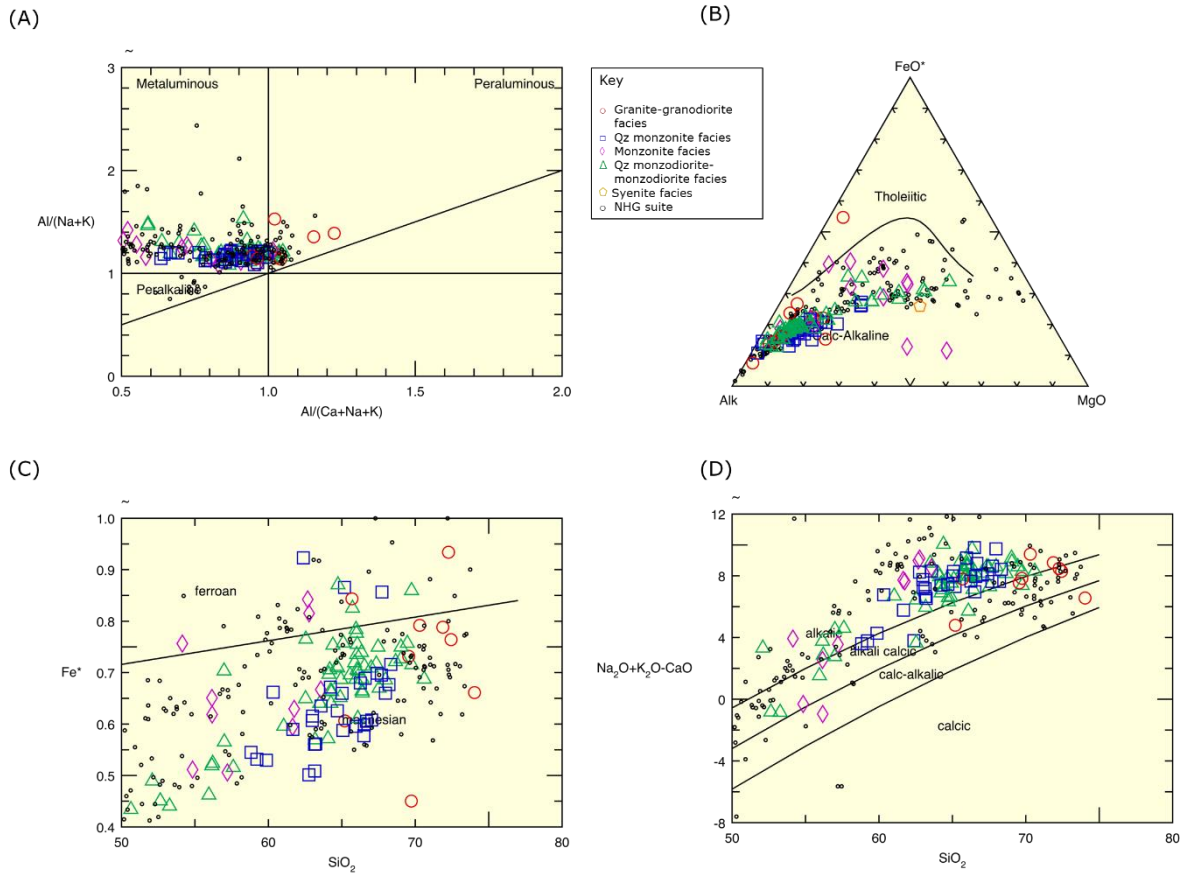


Figure 3.6 Geochemical characteristics of the various facies in the Ratagain Complex. Also plotted are data from Thompson & Fowler 1986, Thirlwall & Burnard 1990, Fowler, 1992, Fowler & Henney (1996), Fowler et al. (2001, 2008). Coloured symbols are data from this investigation and open black circles are compiled literature data for the Northern Highland Granite Suite (NHG). (A) Alumina Saturation index diagram after Maniar & Piccoli (1989); (B) AFM diagram of Irvine & Baragar (1971); (C)FeOt/ (FeOt+ MgO) versus SiO2 diagram; fields of ferroan and magnesian series from Frost et al. (2001); (D) Modified Alkali Lime Index diagram of Frost et al. (2001).

Variation diagrams demonstrate that the SiO_2 concentrations for the various intrusive units of the complex range from a minimum of 43.60 wt% for a monzonite sample to a maximum of 81.92 wt% in a quartz-rich granitoid sample. In all intrusive units, SiO_2 correlates negatively with TiO_2 (0.26-2.42 wt%, Figure 3.7A), Fe_2O_3 (0.91 - 13.5 wt%, Figure 3.7B), MnO (bdl - 0.14 wt%, Figure 3.7D), MgO (0.14 - 9.57 wt%, Figure 3.7E) and CaO (0.48-13.87 wt%, Figure 3.7F). Al_2O_3 (Figure 3.7C) shows the characteristic convex-up distribution delineating a positive correlation from ca. 40 to ca 65 wt % silica, then a negative correlation towards the silicic extremes. Na_2O (2.17 - 6.91 wt%, Figure 3.7G) and K_2O(1.47 -8.06 wt%, Figure 3.7H) are rather scattered across SiO_2 concentrations but both elements generally mimic Al_2O_3, with highest values close to 65% SiO_2.

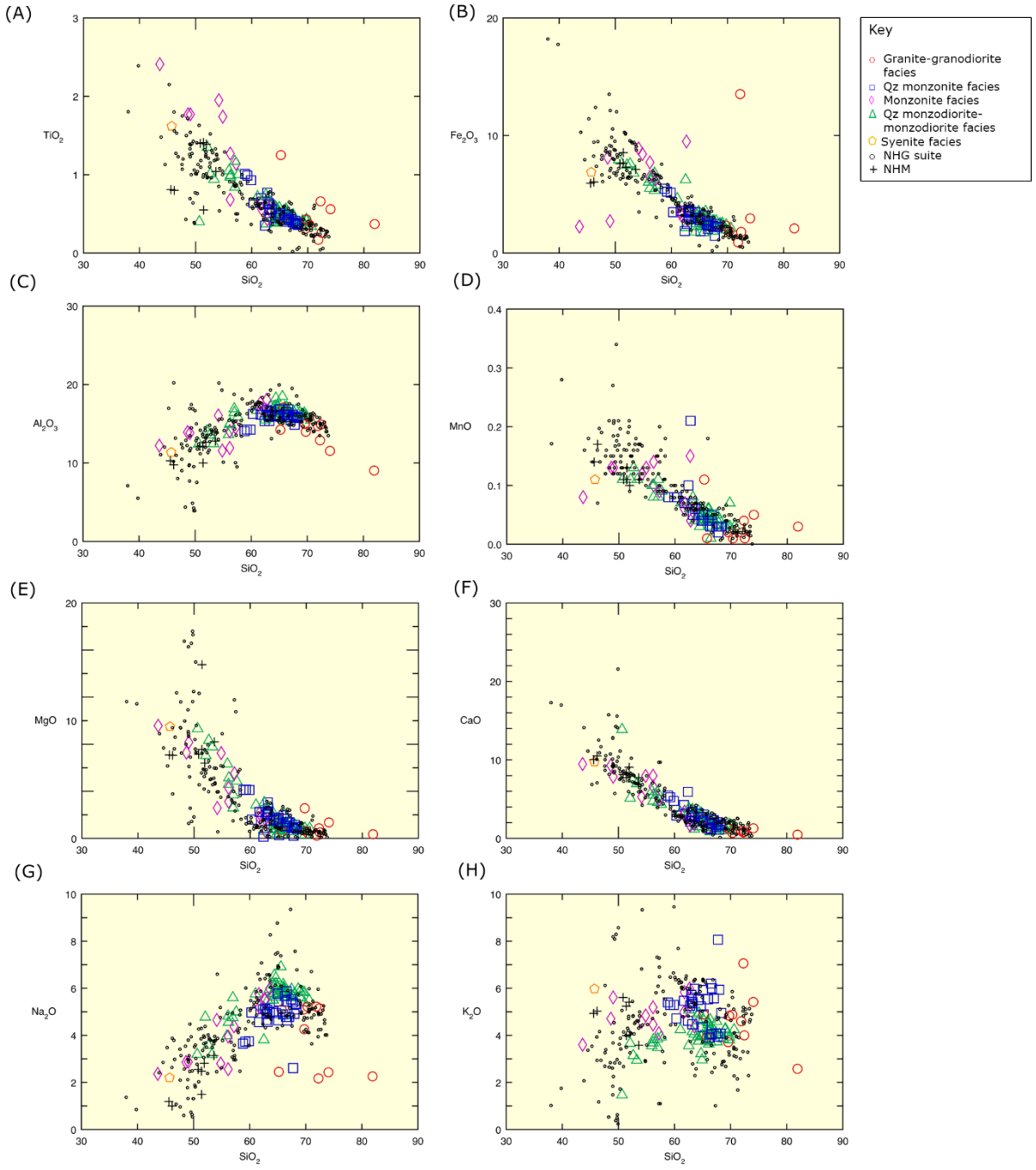


Figure 3.7 Variation diagrams for major element oxides (in weight %) plotted against SiO_2 for the Ratagain Complex and NHG suite. Also included for comparison are data for Northern Highland minettes (NHM) (Canning et al., 1996).

Data for trace elements are also presented as Harker-style plots for a selection of LILEs, transition metals and HFSEs to illustrate the variation within the suite (Figure 3.8). The rocks of the Ratagain Complex exhibit remarkably high Sr and Ba abundances, which can reach up to 4101 ppm and 5812 ppm respectively, comparable to measured values in other High Ba-Sr granites, both in the Late Caledonian NHG suite (Fowler et al., 2008) and worldwide (e.g. Tarney and Jones, 1994; Ye et al., 2008; Lara et al., 2017; Lima et al., 2021). In addition, high Cr (up to 407 ppm) and Ni (up to 433 ppm) contents, across the range of rock types that the Ratagain Complex comprises, signals mantle derivation and further confirms magma mixing between mantellic mafic and crustal silicic end members (e.g. Tarney & Jones, 1994; Fowler & Henney, 1996; Fowler et al., 2001, 2008; Peng et al., 2013; Lara et al., 2017).

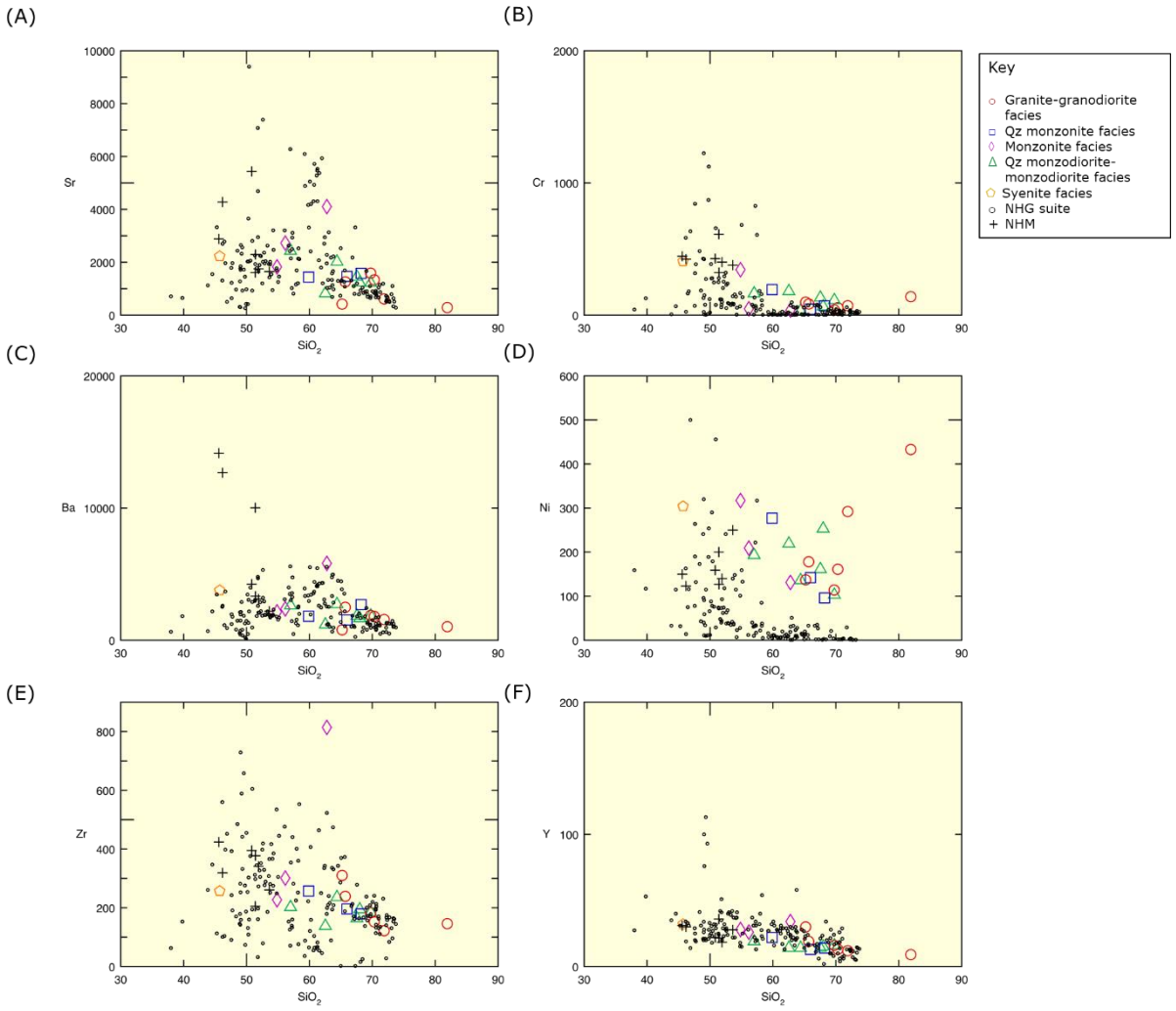


Figure 3.8 Variation diagrams for selected trace elements (in ppm) plotted against SiO_2 for the Ratagain Complex, NHM and NHG suite.

Chondrite-normalized diagrams (Sun & McDonough 1989; Figure 3.9A) indicate a depletion of heavy REEs (HREEs) relative to the light REEs (LREEs) in all the studied facies, as HREE concentrations are typically around 10× chondrite values, whilst the LREE concentrations mainly lie between 100-1000× chondrite values. There is a conspicuous absence of significant Eu anomalies. The most pronounced depletions occur in the granite-granodiorite facies whilst the quartz monzodiorite-monzodiorite facies and monzonites have less-depleted HREE patterns.

Primitive-mantle-normalized trace-element spider diagrams (McDonough & Sun, 1995; Figure 3.9B) show enrichment in large-ion lithophile elements (LILEs) including Rb, Ba, K and Sr, suggesting that feldspar was not a fractionated and/or residual phase.

Notable depletions occur in high field strength elements (HFSEs) including U, Th, Nb, Zr and are particularly pronounced in P and Ti. The deep P and Ti troughs relative to the other HFSE are indicative of selective removal of Ti and P by one or more mineral phases; in the Late Caledonian Rogart and Ach'Uaine intrusives such elemental characteristics have been ascribed to apatite and titanite fractionation (Fowler et al., 2008).

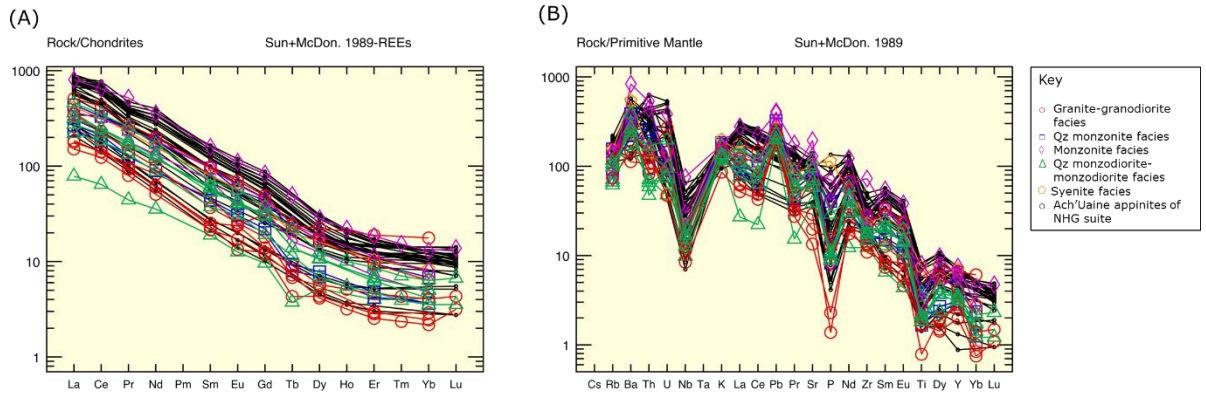


Figure 3.9 (A) Chondrite-normalized REE diagrams and (B) primitive-mantle-normalized trace-element spider diagrams for samples from the Ratagain Complex. Open black circles are literature data for the Ach'Uaine appinites of the NHG suite. Normalizing values are from Sun & McDonough (1989) and McDonough & Sun (1995).

Radiogenic isotopes

New Rb-Sr and Sm-Nd radiogenic isotope data for five samples are presented in Table 3.2. The isotopic compositions, when recalculated using Rogers and Dunning's (1991) crystallisation age of 425 Ma yield a range of $^{87}Sr/^{86}Sri$ values from 0.7056 to 0.7062. $143Nd/144Nd_i$ values fall between 0.511409 and 0.511485 and negative εNd values (ca.− 11.8 to − 13.3) point to an enriched source region for the Ratagain Complex. This is confirmed by the εNd vs $^{87}Sr/^{86}Sr_i$ diagram (Figure 3.10), which plots the new isotope data alongside published isotope work for the NHG high Ba-Sr suite. The Ratagain samples investigated in this study form an enriched cluster comparable to the syenite-dominated intrusions (e.g. Loch Loyal and the Loch Borralan syenite).

Table 3.2 Representative whole-rock radiogenic isotope data for samples from the Ratagain Complex. Key to abbreviations: G is granite; Mz is monzonite; Qmz is quartz monzonite. *U-Pb baddeleyite age after Rogers & Dunning (1995)- see discussion for limitations of older geochronology studies

Sample	Facies	Sr	Rb	$^{87}Sr/^{86}Sr$	$^{87}Sr/^{86}Sr_i$	Sm	Nd	$^{143}Nd/^{144}Nd$	$^{143}Nd/^{144}Nd_i$	$\varepsilon Nd(t)$	t(Ma)*
AL013	G	589	54.7	0.707413	0.705784	2.88	23.2	0.511618	0.511409	-13.3	425
AL059	Mz	7014	57.7	0.706021	0.705789	35.9	203	0.511782	0.511485	-11.8	425
AL063	Qmz	1613	50.9	0.706068	0.705515	5.96	41.5	0.511651	0.511410	-13.3	425
AL074	G	2844	53.5	0.706516	0.706187	13.6	87.6	0.511679	0.511418	-13.1	425
AL092	G	1980	53.4	0.706231	0.705759	7.23	49.3	0.511658	0.511420	-13.1	425

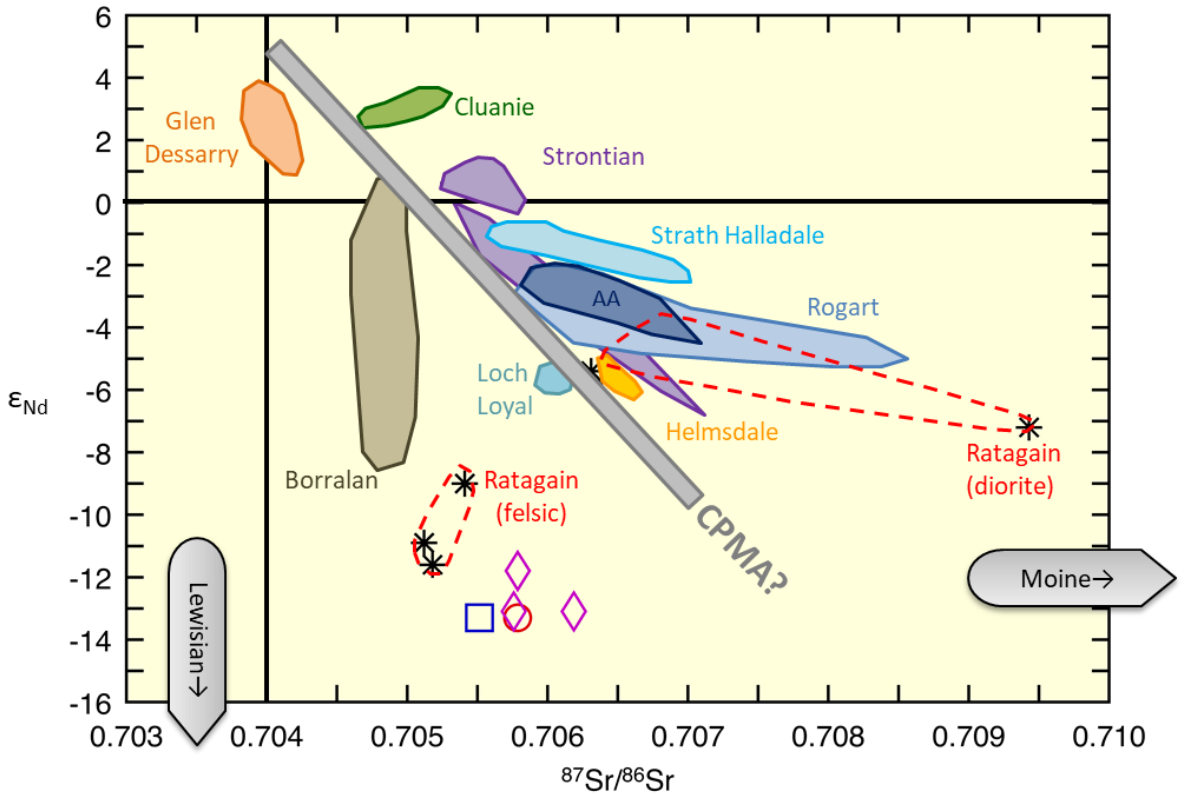


Figure 3.10 Initial Nd vs initial Sr isotope plot for selected samples from the Ratagain Complex. Also plotted are selected samples from the NHG suite (Fowler et al., 2008) and the hypothetical Caledonian Parental Magma Array (CPMA). Asterisks are literature data for the Ratagain Complex.

Discussion

The major element data presented above from the Ratagain Complex overlap with the entire compositional range of the Northern Highlands high Ba-Sr suite (Fowler et al., 2008). In terms of trace elements, the rocks closely resemble the mingled and mixed appinites at Ach'Uaine ca. 100 km to the NE. Further, the field observations and rock magnetic data of Lawrence et al. (2022) evidence that the Ratagain Complex bears a primary (i.e. magmatic) magnetic fabric with a subtle tectonic overprint imparted by sinistral transpressive strain. Critically, this overprint did not develop into a full tectonic fabric (Lawrence et al., 2022). The authors interpreted this magnetic fabric as being formed post-emplacement when the granite was near solidus temperature and in a crystal-rich but magmatic state. Taken in context with previous radiometric ages for the intrusion (Turnell, 1985; Thirlwall, 1988; Rogers & Dunning, 1991) and knowledge of the timing of Acadian regional deformation (Miles et al., 2016; Woodcock et al., 2019) the magnetic characteristics of Ratagain suggest that the complex is either younger than previously proposed and records only Acadian transpression, or that it was intruded and emplaced incrementally over a protracted time period, whereby incremental remobilisation by successive magma pulses accommodated most of the ambient tectonic strain, enabling the preservation of the primary magmatic fabric whilst simultaneously preventing the full development of a solid-state tectonic fabric. Thus, the Ratagain Complex's petrogenesis and emplacement are consistent with transcrustal crystal mush models that have advanced granite emplacement and magma evolution understanding in recent years (Cashman et al., 2017; Jackson et al., 2018; Sparks et al., 2019).

Petrogenetic models for high Ba-Sr magmas fall largely into two camps for the Caledonian examples and worldwide. The first (e.g. Fowler et al, 2008, Bao et al., 2019) holds that

compositional continuity between felsic and mafic members of the suite require a genetic relationship and that a significant component of the granite magmatism is ultimately juvenile. The second (e.g. Nielsen et al., 2009, Ye et al., 2008) argues that the mafic components are mantle-derived but that the granites represent crustal melts which subsequently interact with the contemporaneous mafic magmas. This model requires no genetic relationship, no juvenile input to the felsic magmas and fundamentally different sources for the mafic and felsic extremes. However, both hypotheses for the Caledonian examples are consistent with slab failure being responsible for the magmatism, a tectonic setting which is also commonly proposed for similar magmas elsewhere (Ye et al., 2008; Leite et al., 2021). The latter arguments have been considerably strengthened recently, with a regional study of Caledonian magmas (Archibald et al., 2022) in the light of the slab failure tectonomagmatic discrimination diagrams of Hildebrand and Whalen (2017) and Whalen and Hildebrand (2019).

All felsic samples from the Ratagain Complex with SiO_2 concentrations between 55 and 70 wt% and an alumina saturation index (ASI) of less than 1.1 fall within the slab failure field on the tectonomagmatic discrimination diagrams of Hildebrand and Whalen (2017) and Whalen and Hildebrand (2019), showing high Nb/Y and La/Yb vs. Gd/Y (Figure 3.11A, B) and La/Sm vs. Sm/Yb (Figure 3.11C) ratios. On the Nb vs. Y plot (Figure 3.11D) two monzonite samples display A-type affinities and two samples of the granite-granodiorite and quartz monzodiorite facies respectively plot within the arc field. This is could be accounted for by the alteration of Rb-bearing mineral phases such as alkali feldspar, which shows varying degrees of sericitization in all samples (Figure 3.5A-D).

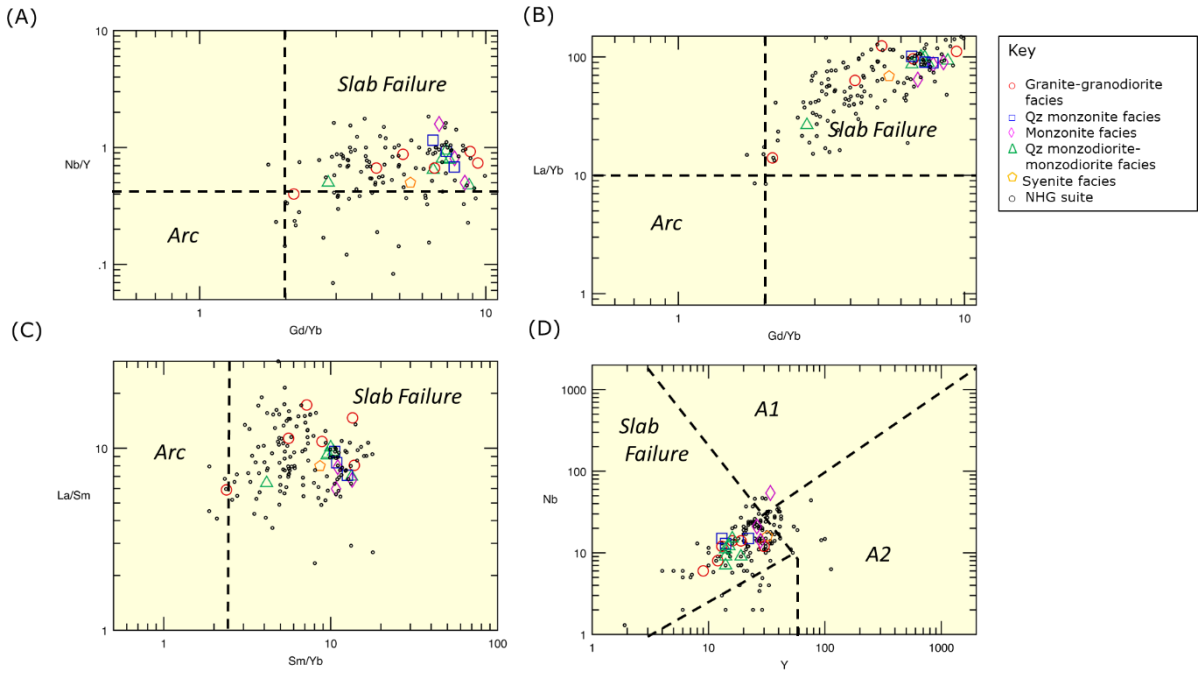


Figure 3.11 Tectonomagmatic discrimination diagrams showing slab-failure, arc and A-type fields (Hildebrand & Whalen, 2017; Whalen & Hildebrand, 2019) for samples from the Ratagain Complex with 55 to 70 wt. % SiO2 and an ASI value of 1.1 or less. Open black circles are NHG data. (A) Nb/Y vs. Gd/Yb plot (B) La/Yb vs.Gd/Yb (C) La/Sm vs. Sm/Yb. A1 and A2 fields for A-type granites are after Eby (1992). (D) Nb vs. Y

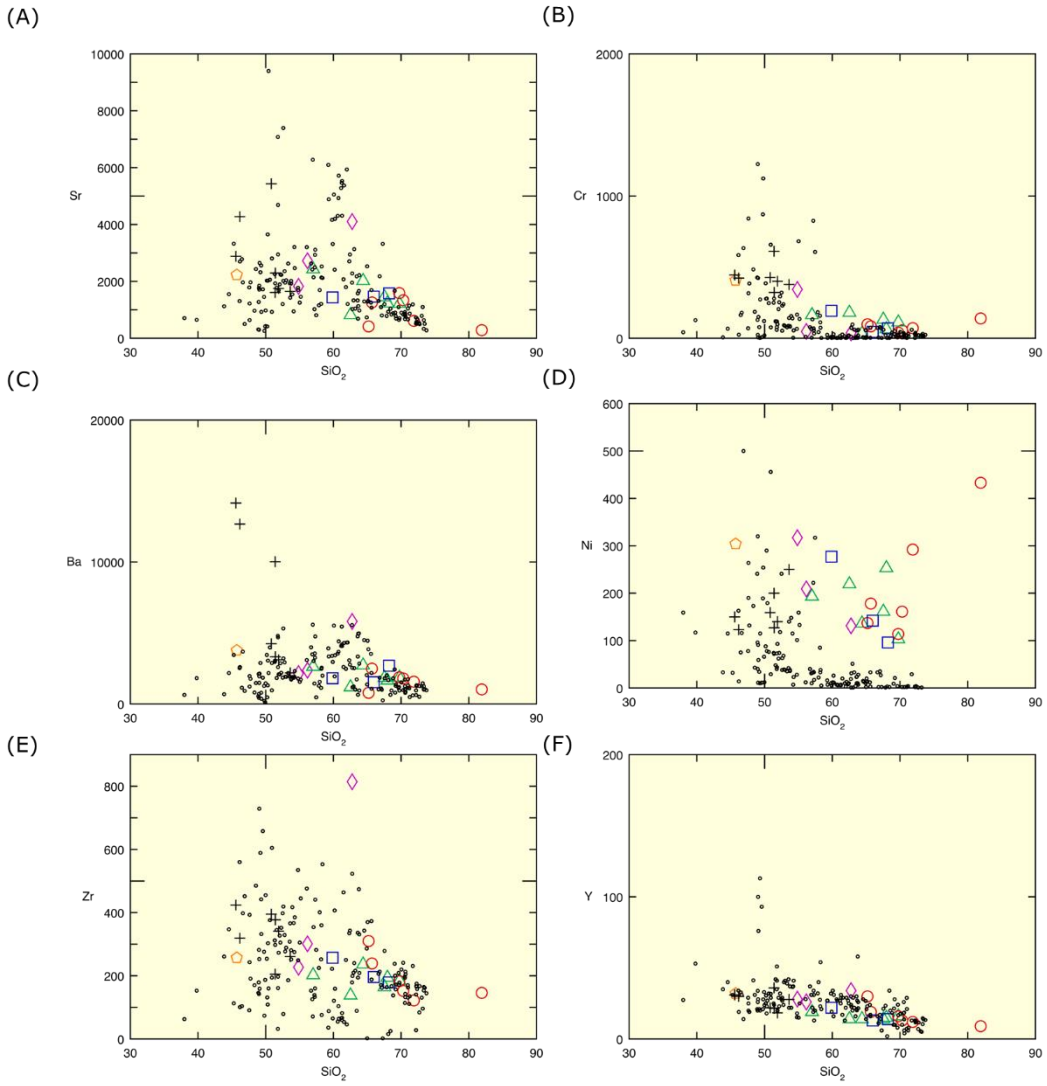


Figure 3.12 Tectonomagmatic discrimination diagrams (Hildebrand & Whalen, 2017; Whalen & Hildebrand, 2019) plotting samples from the Ratagain Complex with a SiO_2 concentration between 55 and 70 wt% and ASI of less than 1.1. Also shown for comparison are the NHG data. (A) Rb vs. Nb+Y (B) Rb vs. Ta+Yb (C) Nb/Sr vs. Sr/Y (D) La/Yb vs. Sr/Y

Nearly all of the Ratagain samples exhibit slab-failure signatures according to the Rb vs. Ta+Yb diagram (Figure 3.12B) and La/Yb vs. Sr/Y plot (Figure 3.12D) The Rb vs. Nb + Y (Figure 3.12A) and Nb/Yb vs. Sr/Y (Figure 3.12C) show more scatter; as before, this can be accounted for by the mobility of Sr and Rb and related feldspar alteration.

Therefore, the following discussion assesses the new data from Ratagain in the context of slab failure, and highlights new constraints and insights from this unique Caledonian intrusion.

Constraints on magmatic sources and evolution

One of the most noticeable aspects of the Ratagain Complex is the relative abundance of exposed intermediate and mafic rocks (Figure 3.2), which are generally subordinate in other members of the Northern Highland high Ba-Sr suite. Fowler et al. (2008) argue that equivalent mafic rocks are likely to be mantle derived, and so offer information on the SCLM reservoir(s) from which they

originated, while Nielsen et al. (2009) suggest that the intermediate rocks are derived by "partial melting of heterogeneous mafic to intermediate lowermost crust that had high Ba–Sr derived from previous melting of large ion lithophile element (LILE)-enriched mantle". Assuming that extensive melting of mafic-intermediate rocks is required to derive mafic-intermediate rocks, the only substantive difference is the number of melting events, one in the former hypothesis and two in the latter. In both hypotheses the origin of the distinctive chemistry lies in the SCLM. It should also be noted that Thirlwall (1981,1982) regards the Lorne high Cr-Ni andesitic (thence intermediate) lavas to be mantle-derived, little modified from primary melt compositions (cf. Nielsen et al, 2009). Similarly, calc-alkaline lamprophyres (minettes) from the Northern Highlands (Canning et al., 1996) are thought to represent primary mantle melts and overlap considerably with the more mafic Ratagain samples, as do the monzogabbros and monzodiorites of the Ach'Uaine appinite suite (Fowler, 1998; Fowler & Henney, 1996) which are regarded as hypabyssal equivalents of the lamprophyres (Figures 3.7-3.9).

Given that these are plutonic rocks, the major element variations between the intermediate and felsic rocks can likely be attributed, at least partly, to crystal-liquid equilibration and variable, incomplete mineral separation. Simple least-squares calculations demonstrate residual differences for example evolutionary models, from monzonite to quartz monzonite by separation of amphibole and plagioclase plus biotite or pyroxene, and from monzonite or quartz monzonite to granite by separation of K-feldspar, plagioclase and amphibole (Table 3.3). This is consistent with the observed petrography (Figures 3.4 and 3.5). Principal component analysis (PCA) conducted on the major element oxides results in ten principal components (see Supplementary Table SC2); the first principal component (PC1) accounts for 66.7% of the overall variance, the second principal component (PC2) accounts for 12.9% of the overall variance and the third principal component (PC3) accounts for 9.6% of the overall variance. Accordingly, the first three out of the ten principal components are responsible for 90% of the overall variation of the major element oxides and only the first two components have eigenvalues greater than 1 (and ~80% of the overall variance). Heavily loaded on PC1 are silica (negative) and all the mafic mineral components (MgO, Fe_2O_3, MnO, CaO: all positive). TiO_2 (titanite) and P_2O_5 (apatite) are also both positively loaded onto PC1. PC2 separates the felsic components, Na_2O and Al_2O_3 (negative) with K_2O positive. The associated scores plot (Figure 3.13) separates monzodiorites and monzonites along the mafic vectors, quartz monzonites broadly around the origin (quartz monzonite dominates the sample set) and granites along the K_2O vector on PC2. Importantly, there is a continuum between the different samples, from most mafic to most felsic. Thus, this objective statistical technique is also consistent with variable mineral separation within genetically-related evolving magmas.

Table 3.3 Summary least-squares mixing models of crystal fractionation in the Ratagain Complex

Fractionation step	Samples	Major fractionating minerals	Sum r^2
Monzonite to monzonite	AL092 - AL059	Amphibole, plagioclase, pyroxene	2.48
Monzonite to quartz monzonite	AL092 – AL063	Amphibole, plagioclase, biotite	3.05
Monzonite to granite	AL059 – AL013	Alkali feldspar, plagioclase, amphibole	0.17
Monzonite to granite	AL059 - AL703	Alkali feldspar, plagioclase, amphibole	0.23
Quartz monzonite to granite	AL063 – AL013	Alkali feldspar, plagioclase, amphibole	1.57
Quartz monzonite to granite	AL063 – AL073	Alkali feldspar, plagioclase, amphibole	1.84

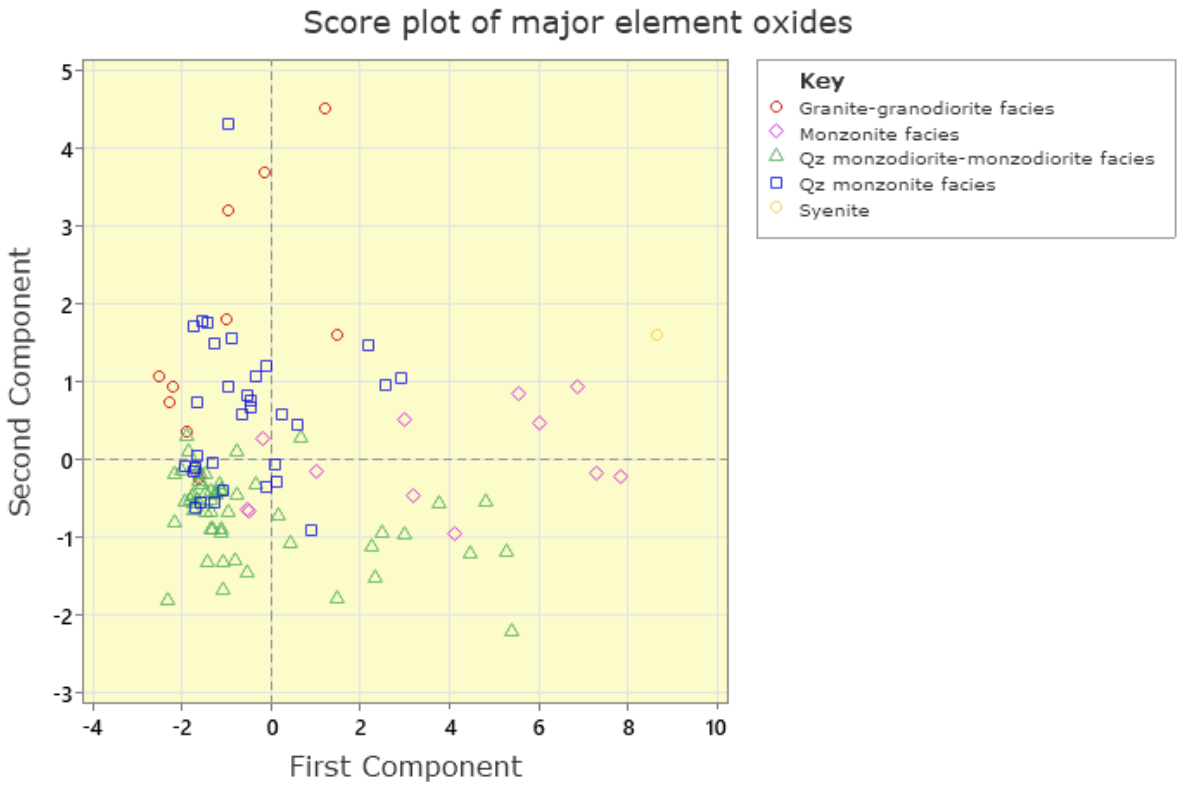


Figure 3.13 Principal component analysis (PCA) biplot of PC1 vs. PC2 scores for samples from the Ratagain Complex

Previous isotopic evidence (Fowler et al., 2008) suggests concurrent crustal contamination affected the NHG, but to an extent that does not obscure the enriched mantle origin if the elemental coherence of the suite is accepted as evidence of a genetic relationship. Our new isotope data indicates that the generation of the Ratagain magmas did involve recycling of ancient continental crust. The Nd-Sr isotope covariations for our studied samples (Figure 3.10) diverge from the fractionation pathways of the other calc-alkaline granites, including previously-sampled "diorites" from the Ratagain Complex that trend towards the local Moine metasediments (Fowler et al., 2008). Our samples instead plot similar trajectories to the NHG syenites, exhibiting $^{87}Sr/^{86}Sr_i$ values and very low εNd values (ca.− 11.8 to − 13.3) that are likely the result of contamination with Rb-depleted Lewisian granulite facies rocks. This suggests significant incorporation of Archean-Paleoproterozoic Lewisian granulite at lower crustal depths as opposed to in-situ contamination in upper crustal magma chambers by Neoproterozoic Moine rocks (Fowler et al., 2008).

Implications for the Late Caledonian granite suite

The Caledonian granites of the Northern Highlands high Ba-Sr suite have previously been interpreted to have been rapidly emplaced at shallow crustal depths following Iapetus subduction and were later subjected to brittle, upper crustal thrusting and strike-slip faulting (Strachan et al., 2020; Searle, 2022).

As previously mentioned, rock magnetic investigations (Lawrence et al., 2022) evidence that the Ratagain Complex records a subtle tectonic overprint indicative of transpression, the absence of a fully-developed solid-state tectonic fabric, precludes the final emplacement, crystallisation and

brittle deformation of the Ratagain Complex during the late Silurian. Lawrence et al. (2022) propose that the complex is therefore either younger than the reported 425±3 Ma age (Rogers & Dunning, 1991) and was affected by later Acadian transpression (see Mendum, 2012; Miles & Woodcock, 2018; Woodcock et al., 2019) or that it was emplaced incrementally with crystallisation of different magma batches over a protracted period, with the complex existing in a crystal-rich but rheologically-magmatic state into the Acadian.

This is more likely to occur at mid-crustal levels wherein the accreting intrusion was remobilized periodically by succeeding replenishments of magma, with exchange of crystals and melt between resident material and each successive magmatic pulse resulting in highly diffuse or indistinguishable internal contacts (Miller et al., 2011).

The emplacement of new magma pulses into partially-crystallised magma mush at mid-crustal depths could also have accommodated most of the strain and temperature increase (Lui et al., 2018) and offers a plausible explanation as to why the Ratagain Complex bears no obvious solid-state fabric (Lawrence et al., 2022), contacts the host Precambrian rock without a thermal aureole (Figure 3.3A, E,) and carries isotopic signatures consistent with a lower-crustal Lewisian granulite contaminant as well as the overlying Moine rocks (Figure 3.10).

In addition to the Ratagain Complex, other Caledonian granites show evidence for long-lived, pulsatory magmatism. Re-examination of the emplacement history of the Shap granite, Lake District through high-precision U-Pb zircon dating, suggests a protracted history of magmatic activity in the order of 106 Ma and zircon crystallisation at deep crustal levels in a crystal-mush system (Miles & Woodcock, 2018). The Shap granite also offer evidence of repeated rejuvenation of this crystal mush in its field features ranging from macroscopic enclaves to microscopic complex zoning patterns in magmatic alkali-feldspar phenocrysts, the former representing voluminous magmatic pulses and the later resulting from smaller magmatic injections (Miles & Woodcock, 2018).

Further, parallels can also be drawn with the Donegal Batholith, Ireland, which has a similar compositional variation and magmatic evolution to the Ratagain Complex (Archibald et al. 2021a). Of note here is that the Donegal Batholith is composed of a number of discrete intrusive bodies, each recording pulsed emplacement. Each intrusion is quite homogeneous, especially the younger ones, and all the intrusions were emplaced rapidly over a period of ca. 30 Myr (Archibald et al., 2021b). The exception is the highly heterogeneous Main Donegal Granite, which contains units that seem to represent each of the surrounding intrusions and its emplacement spans the time frame of the other intrusions (Stevenson et al. 2008). Stevenson et al. (2008) developed a model where the Main Donegal Granite represents the long lived and deeply penetrating feeder zone for the surrounding satellite plutons in the upper crust. Although the Ratagain Complex does not have a suite of satellite plutons, we draw the comparison of a mid-crustal feeder zone and propose that the intrusive body existed as a part of a vertically-linked sheeted-system potentially controlled by sinistral shearing (Lawrence et al., 2022).

We therefore suggest that many Caledonian granites previously interpreted as rapidly-emplaced, shallow-crustal intrusions (e.g. Watson, 1984) actually represent more long-lived, mid-crustal intrusions and that the large, euhedral zircons selected for analysis in the older geochronology studies (e.g. Rogers & Dunning, 1991) represent grains formed in the deep crust, early in the magmatic history. Thus whilst the early U-Pb zircon ages need not be discounted, they can be viewed as maxima for the timing of granite emplacement. Our interpretation is consistent with the large spread of crystallisation ages between c.435–390 Ma (Soper, 1986) for the Caledonian intrusives and could also account for the extended magmatism after active Iapetan subduction and slab failure.

Implications for slab failure magmatism and granite petrogenesis

The Ratagain intrusion and other members of the Northern Highland high Ba-Sr suite plot firmly in the slab failure fields on the appropriate tectonomagmatic discrimination diagrams (Figures 3.11 and 3.12) and indeed have been interpreted previously as the magmatic consequence of slab break-off (Atherton & Ghani, 2002; Fowler et al., 2008; Nielsen et al., 2009; Miles et al., 2016). This is essentially a result of their characteristic enrichment in LILEs and depletion in HFSEs, generating high Sr/Y and La/Yb ratios. Such ratios and associated characteristics are normally ascribed to melting processes involving garnet and/or amphibole stability in the residue, effectively withholding HREEs and associated elements from any equilibrated melt. These are amongst the definitive characteristics of adakitic rocks derived from intra-crustal melting of basalts, and Whalen and Hildebrand (2019) attribute them similarly to ocean crust melting during slab failure at mantle depths. However, there is an alternative to garnet/amphibole residual control that is capable of generating the same characteristic element ratios - extreme enrichment in LILEs without active "depletion" in HFSEs. The characteristic REE pattern of adakite (and TTG which are widely agreed to have been generated by basalt melting) has high LREE and low to very low HREE (<<10x chondrites). The Ratagain Complex (and other Northern Highland high Ba-Sr intrusions) have Yb values that range either side of 10 and up to ca. 20, are extremely enriched in LREE (Ce commonly several hundred and up to 1000x chondrites). Total REE concentrations start high and ultimately decrease with silica concentration, generating genuinely-depleted HREE only as a result of crystal fractionation removal of observed and abundant amphibole, titanite, apatite and zircon. Importantly, the mafic rocks also carry the isotopic signature of extreme LILE enrichment and $^{87}Sr/^{86}Sr$ up to 0.7062 and εNd as low as -13.3. If the slab failure signature were in this case generated by garnet/amphibole in the residue of ocean crust melting, the isotopic character should reflect long-term incompatible element depletion. The simplest explanation is that slab melting also affected the subducted sediment carapace, which infused the overlying SCLM with (possibly additional) enrichment, before being fused by the thermal anomaly resulting from asthenosphere encroachment (Fowler et al., 2008). The elemental and isotopic similarity between the slab failure magmas and broadly coeval lamprophyres, which are generally considered to be primary melts from the SCLM, supports this interpretation.

The felsic rocks of the Ratagain intrusion exhibit such strong elemental similarities to those of the mafic-intermediate rocks that a fundamentally different source is unlikely. Furthermore, any source within the stability range of plagioclase would not generate very high Sr in equilibrated magmas, and would produce negative Eu anomalies - which are conspicuous by their absence here (but are otherwise very common in "I-type" granites). Thus, the felsic rocks represent fractionated versions of "post-collisional mafic magmas", whose origin has been linked to unrecognised crustal growth since the Archaean (Couzinie et al, 2016). Such magmas have zircon Hf-O compositions appropriate to crustal derivation (i.e. negative εHf associated with elevated δ18O), but are dominated in terms of bulk mass by the mantle component (62-85%, Couzinie et al., 2016). The whole-rock Nd and O isotope compositions of Northern Highland high Ba-Sr felsic magmas are reflected in equivalent Hf-O systematics in zircons (Bruand et al., 2019). It therefore seems important to constrain the crust vs. mantle proportions in the high Ba-Sr microcosm that is the Ratagain intrusion (cf. Moyen et al, 2021; Jacob et al, 2021). Outline calculations in Fowler et al. (2008) constrained an average source sedimentary contribution to less than ca. 10% and a crustal contamination contribution via AFC to less than ca. 20%. A combination of both maxima gives a broadly similar estimate to the more rigorous result of Couzinie et al (2016).

As discussed above, the Nd and Sr isotope data included in Fowler et al. (2008) combined with those presented in this study, show that whilst some diorites from the Ratagain Complex define a trend from an enriched mantle source towards the local Moine metasediments, others and the

more “felsic” compositions are consistent with contamination with Lewisian granulite, from a similar point on the “Caledonian Parental Magma Array” (CPMA). The Ratagain source composition on that array is towards the enriched end (though not quite the extreme represented by Loch Loyal syenites and the Helmsdale granite) and is consistent with 5-10% sediment contribution, with a variable local crustal component of a few tens percent in the exposed rocks, but around 30% at maximum.

Conclusions

Our new lithogeochemical data for the Ratagain Complex, NW Scotland, indicate that it is a high Ba-Sr, slab-failure intrusion and thus support regional geological syntheses invoking slab-failure origin for the Northern Highland high Ba-Sr and wider Late Caledonian intrusive suites.

The major element data presented in this study overlap with the entire compositional range of the Northern Highlands high Ba-Sr suite, and the Ratagain intrusion is transitional between the granites and syenites of the Northern Highlands Terrane.

The $^{87}Sr/^{86}Sr$ values (0.7055 to 0.7062) and low initial εNd values (− 11.8 to − 13.3) indicate that contamination by Lewisian continental crust was volumetrically more significant than evident in previous studies.

The geochemical characteristics may be attributable to a long-lived, incremental emplacement of the complex with crystallisation of successive magma batches originating from the same Caledonian Parental Magma Array but differing in age and extent of assimilation-fractionation.

We therefore propose that literature dates for the Late Caledonian intrusions, particularly those obtained from older geochronology studies, may record crystallisation in the deep crust and not be a valid proxy for granite emplacement. There is thus a need for careful review of previous dates for the Late Caledonian intrusions, to better resolve the links between their petrogenesis, crustal tectonics, the geodynamics of Iapetus subduction, collision and slab break-off.

Acknowledgements

AL thanks the Open University, Edinburgh Geological Society and Geologists’ Association for the award of the Ian Gass Bursary, Fieldwork Grant and New Researcher’s Award, respectively, to conduct field work in the Scottish Highlands. AL also thanks parent carers Paul and Mannpreet Lawrence for facilitating fieldwork in the remote Scottish Highlands- no small undertaking!

The assistance provided by Zoe Whittaker in XRF and LAICPMS sample preparation and analysis is gratefully acknowledged.

List of references

Archibald, D.B., Murphy, J.B., Fowler, M., Strachan, R.A. & Hildebrand, R.S. 2022. Testing petrogenetic models for contemporaneous mafic and felsic to intermediate magmatism within the —Newer Granitell suite of the Scottish and Irish Caledonides. In Kuiper, Y.D., Murphy, J.B., Nance, R.D., Strachan, R.A. & Thompson, M.D. (Eds.), New Developments in the Appalachian-Caledonian- Variscan Orogen, *Geological Society of America Special Paper* **554** (p. 1–XXX). Available from: https://doi.org/10.1130/2021.2554(15)

Archibald, D.B. & Murphy, J.B. 2021. A slab failure origin for the Donegal composite batholith, Ireland as indicated by trace-element geochemistry. *Geological Society, London, Special Publications*, **503**, 347-370. Available from: https://doi.org/10.1144/SP503-2020-6

Alderton, D. H. M. 1988. Ag-Au-Te mineralisation in the Ratagain complex, northwest Scotland. *Transactions of the Institution of Mining and Metallurgy (Section B: Applied Earth Sciences)*, **97**, B171–B180.

Atherton, M.P. & Ghani, A.A. 2002. Slab breakoff: a model for Caledonian, Late Granite syn-collisional magmatism in the orthotectonic (metamorphic) zone of Scotland and Donegal, Ireland. *Lithos*, **62**, 65-85. Available from: https://doi.org/10.1016/S0024-4937(02)00111-1

Brown, P. E. & Ryan, P. D. and Soper, N. J. & Woodcock, N. H. 2008. The Newer Granite problem revisited: a transtensional origin for the Early Devonian Trans-Suture Suite. *Geological Magazine*, **145**, 235-256. Available from: https://doi:10.1017/S0016756807004219

Bruand, E., Storey, C. & Fowler, M. 2014. Accessory mineral chemistry of high Ba-Sr granites from Northern Scotland: Constraints on petrogenesis and records of whole-rock Signature. *Journal of Petrology*, **55**(8), 1619-1651. Available from: https://doi.org/10.1093/petrology/egu037

Bruand, E., Storey, C., Fowler, M. & Heilimo, E., 2019. Oxygen isotopes in titanite and apatite, and their potential for crustal evolution research. *Geochimica et Cosmochimica Acta*, **255**, 144-162. Available from: https://doi.org/10.1016/j.gca.2019.04.002

Canning, J., Henney, P., Morrison, M., & Gaskarth, J. 1996. Geochemistry of late Caledonian minettes from Northern Britain: Implications for the Caledonian sub-continental lithospheric mantle. *Mineralogical Magazine*, **60**(398), 221-236. Available from: https://doi.org/10.1180/minmag.1996.060.398.15

Cashman, K. V., Sparks, R. S. J. & Blundy, J. D. 2017. Vertically extensive and unstable magmatic systems: A unified view of igneous processes. *Science*, **355** (6331). Available from: https://doi.org/10.1126/science.aag3055

Conliffe, J., Selby, D., Porter, S. & Feely, M. 2010. Re-Os molybdenite dates from the Ballachulish and Kilmelford Igneous Complexes (Scottish Highlands): age constraints for late Caledonian magmatism. *Journal of the Geological Society, London*, **167**(2), 297-302. Available from: https://doi.org/10.1144/0016-76492009-077

Couzinié, S., Laurent, O., Moyen, J. F., Zeh, A., Bouilhol, P. & Villaros, A. 2016. Post-collisional magmatism: Crustal growth not identified by zircon Hf–O isotopes. *Earth and Planetary Science Letters*, **456**, 182-195. Available from: https://doi.org/10.1016/j.epsl.2016.09.033

De Paolo, D.J. 1988. *Neodymium isotope geochemistry*. Berlin: Springer-Verlag.

Dewey, J.F., Dalziel, I.W. D., Reavy, R. J. & Strachan, R.A. 2015. The Neoproterozoic to Mid-Devonian evolution of Scotland: a review and unresolved issues. *Scottish Journal of Geology*, **51**(1), 5-30. Available from: https://doi.org/10.1144/sjg2014-007

Eby G.N. 1992. Chemical subdivision of the A-type granitoids: *Petrogenetic and tectonic implications*. Geology, **20**(7), 641–644. Available from: https://doi.org/10.1130/0091-7613(1992)020<0641:CSOTAT>2.3.CO;2

Fowler, M. B., & Henney, P. J. 1996. Mixed Caledonian appinite magmas: implications for lamprophyre fractionation and high Ba-Sr granite genesis. *Contributions to Mineralogy and Petrology*, **126**(1), 199-215. Available from: https://doi.org/10.1007/s004100050244

Fowler M., Henney P., Darbyshire D. & Greenwood P. 2001. Petrogenesis of high Ba–Sr granites: the Rogart pluton, Sutherland. *Journal of the Geological Society, London*, **158**(3), 521–534. Available from: https://doi.org/10.1144/jgs.158.3.521

Fowler, M.B., Kocks, H., Darbyshire, D.P.F. & Greenwood, P.B. 2008. Petrogenesis of high Ba-Sr plutons from the Northern Highlands Terrane of the British Caledonian Province. *Lithos*, **105**, 129-148. Available from: https://doi.org/10.1016/j.lithos.2008.03.003

Fowler, M. & Rollinson H. 2012. Phanerozoic sanukitoids from Caledonian Scotland: Implications for Archean subduction. *Geology*, **40**, 1079-1082. Available from: https://doi.org/10.1130/G33371.1

Frost, B. R., Barnes, C. G., Collins, W. J., Arculus, R. J., Ellis, D. J., & Frost, C. D. 2001. A geochemical classification for granitic rocks. *Journal of petrology*, **42**(11), 2033-2048. Available from: https://doi.org/10.1093/petrology/42.11.2033

Goodenough, K., Millar, I., Strachan, R., Krabbendam, M. & Evans, J. 2011. Timing of regional deformation and development of the Moine Thrust Zone in the Scottish Caledonides: constraints from the U–Pb geochronology of alkaline intrusions. *Journal of the Geological Society, London*, **168**(1), 99–114. Available from: https://doi.org/10.1144/0016-76492010-020

Hawkesworth, C., Cawood, P., Kemp, T., Storey, C. & Dhuime, B., 2009. A matter of preservation. *Science*, **323**(5910), 49-50. Available from: https://doi.org/10.1126/science.1168549

Harmon, R.S., Halliday, A.N., Clayburn, J. & Stephens, W.E. 1984. Chemical and isotopic systematics of the Caledonian intrusions of Scotland and northern England: a guide to magma source region and magma-crust interaction. *Philosophical Transactions of the Royal Society of London. Series A, Mathematical and Physical Sciences*, **310**(1514), 709–42. Available from: https://doi.org/10.1098/rsta.1984.0016

Highton, A. J. 1999. Late Silurian and Devonian granitic intrusions of Scotland. In Stephenson, D., Bevins, R. E., Millward, D., Highton, A. J., Parsons, I., Stone, P. & Wadsworth, W. J. (Eds.), *Caledonian Igneous Rocks of Britain* (pp.397–404). Geological Conservation Review Series, Peterborough: JNCC.

Hildebrand, R.S. & Whalen J.B. 2017. The Tectonic Setting and Origin of Cretaceous Batholiths Within the North American Cordillera: The Case for Slab Failure Magmatism and Its Significance for Crustal Growth. *Geological Society of America Special Papers*, **532**, 1-113. Available from: https://doi.org/10.1130/SPE532

Hildebrand R.S., Whalen J.B., & Bowring S.A. 2018. Resolving the crustal composition paradox by 3.8 billion years of slab failure magmatism and collisional recycling of continental crust. *Tectonophysics*, **734–735**, 69–88. Available from: https://doi.org/10.1016/j.tecto.2018.04.001

Hutton, D.H.W. & McErlean, M. 1991. Silurian and early Devonian sinistral deformation of the Ratagain granite, Scotland: constraints on the age of Caledonian movements on the Great Glen fault system. *Journal of the Geological Society, London*, **148**, 1-4. Available from: https://doi.org/10.1144/gsjgs.148.1.0001

Hutton, D. H. W. Stephens, W. E., Yardley, B., McErlean, M. & Halliday, A. N., 1993. Ratagain Plutonic complex. In May, F., Peacock, J. D., Smith, D. I. and Barber, A. J. (Eds.), *Geology of the Kintail district* (pp.52-56). Memoir of the British Geological Survey, London: HMSO.

Irvine, T.N. & Baragar, W.R.A. 1971. A guide to the chemical classification of the common volcanic rocks. *Canadian Journal of Earth Sciences*, **8**(5), 523–548. Available from: https://doi.org/10.1139/e71-055

Jackson, M.D., Blundy, J. & Sparks, R.S.J. 2018. Chemical differentiation, cold storage and remobilization of magma in the Earth's crust. *Nature*, **564**, 405–409. Available from: https://doi.org/10.1038/s41586-018-0746-2

Jacob, J. B., Moyen, J. F., Fiannacca, P., Laurent, O., Bachmann, O., Janoušek, V., Farina, F. & Villaros, A. 2021. Crustal melting vs. fractionation of basaltic magmas: Part 2, Attempting to quantify mantle and crustal contributions in granitoids. *Lithos*, **402-403**, 106292. Available from: https://doi.org/10.1016/j.lithos.2021.106292

Jacobsen, S.B. & Wasserburg, G.J. 1980. Sm–Nd evolution of chondrites. *Earth and Planetary Science Letters*, **50**(1), 139–155. Available from: https://doi.org/10.1016/0012-821X(80)90125-9

Johnson, T.E., Kirkland, C.L., Viete, D.R., Fischer, S., Reddy, S.M., Evans, N.J. & McDonald, B.J. 2017. Zircon geochronology reveals polyphase magmatism and crustal anatexis in the Buchan Block, NE Scotland: Implications for the Grampian Orogeny. *Geoscience Frontiers*, **8**(6), 1469-1478. Available from: https://doi.org/10.1016/j.gsf.2017.02.002

Kinny P., Strachan R., Friend C., Kocks H., Rogers G. & Paterson B. 2003. U–Pb geochronology of deformed metagranites in central Sutherland, Scotland: evidence for widespread late Silurian metamorphism and ductile deformation of the Moine Supergroup during the Caledonian orogeny. *Journal of the Geological Society, London*, **160**(2), 259–269. Available from: https://doi.org/10.1144/0016-764901-087

Lancaster, P. J., Strachan, R. A., Bullen, D., Fowler, M., Jaramillo, M., and Saldarriaga, A. M. 2017. U–Pb zircon geochronology and geodynamic significance of 'Newer Granite' plutons in Shetland, northernmost Scottish Caledonides. *Journal of the Geological Society, London*, **174**(3), 486-497. Available from: https://doi.org/10.1144/jgs2016-106

Lara, P. Oyhantçabal, P. & Dadd, K. 2017. Post-collisional, Late Neoproterozoic, high-Ba-Sr granitic magmatism from the Dom Feliciano Belt and its cratonic foreland, Uruguay: Petrography, geochemistry, geochronology, and tectonic implications. *Lithos*, **277**, 178-198. Available from: https://doi.org/10.1016/j.lithos.2016.11.026

Lawrence, A., Maffione, M. & Stevenson, C.T.E. (2022) Mush ado about the Ratagain Complex, NW Scotland: Insights on Caledonian granitic magmatism and emplacement from magnetic fabric analyses. *Scottish Journal of Geology*, **58**(1), p.XXX. Available from: https://doi.org/10.1144/sjg2021-018

Lee, C. T. A., Morton, D. M., Kistler, R. W. & Baird, A. K. 2007. Petrology and tectonics of Phanerozoic continent formation: From island arcs to accretion and continental arc magmatism. *Earth and Planetary Science Letters*, **263**(3-4), 370-387. Available from: https://doi.org/10.1016/j.epsl.2007.09.025

Leite, A.F.G.D., Fuck, R.A, Dantas, E.L. & Ruiz, A.S. 2021. Appinitic and high Ba-Sr magmatism in central Brazil: Insights into the late accretion stage of West Gondwana. *Lithos*, **398-399**, 106333. Available from: https://doi.org/10.1016/j.lithos.2021.106333

Liu, H., Martelet, G., Wang, B., Erdmann, S., Chen, Y., Faure, M., Huang, F., Scaillet, B., le-Breton, N., Shu, L., Wang, R. & Zhu, J. 2018. Incremental emplacement of the Late Jurassic midcrustal, lopolith-like Qitianling pluton, South China, revealed by AMS and Bouguer gravity data. *Journal of Geophysical Research: Solid Earth*, **123**(10), 9249– 9268. Available from: https://doi.org/10.1029/2018JB015761

Lugmair, G.W. & Marti, K.1978. Lunar initial 143Nd/144Nd: differential evolution line of the lunar crust and mantle. *Earth and Planetary Science Letters*, **39**(3), 349–357. Available from: https://doi.org/10.1016/0012-821X(78)90021-3

MacDonald, R. & Fettes, D.J. 2006. The tectonomagmatic evolution of Scotland. *Earth and Environmental Science Transactions of The Royal Society of Edinburgh*, **97**(3), 213-295. Available from: https://doi.org/10.1017/S0263593300001450

Macera, P., Gasperini, D., Ranalli, G. & Mahatsente, R., 2008. Slab detachment and mantle plume upwelling in subduction zones: an example from the Italian South-Eastern Alps. *Journal of Geodynamics*, **45**(1), 32-48. Available from: https://doi.org/10.1016/j.jog.2007.03.004

Maniar, P. D., & Piccoli, P. M. 1989. Tectonic discrimination of granitoids. *Geological Society of America Bulletin*, **101**(5), 635-643. Available from: https://doi.org/10.1130/0016-7606(1989)101<0635:TDOG>2.3.CO;2

Marshall, D. 1996. Ternplot: An excel spreadsheet for ternary diagrams. *Computers & Geosciences*, **22**(6), 697-699. Available from: https://doi.org/10.1016/0098-3004(96)00012-X

McDonough, W.F. & Sun, S.S. 1995. The composition of the Earth. *Chemical Geology*, **120**(3-4), 223-253. Available from: https://doi.org/10.1016/0009-2541(94)00140-4

McKerrow W.S., MacNiocail C. & Dewey J.F. 2000. The Caledonian Orogeny redefined. *Journal of the Geological Society, London*, **157**(6), 1149–1154. Available from: https://doi.org/10.1144/jgs.157.6.1149

Mendum, J.R. 2012. Late Caledonian (Scandian) and Proto-Variscan (Acadian) orogenic events in Scotland. *OUGS Journal*, **33**, 37–51.

Mendum, J. R. & Noble, S. R. 2010 'Mid-Devonian sinistral transpressional movements on the Great Glen Fault: the rise of the Rosemarkie Inlier and the Acadian Event in Scotland', in Moyen, J.F., Laurent, O., Chelle-Michou, C., Couzinié, S., Vanderhaeghe, O., Zeh, A., Villaros, A. & Gardien, V. 2017. Collision vs. subduction-related magmatism: two contrasting ways of granite formation and implications for crustal growth. *Lithos*, **277**,154-177. Available from: https://doi.org/10.1016/j.lithos.2016.09.018

Miles, A. J., Woodcock, N. & Hawkesworth, C. 2016. Tectonic controls on postsubduction granite genesis and emplacement: The late Caledonian suite of Britain and Ireland. *Gondwana Research*, **39**, 250-260. Available from: https://doi.org/10.1016/j.gr.2016.02.006

Miles, A.J. & Woodcock, N.H. 2018. A combined geochronological approach to investigating long lived granite magmatism, the Shap granite, UK. *Lithos*, **304–307**, 245-257. Available from: https://doi.org/10.1016/j.lithos.2018.02.012

Miller, C.F., Furbish, D.J., Walker, B.A., Claiborne, L.L., Koteas, G.C., Bleick, H.A. & Miller, J.S. 2011. Growth of plutons by incremental emplacement of sheets in crystal-rich host: Evidence

from Miocene intrusions of the Colorado River region, Nevada, USA. *Tectonophysics*, **500**, 65–77. Available from: http://doi.org/10.1016/j.tecto.2009.07.011

Moyen, J.F., Janoušek, V., Laurent, O., Bachmann, O., Jacob, J.B., Farina, F., Fiannacca, P. & Villaros, A., 2021. Crustal melting vs. fractionation of basaltic magmas: Part 1, The bipolar disorder of granite petrogenetic models. *Lithos*, **402-403**, 106291. Available from: https://doi.org/10.1016/j.lithos.2021.106291

Neilson J.C., Kokelaar B.P. & Crowley Q.G. 2009. Timing, relations and cause of plutonic and volcanic activity of the Siluro-Devonian post-collision magmatic episode in the Grampian Terrane, Scotland. *Journal of the Geological Society, London*, **166**(3), 545–561. Available from: https://doi.org/10.1144/0016-76492008-069

Oliver G.J., Wilde S.A. & Wan Y. 2008. Geochronology and geodynamics of Scottish granitoids from the late Neoproterozoic break-up of Rodinia to Palaeozoic collision. *Journal of the Geological Society, London*, **165**(3), 661–674. Available from: https://doi.org/10.1144/0016-76492007-105

Pidgeon, R. T. and Aftalion, M. 1978. Cogenetic and inherited zircon U-Pb systems in Palaeozoic granites from Scotland and England. In Bowls, D. R. and Leake, B.E. (Eds.), *Crustal evolution in northwestern Britain and adjacent regions* (pp.183-220). Liverpool: Seal House Press.

Read, H.H. 1961. Aspects of Caledonian magmatism in Britain. *Geological Journal*, **2**(4), 653–683. Available from: https://doi.org/10.1002/gj.3350020408

Rock, N. M. S., Gaskarth, J. W., Henney, P. J. & Shand, P. 1988. Late Caledonian dyke swarms of northern Britain; some preliminary petrogenetic and tectonic implications of their province-wide distribution and chemical variation. *Canadian Mineralogist*, **26**(1), 3–22.

Rogers, G. & Dunning, G. R. 1991. Geochronology of appinitic and related granitic magmatism in the W Highlands of Scotland: constraints on the timing of transcurrent fault movement. *Journal of the Geological Society, London*, **148**,17-27. Available from: https://doi.org/10.1144/gsjgs.148.1.0017

Rudnick, R. 1995. Making continental crust. *Nature*, **378**, 571–578. Available from: https://doi.org/10.1038/378571a0

Searle, M.P. 2022. Tectonic evolution of the Caledonian orogeny in Scotland: a review based on the timing of magmatism, metamorphism and deformation. *Geological Magazine*, **159**(1), 124–152. Available from: https://doi.org/10.1017/S0016756821000947

Soper, N. J. 1986. The Newer Granite problem: a geotectonic view. *Geological Magazine*, **123**(3), 227–36. Available from: https://doi.org/10.1017/S0016756800034725

Sparks, R. S. J., Annen, C., Blundy, J. D., Cashman, K. V., Rust, A. C. & Jackson, M. D. 2019. Formation and dynamics of magma reservoirs. *Philosophical Transactions of the Royal society A*, **377**(2139), 20180019. Available from: https://doi.org/10.1098/rsta.2018.0019

Steiger, R.H. & Jäger, E. 1977. Subcommission on geochronology: convention on the use of decay constants in geo- and cosmochronology. *Earth and Planetary Science Letters*, **36**(3), 359–362. Available from: https://doi.org/10.1016/0012-821X(77)90060-7

Stephenson, D., Bevins, R.E., Millward, D., Stone, P., Parsons, I., Highton, A.J. & Wadsworth, W.J. 1999. *Caledonian Igneous Rocks of Great Britain*, Peterborough: JNCC.

Streckeisen, A. 1976. To each plutonic rock its proper name. *Earth-Science Reviews*, **12**(1), 1–33. Available from: https://doi.org/10.1016/0012-8252(76)90052-0

Sun S.-S. & McDonough W.F. 1989. Chemical and isotopic systematics of oceanic basalts: implications for mantle composition and processes. *Geological Society, London, Special Publications*, **42**, 313–345. Available from: https://doi.org/10.1144/GSL.SP.1989.042.01.19

Tarney, J. & Jones C.E. 1994. Trace Element Geochemistry of Orogenic Igneous Rocks and Crustal Growth Models. *Journal of the Geological Society, London*, **151**(5), 855-868. Available from: https://doi.org/10.1144/gsjgs.151.5.0855

Thompson R.N. & Fowler M.B. 1986. Subduction-related shoshonitic and ultrapotassic magmatism: a study of Siluro-Ordovician syenites from the Scottish Caledonides. *Contributions to Mineralogy and Petrology*, **94**, 507-522. Available from: https://doi.org/10.1007/BF00376342

Thirlwall, M.F. 1981. Implications for Caledonian plate tectonic models of chemical data from volcanic rocks of the British Old Red Sandstone. *Journal of the Geological Society, London*, **138**(2), 123-138. Available from: https://doi.org/10.1144/gsjgs.138.2.0123

Thirlwall, M.F. 1982. Systematic variation in chemistry and Nd-Sr isotopes across a Caledonian calc-alkaline volcanic arc: implications for source materials. *Earth and Planetary Science Letters*, **58**(1), 27-50. Available from: https://doi.org/10.1016/0012-821X(82)90101-7

Thirlwall, M. F. 1988. Geochronology of late Caledonian magmatism in northern Britain. *Journal of the Geological Society, London*, **145**(11), 951-967. Available from: https://doi.org/10.1144/gsjgs.145.6.0951

Thirlwall, M.F. & Burnard, P. 1990. Pb-Sr-Nd isotope and chemical study of the origin of undersaturated and oversaturated shoshonitic magmas from the Borralan pluton, Assynt, NW Scotland. *Journal of the Geological Society, London*, **147**(2), 259-269. Available from: https://doi.org/10.1144/gsjgs.147.2.0259

Troll, V.R., Emeleus, H., Nicoll, G.R., Mattsson, T., Ellam, R., Donaldson, C.H. & Harris, C. 2019. A large explosive silicic eruption in the British Palaeogene Igneous Province. *Scientific Reports*, **9**, 494. Available from: https://doi.org/10.1038/s41598-018-35855-w

Turnell, H. B. 1985. Palaeomagnetism and Rb-Sr ages of the Ratagan and Comrie intrusions. *Geophysical Journal International*, **83**, 363–378. Available from: https://doi.org/10.1111/j.1365-246X.1985.tb06492.x

Whalen J.B. & Hildebrand R.S. 2019. Trace element discrimination of arc, slab failure, and A-type granitic rocks. *Lithos*, **348–349**, 105179. Available from: https://doi.org/10.1016/j.lithos.2019.105179

Watson, J. 1984. The ending of the Caledonian orogeny in Scotland. *Journal of the Geological Society, London*, **141**(2), 193-214. Available from: https://doi.org/10.1144/gsjgs.141.2.0193

Whitney, D. L., & Evans, B. W. 2010. Abbreviations for names of rock-forming minerals. *American Mineralogist*, **95**, 185–187. Available from: https://doi.org/10.2138/am.2010.3371

Woodcock, N.H., Soper, N.J. and Miles, A.J. 2019. Age of the Acadian deformation and Devonian granites in northern England: a review. *Proceedings of the Yorkshire Geological Society*, **62**, 238–253. Available from: https://doi.org/10.1144/pygs2018-009

Ye, H.-M., LI, X.-H., Li, Z.-X. & Zhang, C.-L. 2008. Age and origin of high Ba–Sr appinite–granites at the northwestern margin of the Tibet Plateau: Implications for early Paleozoic

tectonic evolution of the Western Kunlun orogenic belt. *Gondwana Research*, **13**(1), 126-138. Available from: https://doi.org/10.1016/j.gr.2007.08.005

Chapter 4

A UK perspective on tackling the geoscience racial diversity crisis in the Global North

Published paper

Dowey, N.[1], Barclay, J. [2], Fernando, B. [3], Giles, S.[4], Houghton, J.[5], Jackson, C.[6], Khatwa, A.[7], **Lawrence, A. [4]**, Mills, K.[8], Newton, A.[9], Rogers, R.[10] and Williams, R.[11]

Nature Geoscience, 2021. 14, 256–259. https://doi.org/10.1038/s41561-021-00737-w

This paper combines many different approaches and lived experiences relating to matters of equality, diversity and inclusivity in the Geosciences. Whilst the detailed input and standpoint of each author involved is too personal and nuanced to discuss here, their contributions are broadly summarised below.

Natasha Dowey as lead-author was responsible for conceptualising, planning and writing the manuscript, as well as coordinating inputs from different authors and all communications relating to the editorial process. Jenny Barclay offered perspectives on the colonial history of Geoscience, whilst Ben Fernando brought his lived experience as a minority ethnic student, postgraduate student representative and coordinator of undergraduate access and outreach programs at the University of Oxford to the paper. Anjana Khatwa, Keely Mills and Alicia Newton brought to the paper valuable non-academic perspectives from cultural heritage sectors, governmental organisations and Professional Statutory and Regulatory Bodies, respectively. Sam Giles collated much of the UK census and higher education statistical data as well as contributing her insight into poor recruitment practices of CDTs and DTPs. Jaqueline Houghton, Steven Rogers and Rebecca Williams all added to the discussion on inclusive teaching methods and removing frequently-encountered barriers to ethnic minority students in the Geosciences. Chris Jackson, as one of the few Black Professors of Geology in the UK, offered his detailed insight into structural inequality and systemic racism in the context of academia.

My contributions included: reviewing existing EDI literature, analysing higher education statistical data, contributing my direct lived experiences as a minority ethnic student to inform the paper's proposed actions and writing the manuscript.

[1]Department of the Natural and Built Environment, Sheffield Hallam University, Sheffield, UK

[2]School of Environmental Sciences, University of East Anglia, Norwich, UK

[3]Department of Earth Sciences, University of Oxford, Oxford, UK

[4]School of Geography, Earth and Environmental Sciences, University of Birmingham, Birmingham, UK

[5]School of Earth and Environment, University of Leeds, Leeds, UK

[6]Department of Earth and Environmental Sciences, University of Manchester, Manchester, UK

[7]Wessex Museums, Poole, UK

[8]British Geological Survey, Keyworth, UK

[9]Geological Society of London, London, UK

[10]School of Geography, Geology and the Environment, Keele University, Keele, UK

[11]Department of Geography, Geology and Environment, University of Hull, Hull, UK

Abstract

Geoscientists will play key roles in the grand challenges of the twenty-first century, but this requires our field to address its past when it comes to diversity and inclusion. Considering the bleak picture of racial diversity in the UK, we put forward steps institutions can take to break down barriers and make the geosciences equitable.

Introduction

The roots of modern geoscience lie in early colonial principles stating that land could belong to those willing to use its products, regardless of indigenous territories and practices. The production of geoscience knowledge has therefore been historically tied to a desire to explain the distribution and extractability of resources, largely for the benefit of the colonizing force (Stafford, 1984). This knowledge now has an essential role to play in equitable and sustainable development, but it cannot be successfully applied without diverse representation among geoscientists. Addressing global problems that impact people from all walks of life means we must work within and across a wide array of communities.

A robust approach to diversity and inclusion needs to begin at home, especially in the very countries that have benefited from the structures and wealth of a colonial past. Geoscience in the Global North is disproportionately white, a result of both historic systemic racism that impacts academia as a whole (Gillborn, 2005) and subject-specific issues that make our discipline less inclusive to many under-represented groups (Marín-Spiotta et al., 2020). In the United States, for example, just 6% of geoscience doctorate degrees are awarded to students from under-represented minorities (defined as American Indian or Alaska Native, Black or African American, Hispanic or Latino) despite 31% of the population belonging to these groups (Bernard & Cooperdock, 2018; Dutt, 2020). Moving forwards, we must remove the bias and hostile environments that have led to inequality in our discipline, attract researchers from a variety of backgrounds and retain them throughout their careers.

The lack of diversity in geoscience has been documented in North America (Bernard & Cooperdock, 2018; Dutt, 2020), but there has been little focus on diversity trends in geoscience postgraduate research (PGR; PhD and MRes courses) in other regions of the Global North. This work aims to highlight issues facing UK geoscience in a similar way to Bernard and Cooperdock's work (2018) in the United States, to give international perspective to these discussions. The data we present from the UK Higher Education Statistics Agency (HESA, 2019a) paint a similarly dismal picture (see Figure 4.1). It is difficult to expand this approach to other Global North countries because demographic data are not collected in much of Europe (European Commission, 2017).

To provide context for our discussion, we must reflect on our own experiences. Of the twelve authors of this paper, four identify as BAME (we use the term 'BAME' for Black, Asian and minority ethnic throughout this piece for consistency with HESA terminology, but recognize that this homogenizes different identities and obscures experiences felt by one race or ethnicity). The majority of us have not been the victim of direct racism. We approach this from the perspective of concerned geoscience academics rather than scholars in equity, diversity and inclusion (EDI), although a number of us have EDI responsibilities in institutions or charities. Our aim is to highlight the situation and promote the need for action. Geoscientists in both industry and academia should work together to listen to diverse voices, challenge biases and transform geoscience culture to be more inclusive and accountable.

Factors involved in racial inequity in UK geoscience

The data

While the absolute number of UK-domiciled students who identify as BAME (defined as Black, Asian, 'mixed' and 'other' in UK Census and HESA ethnicity data) in UK higher education (HE) has grown by >150,000 since 2003, there remain pronounced disparities between white and BAME students in their retention into postgraduate research (AdvanceHE, 2019b) These disparities vary between disciplines, and between ethnic groups within the BAME identifier.

Physical geography, geology and environmental sciences are the three worst physical science subjects for BAME student undergraduate participation in UK HE, and are very poor for retention of these students into PGR (HESA, 2019a). In the 2011 UK Census, 18.5% of UK 18–24-year-olds were from BAME backgrounds (ONS, 2011). However, just 5.2% of physical geography, 6.9% of environmental science and 10.4% of geology PGR students identified as BAME in 2018/19. These statistics are far lower than physical science subjects with the highest BAME PGR representation (22.5% in materials science and 14.8% in chemistry).

On average, over the past five years just 1.4% of geology PGR students were Black (HESA, 2019a), even though 3.8% of UK 18–24-year-olds identify as Black (ONS, 2011). During the last five years, there have been two years for both geology and physical geography when *no* Black women took up full-time PGR study. Retention of BAME physical geography and environmental science students into PGR was worse in 2018/19 than over the five years from 2014/15 to 2018/19 (five-year mean shown in Figure 4.1); the situation is not improving with time (HESA, 2019a).

Notes on the data

HESA publish 'subject of study by ethnicity' data broken down by level of study for 2014/15 to 2018/19 on their website (HESA, 2019a). Data from 1994/95 to 2014/15 are available (HESA, 2021), but are not broken down by type of postgraduate study (research versus taught), or fully by ethnicity ('mixed' and 'other' ethnic categories are grouped); these archive data are therefore not used here. We use the term 'geoscience' here to group physical geography, geology and environmental science (due to HESA categories), but recognize our recommendations are applicable to a variety of allied disciplines. Note that the 'physical sciences' HESA subject area includes chemistry, materials science, physics, forensic and archaeological sciences, astronomy, geology, science of aquatic and terrestrial environments (equivalent to environmental science), and physical geographical sciences. Although we present quantitative data up front, we acknowledge that qualitative studies (some of which we reference herein; see our extended reference list in the Appendix 3 Supplementary Information), voices and insights are vital in this discussion.

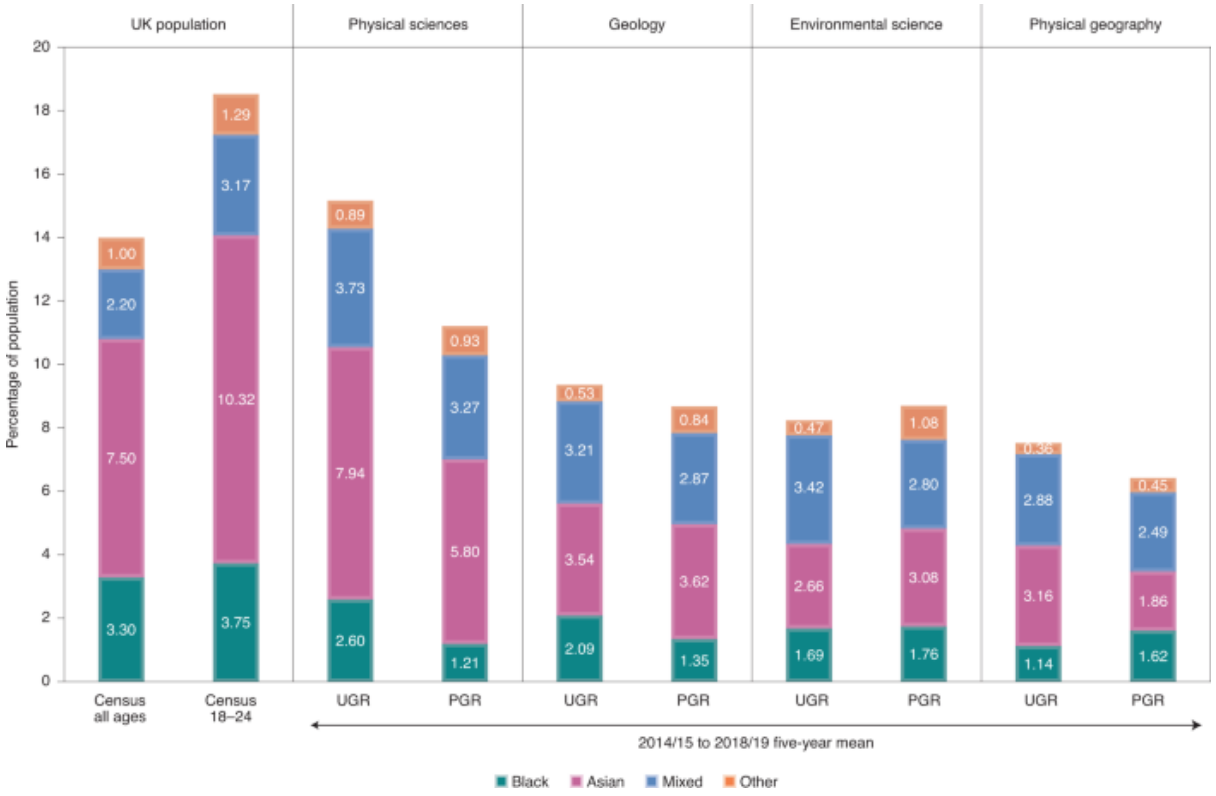


Figure 4.1 Representation of BAME students in geology, environmental science and physical geography. Data taken from UK HESA (2019a). Shown alongside data for the overall physical sciences subject area and ethnicity data from the 2011 UK Government Census (ONS, 2011). HESA data are based on full-time 'all undergraduate' (UGR) and full-time 'postgraduate research' (PGR) categories and are a five-year mean of data from 2014/15 to 2018/19.

Pre-university

Fundamental lack of acknowledgement that geoscience is deeply rooted in, and built on, colonialism, white power, violence, exploitation and slavery pervades relationships in the present and is a barrier to forging equitable partnerships (Marín-Spiotta et al., 2020).The stereotype of a geoscientist as a white man, compounded by the perception that geoscience is an outdoors-only activity (and perpetuated by marketing materials that feature white students in rugged backgrounds), is particularly discouraging to those from minority ethnic backgrounds.

In a recent Geological Society of London survey, 60% of undergraduate geology students mentioned a lifelong interest in the natural environment. Natural environments are less accessible to children from urban settings (which are more ethnically diverse; over 98% of Black African, Pakistani and Bangladeshi people live in urban locations in the United Kingdom (ONS, 2018)) and children from low-income households (more likely to be Pakistani, Bangladeshi, Chinese or Black than white in the United Kingdom (ONS, 2020)). The UK Department for Environment, Food and Rural Affairs report that 18% of children living in the most deprived areas never visit the countryside, with Black and Asian families the least likely group to visit rural areas.

Furthermore, a career in postgraduate geoscience research may not be seen to offer the financial security of other professions, such as medicine, by some communities (Fernando & Antell, 2020).

Retention into postgraduate research and beyond

BAME students applying to high-tariff, research-intensive, institutions are less likely to be accepted than white students with comparable qualifications. For example, BAME applicants to mathematical, physical and life sciences subjects at Oxford are 5.8% less likely to receive an offer than their white counterparts, even after accounting for prior attainment and course choice (Inge, 2020). In 2018/19, Black students made up just 3.9% of students at high-tariff universities, compared to 12.2% at low-tariff universities (HESA, 2019a).

Once at university, BAME students are less likely to gain a first or 2:1 degree classification than their white peers. A range of factors have been proposed to explain this but an *unexplained* gap still exists, probably due to unconscious bias and inequitable frameworks within HE that disadvantage Black and minority ethnic students (Leading Routes, 2019).

Aspects of the PhD application process, such as preference for high-tariff university graduates and selection using metrics that reflect access and resource availability more than student achievement, disproportionately detriment marginalized and under-represented students (Giles et al., 2020). Just 9% of UK Research and Innovation (a UK national funding body) studentships were awarded to ethnic minorities in 2018/19 (UK Research and Innovation, 2020); a dismal statistic considering that 19.4% of 18–34-year-olds identify as BAME (ONS, 2011). These numbers are even lower for the Natural Environment Research Council (a UK national funder of natural science), with just 6% of studentships going to ethnic minorities (UK Research and Innovation, 2020).

Having role models to identify with is important to foster a sense of belonging in the scientific community; a lack of BAME representation at faculty level has been linked to BAME students not continuing to PGR. Across the United Kingdom just 10.8% of professors are BAME (Higher Education Statistics Agency, 2019b), but of the 2,390 staff working in Earth, marine and environmental sciences in 2018/19 only 90 (3.9%) were BAME, the second lowest figure of all science, engineering and technology disciplines (AdvanceHE, 2019a). This 'institutional whiteness' can result in feelings of isolation, and the few BAME staff present being relied upon to be representative of all BAME issues and burdened with advancing equality without meaningful reward.

The geosciences have additional subject-specific hostile environments (Marín-Spiotta et al., 2020) that may deter BAME students from continuing in PGR. Fieldwork requirements create barriers to ethnic minorities, for reasons including cultural sensitivity (for example, co-educational residential trips), cost, inclusivity and racial harassment (Giles, Jackson, & Stephen, 2020; Anadu, Ali, & Jackson, 2020). The 'alcohol culture' in many geoscience departments and at conferences presents barriers to inclusivity for students who do not drink, who are more likely to be from BAME backgrounds (Fernando & Antell, 2020).

Note that some of the above issues are intersectional; BAME students may experience overlapping barriers depending on their gender, sexuality, disability, class, or nationality (Crenshaw, 1989), particularly in the field. Building a culture more inclusive to BAME students can broaden participation to a range of minority groups.

What can we do about it?

Decolonization

There has been a growing demand for academia to contend with its colonial links and institutional whiteness (Peters, 2015). In geoscience we reference the likes of Adam Sedgwick and Henry de

la Beche in our teaching but rarely mention their links to slavery, which are now being recognized. We teach mapping, surveying and mining geology but we rarely explain how these activities link to the growth of the British Empire (Stafford, 1984), or modern destruction of Indigenous sites. Moving forward geoscientists must reflect and engage with social scientists and historical scientists to explore these links, so that they can be taught through the positive lens of geoethics (Di Capua, G., Peppoloni, S. & Bobrowsky, 2017).

The relationship of field-based disciplines with the land has typically taken a colonial approach of white, Western field scientists visiting a location, removing samples (often with the help of local people), then extricating this knowledge and publishing it in paywalled, Western journals (often without local co-authors). This work may disrespect the customs and beliefs of Indigenous communities (Reano, 2020). In a study focussed on First Nation communities, Datta (2018) explains successful, sustainable 'land-based education', which understands the land as dynamic, as relational (for example, spiritual), and as linked to well-being. We can learn from studies like this and be more cognizant of the cultural backgrounds of both our field sites and students during fieldwork, particularly if work is conducted in the Global South or Indigenous lands.

Inclusive teaching

Geoscience is vital in developing a more sustainable society, and a critical aspect of sustainable development is the reduction of inequalities (goal 10 of the United Nations Sustainable Development Goals). Sustainability in geography, Earth and environmental science in HE is considered by Gormally (2019) who advocates for interdisciplinarity, diversity of approach, and moving beyond environmental sustainability to include social, cultural and political perspectives.

By teaching a geoscience curriculum more focussed on global perspectives of sustainability, and less on (typically white) traditional geoscience perspectives, we can create a more relevant and inclusive curriculum to students of all races and ethnicities (Stewart & Gill, 2017).

Representation

We can invest resources in racially diverse promotional materials and ambassador schemes that reward outreach work (Bernard & Cooperdock, 2018) and do not disproportionately place the burden on BAME students (Gewin, 2020). We can also support grass-roots initiatives to amplify BAME voices in geoscience (for example, Black In Geoscience and Black Geographers), and invite diverse geoscience researchers to deliver departmental seminars and showcase innovative science. Crucially, we must increase the diversity of our faculty staff, by implementing BAME staff development opportunities (like StellarHE) to counterbalance structural racism, mitigating under-representation and facilitating career progression.

Subject awareness

By working further back along the student life cycle, we can make it easier for those from BAME communities to connect with nature. Natural heritage organizations need to work closely with community leaders to welcome and nurture positive experiences for BAME children and young people in green spaces. Black2Nature camps run by youth campaigner and environmentalist Mya-Rose Craig have opened pathways that have enabled young people from deprived areas in Bristol to learn about birding, conservation and wildlife; universities can play a part in similar activities through outreach.

Removing barriers

A variety of practical steps can be taken to make field trips more inclusive for ethnic minority students. By fully subsidizing trips and equipment costs, departments can remove barriers to students from low-income backgrounds. To ensure students feel safe from discrimination, field leaders can incorporate recommendations laid out by Anadu and others (2020), including racial risk assessments, anti-discrimination and allyship training, and full documentation of race-related incidents. Trips should be developed with a careful focus on the skills and learning outcomes needed for modern geoscience employment, with mitigations in place to allow all students to achieve them. Professional bodies should reform accreditation requirements around mandatory days in the field. We can create a more inclusionary space by promoting positive accounts and perspectives of fieldwork from minority groups, challenging and disrupting the dominant white, male image of fieldwork.

Ring-fenced opportunities, such as funded research experiences, summer schools, internships and studentships, are clear and evidenced pathways to increased chances of progression for under-represented groups (Dutt, 2019). Working collaboratively with schools, colleges and other universities can make such initiatives more viable and increase their reach.

We can hold funding organizations and institutions accountable for transparency in their recruitment processes (Giles et al., 2020) and form interview panels that understand these barriers, helping to ensure improved diversity in successful applicants (Dutt, 2019). We can push for the publication of candidate demographic data at application, interview, offer and acceptance stages, to provide a clearer picture of postgraduate recruitment diversity (Giles et al., 2020).

Effective, long-lived initiatives

Initiatives do not end at recruitment. Allocating more resources to training in equity and inclusion, and creating more ‘champions’ of diversity to support the interests of minority groups and encourage reflection within geoscience departments, would be a significant step forward in removing hostile environments.

To ensure our efforts are effective and long-lived, we must submit funding bids for evidence-driven action research that works to address data gaps, advocates for real change and develops strategies to broaden participation. We can work with other subjects and bodies facing similar challenges, sharing transferable solutions across the HE sector.

Crucially, we need to acknowledge the hostile environments that deter BAME students from both applying to, and continuing with, our discipline. These problems are real and felt by many (Ali, 2021). We must address personal and structural biases, and go beyond this to be actively anti-racist. The less diverse a field is, the more prevalent implicit biases become (Dutt, 2020). We must act now, and have those difficult conversations, to create a modern geoscience research culture that reflects the diverse nature of the planet we study.

Acknowledgements

We thank C. Souch of the Royal Geographical Society, L. Herringshaw and L. Gallant.

Competing interests

The authors declare no competing interests.

Additional information

Supplementary information

The online version contains supplementary material available at https://doi. org/10.1038/s41561-021-00737-w.

Peer review information

Nature Geoscience thanks Kathleen Quardokus Fisher and the other, anonymous, reviewer(s) for their contribution to the peer review of this work. Primary Handling Editor: James Super.

List of references

AdvanceHE. 2019a. *Equality in Higher Education: Staff Statistical Report 2019*. Available from: https://www.advance-he.ac.uk/knowledge-hub/equality-higher-education-statistical-report-2019.

AdvanceHE. 2019b. *Equality in Higher Education: Students Statistical Report 2019*. Available from: https://www.advance-he.ac.uk/knowledge-hub/equality-higher-education-statistical-report-2019

Ali, H. 2021. Call for a robust anti-racism plan for the geosciences. *Change.org*. Available from: https://www.change.org/p/geoscientists-call-for-a-robust-anti-racism-plan-for-the-geosciences

Anadu, J., Ali, H. & Jackson, C. 2020. Ten steps to protect BIPOC scholars in the field. *Eos*, **101**, 30– 31. Available from: https://doi.org/10.1029/2020EO150525

Bernard, R.E. & Cooperdock, E.H.G. 2018. No progress on diversity in 40 years. *Nature Geoscience*, **11**, 292– 295. Available from: https://doi.org/10.1038/s41561-018-0116-6

Crenshaw, K. 1989. Demarginalizing the Intersection of Race and Sex: A Black Feminist Critique of Antidiscrimination Doctrine, Feminist Theory and Antiracist Politics. *University of Chicago Legal Forum*, **1989**(1), 139-167.Available from: http://chicagounbound.uchicago.edu/uclf/vol1989/iss1/8

Datta, R.K. 2018. Rethinking environmental science education from indigenous knowledge perspectives: an experience with a Dene First Nation community. *Environmental Education Research*, **24**(1), 50–66. Available from: https://doi.org/10.1080/13504622.2016.1219980

Di Capua, G., Peppoloni, S. & Bobrowsky, P.T. 2017. The Cape Town statement on geoethics. *Annals of Geophysics*, **60**, 1– 6. Available from: https://doi.org/10.4401/ag-7553

Dutt, K. 2019. Promoting racial diversity in geoscience through transparency. *Eos*, **100**. Available from: https://doi.org/10.1029/2019EO136977

Dutt, K. 2020. Race and racism in the geosciences. *Nature Geoscience*, **13**, 2– 3. https://doi.org/10.1038/s41561-019-0519-z

European Commission. 2017. *Analysis and comparative review of equality data collection practices in the European Union: Data collection in the field of ethnicity*. Available from: https://data.europa.eu/doi/10.2838/447194

Fernando, B., & Antell, G. 2020. *Recommendations for improving racial equality, diversity, and inclusion in the Department of Earth Sciences, University of Oxford*. Available from: https://www.earth.ox.ac.uk/wp-content/uploads/2020/06/BAME-EDI-Report.pdf

Gewin, V. 2020. The time tax put on scientists of colour. *Nature*, **583**, 479–481 Nature 583, 479-481. Available from: https://doi.org/10.1038/d41586-020-01920-6

Giles, S., Bond, A., Britton, B., Ford, H., Greene, S., Grieve, S., Jackson, C., Lengger, S., Littler, K., & Pancost, R. 2020. Open letter concerning CDT and DTP student recruitment across the UK [Open letter]. Available from: https://docs.google.com/document/d/1EInAKFl7px2DxYv-sAZxVOyTjkm-AE29CzFFnjxw6hg/edit.

Giles, S., Jackson, C., & Stephen, N. 2020. Barriers to fieldwork in undergraduate geoscience degrees. *Nature Reviews Earth & Environment*, **1**, 77–78. Available from: https://doi.org/10.1038/s43017-020-0022-5.

Gillborn, B.D. 2005. Education policy as an act of white supremacy: Whiteness, critical race theory and education reform. *Journal of Education Policy*, **20**(4), 485–505, Available from: https://doi.org/10.1080/02680930500132346

Gormally, A. 2019. The role of sustainability in HE and the GEES disciplines; recommendations for future practice. *Journal of Geography in Higher Education*, **43**(4),599–608. Available from: https://doi.org/10.1080/03098265.2019.1660627

Higher Education Statistics Authority. 2019a. *Higher Education Staff Data*. Available from: https://www.hesa.ac.uk/data-and-analysis/staff.

Higher Education Statistics Authority. 2019b. *Personal Characteristics by Subject of Study*. Available from: https://www.hesa.ac.uk/data-and-analysis/students/what-study/characteristics.

Higher Education Statistics Authority. 2021. *Publications archive*. Available from: https://www.hesa.ac.uk/data-and-analysis/publications.

Inge, S. (2020, June 11). Scale of Oxford's 'white bias' laid bare by internal report. *Research Professional News*. Available from: https://www.researchprofessionalnews.com/rr-he-student-trends-2020-6-scale-of-oxford-s-white-bias-laid-bare-by-internal-report/

Leading Routes. 2019. *The Broken Pipeline*. Available from: https://leadingroutes.org/mdocs-posts/the-broken-pipeline-barriers-to-black-students-accessing-research-council-funding.

Marín-Spiotta, E., Barnes, R.T., Berhe, A.A., Hastings, M.G., Mattheis, A., Schneider, B., & Williams, B.M. 2020. Hostile climates are barriers to diversifying the geosciences. *Advances in Geosciences*, **53**, 117–127. Available from: https://doi.org/10.5194/adgeo-53-117-2020

Office for National Statistics. 2018. *Regional Ethnic Diversity*. Available from: https://www.ethnicity-facts-figures.service.gov.uk/uk-population-by-ethnicity/national-and-regional-populations/regional-ethnic-diversity/latest

Office for National Statistics. 2020. *Child poverty and education outcomes by ethnicity*. Available from:

https://www.ons.gov.uk/economy/nationalaccounts/uksectoraccounts/compendium/economicreview/february2020/childpovertyandeducationoutcomesbyethnicity#child-poverty-and-ethnicity.

Office for National Statistics. 2011. *Population of England and Wales*. Available from: https://www.ethnicity-facts-figures.service.gov.uk/uk-population-by-ethnicity/national-and-regional-populations/population-of-england-and-wales/latest

Peters, M.A. 2015. Why is My Curriculum White? *Educational Philosophy and Theory*, **47**(7), 641-646. Available from: https://doi.org/10.1080/00131857.2015.1037227

Reano, D. 2020. Using Indigenous Research Frameworks in the Multiple Contexts of Research, Teaching, Mentoring, and Leading. *The Qualitative Report*, **25**(11), 3902-3926. Available from: https://doi.org/10.46743/2160-3715/2020.4317

Stafford, R.A. 1984. Geological Surveys, Mineral Discoveries, and British Expansion, 1835–71. *The Journal of Imperial and Commonwealth History*, **12**(3), 5–32. Available from: https://doi.org/10.1080/03086538408582669.

Stewart, I.S., & Gill, J.C. 2017. Social geology — integrating sustainability concepts into Earth sciences. *Proceedings of the Geologists' Association*, **128**(2),165–172, Available from: https://doi.org/10.1016/j.pgeola.2017.01.002

UK Research and Innovation. 2020. *Diversity Results for UKRI funding data 2014/15 to 2018-19*. Available from: https://www.ukri.org/files/about/ukri-diversity-report/

Chapter 5

Between a rock and a workplace

Published paper

Lawrence, A.[1]

Nature Geoscience, 2021. 14, 454-455. https://doi.org/10.1038/s41561-021-00775-4

I am the sole author of this work. Thanks is offered to my parents and Carl Stevenson for their unwavering support and to Jon Oldfield for his illuminating discussions and encouragements to aim high in terms of outlets for publication. Chris Atchison is also thanked for giving an affirmative nod to an early version of this manuscript. Further acknowledgement is given to James Super and Simon Harold for their editorial assistance, for being sensitive and deeply respectful in their communication and, most of all, for inviting someone with lived experience of disability to contribute to the discussion on disability in the geosciences.

[1]School of Geography, Earth and Environmental Sciences, University of Birmingham, Birmingham, UK

Working spaces and cultures in the geosciences need to change in order to attract, safeguard and retain people with disabilities.

Introduction

The one billion or so people living with disabilities represents one of the planet's largest minorities, making up 15% of the global population (United Nations, 2021). Physical, learning, sensory and unseen disabilities are present throughout societies regardless of race, ethnicity, age, religion, gender or sexual orientation. Students, staff and researchers who identify as disabled, however, remain sorely under-represented in academia, and the geosciences are no exception (Carabjal et al., 2017).

Field-based disciplines like the geosciences present well-established challenges to those with disabilities. As such, over the past decade, increasing emphasis has been placed on making fieldwork more accessible and also on promoting office- or laboratory-based careers within the geosciences that do not involve a fieldwork component (Stokes et al., 2019). Yet, for disabled geoscientists, fieldwork isn't the whole story. The institutional workplace and its cultures can prove just as inaccessible and exclusionary as the most rugged and inhospitable environs.

Exclusion from the outset

When one has a disability, starting out in academic geoscience can feel like an impossible task. Workplaces often present a host of physical and sensory issues ranging from a lack of accessible bathrooms to laboratories with flickering lights to lecture halls that are unable to accommodate wheelchair users (De Picker, 2020).

While it's easy to assume that home-based working, which has proliferated during the COVID-19 pandemic, could augment all accessibility problems, this is not necessarily the case. Geoscientists often require access to specialist equipment and facilities to carry out their research; one cannot readily run rock powders through an XRF spectrometer, take CT scans of fossils or conduct thermogravimetric analyses of clay minerals at home.

It follows that many disabled geoscientists face a dilemma from the outset. Staying at home offers more flexibility in work patterns and control over the working environment, but substantially constrains the scope of one's research. In contrast, at the institutional workplace the research possibilities can be almost limitless but one has to endure being in an environment that often wasn't built with disability in mind — a feat that requires great emotional labour and resilience on the disabled individual's part (Inckle, 2018).

Falling flat when fitting in

As well as the inaccessibility of the physical workplace, departmental attitudes can be a source of exclusion for disabled people. Outward indications of disabilities can draw negative responses; inability to verbalize or give eye contact may be perceived as disinterest or, worse, incompetence (Kingsbury et al., 2020), and similarly academic ability may be judged on the basis of physical appearance alone (Brown and Boardman, 2011)

Furthermore, workplace cultures aren't always inclusive. For example, the ubiquitous morning coffee break, often perceived to promote wellbeing, good conversation and networking amongst staff, can actually present an anxiety-provoking test of endurance to those with sensory or neurological disabilities rather than something to look forward to.

It is in such seemingly simple situations as these that disabled people must make the most difficult decisions. Trying to fit in with the normative departmental culture risks one's mental and physical health but bears the allure of potential social acceptance and inclusion. Likewise, playing it safe and staying away can lead to being typecast as the office recluse and forever met with fear, suspicion and pity (or combinations thereof) from one's able colleagues (Stone & Colella, 1996).

Ableist academic systems

Many of the building blocks of academic systems are inherently ableist. The requirement to continuously produce research makes little allowance for those who need more time to process information (Olsen et al., 2020) or need to pace their work to manage chronic pain and fatigue. Pressure to disseminate research through seminars, conferences and public outreach talks (in both virtual and face-to-face formats) automatically excludes those who are non-verbal or verbally limited from making positive contributions.

It can thus be seen that the sustained demonstration of 'excellence' that modern academia incessantly demands (Moore et al., 2017) is at odds with disabled people whose very appearance, communication style or work patterns defy notions of convention and normality.

Gaining ground

In recent years, especially during the pandemic, there has been much looking-inwards from the geoscience community regarding systemic barriers to inclusion for disabled people and other marginalized groups. However, while it's important to discuss problems pertaining to diversity, action is needed to gain ground in addressing these issues. The time has come for looking outwards, as so often solutions already exist; it's just knowing where to find them and how they can be recontextualised.

Embedding inclusion in the workplace is by no means a novel idea; numerous social enterprises and consultancy firms can offer bespoke guidance, assessments and coaching to help organizations, including multinational corporations like Microsoft and JPMorgan Chase and Co., to create and maintain working environments and practices that accommodate those with disabilities (Annabi et al., 2019). Therefore, while bold disability statements are a start, realizing these ambitions will depend on institutional leaders seeking and listening to the readily available advice from outside agencies and following the examples of best practice in other sectors.

Alongside institution-wide change, funding bodies and departmental managers specifically involved with the geosciences must also make visible commitments to disability-hiring initiatives (Erickson et al., 2014). More managerial positions need to be filled by disabled people, who have personal insight into the everyday realities of being 'other'. In this way, those with lived experience are actively involved in decision-making and can help create respectful cultures and welcoming spaces within departments where disabled scholars can thrive.

We, as geoscientists, can also learn much from our colleagues in the humanities and social sciences who are increasingly exploring collaborative research involving mixed groups of disabled and non-disabled academics, in which the strengths of different members are used to make up for the challenges experienced by other individuals within the group (Rosqvist et al., 2019).

Finally, in the geosciences, we are well-versed in time — after all, we have even managed to categorize the entire history of Earth into comprehensible intervals, each marked by key events. It is therefore essential that, starting today, we make meaningful changes so that the systemic exclusion of disabled people from the geosciences doesn't become the lasting legacy of the Anthropocene.

List of references

Annabi, H., Crooks, E.W., Barnett, N., Guadagno, J., Mahoney, J.R., Michelle, J., Pacilio, A., Shukla, H. & Velasco, J. 2019. *Autism @ Work Playbook: Finding talent and creating meaningful employment opportunities for people with autism.* ACCESS-IT, The Information School, University of Washington. Available from: https://access-it.ischool.uw.edu/wordpress/access-it-for-individuals-with-autism/autism-work-playbook/

Brown, L. & Boardman, F. 2011. Accessing the field: Disability and the research process. *Social Science & Medicine,* **72**(1), 23–30. Available from: https://doi.org/10.1016/j.socscimed.2010.09.050

Carabajal, I. G., Marshall, A. M. & Atchison, C. L. 2017. A Synthesis of Instructional Strategies in Geoscience Education Literature That Address Barriers to Inclusion for Students With Disabilities. *Journal of Geoscience* Education, **65**(4), 531–541. Available from: https://doi.org/10.5408/16-211.1

De Picker, M. 2020. Rethinking inclusion and disability activism at academic conferences: strategies proposed by a PhD student with a physical disability. *Disability & Society*, **35**(1), 163–167. Available from: https://doi.org/10.1080/09687599.2019.1619234

Erickson, W. A., von Schrader, S., Bruyère, S. M., VanLooy, S. A. & Matteson, D. S. 2014. Disability-Inclusive Employer Practices and Hiring of Individuals With Disabilities. *Rehabilitation Research, Policy, and Education*, **28**(4), 309–328. Available from: http://doi.org/10.1891/2168-6653.28.4.309

Inckle, K. 2018. Unreasonable adjustments: the additional unpaid labour of academics with disabilities. *Disability & Society,* **33**(8), 1372–1376. Available from: https://doi.org/10.1080/09687599.2018.1480263

Kingsbury, C. G., Sibert, E. C., Killingback, Z. & Atchison, C. L. 2020. "Nothing about us without us:" The perspectives of autistic geoscientists on inclusive instructional practices in geoscience education. *Journal of Geoscience Education*, **68**(4), 302–310. Available from: https://doi.org/10.1080/10899995.2020.1768017

Moore, S., Neylon, C., Paul Eve, M., O'Donnell, D. P. & Pattinson, D. 2017. "Excellence R Us": university research and the fetishisation of excellence. *Palgrave Communications*, **3**, Article 16105. Available from: https://doi.org/10.1057/palcomms.2016.105

Olsen, J., Grifths, M., Soorenian, A. & Porter, R. 2020. Reporting from the Margins: Disabled Academics Reflections on Higher Education. *Scandinavian Journal of Disability Research,* **22**(1), 265–274. Available from: http://doi.org/10.16993/sjdr.670

Rosqvist, H. B., Kourti, M., Jackson, D., Brown, C., Fletcher, K., Bendel, D. and O'Dell, L. 2019. Doing it differently: emancipatory autism studies within a neurodiverse academic space. *Disability & Society*, **34**(7-8), 1082-1101. Available from: https://doi.org/10.1080/09687599.2019.1603102

Stokes, A., Feig, A. D., Atchison, C. L. & Gilley, B. 2019. Making geoscience fieldwork inclusive and accessible for students with disabilities. *Geosphere*, **15**(6),1809–1825. Available from: https://doi.org/10.1130/GES02006.1

Stone, D. L. & Colella, A. 1996. A Model of Factors Affecting the Treatment of Disabled Individuals in Organizations. *The Academy of Management Review*, **21**(2), 352–401. Available from: https://doi.org/10.2307/258666

United Nations. (2021, July 27). *Disability and Higher Education: Workforce Preparedness for Students with Disabilities.* United Nations Academic Impact, United Nations. https://www.un.org/en/disability-higher-education-workforce-preparedness-students-disabilities

Competing interests

The author declares no competing interests.

Chapter 6

Six simple steps towards making GEES fieldwork more accessible and inclusive

Published paper

Lawrence, A.[1] and Dowey, N.[2]

Area, 2021. 54, 52-59. https://doi.org/10.1111/area.12747

This publication originated as ideas shared over cups of lukewarm flask coffee and squished flapjack bars during fieldwork, which were later expressed in small seminars between earth science and geography colleagues, and a subsequent a blog post, before finally being committed to writing.

My contributions included: conceptualization of the paper, writing the paper and subsequently reviewing and editing the paper. Assistance in editing the initial manuscript for brevity and clarity and navigating the peer-review process was provided by Natasha Dowey.

[1]School of Geography, Earth and Environmental Sciences, University of Birmingham, Birmingham, UK

[2]Department of Natural and Built Environment, College of Social Sciences and Arts, Sheffield Hallam University, Sheffield, UK

Abstract

Fieldwork is a defining aspect of Physical Geography, Earth and Environmental Science (GEES) programme curricula. At its best, fieldwork offers students valuable opportunities to develop independent research skills in real- world situations, examine analogues for a range of scientific concepts, and socialise with peers. It offers experiences that are challenging to replicate using virtual/remote learning. However, at its worst, traditional fieldwork practice and culture can present barriers to access and hostile environments that epitomise the broader equity, diversity, and inclusivity problems faced by GEES disciplines. With the role of fieldwork increasingly being called into question, here we promote simple adaptations that can make fieldwork more accessible and enjoyable for all.

Keywords

accessibility, diversity, equity, fieldwork, GEES, inclusivity

Introduction

Fieldwork is a key aspect of most Physical Geography, Earth and Environmental Science (GEES) degrees. From sampling Caledonian granites in Ireland, to measuring water turbidity in the Zambezi River, to logging sedimentary sequences in Utah, to using drones to analyse glaciers in Iceland, fieldwork means so many different things to geographers, earth, and environmental scientists.

Yet this diversity of field environments is not mirrored by the wider GEES community itself. Numerous publications have now demonstrated that these disciplines have alarmingly poor representation of disabled, ethnic minority, and LGBTQ+ scientists (e.g., Bernard & Cooperdock, 2018; Dowey et al., 2021; Dutt, 2020; Stokes et al., 2015). This growing awareness of the need for improved equity, diversity, and inclusivity (EDI), together with the unprecedented travel disruption wrought by COVID-19, has led to the role of fieldwork in GEES education increasingly being the subject of debate (e.g., Dzombak, 2020a; Pickrell, 2020; Giles et al., 2020).

Fieldwork has been the subject of significant criticism for its “masculine, eurocentric origins, assumptions and languages” (Bracken & Mawdsley, 2004). In their 2014 survey of field scientists from some 30 different countries, Clancy et al. (2014) found mistreatment of female early career academics to be widespread, with 71% of female respondents having experienced sexual harassment during fieldwork and over a quarter reporting sexual assault. Frequently encountered fieldwork cultures, including heavy drinking, partying, and “banter” (Nairn, 1996), have served to exclude those with markers of difference, especially ethic minority, LGBTQ+, and disabled scientists (Hall et al., 2004; Nairn, 2003; Pickrell, 2020).

GEES fieldwork involves inherent barriers to individuals from minority groups, including expense, physical exertion, alcohol culture, and access to toilets (Abeyta et al., 2021; Dowey et al., 2021; Greene et al., 2020). Even where fieldwork costs are covered, the expense of field equipment and clothing is a problem for researchers from low socio-economic upbringings, who are disproportionately from minority ethnic backgrounds in Global North countries like the UK (Office for National Statistics, 2020). For some cultures, residential stays in mixed accommodation (Nairn, 2003), or the scheduling of field courses with regards to the religious calendar, may cause concern. Furthermore, fieldwork traditionally takes place in remote, rural, racially homogenous

locations, where ethnic minority researchers may be more likely to face racism (Anadu et al., 2020).

In taught fieldwork, these barriers may be heightened by a lack of flexibility to adapt field locations or sites to be more inclusive for all and by employing the standard “transmission” model of teaching, which is not conducive to active participation of students and student-centred learning (Barr & Tagg, 1995; Michael, 2006).

Many authors maintain that fieldwork is a defining and indispensable aspect of GEES curricula. While it may be supplemented through virtual or non-field-based activities (particularly during the current conditions of the COVID-19 pandemic), these alternatives cannot replicate the learning experiences from outdoor fieldwork (Giles et al., 2020; Sima, 2020; Stokes et al., 2019). Fieldwork is a compulsory part of GEES curricula; in the UK, the Quality Assurance Agency for Higher Education Benchmark Statements for these disciplines refer to fieldwork as “core” and “essential” (QAA, 2019a, 2019b). We cannot, therefore, make GEES disciplines more inclusive by simply removing outdoors working, or by converting it wholesale into something different. We instead must adapt our practice in the field to create more inclusive outdoor working experiences. Embedding EDI considerations into fieldwork is ethical best-practice, and a crucial step in removing the barriers that fieldwork poses to access, participation, and retention of minority researchers in GEES.

In this contribution we draw on our lived experiences as a mixed ethnicity, autistic, non-binary, early career geoscientist and a white, female, physical geography lecturer with experience in industry, respectively. We do not seek to focus on any particular minority or marginalised identity but rather to offer straightforward, holistic recommendations for removing some frequently overlooked barriers and stressors that can occur in the field. Our hope is that these proposed adaptations will help make fieldwork a more accessible and rewarding experience for all.

The Six Steps

Planning is key

Fieldwork has always been prone to challenges. Poor weather, unexpected lack of access to outcrops, vehicle breakdown, a lack of toilets. Overcoming such setbacks is arguably part of the “hidden curriculum” (Jackson, 1968), building resilience and transferable skills in students that they can draw on in future careers. However, for some students, simply participating in a field trip can be challenging, due to pre-existing financial, physical, racial, and/or emotional barriers (Stokes et al., 2019). It follows that if participants experience further adversity in the field, it may affect confidence and be a deterrent to undertaking future fieldwork or pursuing careers in field-based disciplines.

GEES educators are trained to undertake broad planning for health and safety scenarios in the field. However, more can be done to ensure preparedness for a wide range of other challenging situations, some of which have serious health and safety implications. For example, Prior-Jones et al. (2020) recommend embedding inclusion into risk assessments so that greater consideration is given to hazards and appropriate mitigations that particularly affect those from minorities with protected characteristics such as disability, gender reassignment, marriage and civil partnership, religion or belief, sex, and sexual orientation. Anadu et al. (2020) provide detailed recommendations to protect fieldwork participants from racism and prejudice, including racial risk assessments and antidiscrimination training for field leaders.

Kingsbury et al. (2020) advocate creating daily schedules that factor in non-academic aspects of working in the field, such as taking breaks from working in groups to preclude overstimulation and related meltdowns/shutdowns in autistic individuals.

Considered logistical preparation, involving lists of alternative accessible outcrops, digital resources, and plans B, C, and D, may be crucial in avoiding demoralisation and disengagement, particularly for students with disabilities. Although devising backup plans may require creativity and additional effort on the trip organiser's part, having alternatives such as wet-weather activities can be beneficial for entire student cohorts and can easily be reused for each presentation of the field course (Houghton et al., 2020; Figure 6.1).

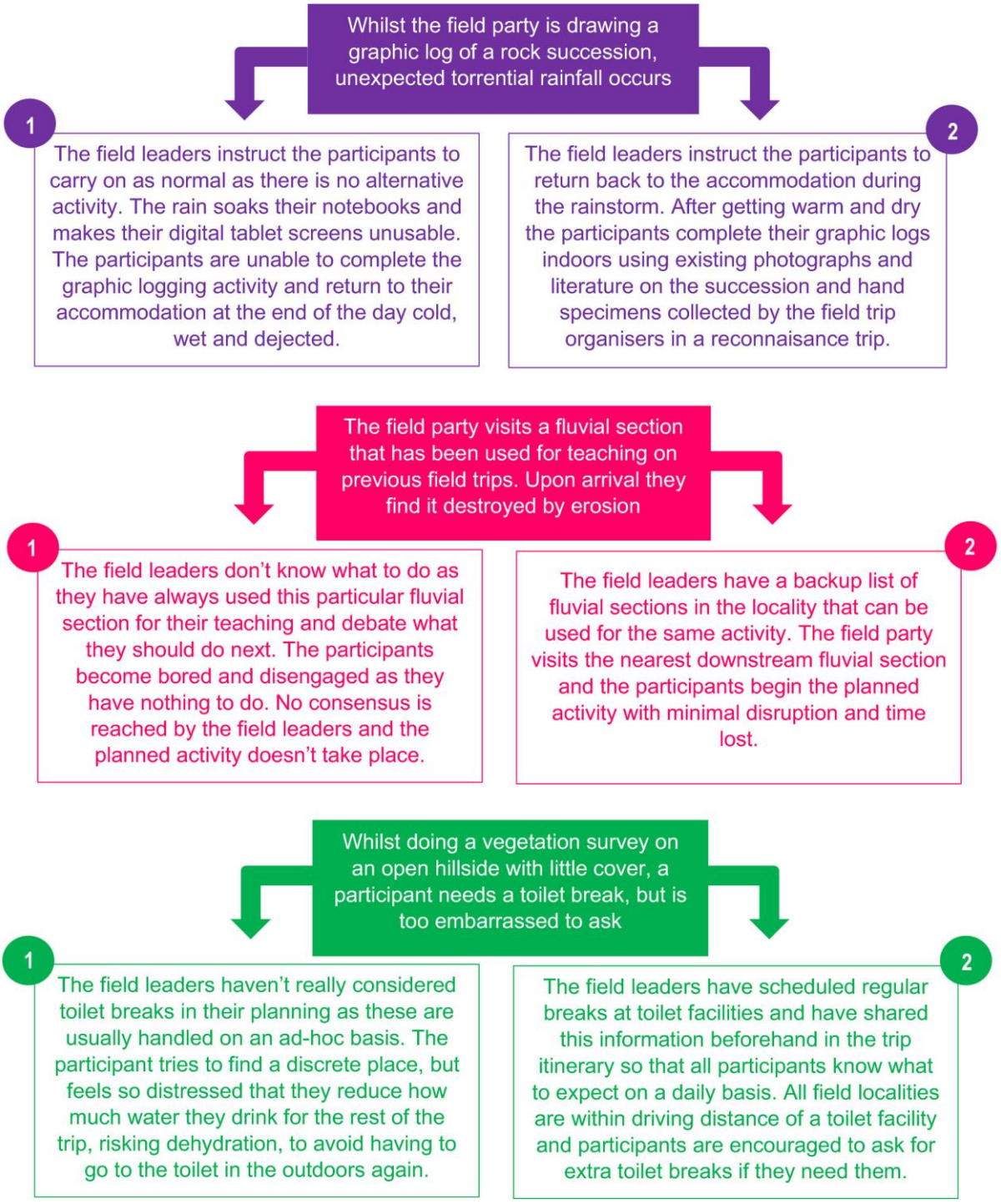


Figure 6.1 Example problems in the field and outcomes. Outcome 1 results from rudimentary fieldwork planning while outcome 2 reflects more considered planning

Field leaders can be open about their mitigations and planning, promoting measures made to improve accessibility and also training students on how to problem-solve when planning their own independent field activities.

Fun not fear

Experiences shared on social media in recent years have revealed a glimpse of the discrimination faced by minority geoscientists in the field (e.g., Anadu, 2020; Larson, 2020; Litchfield, 2020). Even where comprehensive fieldwork planning and preparation is undertaken, such experiences could understandably discourage some, leading them to forgo fieldwork altogether because of fear. For LGBTQ+ geographers, fear of travelling to countries where their status is criminalised (Mackay, 2021; Olcott & Downen, 2020); for ethnic minority geoscientists, fear of experiencing racism (Anadu et al., 2020); for disabled environmental scientists, fear of being in unfamiliar and poorly accessible areas far from the safety net of home and professional healthcare support (Hall & Healy, 2005; Stokes et al., 2019; Tucker & Horton, 2018).

Although these concerns may be difficult to fully address, a good first step is to remove problematic destinations, such as countries that criminalise homosexuality, from field itineraries altogether (Jackson, 2021; Murphy, 2020). To further ensure that all participants can feel safe and find fun in their field experiences, a complete package of support should be offered that goes beyond the standard field trip leader, health and safety officer, or informal buddy schemes.

Assigning personal assistants or mentors to vulnerable individuals can enhance inclusion and access in field environments, especially if the mentor is someone with shared experiences that allow them to relate well to their mentees (Olcott & Downen, 2020). This mentor/assistant can liaise with their mentees prior to the field course, to gain understanding of their personal and cultural circumstances and abilities. As well as ensuring that all prospective mentors and field staff are offered general training in allyship (Anadu et al., 2020), institutions must adopt a flexible approach to fieldwork mentoring, working on a case-by-case basis. Institutional disability service providers may not have the pedagogic experience or familiarity with GEES disciplines required to provide appropriate mentoring support for academics outside of traditional workplace settings (Feig et al., 2019). For example, the first author of this study is provided assistance by their parents in the field as, being full-time carers, they have the greatest insight into the author's disability, including how it affects them on a day-to-day basis and their specific needs in the context of geoscience fieldwork.

On arrival at the field locality, mentors could offer a meet-and-greet service for their mentees to replace any initial feelings of trepidation and anxiety with a sense of welcome and belonging. During the fieldwork itself, mentors should maintain regular communication with their mentees to assess how much support they require to feel comfortable and effectively engage in the learning experience (Hendricks et al., 2017).

While universities and colleges may not consider it their responsibility to provide off-campus support (Anadu et al., 2020), they do have a duty of care to ensure the safety and wellbeing of all staff and students, and it is important that individuals who need it have the safety net of a designated person who can listen and respond to their concerns as they arise.

Skills over hills

A key aim of field training is to allow scientists to gain practical, transferable skills that they can reuse in the future when independently gathering primary data.

However, skills development can be undermined not only by safety concerns but also by fieldwork cultures. It is well reported that a machismo culture of “we must visit that outcrop because it's there” pervades fieldwork in many physical science disciplines (e.g., Fitzpatrick, 2020; Hall et al.,

2004; Maguire, 1998). This may lead to a focus on who can “bag” the most locations, rather than who is able to accurately conduct the analyses necessary. Where fieldwork grades into adventure tourism rather than a purposeful, educative experience, it reinforces casual ableism and excludes people with disabilities (Pickrell, 2020; Tucker & Horton, 2018).

To create more inclusive instructional environments and equitable access to the field, these traditional attitudes and hostile climates must be dismantled. Part of this effort involves institutions reviewing materials used to promote fieldwork, which routinely depict white, physically fit scientists in rugged outdoor settings (Atchison & Libarkin, 2016; Dowey et al., 2021; Hall et al., 2004).

Careful and considered field work design is also needed (Gilley et al., 2015). For example, where a field locality presents accessibility issues, the trip organisers should endeavour to find an alternative that is easily reachable for those with mobility issues or lower levels of physical fitness. Where this isn't feasible, portable Wi-Fi networks and mobile technology can provide students remote access to the inaccessible field site and thereby create an environment conducive to active participation and social inclusion, as demonstrated through the Enabling Remote Activity (ERA) approach pioneered by the Open University (Collins et al., 2016).

In this way, no students need to miss out on experiencing outdoor field activity and related opportunities to build skills just because they are unable to reach the outcrop at the end of a slippery, rocky beach, or atop the highest, most difficult hill.

One size never fits all

Another factor that can deter GEES scientists from participating in outdoor field activities is the course length. The prospect of spending many days or even weeks in the field can raise significant anxieties, not just for students but for scientists at various different levels within the academic hierarchy (Tucker & Horton, 2018).

Whereas postgraduates and more senior academics often have independence to determine the duration of fieldwork that they undertake for their own research, undergraduates and teaching staff involved in field courses rarely have the autonomy to decide.

Therefore, institutions should be open to creating more flexible fieldwork timetables that allow for several shorter field courses or daytrips. This may be preferable to the concentrated social environment, typically long working hours and intense nature of a multiday residential trip, which for some is an “ordeal” rather than a constructive experience (Tucker & Horton, 2018). This has the added advantage of providing thinking and planning time in between field trips; students and staff can reflect on what worked well for them on a trip and whether this can be replicated during their next field visit. Likewise, they can consider what didn't work so well and how this could be improved next time.

Another consideration here is financial (Abeyta et al., 2021). Field skills training in overseas locations, when not fully subsidised, is an expensive and inaccessible option for many researchers. The feasibility of offering domestic trips, that offer the same degree of pedagogic rigour and generate similar learning outcomes (Figure 6.2), should be considered for those with caring responsibilities, on a restricted budget, and/or not wanting to stray too far from home.



Figure 6.2 Different destinations, same aims. The authors of this study photographing field exposures of igneous rocks in overseas (left) and domestic (right) destinations

Embracing diversity – and being actively anti-prejudice

As well as offering flexibility in terms of field work destinations and course lengths, when working with those from diverse backgrounds it is important to show open-mindedness and acceptance towards different personal needs and requirements.

For example, autistic individuals may need to carry a tactile object like a blanket, engage in stimming, or use toys such as fidget spinners, to help maintain focus and cope with the myriad of external sensory stimuli in field environments (Kingsbury et al., 2020).

Researchers who are practising religious fasting may have eating patterns that differ from the traditional meal times that many field courses are structured around. In these cases, leaders should avoid scheduling trips during religious fasting periods such as Ramadan, where possible. If this is unavoidable, and students practising fasting are participating in the fieldwork, leaders must ensure that suitable food is available at the appropriate times (including suitable gluten-free, vegetarian, vegan, halal, and kosher options), and that the trip does not involve an unnecessarily high level of strenuous physical exertion. The risk assessment of the trip should be adapted to include the possibility of students experiencing acute dehydration or fainting. Furthermore, to promote the positive wellbeing of those from various religious groups, it is essential that the accommodation in residential field courses contains quiet, suitable spaces for worship and prayer that can be used in between field activities (Advance HE, 2018; Equality Change Unit, 2009).

Research indicates that 40% of trans and 52% of non-binary people in the UK feel they must adjust the way they dress to avoid discrimination or harassment (Stonewall, 2018). Being given the freedom to dress in outdoor gear and clothing that they feel comfortable and confident wearing is essential for trans and non-binary individuals (Dzombak, 2020b). Furthermore, careful consideration of toilet and changing facilities on fieldtrips is necessary to ensure that everyone can safely use these spaces. Fieldwork leaders should avoid unnecessary gender divisions (e.g., girls queue on the left), ensure that there is universal provision available at the accommodation, and bear in mind that not all trans people feel comfortable using public conveniences (Gendered Intelligence, 2020).

Whatever the difference, tolerance must be extended towards those from underrepresented groups to make the field a more welcoming and diverse place.

Carry on the conversation

It is imperative that the critical thought provoked by the coronavirus pandemic about field work accessibility and inclusion remains at the forefront of our minds long after lockdowns and travel restrictions have ceased. The momentum must continue in order to improve equity, diversity, and accessibility within GEES and associated field work (Sima, 2020).

To see positive, lasting change take effect, those who have been previously excluded should be included in the dialogue and lead the conversation going forward (Scarpelli, 2017). Social media, focus groups, and workshops (Pickrell, 2020) are powerful forums through which academics, fieldwork leaders, and those in management roles can be educated on the challenges faced by minority groups. Conferences, such as those held on accessible virtual platforms during the pandemic (see Batty & Worsfold, 2021; iCRAG, 2021), can enable solution-focused discussions to take place within the wider GEES community and provide opportunities for disseminating information on best practice to broad, international audiences.

Summary

The six steps outlined here (Figure 6.3) have the potential to create meaningful change and transform the nature of fieldwork. They can also form part of broader conversations about ethical code of conduct within departments. Increasing accessibility of GEES subjects is very much aligned to the Cape Town Statement of Geoethics, one of the fundamental values of which is to "promote geoeducation for all" (Di Capua et al., 2017). Our suggestions are broad, and what is perceived as "ethical practice" may differ among different groups and individuals. For that reason, it is important that we listen to diverse groups, and are flexible to actioning their thoughts and ideas where possible. If we do not act on their concerns, we risk losing unique and irreplaceable geographers, earth scientists, and environmental scientists not only from the field, but from our disciplines altogether.



Figure 6.3 Summary of the six simple steps towards making fieldwork more accessible and inclusive

Acknowledgements

The authors kindly acknowledge Chris Jackson and Jaqueline Houghton for reading an early draft and providing encouraging feedback. We are grateful to Alison Stokes and two other anonymous

reviewers for their very detailed, insightful, and constructive comments, which helped us greatly improve our text. We would also like to thank Phil Emmerson and Julian Leyland for their editorial assistance.

Data availability statement

No new data were created.

List of references

Abeyta, A., Fernandes, A.M., Mahon, R.C. & Swanson, T.E. 2021. The true cost of field education is a barrier to diversifying geosciences. *EarthArXiv*. Available from: https://doi.org/10.31223/X5BG70

Advance, H.E. 2018. *Religion and belief: Supporting inclusion of staff and students in higher education and colleges*. Available from: https://www.advance-he.ac.uk/knowledge-hub/religion-and-belief-supporting-inclusion-staff-and-students-higher-education-and.

Anadu, J. (2020, June 22). Black thoughts: Hazards of field work while Black [Video]. *Youtube*. Available from: https://www.youtube.com/watch?v=W0B7xwGkl00

Anadu, J., Ali, H. & Jackson, C. 2020. Ten steps to protect BIPOC scholars in the field. *Eos*, **101**, 30– 31. Available from: https://doi.org/10.1029/2020EO150525

Atchison, C.L. & Libarkin, J.C. 2016. Professionally held perceptions about the accessibility of the geosciences. *Geosphere,* **12**(4), 1154– 1165. Available from: https://doi.org/10.1130/ges01264.1

Barr, R.B. & Tagg, J. 1995. From teaching to learning – A new paradigm for undergraduate education. *Change*, **27**(6), 13– 25.

Batty, L. & Worsfold (2021, March 17). Post-COVID teaching in ecology – Reflections from our BES Festival of Ecology workshop. *BES Teaching and Learning*. Available from: https://besteachingandlearning.wordpress.com/2021/03/17/post-covid-teaching-in-ecology-reflections-from-our-bes-festival-of-ecology-workshop/

Bernard, R.E. & Cooperdock, E.H.G. 2018. No progress on diversity in 40 years. *Nature Geoscience*, **11**, 292– 295. Available from: https://doi.org/10.1038/s41561-018-0116-6

Bracken, L. & Mawdsley, E. 2004. 'Muddy glee': Rounding out the picture of women and physical geography fieldwork. *Area*, **36**(3), 280– 286. Available from: https://doi.org/10.1111/j.0004-0894.2004.00225.x

Clancy, K.B.H., Nelson, R.G., Rutherford, J.N. & Hinde, K. 2014. Survey of Academic Field Experiences (SAFE): Trainees report harassment and assault. *PLoS One*, **9**(7), e102172. Available from: https://doi.org/10.1371/journal.pone.0102172

Collins, T., Davies, S. & Gaved, M. 2016. Enabling remote activity: Widening participation in field study courses. In: D. Kennepohl (Ed.) *Teaching science online: Practical guidance for effective instruction and lab work* (pp. 183– 195). Sterling, VA: Stylus Publishing.

Di Capua, G., Peppoloni, S. & Bobrowsky, P.T. 2017. The Cape Town statement on geoethics. *Annals of Geophysics*, **60**, 1– 6. Available from: https://doi.org/10.4401/ag-7553

Dowey, N., Barclay, J., Fernando, B., Giles, S., Houghton, J., Jackson, C., Khatwa, A., Lawrence, A., Mills, K., Newton, A., Rogers, R. & Williams, R. 2021. A UK perspective on tackling the geoscience racial diversity crisis in the Global North. *Nature Geoscience*, **14**, 256– 259. Available from: https://doi.org/10.31223/osf.io/z4cju

Dutt, K. 2020. Race and racism in the geosciences. *Nature Geoscience*, **13**, 2– 3. https://doi.org/10.1038/s41561-019-0519-z

Dzomback, R. (2020a, July 22). It's time to change the geosciences' outdated, exclusionary, and ableist field requirements [Blog post]. *Sister*. Available from: https://sisterstem.org/2020/07/22/its-time-to-change-the-geosciences-field-requirements/

Dzomback, R. (2020b, October 28). Queer visibility in geoscience has been almost nonexistent for decades. A new generation is working to change that [Blog post]. *Speaking of Geoscience*™. Available from: https://speakingofgeoscience.org/2020/10/28/queer-visibility-in-geoscience-has-been-almost-nonexistent-for-decades-a-new-generation-is-working-to-change-that/

Equality Change Unit 2009. *Religious observance in higher education: Facilities and services.* Available from: https://www.ecu.ac.uk/publications/religious-obs-facilities.

Feig, A.D., Atchison, C.L., Stokes, A. & Gilley, B. 2019. Achieving inclusive field-based education: Results and recommendations from an accessible geoscience field trip. *The Journal of Scholarship of Teaching and Learning*, **19**(2), 66– 87. Available from: https://doi.org/10.14434/josotl.v19i1.23455

Fitzpatrick, A. (2020, March 17). You will never be Indiana Jones. *Lady Science* [Blog post]. Available from: https://www.ladyscience.com/essays/you-will-never-be-indiana-jones-toxic-masculinity-archaeology.

Gendered Intelligence. 2020. *All gender toilet signs*. Available from: http://genderedintelligence.co.uk/professionals/resources/toilets.

Giles, S., Jackson, C. & Stephen, N. 2020. Barriers to fieldwork in undergraduate geoscience degrees. *Nature Reviews Earth & Environment*, **1**, 77– 78. Available from: https://doi.org/10.1038/s43017-020-0022-5

Gilley, B.H., Atchison, C.L., Feig, A. & Stokes, A. 2015. Impact of inclusive field trips. *Nature Geoscience*, **8**, 579– 580. Available from: https://doi.org/10.1038/ngeo2500

Greene, S., Ashley, K., Dunne, E., Edgar, K., Giles, S. & Hanson, E. (2020). Toilet stops in the field: An educational primer and recommended best practices for field-based teaching. *OSF Preprints*. https://doi.org/10.31219/osf.io/gnhj2

Hall, T., Healey, M. & Harrison, M. 2004. Fieldwork and disabled students: Discourses of exclusion and inclusion. *Journal of Geography in Higher Education*, **28**(2), 255– 280. Available from: https://doi.org/10.1080/0309826042000242495

Hall, T. & Healey, M. 2005. Disabled students' experiences of fieldwork. *Area*, **37**(4), 446– 449. https://doi.org/10.1111/j.1475-4762.2005.00649.x

Hendricks, J.E., Atchison, C.L. & Feig, A.D. 2017. Effective use of personal assistants for students with disabilities: Lessons learned from the 2014 accessible geoscience field trip. *Journal of Geoscience Education*, **65**(1), 72– 80. https://doi.org/10.5408/16-185.1

Houghton, J.J., Morgan, D.J., Gordon, C.E., Stokes, A., Atchison, C.L., Collins, T.D., Craven, B. & Willis, K. 2020. Access Anglesey 2018: Lessons from an inclusive field course. *Advances in Geosciences*, **53**, 183– 194. https://doi.org/10.5194/adgeo-53-183-2020

iCRAG. 2021. EDIG Conference. https://www.icrag-centre.org/edig/conference/

Jackson, P. 1968. *Life in classrooms*. New York, NY: Holt, Rinehart and Winston.

Jackson, C. (2021, March 1). Some barriers are invisible. *Geoscientist*, Spring, 202, 16. Available from: https://geoscientist.online/wp-content/uploads/2021/03/GEO_SPRING_2021_WEB.pdf.

Kingsbury, C.G., Sibert, E.C., Killingback, Z. & Atchison, C.L. 2020. “Nothing about us without us:” The perspectives of autistic geoscientists on inclusive instructional practices in geoscience education. *Journal of Geoscience Education*, **68**(4), 302– 310. Available from: https://doi.org/10.1080/10899995.2020.1768017

Larson, C. (2020, September 15). Calling out racism, Black scientists say they face discrimination while doing fieldwork. *Chicago Sun Times*. Available from: https://chicago.suntimes.com/2020/9/15/21436543/black-scientists-racism.

Litchfield, E. 2020. ‘Widespread ableism is exhausting’: What it’s like being a disabled student at Soton. *The Southampton Tab*. Available from: https://thetab.com/uk/soton/2020/10/20/how-soton-uni-are-failing-disabled-students-84771.

Mackay, A. (2021, April, 27). Out in the field. *Geography Directions: Pride in the field*. Available from: https://blog.geographydirections.com/2021/04/27/out-in-the-field/

Maguire, S. 1998. Gender differences in attitudes to undergraduate fieldwork. *Area*, **30**(3), 207–214. Available from: https://doi.org/10.1111/j.1475-4762.1998.tb00065.x

Michael, J. 2006. Where’s the evidence that active learning works? *Advances in physiology education*, **30**(4), 159– 167. Available from: https://doi.org/10.1152/advan.00053.2006

Murphy, V. (2020, July 3). Geoscience course stops running Oman fieldtrip to be more inclusive. [Press release]. Available from: https://www.imperial.ac.uk/news/198915/geoscience-course-stops-running-oman-fieldtrip/

Nairn, K. 1996. Parties on geography fieldtrips: Embodied fieldwork? *Women's Studies Journal*, **12**(2), 86– 97.

Nairn, K. 2003. What has the geography of sleeping arrangements got to do with the geography of our teaching spaces? Gender, place and culture. *A Journal of Feminist Geography*, **10**(1), 67–81. Available from: https://doi.org/10.1080/0966369032000052667

Office for National Statistics. 2020. *Child poverty and education outcomes by ethnicity*. Available from: https://www.ons.gov.uk/economy/nationalaccounts/uksectoraccounts/compendium/economicreview/february2020/childpovertyandeducationoutcomesbyethnicity#child-poverty-and-ethnicity.

Olcott, A.N. & Downen, M.R. 2020. The challenges of fieldwork for LGBTQ+ geoscientists. *Eos*, **101**, 22– 24. Available from: https://doi.org/10.1029/2020EO148200

Pickrell, J. (2020, March 11). Scientists push against barriers to diversity in the field sciences. *Science*, **374**. Available from: https://doi.org/10.1126/science.caredit.abb6887

Prior-Jones, M., Pinnion, J., Millet, M.-A., Bagshaw, E., Fagereng, A. & Ballinger, R. (2020, May 4-8). An inclusive risk assessment tool for travel and fieldwork. [Conference presentation]. *EGU*

General Assembly 2020, Online. Available from: https://doi.org/10.5194/egusphere-egu2020-7678.

Quality Assurance Agency. 2019a. *Subject Benchmark Statement: Earth Sciences, Environmental Sciences and Environmental Studies*. Available from: https://www.qaa.ac.uk/docs/qaa/subject-benchmark-statements/subject-benchmark-statement-earth-sciences-environmental-sciences-and-environmental-studies.pdf.

Quality Assurance Agency. 2019b. *Subject Benchmark Statement: Geography*. Available from: https://www.qaa.ac.uk/docs/qaa/subject-benchmark-statements/subject-benchmark-statement-geography.pdf.

Scarpelli, A. (2017, 19 October). How I realized that LGBT+ scientists like me can inspire others in their field. *Massive. Science*. [Blog post]. Available from: https://massivesci.com/articles/stem-lgbt-diversity-science/

Sima, R.J. 2020. Accessibility and fieldwork in the time of coronavirus. *Eos*, **101**. Available from: https://doi.org/10.1029/2020EO147056

Stokes, A., Feig, A., Atchison, C. & Gilley, B. 2019. Making geoscience fieldwork inclusive and accessible for students with disabilities. *Geosphere*, **15**(6), 1809– 1817. Available from: https://doi.org/10.1130/GES02006.1

Stokes, P., Levine, R. & Flessa, K.W. 2015. Choosing the geoscience major: Important factors, race/ethnicity, and gender. *Journal of Geoscience Education*. **63**(3), 250– 263. Available from: https://doi.org/10.5408/14-038.1

Stonewall. 2018. *LGBT in Britain - Trans report*. Available from: https://www.stonewall.org.uk/lgbt-britain-trans-report.

Tucker, F. & Horton, J. 2018. “The show must go on!” Fieldwork, mental health and wellbeing in Geography, Earth and Environmental Sciences. *Area*, **51**(1), 84– 93. Available from: https://doi.org/10.1111/area.12437

Chapter 7

Muddy Glee at the crossroads: How can we consider intersectionality more holistically in fieldwork?

Invited submission

Lawrence, A.[1]

Area

Following the publication of Lawrence and Dowey (2021; see also Chaper 6) I was invited to author a *Classics Revisited* feature by the editors of *Area* journal. The classical article in question was Bracken and Mawdsley's paper "Muddy Glee" (published in 2004), a paper which sought to both explore the reasons behind gender discrimination for women involved in physical geography fieldwork *and* celebrate the positive field experiences and accounts of female physical geographers.

Whilst Bracken and Mawdsley (2004) most certainly did critique the masculinist frame of reference that dominated physical geography fieldwork at the time, gender is not the sole axis of marginalisation that can be encountered in field-based disciplines, as I found through my own field experiences as a disabled and minority ethnic scientist. Therefore, I naturally took an interest in revisiting "Muddy Glee" to offer an intersectional perspective that, much in keeping with the original paper, sought to 'disrupt' traditional views of fieldwork.

However, as someone who does not neatly conform to the male/female binary, one could argue that my 'disruption' extends to "Muddy Glee" in itself, as a paper that follows mainstream Western society's crude classification of gender into two distinct, opposing forms.

I am the sole author of the manuscript, responsible for conceptualising and writing the piece and navigating the editorial process. Guidance and advice was kindly provided by Natasha Dowey.

[1]School of Geography, Earth and Environmental Sciences, University of Birmingham, Birmingham, UK

Abstract

Almost two decades after its original publication, I revisit Bracken and Mawdsley's (2004) *Muddy Glee*; a landmark paper concerned with the inclusion of women in fieldwork. Whilst *Muddy Glee* made great strides towards raising awareness of gender discrimination in field-based disciplines, I argue that greater understanding of intersectionality is needed to address the exclusion(s) that those with multiple markers of difference, including but not limited to gender, continue to face in fieldwork.

Introduction

I was interested to get involved in this Classics Revisited piece because even 17 years after *Muddy Glee* was written, fieldwork is still not a truly 'shared space'. In this contribution I argue that to 'promote a wider view' of fieldwork, as Bracken and Mawdsley (2004) endeavoured in *Muddy Glee*, an understanding of the intersecting forms of marginalisation and gatekeeping at play in fieldwork is critical. I consider this by reflecting on how my own intersectionality has shaped my experiences of fieldwork. I conclude that greater awareness of intersectionality is needed by fieldwork leaders and participants if we are to 'reclaim the field' for underrepresented groups; including, but not limited to, women.

Intersectionality in action

Bracken and Mawdsley's (2004) seminal piece was a positive step forward in disrupting and critiquing the image of Physical Geography fieldwork as a masculine endeavour. The paper gave important female viewpoints on fieldwork, and advocated normalising modern and diverse methods of fieldwork that could be more inclusive than the "arduous activity", "long stays in remote, inhospitable and often hazardous environments" and social cultures characterised by "heavy drinking and general 'homo-sociability' " that may deter women from fieldwork.

However, what *Muddy Glee* didn't fully consider is that challenging this 'mainly-male' frame of reference and traditional way of working in the field can benefit many other minority groups aside from women. The groups and hierarchies issues raised in the original paper are very much relatable to the feelings of isolation, lack of support, discrimination, or outright harassment that those from other groups have reported in field contexts (e.g. Carabajal et al., 2017; Olcott & Downen, 2020; Jackson, 2021; Rackley, 2021). In highlighting these issues, it would perhaps be more inclusive to discuss these challenges intersectionally, acknowledging the overlaps and variants between groups- for example, a woman of colour may experience the challenges described in *Muddy Glee*, whilst also dealing with threats of racism, racial exclusion or isolation. In order to change the perception of what fieldwork is, and what it involves, it is paramount that we apply an intersectional lens, acknowledging the overlaps and variants in the oppressions and challenges faced by different marginalised identities (Crenshaw, 1991).

Stretching our definitions of what fieldwork is makes it more inclusive to a range of diverse groups. Those with chronic illnesses may be reassured that fieldwork does not have to entail trekking up mountains or other such ardour. Those from cultures who have been historically excluded from nature, may be heartened that fieldwork does not necessitate visiting green spaces where racial prejudice can be encountered. Those with disabilities may be relieved to know that fieldwork does not have to involve long stays away from home support networks and healthcare services. Fieldwork can entail visits to repositories as part of a data collection strategy. It can include

working in urban spaces. It can involve virtual trips or, as suggested in *Muddy Glee*, the use of GIS.

Gatekeepers to the field

Muddy Glee challenges the coding and perception of fieldwork as a masculine endeavour, and explains that societal boundaries continue to be "drawn around women and the other". This disruption is needed, for sure- but how can it take place holistically, so that multiple groups, and those who identify with intersectional identities, benefit?

If efforts to make fieldwork more inclusive for all are to be successful, it is critical to question who the gatekeepers of fieldwork are. Whilst this line of inquiry isn't actively pursued in Bracken and Mawdsley's (2004) original contribution, the authors do hint at its answer in their nod to the institutional environment. Overlooking intersectionality at an institutional level has potential to impact negatively in a multiplier effect further down the academic hierarchy, into workspaces including the field. This is one of the reasons fieldwork remains "one of the key sites of…discrimination" in Physical Geography and related disciplines 17 years after *Muddy Glee* was written.

Furthermore, systemic discrimination towards a range of protected characteristics impacts upon fieldwork as it is those in positions of power within the institution who are the gatekeepers and policymakers; and most institutional gatekeeping and policymaking fails to consider intersectionality (Miles et al., 2017; Bhakta, 2020). In equality agendas all too often gender is considered as the sole axis of marginalisation (Johnson, 2020) or, worse still, conflated with race such that white women have seen a meteoric rise in representation, power and status in the academy (Bhopal & Henderson, 2019) whilst their LGBTQ+, disabled and ethnic minority counterparts, be they male, female, non-binary or any other gender identity, continue to be underrepresented (Núñez et al., 2019). Expectations of sustained excellence (Moore et al., 2017; Gourlay & Stevenson, 2017) and the intense and seemingly relentless demands of contemporary academic employment (Gill, 2010; Morrish, 2019) can also translate into taught fieldwork, rendering it a focal point of distress and 'ordeal' for staff from underrepresented groups (Tucker & Horton, 2019). For fieldwork to be more inclusive for all, the institutional structures in which fieldwork is planned and carried out need also to be equitable and inclusive.

Personal accounts and framing

Bracken and Mawdsley (2004) seek to 'reclaim' positive accounts and perspectives of women in physical geography fieldwork. They argue that positive framing is vital, in order to reposition the social boundaries that are drawn around the "normal" and the "other" (Nairn, 1998, within Bracken & Mawdsley, 2004). But a fine balance to tread is striving to make those positive stories heard, whilst being open and ready to hear the challenges that underrepresented groups face, and make meaningful changes to address the situation.

As an intersectional individual who has undertaken various fieldwork over the years, and experienced my fair share of muddy and gleeful moments too, I have come to realise that it is not the field that I feel out of place with but rather the practises, politics and power-dynamics that come with it.

For example, I find it disconcerting how prior to each field trip I have to describe the daily struggles and intricacies of my condition to yet another person that I have never even seen, from another committee that I have never heard of, so that they can deem if I am physically and mentally 'fit' to undertake fieldwork. I find it frustrating that I have to provide a dossier of evidence on every risk assessment to justify that I am 'disabled enough' to require my parent carers to assist me in the field. I find it humiliating in group toilet breaks when, due to lack of gender-neutral facilities, I am forced to choose between the 'Ladies' and 'Mens', knowing that my choice doesn't reflect my identity yet will be judged by everyone else all the same. I find it upsetting when senior academics, who are the leaders and mainstays of departmental field trips, greet my white father but turn their faces away and take a sidestep when they see me and my brown mother, as if to avoid walking into the mud. I find it exhausting that I repeatedly ask and then implore and then plead for more holistic, inclusive practices around fieldwork (Lawrence & Dowey, 2021) yet progress in this area, to me, seems haltingly slow. I am sometimes so disappointed in my futile attempts to make change happen that I think I should just give up.

There are others like me that feel the same; tired and battleworn from constantly fighting for their right to exist in academic spaces, weakened from having to report their trauma to unlistening or incredulous ears (Inckle, 2019; Bumpus, 2020; Scarlett, 2021). Some actively avoid or have opted-out of fieldwork altogether, after coming up against barrier after barrier (Tucker & Horton, 2019; Peasland et al., 2021). And I often wonder whether it would just be easier to withdraw from the field altogether and its bounding space of academia, so that I don't have to keep struggling in a place where I don't belong.

But then I ask myself, if I give in then who else will 'reclaim the field' for people like me? Who else will speak these uncomfortable truths in the world of academia where reputation is currency and lip service pays well? Who else will remind the leaders in both the field and the academy that intersectionality isn't simply about buzzwords and box-ticking, numbers and statistics, but different knowledge and unique approaches, lived experiences and personal stories? Who else will talk candidly about the mud and the glee that life at the crossroads brings?

Conclusion

By challenging the persistent cultural framing of GEES disciplines as male domains (Kass-Simon & Farnes, 1993; Blickenstaff, 2005; Hulbe et al., 2010), together with our definitions of what fieldwork is, and indeed what 'place(s)' it plays out in, fieldwork can be made more inclusive to a diverse range of groups. In this way, we can consign Bracken and Mawsdley's (2004) words "Women, people of colour, the unfit, the disabled and the non-heterosexual are out of place when they are 'in' the field" from an everyday reality to a distant memory.

But alongside this reframing and redefining, there is a need to move beyond simple categorisation of identity, lived experience and discrimination in the context of fieldwork and wider academia. Too often, the institution deals with these characteristics separately, or even worse, pits them against one another in a race to the bottom, which invariably privileges gender at the expense of ethnicity, (dis)ability and LGBTQ+ identities (e.g. Johnson & Otto, 2019; Bhopal, 2020).

The gatekeepers to fieldwork- from instructors and assistants; to academic staff and course conveners; to inter-departmental committees and institutional leaders- must further their understanding of the multiple forms of exclusion that are barriers to access and participation in field-based disciplines.

It IS important to reclaim fieldwork- but this can only truly be achieved for women if we take an intersectional approach to the problems raised in *Muddy Glee* and reclaim the field for ALL.

Acknowledgements

Gracious acknowledgement is given to Dr Natasha Dowey for her helpful advice, insightful suggestions and unwavering support- it is because of people like Natasha that people like me CAN find a place in the field, academia and the wider world. No reflection on fieldwork would be complete without mention of plant ecologist Sara Middleton; who embodies “Muddy Glee” to me today, just as the paleoecologist Cathy Whitlock did to Bracken and Mawdsley in years gone by. Special thanks is also given to Dr Carl Stevenson and Dr Luis Escobedo who, between them, have taught me pretty much all that I know about fieldwork methodologies in the physical and social sciences, respectively. And, as always, to mum and dad- the best grumpy field assistants anyone could wish for!

List of references

Bhakta, A. 2020. “Which door should I go through?” (In) visible intersections of race and disability in the academy. *Area*, **52**(4), 687–694. Available from: https://doi.org/10.1111/area.12554

Bhopal, K. & H. Henderson. 2019. Competing Inequalities: Gender versus Race in Higher Education Institutions in the UK. *Educational Review*, **73**(2) 1–17. Available from: https://doi.org/10.1080/00131911.2019.1642305

Bhopal, K. 2020. Confronting white privilege: The importance of intersectionality in the sociology of education. *British Journal of Sociology of Education*, **41**(6), 807–816. Available from: https://doi.org/10.1080/01425692.2020.1755224

Blickenstaff, J.C. 2005. Women and science careers: leaky pipeline or gender filter? *Gender and Education,* **17**(4), 369-386. Available from: https://doi.org/10.1080/09540250500145072

Bracken, L. & Mawdsley, E. 2004. ‘Muddy glee’: Rounding out the picture of women and physical geography fieldwork. *Area*, **36**(3), 280– 286. Available from: https://doi.org/10.1111/j.0004-0894.2004.00225.x

Bumpus, N. 2020. Too many senior white academics still resist recognizing racism. *Nature*, **583**, 661. Available from: https://doi.org/10.1038/d41586-020-02203-w

Carabajal, I.G., Marshall, A.M. & Atchison, C.L. 2017. A Synthesis of Instructional Strategies in Geoscience Education Literature That Address Barriers to Inclusion for Students With Disabilities. *Journal of Geoscience Education*, **65**(4) 531-541. Available from: https://doi.org/10.5408/16-211.1

Crenshaw, K. 1991. Mapping the margins: Intersectionality, identity politics, and violence against women of color. Available from: https://heinonline.org/HOL/LandingPage?handle=hein.journals/stflr43&div=52&id=&page=

Gill, R. 2010. "Breaking the silence: The hidden injuries of neo-liberal academia" *Feministische Studien*, **34**(1), 39-55. Available from: https://doi.org/10.1515/fs-2016-0105

Gourlay, L. & Stevenson, J. 2017. Teaching excellence in higher education: critical perspectives. *Teaching in Higher Education*, **22**(4), 391-395. Available from: https://doi.org/10.1080/13562517.2017.1304632

Hulbe, C., Wang, W., & Ommanney, S. 2010. Women in glaciology, a historical perspective. *Journal of Glaciology*, **56**(200), 944-964. Available from: https://doi.org/10.3189/002214311796406202

Inckle, K. 2018. Unreasonable adjustments: the additional unpaid labour of academics with disabilities. *Disability & Society*, **33**, 1372-1376. Available from: https://doi.org/10.1080/09687599.2018.1480263

Jackson, C. 2021. Some barriers are invisible. *Geoscientist*, Spring 2021, 16. Available from: https://geoscie ntist.online/sections/viewpoint/some-barriers-are-invisible/

Johnson, A. 2020. Refuting “How the other half lives”: I am a woman’s rights. *Area*, **52**(4), 801–805. Available from: https://doi.org/10.1111/area.12656

Johnson, C.P.G. & Otto, K. 2019. Better together: A model for women and LGBTQ equality in the workplace. *Frontiers in Psychology*, **10**, 272. Available from: https://doi.org/10.3389/fpsyg.2019.00272

Kass-Simon, G. & Farnes, P. (Eds.) 1993. *Women of science: righting the record*. Indiana University Press.

Lawrence, A. & Dowey, N. 2021. Six simple steps towards making GEES fieldwork more accessible and inclusive. *Area*, **54**(1), 52-59. Available from: https://doi.org/10.1111/area.12747

Miles, A. L., Nishida, A. & Forber-Pratt, A. J. 2017. An open letter to White disability studies and ableist institutions of higher education. *Dis-ability Studies Quarterly*, **37**(3). Available from: http://dx.doi.org/10.18061/dsq.v37i3.5997

Moore, S., Neylon, C., Eve, M.P., O'Donnell, D.P. & Pattinson, D. 2017. “Excellence R Us”: university research and the fetishisation of excellence. *Palgrave Communications*, **3**, 16105 . Available from: https://doi.org/10.1057/palcomms.2016.105

Morrish, L. 2019. *Pressure Vessels: The epidemic of poor mental health among higher education staff*. Higher Education Policy Institute. Available from: https://www.hepi.ac.uk/wp-content/uploads/2019/05/HEPI-Pressure-Vessels-Occasional-Paper-20.pdf

Nairn, K. 1998. *Disciplining identities: geography, gender and the culture of fieldtrips*. [Unpublished PhD dissertation]. University of Waikato, New Zealand.

Núñez, A.M., Rivera, J & Hallmark, T. 2019. Applying an intersectionality lens to expand equity in the geosciences. *Journal of Geoscience Education*, **68**(2), 97-114. Available from: https://www.tandfonline.com/doi/full/10.1080/10899995.2019.1675131

Olcott, A.N. & Downen, M.R. 2020. The challenges of fieldwork for LGBTQ+ geoscientists. *Eos*, **101**, 22– 24. Available from: https://doi.org/10.1029/2020EO148200

Peasland, E.L., Henri, D.C., Morrell, L.J. & Scott, G.W. 2021. Why do some students opt out of fieldwork? Using expectancy-value theory to explore the hidden voices of non-participants. *International Journal of Science Education*, **43**(10), 1576-1599. Available from: https://doi.org/10.1080/09500693.2021.1923080

Rackley, K. 2021. My experience of geography fieldwork as a trans kid: A call for reflection. *Geography Directions: Pride in the field*. Available from: https://blog.geographydirections.com/2021/09/21/my-experience-of-geography-fieldwork-as-a-trans-kid-a-call-for-reflection/

Scarlett, J.P. 2021. A minority within a minority. *Nature Reviews Earth and Environment*, **2**, 455. Available from: https://doi.org/10.1038/s43017-021-00184-6

Smidt, B.T., Bondestam, F., Pétursdóttir, G. M., & Einarsdóttir, Þ. 2020. Expanding gendered sites of resistance in the neoliberal academy. *European Journal of Higher Education*, **10**(2), 115-129. Available from: https://doi.org/10.1080/21568235.2018.1541753

Tucker, F. & Horton, J. 2019. “The show must go on!” Fieldwork, mental health and wellbeing in Geography, Earth and Environmental Sciences. *Area*, **51**, 84– 93. Available from: https://doi.org/10.1111/area.12437

Chapter 8

Conclusions and outlook

Introduction

Since all the papers that comprise this thesis have their own conclusions, I will avoid repeating them here and instead offer some reflections on the contributions to our understanding offered by each chapter and suggest potential avenues of inquiry and action for the future.

Summary

This thesis has shown that one can draw parallels between constructing the continental crust and building diversity in the Geosciences. Just as granite petrogenesis and emplacement is often pulsatory and incremental in nature, efforts to address structural inequalities, systemic discrimination and exclusionary cultures within academic Geoscience can be equally episodic and prolonged by institutional inaction, departmental unaccountability and personal biases deeper-seated than the continental crust itself.

Diversity of thought and experience are prerequisites for innovation, yet it has been my experience throughout this PhD project that different ways of thinking, working and being in Geoscience, and indeed wider academia itself, are only accommodated by the open-minded few. Divergence may be acknowledged by one's immediate colleagues, and tolerated at a departmental level, but any further up the academic hierarchy it is dismissed or, worse still, actively ridiculed. This is one of the many reasons why academic Geoscience, as it stands, is represented and ruled by a restricted demographic rather than the wider society it serves.

We often talk about systemic discrimination, institutional barriers and colonial epistemologies as if they are abstract concepts, but for those of us who are different they are everyday realities. They are in the office next door, the laboratory down the hallway, the lecture theatre on the ground floor. They are at the end of every email, every manuscript submission, every grant application.

If the Geoscience community is willing to challenge the traditional paradigms growth can occur, but doing so often involves tremendous strain, both for those from minorities, who are burdened with advancing equalities by virtue of their simply being different, and for the ruling powers, who may experience difficulty in recognizing their own privilege and unease in using it to promote more equitable outcomes for others.

Chapter 2

As far as we are aware, this publication represents the most comprehensive multidisciplinary study of an intrusion in the British Caledonides to date, combining geophysical, petrographical and field methods. Our rock magnetic analyses revealed that regional transpression imparted a subtle overprint only on the Ratagain Complex as opposed to a solid-state tectonic fabric. This led us to question earlier worker's interpretations of the crystallisation and emplacement history of the complex, which were typically informed by a singular line of investigation as opposed to the multiple, intersecting lines of evidence that our study generated.

Future workers are encouraged to consider adopting similar approaches which comprise different rock magnetic techniques used in tandem with field studies and petrological work, to provide richer insights on the emplacement histories of igneous intrusions and their siting within regional tectonic regimes.

Chapter 3

As is the case for Chapter 2, the various geoscientific methods in this chapter, whilst often employed in isolation, are complimentary to one another. The geochemical analyses used to establish mantle- and crust-derived contributions to granitic magmas, can be combined with petrological, field and structural methods to gain further insights into the timing and duration of slab breakoff magmatism and its relationship to the varying regional tectonic regimes operating in post-collision orogenic settings. The use of the geoscientific methods in combination provides a thorough, holistic understanding of the growth of continental crust by the emplacement of granitic bodies.

In the specific case of the Late Caledonian granites of Scotland, and indeed the wider British Isles, Chapter 3 has demonstrated that new investigations, involving high-precision geochronology, field studies, petrological analyses and rock structural geology work are needed to better resolve the links between granite petrogenesis, crustal tectonics, the geodynamics of Iapetus subduction, collision and slab breakoff.

Chapter 4

This publication was the first in the growing body of EDI literature to document the lack of racial diversity in UK Geoscience, as previous studies have been concerned with the USA only. A major fallout from this publication was the formation of the EQUATOR Research Group; a collaboration between academics from Sheffield Hallam University, the University of Manchester, the University of Hull and the University of Birmingham with additional partners including the Geological Society of London, the British Geological Survey, the Institution of Environmental Sciences, the Royal Geographical Society and Black Geographers, amongst other professional bodies and grassroots organisations (EQUATOR, 2021). The group's primary focus was to work towards justice, equity, diversity and inclusion in UK GEES disciplines. In the period December 2021-May 2022, EQUATOR secured funding from the Natural Environmental Research Council's "Making environmental science equal, diverse and inclusive" call (UKRI, 2022) to undertake work to improve the engagement and participation of students from ethnic minority backgrounds in UK GEES postgraduate research. Our publication formed the groundwork for all of EQUATOR's proposed interventions to improve the experience and increase retention of ethnic minority students in GEES, including setting up a mentoring network to link students to academic and industry GEES professionals and running a fully-funded, residential training school for undergraduates, postgraduates and postdoctoral researchers from the 9th-13th April 2022. Preliminary participant survey data indicates that the EQUATOR project was a resounding success and we hope to see more of our original published recommendations translate from theoretical to practical action in the future so that we can continue in our work towards building diversity in the Geosciences and related disciplines.

Chapter 5

In Chapter 5, I explain through the lens of my lived experience as a disabled academic, how inaccessible workplaces, normative departmental cultures and 'ableist' academic systems have all contributed to the continued underrepresentation and exclusion of those with disabilities in the Geosciences. It is argued that changes to both working spaces and attitudes are urgently needed if institutions are to attract, safeguard and retain people with disabilities. The chapter makes a series of suggestions about how those with disabilities can be attracted, supported and retained in academic Geosciences. Firstly, it recommends that university leaders taking advice from

outside agencies with experience in embedding inclusion in the workplace, as whilst the routes towards expanding the representation of those with disabilities in employment are well-trodden by other sectors, such as information technology and finance, these pathways are still somewhat unexplored by the academic sector. Visible commitments to disability-hiring initiatives, in particular giving more leadership roles to those with disabilities, are proposed to help create more respectful departmental cultures. Another potential initiative outlined in the article is greater collaboration between disabled and non-disabled geoscientists in research groups. In this way, the strengths and talents of the various researchers can be fully realised whilst the different challenges experienced by each group member can be simultaneously overcome. If implemented readily and thoroughly, all of the above measures could increase the participation, inclusion and empowerment of those with disabilities in the Geosciences.

Chapter 6

In this article we aimed to provide uncomplicated and readily-implementable adaptations to traditional fieldwork practice that can enhance the accessibility of fieldwork for all and help it to become an enjoyable experience. As it ultimately falls to GEES educators and practitioners to uptake our advice, an important conclusion to draw is that widespread dissemination of the Six Simple Steps, and publications like it, is key to prompting meaningful changes to how fieldwork is organised and delivered. To this end, the findings of this publication were arguably the mostly widely communicated of all the papers in this thesis, being presented at some four workshops, three national conferences and two international symposia.

Chapter 7

In Chapter 7, I argue that greater understanding of intersectionality is desperately needed for those with multiple markers of difference, beyond just gender, to be fully included in fieldwork. Whilst Bracken and Mawdsley's (2004) words on physical Geography provided the background for this piece, at its forefront were my lived and learned experiences of undergraduate environmental science and postgraduate geoscience fieldwork. Thus, the concerns raised, challenges described and recommendations proposed are universally applicable to GEES disciplines involving field-based study.

Further work issuing from this publication could involve providing consultancy and training to HEIs on a case-by-case basis, to help fieldwork leads in GEES apply an intersectional lens in assessing their programmes. In this way, existing examples of fieldwork best practice can be acknowledged and celebrated, whilst those areas in need of attention can be modified, drawing on my suggested lines of action as inspiration.

Concluding remarks

Like granitic magmas, the building blocks of the Earth's continental crust, can originate from a plethora of source materials, increasing participation of underrepresented scholars in Geoscience is contingent on multiple stakeholders and an intersectional, multifaceted approach towards socio-cultural identification. And more often than not, in order to make 'room' for both granites in the continental crust and minorities in the Geosciences, considerable tectonic forces are required. But I hope that for all my readers in the Geosciences and beyond, this thesis serves as a rallying cry to create equitable academic spaces in which diversity can flourish, no matter how difficult or uncomfortable breaking from tradition and making meaningful change may seem. For after all, no strain, no gain.

List of references

Bracken, L. & Mawdsley, E. 2004. ‘Muddy glee’: Rounding out the picture of women and physical geography fieldwork. *Area*, **36**(3), 280– 286. Available from: https://doi.org/10.1111/j.0004-0894.2004.00225.x

EQUATOR. 2021. *NERC-Funded Project*. Available from: https://equatorresearchgroup.wordpress.com/nerc-funded-project/

UKRI. (2022, February 17). *Diversity, equity and inclusion research in environmental science.* Available from: https://www.ukri.org/news/diversity-equity-and-inclusion-research-in-environmental-science/

Appendices

APPENDIX 1

Supplementary materials for Chapter 2

Table S1 Summary of anisotropy of magnetic susceptibility data from the Ratagain Complex

Lat/Long decimal				Sample no.	susceptibility data				K1 normalised with directions					K2 normalised with directions					K3 normalised with directions					95% angles in plane		Owens (1974) parameters					Jelenick (1981) parameters						
Lat	Long	Rock type	Description	n	Kmean	K1	K2	K3	K1norm	dec	plunge	K1-K2	K1-K3	K2norm	dec	plunge	K1-K2	K2-K3	K3norm	dec	plunge	Foliation dip azimuth	dip	K1-K3	K2-K3	L	F	M	Mu	H	Lj	Fj	P	P'	T1	Shape	T2
57.221815	-5.487339	Qmd	Qz monzodiorite	12	16170	17188.71	16897.65	14439.81	1.063	209.2	11.4	14.7	8.1	1.045	40.8	78.3	14.5	3.3	0.893	300	2.3	119.7	87.7	9	4	2%	15%	0.1	7	17%	1.02	1.17	1.19	1.21	0.80	oblate	0.80
57.221761	-5.487693	Qmd	Qz monzodiorite	6	21230	23268.08	21590.91	18831.01	1.096	292.8	16.6	11	8.3	1.017	39.9	44.5	12.6	4.5	0.887	188	40.8	7.8	49.2	10.3	5.7	8%	13%	0.6	31	21%	1.08	1.15	1.24	1.24	0.29	oblate-triaxial	0.29
57.221635	-5.488301	Qmd	Qz monzodiorite	11	21900	23980.5	23411.1	18308.4	1.095	193.6	1.5	17.7	5.3	1.069	98	75.2	17.5	6.8	0.836	284	14.7	104	75.3	8.2	3.7	3%	23%	0.1	6	26%	1.02	1.28	1.31	1.35	0.82	oblate	0.82
57.221449	-5.489031	Qmd	Qz monzodiorite	7	19030	21313.6	19962.47	15813.93	1.12	350.8	25.4	35.6	3	1.049	184	64	36.6	4.6	0.831	83	5.2	263.3	84.8	12.7	2.7	7%	22%	0.3	18	29%	1.07	1.26	1.35	1.37	0.56	oblate	0.56
57.22128	-5.489687	Qmd	Qz monzodiorite	7	14440	16071.72	14656.6	12591.68	1.113	353.2	16.6	14.5	4.9	1.015	145	71.3	16.8	5.1	0.872	261	8.3	80.8	81.7	11.4	5.2	10%	14%	0.7	34	24%	1.10	1.16	1.28	1.28	0.24	oblate-triaxial	0.24
57.221181	-5.490095	Qmd	Qz monzodiorite	12	19580	20559	20304.46	17896.12	1.05	144	10	24.1	3.1	1.037	23.7	70.8	24.3	9.9	0.914	237	16.3	56.9	73.7	10.4	3.1	1%	12%	0.1	6	14%	1.01	1.13	1.15	1.17	0.82	oblate	0.82
57.220789	-5.490688	Md	Monzodiorite	10	16090	16556.61	16170.45	15542.94	1.029	341.1	81	13.6	5.3	1.005	87.3	2.5	10.8	2.6	0.966	178	8.7	357.7	81.3	10.3	2.9	2%	4%	0.6	32	6%	1.02	1.04	1.07	1.07	0.25	oblate-triaxial	0.25
57.22053	-5.491227	Qmd	Qz monzodiorite	6	22420	23339.22	23070.18	20850.6	1.041	348	54.2	8.5	5.7	1.029	176	35.5	8.5	3.7	0.93	83	3.6	263.1	86.4	6.8	1.2	1%	10%	0.1	7	11%	1.01	1.11	1.12	1.13	0.79	oblate	0.79
57.224358	-5.522887	Qmd	Qz monzodiorite	6	6055	6176.1	6115.55	5873.35	1.02	241.9	66.2	12.6	7.4	1.01	138	6.2	12.6	2.9	0.97	45	22.8	224.9	67.2	7.5	2.8	1%	4%	0.3	14	5%	1.01	1.04	1.05	1.05	0.61	oblate	0.61
57.22646	-5.523792	Md	Monzodiorite	7	8361	8829.216	8636.913	7616.871	1.056	14.9	45.8	10.3	3.3	1.033	143	30.7	11.1	1.6	0.911	251	28.3	71.2	61.7	4.5	3.3	2%	12%	0.2	11	15%	1.02	1.13	1.16	1.17	0.70	oblate	0.70
57.219817	-5.52528	Qrg	Qz granitoid	11	22070	23350.06	23107.29	19752.65	1.058	179.9	12.2	53.3	3.4	1.047	52	70.6	53.3	5.8	0.895	273	14.8	93.2	75.2	8.5	3.7	1%	15%	0.1	4	16%	1.01	1.17	1.18	1.21	0.88	oblate	0.88
57.220827	-5.416701	Qmd	Qz monzodiorite	7	23420	23911.82	23326.32	23021.86	1.021	162.9	49.8	11.3	3.5	0.996	29.3	30.2	11.3	5.6	0.983	284	23.8	104.4	66.2	5.6	3.5	2%	1%	1.9	63	4%	1.03	1.01	1.04	1.04	-0.31	prolate-triaxial	-0.31
57.221124	-5.416417	G	Granite	6	245.7	251.1054	246.6828	239.3118	1.022	123.8	88.1	25.1	6.3	1.004	223	0.3	25.7	11.6	0.974	313	1.9	133.4	88.1	14.2	8.2	2%	3%	0.6	31	5%	1.02	1.03	1.05	1.05	0.26	oblate-triaxial	0.26
57.221628	-5.416004	Qmd	Qz monzodiorite	7	2230	2294.67	2230	2165.33	1.029	4.7	68.8	11	3.8	1	221	17.4	25.6	6.1	0.971	127	11.8	307.2	78.2	24.4	4.1	3%	3%	1.0	45	6%	1.03	1.03	1.06	1.06	0.01	triaxial	0.01
57.222004	-5.41558	Qmz	Qz monzonite	8	555	581.64	566.1	517.26	1.048	47	68.1	15.5	6.1	1.02	236	21.6	15.6	9.6	0.932	145	3.1	324.8	86.9	9.9	6.4	3%	9%	0.3	18	12%	1.03	1.09	1.12	1.13	0.54	oblate	0.54
57.222954	-5.414447	Qmd	Qz monzodiorite	9	21780	23326.38	22869	19144.62	1.071	268.4	67.2	11	2.8	1.05	98.1	22.5	10.8	5.5	0.879	6.6	3.5	186.6	86.5	5.6	3.1	2%	17%	0.1	7	19%	1.02	1.19	1.22	1.24	0.80	oblate	0.80
57.197948	-5.49609	Mz	Monzonite	10	55140	55415.7	55250.28	54754.02	1.005	73.9	37.6	61.3	25.9	1.002	251	52.4	61.5	36.4	0.993	343	1.2	162.9	88.8	39	25.2	0%	1%	0.3	18	1%	1.00	1.01	1.01	1.01	0.50	oblate	0.50
57.21977	-5.512273	Qmd	Qz monzodiorite	11	1181	1206.982	1183.362	1152.656	1.022	48.4	13.5	17.8	9.7	1.002	140	6.2	17.7	15.8	0.976	254	75.1	74.1	14.9	17.4	6.6	2%	3%	0.8	38	5%	1.02	1.03	1.05	1.05	0.14	triaxial	0.14
57.219379	-5.508627	Md	Monzodiorite	12	9040	9663.76	9320.24	8136	1.069	95.5	42.6	9.3	2	1.031	345	20.5	9.2	1.4	0.9	237	40.4	56.9	49.6	2.5	1.2	4%	13%	0.3	16	17%	1.04	1.15	1.19	1.20	0.58	oblate	0.58
57.218181	-5.50266	Gd	Granodiorite	18	15320	16423.04	15396.6	14140.36	1.072	99.8	56.1	8.2	4.2	1.005	218	17.4	6.9	4.3	0.923	317	28.1	137.3	61.9	8.8	5.8	7%	8%	0.8	39	15%	1.07	1.09	1.16	1.16	0.14	triaxial	0.14
57.221687	-5.473359	Qmd	Qz monzodiorite	8	21470	22564.97	21598.82	20246.21	1.051	359.6	50.7	19.9	4.3	1.006	177	39.3	21.6	3	0.943	268	1.1	88.2	88.9	10	4.2	4%	6%	0.7	36	11%	1.04	1.07	1.11	1.12	0.19	triaxial	0.19
57.221676	-5.473384	Qmd	Qz monzodiorite	8	19610	20139.47	20100.25	18609.89	1.027	14.9	41.4	74	6.8	1.025	161	43.3	74	10.3	0.949	269	17.7	88.5	72.3	14.7	6.6	0%	8%	0.0	2	8%	1.00	1.08	1.08	1.09	0.95	oblate	0.95
57.221753	-5.473324	Qmd	Qz monzodiorite	10	27470	29200.61	28486.39	24695.53	1.063	177.3	10.9	7.8	3.4	1.037	31.1	77	9.5	2.9	0.899	269	7.1	88.7	82.9	6.2	3.4	3%	14%	0.2	11	16%	1.03	1.15	1.18	1.20	0.70	oblate	0.70
57.221883	-5.47331	Qmz	Qz monzonite	7	23760	25637.04	24876.72	20766.24	1.079	346.9	0.1	18.5	5.4	1.047	80.5	87.9	18.5	2.8	0.874	257	2.1	76.9	87.9	5.6	2.8	3%	17%	0.2	10	21%	1.03	1.20	1.23	1.26	0.71	oblate	0.71
57.221858	-5.473368	Gd	Granodiorite	N/A																																
57.222095	-5.473218	Qmn	Qz monzonite	5	14740	15432.78	14784.22	14003	1.047	151.3	77.8	12.8	7.8	1.003	6.8	10	42.2	12.6	0.95	276	7	95.6	83	42.2	8.2	4%	5%	0.8	40	10%	1.04	1.06	1.10	1.10	0.12	triaxial	0.12
57.22213	-5.473193	Qmd	Qz monzodiorite	7	18370	19545.68	19104.8	16459.52	1.064	347	16	14.5	4.6	1.04	176	73.8	15.7	3.3	0.896	78	2.4	257.7	87.6	8.3	5	2%	14%	0.2	9	17%	1.02	1.16	1.19	1.21	0.73	oblate	0.73
57.222171	-5.473074	Qmd	Qz monzodiorite	7	18680	19912.88	19352.48	16774.64	1.066	159.6	55.4	14.7	8.1	1.036	295	26	14.5	3.3	0.898	35	21.2	215.4	68.8	9	4	3%	14%	0.2	12	17%	1.03	1.15	1.19	1.20	0.67	oblate	0.67
57.222337	-5.472689	Qmd	Qz monzodiorite	7	22390	23442.33	22658.68	21068.99	1.047	31.6	63.8	5.1	3.2	1.012	260	18	4.5	1.7	0.941	164	18.4	344.1	71.6	4	1.7	3%	7%	0.5	26	11%	1.03	1.08	1.11	1.12	0.36	oblate-triaxial	0.36
57.222483	-5.472488	Qmd	Qz monzodiorite	10	22380	23275.2	22536.66	21328.14	1.04	220.7	73.6	14.4	3.7	1.007	31.7	16.2	14.2	6.9	0.953	122	2.4	302.4	87.6	7.2	4.8	3%	5%	0.6	31	9%	1.03	1.06	1.09	1.09	0.26	oblate-triaxial	0.26
57.222542	-5.47226	Md	Monzodiorite	11	26520	27925.56	27209.52	24424.92	1.053	1.8	26.1	6.7	4.6	1.026	164	62.7	10.6	6.3	0.921	268	7.2	88.2	82.8	10.7	3.9	3%	11%	0.3	14	13%	1.03	1.11	1.14	1.15	0.61	oblate	0.61
57.222667	-5.472003	Qmd	Qz monzodiorite	12	19920	20756.64	20039.52	18963.84	1.042	19.4	82.1	14.9	3.9	1.006	196	7.9	15.4	8.5	0.952	286	0.5	106	89.5	9.7	4.1	4%	5%	0.7	34	9%	1.04	1.06	1.09	1.10	0.22	oblate-triaxial	0.22
57.223223	-5.464256	Qmd	Qz monzodiorite	6	27470	28898.44	28623.74	24887.82	1.052	258.9	52.7	27	3.1	1.042	111	32.7	27.3	6	0.906	11	15.9	190.8	74.1	7.5	2.6	1%	14%	0.1	4	15%	1.01	1.15	1.16	1.18	0.87	oblate	0.87
57.222709	-5.464695	Qmd	Qz monzodiorite	9	24230	26071.48	24884.21	21758.54	1.076	28.8	14.4	7.5	6.1	1.027	232	74.5	8.8	1.6	0.898	120	5.7	300.3	84.3	6.6	4.9	5%	13%	0.4	21	18%	1.05	1.14	1.20	1.21	0.48	oblate-triaxial	0.48
57.222705	-5.46485	Qmd	Qz monzodiorite	11	19130	20507.36	19703.9	17178.74	1.072	22	7.7	6.1	1.9	1.03	226	81.5	10.8	4.9	0.898	113	3.4	292.5	86.6	10.4	1.5	4%	13%	0.3	18	17%	1.04	1.15	1.19	1.20	0.55	oblate	0.55
57.222623	-5.466385	Qmd	Qz monzodiorite	12	23930	25294.01	24911.13	21584.86	1.057	12.6	13.4	13.2	1.6	1.041	231	73.1	13.5	7.4	0.902	105	10.1	285	79.9	8.1	1.1	2%	14%	0.1	7	16%	1.02	1.15	1.17	1.19	0.81	oblate	0.81
57.222032	-5.46702	Qmz	Qz monzonite	5	22330	23558.15	22888.25	20543.6	1.055	5.2	47.7	12.6	8.5	1.025	189	42.2	12	6.1	0.92	97	2	277.4	88	10.7	2.6	3%	11%	0.3	16	14%	1.03	1.11	1.15	1.16	0.58	oblate	0.58
57.222099	-5.467591	G	Granite	9	14240	15051.68	14652.96	13015.36	1.057	177.6	5.1	11.4	7	1.029	295	79.1	10.6	4.3	0.914	87	9.6	266.7	80.4	11.3	7.4	3%	12%	0.2	14	14%	1.03	1.13	1.16	1.17	0.63	oblate	0.63
57.222101	-5.468449	Qmd	Qz monzodiorite	6	17290	19001.71	17912.44	14955.85	1.099	14.9	3.2	7.6	2.7	1.036	268	79.1	8.3	6	0.865	106	10.4	285.5	79.6	8.4	4.9	6%	17%	0.4	20	23%	1.06	1.20	1.27	1.28	0.51	oblate-triaxial	0.51
57.221015	-5.467648	Qmd	Qz monzodiorite	9	18450	19612.35	19132.65	16605	1.063	347.1	7.7	17.8	3	1.037	134	80.8	17.9	3.7	0.9	256	5	76.4	85	5.7	1.8	3%	14%	0.2	11	16%	1.03	1.15	1.18	1.20	0.70	oblate	0.70
57.220933	-5.467996	Qmd	Qz monzodiorite	5	444.6	446.3784	444.6	442.8216	1.004	317.6	17.4	31.3	5	1	209	45.7	26	7	0.996	62	39.2	242.4	50.8	34.8	7.5	0%	0%	1.0	45	1%	1.00	1.00	1.01	1.01	0.00	triaxial	0.00
57.218987	-5.453933	Qmd	Qz monzodiorite	10	26620	28350.3	27924.38	23611.94	1.065	330.3	44.9	20.6	5.2	1.049	152	45.1	20.6	4.6	0.887	61	0.9	241.2	89.1	6.7	2.3	2%	16%	0.1	6	18%	1.02	1.18	1.20	1.23	0.83	oblate	0.83
57.2189	-5.453182	Qmd	Qz monzodiorite	16	23600	24355.2	24072	22372.8	1.032	352.7	84.2	17	4.3	1.02	231	3	17	5.3	0.948	141	5	321.1	85	6.2	2.9	1%	7%	0.2	9	8%	1.01	1.08	1.09	1.10	0.72	oblate	0.72
57.218999	-5.453234	Qmd	Qz monzodiorite	7	19340	20307	19494.72	18218.28	1.05	310.9	62.5	9.4	2.1	1.008	152	26	0.2	4.3	0.942	57	8.4	237.4	81.6	4.3	2.4	4%	7%	0.6	32	11%	1.04	1.07	1.11	1.12	0.25	oblate-triaxial	0.25
57.214756	-5.439147	Qmd	Qz monzodiorite	8	418.6	427.3906	420.2744	408.135	1.021	208.3	37.3	30	3.5	1.004	329	33.9	30.7	10.9	0.975	87	34.5	266.7	55.5	16.1	6.9	2%	3%	0.6	30	5%	1.02	1.03	1.05	1.05	0.27	oblate-triaxial	0.27
57.219439	-5.461624	Qmd	Qz monzodiorite	5	21400	22405.8	22149	19645.2	1.047	356.5	8.7	28.8	5.7	1.035	143	79.6	27.7	14.6	0.918	266	5.8	85.7	84.2	15.4	10.2	1%	12%	0.1	6	13%	1.01	1.13	1.14	1.16	0.82	oblate	0.82
57.219971	-5.462026	Qmd	Qz monzodiorite	6	20350	21733.8	21021.55	18294.65	1.068	324.5	48.5	9	4	1.033	174	37.5	5.2	1.4	0.899	72	15.1	252.3	74.9	8.9	2.9	4%	13%	0.3	15	17%	1.03	1.15	1.19	1.20	0.61	oblate	0.61
57.220584	-5.460934	Qmd	Qz monzodiorite	5	20640	22518.24	21672	17729.76	1.091	174.5	11.8	20.5	3.4	1.05	294	67.2	19.5	7.2	0.859	80	19.2	260.3	70.8	8.9	5.4	4%	19%	0.2	12	23%	1.04	1.22	1.27	1.29	0.68	oblate	0.68
57.220032	-5.450654	Qmd	Qz monzodiorite	7	15440	16474.48	15717.92	14112.16	1.067	260.8	60.8	5.8	4.7	1.018	358	4	7.3	4.7	0.914	90	28.8	270.3	61.2	9.1	2.1	5%	10%	0.5	25	15%	1.05	1.11	1.17	1.17	0.39	oblate-triaxial	0.39
57.220017	-5.450733	Qmd	Qz monzodiorite	6	12250	13046.25	12654.25	11049.5	1.065	57.7	44.8	10.6	3.1	1.033	181	29.1	10.4	6.1	0.902	291	31.1	110.8	58.9	7.8	4	3%	13%	0.2	14	16%	1.03	1.15	1.18	1.19	0.63	oblate	0.63
57.220029	-5.45079	Qmz	Qz monzonite	7	189.5	193.29	189.879	185.331	1.02	323.7	6.9	13.9	6.8	1.002	57.6	29.3	16.9	8	0.978	222	59.8	41.7	30.2	16.2	12	2%	2%	0.8	37	4%	1.02	1.02	1.04	1.04	0.15	triaxial	0.15
57.220077	-5.450834	Qmd	Qz monzodiorite	8	56360	61545.12	58219.88	49315	1.092	253.2	46.7	10.6	5.4	1.033	57.3	42.2	10.5	3.9	0.875	155	8	334.6	82	5.9	3.7	6%	16%	0.4	20	22%	1.06	1.18	1.25	1.26	0.50	oblate-triaxial	0.50
57.220154	-5.450907	Qmz	Qz monzonite	5	264.9	270.7278	264.6351	259.3371	1.022	349	15.8	11.6	3.8	0.999	240	48.4	20.2	11.4	0.979	91	37.2	271.4	52.8	20.2	3.5	2%	2%	1.2	49	4%	1.02	1.02	1.04	1.04	-0.06	triaxial	-0.06
57.219846	-5.450228	Gd	Granodiorite	7	24110	24809.19	24399.32	23097.38	1.029	225.3	51.2	30.7	7.5	1.012	36.8	38.5	31	11.8	0.958	130	4.2	310.1	85.8	13.9	5.9	2%	5%	0.3	17	7%	1.02	1.06	1.07	1.08	0.53	oblate	0.53
57.22744	-5.466392	Mn	Monzonite	14	25500	27285	25831.5	23383.5	1.07	89.8	38.3	10.6	3.8	1.013	211	33.4	7.1	2.5	0.917	328	34	147.6	56	9.1	2.6	6%	10%	0.6	31	15%	1.06	1.10	1.17	1.17	0.29	oblate-triaxial	0.29

Table S1 Continued

					Sample no.	susceptibility data				K1 normalised with					K2 normalised with					K3 normalised with					Owens (1974) parameters					Jelenick (1981) parameters						
	Lat/Long decimal												95% angles					95% angles		Foliation		95% angles in													
Site no.	Lat	Long	Rock type	Description	n	Kmean	K1	K2	K3	K1norm	dec	plunge	K1-K2	K1-K3	K2norm	dec	plunge	K1-K2	K2-K3	K3norm	dec	plunge	dip azimuth	dip	K1-K3	K2-K3	L	F	M	Mu	H	Lj	Fj	P	P'	T1	Shape	T2
AL056	57.227728	-5.467116	Qmn	Qz monzonite	10	14480	16014.88	14595.84	12829.28	1.106	83.6	27.2	5.8	4.1	1.008	206	46.3	7.3	4	0.886	336	31.2	155.5	58.8	7.5	5.4	10%	12%	0.8	39	22%	1.10	1.14	1.25	1.25	0.16	triaxial	0.16
AL057	57.228103	-5.468107	Qmn	Qz monzonite	9	17030	18239.13	17183.27	15667.6	1.071	345.9	38.7	8.2	6.5	1.009	117	39.2	14.1	7.9	0.92	232	27.1	51.6	62.9	14.2	6	6%	9%	0.7	35	15%	1.06	1.10	1.16	1.17	0.22	oblate-triaxial	0.22
AL058	57.228861	-5.469306	Mz	Monzonite	7	13670	14804.61	13902.39	12316.67	1.083	283.4	9.1	8.8	4.7	1.017	161	73.2	17.5	7.9	0.901	16	14	195.7	76	17.2	4.7	7%	12%	0.6	30	18%	1.06	1.13	1.20	1.21	0.32	oblate-triaxial	0.32
AL059	57.23	-5.472111	Mz	Monzonite	12	29950	31986.6	29830.2	28033.2	1.068	173.9	52.5	5.2	3.8	0.996	316	31.1	11.8	4.5	0.936	58	18.8	237.5	71.2	11.7	3.4	7%	6%	1.2	50	13%	1.07	1.06	1.14	1.14	-0.06	triaxial	-0.06
AL060	57.230056	-5.473861	Qmz	Quartz monzonite	6	17130	17695.29	17472.6	16204.98	1.033	115	64.3	45.9	2.5	1.02	276	24.6	45.9	2.4	0.946	9.7	7.2	189.7	82.8	5.1	1	1%	7%	0.2	10	9%	1.01	1.08	1.09	1.10	0.71	oblate	0.71
AL061	57.197889	-5.495778	Mz	Monzonite	6	53850	58265.7	53096.1	50188.2	1.082	247.8	78.8	10.5	7.8	0.986	42.7	10.1	13.4	7.1	0.932	134	4.6	313.5	85.4	13.7	6.6	10%	5%	1.8	61	15%	1.10	1.06	1.16	1.16	-0.25	prolate-triaxial	-0.25
AL062	57.213496	-5.509558	Md	Monzodiorite	9	17290	18880.68	17791.41	15197.91	1.092	37.9	43.4	7.9	3.3	1.029	293	15.4	7.9	4	0.879	188	42.5	8.2	47.5	4.5	3.4	6%	15%	0.4	23	21%	1.06	1.17	1.24	1.25	0.45	oblate-triaxial	0.45
AL063	57.219319	-5.489742	Qmz	Qz monzonite	11	16120	17329	16732.56	14282.32	1.075	349.2	6.1	20	1.6	1.038	194	83.2	20	2	0.886	80	2.9	259.6	87.1	2.1	1.6	4%	15%	0.2	14	19%	1.04	1.17	1.21	1.23	0.64	oblate	0.64
AL064	57.219384	-5.489696	Qmz	Qz monzonite	8	21850	23750.95	22396.25	19402.8	1.087	354.9	4.2	7.8	2.2	1.025	107	78.8	7.9	3.6	0.888	264	10.3	84.1	79.7	5.9	4	6%	14%	0.5	24	20%	1.06	1.15	1.22	1.23	0.42	oblate-triaxial	0.42
AL065	57.219555	-5.48979	Qmz	Qz monzonite	9	17750	19294.25	18424.5	15549	1.087	157	15.6	7.5	1.8	1.038	25.5	67.1	7.6	1.8	0.876	252	16.3	71.7	73.7	2.3	1.9	5%	16%	0.3	17	21%	1.05	1.18	1.24	1.26	0.57	oblate	0.57
AL066	57.219565	-5.490024	Qmz	Qz monzonite	7	18100	19312.7	18516.3	16471	1.067	58.5	19	12.8	3.7	1.023	153	12.9	12.8	6.2	0.91	275	66.7	95.4	23.3	7	2.5	4%	11%	0.4	21	16%	1.04	1.12	1.17	1.18	0.47	oblate-triaxial	0.47
AL067	57.217814	-5.496885	Mz	Monzonite	9	27530	29594.75	28053.07	22657.19	1.075	35	60.7	3.4	0.8	1.019	145	10.6	3.7	2.4	0.823	240	26.9	60	63.1	2.9	0.5	6%	20%	0.3	16	25%	1.05	1.24	1.31	1.34	0.60	oblate	0.60
AL068	57.215167	-5.5225	Mz	Monzonite	13	74410	78800.19	74112.36	70317.45	1.059	230.2	47.5	7.5	6.3	0.996	334	12.7	9.9	2.6	0.945	75	39.7	255.1	50.3	8.1	6.4	6%	5%	1.2	51	11%	1.06	1.05	1.12	1.12	-0.08	triaxial	-0.08
AL069	57.214611	-5.52125	Mz	Monzonite	7	27020	27992.72	26884.9	26182.38	1.036	165.1	71.2	6.5	5.3	0.995	50.5	8.1	38.4	6.2	0.969	318	16.9	138.1	73.1	38.4	5.6	4%	3%	1.6	58	7%	1.04	1.03	1.07	1.07	-0.21	prolate-triaxial	-0.21
AL070	57.197889	-5.495528	G	Granite	6	13720	14845.04	14639.24	11675.72	1.082	84.5	77.5	25.3	2.8	1.067	227	9.9	25.5	4.7	0.851	318	7.5	137.8	82.5	5.9	2.7	2%	22%	0.1	4	23%	1.01	1.25	1.27	1.31	0.88	oblate	0.88
AL071	57.210496	-5.502929	Sy	Syenite	10	31610	33569.82	31451.95	29808.23	1.062	61.8	29.2	8.3	2.3	0.995	243	60.8	8.9	3.6	0.943	152	0.4	332	89.6	9.1	3.8	7%	5%	1.3	52	12%	1.07	1.06	1.13	1.13	-0.10	triaxial	-0.10
AL072	57.201788	-5.487612	G	Granite	6	366.3	380.5857	373.9923	344.322	1.039	180.5	86.6	7.2	4.1	1.021	61.6	1.7	7.1	3.2	0.94	332	3	151.5	87	5.2	2.3	2%	8%	0.2	13	10%	1.02	1.09	1.11	1.11	0.65	oblate	0.65
AL073	57.201954	-5.487653	G	Granite	5	984.6	1038.753	993.4614	921.5856	1.055	140.5	52.7	9.1	4.3	1.009	32.6	13.3	5	2.2	0.936	294	34.1	113.5	55.9	9.2	1.2	5%	7%	0.6	32	12%	1.05	1.08	1.13	1.13	0.25	oblate-triaxial	0.25
AL074	57.210391	-5.485191	Mz	Monzonite	8	22670	23916.85	22579.32	21513.83	1.055	110.2	67.2	21.4	5	0.996	339	15.5	54.3	12.4	0.949	244	16.3	64.3	73.7	53.6	5.8	6%	5%	1.3	51	11%	1.06	1.05	1.11	1.11	-0.09	triaxial	-0.09
AL075	57.226367	-5.46714	Qmz	Qz monzonite	5	21070	23830.17	21596.75	17783.08	1.131	64.3	34.9	36.1	5	1.025	239	55	37.3	4.7	0.844	333	2.4	152.7	87.6	31.7	4.6	11%	18%	0.6	30	29%	1.10	1.21	1.34	1.35	0.33	oblate-triaxial	0.33
AL076	57.226017	-5.46612	Qmz	Qz monzonite	7	1924	2006.732	1929.772	1835.496	1.043	33.8	60.4	16.7	8.5	1.003	238	27.5	20.6	3.2	0.954	142	10.2	322.2	79.8	13.4	8.3	4%	5%	0.8	39	9%	1.04	1.05	1.09	1.09	0.12	triaxial	0.12
AL077	57.225798	-5.465244	Qmz	Qz monzonite	8	19700	21591.2	20428.9	17079.9	1.096	57.4	48.5	31.7	2.3	1.037	230	41.3	31.8	5.6	0.867	323	3.7	143.2	86.3	7.3	2.3	6%	17%	0.3	19	23%	1.06	1.20	1.26	1.28	0.53	oblate	0.53
AL078	57.225493	-5.464711	Qmz	Qz monzonite	9	17030	18358.34	17847.44	14884.22	1.078	31.4	32.6	22	8.2	1.048	230	56	21.5	2.3	0.874	127	8.6	306.9	81.4	9.7	2	3%	17%	0.2	10	20%	1.03	1.20	1.23	1.26	0.73	oblate	0.73
AL079	57.224505	-5.463168	Qmz	Qz monzonite	6	19430	21275.85	20207.2	16806.95	1.095	22.9	42.3	10.6	2.5	1.04	208	47.5	11	2.8	0.865	115	2.7	295.4	87.3	5.1	1.2	5%	18%	0.3	17	23%	1.05	1.20	1.27	1.28	0.56	oblate	0.56
AL080	57.224425	-5.462896	Mz	Monzonite	5	30470	32206.79	30652.82	28550.39	1.057	43.2	18.6	20.4	8.5	1.006	265	65.9	30.1	12.9	0.937	138	14.8	318.2	75.2	30.4	1.7	5%	7%	0.7	36	12%	1.05	1.07	1.13	1.13	0.18	triaxial	0.18
AL081	57.220764	-5.50226	Qmz	Qz monzonite	5	12830	14241.3	13625.46	10623.24	1.11	334.9	45.5	10.4	0.2	1.062	168	43.7	10.2	2.2	0.828	72	6.6	251.6	83.4	4.9	1.8	5%	23%	0.2	12	28%	1.05	1.28	1.34	1.37	0.70	oblate	0.70
AL082	57.220471	-5.499908	Qmz	Qz monzonite	7	9621	10313.71	10150.16	8408.754	1.072	358	28.1	17.3	4.5	1.055	121	45.5	17.2	3.9	0.874	249	31.3	69	58.7	4.7	3.9	2%	18%	0.1	5	20%	1.02	1.21	1.23	1.26	0.84	oblate	0.84
AL083	57.220471	-5.499908	Qmz	Qz monzonite	9	10160	10668	10292.08	9530.08	1.05	137.5	36.2	21.5	7.6	1.013	25.5	27	23.6	6.4	0.938	268	41.8	88.4	48.2	13.3	8	4%	8%	0.5	26	11%	1.04	1.08	1.12	1.12	0.36	oblate-triaxial	0.36
AL084	57.223002	-5.486888	Qmz	Qz monzonite	6	20520	21299.76	20745.72	19514.52	1.038	192.4	43.1	20	9	1.011	56.3	37.6	25.9	16.6	0.951	307	23.6	126.6	66.4	26.9	10.9	3%	6%	0.5	24	9%	1.03	1.06	1.09	1.09	0.40	oblate-triaxial	0.40
AL085	57.222873	-5.486076	Qmz	Qz monzonite	5	19000	19836	19494	17670	1.044	220.9	20.8	8.4	3.2	1.026	95.6	56.8	8.7	1.7	0.93	321	24.7	141	65.3	3.9	2	2%	10%	0.2	11	11%	1.02	1.10	1.12	1.13	0.70	oblate	0.70
AL086	57.222828	-5.485258	Qmz	Qz monzonite	6	25330	25963.25	25380.66	24620.76	1.025	80.1	36	42.5	15.3	1.002	299	47	41.8	21.9	0.972	186	20.2	5.7	69.8	26.3	19.1	2%	3%	0.8	37	5%	1.02	1.03	1.05	1.05	0.15	triaxial	0.15
AL087	57.222844	-5.484521	Qmz	Qz monzonite	7	25080	25932.72	25606.68	23700.6	1.034	57.4	41.4	39	4.3	1.021	190	37.4	39.1	4.3	0.945	302	26.1	121.9	63.9	6.7	4.4	1%	8%	0.2	10	9%	1.01	1.08	1.09	1.10	0.72	oblate	0.72
AL088	57.222888	-5.482509	Qmz	Qz monzonite	6	18950	20655.5	19310.05	16884.45	1.09	24.7	1.2	5.5	4.6	1.019	118	68.6	9.9	4.2	0.891	294	21.4	114.3	68.6	10	4.4	7%	13%	0.6	29	20%	1.07	1.14	1.22	1.23	0.33	oblate-triaxial	0.33
AL089	57.222849	-5.482218	Qmz	Qz monzonite	8	22920	24203.52	23974.32	20582.16	1.056	68	80.5	40.3	9.2	1.046	223	8.6	40.3	4.9	0.898	313	4	133.1	86	9.8	4.7	1%	15%	0.1	4	16%	1.01	1.16	1.18	1.20	0.88	oblate	0.88
AL090	57.222355	-5.482694	Qmz	Qz monzonite	5	25650	27291.6	26368.2	23290.2	1.064	210.3	24.8	11.2	1.4	1.028	94.8	42.9	11.1	2.4	0.908	321	36.9	140.6	53.1	2.6	2.5	4%	12%	0.3	17	16%	1.04	1.13	1.17	1.18	0.57	oblate	0.57
AL091	57.23331	-5.486065	Qmz	Qz monzonite	10	20010	21030.51	20150.07	18849.42	1.051	120.4	74.3	10.9	3	1.007	252	10.6	11	7.1	0.942	345	11.4	164.5	78.6	7.4	2.7	4%	6%	0.7	34	11%	1.04	1.07	1.12	1.12	0.22	oblate-triaxial	0.22
AL092	57.235173	-5.496445	Mz	Monzonite	10	4206	4315.356	4218.618	4088.232	1.026	97.4	27.4	37	7.7	1.003	234	54.4	39.6	15.6	0.972	356	21	176	69	31.5	9.8	2%	3%	0.7	37	5%	1.02	1.03	1.06	1.06	0.16	triaxial	0.16
AL093	57.235859	-5.496456	Qmz	Qz monzonite	9	2019	2083.608	2006.886	1964.487	1.032	106.7	62.6	6.7	3.6	0.994	330	20.7	11.1	5.2	0.973	233	17.1	53.2	72.9	10.4	3.4	4%	2%	1.8	61	6%	1.04	1.02	1.06	1.06	-0.27	prolate-triaxial	-0.27
AL094	57.23874	-5.495943	Md	Monzodiorite	8	56810	63059.1	59025.59	48288.5	1.11	104.4	27.6	15.2	2	1.039	5.9	15.9	15.6	4.2	0.85	250	57.4	69.5	32.6	5.6	1.9	7%	19%	0.4	21	26%	1.07	1.22	1.31	1.32	0.50	oblate-triaxial	0.50
AL095	57.241022	-5.495024	Mz	Monzonite	5	29990	33228.92	32329.22	24411.86	1.108	72.2	54.6	13.7	10.9	1.078	215	29.3	16.4	12.5	0.814	315	18	135	72	18.3	5	3%	26%	0.1	6	29%	1.03	1.32	1.36	1.41	0.82	oblate	0.82
AL096	57.236872	-5.482083	Qmd	Qz monzodiorite	6	34850	38788.05	36871.3	28855.8	1.113	68	81.4	18.9	2.6	1.058	256	8.5	18.7	4.4	0.828	166	1.2	345.7	88.8	5.2	3.7	5%	23%	0.2	13	29%	1.05	1.28	1.34	1.37	0.66	oblate	0.66
AL097	57.233338	-5.476942	Md	Monzodiorite	7	430.3	433.7424	430.7303	426.4273	1.008	334.2	41.2	15.5	6.4	1.001	208	34	23.5	12.9	0.991	95	30.2	274.9	59.8	22.5	7.9	1%	1%	0.7	35	2%	1.01	1.01	1.02	1.02	0.18	oblate-triaxial	0.18
AL098	57.231491	-5.47129	Qmz	Qz monzonite	6	1319	1452.219	1341.423	1163.358	1.101	89.8	1.5	5.3	2.6	1.017	182	51.5	4.2	2.7	0.882	359	38.5	178.6	51.5	4.8	3.5	8%	14%	0.6	32	22%	1.08	1.15	1.25	1.25	0.28	oblate-triaxial	0.28
AL099	57.224756	-5.453306	Qmz	Qz monzonite	10	24990	26539.38	25839.66	22590.96	1.062	51.7	50.6	14.5	1.8	1.034	217	38.5	14.5	2.7	0.904	313	7.2	132.9	82.8	3.1	1.3	3%	13%	0.2	12	16%	1.03	1.14	1.17	1.19	0.67	oblate	0.67
AL100	57.227335	-5.459322	G	Granite	6	7797	8311.602	7828.188	7251.21	1.066	58.3	66.9	6.8	1.5	1.004	215	21.4	7.6	6.5	0.93	308	8.3	128.3	81.7	7.4	1.4	6%	7%	0.8	40	14%	1.06	1.08	1.15	1.15	0.12	triaxial	0.12

T1 after Borridale & Jackson (2005)
T2 from Kappabridge manual (Agico, 2018)

Table S2 Summary of anhysteretic remanent magnetization data from the Ratagain Complex

	Lat/Long decimal					Normalised principal magnitudes				Principal axes						
Site no.	**Lat**	**Long**	**Rock Type**	**N**	**R Mean**	***AARMmax***	***AARMint***	**AARMmin**		***AARMmax***	***AARMint***	**AARMmin**	**L**	**F**	**Pj**	**T**
AL002	57.2218	-5.4877	Qmd	6	3574	1.320	1.007	0.673		204/04	102/69	295/20	1.323	1.505	1.999	0.189
AL009	57.2244	-5.5229	Qmd	6	2869	1.061	0.994	0.946		142/34	318/56	051/02	1.078	1.064	1.15	-0.151
AL011	57.2198	-5.5253	Qg	11	5748	1.154	1.032	0.815		175/014	041/71	268/13	1.137	1.283	1.469	0.327
AL017	57.1979	-5.4961	Mz	10	1346	1.044	1.003	0.953		110/40	208/09	308/49	1.05	1.106	1.1.69	0.32
AL031	57.2225	-5.4723	Md	10	3284	1.098	1.013	0.889		355/17	153/72	263/06	1.105	1.161	1.294	0.162
AL038	57.2221	-5.4676	G	9	2919	1.120	1.025	0.855		175/08	287/80	083/18	1.129	1.214	1.378	0.23
AL045	57.2148	-5.4391	Qmd	8	377.7	1.031	0.998	0.972		198/53	004/37	099/07	1.044	1.081	1.132	0.222
AL048	57.2206	-5.4609	Qmd	5	4605	1.222	1.032	0.746		162/08	293/79	070/08	1.218	1.366	1.671	0.227
AL054	57.2198	-5.4502	Gd	7	1129	1.036	0.999	0.965		222/32	047/58	314/02	1.01	1.04	1.113	-0.112
AL062	57.2135	-5.5096	Md	9	3332	1.226	1.065	0.709		027/45	284/12	183/43	1.17	1.52	1.821	0.467
AL067	57.2178	-5.4969	Mz	9	1409	1.093	0.990	0.918		110/24	334/58	209/20	1.12	1.088	1.226	-0.098
AL079	57.2245	-5.4632	Qmz	6	5267	1.190	1.055	0.755		027/28	201/62	296/02	1.144	1.404	1.631	0.438
AL081	57.2208	-5.5023	Qmz	5	2502	1.290	1.035	0.675		335/41	165/48	069/05	1.25	1.564	1.982	0.35
AL094	57.2387	-5.4959	Md	7	9256	1.246	1.093	0.661		116/23	018/19	253/59	1.16	1.656	1.989	0.584
AL096	57.2369	-5.4821	Qmd	6	6098	1.247	1.033	0.720		070/68	254/22	164/01	1.216	1.467	1.814	0.352
AL100	57.2273	-5.4593	G	6	1799	1.142	0.995	0.864		056/64	210/23	304/10	1.148	1.181	1.368	0.087

Table S3 Summary thin-section microstructural analyses from the Ratagain Complex

Site no.	Lat/Long decimal: Lat	Lat/Long decimal: Long	Rock type	Microstructural category
AL001	57.221815	-5.487339	Qmd	1
AL002	57.221761	-5.487693	Qmd	1
AL003	57.221635	-5.488301	Qmd	4
AL004B	57.221449	-5.489031	Qmd	1
AL005	57.22128	-5.489687	Qmd	1
AL006	57.221181	-5.490095	Qmd	1
AL007	57.220789	-5.490688	Md	1
AL008	57.22053	-5.491227	Qmd	1
AL009	57.224358	-5.522887	Qmd	2
AL010	57.22646	-5.523792	Md	2
AL011	57.219817	-5.52528	Qrg	1
AL012	57.220827	-5.416701	Qmd	4
AL013	57.221124,0	-5.416417	G	4
AL014	57.221628	-5.416004	Qmd	4
AL015	57.222004	-5.41558	Qmz	4
AL016	57.222954	-5.414447	Qmd	4
AL017	57.197948	-5.49609	Mz	3
AL018	57.21977	-5.512273	Qmd	1
AL019	57.219379,0	-5.508627	Md	1
AL020	57.218181	-5.50266	Gd	1
AL021	57.221687	-5.473359	Qmd	1
AL022	57.221676	-5.473384	Qmd	1
AL023	57.221753	-5.473324	Qmd	1
AL024	57.221883	-5.47331	Qmz	1
AL025	57.221858	-5.473368	Gd	1
AL026	57.222095	-5.473218	Qmn	1
AL027	57.22213	-5.473193	Qmd	1
AL028	57.222171	-5.473074	Qmd	1
AL029	57.222337	-5.472689	Qmd	1
AL030	57.222483	-5.472488	Qmd	1
AL031	57.222542	-5.47226	Md	3
AL032	57.222667	-5.472003	Qmd	1
AL033	57.223223	-5.464256	Qmd	1
AL034	57.222709	-5.464695	Qmd	1
AL035	57.222705	-5.46485	Qmd	1
AL036	57.222623	-5.466385	Qmd	1
AL037	57.222032	-5.46702	Qmz	1
AL038	57.222099	-5.467591	G	1
AL039	57.222101	-5.468449	Qmd	1
AL040	57.221015	-5.467648	Qmd	1
AL041	57.220933	-5.467996	Qmd	1
AL042	57.218987	-5.453933	Qmd	4
AL043	57.2189	-5.453182	Qmd	4
AL044	57.218999	-5.453234	Qmd	4
AL045	57.214756	-5.439147	Qmd	4
AL046	57.219439	-5.461624	Qmd	4
AL047	57.219971	-5.462026	Qmd	4
AL048	57.220584	-5.460934	Qmd	4
AL049	57.220032	-5.450654	Qmd	4
AL050	57.220017	-5.450733	Qmd	4
AL051	57.220029	-5.45079	Qmz	4
AL052	57.220077	-5.450834	Qmd	4
AL053	57.220154	-5.450907	Qmz	4
AL054	57.219846	-5.450228	Gd	4
AL055	57.22744	-5.466392	Mn	4
AL056	57.227728	-5.467116	Qmn	4
AL057	57.228103	-5.468107	Qmn	4
AL058	57.228861	-5.469306	Mz	4
AL059	57.23	-5.472111	Mz	4
AL060	57.230056	-5.473861	Qmz	4
AL061	57.197889	-5.495778	Mz	3
AL062	57.213496	-5.509558	Md	1
AL063	57.219319	-5.489742	Qmz	1
AL064	57.219384	-5.489696	Qmz	1
AL065	57.219555	-5.48979	Qmz	1
AL066	57.219565	-5.490024	Qmz	1
AL067	57.217814	-5.496885	Mz	1
AL068	57.215167	-5.5225	Mz	1
AL069	57.214611	-5.52125	Mz	1
AL070	57.197889	-5.495528	G	1
AL071	57.210496	-5.502929	Sy	1
AL072	57.201788	-5.487612	G	2
AL073	57.201954	-5.487653	G	2
AL074	57.210391	-5.485191	Mz	3
AL075	57.226367	-5.46714	Qmz	4
AL076	57.226017	-5.46612	Qmz	4
AL077	57.225798	-5.465244	Qmz	4
AL078	57.225493	-5.464711	Qmz	4
AL079	57.224505	-5.463168	Qmz	4
AL080	57.224425	-5.462896	Mz	4
AL081	57.220764	-5.50226	Qmz	1
AL082	57.220471	-5.499908	Qmz	1
AL083	57.220471	-5.499908	Qmz	1
AL084	57.223002	-5.486888	Qmz	2
AL085	57.222873	-5.486076	Qmz	2
AL086	57.222828	-5.485258	Qmz	1
AL087	57.222844	-5.484521	Qmz	2
AL088	57.222888	-5.482509	Qmz	2
AL089	57.222849	-5.482218	Qmz	1
AL090	57.222355	-5.482694	Qmz	2
AL091	57.23331	-5.486065	Qmz	1
AL092	57.235173	-5.496445	Mz	1
AL093	57.235859	-5.496456	Qmz	1
AL094	57.23874	-5.495943	Md	1
AL095	57.241022	-5.495024	Mz	1
AL096	57.236872	-5.482083	Qmd	4
AL097	57.233338	-5.476942	Md	4
AL098	57.231491	-5.47129	Qmz	4
AL099	57.224756	-5.453306	Qmz	4
AL100	57.227335	-5.459322	G	4

KEY

Category	Temperature	Diagnostic microstructures
(1) Magmatic	T>700°C	No/ rare undulatory quartz extinction Compositionally zoned euhedral to subhedral plagioclase Euhedral to subhedral biotite
(2) High-T solid state	T>650°C	Chessboard extinction in quartz Quartz grain boundary migration recrystallisation Myrmekite Deformation twinning in plagioclase Bent biotite
(3) Medium-T solid state	400°C<T<500°C	Subgrain rotation recrystallisation in quartz Myrmekite Kinked plagioclase twins Kinked biotite cleavage
(4) Low-T solid state	T<400°C	Bulging recrystallisation in quartz Sericitized plagioclase Kinked biotite cleavage

Table S4 Summary of isothermal remanent magnetization component analysis for representative samples

Sample AL002

Component 1 linear												Component 1 log											
EC (%)	EC sd	Bh (mT)	Bh sd	DP	DP sd	P	P sd	S	S sd	OC	OC sd	EC (%)	EC sd	Bh (mT)	Bh sd	DP	DP sd	P	P sd	S	S sd	OC	OC sd
0.95	0.06	16.81	1.28	3.21	1.20	0.98	0.01	0.66	0.03	0.98	0.01	0.95	0.06	1.23	0.11	0.51	0.08	0.98	0.01	0.66	0.03	0.98	0.01

Component 2 linear												Component 2 log											
EC (%)	EC sd	Bh (mT)	Bh sd	DP	DP sd	P	P sd	S	S sd	OC	OC sd	EC (%)	EC sd	Bh (mT)	Bh sd	DP	DP sd	P	P sd	S	S sd	OC	OC sd
0.05	0.06	2922.10	2.10	2.27	1.72	0.07	0.01	0.89	0.38	0.02	0.01	0.05	0.06	3.47	0.32	0.36	0.23	0.07	0.01	0.89	0.38	0.02	0.01

Sample AL009

Component 1 linear												Component 1 log											
EC (%)	EC sd	Bh (mT)	Bh sd	DP	DP sd	P	P sd	S	S sd	OC	OC sd	EC (%)	EC sd	Bh (mT)	Bh sd	DP	DP sd	P	P sd	S	S sd	OC	OC sd
0.52	0.12	39.66	1.18	3.30	1.15	0.67	0.05	0.78	0.09	0.62	0.19	0.52	0.12	1.60	0.07	0.52	0.06	0.67	0.05	0.78	0.09	0.62	0.19

Component 2 linear												Component 2 log											
EC (%)	EC sd	Bh (mT)	Bh sd	DP	DP sd	P	P sd	S	S sd	OC	OC sd	EC (%)	EC sd	Bh (mT)	Bh sd	DP	DP sd	P	P sd	S	S sd	OC	OC sd
0.21	0.10	107.89	1.12	2.01	1.07	0.44	0.08	0.94	0.09	0.28	0.17	0.21	0.10	2.03	0.05	0.30	0.03	0.44	0.08	0.94	0.09	0.28	0.17

Component 3 linear												Component 3 log											
EC (%)	EC sd	Bh (mT)	Bh sd	DP	DP sd	P	P sd	S	S sd	OC	OC sd	EC (%)	EC sd	Bh (mT)	Bh sd	DP	DP sd	P	P sd	S	S sd	OC	OC sd
0.28	0.08	3885.42	1.26	5.62	1.21	0.26	0.02	2.40	0.22	0.09	0.04	0.28	0.08	3.59	0.10	0.75	0.08	0.26	0.02	2.40	0.22	0.09	0.04

Sample AL048

Component 1 linear												Component 1 log											
EC (%)	EC sd	Bh (mT)	Bh sd	DP	DP sd	P	P sd	S	S sd	OC	OC sd	EC (%)	EC sd	Bh (mT)	Bh sd	DP	DP sd	P	P sd	S	S sd	OC	OC sd
1.00	0.00	2.05	4.51	15.45	3.08	1.00	0.00	0.47	0.06	1.00	0.00	1.00	0.00	0.31	0.65	1.19	0.49	1.00	0.00	0.47	0.06	1.00	0.00

Thermomagnetic results for sample AL002

TEMP (°C)	TSUSC (°C)	TIME (s)	TEMP (°C)	TSUSC (°C)	TIME (s)	TEMP (°C)	TSUSC (°C)	TIME (s)	TEMP (°C)	TSUSC (°C)	TIME (s)	TEMP (°C)	TSUSC (°C)	TIME (s)	TEMP (°C)	TSUSC (°C)	TIME (s)
22.1	210.6	0	214.9	224.4	1465	472.5	177.2	2970	681.9	-4.9	4462	450	140.6	5956	312.6	134.2	7443
22.3	210.6	17	216.8	224.7	1480	475.2	176.3	2986	679.6	-4.7	4478	448.8	140.4	5972	311.2	134.2	7458
23.9	210.7	32	219.3	224.8	1495	477.9	175.2	3001	677.7	-3.8	4494	447.3	140.4	5987	310.1	134.3	7473
25.9	210.6	47	221.2	225.2	1510	480.5	174.2	3017	675.5	-4.7	4509	445.2	140.5	6003	309	134.3	7488
28.3	210.8	62	223.6	225.5	1525	483.8	173.4	3032	672.9	-4.3	4525	443.5	140.2	6018	307.8	134	7504
30.6	210.8	77	226.1	225.6	1540	487.1	172.7	3047	670.3	-4	4540	442	140.4	6034	306.7	134.2	7519
32.7	211	92	228.6	226	1556	490.1	171.9	3062	668.1	-4	4556	440.2	140.3	6049	305.6	134.1	7534
34.7	211.1	108	231.1	226.1	1571	493.1	171.3	3078	665.6	-3.1	4571	438.8	139.8	6064	303.9	134.1	7549
36.8	211.2	123	233.8	226.5	1585	495.8	170.7	3093	663	-3.2	4586	437.6	139.9	6080	302.2	133.8	7565
38.9	211.2	138	236.3	226.8	1601	497.9	170.1	3108	660.8	-2.6	4602	436.1	140	6095	300.5	134	7580
40.7	211.3	153	238.5	226.6	1616	500	169.4	3124	658.2	-2.5	4617	434.6	139.8	6110	298.5	133.9	7595
42.5	211.4	168	241.2	225.7	1633	501.8	169.1	3139	655.7	-1.8	4633	433.2	139.8	6126	296.6	133.7	7611
44.3	211.4	183	243.4	227.6	1648	503.9	168.5	3154	653.2	-1.5	4648	431.7	139.7	6141	294.6	133.2	7626
46.1	211.6	198	245.9	227.4	1663	505.7	168.4	3170	650.3	-1.4	4664	430.5	139.9	6156	292.7	133.4	7641
47.7	211.9	214	248.1	227.9	1678	507.8	168	3185	647.8	-1	4679	429.1	139.5	6172	290.4	133.3	7657
49.2	211.9	229	250.6	228.1	1693	509.9	167.9	3200	645.2	-0.9	4694	427.6	139.4	6187	288.5	133.5	7672
50.8	211.9	244	252.8	228.2	1708	512.4	167.2	3216	642.4	-0.3	4710	426.1	139.7	6202	286.5	133.2	7687
52.4	211.9	259	255.3	228.4	1723	515.1	167.2	3231	639.9	0	4725	424.7	139.5	6218	284.5	133.2	7703
54.2	212.1	274	257.8	228.9	1738	518.1	167.1	3246	637	-0.1	4741	423.5	139.4	6233	282.6	132.8	7718
55.7	212.2	289	260.3	228.9	1753	520.8	166.6	3262	634.2	0.2	4756	422.3	139.2	6248	280.6	132.9	7733
57.3	212.2	305	262.8	229.3	1768	523.2	166.4	3277	632	0.2	4772	421.5	139.1	6264	278.7	132.7	7748
58.9	212.3	320	265	229.3	1783	525.7	166.6	3292	629.4	0.2	4787	420.3	139.1	6279	276.7	132.6	7764
60.4	212.4	335	267.5	229.5	1798	528.1	166.3	3308	627.2	0.3	4802	419.1	139.3	6294	274.5	132.6	7779
62.2	212.4	350	270	229.8	1813	530.8	166.4	3323	624.7	0.5	4818	417.7	138.9	6310	272.5	132.2	7794
63.8	212.6	365	272.3	229.9	1828	533.9	166.5	3338	622.8	0.8	4833	416.2	139	6325	270.9	132.5	7809
65.4	212.7	380	275	230.1	1843	536.6	166.2	3354	620.6	1.3	4849	415	139	6341	268.9	132.4	7825
66.9	212.8	395	277.6	230.5	1858	539.7	166.2	3369	617.8	1.6	4864	414.2	138.7	6356	267	132.3	7840
68.5	212.9	410	280.1	230.8	1873	542.7	166.7	3384	615.6	2.1	4879	413	138.9	6371	265	132.1	7855
70.1	213	425	282.6	230.9	1888	546.1	166.3	3399	613.1	2.7	4895	411.8	138.8	6387	263.1	132.2	7870
71.6	213	440	285.4	231.9	1906	548.8	166.5	3415	610.9	4.5	4910	410.7	138.7	6402	260.9	131.8	7886
73.5	213.3	455	287.9	231.5	1921	551.6	166.6	3430	608.4	7.7	4926	409.5	138.6	6417	258.7	131.9	7901
75	213.3	471	290.4	231.8	1936	554.3	166.7	3445	605.9	12.3	4941	408.3	138.3	6433	256.4	131.7	7916
76.9	213.4	486	292.9	231.9	1951	557.1	166.7	3461	603.1	19.8	4956	407.5	138.6	6448	254.2	131.6	7931
78.7	213.7	501	295.7	232.2	1966	560.1	166.2	3476	600.3	29.3	4972	406.6	138.5	6463	252	131.5	7946
80.3	213.7	516	298.8	232	1983	563.2	163.4	3491	597.5	40.1	4987	405.4	138.5	6479	250.3	131.2	7962
82.1	214	531	301.4	232.6	1998	566.6	159.8	3507	595	51.3	5003	404.3	138.2	6494	248.4	131.2	7977
84	213.9	546	303.9	232.9	2013	569.7	154.6	3522	592.6	63	5018	402.5	138.4	6509	246.8	131.3	7992
85.8	214.1	561	306.4	233	2028	572.8	145.3	3537	590.1	75.4	5034	401.1	138.1	6525	244.8	131	8007
87.6	214.3	576	308.7	233.2	2043	575.8	132.7	3553	587.3	88.1	5049	399.6	138.2	6540	242.9	131	8023
89.5	214.3	591	311.2	233.3	2059	578.9	121.3	3568	584.8	102.8	5065	398.4	138.2	6555	241	131	8038
91.3	214.5	606	314	232.5	2076	581.4	110.5	3583	582	117	5080	397.3	138.3	6571	238.8	130.8	8053
93.2	214.3	621	316.8	233.6	2093	584.5	99.2	3599	579.2	130.1	5095	396.4	138	6586	236.8	130.7	8068
95	214.6	636	320	234.3	2110	587.3	86	3614	576.8	140.9	5111	395.3	138.2	6601	234.6	130.5	8084
96.8	214.6	651	322.8	234.3	2127	590.1	73.8	3630	574	151.1	5126	394.1	138.1	6617	232.4	130.3	8099
98.7	214.8	666	325.3	234.5	2142	592.9	61.5	3645	571.2	159.9	5141	392.9	137.9	6632	230.2	130.2	8114
100	215	681	327.9	234.2	2159	595.4	50.2	3660	568.8	165.5	5157	391.5	138.1	6647	227.8	130	8129
100.8	215.1	697	330.4	233.5	2175	598.2	41.1	3675	566	167.2	5172	390.3	138.2	6663	225.3	130	8145
101.1	215.3	712	333	235.3	2192	600.6	31.2	3691	563.5	167	5188	388.6	137.8	6678	222.8	129.9	8160
101.1	215.1	727	335.5	233.2	2209	603.1	23.1	3706	561.1	165.5	5203	386.9	137.9	6693	220.4	129.7	8175
101.3	215.4	742	338.1	234.2	2225	605.9	16.5	3722	558.6	163.6	5218	385.1	137.7	6709	217.9	129.5	8190
101.6	215.5	757	340.7	234.7	2241	609.1	12.6	3737	555.8	161.3	5234	383.7	137.4	6724	215.4	129.4	8206
101.8	215.9	772	342.9	234.6	2256	611.6	10.1	3753	553.4	159	5249	382.2	137.6	6739	212.7	129.4	8221
102.9	215.8	787	345.5	233.8	2272	614.4	8.7	3768	550.6	156.4	5264	380.5	137.3	6755	210.2	129.5	8236
105.8	215.8	802	348.4	234.4	2289	617.5	7.6	3783	548.2	153.8	5280	378.8	137.4	6770	207.8	129.2	8251
109.8	216.2	817	350.9	235.1	2306	621	6.3	3799	545.8	151.2	5295	377	137.4	6785	205.1	129	8267
113.5	216.5	832	353.8	235.4	2323	623.8	5.7	3814	543	149.2	5311	375.3	137.6	6800	202.6	128.9	8282
116.7	216.7	847	356.7	232.6	2340	627.2	4.8	3829	540.6	148.9	5326	373.6	137.3	6816	200.2	128.8	8297
119.8	217.1	862	359.2	233.1	2355	630.7	3.9	3845	538.4	148.3	5341	372.1	137.3	6831	198	128.5	8312
122.8	217	877	362.4	232.7	2370	634.2	3.2	3860	536	147.7	5357	371	137.1	6846	195.5	128.5	8327
125.7	217	892	366.1	231.8	2388	637	2.8	3875	533.9	147.2	5372	369.8	137	6862	193.4	128.6	8342
128.3	217.4	908	369.6	231.3	2403	640.2	1.8	3891	531.4	147	5387	368.7	137	6877	190.9	128.5	8358
131	217.3	923	372.7	230.4	2419	643	0.9	3907	529	146.3	5403	367	136.8	6892	188.8	128.2	8373
133.7	217.5	938	375.6	229.8	2434	645.9	0.6	3922	526.3	146.2	5418	365.3	136.7	6908	186.6	128.2	8388
136.1	218	953	379.1	228.6	2449	649	-0.2	3938	523.5	145.8	5434	363.2	136.7	6923	184.4	128.1	8403
138.7	217.7	968	382.2	227.1	2464	652.5	-0.9	3953	520.8	145.4	5449	361.2	136.6	6938	182.3	128	8418
141.4	218.3	983	385.1	226.4	2480	655.7	-1.1	3968	518.1	145.1	5464	359.2	136.6	6954	179.8	127.9	8433
143.8	218.2	998	388.3	224.2	2497	658.9	-2.2	3984	515.4	144.9	5480	357.5	136.7	6969	177.7	127.8	8449
146.2	218.3	1013	390.9	223.6	2513	662.1	-2.2	3999	513	144.5	5495	355.5	136.4	6984	175.2	127.8	8464
148.6	218.5	1028	393.5	222.2	2528	665.6	-2.9	4015	510.2	144.4	5511	353.8	136.5	6999	172.5	127.6	8479
151	218.8	1043	395.8	220.9	2543	668.8	-3.2	4030	507.8	144.2	5526	352.1	136.2	7015	170.1	127.7	8494
153.2	218.9	1059	398.4	219.1	2558	671.9	-4.2	4045	505.1	144.1	5541	350.6	136.3	7030	167.7	127.5	8509
155.6	219	1074	401.1	217.9	2574	675.5	-4	4060	502.7	143.8	5557	349.2	136.3	7045	165.3	127.4	8524
158	219.5	1089	404	216.3	2589	678.7	-4.6	4076	500.3	143.7	5572	347.5	136	7061	162.8	127.4	8540
160.2	219.4	1104	406.6	214.8	2604	682.2	-4.8	4091	498.5	143.4	5588	345.8	136	7076	160.4	127.2	8555
162.3	219.8	1119	409.5	213	2619	685.4	-5.6	4107	496.1	143	5603	344.4	135.9	7091	158.3	127.2	8570
164.5	219.8	1134	412.4	211.2	2635	688.6	-5.8	4122	494	143.2	5618	342.7	135.7	7106	156.1	127.3	8585
166.6	220.2	1149	414.7	209.4	2650	691.5	-6.2	4138	491.9	142.9	5634	341	135.8	7122	154	127.3	8600
168.8	220.4	1164	417.1	207.8	2665	694.4	-6.5	4153	489.5	142.9	5649	339.5	135.7	7137	151.8	127.2	8615
170.9	220.3	1179	419.7	206	2680	697.6	-7	4169	486.8	142.6	5664	337.5	135.7	7152	149.7	127.1	8631
173.3	220.6	1194	422	204.3	2696	700.9	-7.3	4184	484.1	142.6	5680	335.8	135.4	7168	147.6	127.1	8646
175.8	220.6	1209	424.4	202.5	2711	703.8	-7.9	4200	481.7	142.6	5695	334.4	135.4	7183	145.4	127.1	8661
177.9	221	1224	427	200.9	2726	705.7	-7.8	4215	479.4	142.4	5711	333	135.1	7198	143	127.2	8676
180.1	221.3	1239	430	199.5	2741	706.7	-7.7	4231	477.3	142.3	5726	331.6	135.5	7214	140.9	127.1	8691
182.8	221.6	1254	432.6	197.8	2756	707.3	-7.7	4246	475.8	142.2	5741	329.9	135.2	7229	138.5	127.1	8706
185	221.7	1269	435.2	195.6	2772	707.3	-7.9	4262	474.3	142	5757	328.7	134.9	7244	136.3	126.9	8721
187.4	221.8	1284	437.9	194.4	2787	707	-8	4277	472.5	141.7	5772	327.3	135.2	7260	134.2	127	8736
189.8	222.2	1300	440.5	192.8	2802	705.4	-7.8	4293	470.7	141.6	5787	326.2	135.3	7275	132.1	127	8751
192.3	222.3	1315	443.5	190.9	2818	703.8	-7.9	4308	468.6	141.6	5803	324.8	135.2	7290	129.7	127.1	8766
194.7	222.6	1330	446.1	189.5	2833	702.5	-7.7	4323	466.3	141.6	5818	323.6	135	7305	127.3	126.9	8782
197.2	222.8	1345	449.1	187.8	2848	700.5	-7.2	4339	463.9	141.3	5834	322.2	135	7321	124.9	126.9	8797
199.3	222.8	1360	452	186.4	2864	698.3	-7.2	4354	461.8	141.3	5849	321.1	134.8	7336			
201.5	223.3	1375	455	185.1	2879	696	-7	4370	459.7	141	5864	320	135	7351			
204	223.3	1390	458.2	183.6	2894	693.4	-6.8	4385	458	141.2	5880	318.8	135.1	7366			
206.2	223.6	1405	461.2	182.4	2909	691.2	-6.3	4401	455.9	140.9	5895	317.7	134.8	7382			
208.3	224	1420	464.2	181.1	2925	688.9	-6.5	4416	454.4	140.8	5910	316.3	134.9	7397			
210.5	224.1	1435	467.4	179.5	2940	686.7	-5.9	4431	452.6	140.5	5926	314.9	134.5	7412			
212.7	224.4	1450	469.8	178.3	2955	684.1	-5.4	4447	451.1	140.5	5941	313.7	134.5	7427			

Thermomagnetic results for sample AL009

TEMP (°C)	TSUSC (°C)	TIME (s)	TEMP (°C)	TSUSC (°C)	TIME (s)	TEMP (°C)	TSUSC (°C)	TIME (s)	TEMP (°C)	TSUSC (°C)	TIME (s)	TEMP (°C)	TSUSC (°C)	TIME (s)	TEMP (°C)	TSUSC (°C)	TIME (s)
22.6	49.8	0	222.3	66.1	1472	465.4	36.6	2952	677.7	-115.3	4443	447	-13.7	5935	278.7	-13.8	7417
22.6	51.8	17	224.5	66.5	1487	468.3	36.3	2968	675.5	-115.5	4458	445	-13.6	5950	276.2	-13.7	7433
23.9	51.9	32	226.7	66.7	1502	471	35.8	2983	673.2	-115	4474	443.2	-13.7	5965	273.9	-13.8	7448
25.7	51.8	47	229.1	67	1517	473.7	35.2	2998	671	-114.7	4489	441.7	-13.7	5981	271.4	-13.7	7463
27.7	51.9	62	231.9	67.3	1533	476.1	34.6	3013	668.8	-114.6	4504	439.9	-13.7	5996	268.9	-14	7478
29.8	52	77	234.4	67.5	1548	478.8	34	3029	666.2	-114.2	4520	438.8	-13.9	6011	266.4	-13.8	7493
31.9	51.9	92	236.8	67.8	1563	481.1	33.7	3044	663.6	-114.3	4535	437.3	-13.6	6026	264.2	-13.8	7509
33.9	52.1	107	239.6	67.8	1578	484.1	33.1	3059	661.1	-113.9	4551	436.1	-13.7	6042	262	-14	7524
36	52.2	122	242.3	68.3	1593	487.1	32.3	3075	658.9	-113.5	4566	434.6	-13.9	6057	259.8	-13.9	7539
38.1	52.2	137	244.8	68.4	1609	489.8	31.8	3090	656.3	-113.5	4581	433.2	-13.9	6073	257.8	-13.9	7554
39.9	52.4	152	247.6	68.7	1624	492.5	31.6	3105	654.1	-113	4597	431.7	-13.9	6088	255.6	-14	7569
41.7	52.4	168	250.1	69.2	1639	495.5	31	3121	651.9	-112.9	4612	429.7	-14	6103	253.4	-13.9	7584
43.5	52.3	183	252.6	69.3	1655	498.2	30.4	3136	649.7	-112.5	4627	427.9	-13.9	6119	251.2	-13.8	7600
45.3	52.5	198	255.1	69.4	1670	501.2	29.6	3152	647.1	-112.1	4643	425.8	-13.9	6134	249.2	-13.9	7615
47.2	52.6	213	257.5	69.6	1685	503.9	29.1	3167	644.9	-112	4658	424.1	-14.1	6149	247	-14.1	7630
49	52.8	228	260	69.8	1700	506.6	28.7	3182	642.4	-111.7	4673	422.6	-14.2	6165	244.5	-14.1	7645
50.5	52.6	243	262.3	70.2	1715	509	28.4	3198	640.2	-111.3	4689	420.9	-13.9	6180	242.3	-14	7660
52.4	52.7	258	264.8	70.3	1731	511.8	27.4	3213	637.6	-110.8	4704	419.4	-14	6195	240.1	-14	7675
53.9	52.7	273	267.3	70.3	1746	514.5	27.3	3228	635.1	-110.6	4720	418	-13.9	6211	237.9	-14.1	7690
55.7	52.9	288	269.8	70.7	1761	517.2	26.7	3244	632.6	-110.3	4735	416.5	-13.9	6226	235.7	-14.3	7706
57.6	53.1	304	272.3	70.6	1776	520.2	26.1	3259	630.1	-110.2	4751	415	-14.3	6241	233.3	-14.3	7721
59.4	53	319	274.5	71	1792	522.9	25.5	3274	627.6	-109.5	4766	413.3	-14.1	6256	231.1	-14.6	7736
60.9	53.2	334	276.7	70.8	1807	526	25	3290	625	-109	4782	411.8	-14.3	6272	228.6	-14.1	7751
62.8	53.3	349	279.5	70.9	1822	529	24.5	3305	622.5	-108.7	4797	410.1	-14.2	6287	226.1	-14.3	7766
64.6	53.4	364	282	71.1	1837	532	23.9	3321	620.3	-108.4	4812	408.9	-14.2	6302	223.6	-14.3	7781
66.4	53.4	380	284.3	70.9	1852	534.8	23.4	3336	618.1	-107.6	4828	407.5	-14.5	6318	221.5	-14.3	7797
68	53.5	395	286.8	71.1	1868	537.8	22.9	3351	615.6	-107.1	4843	406	-14.1	6333	219	-14.4	7812
69.8	53.6	410	289.3	71.2	1883	540.6	22.1	3367	612.8	-105.5	4859	404.3	-14.2	6348	216.5	-14.6	7827
71.4	53.6	425	291.8	71.3	1898	543	21.5	3382	610.3	-103.6	4874	402.5	-14.2	6364	214.1	-14.4	7842
73.2	53.7	440	294.1	71.2	1913	545.4	21.1	3397	607.5	-98.7	4890	400.8	-14.4	6379	211.3	-14.5	7857
75	53.7	455	296.6	71.4	1929	548.2	20.4	3413	605	-92.9	4905	398.7	-14.4	6394	208.9	-14.6	7872
76.9	53.8	470	298.8	71.1	1944	551	20	3428	602.2	-86.8	4920	396.7	-14.4	6410	206.2	-14.8	7888
79	54	485	301.1	71.2	1959	553.4	19.4	3444	599.7	-79.4	4936	394.7	-14.3	6425	203.7	-14.7	7903
80.8	54.1	501	303.6	71	1974	556.2	18.9	3459	597.2	-71.9	4951	392.9	-14.4	6440	201.3	-14.8	7918
82.6	54.2	516	306.4	70.8	1990	558.9	18.2	3474	594.7	-63.7	4967	390.6	-14.6	6456	198.8	-14.7	7933
84.5	54.2	531	309.2	70.7	2005	562	17.6	3490	592.2	-55.3	4982	388.3	-14.2	6471	196.4	-14.9	7948
86.3	54.4	546	311.8	70.7	2020	565.1	17	3505	589.5	-45.9	4998	386	-14.3	6486	194.2	-14.9	7963
88.4	54.4	561	314	70.7	2035	568.4	16.1	3520	587	-37.3	5013	384	-14.2	6502	191.7	-15.1	7978
90.3	54.5	576	316.6	70.5	2050	571.5	15	3535	584.5	-29.8	5028	381.7	-14.3	6517	189.3	-14.9	7994
92.1	54.6	591	318.5	70.3	2066	574.3	12.6	3551	581.7	-24.8	5044	379.3	-14.3	6532	186.9	-15.1	8009
94.2	54.6	607	320.8	70	2081	577.4	8.4	3566	579.2	-20.8	5059	377.3	-14.3	6548	184.7	-15.2	8024
96.3	54.7	622	323.1	69.9	2096	580.2	3.2	3582	576.8	-18	5074	375.3	-14.2	6563	182.3	-15.3	8039
98.4	54.7	637	325.6	69.7	2112	583.3	-4.3	3597	574.3	-15.4	5090	373	-14.1	6578	180.1	-15.1	8054
100.8	55	652	327.9	69.3	2127	586	-14.3	3612	571.8	-14.3	5105	371.3	-14.3	6593	177.7	-15.3	8069
102.9	55.3	667	330.2	69.1	2142	589.5	-27.9	3628	569.4	-13.7	5120	369.6	-14.2	6609	175.2	-15.3	8084
105	55.4	682	332.4	68.5	2157	592.6	-43.7	3643	566.9	-13.5	5136	367.8	-14.3	6624	172.8	-15.2	8100
107.1	55.4	697	334.7	68.3	2173	595.4	-57.2	3658	564.4	-13	5151	365.8	-14.3	6639	170.4	-15.5	8115
109.5	55.3	712	337	67.7	2188	598.5	-70.3	3674	562	-12.7	5167	364.1	-14.2	6654	168	-15.4	8130
111.9	55.6	728	339.2	67.7	2203	601.3	-81.2	3689	559.5	-12.9	5182	362.1	-14.2	6670	165.5	-15.4	8145
114.3	55.8	743	341.2	67.1	2218	603.8	-88.9	3704	557.1	-12.9	5197	360.4	-14.1	6685	163.1	-15.5	8160
116.4	56	758	343.2	66.5	2234	606.6	-95.1	3720	554.6	-12.7	5213	358.7	-14.1	6700	160.7	-15.3	8175
118.5	56.2	773	344.9	66.2	2249	609.7	-99.6	3735	552.5	-13	5228	356.9	-14	6716	158.5	-15.2	8191
120.6	56.5	788	347.2	65.6	2264	613.1	-101.4	3750	549.7	-12.8	5243	355.5	-13.9	6731	156.4	-15.4	8205
122.8	56.2	804	349.2	65	2279	616.3	-102.8	3766	547.3	-12.8	5259	354.4	-14	6746	154.5	-15.3	8221
124.9	56.4	819	351.5	64.1	2295	619.7	-104	3781	544.8	-12.8	5274	352.9	-13.7	6761	152.1	-15.5	8236
126.7	57.1	834	353.8	63.7	2310	622.8	-104.9	3796	542.4	-12.7	5290	351.8	-13.9	6777	150	-15.4	8251
128.9	56.7	849	356.4	63	2325	626.3	-105.8	3812	540	-12.7	5305	350.9	-13.8	6792	148.1	-15.4	8266
131	57	864	358.7	62.2	2340	629.8	-106.6	3827	537.5	-12.8	5320	349.8	-13.8	6807	145.9	-15.4	8281
132.9	57.1	879	360.9	61.7	2356	632.9	-107.3	3843	534.5	-12.8	5336	348.9	-13.7	6823	144.1	-15.3	8296
134.7	57.3	895	363.5	61.1	2371	636.4	-108	3858	531.7	-12.6	5351	348.1	-13.7	6838	141.9	-15.4	8311
136.9	57.6	910	366.1	60.3	2386	639.5	-108.6	3874	528.7	-12.8	5366	346.9	-13.7	6853	139.8	-15.3	8326
138.7	57.7	925	368.7	59.7	2401	642.7	-109.1	3889	525.7	-12.9	5382	345.8	-13.8	6868	137.7	-15.4	8341
140.9	57.8	940	371.3	58.9	2417	646.2	-109.7	3904	523.2	-12.8	5397	344.1	-13.8	6884	135.5	-15.5	8356
143	58.1	955	373.9	57.9	2432	649.7	-110.3	3920	520.5	-12.8	5413	342.4	-13.8	6899	133.4	-15.4	8371
145.1	58.4	971	376.5	57	2447	653.2	-110.7	3935	518.1	-12.7	5428	340.4	-13.9	6914	131	-15.5	8387
147.3	58.6	986	379.1	56.3	2463	656.6	-111.2	3950	515.7	-13	5444	338.4	-13.4	6930	128.6	-15.2	8402
149.4	58.7	1001	381.7	55.4	2478	660.5	-111.6	3966	513	-12.8	5459	336.4	-13.6	6945	126.5	-15.4	8417
151.8	58.9	1016	384.5	54.9	2493	664	-112.1	3981	510.6	-12.8	5474	334.1	-13.7	6960	124.4	-15.4	8432
154	59.1	1031	387.1	53.9	2509	667.2	-113	3997	507.8	-12.8	5489	332.1	-13.7	6975	122.2	-15.3	8447
156.1	59.4	1047	389.7	53	2524	670.3	-113.2	4012	505.4	-12.9	5505	329.9	-13.6	6991	119.8	-15.2	8462
158.5	59.6	1062	392.4	52.5	2539	673.5	-113.7	4027	502.7	-13.1	5520	328.2	-13.6	7006	117.7	-15.1	8477
161	59.7	1077	395	51.6	2555	676.7	-114	4043	500.3	-13.1	5536	326.8	-13.6	7021	115.6	-15.2	8492
163.4	60.1	1092	397.9	51.2	2570	679.9	-114.5	4058	497.6	-12.8	5551	325.3	-13.8	7036	113.5	-15.3	8507
165.8	60.4	1107	400.8	50.3	2585	682.8	-114.7	4073	495.2	-13	5566	323.6	-13.6	7052	111.6	-15.1	8522
168.2	60.5	1122	403.1	49.9	2600	686	-114.7	4089	492.5	-12.8	5582	322.2	-13.7	7067	109.5	-15	8537
170.4	60.7	1138	405.7	49.1	2616	689.3	-115.2	4104	490.1	-13.1	5597	320.8	-13.6	7082	107.7	-15	8552
172.5	60.9	1153	408	48	2631	692.5	-115.8	4120	487.4	-13.2	5612	319.4	-13.8	7097	105.5	-15	8567
175	61.1	1168	410.9	47.6	2646	695.4	-116.1	4135	485.3	-13.1	5628	318	-13.6	7113	103.7	-14.8	8582
177.4	61.3	1183	413.6	47.1	2662	698.6	-116.2	4150	482.9	-13.1	5643	316.6	-13.4	7128	101.6	-14.9	8597
179.8	61.4	1198	415.9	46.6	2677	701.2	-116.6	4166	481.1	-13	5658	315.4	-13.7	7143	99.7	-15	8612
182.3	61.8	1214	418.5	46	2692	703.1	-117	4181	479.4	-13.1	5674	314	-13.8	7158	97.9	-14.8	8627
184.7	62.2	1229	421.2	45.4	2707	704.4	-117.1	4196	477.6	-13	5689	312.6	-13.7	7174	95.8	-14.7	8642
187.1	62.3	1244	423.8	44.9	2723	704.8	-117	4212	475.5	-13.2	5704	310.9	-13.7	7189	93.7	-14.7	8657
189.6	62.7	1259	426.7	44.3	2738	704.1	-117.2	4227	473.4	-13.3	5720	309.2	-13.9	7204	91.8	-14.6	8672
192	62.9	1274	429.4	43.8	2753	703.1	-117.2	4242	471.6	-13.3	5735	307.3	-13.7	7219	90.3	-14.8	8687
194.2	63.1	1290	432	43.3	2769	702.2	-117.2	4258	469.8	-13.4	5751	305	-13.7	7234	88.7	-14.5	8702
196.4	63.4	1305	434.6	42.8	2784	700.5	-117.1	4273	468	-13.4	5766	302.8	-13.6	7250	87.1	-14.6	8718
198.8	63.6	1320	437.3	42.2	2799	698.9	-117.2	4289	466	-13.3	5781	300.5	-13.8	7265	85.5	-14.4	8732
201.3	64	1335	440.2	41.7	2814	697	-117	4304	463.9	-13.4	5797	298.3	-13.7	7280			
203.7	64.2	1350	442.9	41	2830	695.1	-116.6	4320	461.8	-13.4	5812	296	-13.7	7296			
205.9	64.6	1366	445.5	40.6	2845	693.1	-116.3	4335	459.7	-13.4	5827	293.5	-13.6	7311			
208.3	64.8	1381	448.5	40.2	2860	690.9	-116.5	4350	458	-13.5	5843	291.5	-13.7	7326			
210.8	65	1396	451.4	39.6	2876	688.6	-116.5	4366	456.2	-13.4	5858	289.6	-13.9	7341			
213.3	65.4	1411	454.4	38.9	2891	686.4	-116.1	4381	454.7	-13.4	5873	287.3	-13.8	7356			
215.4	65.7	1426	457.1	38.7	2906	683.8	-115.9	4397	452.9	-13.5	5889	285.4	-13.5	7372			
217.9	65.7	1442	459.7	38.1	2921	681.9	-116	4412	450.9	-13.6	5904	283.1	-13.8	7387			
220.1	66	1457	462.4	37.2	2937	679.6	-115.9	4427	449.1	-13.6	5919	280.9	-13.8	7402			

Thermomagnetic results for sample AL011

TEMP (°C)	TSUSC (°C)	TIME (s)	TEMP (°C)	TSUSC (°C)	TIME (s)	TEMP (°C)	TSUSC (°C)	TIME (s)	TEMP (°C)	TSUSC (°C)	TIME (s)	TEMP (°C)	TSUSC (°C)	TIME (s)	TEMP (°C)	TSUSC (°C)	TIME (s)
16.2	216.8	0	217.6	246.7	1510	491.6	227.2	3134	654.1	-92	4663	425.8	128	6154	280.1	126	7629
16.4	211.1	16	220.4	246.9	1527	494.3	228.4	3151	652.2	-90.6	4678	424.4	128.3	6170	278.4	125.7	7644
17.7	212.2	31	223.4	247.5	1543	497.6	227	3168	650	-90.2	4694	422.6	128	6185	277	125.7	7659
19.2	212.3	46	226.4	249.4	1560	500.6	226.4	3185	647.8	-89.9	4709	421.2	127.8	6200	275.6	125.9	7674
21.3	212.4	61	229.4	249.9	1577	503.6	231.6	3202	645.9	-89.1	4725	419.4	128.1	6215	274.2	126	7690
23.4	212.6	76	232.7	250.4	1594	506.9	228.7	3219	643.6	-88.1	4740	418	127.9	6230	273.1	125.8	7705
25.2	212.5	92	235.7	250.9	1610	509.9	228.9	3236	641.4	-87.2	4755	416.5	127.5	6246	272	125.9	7720
27	212.6	106	238.5	251.8	1627	513.6	228.4	3253	638.9	-85.4	4771	415	127.8	6261	270.9	125.5	7735
29	212.9	122	241.5	250.9	1644	516.9	229.1	3270	636.1	-84.6	4786	413.9	127.5	6276	269.8	125.6	7750
30.8	213	137	244.3	252.7	1661	519.9	230.7	3287	633.9	-83.6	4802	412.7	127.3	6292	268.4	125.9	7765
32.4	213.2	152	247.3	253.4	1677	523.2	230.9	3303	631.3	-82.2	4817	411.8	127.5	6307	267	125.6	7781
34.2	213.2	167	250.3	254.3	1694	526.6	233.2	3320	628.8	-81.2	4833	410.7	127.9	6322	265.9	125.6	7796
35.8	213.4	182	253.1	254.1	1711	529.6	229.3	3337	626.3	-78.9	4848	409.5	127.4	6338	264.5	125.2	7811
37.3	213.5	197	255.9	255	1728	532.4	232.1	3354	623.8	-77.2	4863	408	127.1	6353	262.8	125.4	7826
38.9	213.9	212	258.7	256	1744	535.4	231.9	3371	621.6	-74.8	4879	406.6	127.7	6368	260.9	125.2	7841
40.4	213.9	227	261.4	255.6	1761	537.8	232	3388	618.8	-71.8	4894	405.4	127.6	6383	258.9	125	7856
42	214.2	242	264.2	256	1778	541.2	233.2	3405	616.3	-69.1	4910	404.3	127.5	6398	257	125	7871
43.5	214.1	257	267	256.2	1795	544.5	233.2	3422	613.8	-66.4	4925	403.4	127.3	6414	254.8	125	7886
44.8	214.4	272	269.8	256.6	1812	547.6	235.4	3439	611.3	-61.9	4941	401.9	127.5	6429	252.8	124.8	7901
46.4	214.6	287	272.5	258.9	1829	551	236.6	3456	608.8	-56.4	4956	400.5	127.5	6444	251.2	124.7	7916
47.9	214.9	302	275.6	257.6	1845	554.3	234.5	3473	605.9	-48.9	4971	399	127.4	6460	249.2	124.9	7932
49.5	215.3	317	278.7	256.1	1862	557.7	235.6	3490	603.8	-41.1	4987	397.3	127.4	6475	247.3	124.6	7947
51.1	215.3	332	281.2	258.4	1879	561.1	232.8	3507	601.3	-32.1	5002	395.3	127	6490	245.4	124.7	7962
52.6	215.5	347	284.3	258.7	1896	564.1	221.4	3522	598.8	-21.3	5018	392.9	127.3	6505	243.2	124.6	7977
54.2	215.9	363	286.8	259.8	1912	567.5	200.2	3538	596.3	-8.8	5033	390.9	127.3	6520	241.2	124.4	7992
56	215.9	378	289.6	257.4	1929	570.6	167.1	3553	594.1	4.5	5048	389.2	127.2	6536	239.3	124.3	8007
57.6	216.3	393	292.4	259.5	1946	573.7	128.2	3568	591.3	20	5064	387.1	127.2	6551	237.1	124.2	8022
59.4	216.5	408	295.2	260.2	1963	576.8	97.9	3584	588.5	36.5	5079	384.8	127.1	6566	235.2	124.2	8037
61.2	216.6	423	298	259.2	1979	579.5	73	3599	585.7	54.1	5095	382.8	127.2	6582	233.3	124.2	8052
63	217	438	300.8	259.2	1996	582.9	51.5	3615	582.9	73.3	5110	381.1	127.3	6597	231.1	124.1	8067
64.9	217.2	453	303.9	259.2	2013	586	31	3630	580.5	93.9	5125	379.3	127.4	6612	229.1	123.9	8082
66.7	217.4	468	307	259	2030	588.8	13.4	3645	577.7	114.8	5141	377.9	127.2	6627	227.2	123.9	8097
68.2	217.7	483	309.8	260.8	2047	591.6	-2.3	3661	575.5	135.9	5156	376.5	127.6	6642	225.3	123.7	8112
70.1	217.8	498	312.6	259.1	2064	594.1	-16.9	3676	573.4	161.2	5172	375.3	127.3	6658	223.6	123.5	8127
71.6	218.3	513	315.2	258.3	2080	596.9	-31	3692	570.9	187.1	5187	373.9	127.6	6673	221.5	123.3	8142
73.2	218.5	528	318	258.5	2097	599.4	-41.7	3707	568.4	204.8	5203	372.4	127.6	6688	219.5	123.5	8157
75	218.8	543	321.1	259.5	2114	602.2	-50.9	3723	566	209.5	5218	370.7	127.9	6703	217.4	123.3	8173
77.1	219.2	558	323.9	259.1	2131	604.7	-58.5	3738	563.2	208.7	5233	369	127.9	6719	214.9	123.2	8188
78.7	219.6	573	326.8	259.9	2148	607.2	-64.1	3753	560.5	206.5	5249	367.5	127.6	6734	212.4	123	8203
80.5	220	588	329.6	261	2164	610	-67.6	3769	558	203.8	5264	366.1	127.9	6749	210.2	122.9	8218
82.4	220	604	332.4	258.5	2181	613.1	-70.9	3784	555.2	201.4	5279	364.7	128.2	6764	207.8	122.8	8233
84.2	220.6	619	335.3	259.1	2198	616.6	-73.9	3799	552.5	198.1	5295	363.5	128.2	6779	205.3	122.4	8248
86.3	220.7	634	338.1	259.7	2215	619.4	-76.3	3815	550	195.5	5310	362.4	128.2	6795	203.2	122.3	8263
88.4	221.2	649	341	259.1	2232	622.5	-78.1	3830	547.9	192.7	5325	360.9	128.2	6810	200.7	122.1	8278
90.8	221.6	664	343.8	260.8	2248	625.7	-79.4	3846	545.8	189.7	5341	359.5	128	6825	198.5	122	8293
93.2	221.9	679	346.9	260.7	2265	629.1	-81.5	3861	543.3	188.4	5356	358.1	128.4	6841	196.1	122	8308
95.5	222.6	694	350.1	260	2282	632	-82.8	3877	540.6	185.4	5372	356.7	128.5	6856	193.9	121.8	8323
97.9	222.9	709	353.2	260.6	2299	634.8	-84.1	3892	538.4	183.3	5387	355.2	128.2	6871	191.5	121.6	8338
100	223.3	724	356.1	259.5	2316	638.3	-85.5	3907	536	180.5	5402	353.8	128	6886	189	121.4	8353
102.1	223.8	739	359.2	259.6	2333	641.4	-87.4	3923	533.6	177.6	5418	352.6	128.4	6901	186.9	121.3	8368
104	224.3	755	362.4	260.3	2349	644.9	-88.2	3938	531.1	175.2	5433	351.2	128.4	6916	184.4	121.2	8383
106.3	224.5	770	365.3	260.5	2366	648.7	-89.1	3954	528.7	172.4	5449	349.8	128.4	6931	182.3	121	8398
108.5	225.2	785	368.4	259.2	2383	651.9	-90.9	3969	525.7	169.7	5464	348.4	128.4	6946	179.8	120.9	8413
110.8	225.6	800	371	258.5	2400	655.1	-91.4	3985	522.9	166.9	5479	346.7	128.3	6962	177.4	120.9	8428
112.9	226	815	373.3	259.2	2416	657.9	-93.1	4000	520.2	164.1	5495	344.7	128.2	6977	175.2	120.7	8443
115.1	226.6	830	375.9	258	2433	660.8	-94.2	4015	517.8	161.4	5510	342.7	128.1	6992	172.8	120.6	8458
117.2	227.1	845	378.5	257.2	2450	664	-95.4	4031	515.4	158.6	5526	341	128.1	7007	170.4	120.4	8473
119	227.6	861	381.1	257	2467	667.2	-96.2	4046	513.3	156.5	5541	339.5	128.2	7022	168	120.6	8488
120.9	227.3	876	383.4	255.8	2484	670.3	-97.5	4062	510.9	154	5557	338.1	128.2	7037	165.3	120.2	8503
123	228.1	891	386	254.4	2501	673.2	-98.1	4077	508.4	150.7	5572	336.4	128.1	7053	162.8	120.1	8518
125.2	228.6	906	388.3	255.1	2517	676.4	-98.9	4092	506	147.9	5587	335	127.9	7068	160.4	120.1	8533
127.3	228.7	921	390.3	252.5	2534	679.6	-99.9	4108	503.9	143.9	5603	333.8	127.9	7083	158	120.1	8548
129.7	229	936	392.4	252.3	2551	682.8	-100.5	4123	501.5	139.8	5618	332.4	128.1	7098	155.9	120	8563
132.1	229.9	951	394.4	250.9	2568	686	-101.4	4139	499.1	138.1	5633	330.7	128.1	7113	153.7	119.7	8578
134.2	230.1	966	396.4	249.4	2585	689.6	-101.9	4154	496.7	137.1	5649	329.3	128	7129	151.8	119.8	8593
136.6	230.5	982	398.7	248.9	2601	692.8	-102.6	4169	494.3	136.1	5664	327.9	128	7144	149.4	119.9	8608
139	230.7	997	401.1	247.5	2618	696	-103.4	4185	491.9	135.2	5679	326.5	127.6	7159	147.3	119.9	8623
141.1	230.9	1012	403.7	241.8	2635	699.3	-103.6	4200	489.2	134.8	5695	325.1	127.8	7174	145.1	119.8	8638
143.3	231.6	1027	406.3	244.4	2652	702.5	-103.6	4216	486.8	134	5710	323.9	127.7	7189	143	119.9	8653
145.7	231.9	1042	408.9	242.6	2669	704.1	-104.3	4231	484.4	133.8	5725	322.8	127.4	7205	140.6	119.7	8668
148.1	231.9	1057	411.5	239	2686	704.4	-104.5	4247	482	133.2	5741	321.4	127.5	7220	138.5	119.6	8683
151	231.6	1075	414.4	237.4	2702	704.1	-104.6	4262	479.4	132.6	5756	320.2	127.5	7235	136.3	119.7	8698
153.7	232.5	1093	417.7	235.3	2719	703.1	-104.4	4277	476.7	132.4	5771	318.8	127.4	7250	134.2	119.6	8713
155.9	233.8	1108	420.9	236.5	2736	701.5	-104.4	4293	473.7	132.4	5787	317.7	127.4	7265	132.1	119.5	8728
158.5	234.3	1124	423.8	235.7	2753	699.9	-104.5	4308	470.7	131.9	5802	316	127.3	7280	129.9	119.6	8743
161.2	234.8	1142	426.7	233.2	2770	698.3	-104.5	4324	468	131.7	5818	314.6	127.5	7295	127.5	119.6	8758
163.6	234.8	1158	429.7	231.9	2787	696.4	-104.2	4339	465.7	131.3	5833	313.2	127.5	7311	125.4	119.5	8773
166.1	234.5	1175	432.6	231.4	2804	694.7	-104.3	4355	463.3	130.9	5848	311.8	127.1	7326	123	119.6	8788
168.8	235.7	1192	435.5	230.3	2821	692.8	-103.7	4370	461.2	131	5863	310.1	127.3	7341	120.9	119.4	8803
171.5	235.7	1208	438.2	229.4	2838	690.9	-103.5	4385	459.4	130.7	5879	308.4	127.1	7356	118.8	119.4	8818
173.9	236.3	1225	441.1	227.3	2854	688.9	-102.7	4401	457.7	130.4	5894	306.4	127	7371	116.9	119.5	8833
176.9	236.7	1242	444.4	228.4	2871	687.3	-102.4	4416	455.9	130.4	5909	305	127	7386			
179.3	236.6	1259	447.3	227.4	2888	684.8	-102.5	4432	453.8	130	5925	303.6	126.9	7402			
182	237.6	1276	450.3	228.5	2905	682.5	-101.8	4447	451.7	129.8	5940	301.9	127.3	7417			
184.4	240.1	1292	453.5	226.6	2922	680.9	-100.8	4463	450	129.8	5955	300.2	126.9	7432			
187.1	240	1309	456.5	227	2939	679	-100.6	4478	447.9	129.5	5971	298.5	126.7	7447			
189.8	239	1326	459.1	227	2955	676.7	-100.2	4493	445.5	129.4	5986	296.9	126.5	7462			
192.6	240.4	1343	461.5	226.3	2971	674.8	-99.6	4509	443.5	129.4	6001	295.5	126.3	7478			
195.3	240.7	1359	464.8	225.7	2988	672.9	-98.8	4524	441.4	129.4	6016	294.1	126.5	7493			
197.7	240.9	1376	467.7	226.4	3004	671	-97.6	4539	439.6	129.4	6032	292.7	126.8	7508			
200.2	241.4	1393	471	226.4	3019	669.1	-97.5	4555	437.6	128.8	6047	290.7	126.3	7523			
202.6	244.8	1410	474	226.3	3034	666.8	-96.7	4570	435.5	129.3	6062	289	126.4	7538			
204.8	245.2	1426	477.6	227.7	3052	664.9	-95.8	4586	433.8	128.9	6078	287.6	126.2	7553			
207.2	243.9	1443	480.2	226.2	3067	662.7	-95.2	4601	432	128.7	6093	285.9	126.1	7568			
210	244.3	1460	482.9	225.1	3084	660.5	-94	4617	430.2	128.4	6108	284.5	126.1	7584			
212.4	245.4	1476	485.9	226.4	3101	658.6	-92.8	4632	428.8	128.3	6124	282.9	126	7599			
214.9	246.3	1493	488.6	228.6	3118	656.6	-92.7	4647	427.3	128.4	6139	281.5	126	7614			

Thermomagnetic results for sample AL017

TEMP (°C)	TSUSC (°C)	TIME (s)	TEMP (°C)	TSUSC (°C)	TIME (s)	TEMP (°C)	TSUSC (°C)	TIME (s)	TEMP (°C)	TSUSC (°C)	TIME (s)	TEMP (°C)	TSUSC (°C)	TIME (s)	TEMP (°C)	TSUSC (°C)	TIME (s)
17.4	651.2	0	238.2	697.3	1615	511.8	509.2	3248	645.9	-122	4774	403.1	308.7	6370	159.9	275.3	7998
17.4	651.5	18	240.7	698.2	1632	514.8	509.3	3265	643.6	-121.7	4789	401.1	305.9	6387	157.2	275.1	8015
18.7	651.7	35	243.2	697.7	1649	517.5	510.3	3281	641.1	-121	4804	398.7	308.2	6404	154.5	274.6	8031
21	652.2	52	245.9	700.6	1666	520.5	511	3298	638.6	-120.9	4820	396.4	306.5	6420	152.1	274	8048
23.9	651.9	68	249	699.5	1682	523.2	511.4	3315	636.4	-120.3	4835	394.4	307.5	6437	149.7	275	8065
26.2	652.3	85	251.7	700.2	1699	526	510.6	3332	634.2	-119.8	4851	392.1	307.5	6454	147.3	272.4	8082
28.8	652.6	101	254.5	701.6	1716	529	512	3349	631.6	-119.3	4867	389.5	307.2	6471	145.1	272.2	8098
31.1	653.1	118	257	702.6	1733	531.7	513.5	3366	629.4	-118.7	4882	387.4	305.5	6488	142.7	272.8	8115
33.2	653.2	134	259.8	703	1749	534.8	511.9	3383	627.2	-118.3	4897	385.1	305.6	6505	140.3	272.9	8132
35.5	653.1	151	262.5	704.7	1766	537.5	515.3	3400	625	-117.7	4913	383.1	306	6522	138.2	274	8148
37.6	654.2	168	265	703.7	1783	540.3	516.5	3417	622.5	-117	4928	381.7	306.5	6538	135.8	273.8	8165
39.4	654.2	184	267.8	705.1	1800	543.3	515.3	3434	620.3	-115.9	4944	379.9	305.7	6555	133.1	273.6	8181
41.5	653.6	201	270.3	706.1	1816	546.7	517.8	3450	618.1	-115.2	4959	378.5	304.7	6572	130.7	272.7	8198
43.3	653.9	217	273.1	707.4	1833	549.4	517.5	3467	615.6	-113.9	4975	377	305.3	6589	128.3	272.5	8215
45.1	653.7	234	275.9	707.6	1850	552.5	519	3484	613.1	-111	4990	375.6	305.1	6606	125.7	272.6	8231
46.9	654.9	250	278.4	709.6	1867	555.8	517.5	3501	610.3	-105.2	5006	373.9	304.5	6623	123	273.8	8248
48.7	655.1	266	281.2	709.7	1884	558.9	511.3	3518	607.2	-96.5	5021	372.1	306	6639	120.6	274.3	8265
50.5	655	283	283.7	710.3	1900	562.3	470.8	3535	604.4	-84.9	5036	370.4	302.8	6656	118	274.1	8281
52.4	655.4	300	286.2	711.7	1917	565.7	400.3	3552	601.6	-70.5	5052	368.7	304.3	6673	115.6	274.6	8298
54.2	654.7	316	289	714.1	1934	569.4	325	3569	598.8	-54.6	5067	366.4	304.1	6690	113.2	274.6	8314
56.3	655.5	333	291.5	713.6	1951	572.8	265.5	3586	596	-35.1	5083	364.4	302.8	6707	110.8	273	8331
58.1	655.7	349	294.3	714.3	1967	576.5	222.2	3601	593.2	-14.9	5098	362.7	303.2	6724	108.7	274.6	8348
59.9	656.4	365	297.1	714.7	1984	579.9	173	3617	590.7	5.9	5114	360.4	302.3	6741	106.3	273.7	8364
61.7	656.4	382	299.9	716.4	2001	583.6	121.9	3632	588.2	28.4	5129	358.4	302	6757	104	275.6	8381
63.5	657.3	399	302.8	716.5	2018	586.7	75.8	3647	585.7	56.7	5144	356.4	302.4	6774	101.8	274.7	8398
65.6	656.7	415	305.3	717.7	2034	589.5	33.5	3663	583.6	81	5160	354.1	302.4	6791	99.7	274.4	8414
67.5	656.8	432	308.1	718.3	2051	592.2	-2.9	3678	580.8	104.8	5175	351.8	302.2	6808	97.4	275.6	8431
69.6	657.7	448	310.9	719.5	2068	594.7	-34.9	3694	578.3	129.7	5191	348.9	300.8	6825	95.3	275.1	8447
71.4	656.9	465	313.7	719.5	2085	597.5	-62.3	3709	575.5	155.5	5206	345.8	302	6841	93.2	273.7	8464
73.2	658.2	481	316.6	719.5	2102	600.6	-86.3	3724	573.1	178.5	5222	342.9	302.4	6858	91	274.9	8481
75	658.4	498	319.4	719.4	2119	603.4	-100.6	3740	570.9	206.3	5237	340.4	300.8	6875	88.9	275.7	8497
76.9	658.5	515	322.5	720.9	2135	606.3	-107.3	3755	568.1	252.1	5254	337.8	299.8	6892	86.8	276	8514
78.7	659.5	531	325.6	721.3	2152	608.8	-111.4	3771	565.7	287.2	5271	335.3	299.9	6909	84.5	276.1	8530
80.5	658.4	548	328.5	721.1	2169	611.6	-113.7	3786	563.2	311.4	5288	333	301	6926	82.4	275.5	8547
82.6	658.2	564	331.3	720.5	2186	614.7	-115.6	3802	560.8	320.5	5305	330.7	298.7	6942	80.3	275.9	8563
84.5	658.3	581	334.1	722.3	2203	617.8	-117.1	3817	557.7	323.8	5322	328.7	299.3	6959	78.2	275.6	8580
86.3	658.7	598	336.7	721.6	2219	620.6	-118.1	3832	554.9	324.2	5338	326.8	299	6976	76.4	275.2	8596
88.2	659.9	614	339.5	720.1	2236	623.5	-118.3	3848	552.2	324.8	5355	324.5	298.8	6993	74.3	276	8613
90	660.1	631	342.4	720.2	2253	626.3	-119.5	3863	550	323.9	5372	321.9	297.4	7010	72.4	276.8	8629
92.4	660.1	648	345.2	718.3	2270	629.4	-119.7	3879	547.6	324.1	5390	319.4	298.2	7027	70.6	276.5	8646
94.7	660.4	664	348.1	715.2	2286	632.3	-120.6	3894	545.8	323.6	5406	316.8	298.3	7043	68.8	275.7	8663
97.1	661.3	681	350.9	714.5	2303	635.4	-120.8	3909	543.9	325	5423	314	297.2	7060	66.9	276.2	8679
99.7	661.8	697	353.8	711.2	2320	638.6	-121.6	3925	541.8	322.9	5440	311.5	296.3	7077	65.1	276.4	8696
102.1	662.8	714	356.4	709.2	2337	641.7	-121.7	3940	539.7	323.4	5457	309	295.7	7094	63.3	277.3	8712
104.8	662.1	730	359.5	703.8	2354	645.2	-122.4	3956	537.5	320.7	5474	306.1	298	7111	61.5	276.8	8729
107.4	663.2	747	362.4	699.3	2371	648.4	-122.8	3971	535.4	322.3	5491	303.6	294.6	7127	59.6	276.6	8745
110	664	764	365.3	692.8	2387	651.6	-123.4	3986	532.4	321	5508	300.8	296	7144	57.6	276.1	8763
112.4	664.3	781	367.8	685	2404	655.1	-123.7	4002	529.3	322.5	5525	298	293.9	7161	54.2	276.3	8779
115.1	664	797	370.7	678.3	2421	658.2	-124.9	4017	526.6	319.8	5542	295.5	296.9	7178	50.3	276.9	8796
117.2	665.3	814	373.3	671.3	2438	661.1	-125.2	4033	523.2	321.1	5559	292.7	295.7	7195	46.4	276.8	8812
119.6	665.6	830	376.2	661.9	2455	663.3	-125.8	4048	520.2	321	5576	289.9	293.6	7212			
121.7	666.8	847	378.8	654.2	2472	665.9	-126.5	4063	517.8	319	5593	287.1	293.9	7228			
123.8	667.5	864	381.4	644.2	2488	669.1	-127.2	4079	515.4	319.7	5609	284.3	294.1	7245			
125.9	667.6	880	384.3	635.1	2505	671.9	-127.9	4094	512.7	319.5	5626	281.5	293.9	7262			
128.1	667.8	897	386.9	627.3	2522	675.1	-128.3	4110	509.9	319.3	5644	278.7	294.2	7279			
130.5	668.8	914	390	618.5	2539	679	-128.6	4125	507.5	318.1	5660	275.9	291.2	7295			
132.9	668.4	930	393.2	609.3	2556	682.5	-128.9	4141	504.5	318	5677	273.1	292.3	7312			
135.5	670.1	947	396.1	600.3	2572	686.4	-129.6	4156	502.1	317.9	5694	270	291	7329			
138.2	670.3	964	399	593	2589	689.9	-130.1	4172	499.4	317.8	5711	267	292.2	7346			
140.6	671	980	401.9	586.9	2606	692.8	-130.4	4187	496.7	316.1	5728	264.2	291.4	7363			
143.3	671.2	997	404.8	581.7	2623	695.7	-131.2	4202	493.7	317	5745	261.4	291.5	7379			
145.9	672	1014	407.5	574.3	2640	699.3	-132.3	4218	491.3	316.5	5762	258.4	290.3	7396			
148.4	671.9	1030	410.4	570	2657	702.5	-133.1	4233	488.6	314.3	5779	255.6	291.7	7413			
150.8	672.4	1047	413	562.9	2674	705.4	-133.3	4249	485.6	314.5	5796	252.6	290.4	7430			
153.4	673.3	1064	415.9	558.5	2690	707.3	-133.7	4264	482.9	315.5	5813	249.8	290	7447			
156.1	673.6	1080	418.5	549.5	2707	708.6	-133.9	4280	480	317.3	5830	247	290.9	7463			
158.5	675	1097	421.5	547.4	2724	708.6	-133.7	4295	477	313.8	5846	244.3	288.9	7480			
161	674.6	1114	424.4	544.6	2741	708	-133.7	4310	474	314.8	5863	241.5	289.7	7497			
163.4	675.7	1130	427.6	541	2758	707	-133.7	4326	471	315.4	5880	238.8	288.7	7513			
165.8	676	1147	430.5	535.3	2775	705.1	-133.3	4341	468	314.5	5897	236	287.9	7530			
168.2	675.3	1164	433.8	533.3	2791	703.5	-132.8	4357	465.7	314	5914	233.3	286.7	7547			
170.9	677.1	1180	436.7	528.6	2808	701.5	-132.7	4372	463.9	314.8	5931	230.5	286.9	7564			
173.3	677.6	1197	439.6	526.2	2825	699.9	-132.7	4388	462.1	313.7	5948	227.8	287	7581			
176	678.2	1214	442.6	522.2	2842	698	-132	4403	460	313.9	5965	225.3	286.1	7597			
178.5	678.8	1230	445.5	521.2	2859	696	-130.8	4418	458.2	313.6	5982	222.6	287.2	7614			
180.9	679.9	1247	448.2	517.9	2876	694.1	-130.7	4434	455.9	312.6	5998	219.8	284	7631			
183.6	679.7	1264	451.1	516.3	2893	692.2	-130.3	4449	453.2	313.7	6016	217.1	284.6	7647			
186.3	680.8	1281	453.8	515.2	2910	690.2	-130	4465	450.9	313.5	6032	214.3	283.9	7664			
188.5	681.8	1297	457.1	512.7	2927	688	-129.7	4480	447.9	311.9	6049	211.9	283.5	7681			
190.9	682.3	1314	459.7	510.8	2944	685.7	-129.4	4496	445	312	6066	209.2	282.2	7698			
193.4	682.7	1331	462.7	510.9	2961	683.2	-128.9	4511	441.7	311.8	6083	206.2	281.7	7714			
195.8	683.9	1347	465.7	510.1	2978	680.9	-128.7	4527	439.1	311.9	6100	203.2	281	7731			
198.5	685	1364	468.3	509.6	2994	678.7	-128.5	4542	436.4	310.9	6117	200.4	281.5	7748			
201	686.2	1381	471.3	508.6	3011	677.1	-127.8	4558	434.1	310	6134	197.4	280.5	7764			
203.4	685.4	1398	474	506.2	3028	674.8	-127.3	4573	431.7	310.9	6150	194.7	280.9	7781			
205.9	687.7	1415	477.3	508.8	3045	672.6	-126.6	4588	429.1	310.8	6167	192	277.5	7798			
208.3	687.9	1431	480	507.1	3062	670.3	-126.4	4604	426.4	308.3	6184	189.3	278.6	7814			
211.1	688.5	1448	482.6	507.3	3079	668.1	-125.7	4619	423.8	310.8	6201	186.6	278.3	7831			
213.5	689.2	1465	485.3	507.6	3096	665.9	-125.7	4635	421.8	311	6218	183.9	278.3	7848			
216.5	690.6	1481	488	507.7	3113	663.6	-125.2	4650	419.7	308.9	6235	181.2	279.3	7865			
219.3	691.2	1498	491	509.1	3129	661.4	-125.1	4666	417.7	310.5	6252	178.7	276.2	7881			
222	692	1515	494	508.4	3146	659.2	-124.6	4681	415.3	310.3	6268	176	275.7	7898			
225	692.9	1532	496.7	507.9	3163	656.6	-124.2	4697	413.3	309.1	6285	173.6	275.2	7915			
227.8	693.2	1548	499.7	509.5	3180	654.4	-123.8	4712	411.2	308.8	6302	170.9	274.7	7931			
230.5	694.6	1565	503	508.9	3197	652.2	-123.5	4727	409.2	309	6319	168.2	274.6	7948			
233.3	696.1	1582	505.7	508.6	3214	650	-123.1	4743	407.5	308.6	6336	165.5	274.1	7965			
235.7	695.9	1599	508.7	509.3	3231	647.8	-122.3	4758	405.1	308.6	6353	162.6	273.6	7981			

Thermomagnetic results for sample AL031

TEMP (°C)	TSUSC (°C)	TIME (s)	TEMP (°C)	TSUSC (°C)	TIME (s)	TEMP (°C)	TSUSC (°C)	TIME (s)	TEMP (°C)	TSUSC (°C)	TIME (s)	TEMP (°C)	TSUSC (°C)	TIME (s)	TEMP (°C)	TSUSC (°C)	TIME (s)
15.4	150.4	0	210.8	168.8	1467	462.1	136.8	2948	688.9	-94	4442	458.8	70.5	5936	296	64.4	7421
15.6	151.6	16	213	169.1	1482	464.8	136.4	2963	686.7	-93.8	4457	457.4	70.5	5952	293.8	64.4	7436
17.2	151.8	31	215.4	169.4	1497	467.4	136	2978	684.4	-93.7	4473	455.9	70.4	5967	291.5	64.2	7451
19.2	151.7	46	217.9	169.7	1513	469.8	135.6	2994	682.2	-93.1	4488	454.1	70.3	5983	289	64.1	7467
21.3	151.7	61	220.6	170.1	1528	473.1	135.6	3009	680.3	-93	4504	452.3	70.1	5998	286.5	64.2	7482
23.6	151.6	76	223.4	170.4	1543	475.8	133.8	3024	678.7	-92.6	4519	450.9	70.1	6013	283.7	63.8	7497
25.7	151.9	91	225.8	170.7	1558	478.8	134.3	3040	676.7	-92.2	4535	449.1	70.1	6029	281.2	63.8	7512
27.7	152	106	228.6	170.9	1573	481.7	134.1	3055	674.5	-91.6	4550	447.3	69.9	6044	278.4	64.2	7528
29.8	151.9	121	231.1	171.2	1588	484.4	133.1	3071	672.6	-92	4565	445.2	69.9	6059	275.9	63.6	7543
31.6	152.1	136	233.5	171.5	1604	486.8	133.3	3086	670.7	-91.8	4581	443.2	70	6075	273.4	63.4	7558
33.7	152.3	152	236.3	171.8	1619	489.2	132	3101	668.4	-91.4	4596	440.8	69.9	6090	271.2	62.9	7573
35.2	152.2	167	238.8	172	1634	491.3	131.9	3117	666.5	-91.6	4612	439.1	69.6	6105	268.6	63	7588
37.1	152.6	182	241.2	172.6	1649	494	131.6	3132	664.3	-90.9	4627	437.3	70	6120	266.1	62.9	7604
38.9	152.7	197	244	172.7	1664	496.4	130.6	3147	662.1	-91.3	4642	435.2	69.7	6136	263.6	62.9	7619
40.4	152.8	212	246.8	173	1680	499.1	130.2	3162	660.1	-91.4	4658	433.5	69.9	6151	260.9	62.8	7634
42.2	153	227	249.2	173.1	1695	501.8	130.6	3178	657.9	-91	4673	431.7	69.6	6167	257.8	62.7	7649
43.8	153	242	251.5	173.5	1710	504.8	129.8	3193	655.7	-91.4	4688	430.2	69.5	6182	255.1	62.5	7664
45.6	153.2	257	253.9	173.9	1725	507.5	129.2	3209	653.5	-91.1	4704	428.8	69.2	6197	252.3	62.1	7680
47.2	153.3	272	256.7	174	1741	510.2	128.5	3224	651.2	-90.9	4719	427.3	69.4	6213	249.8	62.2	7695
48.5	153.6	287	259.2	174.6	1756	513	128.6	3239	649	-90.1	4735	425.6	69.2	6228	247.6	62	7710
50.3	153.7	302	261.7	174.7	1771	516	128	3255	646.8	-90.1	4750	423.5	69.3	6243	245.4	62.1	7725
51.8	153.9	317	264.2	175	1786	519	127.5	3270	644.6	-90.2	4765	421.5	69.1	6258	242.9	61.8	7740
53.4	154.1	332	266.7	175.4	1801	521.7	127.3	3285	642.1	-90.3	4781	419.7	69.3	6274	240.4	61.7	7756
55	154.3	348	268.9	175.3	1817	524.2	126.2	3301	639.5	-89.5	4796	418.5	69.1	6289	237.7	61.5	7771
56.8	154.2	363	271.4	175.7	1832	526.6	125.9	3316	637	-89.4	4812	417.4	69.3	6304	235.5	61.4	7786
58.3	154.5	378	273.9	175.9	1847	529.3	126	3332	634.5	-88.9	4827	416.2	69.1	6320	232.7	61.3	7801
59.9	154.7	393	276.4	176.1	1863	531.7	125.2	3347	632.3	-88.6	4843	415	68.9	6335	230.5	61.1	7816
61.5	154.7	408	279	176.2	1878	534.2	124.9	3362	630.1	-88.5	4858	413.9	69	6350	228	60.8	7832
63	154.8	423	281.5	176.6	1893	536.6	124.4	3378	627.6	-88.5	4874	412.7	68.9	6366	225.8	60.7	7847
64.9	155.1	438	284	176.8	1908	539	124	3393	625.7	-88.1	4889	411.2	68.9	6381	223.4	60.4	7862
66.4	155.1	453	286.2	176.8	1923	541.2	123.4	3409	624.4	-88	4904	410.1	68.6	6396	220.9	60.3	7877
68.2	155.3	468	288.7	177	1939	543.6	123.4	3424	623.5	-88	4920	409.2	68.7	6411	218.4	60.2	7893
70.1	155.3	483	291.3	177	1954	546.1	122.8	3439	622.2	-87.7	4935	408	68.9	6427	216	59.9	7908
71.6	155.6	498	293.8	177.1	1969	548.8	122.2	3455	620.6	-86.9	4951	406.3	68.7	6442	213.5	59.8	7923
73.2	155.8	513	296.3	177.5	1984	551.9	121.9	3470	618.8	-86.5	4966	404.8	68.6	6457	211.3	59.7	7938
75	156.1	528	298.5	177.5	2000	554.6	121.7	3486	616.6	-86.2	4981	403.1	68.5	6473	208.9	59.8	7953
76.6	156.3	544	301.1	177.5	2015	557.7	121	3501	614.7	-85.2	4997	401.3	68.4	6488	206.4	59.7	7969
78.4	156.4	559	303.3	177.6	2030	561.1	120	3516	612.5	-83.6	5012	399.9	68.4	6503	204	59.2	7984
80.5	156.6	574	305.9	177.7	2045	564.1	116.3	3532	610.3	-81.9	5028	398.4	68.4	6519	201.5	59.1	7999
82.4	156.7	589	308.4	177.6	2061	567.2	110.1	3547	608.1	-79	5043	396.7	68.1	6534	199.1	58.8	8014
84.2	157	604	310.6	177.7	2076	569.7	101.9	3562	605.9	-72.7	5059	395	68.2	6549	196.6	58.6	8029
86.1	157.4	619	313.2	177.3	2091	572.4	86.8	3578	603.8	-67.2	5074	393.5	68.3	6565	194.2	58.6	8044
88.2	157.3	634	315.7	177.2	2106	575.5	71.3	3593	601.3	-62	5090	391.8	68.1	6580	191.7	58.7	8060
90.3	157.5	649	318.5	177.1	2122	578.9	55.7	3609	599.1	-53.1	5105	390.3	68.3	6596	189.3	58.3	8075
92.6	157.6	664	321.1	176.9	2137	581.7	40.1	3624	596.3	-44.9	5120	388.6	67.9	6611	187.1	58	8090
94.7	157.8	680	323.6	176.9	2152	585.1	24.7	3639	594.1	-36.6	5136	386.9	67.8	6626	184.7	58.1	8105
96.8	157.9	695	326.2	176.4	2167	587.9	10.5	3655	591.6	-27.8	5151	385.1	67.9	6642	182.3	57.9	8120
98.9	158.2	710	328.7	175.8	2183	590.7	-3	3670	589.1	-19.6	5167	383.4	67.6	6657	179.8	57.6	8136
101.1	158.5	725	331.3	175.6	2198	593.5	-16.9	3685	587.3	-11.9	5182	381.9	67.6	6672	177.1	57.5	8151
103.4	158.6	740	333.8	175.2	2213	596.6	-29.8	3701	585.1	-5	5197	380.5	67.6	6688	175	57.6	8166
105.5	158.9	755	336.4	174.6	2228	599.4	-42.2	3716	583.3	1.3	5213	379.1	67.8	6703	172.5	57.3	8181
107.9	159.2	770	339	173.6	2244	602.2	-53.7	3732	580.8	8.5	5228	377	67.5	6718	170.1	57.2	8196
110	159.4	785	341.5	173.1	2259	605	-62.1	3747	578.6	18.9	5244	375	67.7	6733	167.7	57.1	8211
112.4	159.5	801	344.1	172.2	2274	607.5	-70.4	3762	576.1	29.4	5259	373.3	67.3	6749	165.3	57	8227
114.5	159.7	815	346.7	171.4	2289	610	-74.2	3778	573.7	42.7	5275	371.6	67.3	6764	162.6	56.9	8242
116.7	160.1	831	349.5	170.5	2305	612.8	-76.6	3793	571.2	56.7	5290	370.1	67.3	6779	160.2	56.9	8257
118.5	160.1	846	351.8	169.5	2320	615.9	-78.7	3809	568.8	66.4	5305	368.7	67.2	6795	157.7	57	8272
120.6	160.3	861	354.4	168.3	2335	618.8	-80.2	3824	566	71.3	5321	367.3	67.1	6810	155.3	56.6	8287
122.5	160.5	876	357.2	167.2	2351	621.6	-80.8	3839	563.2	73.1	5336	365.5	67.3	6825	153.2	56.7	8302
124.6	160.5	891	360.1	165.4	2366	624.4	-81.2	3855	560.8	73.3	5351	363.5	67.4	6841	151	56.8	8317
126.5	160.6	906	362.7	164.4	2381	626.9	-81.9	3870	558.3	74.1	5367	361.8	67	6856	148.9	56.6	8332
128.9	161	922	365.3	162.8	2396	630.1	-83.1	3885	555.8	73.7	5382	360.4	67.2	6871	146.7	56.7	8348
131	161.1	936	367.8	161.5	2412	632.9	-84	3901	553.4	73.9	5397	358.9	66.7	6886	144.9	56.4	8363
133.1	161.2	952	370.7	160.2	2427	636.1	-84.3	3916	550.6	73.4	5413	357.2	66.8	6902	142.7	56.6	8378
135.3	161.5	967	373.6	159	2442	639.2	-83.6	3932	548.2	73	5428	355.8	67	6917	140.6	56.6	8393
137.7	161.6	982	376.2	157.9	2458	642.4	-85.2	3947	545.4	73.2	5444	354.4	66.4	6932	138.2	56.7	8408
139.8	161.9	997	378.8	156.5	2473	645.2	-85.3	3963	542.7	73.1	5459	352.9	66.8	6948	136.1	56.8	8423
141.9	162.1	1012	381.4	155.5	2488	648.1	-86	3978	540	73	5474	351.8	66.9	6963	133.9	56.7	8438
144.3	162	1027	384.3	154.4	2503	650.3	-86.5	3993	536.9	72.8	5490	350.6	66.8	6978	131.8	57	8453
146.5	162.1	1043	386.9	153.2	2519	651.2	-86.4	4009	533.9	72.8	5505	349.5	66.7	6994	129.7	56.9	8468
148.9	162.6	1058	389.5	152.4	2534	652.2	-86.6	4024	529.6	72.4	5521	348.4	66.3	7009	127.3	56.8	8484
151	162.9	1073	392.4	151.5	2549	653.5	-87.6	4040	525.7	72.4	5536	346.9	66.3	7024	125.2	56.9	8499
153.4	163.2	1088	395.3	150.6	2565	656	-87	4055	522	72.5	5551	345.2	66.4	7039	122.8	57.2	8514
155.6	163.1	1103	398.2	149.7	2580	659.2	-87.7	4070	518.4	72	5567	343.5	66.3	7055	120.4	57.1	8529
157.7	163.2	1118	400.8	149.2	2595	662.7	-88.4	4086	515.1	72.1	5582	341.8	66	7070	118.2	57.2	8544
160.2	163.4	1133	403.7	148.1	2611	666.8	-88.8	4101	511.8	72.1	5598	339.8	65.8	7085	116.1	57	8559
162.3	163.6	1148	406.3	147.8	2626	671.6	-89.8	4117	508.7	71.8	5613	338.1	66.2	7100	113.7	57.1	8574
164.7	163.6	1163	408.9	146.8	2641	677.4	-90.5	4132	506	71.9	5628	335.8	66.3	7116	111.6	57.2	8589
167.1	164.2	1179	411.2	146.4	2657	683.5	-91.1	4148	503.3	71.9	5644	333.6	65.8	7131	109.5	57.4	8604
169.6	164.3	1194	413.9	145.9	2672	688	-91.6	4163	500.6	71.8	5659	331.6	66	7146	107.4	57.4	8619
172	164.3	1209	416.5	145.1	2687	692.5	-92.2	4178	497.9	71.4	5675	329.6	65.7	7162	105.5	57.3	8634
174.4	164.7	1224	419.1	144.8	2702	695.7	-92.6	4194	495.2	71.5	5690	327.9	65.6	7177	103.4	57.4	8649
176.9	165.2	1239	421.8	144	2718	699.6	-92.5	4209	492.5	71.6	5706	325.9	65.7	7192	101.6	57.3	8664
179	165.2	1255	424.4	143.3	2733	703.1	-93.6	4225	489.8	71.6	5721	323.9	65.6	7207	99.5	57.7	8679
181.4	165.5	1270	427	142.9	2749	706	-93.4	4240	487.1	71.4	5736	322.2	65.5	7223	97.4	57.3	8694
183.9	165.6	1285	430	142.5	2764	707.7	-94.1	4256	484.4	71.4	5752	320.5	65.3	7238	95.5	57.6	8709
186.3	165.9	1300	432.6	141.9	2779	708.3	-94.3	4272	481.7	71.6	5767	318.5	65.5	7253	93.4	57.5	8724
188.5	166.3	1315	435.2	141.4	2794	708	-94.3	4287	479.1	71.2	5783	316.6	65.4	7268	91.3	57.7	8739
190.9	166.5	1330	437.6	141.3	2810	707	-93.8	4303	476.7	71	5798	314.6	65.1	7284	89.5	57.7	8754
193.1	166.8	1346	440.2	140.6	2825	705.4	-94.8	4318	474.3	71	5813	312.3	65.2	7299	87.4	57.9	8770
195.3	167.1	1361	442.9	139.9	2840	703.8	-94.4	4334	472.5	70.9	5829	310.4	64.9	7314	85.5	57.9	8785
197.7	166.9	1376	445.5	139.6	2855	702.5	-94.8	4349	470.4	70.5	5844	308.1	65	7329	83.7	57.9	8800
199.9	167.6	1391	448.2	139	2871	700.5	-95	4365	468	71	5859	306.4	64.8	7345	81.6	57.9	8815
202.1	167.6	1406	451.1	138.5	2886	698.3	-94.8	4380	466	70.5	5875	304.4	64.5	7360	79.8	58	8830
204.2	167.9	1421	453.8	138.3	2902	695.7	-94.6	4396	463.9	70.5	5890	302.2	64.9	7375	77.9	58	8845
206.4	168.6	1437	456.5	137.7	2917	693.4	-94	4411	462.1	70.4	5905	300.2	64.5	7390			
208.6	168.6	1452	459.4	137.2	2932	691.2	-94.2	4427	460.3	70.3	5921	298.3	64.7	7406			

Thermomagnetic results for sample AL038

TEMP (°C)	TSUSC (°C)	TIME (s)	TEMP (°C)	TSUSC (°C)	TIME (s)	TEMP (°C)	TSUSC (°C)	TIME (s)	TEMP (°C)	TSUSC (°C)	TIME (s)	TEMP (°C)	TSUSC (°C)	TIME (s)	TEMP (°C)	TSUSC (°C)	TIME (s)
22.1	-3.3	0	214.3	9.7	1474	455	-14.6	2957	686.4	-130.8	4452	460.3	6.3	5947	323.4	3.5	7431
22.3	0.7	16	216.5	10	1489	458	-15	2972	685.4	-130.7	4467	458.2	6.5	5963	322.2	3.5	7447
23.6	-2.7	31	219	10.3	1504	460.6	-15.5	2987	684.1	-130.6	4483	456.5	6.7	5978	320.8	3.4	7462
25.4	-2.5	46	221.5	10.5	1520	463.6	-15.7	3003	682.8	-130.2	4498	454.7	6.7	5993	319.7	3.3	7477
27.7	-2.3	62	224.2	10.6	1535	466.9	-15.9	3018	680.9	-129.7	4514	452.9	7	6009	318.5	3.2	7492
30.1	-2.3	77	226.9	11	1550	469.8	-16.3	3034	679	-129.5	4529	451.1	7.3	6024	317.4	3	7508
32.1	-2.3	92	229.7	11.1	1565	473.1	-16.4	3049	676.7	-128.7	4545	449.4	7.3	6039	316.3	3.2	7523
34.2	-2.1	107	232.4	11.3	1581	475.8	-16.6	3064	674.5	-128.5	4560	448.2	7.6	6055	315.4	2.9	7538
36.3	-2.1	122	234.9	11.5	1596	478.8	-17.2	3080	672.6	-128.2	4575	446.7	7.6	6070	314.3	3.1	7554
38.3	-1.9	137	237.1	11.9	1611	481.4	-16.7	3095	670.7	-128	4591	445.5	7.8	6085	313.5	2.9	7569
40.2	-1.8	153	239.6	11.9	1626	484.1	-17	3110	668.8	-127.6	4606	443.8	7.8	6101	312.9	3.1	7584
42	-1.8	168	242.1	12.1	1642	486.8	-17.1	3126	666.5	-127.3	4622	442.6	7.8	6116	311.8	2.7	7599
43.8	-1.6	183	244.3	12.4	1657	489.2	-17.1	3141	664.3	-126.9	4637	441.1	8	6132	310.9	2.7	7614
45.6	-1.5	198	246.8	12.4	1672	491.9	-17	3157	661.7	-126.6	4653	439.6	8	6147	309.8	2.7	7630
47.2	-1.5	213	249.2	12.6	1687	494.3	-17	3172	659.2	-126.1	4668	437.9	8	6162	308.7	2.8	7645
48.7	-1.4	228	251.7	12.8	1703	497	-17.2	3188	656.6	-125.3	4684	436.4	8.3	6177	307.5	2.5	7660
50.5	-1.5	243	253.9	13.1	1718	499.7	-16.9	3203	654.4	-124.8	4699	434.9	8	6193	306.1	2.4	7675
52.1	-1.2	259	256.2	13.1	1733	502.7	-16.6	3218	651.9	-124.3	4714	433.2	8	6208	304.7	2.3	7690
53.7	-1.2	274	258.4	13.2	1748	505.4	-16.7	3234	649.3	-124.1	4730	432	8.2	6223	303.6	2.5	7706
55.2	-1.2	289	260.9	13.5	1763	508.4	-16.4	3249	646.5	-123.7	4745	430.5	8.2	6239	302.5	2.4	7721
56.8	-0.9	304	263.4	13.5	1779	511.5	-16.1	3265	644.3	-122.8	4761	429.4	8.2	6254	301.4	2.1	7736
58.3	-0.8	319	265.6	13.7	1794	513.9	-16	3280	641.7	-121.9	4776	427.9	8.2	6269	300.5	1.9	7751
59.9	-1	335	268.1	13.6	1809	516.6	-15.7	3295	639.2	-119.9	4792	426.1	8.1	6285	299.7	2	7767
61.5	-0.9	350	270.6	13.8	1824	519	-15.3	3311	636.7	-117.2	4807	424.7	8.6	6300	299.1	1.7	7782
63	-0.5	365	273.1	13.9	1840	521.7	-14.8	3326	633.9	-113.7	4823	423.2	8.3	6316	298	2	7797
64.9	-0.6	380	275.3	13.9	1855	524.2	-15.1	3342	631	-111.4	4838	422	8.3	6331	296.6	2	7812
66.4	-0.4	395	277.6	13.7	1870	526.6	-14.1	3357	628.5	-108.8	4853	420.9	8.2	6346	295.2	1.5	7828
68	-0.3	410	279.8	14	1885	529.6	-13.5	3372	626.3	-107.4	4869	419.4	8.4	6361	294.1	1.7	7843
69.6	-0.1	425	282	13.8	1901	532.4	-13	3388	623.8	-105.5	4884	417.7	8.4	6377	292.7	1.2	7858
71.1	-0.1	441	284.5	14.1	1916	535.1	-12.1	3403	621.3	-103.8	4900	416.2	8.1	6392	291.5	1.5	7873
72.9	0.1	456	286.8	13.7	1931	537.8	-11.7	3419	619.1	-102.4	4915	414.7	8	6408	290.1	1.3	7889
74.5	0.2	471	289	13.8	1946	540.9	-10.7	3434	617.2	-100.1	4931	413.6	8.2	6423	288.5	1	7904
76.4	0.2	486	291.3	13.6	1961	543.6	-10.2	3449	615	-98.4	4946	412.7	8.2	6438	287.1	1.3	7919
78.2	0.4	501	293.8	13.5	1977	546.4	-9	3465	613.4	-97.3	4961	411.5	8.2	6453	285.7	1.1	7934
79.8	0.6	516	296	13.6	1992	549.4	-7.5	3480	611.9	-95.8	4977	410.4	8.2	6469	284.5	1.1	7949
81.6	0.7	532	298.8	13.4	2007	552.8	-6.3	3496	610	-93.8	4992	409.2	8.2	6484	283.4	0.8	7964
83.4	0.8	547	301.6	13.3	2023	556.2	-4.8	3511	607.8	-90.7	5008	407.5	8.1	6500	282	0.9	7980
85.3	1	562	304.4	13.1	2038	559.2	-3.3	3526	605.3	-87.7	5023	406.3	8.4	6515	280.9	0.4	7995
87.1	0.9	577	307	13	2053	562.3	-2	3542	603.1	-84.4	5039	405.1	8	6530	279.5	0.4	8010
88.9	1.2	592	309.5	12.8	2068	565.4	-4.6	3557	601.3	-81.9	5054	404.3	8.1	6546	277.8	0.3	8025
90.8	1.2	607	312.1	12.5	2084	568.8	-10.7	3573	599.7	-79.2	5069	403.4	8.1	6561	276.2	0.2	8041
92.9	1.3	623	314.6	12.5	2099	572.1	-21.5	3588	598.2	-77	5085	402.8	8	6576	274.2	0.1	8056
95	1.7	638	317.1	12.4	2114	575.2	-35.4	3603	596.3	-73.8	5100	401.9	7.9	6591	272.5	0	8071
97.4	1.8	653	320	12.3	2130	578	-46.5	3619	594.4	-69.9	5116	400.8	8	6606	270.6	0	8086
99.5	1.7	668	322.5	11.8	2145	581.1	-55.3	3634	591.9	-66.5	5131	399	7.9	6622	268.4	-0.1	8101
101.6	1.8	683	325.1	11.6	2160	583.9	-63.1	3649	589.8	-62.3	5146	397.9	7.6	6637	265.9	-0.5	8117
103.7	2.2	698	327.6	11	2176	586.7	-71	3665	587.6	-58.2	5162	396.4	7.8	6652	263.6	-0.6	8132
106.1	2.1	714	330.4	10.7	2191	589.5	-79.2	3680	585.1	-54.6	5177	395.5	7.8	6668	261.1	-0.7	8147
108.2	2.3	729	332.7	10.2	2206	592.6	-87	3696	582.6	-51.4	5193	394.4	7.7	6683	258.4	-0.7	8162
110.6	2.4	744	335.5	9.9	2221	596	-94.8	3711	580.2	-48.4	5208	393.5	7.7	6698	255.6	-0.9	8177
112.7	2.7	759	338.1	9.4	2237	598.8	-100.7	3727	577.4	-44.6	5224	392.6	7.9	6714	253.1	-1.2	8193
114.8	2.8	774	340.7	8.7	2252	601.9	-105.6	3742	574.6	-39.1	5239	391.8	7.6	6729	250.6	-1.3	8208
116.9	3.2	790	342.9	8.2	2267	604.7	-108.6	3757	571.8	-33.6	5254	390.9	7.5	6744	248.4	-1.7	8223
119	3.1	805	345.2	7.7	2283	607.5	-110.5	3773	569.4	-27.6	5270	389.5	7.3	6760	245.9	-1.7	8238
120.9	3.4	820	347.5	7.1	2298	610	-112.4	3788	566.6	-22.2	5285	388	7.5	6775	243.4	-2	8253
123	3.5	835	349.5	6.7	2314	612.8	-113.3	3804	564.1	-17.8	5301	386.6	7.4	6790	241	-2.1	8269
124.9	3.5	851	351.5	5.9	2329	615.3	-114.1	3819	561.1	-15.5	5316	384.8	7.4	6805	238.8	-2.2	8284
126.7	3.7	866	353.8	5.1	2344	618.1	-115.2	3834	558	-14.7	5332	383.4	7.2	6821	236.6	-2.4	8299
128.9	3.8	881	356.1	4.5	2359	621.3	-116.9	3850	554.6	-13.9	5347	382.2	7.1	6836	234.6	-2.8	8314
130.7	3.9	896	358.4	4	2375	624.7	-118.2	3865	551.3	-13.3	5363	380.5	7	6851	232.4	-2.5	8329
132.9	4	912	360.7	3	2390	627.6	-119.1	3881	548.2	-12.8	5378	379.1	6.9	6867	230.2	-2.6	8344
135	4.1	927	362.7	2.4	2405	630.7	-119.7	3896	545.4	-12.7	5393	377.3	6.9	6882	228	-2.8	8360
136.9	4.2	942	365.3	1.7	2420	634.2	-121.3	3912	542.7	-12.1	5409	375.9	6.8	6897	225.8	-3.2	8375
139	4.5	957	367.3	0.9	2436	638	-121.9	3927	540.3	-11.4	5424	374.4	6.8	6912	223.6	-3.7	8390
141.1	4.5	972	369.8	0.1	2451	642.1	-122.7	3943	538.1	-11.2	5439	373	6.6	6928	221.2	-3.4	8405
143.3	4.6	987	372.4	-0.5	2466	645.5	-123.9	3958	535.7	-10.5	5455	371.9	6.7	6943	219.3	-3.6	8420
145.4	4.8	1003	374.7	-1.1	2482	648.4	-124.1	3974	533.6	-10.1	5470	370.7	6.5	6958	217.1	-3.9	8435
147.6	4.8	1018	377.6	-2	2497	651.2	-125.4	3989	531.1	-9.4	5486	369.6	6.6	6974	214.9	-4	8451
149.7	5	1033	379.9	-2.6	2512	654.4	-125.7	4004	528.7	-8.8	5501	368.4	6.4	6989	212.7	-4.3	8466
152.1	5.2	1048	382.5	-3.4	2528	657.6	-126.2	4020	526	-8.3	5516	367.5	6.4	7004	210.5	-4.4	8481
154.2	5.3	1063	384.8	-3.8	2543	660.8	-126.5	4035	522.9	-7.4	5532	366.4	6.4	7019	208.1	-4.8	8496
156.7	5.6	1079	387.4	-4.4	2558	664.3	-127.5	4051	520.2	-6.7	5547	365.3	6.2	7034	205.9	-5.1	8511
158.8	5.7	1094	390.3	-5	2573	667.8	-127.5	4066	517.2	-6.1	5563	364.1	6.2	7050	203.4	-5.3	8526
161.2	5.7	1109	392.9	-5.6	2589	671.3	-128.5	4082	514.8	-5.3	5578	363	6.3	7065	201.3	-5.5	8541
163.4	5.7	1124	395.3	-5.8	2604	674.8	-129.5	4097	512.7	-4.8	5594	361.2	5.9	7080	198.8	-5.7	8557
165.5	5.9	1139	397.9	-6.5	2620	678.7	-130.1	4113	510.9	-4.3	5609	359.2	5.9	7096	196.6	-6	8572
167.7	6	1155	400.5	-6.8	2635	682.2	-130.4	4128	508.7	-3.5	5624	357.5	5.8	7111	194.2	-6.1	8587
169.8	6.2	1170	402.8	-7.3	2650	685.1	-130.6	4143	506.3	-3.1	5640	355.5	5.8	7126	191.5	-6.4	8602
172.3	6.3	1185	405.4	-7.7	2665	688	-131.2	4159	504.5	-2.6	5655	353.2	5.8	7142	189	-6.7	8617
174.7	6.5	1200	408	-8.1	2681	691.2	-131.4	4174	502.4	-1.8	5670	351.2	5.4	7157	186.3	-7	8632
176.9	6.7	1215	410.7	-8.8	2696	694.4	-131.8	4190	500.6	-1.7	5686	349.2	5.4	7172	183.9	-7.2	8647
179	6.8	1230	413.3	-8.9	2711	697.6	-132.3	4205	498.8	-0.9	5701	347.2	5.3	7187	181.4	-7.5	8662
181.4	6.8	1246	415.9	-9.5	2727	700.9	-132.7	4220	496.7	-0.5	5717	345.2	4.9	7203	179	-7.5	8677
183.9	7	1261	418.8	-9.6	2742	704.4	-133	4236	494.3	0.2	5732	343.2	5.1	7218	176.6	-7.8	8692
186.3	7.3	1276	421.5	-10.2	2757	706.7	-133.2	4251	491.9	0.7	5747	341.5	4.7	7233	173.9	-8	8707
188.5	7.6	1291	424.4	-10.6	2773	708.3	-133.1	4267	489.2	1.7	5763	339.8	4.7	7248	170.9	-8.3	8723
190.7	7.9	1307	427	-10.8	2788	709	-133.8	4282	486.2	2.2	5778	338.7	4.6	7264	168.2	-8.4	8738
193.1	8	1322	430	-11.1	2803	709	-133.4	4298	483.2	2.7	5793	337.3	4.6	7279	165.5	-8.6	8753
195.3	8.2	1337	432.3	-11.6	2819	708	-133.2	4313	480	3.4	5809	336.1	4.5	7294	163.1	-8.7	8768
197.4	8.4	1352	434.6	-12.1	2834	705.1	-132.8	4328	477	4.1	5824	335	4.4	7309	160.7	-8.9	8783
199.6	8.3	1367	437	-12.5	2849	702.2	-132.9	4344	474.3	4.3	5840	333.6	4.4	7325	158.3	-9.1	8798
202.1	8.7	1383	439.4	-12.8	2865	699.6	-132.2	4359	471.9	4.9	5855	331.9	4.2	7340	155.9	-9.2	8813
204.2	8.8	1398	442	-13	2880	696.7	-132.4	4375	469.8	5	5870	330.2	3.8	7355	153.7	-9.4	8828
206.4	9	1413	444.7	-13.6	2896	694.1	-131.9	4390	467.7	5.1	5886	328.5	4	7370	151.6	-9.4	8843
208.3	9.1	1428	447.3	-13.9	2911	691.5	-131.5	4406	466	5.6	5901	327	3.8	7386	149.7	-9.5	8858
210.2	9.4	1444	450	-14.1	2926	689.6	-131.3	4421	464.2	5.7	5916	325.9	3.9	7401	147.6	-9.8	8873
212.2	9.7	1459	452.6	-14.6	2942	687.7	-131	4437	462.1	6.4	5932	324.8	3.8	7416			

Thermomagnetic results for sample AL045

TEMP (°C)	TSUSC (°C)	TIME (s)	TEMP (°C)	TSUSC (°C)	TIME (s)	TEMP (°C)	TSUSC (°C)	TIME (s)	TEMP (°C)	TSUSC (°C)	TIME (s)	TEMP (°C)	TSUSC (°C)	TIME (s)	TEMP (°C)	TSUSC (°C)	TIME (s)
20.5	-60.7	0	219.8	-127.2	1470	468.3	-129.7	2949	684.1	-137.3	4440	455.9	-130.8	5931	317.4	-129	7412
21	-121.9	17	222.3	-127.1	1485	471	-129.5	2965	681.9	-137.2	4455	454.7	-130.5	5946	316.3	-129	7427
22.9	-121.8	32	224.5	-126.9	1501	473.4	-129.4	2980	679.3	-137.2	4470	453.8	-130.5	5961	315.2	-128.8	7443
25.2	-121.7	47	226.9	-127	1516	475.8	-129.5	2995	676.7	-137	4486	452.9	-130.8	5977	313.7	-128.8	7458
27.5	-121.9	62	229.4	-127.1	1531	478.5	-129.6	3010	673.2	-136.6	4501	451.7	-130.6	5992	312.3	-128.9	7473
29.8	-122.1	77	232.2	-127.1	1546	481.1	-129.7	3026	669.4	-136.8	4517	450.3	-130.7	6007	310.9	-128.7	7488
32.1	-122.1	92	234.9	-127.1	1561	483.8	-129.6	3041	666.2	-137	4532	448.8	-130.7	6023	309.2	-128.9	7503
34.2	-122	107	237.9	-127.1	1576	486.8	-129.6	3056	663.3	-137.1	4548	447.3	-130.4	6038	307.8	-128.9	7519
36.3	-122.3	122	240.7	-127	1592	489.8	-129.8	3072	660.5	-136.8	4563	445.8	-130.6	6053	306.4	-128.9	7534
38.1	-122.1	137	243.2	-127	1607	492.8	-130.1	3087	657.9	-136.8	4579	444.4	-130.7	6068	304.7	-128.9	7549
39.9	-122.3	152	245.7	-127.2	1622	495.5	-130.1	3102	655.4	-136.5	4594	443.5	-130.5	6084	303.3	-128.8	7564
41.7	-122.3	167	248.1	-127.1	1637	498.2	-130.1	3118	652.8	-136.6	4609	442.3	-130.2	6099	301.4	-128.9	7579
43.5	-122.6	182	250.6	-127.3	1652	500.9	-129.9	3133	650	-136.5	4625	440.8	-130.5	6114	299.4	-128.8	7595
45.3	-122.5	198	253.1	-127	1667	503	-130.2	3148	647.8	-136.4	4640	439.4	-130.6	6130	297.4	-128.8	7610
47.2	-122.5	213	255.9	-127.2	1683	505.7	-130.1	3164	644.9	-136.5	4655	437.9	-130.3	6145	295.2	-128.5	7625
48.7	-122.5	228	258.4	-127.2	1698	508.4	-130	3179	642.4	-136.3	4671	436.7	-130.5	6160	292.9	-128.7	7640
50.5	-122.5	243	260.9	-127.1	1713	510.9	-130.1	3194	639.5	-136.3	4686	435.2	-130.3	6175	290.4	-128.4	7655
52.1	-122.7	258	263.4	-127.3	1728	513.3	-130.3	3210	637	-136.4	4702	434.1	-130.3	6191	287.9	-128.8	7671
53.9	-122.6	273	265.6	-127.2	1744	516.3	-130.5	3225	634.8	-136.3	4717	432.6	-130.6	6206	285.1	-128.5	7686
55.5	-122.8	288	268.1	-127.2	1759	519	-130.6	3240	632.6	-136.3	4732	431.4	-130.2	6221	282.6	-128.5	7701
57	-122.9	303	270.6	-127	1774	522	-130.5	3256	630.1	-136.2	4748	430.5	-130.2	6236	280.1	-128.5	7716
58.9	-122.9	319	273.1	-126.9	1789	524.8	-130.4	3271	627.2	-136.2	4763	429.4	-130.2	6252	277.6	-128.4	7732
60.4	-123	333	275.3	-126.9	1804	527.5	-130.5	3286	624.7	-136.3	4779	428.2	-130.2	6267	275	-128.6	7747
62.2	-123.1	349	278.1	-127.1	1820	530.5	-130.5	3302	621.6	-136	4794	426.7	-130.3	6282	272.8	-128.5	7762
63.8	-123.3	364	280.6	-127.2	1835	533.3	-130.8	3317	619.1	-136.1	4810	425.3	-130.1	6297	270.3	-128.3	7777
65.6	-123.3	379	282.9	-127.2	1850	536	-130.7	3332	616.6	-136	4825	423.2	-130.4	6313	267.5	-128.3	7792
67.2	-123.3	394	285.4	-127.2	1865	539	-130.7	3348	613.8	-135.9	4840	421.5	-130	6328	265	-128.4	7808
68.8	-123.5	409	288.2	-127.1	1881	542.1	-130.7	3363	611.3	-135.8	4856	419.4	-130.1	6343	262.3	-128.1	7823
70.6	-123.5	424	290.7	-127.3	1896	544.5	-130.7	3378	608.8	-135.9	4871	417.7	-130	6359	259.5	-128.4	7838
72.4	-123.8	439	293.2	-127.3	1911	547.6	-130.9	3394	606.3	-135.6	4886	415.6	-130.3	6374	257	-128.2	7853
74	-123.7	454	295.7	-127.2	1927	550.3	-131	3409	603.8	-135.5	4902	413.9	-130.1	6389	254.2	-128.4	7869
75.8	-123.9	470	298	-127.1	1942	553.1	-131	3424	601.3	-135.5	4917	412.1	-130.1	6405	251.7	-128.1	7884
77.7	-124	485	300.8	-127.4	1957	555.8	-131.2	3439	598.8	-135.3	4932	410.4	-130.1	6420	249.2	-128.1	7899
79.5	-124	500	303.3	-127.3	1972	558.6	-131	3455	596.3	-135	4948	408.9	-130	6435	247	-128.2	7914
81.1	-124.1	515	306.1	-127.5	1988	561.4	-131.2	3470	593.8	-134.9	4963	407.5	-130	6450	244.8	-128	7929
82.9	-124.4	530	309	-127.3	2003	564.1	-131.2	3485	591.3	-134.8	4978	406	-130	6466	242.3	-128.3	7945
84.7	-124.4	545	311.5	-127.5	2018	567.2	-131.3	3501	588.8	-134.3	4994	404.5	-130.1	6481	239.9	-128	7960
86.6	-124.6	560	314	-127.1	2033	570.3	-131.8	3516	586.4	-134.6	5009	403.1	-129.9	6496	237.4	-128	7975
88.4	-124.6	575	316.6	-127.3	2048	573.7	-131.8	3531	583.6	-134.2	5025	401.6	-130	6512	234.9	-127.9	7990
90.3	-125	591	319.1	-127.5	2064	576.8	-132.3	3547	581.1	-134.2	5040	400.2	-129.9	6527	232.7	-127.8	8005
92.4	-125	606	321.7	-127.6	2079	579.9	-133	3562	578.3	-133.4	5055	399	-129.8	6543	230.2	-127.7	8020
94.2	-125.2	621	324.5	-127.5	2094	582.9	-133.5	3578	575.8	-133.4	5071	397.6	-130	6558	227.8	-127.8	8035
96.3	-125.3	636	327	-127.4	2109	586	-133.5	3593	573.4	-133.2	5086	396.1	-129.8	6573	225.6	-127.7	8051
98.4	-125.5	651	329.9	-127.6	2125	588.8	-133.7	3609	570.6	-133	5101	394.7	-129.9	6588	223.1	-127.5	8066
100.5	-125.6	666	332.4	-127.7	2140	591.6	-134.1	3624	568.1	-132.5	5117	393.5	-129.8	6603	220.6	-127.8	8081
102.6	-125.8	681	335	-127.6	2155	594.7	-134.6	3639	565.7	-132.2	5132	392.4	-129.9	6619	218.2	-127.6	8096
104.8	-125.8	697	337.3	-127.6	2171	597.5	-134.8	3655	563.2	-132.1	5147	391.2	-129.7	6634	216	-127.5	8111
106.9	-126.1	712	339.5	-127.4	2186	600.6	-135.1	3670	560.5	-132.3	5163	390	-129.7	6649	213.8	-127.5	8127
109.2	-126.2	727	341.5	-127.4	2201	603.8	-135.3	3685	558	-132.3	5178	389.2	-129.8	6665	211.3	-127.2	8142
111.6	-126.3	742	343.5	-127.7	2216	606.6	-135.2	3701	555.5	-132.1	5193	388.3	-129.9	6680	208.9	-127.4	8157
113.7	-126.2	757	345.8	-127.5	2231	609.4	-135.8	3716	553.1	-132.1	5209	387.4	-129.6	6695	206.7	-127.2	8172
115.6	-126.3	772	348.1	-127.9	2246	612.2	-135.8	3731	551	-132.1	5224	386	-130	6710	204.2	-127.4	8187
117.7	-126.4	788	350.4	-127.6	2262	614.7	-135.6	3747	548.2	-132	5240	384.5	-129.9	6726	201.8	-127.2	8202
119.6	-126.3	803	352.6	-127.5	2277	617.8	-135.6	3762	545.8	-131.9	5255	383.1	-129.7	6741	199.3	-127.1	8218
121.7	-126.4	818	355.2	-127.8	2292	620.3	-136	3778	543	-131.9	5270	381.4	-129.7	6756	197.2	-127.2	8233
123.8	-126.5	833	357.5	-127.6	2307	623.5	-136.1	3793	540.6	-132.1	5286	379.9	-129.8	6772	194.7	-127.1	8248
125.9	-126.5	848	359.8	-128	2323	626.3	-136.1	3808	538.1	-131.8	5301	378.2	-129.6	6787	192.3	-127	8263
127.8	-126.7	863	362.1	-128.2	2338	629.8	-135.9	3824	535.7	-132	5317	376.5	-129.7	6802	189.8	-126.9	8278
129.9	-126.6	878	364.4	-127.9	2353	632.9	-136.3	3839	533.3	-132	5332	374.7	-129.8	6818	187.7	-126.9	8293
132.1	-126.7	893	366.7	-127.7	2368	636.4	-136.2	3854	530.8	-131.7	5347	373	-129.7	6833	185.2	-126.9	8309
134.2	-126.8	909	369.3	-128	2384	639.9	-136.2	3870	528.4	-131.4	5363	371	-129.7	6848	182.8	-127.1	8324
136.3	-126.8	924	371.9	-128.1	2399	643	-136.3	3885	525.4	-131.4	5378	369.3	-129.5	6863	180.6	-127.2	8339
138.5	-126.9	939	374.2	-128.1	2414	646.2	-136.5	3900	522.6	-131.4	5393	367.8	-129.6	6878	178.2	-127	8354
140.6	-126.8	954	376.8	-128.2	2429	649	-136.5	3916	519.6	-131.7	5409	366.1	-129.8	6894	175.8	-127	8369
143	-127	969	379.3	-128.1	2445	652.2	-136.5	3931	517.2	-131.5	5424	364.4	-129.5	6909	173.6	-127	8384
145.1	-126.8	985	382.2	-128.3	2460	655.4	-136.6	3947	514.8	-131.7	5439	363	-129.6	6924	171.2	-127.1	8399
147.3	-126.8	1000	384.8	-128.3	2475	658.6	-136.9	3962	512.1	-131.4	5455	361.2	-129.5	6940	168.8	-126.9	8415
149.7	-126.9	1015	387.4	-128.3	2491	662.1	-137.1	3977	509.6	-131.2	5470	360.1	-129.5	6955	166.3	-126.8	8430
151.6	-126.9	1030	390	-128.3	2506	665.2	-136.9	3993	507.2	-131.2	5485	359.2	-129.3	6970	163.9	-126.7	8445
154	-126.9	1045	392.6	-128.3	2521	668.4	-136.6	4008	504.8	-131.3	5501	358.1	-129.4	6985	161.5	-126.9	8460
156.1	-127	1060	395.5	-128.1	2536	671.3	-137.1	4024	502.7	-131.1	5516	356.9	-129.5	7001	159.3	-126.8	8475
158.5	-126.9	1076	397.9	-128.5	2552	674.5	-137.3	4039	500.9	-131.2	5531	356.1	-129.3	7016	156.9	-126.8	8490
161	-126.8	1091	400.5	-128.6	2567	677.7	-137.6	4054	498.8	-131.1	5547	354.9	-129.5	7031	155.1	-126.8	8505
163.4	-127	1106	402.8	-128.5	2582	680.6	-137.1	4070	497	-131.2	5562	353.5	-129.5	7047	152.9	-126.8	8520
165.5	-126.9	1121	405.7	-128.7	2598	683.5	-137.4	4085	495.2	-130.9	5578	352.1	-129.6	7062	151	-126.9	8535
167.7	-127	1136	408.3	-128.8	2613	687	-137.4	4101	493.7	-131.1	5593	350.6	-129.4	7077	148.9	-126.6	8550
169.8	-127	1152	411.2	-128.9	2628	690.2	-137.7	4116	491.9	-131.1	5608	348.9	-129.2	7092	147	-126.6	8565
172	-127.1	1167	414.2	-128.7	2643	693.4	-137.7	4132	490.4	-131	5623	347.5	-129.2	7108	144.9	-126.6	8581
174.7	-127	1182	416.8	-128.8	2659	696.7	-137.6	4147	488.6	-131.1	5639	345.8	-129.3	7123	142.7	-126.6	8596
176.9	-127	1197	419.4	-128.9	2674	699.6	-137.8	4162	487.1	-131	5654	344.4	-129.2	7138	140.6	-126.4	8611
179.3	-127.1	1212	421.8	-128.9	2689	702.5	-137.7	4178	485.3	-131	5670	342.7	-129.3	7154	138.5	-126.5	8626
181.4	-127	1227	424.4	-128.8	2704	704.8	-138	4193	483.8	-131.2	5685	341	-129.3	7169	136.3	-126.4	8641
183.9	-126.9	1243	427	-128.8	2720	706.4	-137.6	4209	482.3	-130.9	5700	339.2	-129	7184	134.2	-126.4	8656
186	-126.9	1258	429.7	-128.8	2735	707.3	-137.9	4224	480.5	-131	5716	337.5	-129.2	7199	131.8	-126.5	8671
188.2	-127	1273	432.6	-128.9	2750	707.7	-138.1	4239	479.1	-131.1	5731	336.4	-129.1	7214	129.7	-126.4	8686
190.4	-126.9	1288	435.5	-129.3	2766	707	-137.5	4255	477.6	-131	5746	335	-129.2	7229	127.3	-126.4	8701
192.6	-127.1	1304	438.2	-129	2781	706.4	-137.5	4270	476.1	-131	5762	333.6	-129	7245	125.2	-126.4	8716
195	-127	1319	441.1	-129.3	2796	704.8	-137.7	4286	474.6	-130.9	5777	331.9	-129	7260	123	-126.1	8731
197.7	-127	1334	443.8	-129.1	2812	702.8	-137.9	4301	472.8	-130.9	5792	330.4	-129.1	7275	120.9	-126.4	8746
200.4	-126.8	1349	446.7	-129.1	2827	700.9	-137.8	4316	470.7	-130.8	5808	328.5	-129.2	7290			
203.2	-127	1364	449.4	-129.5	2842	698.6	-137.8	4332	468.6	-130.5	5823	326.8	-128.9	7306			
205.6	-127	1379	452	-129.3	2857	696.7	-137.4	4347	466.3	-131	5838	325.1	-129	7321			
208.1	-127.2	1394	454.7	-129.2	2873	694.4	-137.7	4363	463.9	-130.8	5854	323.4	-129.1	7336			
210.2	-127	1409	457.4	-129.2	2888	692.5	-137.6	4378	462.1	-130.6	5869	321.9	-128.9	7351			
212.7	-127	1424	460	-129.5	2903	690.5	-137.5	4393	460.3	-130.7	5884	320.5	-128.8	7367			
215.2	-126.9	1440	462.7	-129.6	2919	688.3	-137.4	4409	458.5	-130.7	5900	319.4	-129	7382			
217.6	-127	1455	465.4	-129.4	2934	686	-137.2	4424	457.4	-130.6	5915	318.5	-129	7397			

Thermomagnetic results for sample AL048

TEMP	TSUSC	TIME	TEMP	TSUSC	TIME	TEMP	TSUSC	TIME	TEMP	TSUSC	TIME	TEMP	TSUSC	TIME	TEMP	TSUSC	TIME
(°C)	(°C)	(s)	(°C)	(°C)	(s)	(°C)	(°C)	(s)	(°C)	(°C)	(s)	(°C)	(°C)	(s)	(°C)	(°C)	(s)
12	206.7	0	219	228.8	1461	487.1	181.2	2995	665.2	-74.2	4490	435.5	76.1	5984	234.6	69.2	7466
12.3	203.8	16	221.2	229.1	1476	490.1	180.2	3011	663	-73.8	4506	434.1	76.3	5999	232.2	69.1	7481
13.8	203.7	31	223.6	229.5	1492	493.4	179.2	3026	660.8	-72.8	4521	432.3	76.1	6015	229.7	69.1	7496
15.9	203.9	46	226.4	229.9	1507	496.1	178.4	3041	658.6	-71.8	4536	430.8	75.9	6030	226.9	68.9	7512
18.5	203.9	61	229.1	230.2	1522	498.5	177.6	3057	656	-70.9	4552	429.1	75.8	6045	224.5	68.7	7527
21	204	76	231.9	230.7	1537	501.2	176.8	3072	653.5	-70	4567	427.6	76	6060	222	68.6	7542
23.6	204.2	91	234.6	231.1	1552	503.6	175.9	3087	650.9	-69	4583	426.1	76	6076	219.5	68.5	7557
25.7	204.3	106	237.7	231.5	1567	506.6	174.9	3103	649	-68.2	4598	424.7	75.7	6091	216.8	68.2	7572
28	204.4	120	240.4	231.9	1583	509.3	173.8	3118	646.8	-67.2	4614	422.9	75.5	6106	214.1	68.3	7588
30.3	204.7	136	243.4	232	1600	512.1	173.1	3133	645.2	-66.5	4629	421.2	75.6	6122	211.9	68.2	7603
32.4	204.9	150	246.2	232.8	1616	514.5	172.1	3149	643.3	-65.7	4644	419.4	75.7	6137	209.4	67.9	7618
34.5	205	165	248.7	233.3	1631	517.2	170.8	3164	641.4	-64.8	4660	418	75.5	6152	207	67.9	7633
36.5	205.2	180	251.2	233.6	1646	519.9	169.9	3179	639.2	-64.4	4675	415.9	75.5	6168	204.5	67.7	7648
38.3	205.3	195	253.9	233.1	1663	522.6	169.2	3195	636.7	-63.5	4691	414.2	75.2	6183	202.3	67.7	7664
40.4	205.4	210	257	233.1	1681	525.4	168.4	3210	634.5	-62.4	4706	412.1	75.2	6198	200.2	67.5	7679
42.2	205.5	225	259.5	234.8	1696	528.1	167.4	3226	632	-61.6	4722	410.1	75.1	6214	198	67.4	7694
44	205.8	240	262.5	234.7	1713	531.1	166.4	3241	629.8	-60.1	4737	408.3	75.4	6229	195.8	67.3	7709
45.6	206	255	265.6	235.7	1730	534.2	165.5	3256	627.6	-59.3	4753	406.6	74.9	6244	193.6	67.2	7724
47.4	206.1	270	268.4	235.5	1746	536.9	164.6	3272	625.4	-57.8	4768	404.8	75	6260	191.2	67.1	7739
49.2	206.3	285	271.2	235.7	1763	540	163.6	3287	622.8	-57	4783	402.8	75.2	6275	188.8	67.1	7754
51.1	206.5	300	273.9	236.9	1780	542.7	162.6	3303	620.3	-55.1	4799	401.1	74.7	6290	186.3	67	7770
52.9	206.7	315	277	236.2	1797	545.1	161.8	3318	617.8	-53.3	4814	399	74.8	6306	183.6	67	7785
54.7	206.8	330	279.8	237.3	1814	547.6	160.4	3333	615.6	-50.6	4830	397.3	74.7	6321	180.9	66.7	7800
56.5	207	345	282.9	237.9	1831	549.7	159.8	3349	612.8	-47.2	4845	395.5	74.6	6336	178.2	66.7	7815
58.1	207.3	360	285.7	238.3	1847	552.2	158.9	3364	610.3	-44.2	4861	394.1	74.6	6351	175.5	66.6	7830
59.6	207.6	375	288.7	237.9	1864	554.6	157.7	3379	607.8	-40.7	4876	392.6	74.6	6366	173.1	66.4	7845
61.5	207.6	390	291.5	238.8	1881	557.4	156.8	3395	605.3	-36.5	4892	390.9	74.6	6382	170.4	66.5	7861
63.3	207.7	405	294.3	238.5	1898	560.5	156	3410	602.8	-31.6	4907	389.2	74.6	6397	167.7	66.1	7876
64.9	208	420	297.1	238.6	1914	562.9	154.6	3426	600.6	-26.6	4922	387.4	74.6	6412	165	66.4	7891
66.9	208.3	435	299.9	239.5	1931	565.4	152.7	3441	598.5	-21.2	4938	385.7	74.4	6428	162.3	66.3	7906
68.8	208.5	450	302.8	239	1948	568.1	146	3457	596.3	-15.7	4953	384	74.5	6443	159.6	66.1	7921
70.9	208.6	465	305.6	239.9	1965	571.5	131.3	3472	593.8	-9.5	4968	382.2	74.1	6458	157.2	66	7936
72.7	208.9	480	308.4	239.3	1982	574.3	110.7	3487	591.3	-3.1	4984	380.8	74.1	6474	154.8	66	7951
74.3	209.1	495	311.5	238.9	1998	577.4	90.7	3503	588.8	3.1	4999	379.1	73.9	6489	152.4	66	7967
76.1	209.3	510	314.6	239.1	2015	580.8	73.1	3518	586.4	9.6	5015	377.9	74.1	6504	150.2	66.1	7982
77.9	209.6	525	317.4	239.3	2032	583.9	58.5	3533	583.9	16.1	5030	376.8	74	6520	148.1	65.9	7997
79.8	210	540	320.2	238.7	2049	587.3	45.5	3549	581.4	22.8	5046	375.9	74.1	6535	145.9	66	8012
81.6	210.1	555	323.4	239.1	2065	590.7	31.2	3564	578.9	30.8	5061	374.7	74.2	6550	143.8	66	8027
83.2	210.2	570	326.2	239.1	2082	594.1	17.4	3580	576.8	38.7	5076	373.3	74.1	6566	141.7	65.9	8042
85.3	210.5	585	329	237.9	2099	597.5	4.7	3595	574.6	48.5	5092	371.3	73.9	6581	139.3	66.2	8057
87.1	210.6	600	331.9	236.4	2116	600.6	-6.7	3610	572.4	59.8	5107	369.3	73.8	6596	136.9	66	8072
88.9	211	615	334.7	236.1	2132	603.8	-16.7	3626	570	69.6	5123	367.3	73.8	6612	134.7	66.3	8088
91	211.3	630	337.8	236	2149	606.6	-23.6	3641	567.8	76.4	5138	365	73.8	6627	132.6	66.1	8103
93.2	211.4	645	340.7	234.9	2166	609.4	-28.5	3656	565.7	79.7	5153	363	73.6	6642	130.2	66.1	8118
95.5	211.8	660	343.8	234.3	2183	611.9	-32.9	3672	563.2	80.8	5169	360.9	73.9	6657	127.8	66.4	8133
97.6	212	675	346.7	232.4	2200	614.7	-36.9	3687	560.5	81.5	5184	359.2	73.7	6673	125.7	66.2	8148
99.5	212.4	690	349.5	232.5	2215	617.5	-40.3	3703	558.3	81.5	5200	357.2	73.7	6688	123.6	66.3	8163
101.8	212.6	705	352.4	231.4	2230	620.6	-43.2	3718	555.8	81.7	5215	355.2	73.6	6703	121.4	66.5	8179
104	213	720	355.2	230.1	2245	623.8	-45.9	3734	553.4	81.6	5230	353.5	73.9	6718	119.3	66.3	8194
106.1	213.1	736	357.8	229	2260	626	-47.7	3749	550.6	81.4	5246	352.1	73.5	6734	117.5	66.3	8209
108.2	213.5	751	360.4	227.7	2276	628.8	-49.7	3764	548.2	81.1	5261	350.4	73.4	6749	115.6	66.6	8224
110.3	213.6	766	363.2	226.3	2291	631.3	-51.4	3780	545.8	81	5276	348.9	73.6	6764	113.7	66.8	8239
112.2	213.9	781	365.8	224.9	2306	634.2	-52.9	3795	543	80.9	5292	347.5	73.5	6779	111.9	66.5	8254
114.3	214.2	796	368.4	223.4	2321	637.3	-54.7	3810	540	80.8	5307	345.8	73.4	6795	110	66.7	8269
116.1	214.6	811	371	222	2337	640.5	-56.5	3826	537.2	80.4	5323	344.1	73.3	6810	107.9	66.7	8284
118.2	214.6	826	373.9	220.5	2352	643.3	-58.3	3841	534.5	80.7	5338	342.4	73.5	6825	106.1	66.8	8299
120.4	215	841	376.8	219.2	2367	646.5	-60.6	3857	532	80.3	5353	340.4	73.1	6840	104	66.8	8314
122.5	215.2	856	379.6	217.9	2383	649.7	-61.8	3872	529.3	80.1	5369	338.4	73.1	6856	102.1	66.8	8329
124.6	215.7	871	382.2	216.4	2398	652.8	-63.3	3888	526.9	79.9	5384	336.1	73	6871	100	66.7	8345
126.7	215.8	886	384.8	215.3	2413	656.3	-65.3	3903	524.2	79.9	5400	333.8	72.8	6886			
128.6	215.9	901	387.7	214	2428	659.8	-66.7	3919	521.7	79.4	5415	331.6	73	6902			
130.7	216.2	916	390.6	212.9	2444	663	-68.6	3934	519.3	79.7	5430	329	72.9	6917			
132.6	216.3	931	393.2	211.6	2459	665.9	-69.6	3949	516.9	79.6	5446	326.8	72.7	6932			
134.7	216.7	946	396.1	210.6	2474	669.1	-70.8	3965	514.5	79.4	5461	324.5	72.7	6947			
136.9	217	961	398.7	209.4	2489	672.3	-72.4	3980	512.1	79.5	5476	322.2	72.7	6962			
139.3	217	976	401.6	207.9	2505	675.1	-73.5	3996	509	79.2	5492	319.7	72.5	6978			
141.4	217.5	991	404.3	207	2520	678.3	-74.5	4011	505.7	79.1	5507	317.4	72.5	6993			
143.5	217.8	1007	406.9	205.9	2535	681.9	-75.9	4027	502.7	78.9	5523	314.9	72.3	7008			
145.7	217.9	1022	409.8	205	2551	685.4	-77.2	4042	499.4	78.5	5538	312.1	72.2	7024			
147.8	218.1	1037	412.7	203.7	2566	688.6	-78.3	4057	496.1	78.6	5553	309.5	72.4	7039			
150.2	218.4	1052	415.3	203	2581	691.8	-79.2	4073	493.1	78.6	5569	306.7	72.2	7054			
152.6	218.9	1067	418.5	201.9	2596	695.1	-80	4088	489.8	78.4	5584	304.2	72.2	7070			
154.8	219.4	1082	421.2	201.4	2612	698.3	-80.9	4104	486.8	78.3	5599	301.6	72.2	7085			
157.2	219.4	1097	424.1	200.3	2627	701.2	-82	4119	483.8	77.9	5615	298.8	71.8	7100			
159.6	219.5	1112	426.4	199.4	2642	703.5	-82.8	4135	481.1	77.9	5630	296.3	71.8	7115			
162	219.9	1127	429.1	198.4	2658	705.1	-83.3	4150	478.8	77.5	5646	293.5	71.8	7130			
164.7	220.3	1142	431.4	197.9	2673	705.7	-83.7	4165	476.4	77.8	5661	291	71.6	7146			
167.4	220.7	1157	434.1	197	2688	705.4	-83.8	4181	474	77.7	5677	288.2	71.4	7161			
170.4	221	1173	436.7	196.3	2704	704.4	-83.6	4196	471.6	77.9	5692	285.4	71.2	7176			
173.3	221.3	1188	439.4	195.4	2719	702.8	-83.2	4212	469.2	77.7	5707	282.9	71.2	7192			
176	221.6	1203	442	194.6	2734	701.2	-83.1	4227	467.1	77.5	5723	280.1	71.2	7207			
178.7	222.1	1218	444.4	193.8	2750	699.6	-82.1	4243	464.8	77.4	5738	277.3	71.1	7222			
181.4	222.5	1233	447	193	2765	698.3	-82.2	4258	462.7	77.2	5754	274.2	70.9	7237			
184.2	223	1249	449.7	192.5	2780	696.7	-81.8	4274	460.3	77.3	5769	271.4	71.1	7253			
186.9	223.4	1264	452.6	191.7	2796	694.7	-81.5	4289	458	77.3	5784	268.6	70.8	7268			
189.3	223.6	1279	455.3	190.7	2811	692.8	-81	4305	455.6	77	5800	265.6	70.6	7283			
192	224.2	1294	458	190	2826	690.9	-80.7	4320	453.5	76.7	5815	262.5	70.6	7298			
194.5	224.6	1309	460.6	189	2842	688.9	-80.4	4336	451.1	76.8	5830	259.8	70.4	7314			
196.9	225	1325	463.3	188.6	2857	686.7	-79.5	4351	449.1	76.8	5846	257.3	70.3	7329			
199.6	225.6	1340	465.7	187.7	2872	684.4	-79.4	4367	446.7	76.7	5861	254.8	70	7344			
202.1	225.7	1355	468.3	186.8	2888	681.6	-78.7	4382	444.7	76.4	5876	252.3	70.1	7359			
204.2	226.2	1370	471	186	2903	679	-78.1	4398	442.9	76.3	5892	249.5	70	7374			
206.7	226.7	1385	473.7	185.3	2918	676.4	-77.6	4413	441.4	76.4	5907	247	69.8	7390			
209.2	227.1	1400	476.4	184.2	2934	674.2	-76.9	4428	439.9	76.3	5923	244.8	69.7	7405			
211.6	227.6	1416	479.4	183.7	2949	671.9	-76	4444	438.8	76.3	5938	242.3	69.6	7420			
214.1	227.9	1431	482	182.6	2965	669.7	-75.6	4459	437.9	76.3	5953	239.6	69.5	7435			
216.5	228.3	1446	484.4	181.7	2980	667.5	-74.7	4475	437	76.2	5969	237.1	69.4	7451			

Thermomagnetic results for sample AL054

TEMP	TSUSC	TIME	TEMP	TSUSC	TIME	TEMP	TSUSC	TIME	TEMP	TSUSC	TIME	TEMP	TSUSC	TIME	TEMP	TSUSC	TIME
(°C)	(°C)	(s)	(°C)	(°C)	(s)	(°C)	(°C)	(s)	(°C)	(°C)	(s)	(°C)	(°C)	(s)	(°C)	(°C)	(s)
21.8	-74	0	219.5	-72.6	1469	458.8	-71.4	2952	694.4	-121.2	4446	463	98.1	5944	319.4	36	7429
22.1	-73.4	17	222	-72.5	1484	461.5	-71.2	2967	692.5	-120.6	4461	461.2	97.4	5959	317.7	36.1	7444
23.6	-73.9	32	224.2	-72.4	1499	464.2	-71.4	2982	690.2	-120.5	4476	459.4	97	5975	316	35.7	7459
25.9	-73.8	47	226.4	-72.4	1515	466.9	-71.2	2998	688.3	-120	4492	457.7	96.5	5990	314.6	35.8	7475
28.3	-73.9	62	229.1	-72.4	1530	469.2	-71.3	3013	686	-118.6	4507	456.2	95.9	6006	313.5	35.5	7490
30.6	-73.9	77	231.9	-72.4	1545	471.6	-70.9	3028	683.5	-118.3	4523	455	95.5	6021	312.3	35.5	7505
32.9	-74	92	234.9	-72.4	1560	473.7	-71.3	3044	681.6	-117.8	4538	453.8	95.3	6036	310.9	35.4	7521
35	-73.9	107	237.7	-72.2	1575	476.1	-70.9	3059	679.6	-117.2	4554	452.6	94.6	6052	309.5	35.2	7536
37.1	-74	122	240.7	-72.2	1591	478.8	-71.2	3074	677.1	-116.8	4569	451.1	94.2	6067	308.4	34.9	7551
39.1	-74.1	137	243.4	-72	1606	481.7	-71.1	3090	674.5	-115.4	4585	450	94	6082	307	34.9	7566
41.2	-74.1	152	245.9	-72	1621	485	-71	3105	671.9	-114.9	4600	448.5	93.3	6098	305.6	34.8	7582
43	-74.1	167	248.4	-71.9	1636	488	-70.9	3120	669.7	-114.6	4615	447	92.8	6113	304.2	34.6	7597
44.8	-74.1	182	250.9	-72	1652	490.7	-70.7	3136	667.2	-113.7	4631	445.5	92.4	6129	302.8	34.5	7612
46.6	-74.1	197	253.7	-71.9	1667	493.4	-71	3151	664.6	-113	4646	444.4	92.1	6144	301.4	34.2	7627
48.2	-74	212	256.2	-72	1682	496.4	-70.8	3166	662.1	-112.1	4662	443.2	91.7	6159	299.9	34.4	7642
50	-73.9	227	258.7	-71.7	1697	498.8	-70.5	3182	659.8	-110.9	4677	441.7	91.3	6175	298.3	34.2	7658
51.8	-74	242	261.1	-71.7	1713	501.2	-70.2	3197	657	-109.9	4693	440.2	90.9	6190	296.9	34	7673
53.4	-73.9	257	263.6	-71.7	1728	503.6	-70.6	3212	654.1	-109	4708	438.5	90.2	6205	295.2	33.8	7688
55.2	-74	273	266.1	-71.6	1743	506	-70.3	3228	651.2	-107.9	4723	436.7	89.8	6221	293.5	33.7	7703
56.8	-74	288	268.4	-71.7	1758	508.4	-70.5	3243	648.4	-106.2	4739	435.2	89.8	6236	291.8	33.7	7718
58.3	-74.2	303	271.2	-71.7	1774	510.9	-70.4	3258	645.9	-105.1	4755	433.8	89.1	6251	290.1	33.5	7733
59.9	-74.1	318	273.4	-71.6	1789	513.6	-70.2	3274	643.3	-103.8	4770	432.3	88.8	6267	288.5	33.5	7749
61.7	-74.1	333	276.2	-71.5	1804	516.3	-70.1	3289	640.5	-102.2	4785	430.5	88.3	6282	286.5	33.3	7764
63.3	-73.9	348	278.7	-71.8	1819	518.7	-70.4	3305	638	-100.5	4801	428.8	88.1	6297	284.8	33.2	7779
64.9	-74.1	363	281.5	-71.5	1834	521.4	-70.1	3320	635.4	-99.1	4816	427	87.6	6313	282.6	33.1	7794
66.4	-74.3	378	284	-71.6	1850	524.2	-69.9	3335	633.2	-97.8	4832	425	87.3	6328	280.6	33	7810
68.2	-74	393	286.8	-71.3	1865	526.9	-69.8	3351	631	-95.8	4847	423.2	87.1	6343	278.7	32.8	7825
69.8	-74.1	408	289.3	-71.3	1880	529.6	-69.8	3366	628.8	-94	4863	421.8	86.7	6359	276.7	32.7	7840
71.4	-74.1	423	292.1	-71.3	1895	532.7	-69.7	3382	626.6	-92.5	4878	420.6	86.3	6374	274.8	32.5	7855
73.2	-74.1	438	294.9	-71.1	1911	535.7	-69.4	3397	624.7	-90.7	4894	419.4	85.5	6390	273.1	32.5	7871
75	-74.1	454	297.4	-71.3	1926	538.4	-69.2	3413	622.5	-88.2	4909	418	85.1	6405	271.7	32.3	7886
76.9	-74	469	299.9	-71.1	1941	541.5	-68.5	3428	620	-85.9	4925	416.8	84.5	6420	270	32.3	7901
78.7	-74	484	302.8	-71.1	1956	544.2	-68.3	3443	617.8	-83.5	4940	415.3	83.9	6436	268.1	32	7916
80.3	-74	499	305.3	-71.1	1972	547	-67.8	3459	615.3	-80.3	4956	414.2	83.4	6451	266.1	32.1	7932
82.1	-74	514	307.8	-71.2	1987	549.7	-66.8	3474	612.8	-76.5	4971	412.7	82.8	6466	263.9	31.8	7947
83.7	-73.9	529	310.6	-71	2002	552.5	-66	3489	610	-71.5	4987	410.9	82.3	6482	261.4	31.6	7962
85.5	-74	544	313.5	-71.1	2017	554.9	-64.6	3505	607.5	-66.2	5002	409.2	81.8	6497	259.2	31.6	7977
87.4	-74.1	559	316	-71.1	2033	557.7	-62.9	3520	605	-59.9	5017	408	81.3	6512	256.7	31.4	7992
89.2	-74	574	318.5	-70.7	2048	560.5	-60.5	3536	602.2	-51.8	5033	406.6	80.9	6528	253.9	31.5	8007
91	-74.1	589	321.1	-70.9	2063	563.5	-58.5	3551	599.4	-42.6	5048	405.4	80.4	6543	251.7	31.1	8023
92.6	-74.1	604	323.6	-71.1	2078	566.6	-57.2	3567	596.9	-32.9	5064	404	80	6558	249.5	31	8038
94.2	-74	620	326.5	-70.9	2094	569.4	-58.5	3582	593.8	-22.7	5079	402.5	79.6	6574	247.3	30.9	8053
96.3	-74.1	635	329	-70.8	2109	572.1	-62.3	3598	591.3	-12.4	5095	400.8	79.1	6589	245.1	30.5	8068
98.2	-74	650	331.6	-70.7	2124	574.6	-67.8	3613	588.8	-1.7	5110	399.3	78.8	6604	242.9	30.6	8083
100	-74	665	333.8	-71.1	2140	577.4	-73.8	3628	586	10.2	5125	398.2	78.3	6619	240.4	30.4	8098
101.6	-74	680	335.8	-70.6	2155	580.2	-78.7	3644	583.6	21.7	5141	397.3	78.2	6634	238.2	30.2	8113
103.2	-73.9	695	337.5	-70.8	2170	582.9	-82.7	3659	581.1	33.3	5156	396.1	78	6650	236	29.8	8129
105	-74.1	710	339.2	-70.9	2186	585.7	-86.7	3674	578.9	44.6	5172	395.3	77.8	6665	233.8	29.8	8144
107.1	-73.8	725	340.7	-71	2201	588.5	-90.8	3690	576.1	61.8	5190	394.1	77.5	6680	231.6	29.7	8159
109	-73.9	741	342.4	-70.7	2216	591.3	-94.3	3705	573.4	82.1	5205	392.9	77.3	6695	229.4	29.6	8174
110.8	-73.9	756	343.8	-70.9	2231	594.1	-97.7	3720	570.9	103.3	5220	391.8	76.8	6711	226.9	29.3	8190
112.9	-73.9	771	345.8	-70.7	2247	596.9	-101.2	3736	568.1	118.4	5236	390.3	76.4	6726	224.5	29.2	8205
115.3	-73.7	786	347.5	-70.7	2262	599.4	-104.1	3751	565.4	126.7	5251	388.9	76.1	6741	222	28.8	8220
117.5	-74	801	349.5	-70.9	2277	602.2	-106.8	3767	562.6	127.8	5267	387.7	75.8	6757	219.5	28.6	8235
119.6	-73.7	816	351.2	-70.7	2293	605.6	-109.8	3782	559.8	126.5	5282	386.3	75.6	6772	217.4	28.6	8250
122	-73.8	831	352.9	-71	2308	608.8	-112	3798	556.8	125.6	5298	385.4	75.2	6787	214.9	28.3	8266
124.1	-73.7	846	354.9	-70.8	2323	611.6	-113	3813	554	124.4	5313	384.3	74.8	6802	212.7	28.2	8281
126.2	-73.8	862	357.2	-70.8	2339	614.1	-113.8	3828	551.6	123.4	5328	383.1	74	6818	210.2	27.8	8296
128.3	-73.7	877	359.5	-70.9	2354	616.9	-114.7	3844	549.1	122.6	5344	382.2	72.7	6833	207.5	27.8	8311
130.5	-73.7	892	361.8	-70.8	2369	620	-115.8	3859	546.4	122.1	5359	381.1	71.1	6848	205.1	27.5	8326
132.6	-73.7	907	364.4	-70.8	2384	623.2	-116.4	3875	543.9	121.4	5375	379.9	69.4	6864	202.6	27.1	8341
134.7	-73.6	922	367	-71	2400	626.6	-117.2	3890	541.5	120.8	5390	379.1	66.6	6879	200.2	27	8356
137.1	-73.5	937	369.6	-70.8	2415	630.1	-117.7	3906	539	120.4	5405	377.9	64	6894	197.7	26.9	8372
139.3	-73.6	952	372.1	-71	2430	633.9	-118.2	3921	536.6	120.1	5421	376.8	61.3	6910	195.5	26.6	8387
141.7	-73.4	968	374.7	-70.9	2446	637.3	-118.3	3937	534.2	119.7	5436	375.3	58.9	6925	193.4	26.4	8402
144.1	-73.5	983	377	-71	2461	640.8	-119.1	3952	532	119.3	5451	373.9	56.8	6940	190.9	26.1	8417
146.2	-73.5	998	379.6	-71.2	2476	643.6	-119.4	3967	529.6	118.9	5467	372.4	54.8	6955	188.8	25.8	8432
148.6	-73.4	1013	381.9	-70.9	2492	646.8	-119.7	3983	527.2	118.3	5482	371.3	52.9	6971	186.3	25.5	8448
151	-73.4	1029	384.5	-71	2507	650	-120.2	3998	524.2	117.7	5498	369.8	51.4	6986	183.9	25.5	8463
153.4	-73.5	1044	387.1	-71.1	2522	653.2	-120.1	4014	521.4	117.4	5513	368.1	50	7001	181.7	25.3	8478
155.9	-73.4	1059	389.7	-70.9	2538	656.3	-120.3	4029	518.4	116.8	5529	366.7	48.6	7016	179.3	24.9	8493
158.3	-73.2	1074	392.4	-70.8	2553	659.5	-121	4044	516	116.4	5544	365.3	47.5	7032	176.9	24.7	8508
160.7	-73.3	1089	395	-70.9	2568	662.4	-121.2	4060	513.9	115.7	5559	364.1	46.8	7047	174.4	24.5	8523
163.1	-73.3	1104	397.6	-71.1	2584	665.2	-121.5	4075	511.8	115.6	5575	363.2	45.8	7062	172	24.1	8538
165.3	-73.4	1120	400.2	-71	2599	668.4	-121.7	4091	509.9	115	5590	362.4	44.9	7078	169.3	23.8	8554
167.7	-73.2	1135	402.8	-71.1	2614	671.6	-121.5	4106	507.8	114.4	5606	360.9	44.3	7093	167.1	23.7	8569
169.8	-73.3	1150	405.4	-71.3	2630	674.5	-122.1	4122	505.7	114	5621	359.5	43.7	7108	164.5	23.5	8584
172.3	-73.2	1165	408.3	-71.1	2645	677.7	-122.5	4137	503.6	113.1	5637	357.8	42.9	7124	162	23.1	8599
174.7	-73.1	1180	410.9	-71.1	2660	680.9	-122.3	4152	501.2	112.7	5652	355.8	42.3	7139	159.6	22.8	8614
177.1	-73.2	1195	413.3	-71.3	2676	684.1	-122.6	4168	499.4	111.6	5667	353.8	42	7154	157.5	22.6	8629
179.6	-73.2	1210	415.9	-71.1	2691	687.3	-122.6	4183	497.3	111.2	5683	351.8	41.4	7169	155.3	22.4	8644
181.7	-73.3	1226	418.2	-71	2706	690.5	-122.9	4199	495.2	110.4	5698	350.1	40.9	7185	152.9	22.3	8659
183.9	-72.9	1241	420.3	-71.2	2722	693.8	-122.9	4214	493.1	109.8	5713	348.4	40.5	7200	151	22	8674
186	-73	1256	422.6	-71.3	2737	696.7	-123.2	4229	491.3	109.3	5729	346.9	40.2	7215	148.9	21.9	8689
187.9	-72.9	1271	424.7	-71.3	2752	700.2	-123.4	4245	489.2	108.2	5744	345.8	39.8	7230	147	21.5	8704
190.1	-73	1286	427.3	-71.2	2768	703.8	-123.4	4260	486.8	107.3	5760	344.4	39.5	7246	144.9	21.5	8720
192.6	-73	1302	429.7	-71.4	2783	706	-123.8	4276	484.4	106.6	5775	342.9	39.2	7261	142.7	21.2	8735
195	-72.9	1317	432	-71.1	2798	707.3	-123.8	4291	482.6	105.9	5790	341.2	38.8	7276	140.9	20.9	8750
197.4	-72.9	1332	434.6	-71.2	2814	707.7	-124.1	4307	480.5	104.9	5806	339.2	38.4	7292	138.7	20.7	8765
200.2	-72.9	1347	437.3	-71.5	2829	708	-123.7	4322	478.8	104.2	5821	337.3	38.3	7307	136.6	20.3	8780
202.6	-72.9	1362	439.9	-71.3	2844	707.3	-123.7	4338	476.4	103.5	5837	335	37.9	7322	134.2	20.1	8795
204.8	-72.8	1378	442.6	-71.4	2859	705.7	-123.8	4353	474	102.6	5852	332.7	37.8	7337	132.1	19.9	8810
207.2	-72.7	1393	445.5	-71.5	2875	704.1	-123.2	4368	471.6	101.8	5867	330.4	37.3	7353	129.7	19.6	8825
209.7	-72.7	1408	448.2	-71.3	2890	702.5	-123	4384	469.8	100.8	5883	328.2	37	7368	127.5	19.5	8840
212.2	-72.6	1423	450.9	-71.3	2906	700.5	-122.9	4399	468	100.1	5898	325.9	36.9	7383	125.2	19.4	8855
214.6	-72.6	1438	453.5	-71.3	2921	698.6	-122.4	4415	466.6	99.3	5914	323.6	36.6	7399	123	19.2	8870
217.1	-72.9	1454	456.2	-71.5	2936	696.4	-121.6	4430	464.8	98.8	5929	321.4	36.2	7414	120.9	18.8	8885

Thermomagnetic results for sample AL062

TEMP (°C)	TSUSC (°C)	TIME (s)	TEMP (°C)	TSUSC (°C)	TIME (s)	TEMP (°C)	TSUSC (°C)	TIME (s)	TEMP (°C)	TSUSC (°C)	TIME (s)	TEMP (°C)	TSUSC (°C)	TIME (s)	TEMP (°C)	TSUSC (°C)	TIME (s)
21	305.3	0	241.8	329.6	1612	503.9	284.3	3240	650.9	-10	4760	436.7	238.1	6319	255.3	225.9	7930
21.6	305	19	244.5	328.8	1628	506.9	283.3	3257	648.7	-8.9	4776	434.9	237.9	6336	253.1	225.4	7945
23.4	306.1	35	247.3	329.2	1645	509.9	283	3273	646.5	-7.1	4791	432.9	237.4	6353	250.9	225.2	7960
25.7	305.1	51	250.1	330.3	1662	513.3	282.6	3290	644	-5.9	4807	430.5	240.2	6369	249	225.3	7975
28.3	306.1	68	252.8	331	1678	516.3	280.9	3307	641.4	-4.2	4822	427.9	238.6	6386	246.8	225.1	7993
30.8	305	84	255.6	331.2	1695	519.6	279.5	3324	638.9	-2.9	4837	425.3	238.2	6403	244.8	224.8	8008
33.4	305.5	101	258.1	330.8	1712	522.6	279.7	3341	637	-1.7	4853	422.9	238.6	6420	242.6	224	8025
35.8	305.3	117	260.9	331.8	1728	525.7	279.3	3358	634.8	-0.6	4868	420.6	237.5	6437	240.4	224.4	8042
37.8	306.7	134	263.6	331.7	1745	528.7	275.5	3374	632.6	1.4	4884	418.2	237.9	6454	238.2	224.2	8058
40.2	305.2	150	266.1	332.4	1762	531.4	277	3391	630.1	3.2	4899	415.9	236.6	6470	236	224.2	8073
42	305.5	167	268.9	332.6	1779	534.5	276.6	3408	627.6	5	4914	414.2	236.7	6487	233.5	225.2	8090
44	305.3	183	271.4	333	1795	537.5	274.7	3425	625.4	7.3	4930	412.1	238.4	6504	231.3	223.8	8105
46.1	305.3	200	274.2	334.4	1812	540.6	275.7	3442	622.8	9.4	4945	410.7	236.6	6521	229.1	223.5	8120
47.9	305.1	216	277	334	1829	543.6	273.3	3459	620.3	11.5	4960	409.2	236.9	6537	226.7	223.3	8135
49.8	305.5	233	279.8	333.8	1846	546.7	274.2	3476	617.8	13.8	4976	407.5	237.5	6554	224.5	222.9	8150
51.8	305.6	249	282.9	332.6	1862	549.4	273.2	3492	615.3	16.3	4991	405.4	235.8	6571	222	222.9	8166
53.4	305.4	266	285.4	335.4	1879	552.8	271.5	3509	613.1	18.7	5007	404	238.1	6588	219.5	222.7	8181
55.2	306.5	282	287.6	334.7	1896	555.8	270.2	3526	610.6	21.2	5022	402.2	236.9	6604	217.1	222.3	8196
57	307	298	289.6	335.2	1913	558.9	266.9	3543	608.1	24.2	5037	400.5	236.9	6621	214.9	222.1	8211
58.9	306.8	315	291.5	334.7	1929	562	254.7	3560	605.6	28.8	5053	398.7	236.4	6638	212.7	222	8226
60.9	306.6	332	293.5	336.7	1946	565.1	232.1	3577	602.8	33.4	5068	397	237.6	6655	210.5	221.9	8241
62.8	306	348	295.7	335.1	1963	568.1	205.9	3592	600.3	39.3	5084	395	236.6	6672	208.6	221.6	8257
64.6	306.6	364	298	336.4	1980	571.5	180.8	3608	597.5	46.3	5099	392.9	238.2	6688	206.4	221.5	8272
66.4	306.5	381	300.2	337.3	1997	574.3	160.5	3623	595	53	5114	391.2	236.5	6705	204.2	221.1	8287
68.5	307.3	397	302.8	336.4	2013	577.4	142.6	3638	592.2	60.5	5130	389.5	235.5	6722	202.1	221	8302
70.3	306.9	414	305.3	337.6	2030	580.8	127.4	3654	589.5	69.8	5145	388	235.8	6739	199.9	220.6	8317
72.4	306.6	430	308.1	336.8	2047	583.9	112.9	3669	587	81.4	5161	386.6	235.6	6756	198	220.5	8332
74.5	307.9	447	310.9	337.4	2064	587	97.9	3684	584.2	90.5	5176	385.1	235.4	6773	195.8	220.1	8347
76.4	307.9	464	313.7	338.6	2080	590.1	84.2	3700	582	99.9	5191	383.4	236.5	6790	193.4	219.9	8362
78.4	308.9	480	316.3	338.2	2097	592.9	74.1	3715	579.5	109.3	5207	381.7	236.6	6806	191.2	219.8	8377
80.3	308.6	497	319.1	338.5	2114	595.7	65.7	3730	577.1	120	5222	379.9	236.2	6823	189	219.5	8392
82.4	309	513	321.9	338.4	2131	598.5	57.8	3746	574.6	130.8	5237	377.9	234.3	6840	186.6	219.2	8407
84.2	309.1	530	324.8	338.2	2148	601.3	51.6	3761	572.1	143	5252	375.9	235.7	6856	184.4	219.3	8422
86.3	309.7	546	327.6	338.9	2164	604.1	46	3776	569.7	157.7	5268	373.9	234	6873	182.3	218.8	8438
88.4	308.3	563	330.2	339.5	2181	606.6	42.1	3792	567.2	174.6	5283	371.9	236.2	6890	179.8	218.6	8453
90.3	309.3	579	332.4	338.7	2198	609.4	38	3807	564.8	191.3	5298	369.6	235	6907	177.4	218.6	8468
92.4	310.1	596	334.4	337.7	2214	612.5	34	3822	562.3	203.6	5314	367.5	235.5	6923	175	218.4	8483
94.5	308.9	612	336.4	337.5	2231	615.3	29.7	3838	560.1	209.9	5329	365.5	234.2	6940	172.5	218.3	8498
96.6	309.8	629	338.4	337.1	2248	618.5	26.7	3853	558	214.5	5344	363.5	234.1	6957	170.1	218.2	8513
98.7	309.9	646	340.7	337	2265	621.3	23.4	3868	555.5	216.1	5360	361.5	233.1	6974	167.4	218	8528
100.8	310.3	662	342.9	335.2	2282	624.1	20.8	3884	553.1	217.1	5375	359.8	233.4	6991	165	218	8543
102.9	310.6	679	345.5	335.2	2298	626.9	18.3	3899	551	218	5390	357.8	233.5	7007	162.8	217.8	8558
105	310.8	695	348.1	334.5	2315	630.1	15.8	3914	548.5	218.9	5406	356.1	234	7024	160.4	217.6	8573
107.4	310.7	712	350.4	333.1	2332	632.9	12.2	3930	546.1	219.4	5421	354.4	235.1	7041	158.3	217.7	8588
109.8	311.1	729	352.9	331.7	2349	635.7	10.4	3945	543.6	220.4	5437	352.9	232.9	7058	155.9	217.7	8604
112.4	312.2	745	354.9	331.5	2366	638.6	8.3	3961	541.2	220.9	5452	351.5	233.5	7074	154	217.4	8618
114.8	311.1	762	357.2	332	2383	641.7	6.6	3976	539	222.2	5467	349.8	233.3	7091	151.8	217.7	8634
117.2	312.2	778	359.5	328.1	2399	644.9	4.3	3991	536.6	222.8	5482	347.8	233.6	7108	149.7	217.4	8649
119.6	312.9	795	361.5	328.2	2416	647.8	2	4006	533.9	223.6	5498	345.8	233.8	7124	147.8	217.4	8664
122	313.7	812	363.5	326	2433	650.6	-0.3	4022	531.1	224.8	5513	343.5	233.6	7141	145.7	217.4	8679
124.1	313	828	366.1	328.5	2450	653.8	-2.3	4037	528.1	224.8	5530	341.2	234.4	7158	143.8	217.3	8694
126.2	313	845	368.7	325	2466	657	-5.1	4053	524.8	227.2	5547	339.2	231.3	7175	141.7	217.4	8709
128.6	313.8	861	371.6	324.6	2483	660.1	-6.5	4068	522.3	227.9	5562	337.5	231.5	7191	139.5	217.4	8724
130.7	313.8	878	374.2	323.6	2500	663.3	-8.5	4083	519.6	227	5579	335.8	231.3	7208	137.4	217.5	8739
133.1	314	895	377	322.2	2517	666.5	-10.2	4099	517.5	229.7	5596	334.4	230.5	7225	135.5	217.4	8754
135.3	314	911	379.9	320.4	2534	669.7	-11.9	4114	515.4	229.1	5613	332.7	232.3	7242	133.7	217.5	8769
137.7	314.3	928	383.1	319.2	2550	672.9	-14.1	4130	513	230.1	5629	330.7	231.1	7259	131.5	217.6	8784
140.1	314.7	944	386	318.3	2567	676.4	-16.4	4145	511.2	229.8	5646	328.7	231	7275	129.7	217.4	8799
142.5	315.3	961	388.6	316.6	2584	679.6	-18	4160	508.7	233.6	5663	326.8	231	7292	127.8	217.4	8814
144.9	315.3	978	391.5	316	2601	682.5	-20.3	4176	506	232.8	5680	325.1	231.5	7309	125.9	217.5	8829
147.3	315.3	994	394.1	315.7	2618	685.4	-22.2	4191	503.6	230.4	5697	323.1	230.4	7325	123.8	217.7	8844
149.7	316.1	1011	396.7	314	2634	688.6	-23.7	4206	501.2	231.6	5714	321.7	229.9	7342	122	217.8	8859
152.1	316.1	1027	399.6	314.6	2651	691.8	-25.1	4222	498.8	234.4	5730	320	230.6	7359	120.1	217.9	8874
154.8	315.9	1044	402.5	311.9	2668	694.7	-26.4	4237	496.4	235.5	5747	318.3	230.9	7376	118	218	8889
157.5	315.4	1061	405.4	311.7	2685	698	-27.8	4252	494	236.3	5764	316.8	231	7392	116.1	217.9	8904
160.2	316.5	1078	408.6	311.7	2702	701.2	-29.3	4268	491.6	235.4	5781	315.4	230.2	7409	114.3	218.1	8919
162.8	317.5	1094	411.8	310.3	2718	704.8	-31.1	4283	489.2	235.6	5798	314	231.6	7426	112.2	218.1	8934
165.3	317.4	1111	414.7	309.2	2735	707	-32.5	4299	487.1	236.8	5815	312.9	228.6	7443	110.6	218.2	8949
168	317.1	1127	417.7	308.6	2752	708.3	-33.2	4314	485.3	238	5831	311.8	228.2	7460	109	218.2	8964
170.1	317.8	1144	420.3	307.3	2769	709	-33.5	4330	483.5	236.4	5848	310.6	229.8	7476			
172.5	318.4	1161	423.2	305.5	2786	709.3	-34.3	4345	482	236.8	5865	309	228.6	7493			
175	319.1	1177	426.1	306.5	2802	708	-34.1	4360	480.2	238.2	5882	307.5	229.5	7510			
177.7	319.2	1194	429.1	305	2819	706.4	-34.2	4376	478.8	237.5	5899	306.1	229.7	7527			
180.1	317.8	1211	432	303.2	2836	704.4	-33.9	4391	477.3	237.9	5915	304.7	229.6	7543			
182.3	320.8	1228	434.6	304.5	2853	702.8	-33.5	4406	475.8	237.6	5932	303.3	230.1	7560			
184.7	320.8	1244	437.6	303.7	2870	700.5	-32.6	4422	474.3	238.8	5949	301.6	229.9	7577			
187.1	320.5	1261	440.5	301.8	2886	698.3	-32.2	4437	472.2	238.6	5966	299.7	229.9	7593			
189.8	322	1278	443.5	300.1	2903	696	-31.5	4453	470.4	238.2	5982	298	228.6	7610			
192.3	321.5	1294	446.4	300.6	2920	693.8	-30	4468	468.6	237.7	5999	296.6	228.4	7627			
194.7	320.8	1311	449.7	298.5	2937	691.5	-29.8	4483	467.1	238.3	6016	294.9	228.5	7644			
197.4	320.8	1327	452.6	299.1	2954	689.6	-28.8	4499	466	237.7	6033	293.5	228.8	7661			
199.9	323	1344	455.6	298.4	2970	687.3	-27.8	4514	464.5	238.5	6050	292.1	228.3	7677			
202.6	322.5	1361	458.8	297.6	2987	684.8	-27.4	4530	463.3	239.2	6066	290.1	227.9	7694			
205.1	324.4	1378	461.8	296.3	3004	682.5	-26.4	4545	462.1	238.2	6083	288.2	228.2	7711			
207.5	323.1	1394	464.5	295.7	3021	680.6	-25.7	4560	461.2	238.8	6100	285.9	227.7	7727			
210	324.9	1411	467.7	295.9	3038	678.3	-23.7	4576	460.3	239.2	6117	283.7	227.7	7744			
212.4	325.7	1428	470.7	295.9	3055	675.8	-22.6	4591	459.4	240	6134	281.7	227.7	7759			
214.9	324.5	1444	473.7	293.3	3071	673.2	-21.3	4606	458.2	239.5	6151	279.8	227.7	7775			
217.1	325.4	1461	476.7	292.9	3088	671	-19.8	4622	456.5	238.9	6168	277.6	227.5	7790			
219.5	325.6	1478	479.7	292.4	3105	668.4	-18.6	4637	454.4	237.5	6184	275.3	227.3	7805			
221.7	325.3	1494	482.6	290.9	3122	666.2	-17.9	4653	452.3	239.6	6201	272.5	225.2	7823			
224.2	329	1511	485.9	291.8	3139	664	-16.6	4668	450	240.6	6218	270	226.9	7839			
226.7	325.5	1528	489.2	289	3155	661.7	-15.7	4684	447.3	239.5	6235	267.5	226.8	7854			
229.7	326.8	1545	492.5	288.8	3172	659.8	-14.6	4699	445	239	6252	265	226.6	7869			
232.4	327.1	1561	495.2	288	3189	657.6	-13.6	4714	442.6	240.4	6269	262.8	226.2	7884			
235.7	328.2	1578	498.2	286.8	3206	655.4	-12.3	4730	440.5	239.2	6285	260.3	226.2	7900			
238.8	329.6	1595	501.2	286.5	3223	653.2	-11.5	4745	438.5	238.4	6302	257.5	226	7915			

Thermomagnetic results for sample AL067

TEMP (°C)	TSUSC (°C)	TIME (s)	TEMP (°C)	TSUSC (°C)	TIME (s)	TEMP (°C)	TSUSC (°C)	TIME (s)	TEMP (°C)	TSUSC (°C)	TIME (s)	TEMP (°C)	TSUSC (°C)	TIME (s)	TEMP (°C)	TSUSC (°C)	TIME (s)
14.4	-115.6	0	217.1	-112.9	1470	459.1	-115	2949	695.7	-139.8	4439	466.6	-126.6	5928	326.8	-125.4	7411
14.9	-114.8	17	219.3	-112.9	1485	461.5	-115.5	2964	694.1	-139.6	4455	464.2	-126.6	5943	325.1	-125.7	7426
16.4	-114.5	32	221.5	-112.7	1501	463.9	-115.3	2980	692.5	-139.3	4470	461.8	-126.5	5959	323.4	-125.5	7441
18.5	-114.6	47	223.9	-113	1516	466.6	-115.3	2995	690.5	-139.7	4485	459.7	-126.9	5974	321.4	-125.4	7456
21	-114.4	62	226.4	-112.7	1531	469.2	-115.7	3010	688.6	-139.9	4501	458	-126.9	5989	319.7	-125.5	7472
23.4	-114.4	77	229.1	-112.6	1546	471.9	-115.4	3026	687	-139.4	4516	456.2	-126.8	6005	317.4	-125.7	7487
25.7	-114.4	92	231.6	-112.7	1562	474.6	-115.4	3041	685.4	-139.7	4531	454.4	-126.8	6020	315.4	-125.5	7502
28	-114.3	107	234.6	-112.6	1577	477.3	-115.9	3056	683.8	-139.7	4547	453.2	-126.5	6035	313.2	-125.4	7517
30.1	-114.3	122	237.1	-112.4	1592	480	-116	3072	681.9	-139.7	4562	451.4	-126.6	6051	311.2	-125.3	7533
32.4	-114.3	137	239.6	-112.6	1607	482.3	-115.9	3087	679.9	-139.5	4578	450	-126.6	6066	309	-125.5	7548
34.2	-114.3	152	242.1	-112.8	1622	485	-116	3102	678	-139.8	4593	447.9	-126.9	6081	307	-125.8	7563
36	-114.3	168	244.5	-112.5	1638	487.4	-116.1	3118	675.5	-139.5	4608	445.8	-126.7	6097	304.7	-125.5	7579
38.1	-114.2	182	247	-112.6	1653	490.1	-116.3	3133	673.5	-139.5	4624	444.4	-126.5	6112	302.8	-125.4	7594
39.9	-114.2	198	249.5	-112.6	1668	492.5	-116.2	3149	671.6	-139.6	4639	442.6	-126.6	6127	300.8	-125.3	7609
41.7	-114.2	213	252.3	-112.6	1683	494.6	-116.3	3164	669.7	-139.4	4655	440.8	-126.4	6143	299.4	-125.6	7624
43.5	-114	228	254.8	-112.5	1699	497	-116.6	3179	667.5	-139.8	4670	438.8	-126.5	6158	297.7	-125.6	7639
45.3	-114.3	243	257.3	-112.5	1714	499.1	-116.9	3194	665.2	-139.6	4685	436.4	-126.6	6173	296	-125.6	7655
46.9	-114.2	258	259.8	-112.4	1729	501.5	-116.7	3210	663.3	-139.5	4701	434.6	-126.7	6189	294.3	-125.5	7670
48.7	-114.2	273	262.3	-112.4	1744	503.9	-116.7	3225	661.1	-139.4	4716	433.2	-126.5	6204	292.7	-125.5	7685
50.3	-114	288	264.8	-112.4	1759	506.6	-117.1	3240	658.6	-139.5	4731	431.7	-126.4	6219	291	-125.5	7700
52.1	-114.3	303	267.3	-112.4	1775	509.3	-117.1	3256	656.3	-139	4747	430	-126.6	6234	289	-125.5	7716
53.7	-114.1	319	269.8	-112.5	1790	511.8	-117.1	3271	654.1	-139.4	4762	427.9	-126.4	6250	287.3	-125.2	7731
55.5	-114.1	333	272.5	-112.3	1805	514.2	-117.3	3286	651.6	-139.5	4777	426.1	-126.6	6265	285.7	-125.5	7746
57	-114	349	275	-112.3	1820	516.6	-117.2	3302	649.3	-139.5	4793	424.7	-126.3	6280	284	-125.2	7761
58.9	-114.2	364	277.8	-112.4	1835	519.3	-117.3	3317	646.8	-139.3	4808	423.2	-126.6	6295	282	-125.3	7776
60.7	-114.2	379	280.3	-112.4	1851	522	-117.4	3333	644.3	-139.3	4824	421.8	-126.6	6311	280.1	-125.4	7792
62.2	-114.3	394	283.1	-112.3	1866	524.8	-117.8	3348	641.7	-139.2	4839	420.9	-126.5	6326	278.1	-125.5	7807
63.8	-114.2	409	285.7	-112.4	1881	527.2	-118.4	3363	639.2	-139.1	4854	420	-126.8	6341	276.4	-125.4	7822
65.6	-114.2	424	288.2	-112.2	1897	529.6	-118.5	3379	637	-139.4	4870	418.8	-126.4	6357	274.8	-125.5	7837
67.5	-114.2	439	291	-112.2	1912	532.7	-119.4	3394	634.8	-139.2	4885	417.4	-126.4	6372	273.1	-125.3	7852
69	-114	454	293.2	-112.2	1927	535.4	-120.2	3410	632.3	-139.3	4901	416.2	-126.7	6387	271.4	-125.4	7868
70.9	-114	470	295.7	-112.4	1942	537.8	-121.1	3425	629.8	-139.4	4916	414.4	-126.5	6402	269.8	-125.4	7883
72.7	-114.1	484	298.3	-112.2	1957	540.3	-122.4	3440	627.6	-139.2	4931	412.4	-126.5	6418	268.1	-125.4	7898
74.5	-114	500	300.8	-112.2	1973	543.3	-123.3	3456	625	-139.2	4947	410.9	-126.3	6433	266.4	-125.5	7913
76.4	-114	515	303.6	-112.2	1988	546.4	-124.9	3471	622.5	-138.9	4962	409.5	-126.4	6448	264.5	-125.3	7929
77.9	-114.1	530	306.4	-112	2003	549.4	-126.6	3486	620.3	-138.9	4977	408	-126.4	6464	262.3	-125.4	7944
80	-114.1	545	308.7	-112.1	2018	552.8	-128.2	3502	617.8	-138.7	4993	406.6	-126.3	6479	260	-125.4	7959
81.9	-114	560	310.9	-111.9	2034	556.2	-130.4	3517	615.6	-138.6	5008	405.4	-126.2	6494	257.8	-125.1	7974
83.7	-114	575	313.5	-112.2	2049	558.9	-131.9	3532	613.8	-139.3	5023	404.3	-126.2	6509	255.3	-125.4	7990
85.5	-114	590	316	-112	2064	562	-132.7	3548	611.6	-138.8	5039	402.8	-126.1	6525	253.1	-125.2	8005
87.6	-114.1	605	318.5	-112.1	2079	565.1	-134.6	3563	608.8	-139.3	5054	401.3	-126	6540	250.6	-125.4	8020
89.7	-114.1	620	321.1	-112.3	2095	568.1	-135.5	3579	606.3	-139	5069	399.9	-126.5	6555	248.1	-125.5	8035
91.8	-114.1	636	323.6	-112.2	2110	571.2	-136	3594	603.8	-138.6	5085	398.2	-126.2	6571	245.7	-125.3	8050
94.2	-114	651	326.2	-112.1	2125	574	-136.4	3609	601	-138.7	5100	396.4	-126.3	6586	243.4	-125.3	8065
96.3	-114	666	329	-111.9	2140	576.5	-137.5	3625	598.2	-138.7	5115	394.7	-126.2	6601	241	-125.2	8081
98.7	-114	681	331.6	-112.1	2155	579.2	-137.9	3640	595.7	-138.9	5131	393.2	-126.4	6616	238.5	-125.5	8096
101.1	-114.1	696	334.1	-112.1	2171	582	-138.3	3655	593.2	-138.6	5146	392.1	-126.3	6632	236	-125.2	8111
103.2	-114	711	336.7	-111.8	2186	584.8	-138.3	3671	590.7	-138.4	5161	390.6	-126.1	6647	233.8	-125.3	8126
105.5	-113.9	726	339.2	-112	2201	587.6	-138.5	3686	588.2	-138.5	5177	389.2	-126.3	6662	231.6	-125.3	8141
107.7	-113.5	742	341.8	-112.2	2216	590.7	-138.9	3702	585.7	-138.5	5192	387.7	-126.3	6678	229.1	-125.2	8157
110	-113.4	757	344.7	-111.8	2231	593.5	-138.8	3717	583.3	-137.8	5207	386.3	-126.4	6693	226.7	-125.2	8172
112.2	-113.5	772	347.5	-112.1	2247	596.3	-139.2	3732	581.1	-137.9	5223	384.5	-126.3	6708	224.2	-125.5	8187
114.3	-113.5	787	350.1	-112.2	2262	599.1	-139.1	3748	578.6	-137.5	5238	383.1	-126.3	6723	221.7	-125.3	8202
116.4	-113.5	802	353.2	-112.2	2277	601.6	-139	3763	575.8	-136.9	5253	381.9	-126.1	6739	219.5	-125.1	8217
118.5	-113.5	817	355.8	-112.3	2292	604.1	-139.3	3778	573.4	-137	5269	380.8	-126.4	6754	217.1	-125.4	8232
120.6	-113.5	832	358.7	-112.2	2308	606.6	-139.4	3794	570.9	-136.3	5284	379.3	-126.2	6769	214.6	-125.3	8248
122.8	-113.6	848	360.9	-112.1	2323	609.4	-139.3	3809	568.4	-135.9	5300	377	-126	6784	212.4	-125.1	8263
124.9	-113.3	863	363.5	-112.2	2338	611.9	-139.7	3825	565.7	-135.8	5315	374.7	-126.2	6800	210	-125.1	8278
127	-113.4	878	366.4	-112.1	2353	614.4	-139.1	3840	563.5	-135.3	5330	372.1	-126	6815	207.2	-125.3	8293
129.1	-113.7	893	369.3	-112.4	2369	617.2	-139.6	3856	561.1	-134.8	5346	369.8	-126.1	6830	204.5	-125.2	8308
131.3	-113.6	908	372.1	-112.6	2384	620	-139.4	3871	558.6	-134	5361	367.5	-126	6846	202.1	-125.2	8323
133.7	-113.7	923	375	-112.6	2399	622.8	-139.4	3886	556.2	-133.5	5376	365.3	-126	6861	199.6	-125.4	8339
135.8	-113.4	938	377.6	-112.4	2414	625.7	-139.3	3901	553.7	-132.9	5392	363	-126.1	6876	197.2	-125.3	8354
137.9	-113.4	954	380.5	-112.6	2430	628.5	-139.4	3917	551.3	-132.4	5407	361.2	-126	6891	194.7	-125	8369
140.1	-113.4	969	382.2	-112.5	2445	631.6	-140	3932	548.8	-131.3	5422	359.8	-126	6907	192.3	-125.2	8384
142.2	-113.4	984	383.7	-112.5	2460	635.1	-139.8	3948	546.4	-130.9	5438	359.5	-126	6922	190.1	-125	8399
144.3	-113.7	999	385.1	-112.8	2475	638	-139.6	3963	543.9	-130.5	5453	359.5	-125.9	6937	187.4	-125.1	8414
146.7	-113.5	1014	386.9	-112.9	2491	641.1	-139.7	3978	541.2	-130	5468	359.8	-125.9	6952	185	-125.3	8430
149.2	-113.5	1029	388.6	-113	2506	644.3	-139.4	3994	538.4	-129.2	5484	359.8	-126.2	6968	182.5	-125.1	8445
151.3	-113.4	1045	390.6	-112.9	2521	647.4	-139.6	4009	536	-129	5499	359.8	-125.9	6983	180.1	-125.4	8460
154	-113.5	1060	392.9	-113	2537	650.6	-139.4	4024	533.3	-128.7	5514	359.2	-126.1	6998	177.7	-125.4	8475
156.1	-113.5	1075	395	-113	2552	654.1	-140	4040	530.5	-128.3	5530	358.7	-125.9	7013	175.2	-125.2	8490
158.5	-113.5	1090	397.3	-113.1	2567	657.3	-139.9	4055	527.5	-128	5545	358.1	-126.2	7028	172.8	-125.4	8505
161	-113.3	1105	399.3	-113.1	2583	660.5	-140	4070	524.8	-127.5	5560	357.5	-125.9	7044	170.4	-125	8520
163.4	-113.3	1120	401.6	-113.2	2598	663.3	-140	4086	521.7	-127.8	5576	356.9	-126.1	7059	168	-125.3	8535
165.5	-113.2	1136	404.3	-113.1	2613	666.8	-139.8	4101	518.7	-127.5	5591	356.1	-125.8	7074	165.5	-125.3	8551
167.7	-113.4	1151	406.3	-113.2	2628	670.3	-139.5	4116	516	-127.3	5606	355.2	-125.8	7090	162.8	-125.1	8566
170.4	-113.3	1166	408.9	-113.3	2644	673.5	-139.8	4132	513.9	-127.2	5622	354.4	-125.8	7105	160.7	-125.2	8581
172.8	-113.1	1181	410.9	-113.5	2659	677.4	-139.7	4147	511.5	-127.4	5637	353.2	-125.6	7120	158.3	-125.2	8596
175.2	-113.5	1197	413	-113.4	2674	680.9	-139.5	4163	508.7	-127.2	5652	351.8	-125.8	7136	155.9	-125.2	8611
177.7	-113.3	1212	415.3	-113.7	2689	684.8	-140	4178	506.3	-127.4	5667	350.9	-125.9	7151	153.7	-125	8626
180.1	-113.2	1227	418	-113.9	2705	688.3	-139.9	4193	503.6	-127.4	5683	349.8	-125.6	7166	151.6	-125.2	8641
182.5	-113.2	1242	420.6	-113.9	2720	691.8	-139.6	4209	500.9	-127.1	5698	348.4	-126	7182	149.4	-125.2	8657
184.7	-113.2	1257	423.5	-114	2735	695.4	-140.2	4224	498.2	-127.1	5714	347.2	-125.7	7197	147.3	-125	8672
187.1	-113.1	1272	426.1	-113.9	2750	698.3	-139.9	4240	495.8	-127.2	5729	346.4	-125.8	7212	145.1	-125	8687
189.8	-113.1	1288	428.5	-114.2	2766	700.5	-139.5	4255	493.4	-126.9	5744	344.9	-125.9	7228	143.3	-125.4	8702
192.3	-112.8	1303	431.1	-114.2	2781	702.2	-140.7	4271	491.3	-127.1	5759	343.5	-125.7	7243	141.1	-125	8717
194.7	-113.1	1318	434.1	-114.3	2796	703.5	-140.4	4286	489.5	-127.1	5775	342.1	-125.7	7258	139	-125.2	8732
197.2	-113.2	1333	436.7	-114.4	2812	703.8	-139.8	4301	487.4	-127.1	5790	340.4	-125.9	7274	136.9	-124.9	8747
199.3	-113	1349	439.1	-114.5	2827	703.5	-140	4316	485.6	-126.8	5805	338.7	-125.7	7289	134.7	-125.2	8762
201.8	-112.9	1364	441.7	-114.4	2842	703.5	-140	4332	483.2	-127	5821	337	-125.7	7304	132.6	-125	8777
204	-113.2	1379	444.4	-114.8	2857	703.1	-139.8	4347	480.8	-127.2	5836	335.5	-125.5	7319	130.5	-125.1	8792
206.2	-113.1	1394	446.7	-114.9	2873	701.8	-140	4362	478.2	-126.8	5852	334.1	-125.8	7334	128.1	-124.8	8808
208.3	-113	1409	449.1	-114.7	2888	700.5	-140	4378	475.5	-126.9	5867	332.7	-125.8	7350	125.9	-125	8822
210.5	-112.9	1425	451.7	-114.6	2903	699.9	-140	4393	472.8	-126.7	5882	331.3	-125.6	7365	123.6	-124.9	8838
212.7	-112.8	1440	454.1	-115	2919	698.9	-140.4	4409	470.7	-127.1	5898	329.6	-125.8	7380	121.4	-124.8	8853
214.9	-113	1455	456.8	-114.9	2934	697.6	-140	4424	468.6	-126.8	5913	328.2	-125.6	7395	119.3	-125	8868

Thermomagnetic results for sample AL079

TEMP (°C)	TSUSC (°C)	TIME (s)	TEMP (°C)	TSUSC (°C)	TIME (s)	TEMP (°C)	TSUSC (°C)	TIME (s)	TEMP (°C)	TSUSC (°C)	TIME (s)	TEMP (°C)	TSUSC (°C)	TIME (s)	TEMP (°C)	TSUSC (°C)	TIME (s)
12.8	191.3	0	218.2	204.8	1472	468.3	168.3	2954	686.7	-125.7	4448	451.4	81.2	5943	282.3	74	7425
12.8	190.4	16	220.6	205.1	1487	471	168	2969	684.4	-124.8	4463	449.4	81	5958	279.8	73.8	7441
14.4	190.7	31	223.4	205.4	1502	473.7	167.8	2985	682.2	-123.9	4479	447	80.9	5974	277.3	73.8	7456
16.4	190.6	46	226.1	205.8	1517	476.4	167.6	3000	680.3	-122.8	4494	444.7	80.8	5989	274.8	73.8	7471
18.7	190.8	61	228.9	206.3	1533	479.4	167.1	3015	678	-122.5	4510	442	80.7	6004	272.3	73.6	7487
21.3	190.9	76	231.6	206.9	1548	482.3	166.5	3031	676.1	-121.6	4525	439.6	80.9	6020	269.5	73.3	7502
23.6	191.1	92	234.1	207.1	1563	485.3	166.4	3046	674.2	-121	4540	437.6	80.5	6035	266.7	73.1	7517
25.9	191.2	107	236.8	207.6	1578	487.7	165.9	3061	672.3	-120.1	4556	435.5	80.3	6050	263.9	73	7532
28.3	191.4	122	239.3	208.1	1594	490.1	165.6	3076	670.3	-119.5	4571	433.5	80.3	6066	261.1	73.2	7547
30.3	191.5	137	241.8	208.3	1609	492.2	164.9	3092	668.4	-118.1	4587	432	80.3	6081	258.4	72.6	7563
32.7	191.5	152	244.3	208.6	1624	494.6	164.8	3107	666.2	-116.4	4602	430.5	80.3	6096	255.3	72.8	7578
34.5	191.6	167	246.8	209	1639	497	164.6	3123	664.3	-116.1	4618	429.4	80.3	6111	252.8	72.3	7593
36.5	191.6	182	249.2	209.4	1655	499.4	163.9	3138	662.4	-114.8	4633	427.6	80.1	6127	250.3	72.4	7608
38.3	191.9	197	251.7	209.7	1670	501.8	163.6	3153	660.1	-113.2	4649	425.8	80.1	6142	247.9	72.3	7624
40.4	191.9	212	254.2	210.1	1685	504.5	163.4	3169	657.6	-111.9	4664	424.1	80.1	6157	245.4	72.1	7639
42.2	192.1	228	256.7	210.4	1700	507.2	162.7	3184	655.4	-110.6	4680	422.3	79.7	6173	242.9	72	7654
44	192.3	242	259.2	210.6	1715	509.9	162.3	3199	653.2	-109.4	4695	420.6	79.9	6188	240.4	71.8	7669
45.9	192.3	258	261.7	211	1731	513	162	3215	650.9	-108.3	4711	419.1	79.7	6203	237.9	71.8	7684
47.7	192.4	273	264.2	211.4	1746	515.7	161.5	3230	648.7	-106.6	4726	418	79.5	6219	235.2	71.7	7700
49.5	192.5	288	266.7	211.7	1761	518.4	161	3245	645.9	-105.4	4742	416.5	79.4	6234	232.4	71.3	7715
51.3	192.5	303	269.5	211.9	1777	521.1	160.6	3261	643.3	-103.7	4757	415	79.4	6249	230	71.3	7730
52.9	192.7	318	271.7	212	1792	523.9	160.3	3276	641.1	-101.6	4772	413.6	79.3	6265	227.5	70.9	7745
54.7	192.9	333	274.5	212.1	1807	526.6	159.5	3291	638.9	-99.9	4788	411.8	79.2	6280	225	70.8	7760
56.5	192.8	348	277.3	212.1	1822	529.3	159.1	3307	636.4	-98.1	4803	409.8	79.2	6295	222.6	70.6	7776
58.1	193	364	280.1	212.7	1838	532.4	158.6	3322	633.9	-96.5	4819	407.7	79	6311	219.8	70.7	7791
59.9	193	379	282.6	212.7	1853	535.4	158.3	3338	631.6	-94.9	4834	406.3	78.9	6326	217.4	70.3	7806
61.7	193.1	394	285.4	212.8	1868	538.1	157.9	3353	629.1	-93.1	4849	404.5	78.8	6341	214.6	70.3	7821
63.3	193.3	409	287.9	212.8	1883	540.9	157.3	3369	626.6	-91.6	4865	403.1	78.9	6357	211.9	70	7836
65.1	193.2	424	290.7	212.4	1898	543.9	157	3384	624.1	-89.8	4880	401.9	78.7	6372	209.4	69.7	7852
66.9	193.4	439	293.2	212.6	1914	546.7	156.5	3399	621.9	-87.7	4896	400.8	78.7	6387	206.7	69.5	7867
68.8	193.6	454	295.5	212.4	1929	549.1	155.3	3415	619.7	-86.4	4911	399.9	79	6402	204.2	69.5	7882
70.6	193.5	470	298	211.8	1944	551.6	154.9	3430	617.2	-83.6	4927	399	78.5	6418	201.8	69.3	7897
72.4	193.8	485	300.5	211.7	1959	554	154.6	3445	614.7	-81.4	4942	397.6	78.5	6433	199.1	69.1	7913
74.3	193.7	500	303.3	211.6	1975	556.8	153.8	3461	612.2	-79.4	4957	396.1	78.6	6448	196.6	69	7928
76.1	193.7	515	306.1	210.9	1990	559.8	153	3476	609.7	-77.4	4973	394.7	78.4	6463	194.2	68.8	7943
77.9	193.6	530	309.2	210.3	2005	562.6	150.5	3492	607.2	-74.9	4988	393.2	78.4	6478	191.7	68.5	7958
79.8	194	545	311.8	209.7	2020	565.7	141.8	3507	604.4	-71.4	5004	391.5	78.4	6494	189.3	68.4	7973
81.9	193.9	561	314.6	208.9	2036	568.8	127.4	3522	601.9	-67.1	5019	390	78.3	6509	186.9	68.1	7988
83.7	193.9	576	317.1	207.9	2051	571.5	102.9	3538	599.4	-61.7	5035	388.6	78.2	6524	184.4	68.2	8003
85.5	193.8	591	319.7	206.8	2066	574.6	73.7	3553	596.9	-56	5050	387.4	78.1	6540	182	67.6	8019
87.6	194	606	322.2	205.5	2081	577.7	48.5	3568	594.4	-48.2	5066	385.7	77.9	6555	179.6	67.7	8034
89.5	194	621	324.5	204.3	2097	580.5	30	3584	592.2	-40.1	5081	384.3	78.1	6570	177.1	67.5	8049
91.6	194	636	327	202.9	2112	583.6	14.7	3599	589.5	-31.3	5097	382.5	77.9	6586	174.7	67.3	8064
93.9	193.9	651	329.6	201.1	2127	586.4	0.4	3615	587	-23.3	5112	380.5	77.9	6601	172	67.2	8079
96	194	667	332.1	200.1	2142	589.1	-14.8	3630	584.5	-14.5	5127	379.1	77.7	6616	169.6	67.1	8094
98.2	194	682	335	198.6	2158	592.2	-29	3646	582.3	-5.3	5143	377.3	77.8	6631	166.9	67	8110
100.5	194	697	337.5	197.3	2173	595.4	-41.2	3661	579.9	3.8	5158	375.9	77.8	6647	164.2	66.9	8125
102.9	193.8	712	340.1	195.9	2188	598.2	-52	3676	577.4	13.3	5174	374.4	77.5	6662	161.8	66.9	8140
105	193.9	727	342.7	194.6	2204	601.3	-60.4	3692	575.2	25.4	5189	373	77.5	6677	159.3	66.7	8155
107.4	194.1	742	344.9	193.7	2219	604.7	-67.5	3707	572.4	44.5	5205	371.9	77.5	6693	156.9	66.8	8170
109.5	193.8	757	347.5	192.1	2234	608.4	-71.6	3723	570	61.8	5220	370.4	77.4	6708	154.5	66.9	8185
111.6	193.8	773	350.4	191.2	2249	611.6	-75.6	3738	567.5	74.7	5236	368.7	77.4	6723	152.4	66.5	8200
113.5	193.7	788	352.9	190.2	2265	613.8	-79.2	3753	564.8	81.6	5251	367	77.2	6739	150	66.5	8216
115.6	193.7	803	355.8	189.3	2280	616.6	-81.5	3769	562.3	84	5266	365.3	77.1	6754	147.8	66.5	8231
117.7	193.8	818	358.1	188.2	2295	619.7	-84.6	3784	559.8	84.2	5282	363.5	77.1	6769	145.7	66.5	8246
119.8	193.8	833	360.7	187.2	2311	622.5	-86.9	3800	557.7	84.8	5297	362.1	77	6785	143.5	66.4	8261
121.7	193.9	848	363.2	186.2	2326	625.7	-89.9	3815	555.5	85.1	5313	360.7	77.2	6800	141.4	66.4	8276
123.8	193.8	864	365.8	185.7	2341	628.8	-92.7	3831	553.1	85	5328	359.2	77.1	6815	139.3	66.5	8291
125.9	193.8	879	368.4	184.7	2357	632	-96.5	3846	550.6	84.8	5343	357.8	76.9	6830	137.1	66.4	8306
128.1	193.8	894	371.3	184	2372	635.1	-99.4	3861	548.2	84.9	5359	356.1	77.1	6846	134.7	66.5	8321
130.2	194	909	373.9	183.5	2387	638.3	-101.5	3877	545.4	84.8	5374	354.7	76.9	6861	132.9	66.5	8336
132.3	194.2	924	376.5	182.6	2403	641.4	-103.9	3892	543	84.8	5390	353.2	76.9	6876	130.7	66.5	8351
134.5	194.2	939	379.1	181.8	2418	644.3	-106.1	3907	540.6	84.8	5405	351.5	76.6	6892	128.3	66.5	8366
136.9	194.2	955	381.7	181.2	2433	647.1	-108	3923	538.1	84.7	5420	349.8	76.9	6907	126.2	66.6	8382
139.3	194.5	970	384.5	180.7	2449	650	-110.2	3938	535.4	84.5	5436	348.4	76.6	6922	123.8	66.6	8397
141.4	194.6	985	387.1	180.2	2464	653.2	-112.5	3954	532.7	84.7	5451	346.9	76.7	6937	121.4	66.8	8412
143.8	194.8	1000	389.7	179.6	2479	656	-113.7	3969	529.9	84.1	5467	345.5	76.6	6953	119	66.7	8427
146.2	195.1	1015	392.1	179.2	2494	659.2	-115	3985	526.9	84.5	5482	343.5	76.5	6968	116.9	66.8	8442
148.4	195.1	1031	394.4	178.5	2510	662.4	-117.1	4000	524.2	84.2	5498	341.8	76.6	6983	114.8	66.9	8457
150.8	195.3	1046	397	178.1	2525	665.2	-118.4	4016	521.7	84	5513	340.1	76.7	6998	112.7	66.7	8472
153.4	195.3	1061	399.6	177.2	2540	668.1	-119.7	4031	519.3	83.9	5528	338.4	76.3	7014	110.6	66.9	8487
155.9	195.7	1076	402.2	177.1	2556	671.6	-120.8	4046	516.9	83.9	5543	336.7	76.3	7029	108.5	66.9	8502
158.3	196.2	1091	404.8	176.7	2571	675.1	-121.5	4062	514.5	83.6	5559	335	76.4	7044	106.6	67	8518
161	196.2	1107	407.5	176.2	2586	678	-122.9	4077	512.1	83.8	5574	333.3	76.2	7060	104.5	67	8532
163.4	196.5	1122	410.1	175.9	2601	680.9	-124.2	4092	509.6	83.7	5590	331.3	76.1	7075	102.4	67.2	8547
165.5	196.4	1137	412.7	175.6	2617	684.4	-125.3	4108	506.9	83.5	5605	329.3	76.1	7090	100.3	67.2	8562
167.7	196.9	1152	415	174.9	2632	687.3	-126.1	4123	504.5	83.4	5620	327.9	76	7105	98.4	67.2	8578
170.1	197.1	1168	417.7	174.4	2647	690.2	-127	4139	501.8	83.4	5636	325.9	76	7120	96.3	67.2	8592
172.8	197.4	1183	419.7	174.1	2663	693.4	-127.8	4154	499.1	83.1	5651	324.2	76	7136	94.2	67.4	8608
175.2	197.7	1198	422	173.7	2678	697	-128.7	4170	496.1	83	5667	322.2	75.8	7151	92.4	67.6	8623
177.7	197.8	1213	424.7	173.7	2693	700.2	-129.8	4185	493.4	83.3	5682	320.2	75.6	7166	90.3	67.7	8638
180.4	198.3	1229	427.3	173.1	2708	703.5	-130.7	4201	490.7	83	5697	318	75.5	7181	88.4	67.5	8653
182.8	198.7	1244	430.2	173.1	2724	705.7	-131	4216	488	82.8	5713	316.3	75.5	7196	86.3	67.6	8668
185.5	198.9	1259	432.9	172.8	2739	707.7	-131.5	4232	485	82.3	5728	314.3	75.5	7212	84.5	67.6	8683
188.2	199.5	1274	435.5	172.4	2755	709	-131.5	4247	482	82.6	5744	312.6	75.4	7227	82.4	67.7	8698
190.7	200	1289	437.9	172.3	2770	709	-131.7	4262	479.4	82.7	5759	310.6	75.4	7242	80.5	67.6	8713
193.1	200.1	1305	440.2	171.8	2785	708.3	-131.7	4278	476.1	82.6	5774	308.7	75.3	7257	78.7	67.9	8728
195.8	200.6	1320	442.6	171.5	2800	707.3	-131.7	4293	473.1	82.1	5789	306.7	75.2	7273	76.9	67.7	8743
198.3	201.1	1335	445.2	171.3	2816	706	-131	4309	470.1	82	5805	304.4	74.9	7288	75	67.8	8758
200.7	201.6	1350	447.6	171	2831	703.8	-130.6	4324	467.4	82.2	5820	302.2	74.9	7303	73.2	67.9	8773
202.9	201.8	1365	450	170.7	2846	701.2	-130	4340	465.1	82.1	5835	299.7	74.8	7319	71.4	68	8788
205.6	202.2	1381	452.6	170.3	2862	698.6	-129.3	4355	463.3	82	5851	297.4	74.7	7334	69.8	68	8803
207.8	202.9	1396	455.6	170	2877	696.4	-128.6	4371	461.2	81.7	5866	294.9	74.6	7349			
210	203.2	1411	458.2	169.5	2892	694.4	-128.3	4386	459.4	81.6	5882	292.4	74.4	7364			
212.2	203.5	1426	460.6	169.4	2908	692.5	-127.7	4401	457.1	81.5	5897	289.9	74.3	7380			
214.1	203.8	1441	463.3	169	2923	690.5	-127.1	4417	455	81.5	5912	287.3	74.1	7395			
216.3	204.4	1457	465.7	168.7	2939	688.6	-126.6	4432	452.9	81.3	5928	284.8	73.9	7410			

Thermomagnetic results for sample AL081

TEMP (°C)	TSUSC (°C)	TIME (s)	TEMP (°C)	TSUSC (°C)	TIME (s)	TEMP (°C)	TSUSC (°C)	TIME (s)	TEMP (°C)	TSUSC (°C)	TIME (s)	TEMP (°C)	TSUSC (°C)	TIME (s)	TEMP (°C)	TSUSC (°C)	TIME (s)
20.8	-35.8	0	203.7	-30.6	1458	434.4	-26.1	2932	700.9	-137.7	4421	479.4	-5.6	5914	342.1	-9.7	7401
21	-35.9	16	205.6	-30.5	1473	437	-25.9	2948	698.6	-137.8	4437	477.9	-5.8	5930	341	-9.5	7416
22.3	-36	31	208.1	-30.6	1488	439.9	-25.7	2963	696	-138	4452	476.4	-5.6	5945	340.1	-9.9	7431
24.4	-35.8	46	210.5	-30.6	1503	442.3	-25.6	2978	693.8	-138	4468	475.2	-6.1	5961	339.2	-9.7	7447
26.5	-35.9	61	213.3	-30.2	1518	445	-25.3	2994	691.5	-137.7	4483	474.3	-6	5976	338.1	-9.8	7462
28.5	-35.8	76	216	-30.3	1533	447.6	-25.4	3009	689.6	-137.9	4498	473.1	-6.4	5991	337	-9.8	7477
30.6	-35.8	91	218.4	-30.3	1549	450.3	-25.4	3024	687.7	-137.7	4513	471.9	-6	6006	336.1	-9.9	7493
32.4	-35.8	106	220.9	-30.2	1564	452.9	-25.2	3039	685.4	-137.5	4529	470.7	-5.9	6022	334.7	-9.8	7508
34.5	-35.6	121	223.4	-30.1	1579	455.3	-25.2	3055	683.5	-138	4544	469.2	-6.2	6037	333.3	-9.8	7523
36.3	-35.8	136	225.8	-30	1594	458.2	-25.1	3070	681.6	-137.8	4560	467.7	-6.5	6053	331.9	-9.9	7538
38.1	-35.8	151	228.3	-29.7	1609	460.9	-24.9	3085	679.3	-137.8	4575	466	-6.3	6068	330.2	-10	7553
39.9	-35.8	166	230.5	-29.7	1624	463.6	-24.7	3101	677.1	-137.8	4591	464.5	-6.5	6083	328.2	-10.2	7569
41.5	-35.8	182	233	-29.6	1639	466.3	-24.8	3116	675.1	-137.8	4606	463	-6.3	6099	326.2	-9.9	7584
43	-35.7	196	235.2	-29.5	1654	469.2	-24.7	3131	672.9	-137.4	4621	461.8	-6.3	6114	324.5	-10	7599
44.8	-35.7	212	237.4	-29.5	1669	471.9	-24.7	3146	670.3	-137.4	4637	460.6	-6.6	6130	322.5	-10.1	7615
46.4	-35.7	227	239.9	-29.6	1685	474.9	-24.5	3162	667.8	-137.5	4652	459.1	-6.6	6145	320.8	-10.2	7630
47.9	-35.7	242	242.1	-29.3	1700	477.6	-24	3177	665.6	-137.7	4668	457.7	-6.7	6160	318.8	-10.1	7645
49.5	-35.7	257	244.5	-29.1	1715	480.2	-24.2	3192	663.3	-137.4	4683	456.2	-6.6	6176	316.8	-10.5	7661
51.1	-35.7	272	246.8	-29.4	1730	482.9	-23.9	3207	660.8	-137.5	4698	454.4	-6.6	6191	315.2	-10.5	7676
52.6	-35.5	287	249.2	-29.3	1745	485.6	-23.5	3223	658.6	-137.7	4714	452.9	-7	6206	313.2	-10.4	7691
54.2	-35.5	302	251.5	-29	1760	488.3	-23.2	3238	656.3	-137.5	4729	451.1	-6.8	6222	311.5	-10.4	7706
55.7	-35.6	317	253.9	-28.9	1775	490.7	-23.3	3253	653.8	-137.4	4745	449.4	-6.8	6237	310.4	-10.4	7721
57.3	-35.6	332	256.4	-28.8	1791	493.7	-23.2	3269	651.2	-137.6	4760	447.6	-7.1	6252	309.2	-10.4	7737
58.9	-35.6	347	258.7	-28.6	1806	496.4	-22.9	3284	649	-137.5	4776	446.1	-7	6268	307.8	-10.4	7752
60.4	-35.5	362	261.1	-28.4	1821	499.4	-22.7	3299	646.8	-137.5	4791	444.7	-6.9	6283	306.4	-10.4	7767
62	-35.6	377	263.6	-28.5	1836	502.4	-22.5	3315	644.3	-137.2	4806	442.9	-6.6	6298	304.7	-10.6	7782
63.5	-35.3	392	266.1	-28.3	1851	505.4	-22.4	3330	641.7	-137.4	4822	441.1	-7.1	6314	303	-10.5	7798
65.1	-35.5	407	268.6	-28.2	1866	508.4	-22.2	3345	639.5	-137.1	4837	439.4	-6.9	6329	301.6	-10.6	7813
66.7	-35.4	422	270.9	-28.1	1881	511.8	-21.7	3361	637	-137.3	4852	437.6	-6.9	6344	299.9	-10.6	7828
68.5	-35.4	437	273.1	-28.2	1897	514.5	-21.7	3376	634.5	-137.2	4868	435.8	-7	6360	298.8	-10.6	7843
70.1	-35.3	452	275.3	-28.1	1912	517.2	-21.6	3391	632	-137.2	4883	434.1	-7.2	6375	297.4	-10.7	7859
71.6	-35.2	467	277.6	-28.1	1927	519.6	-21.4	3407	629.8	-137.2	4898	432.6	-7.1	6391	296.3	-10.7	7874
73.5	-35.2	482	279.8	-27.9	1942	522.3	-20.9	3422	627.2	-137.2	4914	431.1	-7.6	6406	294.9	-10.7	7889
75	-35.3	497	282	-27.9	1957	525.1	-20.9	3437	624.7	-137.3	4929	430	-7.1	6421	293.5	-10.8	7904
76.6	-35.1	512	284.5	-27.9	1973	527.8	-20.4	3453	622.5	-137.2	4945	428.8	-7.4	6437	292.1	-10.9	7920
78.4	-35.1	527	286.8	-27.8	1988	530.5	-20.6	3468	620.3	-137.3	4960	427.6	-7.3	6452	290.7	-10.8	7935
80	-35.1	542	289.3	-27.8	2003	533.3	-20.5	3483	617.8	-137.4	4976	426.4	-7.3	6467	289.3	-10.9	7950
81.9	-35.2	557	292.1	-27.7	2018	536.3	-20.8	3499	615.3	-136.8	4991	424.7	-7.2	6482	287.9	-10.9	7966
83.4	-35.1	572	294.3	-27.8	2033	539.3	-21.1	3514	612.8	-137.1	5007	423.2	-7.4	6498	286.8	-10.8	7981
85	-34.9	587	296.3	-27.7	2049	542.4	-21.2	3529	610.9	-136.8	5022	421.5	-7.4	6513	285.1	-10.9	7996
86.8	-34.9	602	298.5	-27.6	2064	545.8	-21.6	3545	608.4	-136.9	5037	420	-7.6	6529	283.7	-10.8	8011
88.4	-34.8	617	300.5	-27.5	2079	548.8	-22.6	3560	605.6	-136.8	5053	418.5	-7.5	6544	281.7	-10.9	8027
90.5	-34.9	632	302.8	-27.6	2094	551.9	-23.4	3575	603.1	-136.8	5068	417.1	-7.6	6559	280.1	-11.1	8042
92.4	-34.8	646	305.3	-27.4	2109	554.9	-24.8	3591	600.3	-136.5	5084	415.6	-7.5	6575	278.1	-11	8057
94.2	-34.7	662	307.8	-27.2	2124	558.3	-29.4	3606	597.2	-136.6	5099	413.9	-7.6	6590	275.9	-11.1	8072
96	-34.7	676	310.4	-27.4	2140	561.7	-37.2	3621	594.4	-136.1	5115	412.4	-7.8	6606	273.9	-11	8087
97.6	-34.5	691	312.6	-27.2	2155	564.8	-51.5	3637	591.3	-135.9	5130	410.9	-8	6621	271.7	-11	8102
99.5	-34.5	706	314.6	-27.3	2170	567.8	-71	3652	588.8	-134.2	5145	409.5	-7.9	6636	269.5	-11.1	8118
101.3	-34.4	721	316.3	-27.3	2185	570.6	-90.3	3667	586	-131.8	5161	408.3	-7.9	6652	267.3	-11.1	8133
103.4	-34.5	736	318	-27.3	2200	573.7	-105.6	3683	583.3	-127.9	5176	406.9	-7.9	6667	265	-11.2	8148
105.5	-34.4	751	320	-27.3	2216	576.5	-116	3698	580.8	-123.1	5192	405.4	-7.8	6682	262.5	-11.2	8163
107.4	-34.2	766	321.9	-27.2	2231	579.5	-124.9	3714	578.3	-117	5207	404	-7.9	6697	260	-11.3	8179
109.2	-34.2	781	324.2	-27.3	2246	582.6	-131.3	3729	575.8	-109.9	5222	402.5	-7.7	6713	257.3	-11.4	8194
111.4	-34.2	796	326.2	-27.3	2261	585.7	-134.5	3744	573.7	-102.4	5238	401.3	-8	6728	254.8	-11.4	8209
113.2	-34.1	811	328.5	-27.2	2277	588.8	-135.9	3759	571.5	-92.2	5253	399.9	-7.9	6743	252.6	-11.3	8224
115.1	-34.2	826	330.7	-27.2	2292	591.6	-136.5	3775	569.1	-78.5	5268	398.2	-8	6759	250.1	-11.5	8239
116.7	-34.1	841	332.4	-27.3	2307	594.7	-136.7	3790	566.9	-62.6	5284	396.4	-8	6774	247.9	-11.4	8255
118.5	-34	856	334.4	-27.2	2322	598.2	-136.7	3805	565.1	-48.6	5299	395	-7.8	6789	245.7	-11.5	8270
120.4	-34	871	335.8	-27.2	2338	601.3	-136.9	3821	563.2	-33.9	5314	393.2	-8.2	6805	243.4	-11.6	8285
122	-34.1	886	337.5	-27.3	2353	604.4	-137.3	3836	561.4	-22.2	5330	392.1	-8.1	6820	241.5	-11.6	8300
123.8	-34	901	339.2	-27.4	2368	607.5	-137.3	3851	559.2	-15.4	5345	390.9	-8.3	6835	239.6	-11.5	8315
125.7	-34	916	340.7	-27.4	2383	610.3	-137.3	3867	557.4	-11.6	5361	389.7	-8.3	6850	237.7	-11.6	8331
127.5	-33.9	931	342.4	-27.2	2399	613.4	-136.9	3882	554.9	-9.5	5376	388.3	-8.2	6866	235.7	-11.5	8346
129.4	-33.9	946	344.1	-27.2	2414	617.2	-137.4	3898	553.1	-7.9	5391	386.9	-8.5	6881	233.8	-11.5	8361
131.5	-33.7	961	346.4	-27.3	2429	620.3	-137.4	3913	551	-6.8	5407	385.1	-8.6	6896	231.9	-11.7	8376
133.4	-33.7	976	348.7	-27.1	2444	623.8	-137.4	3928	548.8	-6	5422	383.4	-8.4	6912	230.2	-11.9	8391
135.5	-33.7	991	350.9	-27.4	2459	626.6	-137.2	3943	547	-5.6	5438	381.7	-8.5	6927	228.3	-11.7	8407
137.7	-33.6	1006	353.5	-27.1	2475	629.8	-137.3	3959	545.1	-4.9	5453	379.9	-8.3	6942	226.4	-11.7	8422
139.8	-33.7	1021	356.1	-27.2	2490	632.9	-137.6	3974	543	-4.2	5468	378.5	-8.6	6958	224.5	-11.8	8437
141.9	-33.6	1036	358.7	-27.1	2505	636.4	-137.6	3990	541.2	-4.3	5484	377	-8.8	6973	222.8	-12	8452
144.1	-29.1	1051	361.5	-27.2	2520	639.5	-137.5	4005	539	-3.9	5499	375.6	-8.6	6988	220.9	-11.8	8467
146.5	-33.6	1066	364.1	-27.4	2536	642.7	-137.7	4020	536.9	-3.7	5514	374.4	-8.9	7004	219.3	-12	8483
148.9	-33.3	1081	366.7	-27.2	2551	646.2	-138	4036	534.5	-3.3	5530	373.3	-8.8	7019	217.4	-11.8	8498
151	-33.1	1096	369	-27.2	2566	649.7	-137.7	4051	532.4	-3.4	5545	372.1	-8.8	7034	215.4	-12	8513
153.2	-33.4	1111	371.6	-27.4	2581	653.2	-137.7	4066	530.2	-3.4	5560	371	-8.8	7049	213.5	-12.3	8528
155.3	-33.3	1126	374.2	-27.3	2597	657	-137.8	4082	527.8	-3.2	5576	369.6	-8.9	7065	211.6	-12.1	8544
157.5	-33.1	1141	376.5	-27	2612	660.5	-137.7	4097	525.4	-3.4	5591	368.4	-8.9	7080	209.7	-12.2	8559
159.6	-33.1	1156	379.1	-27.1	2627	664	-137.6	4113	522.6	-3.6	5607	367.3	-8.9	7095	207.8	-12	8574
161.8	-32.8	1171	381.7	-27	2642	667.2	-137.9	4128	520.5	-3.4	5622	366.1	-9	7110	206.2	-12.2	8589
163.9	-32.8	1187	384.5	-26.9	2657	670.7	-138.1	4144	518.7	-3.3	5637	365	-8.8	7126	204.2	-12.5	8604
166.1	-32.6	1202	387.1	-27	2673	673.9	-138.1	4159	516.9	-3.3	5653	363.8	-8.8	7141	202.1	-12.5	8620
168.5	-32.8	1217	389.7	-27	2688	676.7	-137.7	4174	515.1	-4.1	5668	362.4	-9	7156	200.2	-12.5	8635
170.6	-32.5	1232	392.4	-26.8	2703	679.6	-137.8	4190	513	-3.9	5683	361.2	-9.1	7172	198	-12.5	8650
172.8	-32.5	1247	395	-27.1	2719	682.5	-137.9	4205	510.9	-4	5699	360.1	-9.3	7187	196.1	-12.6	8665
175.2	-32.3	1262	397.6	-26.9	2734	685.7	-137.9	4220	509	-3.9	5714	358.9	-9.1	7202	194.2	-12.6	8680
177.4	-32	1277	399.9	-26.8	2749	688.9	-137.5	4236	506.9	-4.2	5729	357.8	-9.2	7218	192.3	-12.7	8696
179.6	-32.1	1292	402.8	-26.8	2764	691.8	-137.9	4251	504.8	-4.6	5745	356.7	-9.5	7233	190.4	-12.5	8711
181.7	-32	1307	405.7	-26.9	2780	695.4	-138	4267	502.4	-4.7	5760	355.2	-9.3	7248	188.8	-12.7	8726
183.9	-31.8	1322	408.6	-26.8	2795	698.6	-137.9	4282	500.3	-4.9	5776	353.5	-9.1	7264	186.9	-12.7	8741
186.3	-31.8	1337	411.5	-26.7	2810	701.2	-138.1	4298	497.6	-5.2	5791	352.1	-9.5	7279	185	-12.9	8756
188.5	-31.8	1352	414.2	-26.6	2825	703.1	-138	4313	495.2	-4.9	5806	350.6	-9.6	7294	183.1	-12.8	8771
190.7	-31.6	1367	416.8	-26.4	2841	704.4	-138.2	4329	492.5	-5.2	5822	349.2	-9.3	7309	180.9	-12.7	8786
192.8	-31.3	1382	419.7	-26.3	2856	705.4	-138.3	4344	489.8	-5.1	5837	348.1	-9.4	7325	179	-13	8802
195.3	-31.4	1397	422.6	-26.1	2871	705.4	-138	4360	487.1	-5.5	5853	346.7	-9.8	7340	176.9	-13.1	8817
197.4	-31	1412	425.6	-26.3	2886	705.1	-137.9	4375	485	-5.4	5868	345.5	-9.9	7355	174.7	-13.1	8832
199.3	-31.3	1427	428.5	-26.1	2902	703.8	-138	4391	482.9	-5.8	5883	344.4	-9.5	7370	172.5	-13	8847
201.5	-31	1443	431.4	-26.2	2917	702.5	-138	4406	480.8	-5.7	5899	343.5	-9.6	7385	170.4	-13.3	8862

Thermomagnetic results for sample AL094

TEMP (°C)	TSUSC (°C)	TIME (s)	TEMP (°C)	TSUSC (°C)	TIME (s)	TEMP (°C)	TSUSC (°C)	TIME (s)	TEMP (°C)	TSUSC (°C)	TIME (s)	TEMP (°C)	TSUSC (°C)	TIME (s)	TEMP (°C)	TSUSC (°C)	TIME (s)
21.3	1125.1	0	240.7	1244.7	1607	510.6	1064.8	3234	637	128.6	4770	404.8	784.6	6389	251.2	754.6	8016
21.6	1124.2	18	242.9	1245.4	1623	513.9	1063.5	3251	634.8	133.4	4785	402.5	784.7	6406	248.7	755.7	8032
23.4	1124.6	34	245.1	1246.9	1640	516.9	1062.3	3268	632.6	138.7	4800	400.2	783.6	6423	246.5	754.3	8049
25.7	1126.1	51	247.6	1248.7	1657	519.9	1057.4	3285	630.1	144.4	4816	397.9	783.7	6440	244	753.2	8066
28.3	1127	67	250.1	1247.9	1673	523.5	1057.4	3302	627.6	149.6	4831	395.5	783.7	6457	241.5	752.1	8082
30.6	1128.7	84	252.8	1250.2	1690	526.3	1054.8	3319	625.4	155	4847	393.5	784.1	6474	239.3	751.3	8099
32.9	1130.8	100	255.6	1252.4	1707	529.6	1054.2	3335	622.8	161.8	4862	391.2	782.9	6491	236.8	750.3	8116
35	1131.7	117	258.4	1254.9	1724	532.7	1051.9	3352	620.6	169.9	4877	389.2	782.9	6507	234.4	748.4	8133
37.1	1132	134	261.1	1255.2	1740	536	1048.1	3369	618.1	179.2	4893	387.4	781.4	6524	231.9	750.1	8149
39.1	1133.5	150	263.6	1254.4	1757	538.7	1048.8	3386	615.3	191.2	4908	385.7	783.1	6541	229.4	750.8	8166
41.2	1134.8	166	266.4	1257.4	1774	541.8	1046.6	3403	612.8	204.2	4924	384	780.1	6557	226.9	749.2	8183
43	1135.8	183	269.2	1257.1	1790	544.8	1042.7	3419	610.3	217.8	4939	382.2	780.8	6574	224.2	749	8199
45.1	1137.2	200	271.7	1260.6	1807	548.2	1043.5	3436	607.5	236.2	4956	380.5	779.1	6591	221.7	748.6	8216
46.9	1136.9	216	274.5	1260.4	1824	551.3	1039.9	3453	605.3	257.1	4973	379.1	779.5	6608	219	747.6	8232
48.7	1138	233	277.3	1260.4	1840	554.3	1037.2	3470	602.8	279.6	4989	377.3	780.3	6625	216.3	747.2	8249
50.5	1139.4	249	279.8	1261.2	1857	557.4	1032.5	3487	600	304.6	5007	375.6	779.1	6641	214.1	747.6	8266
52.1	1139.7	266	282.6	1262.5	1874	560.1	1031.3	3504	597.2	338.5	5024	374.2	777.8	6658	211.6	745.8	8283
53.9	1139.8	282	284.8	1262	1891	563.2	1016.1	3520	594.1	368.4	5041	372.4	779.9	6675	209.4	746.3	8299
55.7	1142.9	299	287.6	1263.4	1907	566.6	972.5	3537	591.3	400.9	5057	371	779.2	6692	207.2	745.5	8316
57.6	1143.1	315	290.1	1262.7	1924	570	895.1	3554	588.8	429.4	5074	369.3	779.2	6709	204.8	742.6	8333
59.4	1143.8	332	292.7	1263.5	1941	573.4	790.2	3571	586	461.1	5091	368.1	779.1	6725	202.6	741	8349
61.2	1144.8	348	295.5	1261.2	1958	576.8	687.4	3588	583.6	496.4	5108	367	778	6742	200.2	742.3	8366
63	1145.3	365	298.3	1261.4	1974	580.2	615	3605	580.5	538.7	5125	365.5	779.4	6759	198	739.5	8382
64.9	1146.5	382	301.1	1260.5	1991	583.9	544.9	3622	578	584.6	5142	364.1	776.7	6776	195.5	741.7	8399
66.7	1147.9	398	304.2	1261.1	2008	587.3	484.6	3639	575.2	639.4	5159	362.4	777.6	6793	193.1	740.7	8416
68.5	1148.5	414	307	1259.4	2024	590.7	436.3	3656	572.4	700	5176	360.4	775.4	6809	190.7	740.9	8433
70.6	1149.6	431	309.8	1259.1	2041	594.4	388.4	3673	569.7	761.1	5193	358.7	775.2	6826	188.5	740.4	8449
72.4	1150.7	448	312.6	1257.6	2058	597.8	339.6	3690	566.9	795.9	5210	356.7	775.4	6843	186	740.5	8466
74.3	1152.6	464	315.4	1255.1	2075	601.3	304.8	3706	564.1	809	5227	354.9	776.9	6860	183.6	739.7	8482
76.1	1154.5	480	318.3	1253.6	2091	604.7	273.6	3723	561.7	814.5	5244	353.2	776.2	6876	180.9	738.4	8499
77.9	1153.4	497	321.1	1251.2	2108	607.8	241.7	3740	559.2	815.1	5261	351.8	775.7	6893	178.5	738.8	8516
79.8	1155.8	513	323.9	1248.3	2125	611.3	225.9	3755	556.5	814.9	5278	350.6	774.3	6910	176	739.4	8533
81.6	1155.7	530	326.5	1246.7	2142	614.4	208.7	3771	553.7	814.8	5295	349.5	773	6927	173.9	737.8	8549
83.7	1156.8	546	328.7	1243.3	2159	617.5	196.2	3786	551.3	814.3	5311	348.7	774.2	6943	171.5	736.4	8566
85.5	1158	563	331	1239.1	2175	620.6	185.9	3801	548.5	813.5	5328	347.8	774.2	6960	169.3	737.2	8583
87.4	1159.7	579	333.3	1233	2192	623.8	176.4	3816	546.1	812	5345	346.9	772.9	6977	166.9	735.7	8599
89.2	1159.8	596	335.5	1230.3	2209	626.6	167.2	3832	543.6	811.2	5362	345.8	773.7	6994	164.5	735.5	8616
91.3	1160.8	612	338.1	1226.4	2226	630.1	156.7	3847	540.9	810.1	5379	344.4	773.5	7011	162	736.1	8632
93.4	1161.4	629	340.7	1220.7	2243	633.2	148.5	3863	537.8	809.1	5396	342.9	772.9	7027	159.9	736.4	8649
95.5	1163	645	343.2	1214	2259	636.4	140.8	3878	534.5	809.1	5413	341	773.2	7044	157.7	736.1	8666
97.6	1164.2	661	345.5	1210	2276	639.9	132.3	3893	531.4	808.7	5430	338.7	773.5	7061	155.6	737.9	8682
99.7	1165.4	678	348.1	1205.2	2293	643.3	122.7	3909	528.4	807	5447	336.7	771.9	7078	153.4	736	8699
101.8	1166.9	694	350.1	1198.6	2310	646.5	115.8	3924	525.7	806.1	5463	334.1	771.4	7094	151	737.1	8715
104.2	1166.4	711	352.4	1195.5	2326	649.7	108.1	3939	522.9	807.6	5480	331.9	772.1	7111	148.9	737.2	8732
106.6	1167.1	727	354.7	1192.1	2343	653.2	101.8	3955	519.9	807.4	5497	329.9	771.6	7128	146.5	736.9	8748
109	1169.2	744	356.9	1186.8	2360	656.3	95.1	3970	516.9	804.6	5514	327.9	771.2	7145	144.1	737	8765
111.4	1169.9	760	359.2	1184.2	2377	659.5	89	3985	514.2	805.5	5531	325.6	769.6	7162	141.9	737.4	8782
113.7	1171.1	777	361.8	1179.8	2394	663	82.5	4000	511.5	804.4	5548	323.9	770.2	7178	139.5	737.2	8798
115.9	1171.1	793	364.4	1175.5	2410	666.2	77.5	4016	509	801.6	5565	322.2	768.8	7195			
118.2	1172.3	809	367.5	1172.3	2427	669.1	72.7	4031	506.3	801.6	5582	320.5	767.5	7212			
120.6	1172.3	826	370.1	1169.4	2444	671.6	67.7	4047	503.6	803.5	5598	319.1	767.8	7229			
122.8	1173.8	843	373	1167.5	2461	674.5	62.4	4062	501.2	803.7	5615	318	766.4	7245			
124.9	1174.6	859	375.9	1161.7	2478	677.4	56.8	4077	499.1	802.2	5632	316.3	768.4	7262			
127.3	1175.3	876	378.8	1159.9	2494	680.3	52.1	4092	496.7	801.7	5649	314.9	767.6	7279			
129.7	1175.1	892	381.7	1155.3	2511	682.8	47.5	4108	494.3	801.3	5666	313.5	768	7296			
131.8	1174.6	909	384.3	1155.4	2528	685.7	42.5	4123	491.6	801.1	5683	311.8	767.5	7312			
134.2	1178.6	925	387.1	1151.4	2545	689.3	37.6	4138	489.2	801	5700	310.4	767.2	7329			
136.6	1177.6	942	389.7	1148.7	2562	692.5	32.4	4154	486.8	799.5	5716	309	766.3	7346			
139	1178.7	958	392.4	1144.3	2578	695.7	27.3	4169	484.1	800.1	5733	307.5	766.4	7363			
141.4	1180.6	975	395.3	1143.5	2595	698.9	23.2	4185	481.7	800.2	5750	306.1	765.6	7379			
143.8	1180.4	991	398.4	1141	2612	702.2	18.7	4200	479.7	798.1	5767	305	766.2	7396			
146.2	1182.5	1008	401.3	1139.1	2629	704.8	14.8	4215	477	798	5784	303.9	766	7413			
148.6	1182.1	1025	404.5	1136.6	2645	706.7	12	4231	474.3	800.6	5801	303	764.5	7430			
151.3	1183.8	1041	407.7	1134.1	2662	707.3	10.3	4246	471.9	796.1	5818	302.2	764.2	7446			
154	1186.4	1058	410.9	1131.5	2679	707.3	9.7	4261	469.8	796.8	5834	301.4	764.4	7463			
156.7	1187.9	1074	413.6	1129.5	2696	706.7	10	4277	467.7	797.2	5851	300.2	764.3	7480			
159.1	1187.9	1091	416.5	1126.1	2713	705.7	10.7	4292	465.7	796.1	5868	299.1	763.8	7497			
161.5	1189.5	1108	419.4	1125.2	2730	704.4	12.7	4308	463.6	797	5885	298	763.6	7514			
163.9	1190.7	1124	422.3	1122.2	2746	702.8	14.4	4323	461.5	796.3	5901	296.6	764.3	7530			
166.6	1192.8	1141	425.6	1121.4	2763	700.9	17.1	4338	459.4	794.4	5918	295.5	764.5	7547			
169	1194	1157	428.5	1119.2	2780	698.9	19.8	4354	457.4	792.8	5935	294.3	764.8	7564			
171.7	1195.4	1174	431.7	1116.6	2797	697.3	22.5	4369	455.3	793.6	5952	293.2	763.3	7581			
174.4	1196.3	1190	434.6	1115.5	2814	695.1	25.7	4385	453.2	792.5	5969	291.8	763.5	7597			
177.1	1197.7	1207	437.9	1112.6	2831	692.8	29.5	4400	451.1	792.6	5986	291	764	7614			
179.6	1200.3	1224	441.4	1110.4	2847	690.5	33.3	4416	449.1	792.2	6003	289.9	763.1	7631			
182.3	1202.7	1240	444.7	1110	2864	688.3	36.6	4431	447	791.5	6019	288.5	763.3	7648			
184.7	1203.9	1257	447.6	1108	2881	686.4	40.2	4446	445	791.8	6036	287.3	764.1	7664			
187.1	1204.8	1274	450.9	1104.9	2898	684.8	43.7	4462	442.9	791.5	6053	286.2	761.6	7681			
189.6	1206.9	1290	453.8	1102.8	2915	682.2	46.9	4477	440.5	791.4	6070	284.8	760.6	7698			
192.3	1208.5	1307	457.1	1100.2	2932	679.9	51.1	4493	438.5	790.2	6087	283.7	759.8	7715			
195	1210.5	1323	460	1098.8	2948	677.4	54.7	4508	436.1	789.6	6104	282.3	761.1	7732			
197.2	1212.5	1340	463.3	1096.5	2965	675.1	58.1	4523	434.1	789.3	6120	281.2	761.4	7748			
199.6	1214.7	1357	466.3	1096	2982	672.6	62	4539	432.3	788.2	6137	279.8	760.4	7765			
202.1	1216.7	1374	468.9	1093.9	2999	670.3	65.3	4554	430.5	788.2	6154	278.7	760.4	7782			
204.5	1218.4	1390	471.9	1092	3016	667.8	68.8	4569	428.8	788.4	6171	277.3	760.1	7798			
207	1221.6	1407	474.9	1089.5	3033	665.2	72.8	4585	426.7	788.7	6188	276.2	759.2	7815			
209.4	1222.7	1423	478.2	1086.8	3050	663	76.1	4600	425	787.8	6205	274.8	758.6	7832			
211.6	1225.2	1440	481.4	1084.3	3067	661.1	79.2	4616	422.9	787.5	6221	273.1	760	7849			
214.1	1226.8	1457	484.7	1084.2	3083	658.9	83.3	4631	421.2	788.7	6238	271.2	757.8	7865			
223.9	1233.4	1473	488	1082	3100	656.6	87.3	4646	419.4	787.1	6255	269.5	760.1	7882			
225.6	1234.1	1490	490.7	1078.7	3117	654.4	91.6	4662	417.7	787.1	6272	267.8	758.8	7899			
227.2	1234.9	1507	493.7	1076.2	3134	651.9	97	4677	416.5	787.1	6288	265.6	756.5	7915			
229.1	1235.6	1524	496.4	1075.1	3151	649.3	102.4	4692	414.7	787.1	6305	263.4	757	7932			
231.3	1236.9	1540	499.1	1073.3	3167	646.8	108	4708	413	786.3	6322	261.1	756	7949			
233.5	1239.4	1557	501.8	1070	3184	644.3	113.2	4723	411.2	786.9	6339	258.7	756.3	7965			
235.7	1240.7	1574	504.8	1069.1	3201	641.7	118.3	4739	409.5	784.7	6356	255.9	756.4	7982			
238.2	1242.8	1590	507.5	1065.3	3218	639.5	123	4754	407.2	784.3	6373	253.4	754	7999			

Thermomagnetic results for sample AL096

TEMP (°C)	TSUSC (°C)	TIME (s)	TEMP (°C)	TSUSC (°C)	TIME (s)	TEMP (°C)	TSUSC (°C)	TIME (s)	TEMP (°C)	TSUSC (°C)	TIME (s)	TEMP (°C)	TSUSC (°C)	TIME (s)	TEMP (°C)	TSUSC (°C)	TIME (s)
13.6	170.7	0	210.5	185.6	1465	460.9	154.1	2940	685.4	-135.3	4433	460.3	73.7	5927	296	69.6	7410
13.8	171.2	16	213	185.7	1480	463.6	153.7	2956	682.8	-135.4	4448	459.1	73.7	5942	293.5	69.1	7425
14.9	171.4	31	215.2	186	1495	466.3	153.8	2971	680.6	-135.5	4464	457.7	73.7	5957	290.7	69.4	7440
16.9	171.4	46	217.9	186.2	1510	468.6	153.4	2987	678.3	-135.4	4479	455.9	73.5	5973	287.9	69.2	7456
19.2	171.5	62	220.4	186.6	1525	471.6	153.2	3002	676.4	-135.5	4495	454.1	73.5	5988	285.4	69.2	7471
21.6	171.8	77	223.1	187.1	1540	474.6	153.2	3017	674.2	-135.3	4510	452.3	73.4	6003	282.9	69.4	7486
23.9	172	92	225.8	187	1555	477.6	152.7	3033	671.9	-135.3	4525	450.9	73.4	6019	280.3	68.9	7501
25.9	171.9	107	228.3	187.6	1570	480.5	152.3	3048	669.7	-135.3	4541	449.4	73.7	6034	277.8	69	7517
28	172	123	231.1	188	1585	483.5	152.5	3063	667.8	-135.3	4556	447.6	73.4	6049	275.3	69.2	7532
30.1	172.1	138	233.5	188.4	1601	486.2	151.9	3079	665.9	-135.7	4572	445.8	73.3	6065	272.5	69.1	7547
32.1	172.1	153	236	188.5	1616	489.2	151.7	3094	663.6	-135.5	4587	443.8	73.2	6080	269.8	68.8	7562
34.2	172.3	168	238.5	188.8	1631	491.9	151.6	3109	662.1	-135.1	4603	442	73.3	6095	267	68.9	7577
36	172.4	183	240.7	189.1	1646	494.6	151.5	3125	659.8	-135.8	4618	440.2	73.3	6111	264.2	68.8	7593
37.8	172.5	198	243.2	189.2	1661	497.3	151.6	3140	657.6	-135.6	4633	438.8	73	6126	261.4	68.6	7608
39.6	172.6	214	245.9	189.5	1676	499.7	151.4	3155	655.4	-135.2	4649	437	73	6141	258.4	68.6	7623
41.5	172.6	229	248.4	189.9	1691	502.4	151.4	3170	653.2	-135.4	4664	435.5	73.4	6157	255.9	68.2	7638
43	172.7	244	250.9	190.2	1707	505.1	151.4	3186	650.9	-135.3	4679	433.5	73.1	6172	253.1	68.5	7653
44.8	172.8	259	253.4	190.2	1722	508.1	151.4	3201	649	-134.9	4695	431.7	73	6187	250.6	68.8	7669
46.6	172.9	274	256.2	190.7	1737	510.6	151.8	3217	647.1	-134.4	4710	429.7	73	6203	248.1	68.5	7684
48.2	172.9	289	258.9	190.6	1752	513.3	151.5	3232	644.9	-134.1	4726	428.2	73.1	6218	245.4	68.4	7699
50	172.9	305	261.1	191.2	1767	516	151.7	3247	642.7	-133.1	4741	426.7	73	6233	242.9	68.1	7714
51.6	173	320	263.4	191.2	1782	518.7	151.1	3262	640.5	-131.4	4756	425	73.1	6249	240.4	68.2	7730
53.4	173.1	335	265.9	191.4	1797	521.1	151.3	3278	638.3	-130.7	4772	423.2	72.8	6264	238.2	67.9	7745
55	173.1	350	268.4	191.8	1813	523.9	151.1	3293	636.1	-129.8	4787	421.8	72.8	6279	235.7	68.1	7760
56.5	173.3	365	270.9	192.1	1828	526.9	151.4	3308	633.9	-128.9	4803	420.3	73	6295	233.3	67.9	7775
58.3	173.2	380	273.7	192.3	1843	529.9	151.2	3324	632	-127.8	4818	418.8	73.1	6310	230.8	67.6	7790
59.9	173.3	396	276.4	192.4	1858	533	151.3	3339	630.1	-127	4834	417.7	73	6325	228.3	67.6	7806
61.7	173.3	411	278.7	192.7	1873	535.7	151.7	3355	627.9	-126	4849	416.2	72.9	6341	226.1	67.4	7821
63.5	173.5	426	280.9	193	1888	538.4	151.9	3370	625.4	-125	4864	414.7	72.7	6356	223.6	67	7836
65.4	173.4	441	283.4	193	1904	541.8	151.7	3385	623.2	-123.7	4880	413.3	72.8	6371	221.2	67.3	7851
67.2	173.4	456	285.7	193.1	1919	544.8	151.6	3401	620.6	-122.8	4895	411.8	72.7	6387	218.7	67.2	7866
69	173.6	471	288.2	193.3	1934	547.3	151.7	3416	618.1	-121.7	4911	410.4	72.8	6402	216.5	67	7881
70.6	173.8	486	290.7	193.2	1949	550	152.2	3431	615.9	-120.7	4926	408.6	72.6	6418	214.1	66.9	7897
72.4	173.7	501	293.5	193.5	1964	552.8	152.6	3447	613.1	-119.4	4941	406.9	72.6	6433	211.3	66.8	7912
74.3	173.7	517	296	193.1	1980	555.8	153	3462	610.9	-117.4	4957	405.1	72.6	6448	208.9	66.4	7927
76.1	173.9	532	298.5	193.4	1995	559.2	152.3	3477	608.4	-115.3	4972	403.7	72.4	6463	206.2	66.4	7942
77.7	173.9	547	301.1	193.5	2010	562.6	148.6	3493	605.9	-111.8	4988	401.9	72.5	6479	203.7	65.9	7957
79.5	174.1	562	303.6	193.4	2025	565.7	137.5	3508	603.1	-106.4	5003	400.2	72.5	6494	201.3	65.5	7973
81.3	174.1	577	305.9	193.2	2040	568.4	117.2	3524	600.6	-101	5019	398.4	72.5	6509	199.1	65.7	7988
83.2	174.1	592	308.4	193.1	2056	571.5	91.9	3539	597.8	-93.8	5034	396.7	72.2	6525	196.4	65.4	8003
85.3	174.3	607	310.6	192.6	2071	574.6	57.9	3554	595	-85.8	5049	395.3	72	6540	193.9	65.4	8018
87.4	174.3	623	313.2	192.2	2086	577.7	25.8	3570	592.9	-77.2	5065	393.8	72.1	6555	191.5	64.9	8033
89.5	174.5	638	315.7	191.8	2101	580.5	-1.8	3585	590.4	-68.7	5080	392.4	72.4	6571	189	65	8048
91.6	174.8	653	318.3	191.2	2117	583.6	-23.6	3601	587.9	-58.5	5096	390.9	72.4	6586	186.6	65	8064
93.9	174.6	668	320.5	190.5	2132	586.7	-45.4	3616	585.4	-47.5	5111	389.5	72.2	6601	184.2	64.6	8079
96	175	683	322.8	189.8	2147	589.8	-66.9	3631	582.9	-35.5	5127	388	72.1	6616	181.4	64.5	8094
98.2	174.8	698	325.3	189.1	2162	592.9	-85	3647	580.2	-23.7	5142	386.3	72.1	6632	179	64.3	8109
100.3	175.1	713	327.6	188	2177	596	-99.6	3662	578	-12.6	5157	384.8	72.3	6647	176.6	63.9	8124
102.6	174.9	728	329.9	187.1	2193	598.8	-110.4	3677	575.8	-1	5173	383.4	72	6662	173.9	63.9	8139
105	175.2	743	332.1	186	2208	601.6	-119	3693	574	13	5188	381.9	72	6678	171.5	63.8	8154
107.1	175.2	758	335	184.5	2223	604.7	-126.4	3708	571.5	33.5	5204	380.8	71.9	6693	168.8	63.6	8170
109.2	175.2	773	337.5	183.1	2238	607.8	-130.1	3723	569.4	52	5219	379.6	71.9	6708	166.1	63.4	8185
111.4	175.3	788	340.4	181.4	2253	610.6	-132.3	3739	566.6	66.5	5234	378.5	71.9	6723	163.6	63.5	8200
113.2	175.3	803	343.2	179.8	2269	613.1	-133.5	3754	564.1	72.6	5250	377.3	72.1	6739	161	63.2	8215
115.3	175.5	818	345.8	178.1	2284	615.6	-133.9	3770	561.4	74.9	5265	376.2	71.8	6754	158.5	63.3	8230
117.2	175.4	833	348.7	176.3	2299	618.8	-133.9	3785	559.2	75.5	5280	374.7	72	6769	156.1	62.9	8245
119.3	175.6	848	350.9	174.6	2314	621.9	-134.4	3800	557.1	75.9	5296	373.3	71.9	6785	153.7	62.9	8260
121.2	175.6	863	353.5	172.8	2330	625	-134.6	3816	554.6	76.1	5311	371.9	72	6800	151.6	62.9	8275
123.3	175.6	878	356.1	171.6	2345	628.2	-134.5	3831	552.2	76	5327	370.4	71.7	6815	149.4	62.8	8291
125.2	175.9	893	358.9	170.2	2360	631.6	-134.8	3846	549.4	75.6	5342	369	71.9	6831	147.3	62.7	8306
127.3	175.9	908	361.5	168.6	2375	634.8	-134.8	3862	547	75.3	5357	367.8	71.6	6846	145.4	62.5	8321
129.1	176.1	923	364.1	167.7	2391	637.3	-134.8	3877	544.2	75.6	5373	366.1	71.6	6861	143.3	62.7	8336
131.3	176.3	938	366.7	166.8	2406	640.2	-135	3893	541.8	75.2	5388	364.7	71.5	6876	140.9	62.2	8351
133.4	176.4	953	369.3	165.7	2421	643.3	-135.3	3908	539.7	75.3	5403	362.7	71.5	6892	138.7	62.6	8366
135.5	176.5	968	371.9	164.9	2436	646.2	-135	3923	537.2	75.3	5419	360.7	71.3	6907	136.3	62	8381
137.7	176.9	983	374.2	164.1	2451	649	-135	3939	534.8	74.7	5434	358.7	71.4	6922	134.2	62.2	8396
139.8	176.8	998	377	163.2	2467	652.2	-135.1	3954	532	74.8	5450	356.4	71.4	6938	132.1	62.2	8411
141.9	177	1013	379.3	163	2482	655.4	-135.4	3970	529.3	74.6	5465	354.4	71.4	6953	129.9	62.1	8426
144.1	177.3	1028	381.9	162.4	2497	658.9	-135.2	3985	526.6	74.7	5481	352.6	71	6968	127.5	61.9	8441
146.2	177.4	1043	384.5	161.8	2513	662.4	-135.5	4000	523.5	74.6	5496	351.5	71.2	6983	125.4	62	8456
148.4	177.6	1058	387.1	161.4	2528	665.6	-135.4	4016	521.1	74.8	5512	350.1	71.4	6999	123	62.1	8471
150.5	178.2	1073	390	161.1	2543	668.4	-135.3	4031	518.4	74.5	5527	348.7	71	7014	120.9	62.2	8486
152.9	178.1	1088	392.6	160.7	2558	671.6	-135.2	4047	516	74.5	5542	347.2	71.2	7029	118.5	62	8501
155.1	178.4	1103	395.5	160.4	2574	674.2	-135.4	4062	513.6	74.3	5558	345.5	71.3	7044	116.4	62.2	8516
156.9	178.7	1118	398.2	160.1	2589	676.7	-135.5	4077	511.2	74.3	5573	344.1	71	7060	114.3	62	8531
159.1	178.9	1133	400.8	159.7	2604	679.6	-135.7	4093	508.7	74.6	5588	342.9	71	7075	111.9	61.8	8546
161.2	179.2	1148	403.4	159.6	2619	682.8	-135.8	4108	505.7	74.7	5604	341.5	71.1	7090	110	62	8561
163.6	179.4	1163	406	159.3	2635	686	-135.6	4124	503	74.5	5619	340.4	71	7105	107.9	61.8	8577
166.1	179.6	1178	408.6	158.8	2650	688.9	-135.8	4139	500.6	74.5	5634	338.7	70.8	7121	105.8	62	8591
168.8	179.9	1193	411.2	158.5	2665	692.5	-135.9	4155	497.9	74.7	5650	336.7	70.9	7136	103.7	61.7	8607
171.2	180.3	1208	414.2	158.3	2680	696	-135.9	4170	495.5	74.3	5665	335	70.8	7151	101.6	61.9	8621
173.6	180.3	1223	417.1	157.8	2696	699.3	-135.8	4185	492.8	74.6	5681	333	70.8	7166	99.5	61.9	8636
176	180.7	1238	420	158	2711	702.5	-135.9	4201	490.7	74.4	5696	330.7	70.7	7182	97.4	61.8	8651
178.5	180.9	1254	422.9	157.2	2726	704.8	-135.5	4217	488.6	74.1	5712	328.5	70.2	7197	95.5	62	8666
180.9	181.5	1269	425.8	157.2	2742	706.4	-135.7	4232	486.5	74.3	5727	326.5	70.5	7212	93.4	61.6	8681
183.3	181.6	1284	428.8	157.3	2757	707	-135.7	4247	484.1	74.3	5743	323.9	70.5	7227	91.3	61.7	8696
186	181.8	1299	431.4	156.8	2772	706.7	-135.9	4263	481.7	74	5758	321.7	70.5	7243	89.2	61.7	8711
188.5	182.3	1314	434.4	156.5	2787	705.7	-136.1	4278	479.4	74	5773	319.1	70.1	7258	87.4	61.5	8726
190.7	182.3	1329	437.3	156.6	2803	704.8	-135.7	4294	477	73.8	5788	316.6	70.2	7273	85.3	61.7	8741
193.1	182.8	1344	439.9	156	2818	703.1	-135.9	4309	475.2	74	5804	314	70.2	7288	83.4	61.8	8756
195.5	183.2	1359	442.3	155.5	2833	701.5	-135.9	4324	473.1	73.8	5819	312.1	70	7304	81.3	61.4	8771
197.7	183.6	1374	444.7	155.3	2849	699.6	-135.9	4340	471.3	74	5835	309.8	70	7319	79.5	61.5	8786
200.2	183.8	1389	447.3	155.2	2864	697.3	-135	4356	469.2	73.6	5850	307.5	69.9	7334	77.7	61.7	8801
202.3	184.3	1404	450.3	155.2	2879	695.1	-135.9	4371	467.1	74.2	5865	305.3	70.3	7349			
204.2	184.7	1419	452.9	155.1	2895	692.8	-135.9	4387	465.1	73.6	5881	303	69.9	7364			
206.4	184.9	1435	455.6	154.2	2910	690.2	-135.8	4402	463.3	73.5	5896	300.8	69.9	7380			
208.3	185	1449	458.5	154.5	2925	688	-135.7	4417	461.8	73.8	5911	298.3	69.3	7395			

Thermomagnetic results for sample AL100

TEMP (°C)	TSUSC (°C)	TIME (s)	TEMP (°C)	TSUSC (°C)	TIME (s)	TEMP (°C)	TSUSC (°C)	TIME (s)	TEMP (°C)	TSUSC (°C)	TIME (s)	TEMP (°C)	TSUSC (°C)	TIME (s)	TEMP (°C)	TSUSC (°C)	TIME (s)
21.8	177.5	0	217.4	197.1	1465	436.4	163.8	2937	705.7	-95.2	4428	481.4	63.7	5922	348.4	60.3	7409
22.3	177.1	17	219.5	197.6	1480	439.4	163.3	2953	704.4	-94.8	4443	479.4	64	5938	346.9	60.4	7424
23.6	177.3	32	221.7	198	1495	441.7	163.1	2968	702.8	-94.4	4459	477.6	63.6	5953	345.2	60.1	7439
25.7	177.4	47	223.9	198.2	1510	445	162.4	2983	700.9	-94.1	4474	476.1	63.6	5968	343.5	60	7454
28	177.6	62	226.1	198.5	1525	447.6	162.5	2998	698.9	-93.7	4490	474.3	63.6	5984	342.1	60	7470
30.3	177.6	78	228.9	198.9	1540	450.3	161.7	3014	696.7	-93.1	4505	472.5	63.5	5999	340.4	60.2	7485
32.4	177.8	93	231.3	199.4	1555	452.9	161.2	3029	694.4	-92.5	4520	471	63.3	6015	339	59.9	7500
34.7	177.9	108	234.1	199.7	1570	455.6	160.7	3044	692.8	-91.8	4536	469.8	63.4	6030	337.5	60.2	7515
36.8	178.2	123	236.6	200.2	1585	458.2	160.7	3059	690.9	-91.7	4551	468.6	63.2	6046	335.8	60.2	7531
38.6	178.3	139	239	200.4	1600	460.6	160	3075	689.3	-91	4566	467.4	63.4	6061	334.1	60.2	7546
40.7	178.3	154	241.8	201	1615	463	159.3	3090	687	-89.9	4582	466.9	63.5	6077	332.4	60	7561
42.5	178.4	169	244.3	201.2	1630	465.4	159.2	3105	684.8	-89.5	4597	466	63.2	6092	330.7	60.2	7576
44.6	178.8	184	246.5	201.9	1645	467.7	158.4	3121	682.5	-88.8	4613	465.1	63.3	6107	329	59.9	7591
46.1	178.9	199	249.2	201.4	1660	469.8	158.2	3136	680.6	-88.1	4628	463.9	63.2	6122	327.6	60	7607
47.9	179.1	215	251.7	202.5	1675	472.2	157.8	3151	678.3	-87	4644	462.7	63.2	6138	326.2	59.9	7622
49.5	179	230	254.2	202.5	1691	474.9	157.2	3167	676.1	-86.1	4659	461.8	63.3	6153	324.8	60	7637
51.3	179.2	245	256.7	202.9	1706	477.6	156.9	3182	673.9	-85.8	4674	460.6	63.1	6168	323.4	59.8	7652
52.9	179.4	260	259.2	202.9	1721	480.2	156.6	3197	671.6	-84.9	4690	459.4	63.2	6184	322.2	59.9	7668
54.4	179.5	275	262	203.5	1736	483.2	155.9	3213	669.4	-84.7	4705	458.5	63	6199	320.8	60	7683
56	179.7	291	264.5	203.8	1751	486.2	155.3	3228	667.5	-83.9	4721	458	63.2	6214	319.7	60	7698
57.8	179.8	306	266.7	203.8	1766	489.2	154.6	3243	665.6	-82.8	4736	457.1	63.2	6230	318.5	59.8	7714
59.4	179.8	321	268.9	204.1	1781	491.9	154.5	3259	663.3	-82.3	4752	455.9	62.9	6245	317.1	60	7729
60.9	180.1	336	271.4	204.4	1796	494.9	153.9	3274	661.1	-80.9	4767	455	62.9	6260	316	59.6	7744
62.8	180.5	351	273.9	204.8	1811	497.6	153.7	3289	658.9	-80.3	4783	454.1	62.8	6276	314.6	59.5	7759
64.3	180.2	366	276.4	204.6	1826	500.6	152.9	3304	656.6	-79.3	4798	452.9	62.6	6291	313.5	59.7	7775
65.9	180.6	381	279	204.9	1842	503	152.6	3320	654.4	-78.3	4814	452.3	62.8	6306	312.3	59.5	7790
67.5	180.8	397	281.5	205.2	1857	505.7	151.7	3335	652.2	-77.4	4829	451.7	62.9	6322	310.9	59.7	7805
69.3	180.8	412	284	205.6	1872	508.1	151.3	3351	650	-76.6	4845	451.1	62.6	6337	309.8	59.3	7820
71.1	181	427	286.2	205.2	1887	511.2	150.6	3366	647.1	-75.3	4860	450.3	62.8	6353	308.4	59.6	7835
72.9	181.4	442	288.7	205.3	1902	513.9	150	3381	644.6	-74.6	4875	449.1	62.9	6368	307	59.5	7851
74.5	181.3	457	291.3	205.5	1918	516.9	149.3	3397	642.1	-74	4891	447.9	62.6	6383	305.3	59.2	7866
76.1	181.5	473	293.5	205.2	1933	519.9	148.8	3412	639.5	-73.3	4906	447	62.6	6399	303.9	59.6	7881
77.9	181.6	488	296	205.1	1948	522.6	147.8	3427	637.6	-72.4	4922	445.8	62.6	6414	302.5	59.4	7896
79.8	181.6	503	298.5	205.2	1963	525.4	147.8	3443	635.1	-71.6	4937	445	62.5	6429	300.8	59.4	7911
81.3	181.9	518	301.4	204.9	1978	528.1	147	3458	632.9	-70.9	4952	443.8	62.6	6445	299.1	59.1	7927
83.2	182.3	533	303.9	205	1993	530.8	146.4	3473	630.1	-70.2	4968	442.9	62.6	6460	297.4	59.2	7942
85	182.1	548	306.4	204.6	2009	533.6	145.5	3489	627.2	-68.9	4983	441.7	62.6	6475	295.5	59.3	7957
86.8	182.4	563	308.7	204.1	2024	536	145	3504	625	-67.7	4999	440.5	62.5	6490	293.5	59.3	7972
88.7	182.6	578	310.6	203.6	2039	538.4	144.5	3519	622.2	-66	5014	439.4	62.5	6506	291.3	59.1	7987
90.3	182.7	594	312.6	203	2054	540.9	143.8	3534	620	-64.8	5029	438.2	62.5	6521	289.3	59.1	8003
92.1	182.9	609	314.3	202.7	2069	543.3	143.1	3550	617.5	-63.2	5045	436.7	62.4	6536	287.3	59	8018
93.9	182.9	624	316	202	2084	546.4	142.8	3565	615	-61.4	5060	435.2	62.5	6552	285.7	59	8033
96	183.1	639	317.4	201.4	2100	549.1	141.8	3581	612.5	-59.6	5076	433.5	62	6567	284	59.1	8048
98.2	183.4	654	319.1	200.6	2115	552.2	141.3	3596	610	-56.7	5091	431.7	62.1	6582	282	58.9	8064
100	183.6	669	320.8	199.5	2130	554.6	140.2	3612	607.5	-54	5106	430	62.2	6598	279.8	58.9	8079
102.1	183.7	684	322.5	198.9	2145	557.4	138.8	3627	604.7	-51.1	5122	428.5	62.4	6613	277.8	58.6	8094
104.2	183.9	699	324.8	197.9	2160	560.1	136.5	3642	601.9	-47	5137	426.7	62.1	6628	275.6	58.6	8109
106.3	184.2	715	327	197.2	2175	563.2	131.1	3658	599.1	-43.1	5153	425.3	62	6644	273.1	58.7	8124
108.5	184.2	730	329.3	196.3	2191	566.3	120.5	3673	596.6	-37.7	5168	423.8	61.9	6659	270.9	58.6	8139
110.8	184.4	745	331.9	194.7	2206	569.4	101.6	3689	593.8	-31.3	5184	422.3	62	6674	268.4	58.6	8155
112.9	184.5	760	334.1	193.6	2221	572.8	80.8	3704	591	-25.1	5199	420.6	62	6690	265.9	58.6	8170
115.1	184.7	775	336.1	192.4	2236	575.5	62	3719	588.5	-19.7	5214	419.1	62	6705	263.4	58.3	8185
116.9	184.9	790	338.1	191.1	2251	578.3	45.6	3735	586	-14.4	5230	418	61.8	6720	260.9	58.4	8200
119	184.8	805	339.8	189.4	2267	581.4	31.4	3750	583.9	-8.5	5245	416.8	61.9	6736	258.4	58.3	8215
120.9	185.3	820	341.8	188.6	2282	584.5	18.7	3765	581.1	-0.8	5261	415.3	62.1	6751	255.9	58.4	8230
122.8	185.3	835	344.1	187.8	2297	587.6	8.1	3781	578.6	6.5	5276	414.2	61.8	6766	253.7	58.1	8245
124.6	185.3	850	346.1	186.1	2312	590.4	-1.5	3796	575.8	15.6	5291	412.7	61.9	6781	251.5	58.1	8261
126.5	185.5	865	348.4	184.9	2327	593.2	-11.8	3811	573.4	27.1	5307	411.2	61.6	6797	249	58.3	8276
128.6	185.6	880	350.4	184.1	2342	596.3	-20.8	3827	570.6	39.1	5322	409.5	61.7	6812	246.8	58.1	8291
130.5	185.9	896	352.1	183.2	2358	599.1	-29.1	3842	568.4	48.6	5338	408	61.7	6827	244.5	57.8	8306
132.6	186.2	911	353.8	182.2	2373	602.2	-35.9	3858	565.7	56.7	5353	406.3	61.3	6843	242.3	57.9	8321
134.7	186.2	926	355.2	181.1	2388	605	-42.2	3873	562.9	62.4	5369	404.5	61.2	6858	239.9	57.8	8336
136.9	186.4	941	356.4	180.2	2403	608.4	-47.7	3888	560.5	64.2	5384	403.4	61.5	6873	237.4	57.8	8352
139	186.7	956	357.5	179.3	2419	611.6	-51.9	3904	557.7	65.5	5399	401.9	61.2	6889	235.2	57.5	8367
141.4	186.9	971	358.7	178.8	2434	614.7	-55.4	3919	555.2	66.1	5415	400.5	61.3	6904	232.7	57.7	8382
143.8	187.1	986	359.8	177.9	2449	617.5	-58.2	3934	552.8	66.2	5430	399	61.3	6920	230.5	57.5	8397
146.2	187.2	1001	361.2	177.6	2464	620.6	-60.2	3950	550.3	66.5	5446	397.6	61.3	6935	228	57.5	8412
148.6	187.5	1016	362.7	176.6	2480	623.5	-61.7	3965	547.6	66.3	5461	396.1	61.5	6950	225.8	57.4	8427
150.8	187.9	1031	364.4	176	2495	626.6	-63.6	3981	545.1	66.3	5477	395	61	6965	223.4	57.3	8443
153.4	188.1	1046	365.8	175.6	2510	629.4	-65.1	3996	542.4	66.3	5492	393.5	61.1	6981	220.9	57.2	8458
155.9	188.6	1061	367.8	174.8	2525	632.6	-66.3	4012	540	66	5508	392.1	61.1	6996	218.4	57	8473
158.3	188.8	1076	369.8	174.6	2541	635.7	-67.7	4027	537.2	66.1	5523	390.6	60.9	7011	215.7	56.9	8488
160.7	188.9	1091	372.1	174.2	2556	638.9	-69.5	4042	534.5	65.8	5539	388.9	61.1	7027	213.3	57	8503
163.1	189.1	1106	374.7	173.6	2571	642.1	-70.8	4058	532	65.8	5554	387.1	61	7042	211.1	56.9	8518
165.5	189.3	1121	377	173.3	2586	645.2	-71.9	4073	529.3	65.5	5569	385.4	60.9	7057	208.6	56.8	8534
168	189.7	1136	379.6	172.8	2602	648.7	-73.7	4088	526.3	65.8	5585	383.4	61	7072	206.2	56.8	8549
170.1	190	1151	382.2	172.5	2617	651.9	-74.9	4104	523.2	65.3	5600	381.7	60.6	7088	204	56.5	8564
172.5	190.1	1166	384.8	172.2	2632	655.4	-76.4	4119	520.5	65.2	5615	379.9	60.7	7103	201.5	56.5	8579
175	190.6	1181	387.4	171.1	2647	658.6	-77.7	4135	518.1	65.4	5631	378.2	60.9	7118	199.1	56.3	8594
177.4	191.1	1196	389.7	171	2663	661.4	-78.8	4150	516	65.2	5646	376.8	61.1	7134	196.6	56.3	8609
179.8	191.2	1211	392.4	170.9	2678	664.6	-80.5	4165	514.2	65	5662	375.3	60.7	7149	194.2	56.4	8625
182.5	191.6	1226	394.7	170.4	2693	667.8	-81.5	4181	512.1	65.2	5677	374.2	60.8	7164	192	56.2	8640
185	191.9	1241	397.3	169.8	2708	670.7	-82.3	4196	509.9	65	5692	373	60.8	7179	189.6	56.2	8655
187.4	192.3	1256	399.6	169.3	2724	674.2	-83.8	4212	507.5	65	5708	371.9	60.6	7195	187.4	56	8670
189.3	192.5	1271	402.5	168.7	2739	677.7	-84.7	4227	505.7	64.8	5723	370.4	60.5	7210	185	55.9	8685
191.5	192.8	1286	405.1	168.6	2754	680.9	-86.2	4243	503.9	64.9	5738	369	60.6	7225	182.3	56.1	8700
193.6	193	1301	408	167.9	2769	684.1	-87.6	4258	502.4	64.8	5754	367.3	60.6	7240	179.8	55.9	8715
195.8	193.5	1316	410.7	167.9	2784	687.3	-88.5	4273	500.6	64.6	5769	365.3	60.8	7256	177.4	55.8	8731
198	193.9	1331	413.3	167.5	2800	690.5	-89.5	4289	498.8	64.3	5784	363.2	60.7	7271	175	56	8746
199.9	194.1	1346	415.9	167	2815	693.8	-90.6	4304	497	64.4	5800	361.2	60.5	7286	172.3	55.8	8761
202.1	194.6	1361	418.2	166.6	2830	697	-91.4	4320	494.9	64.4	5815	359.2	60.5	7302	169.8	55.6	8776
204.2	194.9	1375	420.6	166.3	2846	699.6	-92.6	4335	493.4	64.4	5830	357.2	60.6	7317	167.4	55.5	8791
206.4	195.3	1390	423.2	165.7	2861	702.5	-92.6	4351	491.3	64.1	5846	355.5	60.5	7332	165	55.5	8806
208.6	195.8	1405	426.1	165.4	2876	704.4	-93.9	4366	489.5	64.2	5861	353.8	60.4	7347	162.6	55.5	8821
211.1	195.9	1420	428.8	164.7	2891	705.7	-94.5	4381	487.4	64.1	5876	352.4	60.3	7363	160.4	55.6	8836
213.3	196.2	1435	431.4	164.6	2906	706.7	-94.6	4397	485.3	64.4	5892	351.2	60.4	7378	158.3	55.4	8851
215.4	196.9	1450	433.8	164.4	2922	706.4	-95	4412	483.2	64.1	5907	349.8	60.4	7393	156.1	55.6	8866

APPENDIX 2

Supplementary materials for Chapter 3

Table SA1 XRF Standards

		Na2O	MgO	Al2O3	SiO2	P2O5	K2O	CaO	TiO2	MnO	Fe2O3	Sc	V	Cr	Ni	Cu	Zn	Ga	Rb	Sr	Y	Zr	Nb	Ba	Pb	La	Ce	Th	U	Sn
		mass%	mass%	mass%	mass%	mass%	mass%	mass%	mass%	mass%	mass%	ppm	ppm	ppm	ppm	ppm	ppm	ppm	ppm	ppm	ppm	ppm	ppm	ppm	ppm	ppm	ppm	ppm	ppm	ppm
JG-1A	**CERT**	3.390	0.690	14.300	72.300	0.083	3.960	2.130	0.250	0.057	2.050	6.21	22.7	17.6	6.91	1.67	36.5	16.5	178	187	32.1	118	11.4	470	26.4	21.3	45	12.8	4.68	4.47
JG-1a	**Traces 2020- fix**	3.39	0.69	14.3	72.3	0.08	3.96	2.13	0.25	0.06	2.05	8	23	19	8	3	38	17	188	187	38	96	10	436	25	22	48	11	5	4
JG-1a	**Traces 2020- fix**	3.39	0.69	14.3	72.3	0.08	3.96	2.13	0.25	0.06	2.05	7	21	16	7	3	38	17	187	187	38	97	9	429	26	23	28	12	5	4
JGB-1	**CERT**	1.200	7.850	17.490	43.660	0.056	0.240	11.900	1.600	0.189	15.160	35.8	635	57.8	25.4	85.7	109	17.9	6.87	327	10.4	32.8	3.34	64.5	1.92	3.6	8.17	0.48	0.13	0.48
JGB-1	**Traces 2020- fix**	1.2	7.85	17.49	43.66	0.06	0.24	11.9	1.6	0.19	15.16	39	579	73	46	85	113	19	11	341	14	4	3	89	1	8	4	1	1	1
JGB-1	**Traces 2020- fix**	1.2	7.85	17.49	43.66	0.06	0.24	11.9	1.6	0.19	15.16	38	575	76	46	84	114	20	10	340	14	3	5	94	1	5	3	1	1	1
JB-1A	**CERT**	2.730	7.830	14.450	52.410	0.260	1.400	9.310	1.280	0.148	9.100	27.9	205	392	139	56.7	82.1	17.9	39.2	442	24.0	114	26.9	504	6.76	37.6	65.9	9.03	1.57	2.24
JB-1A	**Traces 2020- fix**	2.73	7.83	14.45	52.41	0.26	1.4	9.31	1.28	0.15	9.1	23	224	369	132	56	82	18	40	461	24	118	34	530	10	32	79	9	1	2
JB-1A	**Traces 2020- fix**	2.73	7.83	14.45	52.41	0.26	1.4	9.31	1.28	0.15	9.1	23	224	370	131	56	82	18	40	459	25	118	34	532	8	32	63	10	1	2
JGB-1 cert	**CERT**	1.2	7.85	17.49	43.66	0.056	0.24	11.9	1.6	0.189	15.16	35.8	635	57.8	25.4	85.7	109	17.9	6.87	327	10.4	32.8	3.34	64.5	1.92	3.6	8.17	0.48	0.13	0.48
JGB-1	**Measured**	1.2	7.85	17.49	43.66	0.06	0.24	11.9	1.6	0.19	15.16	39	573	77	37	84	113	19	10	339	14	3	5	94	1	4	10	1	1	1
JG-1A cert	**CERT**	3.39	0.69	14.3	72.3	0.083	3.96	2.13	0.25	0.057	2.05	6.21	22.7	17.6	6.91	1.67	36.5	16.5	178	187	32.1	118	11.4	470	26.4	21.3	45	12.8	4.68	4.47
JG-1a	**Measured**	3.39	0.69	14.3	72.3	0.08	3.96	2.13	0.25	0.06	2.05	8	22	14	8	3	38	17	188	186	38	97	11	443	26	25	36	12	5	4
JB-1A cert	**CERT**	2.73	7.83	14.45	52.41	0.26	1.4	9.31	1.28	0.148	9.1	27.9	205	392	139	56.7	82.1	17.9	39.2	442	24	114	26.9	504	6.76	37.6	65.9	9.03	1.57	2.24
JB-1A	**Measured**	2.73	7.83	14.45	52.41	0.26	1.4	9.31	1.28	0.15	9.1	20	220	369	133	55	89	18	40	458	24	118	30	538	10	30	71	10	1	2

Table SA2 XRF data for the Ratagain Complex

		Lat/Long decimal																																							
Rock type	Sample	Lat	Long	SiO2	TiO2	Al2O3	Fe2O3	MnO	MgO	CaO	Na2O	K2O	P2O5	V	Cr	Ni	Zn	Rb	Sr	Y	Zr	Nb	Ba	La	Ce	Pr	Nd	Sm	Eu	Gd	Tb	Dy	Ho	Er	Tm	Yb	Lu	Nb	Th	U	Sc	Pb
Quartz monzodiorite	AL001	57.22182	-5.48734	69.76	0.41	15.84	2.40	0.03	0.86	1.82	5.38	3.81	0.20																													
Quartz monzodiorite	AL002	57.22176	-5.48769	67.54	0.46	16.58	2.75	0.04	1.22	2.10	5.67	3.72	0.22	55	131	161	16	62	1443	14	164	9	1842	51.95	112.2	12.6	40.82	5.7	1.77	3.93	0.43	1.73	0.31	0.79	0.1	0.6	0.09	9	5.57	1.53	3	14
Quartz monzodiorite	AL003	57.22164	-5.4883	66.40	0.48	16.75	2.87	0.04	1.33	2.36	5.77	3.71	0.24																													
Quartz monzodiorite	AL004	57.22145	-5.48903	64.06	0.60	17.13	3.23	0.05	2.18	2.54	5.78	4.87	0.33																													
Quartz monzodiorite	AL005	57.22128	-5.48969	63.18	0.61	15.83	3.67	0.08	2.50	3.69	5.48	4.16	0.38																													
Quartz monzodiorite	AL006	57.22118	-5.4901	70.61	0.34	15.44	2.10	0.03	0.86	1.44	5.49	4.24	0.16																													
Monzodiorite	AL006.1	57.22212	-5.49141	69.46	0.35	16.34	2.18	0.03	0.63	1.36	5.84	4.10	0.16																													
Monzodiorite	AL006.2	57.22212	-5.49141	52.64	1.01	13.57	7.59	0.13	8.33	7.55	3.58	3.14	0.99																													
Monzodiorite	AL007.1	57.22257	-5.49593	57.61	1.00	15.87	5.75	0.09	4.86	4.33	4.99	3.93	0.80																													
Monzodiorite	AL007.2	57.22257	-5.49593	61.04	0.72	16.69	4.63	0.07	2.83	3.31	5.76	4.24	0.58																													
Monzodiorite	AL007.3	57.22257	-5.49593	68.66	0.38	16.43	2.50	0.03	0.87	1.68	5.97	3.85	0.18																													
Quartz monzodiorite	AL008	57.22053	-5.49123	64.26	0.59	17.26	3.36	0.05	1.70	2.40	6.13	3.75	0.28																													
Quartz monzodiorite	AL009	57.22436	-5.52289	67.98	0.40	16.70	2.74	0.04	1.13	1.23	5.78	4.04	0.20	48	64	253	40	68	1223	15	194	12	1657	108.8	213.5	24.6	78.28	10.8	3.28	7.61	0.83	3.2	0.57	1.43	0.18	1.08	0.17	12	14.2	4.11	2	16
Monzodiorite	AL010.1	57.22646	-5.52379	55.95	1.05	13.61	6.03	0.10	6.32	6.02	3.98	3.56	0.84																													
Quartz monzodiorite	AL010.2	57.2269	-5.52326	66.09	0.56	15.70	3.54	0.05	2.03	2.77	4.84	3.63	0.33																													
Qz-rich granitoid	AL011	57.21982	-5.52528	81.92	0.37	9.04	2.10	0.03	0.35	0.48	2.26	2.58	0.05	42	139	433	-22	47	283	9	146	6	1026	35.7	75.41	7.57	23.61	3.28	1	2.45	0.27	1.05	0.18	0.42	0.06	0.37	0.08	6	11	0.99	4	13
Quartz monzodiorite	AL012	57.22083	-5.4167	65.87	0.44	16.19	2.76	0.06	0.97	2.40	5.79	4.58	0.25																													
Granite	AL013	57.22112	-5.41642	71.88	0.17	14.71	0.91	0.02	0.22	0.97	5.22	4.60	0.03	9	71	292	-10	75	610	12	122	8	1570	43.7	85.68	9.09	28.12	3.86	1.38	2.86	0.34	1.46	0.29	0.76	0.11	0.69	0.11	8	12.7	5.61	1	14
Quartz monzodiorite	AL014	57.22163	-5.416	67.47	0.38	15.94	1.86	0.05	0.56	2.00	5.96	4.59	0.18																													
Quartz monzonite	AL015	57.222	-5.41558	60.32	0.64	16.25	3.48	0.08	1.60	2.92	4.97	4.72	0.39																													
Quartz monzodiorite	AL016.1	57.22295	-5.41445	65.73	0.40	15.60	1.73	0.04	0.33	1.45	6.03	3.80	0.18																													
Monzonite	AL017	57.19795	-5.49609	56.16	0.68	14.05	6.46	0.10	3.12	6.60	3.95	5.19	0.90	116	47	209	68	91	2724	26	301	21	2371	190.6	395.9	49.2	165.7	24.2	6.41	17.1	1.86	7.2	1.25	3.05	0.39	2.2	0.35	21	37.5	8.02	0	28
Quartz monzodiorite	AL018	57.21977	-5.51227	53.27	0.94	12.45	6.80	0.11	7.77	6.97	3.18	2.94	0.85																													
Monzodiorite	AL018.1	57.21977	-5.51227	56.21	0.99	15.05	6.28	0.10	5.14	5.50	4.55	3.81	0.79																													
Monzodiorite	AL018.2	57.21992	-5.51336	52.09	1.35	14.06	7.48	0.11	7.03	5.12	4.77	3.66	1.05																													
Quartz monzodiorite	AL018.3	57.21992	-5.51336	69.05	0.41	16.02	2.54	0.03	0.86	0.98	5.59	4.28	0.19																													
Monzodiorite	AL019	57.21938	-5.50863	56.15	0.97	14.93	5.50	0.08	4.59	4.74	4.82	3.68	0.83																													
Granodiorite	AL020	57.21818	-5.50266	69.56	0.31	14.95	2.03	0.02	0.67	1.26	5.09	3.71	0.12																													
Quartz monzodiorite	AL021	57.22169	-5.47336	66.03	0.47	16.88	3.08	0.06	1.16	1.80	5.98	4.55	0.26																													
Quartz monzodiorite	AL022	57.22168	-5.47338	65.56	0.38	18.47	2.31	0.04	0.91	1.73	6.91	3.76	0.17																													
Quartz monzodiorite	AL023	57.22175	-5.47332	66.05	0.46	16.95	2.77	0.04	0.81	1.37	6.03	4.32	0.25																													
Quartz monzonite	AL024	57.22188	-5.47331	66.34	0.49	17.09	2.99	0.01	0.95	0.83	5.89	4.67	0.26																													
Granodiorite	AL025	57.22186	-5.47337	72.44	0.26	14.90	1.80	0.01	0.50	0.86	5.15	4.00	0.12																													
Quartz monzonite	AL026	57.2221	-5.47322	65.19	0.51	16.75	1.86	0.05	0.26	3.03	5.44	4.89	0.28																													
Quartz monzodiorite	AL027	57.22213	-5.47319	65.97	0.51	16.88	2.42	0.03	0.60	1.96	5.88	4.18	0.29																													
Quartz monzodiorite	AL028	57.22217	-5.47307	66.11	0.47	16.22	2.76	0.04	1.05	2.00	5.78	4.18	0.25																													
Quartz monzodiorite	AL029	57.22234	-5.47269	64.32	0.56	16.81	3.41	0.06	1.56	2.79	6.13	3.75	0.34																													
Quartz monzodiorite	AL030	57.22248	-5.47249	64.94	0.52	16.77	3.09	0.05	1.27	2.50	6.02	3.99	0.29																													
Monzodiorite	AL031	57.22254	-5.47226	64.39	0.39	18.27	2.51	0.03	0.74	1.47	6.55	4.95	0.19	39	31	136	33	39	2017	14	236	11	2720	74.91	151.24	16.94	59.3	8.07	2.46	6.26	0.52	2.68	bdl	1.11	bdl	0.84	bdl	11	4	2	5	16
Quartz monzodiorite	AL032	57.22267	-5.472	66.38	0.53	16.62	2.99	0.05	1.36	2.03	5.74	4.31	0.24																													
Quartz monzodiorite	AL033	57.22322	-5.46426	63.50	0.60	17.14	3.38	0.04	1.71	1.19	5.95	4.05	0.37																													
Quartz monzodiorite	AL034	57.22271	-5.4647	66.38	0.46	16.69	2.94	0.05	1.20	1.96	5.83	4.03	0.28																													
Quartz monzodiorite	AL035	57.22271	-5.46485	66.54	0.44	16.29	2.78	0.04	1.01	1.39	5.63	3.96	0.25																													
Quartz monzodiorite	AL036	57.22262	-5.46639	65.95	0.49	16.93	3.07	0.05	1.26	1.94	5.97	3.94	0.29																													
Quartz monzonite	AL037	57.22203	-5.46702	68.34	0.37	15.83	2.24	0.03	0.80	1.63	5.10	4.95	0.18																													
Granite	AL038	57.2221	-5.46759	70.31	0.36	15.78	1.86	0.01	0.44	0.70	5.22	4.88	0.18	51	56	161	23	75	1337	13	152	12	1802	82.52	141.3	13.8	46	5.62	1.48	3.67	0.25	1.4	bdl	.4910	bdl	.4160	bdl	12	7	2	6	17
Quartz monzodiorite	AL039	57.2221	-5.46845	64.89	0.58	15.71	3.53	0.06	1.70	2.43	6.12	2.95	0.44																													
Quartz monzodiorite	AL040	57.22102	-5.46765	67.00	0.42	16.18	2.57	0.04	0.95	1.78	5.76	4.19	0.24																													
Quartz monzodiorite	AL041	57.22093	-5.468	64.74	0.47	16.26	2.84	0.05	0.38	3.24	5.61	3.94	0.30																													
Quartz monzodiorite	AL042	57.21899	-5.45393	66.00	0.44	16.61	2.70	0.04	0.70	1.78	5.89	4.53	0.22																													
Quartz monzodiorite	AL043	57.2189	-5.45318	64.72	0.54	17.07	3.44	0.05	1.27	2.83	6.19	3.22	0.28																													
Quartz monzodiorite	AL044	57.219	-5.45323	69.03	0.39	16.22	2.36	0.03	0.71	0.98	5.89	4.23	0.21																													
Quartz monzodiorite	AL045	57.21476	-5.43915	69.75	0.43	16.07	1.97	0.07	0.29	1.47	5.82	3.93	0.24	53	112	103	17	74	1214	16	184	15	1859	85.39	147.37	16.16	55.69	8.95	2.36	6.25	0.52	2.74	bdl	1.09	bdl	0.86	bdl	15	12	2	7	14
Quartz monzodiorite	AL046	57.21944	-5.46162	64.12	0.45	15.72	2.78	0.05	1.09	1.50	5.50	3.93	0.25																													
Quartz monzodiorite	AL047	57.21997	-5.46203	64.18	0.44	15.82	2.74	0.04	1.03	2.01	5.50	3.93	0.25																													

Table SA2 Continued

		Lat/Long decimal																																							
Rock type	**Sample**	**Lat**	**Long**	**SiO2**	**TiO2**	**Al2O3**	**Fe2O3**	**MnO**	**MgO**	**CaO**	**Na2O**	**K2O**	**P2O5**	**V**	**Cr**	**Ni**	**Zn**	**Rb**	**Sr**	**Y**	**Zr**	**Nb**	**Ba**	**La**	**Ce**	**Pr**	**Nd**	**Sm**	**Eu**	**Gd**	**Tb**	**Dy**	**Ho**	**Er**	**Tm**	**Yb**	**Lu**	**Nb**	**Th**	**U**	**Sc**	**Pb**
Quartz monzodiorite	**AL047.1**	57.22062	-5.46507	64.66	0.50	17.36	2.91	0.05	1.06	2.58	6.44	3.96	0.26																													
Quartz monzodiorite	**AL047.2**	57.22059	-5.4653	66.01	0.41	17.10	2.62	0.04	0.85	2.06	6.16	4.46	0.22																													
Quartz monzodiorite	**AL048**	57.22058	-5.46093	67.35	0.49	16.29	2.70	0.03	0.96	1.14	5.60	4.12	0.26																													
Quartz monzodiorite	**AL049**	57.22003	-5.45065	62.55	0.37	16.26	2.17	0.06	0.60	3.82	5.17	5.08	0.27																													
Quartz monzodiorite	**AL050**	57.22002	-5.45073	65.10	0.41	16.55	2.22	0.04	0.64	2.60	5.69	4.68	0.21																													
Quartz monzonite	**AL051**	57.22003	-5.45079	67.74	0.41	14.87	1.46	0.02	0.22	2.05	2.61	8.06	0.27																													
Quartz monzodiorite	**AL052**	57.22008	-5.45083	64.23	0.38	16.46	1.78	0.06	0.81	3.51	5.78	4.62	0.21																													
Quartz monzonite	**AL053**	57.22015	-5.45091	62.38	0.35	15.34	1.87	0.10	0.14	5.93	5.11	4.62	0.21																													
Granodiorite	**AL054**	57.21985	-5.45023	65.69	0.46	17.06	3.29	0.01	0.55	1.20	5.09	3.90	0.27	59	84	178	41	65	1258	19	239	14	2491	120.42	259.40	25.99	92.77	14.96	4.05	10.13	0.90	4.30	bdl	1.56	bdl	1.08	bdl	14	8	2	5	16
Monzonite	**AL055**	57.22744	-5.46639	63.57	0.62	16.20	3.78	0.06	1.70	1.82	5.98	4.37	0.43																													
Quartz monzonite	**AL056**	57.22773	-5.46712	65.02	0.48	16.84	2.80	0.04	1.30	2.13	5.77	4.35	0.25																													
Quartz monzonite	**AL057**	57.2281	-5.46811	66.54	0.45	16.07	2.75	0.05	1.66	2.52	5.44	4.04	0.20																													
Monzonite	**AL058**	57.22886	-5.46931	61.65	0.63	17.63	3.47	0.06	2.13	3.01	5.75	4.98	0.37																													
Monzonite	**AL059**	57.23	-5.47211	62.77	0.43	18.05	2.89	0.04	0.59	1.66	5.52	5.25	0.18	61	37	131	39	47	4101	34	814	54	5812	87.46	191.27	23.37	86.29	14.63	3.69	9.34	0.92	4.70	bdl	1.87	bdl	1.36	bdl	54	45	2	0	29
Quartz monzonite	**AL060**	57.23006	-5.47386	66.59	0.43	16.84	2.61	0.03	1.06	1.98	5.88	4.06	0.20																													
Monzonite	**AL061**	57.19789	-5.49578	56.17	1.27	11.91	7.71	0.14	4.28	7.98	2.56	4.46	1.23																													
Monzodiorite	**AL062**	57.2135	-5.50956	57.00	0.84	16.42	5.33	0.08	3.69	4.57	5.60	3.48	0.63	117	163	193	71	45	2427	19	202	9	2620	65.07	132.79	15.12	56.05	9.33	2.33	6.12	0.52	2.71	bdl	1.03	bdl	0.70	bdl	9	5	2	2	17
Quartz monzonite	**AL063**	57.21932	-5.48974	68.21	0.36	15.76	2.21	0.03	0.95	1.77	5.33	4.07	0.18	45	70	96	42	70	1579	14	179	13	2693	56.10	111.42	11.96	42.07	6.74	1.78	4.51	0.35	1.98	bdl	0.79	bdl	0.62	bdl	13	8	2	0	21
Quartz monzonite	**AL064**	57.21938	-5.4897	67.40	0.39	16.15	2.32	0.03	0.90	1.48	5.53	4.08	0.19																													
Quartz monzonite	**AL065**	57.21956	-5.48979	67.70	0.37	15.94	2.23	0.03	0.88	1.71	5.39	3.95	0.18																													
Quartz monzonite	**AL066**	57.21957	-5.49002	66.27	0.40	16.49	2.43	0.03	1.03	1.93	5.67	3.91	0.20																													
Monzonite	**AL067**	57.21781	-5.49689	54.84	1.74	11.57	8.42	0.13	7.24	7.95	2.80	4.84	1.52	116	343	317	99	85	1825	28	227	14	2139	72.86	148.49	17.05	61.88	10.88	2.14	6.84	0.61	3.18	bdl	1.18	bdl	0.81	bdl	14	13	3	5	20
Monzonite	**AL068**	57.21517	-5.5225	48.64	1.77	13.92	8.12	0.13	7.28	9.30	2.86	4.71	1.80																													
Monzonite	**AL069**	57.21461	-5.52125	49.06	1.77	13.81	2.71	0.13	8.16	7.85	2.87	5.61	1.37																													
Granite	**AL070**	57.19789	-5.49553	74.04	0.56	11.54	2.95	0.05	1.36	1.29	2.43	5.42	0.15																													
Monzonite	**AL070.1**	57.19789	-5.49553	62.68	0.61	16.74	9.49	0.15	1.60	2.52	5.51	5.99	0.37																													
Syenite	**AL071**	57.2105	-5.50293	45.72	1.62	11.36	6.88	0.11	9.50	9.74	2.20	5.98	2.47	160	407	304	98	97	2228	32	257	16	3778	97.74	195.99	21.73	73.56	12.25	3.33	7.74	0.75	4.05	bdl	1.72	bdl	1.42	bdl	16	12	1	32	19
Granite	**AL072**	57.20179	-5.48761	65.20	1.25	14.23	2.84	0.11	1.66	2.54	2.45	4.88	0.34	129	98	137	46	98	416	30	310	12	786	42.11	86.37	10.2	38.5	7.13	1.41	6.4	0.88	5.72	bdl	3.13	bdl	3	bdl	9	9	3	14	18
Granite	**AL073**	57.20195	-5.48765	72.27	0.66	12.89	13.52	0.04	0.86	0.76	2.17	7.06	0.14																													
Monzonite	**AL074**	57.21039	-5.48519	43.61	2.41	12.21	2.25	0.08	9.57	9.47	2.36	3.60	1.83																													
Quartz monzonite	**AL075**	57.22637	-5.46714	64.22	0.45	16.00	3.48	0.05	1.53	3.14	5.01	5.51	0.41																													
Quartz monzonite	**AL076**	57.22602	-5.46612	62.76	0.77	16.74	2.48	0.21	2.22	2.16	5.14	5.26	0.48																													
Quartz monzonite	**AL077**	57.2258	-5.46524	66.50	0.49	16.08	2.05	0.00	1.35	1.16	4.78	6.20	0.30																													
Quartz monzonite	**AL078**	57.22549	-5.46471	67.97	0.38	15.74	2.48	0.00	1.15	1.11	4.91	5.94	0.24																													
Quartz monzonite	**AL079**	57.22451	-5.46317	65.97	0.49	16.22	3.21	0.04	1.96	1.27	4.89	5.53	0.29	43	45	142	32	59	1464	13	196	15	1533	63.85	128.86	12.13	41.75	6.66	1.58	4.12	0.30	1.75	bdl	0.70	bdl	0.63	bdl	15	15	2	5	17
Monzonite	**AL080**	57.22443	-5.4629	61.76	0.56	16.92	3.21	0.07	1.70	3.40	5.20	5.83	0.46																													
Quartz monzonite	**AL081**	57.22076	-5.50226	59.87	0.93	14.24	5.14	0.08	4.11	4.77	3.75	5.29	0.88	105	193	277	71	99	1437	22	257	15	1816	103.57	203.12	23.11	84.59	14.60	3.24	9.00	0.82	4.21	bdl	1.57	bdl	1.16	bdl	15	22	3	3	23
Quartz monzonite	**AL082**	57.22047	-5.49991	67.03	0.43	15.44	2.36	0.00	1.37	2.30	4.78	5.57	0.30																													
Quartz monzonite	**AL083**	57.22047	-5.49991	59.22	0.99	14.26	5.22	0.00	4.14	5.24	3.73	5.29	0.96																													
Quartz monzonite	**AL084**	57.223	-5.48689	63.22	0.51	15.35	3.60	0.00	2.53	3.40	4.57	5.36	0.53																													
Quartz monzonite	**AL085**	57.22287	-5.48608	63.01	0.62	16.18	3.68	0.00	2.07	2.94	4.65	5.54	0.48																													
Quartz monzonite	**AL086**	57.22283	-5.48526	63.58	0.56	16.59	2.92	0.06	1.51	2.66	4.99	5.98	0.42																													
Quartz monzonite	**AL087**	57.22284	-5.48452	62.99	0.64	16.12	3.43	0.07	2.00	2.88	4.91	5.72	0.60																													
Quartz monzonite	**AL088**	57.22289	-5.48251	58.82	1.01	14.05	5.47	0.08	4.11	5.46	3.65	5.40	0.89																													
Quartz monzonite	**AL089**	57.22285	-5.48222	65.08	0.51	15.94	2.79	0.00	1.76	2.29	4.64	5.93	0.45																													
Quartz monzonite	**AL090**	57.22236	-5.48269	61.67	0.70	16.16	3.59	0.07	2.25	4.26	4.56	5.47	0.49																													
Quartz monzonite	**AL091**	57.23331	-5.48607	66.67	0.42	15.84	2.32	0.00	1.36	1.83	4.63	6.00	0.27																													
Monzonite	**AL092**	57.23517	-5.49645	57.21	1.14	14.51	6.28	0.09	5.52	4.92	4.38	4.09	0.84																													
Quartz monzonite	**AL093**	57.23586	-5.49646	63.16	0.62	15.85	3.52	0.05	3.06	2.82	5.01	4.47	0.44																													
Monzodiorite	**AL094**	57.23874	-5.49594	56.98	1.17	16.90	6.79	0.11	2.58	5.85	4.75	3.85	0.59																													
Monzonite	**AL095**	57.24102	-5.49502	54.14	1.95	16.05	8.90	0.12	2.58	5.29	4.65	4.57	1.05																													
Quartz monzodiorite	**AL096**	57.23687	-5.48208	62.53	0.74	15.48	6.23	0.00	3.03	3.74	3.81	3.56	0.33	105	180	219	51	42	815	14	138	7	1181	18.58	39.35	4.20	16.53	2.89	0.73	1.97	0.14	1.33	bdl	0.66	bdl	0.70	bdl	7	6	1	13	12
Monzodiorite	**AL097**	57.23334	-5.47694	50.64	0.40	12.42	7.94	0.11	9.32	13.87	3.19	1.47	0.09																													
Quartz monzonite	**AL098**	57.23149	-5.47129	64.70	0.48	16.12	3.01	0.04	1.62	2.73	4.95	5.23	0.38																													
Quartz monzonite	**AL099**	57.22476	-5.45331	63.14	0.55	15.98	3.13	0.00	2.21	3.36	5.09	5.43	0.45																													
Granite	**AL100**	57.22734	-5.45932	69.74	0.43	13.98	2.33	0.00	2.56	1.26	4.26	4.83	0.28	47	40	114	39	75	1588	16	183	14	1880	61.37	95.82	8.83	28.7	3.56	0.78	2.55	0.16	1.1	bdl	0.47	bdl	0.5	bdl	11	11	2	12	17

Table SA3 LOI data for the Ratagain Complex

Sample No.	Crucible Wt (g)	Sample Wt (g)	TOTAL (g)	Crucible +Sample Wt after Furnace (g)	*Loss (g)*	*%LOI*
AL001	11.5930	1.1420	12.7350	12.7212	0.0138	1.21
AL002	11.9290	1.0535	12.9825	12.9731	0.0094	0.89
AL003	11.7930	1.1266	12.9196	12.9069	0.0127	1.13
AL004	11.3040	1.0300	12.3340	12.3272	0.0068	0.66
AL005	11.3446	1.2223	12.5669	12.5501	0.0168	1.37
AL006	11.4552	1.0598	12.5150	12.5100	0.0050	0.47
AL006.1	11.4209	1.0408	12.4617	12.4572	0.0045	0.43
AL006.2	11.6407	1.0358	12.6765	12.6582	0.0183	1.77
AL007.1	12.4264	1.2299	13.6563	13.6427	0.0136	1.11
AL007.2	16.7761	1.0815	17.8576	17.8467	0.0109	1.01
AL007.3	12.2330	1.0340	13.2670	13.2600	0.0070	0.68
AL008	11.3880	1.0292	12.4172	12.4117	0.0055	0.53
AL009	16.0117	1.0711	17.0828	17.0683	0.0145	1.35
AL010.1	14.8437	1.0610	15.9047	15.8854	0.0193	1.82
AL010.2	15.8948	1.0459	16.9407	16.9328	0.0079	0.76
AL011	15.2492	1.1450	16.3942	16.3828	0.0114	1.00
AL012	11.4246	1.0935	12.5181	12.4758	0.0423	3.87
AL013	11.9372	1.1312	13.0684	13.0542	0.0142	1.26
AL014	16.0059	1.2629	17.2688	17.2394	0.0294	2.33
AL015	15.9427	1.0219	16.9646	16.9024	0.0622	6.09
AL016.1	11.5926	1.0442	12.6368	12.6182	0.0186	1.78
AL017	11.4564	1.0403	12.4967	12.4928	0.0039	0.37
AL018	15.0343	1.0161	16.0504	16.0341	0.0163	1.60
AL018.1	15.4511	1.0040	16.4551	16.4384	0.0167	1.66
AL018.2	11.5056	1.0020	12.5076	12.4892	0.0184	1.84
AL018.3	12.2354	1.2369	13.4723	13.4644	0.0079	0.64
AL019	15.5702	1.0313	16.6015	16.5906	0.0109	1.06
AL020	16.7776	1.0192	17.7968	17.7802	0.0166	1.63
AL021	15.8190	1.0000	16.8190	16.8163	0.0027	0.27
AL022	15.1656	1.0000	16.1656	16.1588	0.0068	0.68
AL023	16.1027	1.0000	17.1027	17.0943	0.0084	0.84
AL024	15.6234	1.0000	16.6234	16.6113	0.0121	1.21
AL025	11.5250	1.0000	12.5250	12.5203	0.0047	0.47
AL026	11.8552	1.0000	12.8552	12.8255	0.0297	2.97
AL027	11.4689	1.0000	12.4689	12.4550	0.0139	1.39
AL028	11.6203	1.0000	12.6203	12.6101	0.0102	1.02
AL029	12.3888	1.0000	13.3888	13.3776	0.0112	1.12
AL030	16.9748	1.0000	17.9748	17.9630	0.0118	1.18
AL031	15.2394	1.0000	16.2394	16.2350	0.0044	0.44
AL032	16.0674	1.0000	17.0674	17.0618	0.0056	0.56
AL033	16.2336	1.0000	17.2336	17.2180	0.0156	1.56
AL034	12.6985	1.0000	13.6985	13.6925	0.0060	0.60
AL035	11.7421	1.0000	12.7421	12.7319	0.0102	1.02
AL036	11.7821	1.0000	12.7821	12.7749	0.0072	0.72
AL037	11.6815	1.0000	12.6815	12.6648	0.0167	1.67
AL038	15.2225	1.0000	16.2225	16.2138	0.0087	0.87
AL039	15.3648	1.0000	16.3648	16.3432	0.0216	2.16
AL040	16.3446	1.0000	17.3446	17.3305	0.0141	1.41
AL041	16.0262	1.0000	17.0262	16.9942	0.0320	3.20
AL042	11.7241	1.0000	12.7241	12.7104	0.0137	1.37
AL043	11.9958	1.0000	12.9958	12.9852	0.0106	1.06
AL044	11.7502	1.0000	12.7502	12.7429	0.0073	0.73
AL045	11.5473	1.0000	12.5473	12.5310	0.0163	1.63
AL046	12.9429	1.0000	13.9429	13.9338	0.0091	0.91
AL047	12.6814	1.0000	13.6814	13.6620	0.0194	1.94
AL047.1	16.2318	1.0000	17.2318	17.2220	0.0098	0.98

Table SA3 Continued

Sample No.	Crucible Wt (g)	Sample Wt (g)	TOTAL (g)	Crucible +Sample Wt after Furnace (g)	*Loss (g)*	*%LOI*
AL047.2	15.0298	1.0000	16.0298	16.0213	0.0085	0.85
AL048	15.7184	1.0000	16.7184	16.7090	0.0094	0.94
AL049	12.2954	1.0496	13.345	13.3131	0.0319	3.04
AL050	15.7835	1.0000	16.7835	16.7546	0.0289	2.89
AL051	17.0876	1.0000	18.0876	18.0563	0.0313	3.13
AL052	12.2898	1.0000	13.2898	13.2600	0.0298	2.98
AL053	12.0993	1.0000	13.0993	13.0395	0.0598	5.98
AL054	11.3831	1.0000	12.3831	12.3650	0.0181	1.81
AL055	13.0104	1.0104	14.0208	14.0164	0.0044	0.44
AL056	12.6672	1.0487	13.7159	13.7116	0.0043	0.41
AL057	15.925	1.0937	17.0187	17.0151	0.0036	0.33
AL058	15.036	1.0159	16.0519	16.0475	0.0044	0.43
AL059	13.5706	0.5202	14.0908	14.0881	0.0027	0.52
AL060	15.451	1.0433	16.4943	16.4903	0.004	0.38
AL061	11.7852	1.0057	12.7909	12.787	0.0039	0.39
AL062	15.8961	1.0219	16.918	16.9128	0.0052	0.51
AL063	16.0075	1.0288	17.0363	17.0331	0.0032	0.31
AL064	13.5304	1.0087	14.5391	14.5348	0.0043	0.43
AL065	12.4048	1.0146	13.4194	13.4146	0.0048	0.47
AL066	12.6337	1.0259	13.6596	13.6541	0.0055	0.54
AL067	16.7783	1.0504	17.8287	17.8225	0.0062	0.59
AL068	12.2967	1.0784	13.3751	13.3677	0.0074	0.69
AL069	12.0794	1.1003	13.1797	13.1733	0.0064	0.58
AL070	13.0106	1.0404	14.051	14.0468	0.0042	0.40
AL070.1	12.6683	1.0792	13.7475	13.7422	0.0053	0.49
AL071	13.3755	1.0018	14.3773	14.3717	0.0056	0.56
AL072	12.2965	1.0459	13.3424	13.3324	0.01	0.96
AL073	12.0802	1.0467	13.1269	13.1184	0.0085	0.81
AL074	12.405	1.0817	13.4867	13.4736	0.0131	1.21
AL075	13.5711	1.0744	14.6455	14.6398	0.0057	0.53
AL076	15.4513	1.0044	16.4557	16.4477	0.008	0.80
AL077	13.011	1.0045	14.0155	14.01	0.0055	0.55
AL078	12.6687	1.0495	13.7182	13.7126	0.0056	0.53
AL079	15.8968	1.1141	17.0109	17.003	0.0079	0.71
AL080	11.788	1.0085	12.7965	12.7909	0.0056	0.56
AL081	16.7784	1.0219	17.8003	17.7943	0.006	0.59
AL082	15.0369	1.1121	16.149	16.1392	0.0098	0.88
AL083	14.846	1.1802	16.0262	16.0202	0.006	0.51
AL084	16.0083	1.0148	17.0231	17.0185	0.0046	0.45
AL085	15.5707	1.036	16.6067	16.6032	0.0035	0.34
AL086	15.926	1.0001	16.9261	16.9224	0.0037	0.37
AL087	12.6348	1.0447	13.6795	13.6726	0.0069	0.66
AL088	12.429	1.3682	13.7972	13.785	0.0122	0.89
AL089	11.5858	1.062	12.6478	12.6451	0.0027	0.25
AL090	16.0148	1.167	17.1818	17.1662	0.0156	1.34
AL091	12.24	1.0153	13.2553	13.2511	0.0042	0.41
AL092	11.6439	1.0862	12.7301	12.7222	0.0079	0.73
AL093	11.3464	1.1491	12.4955	12.4869	0.0086	0.75
AL094	11.9286	1.1144	13.043	13.0379	0.0051	0.46
AL095	11.4596	1.0423	12.5019	12.4946	0.0073	0.70
AL096	15.2542	1.0625	16.3167	16.3063	0.0104	0.98
AL097	13.3743	1.0219	14.3962	14.3841	0.0121	1.18
AL098	14.8454	1.0888	15.9342	15.9294	0.0048	0.44
AL099	12.0785	1.0953	13.1738	13.1678	0.006	0.55
AL100	15.5704	1.0106	16.581	16.5727	0.0083	0.82

Table SA4 XRF data for the Northern Highlands Granite Suite

Locality	Rock type	Sample	Source	SiO2	TiO2	Al2O3	FeO	MnO	MgO	CaO	Na2O	K2O	P2O5	V	Cr	Co	Ni	Zn	Rb	Sr	Y	Zr	Nb	Ba	La	Ce	Pr	Nd	Sm	Eu	Gd	Dy	Ho	Er	Yb	Lu	Nb	Hf	Ta	Th	U	Sc	Pb
Ach'Uaine	"Appinite"	A254	Fowler & Henney (1996)	51.91	1.01	13.15	5.88	0.09	7.53	7.37	3.92	3.98	1.05	96	99	30	93	131	76	1686	20	273	21	2093	134	285	28	106	15.2	4.05	10.1	4.53	0.73	1.73	1.41	0.18	21			25				
Ach'Uaine	"Appinite"	A256	Fowler & Henney (1996)	60.18	0.57	17.08	3.5	0.06	1.77	2.91	5.48	4.46	0.39	43	29	17	26	68	79	2409	16	407	20	1943	135	261	24.2	82	9.03	2.47	6.02	3.31	0.57	1.43	1.41	0.2	20	12.7	1.8	37.3	6.2			
Ach'Uaine	"Appinite"	A34	Fowler & Henney (1996)	52.29	1.21	11.33	6.47	0.15	7.28	10.21	3.5	4.07	2.11	75	294	24	118	109	85	2230	32	352	30	2199	159	385	38.3	158	23	5.98	15.5		1.12	2.57	2.05	0.27	30			23				
Ach'Uaine	"Appinite"	A34A	Fowler & Henney (1996)	52.79	0.96	13.63	6.47	0.13	6.07	7.99	3.88	4.06	0.9	98	239	25	68	89	104	2360	24	329	23	2932	177	366	33.7	128	18	4.79	11.5	5.15	0.84	2.09	1.81	0.25	23			30				
Ach'Uaine	"Appinite"	A37	Fowler & Henney (1996)	65.62	0.52	16.94	3.32	0.05	0.95	1.58	6.09	4.58	0.17	36	3	25	3	69	63	1694	17	373	21	2187	123	223	20.9	68	8.71	2.4	5.68	3.3	0.59	1.6	1.6	0.24	21	8.4	2.3	23.2	5			
Ach'Uaine	"Appinite"	A38	Fowler & Henney (1996)	50.17	1.01	12.85	6.62	0.12	8.4	8.94	3.51	3.62	0.98	111	386	28	88	86	93	2026	25	254	21	3453	187	390	35.1	135	19.7	5.27	12.7	5.13	0.82	1.99	1.58	0.22	21			26				
Ach'Uaine	"Appinite"	A40	Fowler & Henney (1996)	52.06	0.96	13.48	7.03	0.15	5.54	8.04	4.38	3.26	1.05	101	205	23	62	113	84	1893	29	327	19	2079	216	446	37.8	144	20.2	5.24	13.1	5.94	0.99	2.47	2.16	0.3	19			25				
Ach'Uaine	"Appinite"	A45	Fowler & Henney (1996)	46.15	1.8	10.2	8.25	0.16	9.41	10.08	2.64	3.93	1.88	106	585	31	163	126	100	1306	34	560	32	2527	197	437	39	159	25.2	6.89	17.9	7.88	1.23	2.84	2.15	0.28	32			25				
Ach'Uaine	"Appinite"	A49	Fowler & Henney (1996)	47.75	1.2	11.94	6.08	0.16	7.25	10.54	3.14	3.39	1.25	95	385	29	132	102	115	1966	19	191	27	1772	81.9	205	23.9	96	15.1	4.31	10.4	4.7	0.74	1.8	1.32	0.18	27			10				
Ach'Uaine	"Appinite"	A56	Fowler & Henney (1996)	51.4	1	13.35	6.44	0.13	7.24	8.33	4.3	3.5	1.01	103	280	27	72	83	77	1930	24	298	24	3056	217	421	37.4	143	19.8	5.14	12.5	5.26	0.83	2.02	1.7	0.23	24			37				
Ach'Uaine	"Appinite"	A58	Fowler & Henney (1996)	58.39	0.7	18.16	4.48	0.09	1.63	2.98	5.07	5.54	0.45	57	2	22	5	83	120	2118	21	553	37	1994	166	297	25.2	83	10.4	2.83	6.98	3.92	0.7	1.84	1.85	0.28	37	14.9	3.1	53.6	11.2			
Borralan	Syenite	b27639	Thirlwall & Burnard (1990)	71.01	0.152	16.35	1.24	0.023	0.15	0.51	6.71	3.405	0.016	21	2		3	33	64.5	1045	7.2	131	5.4	1313	14.24	28.06		11.69	1.953	0.555	1.36	1.051		0.568	0.609	0.093	5.4			2.1	0.684	1	16.5	
Borralan	Syenite	b312	Thirlwall & Burnard (1990)	49.58	1.426	16.9	8.03	0.176	1.44	9.22	3.94	8.29	0.287	290	7		11	95	221	1721	93	658	14.3	1846	99.2	256.7		180.9	42.48	11.67	33.5	19.5		7.34	5.29	0.693	14.3			22.9	7.91	5	10.3	
Borralan	"Pyroxenite"	b313	Thirlwall & Burnard (1990)	37.99	1.803	7.1	18.21	0.171	11.62	17.29	1.37	1.022	2.906	529	42		159	84	13.4	708	27.4	63	3.4	645	51.4	131.3		87.13	17.64	4.38		6.32		2.22	1.332	0.22	3.4			4		59	21.8	
Borralan	Syenite	b36	Thirlwall & Burnard (1990)	54.23	0.539	20.19	3.5	0.12	0.56	4.23	6.6	9.33	0.1	124	3		7	98	131	3206	37	275	16.9	1920	154.4	271.2		95.52	16.09	4.44	12.29	7.52		3.14	2.38	0.335	16.9			23.5		2	46	
Borralan	Syenite	b37	Thirlwall & Burnard (1990)	49.99	1.014	16.67	8.74	0.169	1.82	10.36	1.31	8.57	0.273	388	20		12	59	439	975	23.8	455	5.4	1455	64.8	198.2		163.3	24.17	5.11	11.71	4.91		1.731	1.351	0.202	5.4			9.8		6	10.5	
Borralan	Syenite	b37563	Thirlwall & Burnard (1990)	68.1	0.049	18.54	0.56	0.007	0.14	0.13	7.57	5.11	0.021	16	2		3	13	69.8	932	1.9	15.6	1.3	1681	19.85	21.38		5.554	0.662	0.397	0.448	0.227		0.108	0.137	0.026	1.3			3.1	0.811	1	15.1	
Borralan	"Appinite"	b932	Thirlwall & Burnard (1990)	46.48	1.272	13.16	12.39	0.197	7.61	12.53	3.79	1.173	0.971	339	164		75	117	20.1	2782	32.8	104	10.7	1146	87	187.6		97.93	17.84	4.63	12.66	7.17		2.81	2.03		10.7			6.9	1.92	28	14.1	
Loch Loyal	Syenite	BL/C	Fowler et al. (2008)	65.55	0.38	15.27	2.6		0.72	1.01	7.38	6.23	0.18	49		19	12	57	95	1256	24			3530																		3		
Loch Loyal	Syenite	BL/NW	Fowler et al. (2008)	65.16	0.36	15.81	2.52		0.82	1.07	6.89	6.35	0.28	50		15	14	52	91	1306	23			3857																		2		
Loch Loyal	Syenite	BL1	Fowler et al. (2008)	63.6	0.51	13.1	4.83	0.07	3	2.83	6.32	5.29	0.44	29	9		10	55	102	1580	21	336	11	3341	124	247		123	18.4	4.79	13.1	5.52		2.57	1.68		11	12.7	0.91	33.3	4.56			
Loch Loyal	Syenite	BL2	Fowler et al. (2008)	63.68	0.37	16.96	2.6	0.07	0.65	1.52	8.27	6.37	0.18	53	3	30	10	34	91	1134	27			4958	188	319		129	18.7	4.62	12.3	5.9		2.49	1.76							2		
Loch Loyal	Syenite	BL3	Fowler et al. (2008)	65.07	0.49	15.83	3.16	0.06	0.93	1.5	6.87	6.32	0.25	48	5		20	47	88						191	315		141	20.6	5	13.5	5.16		2.59	1.16							4.5		
Loch Loyal	Syenite	BL4	Fowler et al. (2008)	62.75	0.42	15.45	2.58	0.08	1.04	2.03	6.41	5.99	0.24	31	11		19	33	79	1957	30	179	11	5557	236	393		193	24.2	5.98	15.4	6.68		3.29	1.67		11	4.92	0.6	37.2	2.9			
Loch Loyal	Syenite	BL5	Fowler et al. (2008)	64.62	0.4	15.43	2.85	0.06	1	1.71	7.45	6.09	0.19	35	4		13	54	81						244	385		165	22.8	5.08	12.8	5.46		2.46	1.36							4.1		
Loch Loyal	Syenite	BL6	Fowler et al. (2008)	64.94	0.38	15.41	3.3	0.06	0.87	1.46	8.77	5.62	0.2	28	2		10	55	110						180	231		123	16.8	4.16	11.1	4.68		2.43	1.29							4.2		
Loch Loyal	Syenite	BL7	Fowler et al. (2008)	62.11	0.43	16.25	2.73	0.09	1.02	1.95	7.08	6.52	0.24	60	3	16	13	54	76	1204	29			4334	207	385		164	24.2	5.74	15	6.87		2.76	1.68							3		
Loch Loyal	Syenite	BL8	Fowler et al. (2008)	63.58	0.44	16.29	3.19	0.08	1.21	2.27	6.55	6.36	0.33	61	10	17	23	71	93	1330	30			4762	224	519		164	24.7	5.67	14.7	6.47		2.93	1.51							3		
Loch Loyal	Syenite	BL9	Fowler et al. (2008)	64.55	0.41	16.59	3.02	0.07	0.94	1.9	6.13	5.86	0.31	34	7		15	55	88	1292	28	343	16	4502	211	385		179	23.3	5.56	14.6	6.01		2.99	1.47		16	8.66	1.24	43.3	3.53	4.6		
Loch Loyal	Syenite	BLSE	Fowler et al. (2008)	65.06	0.37	15.13	2.58	0.07	0.83	0.94	6.95	6.38	0.17	26	10		13	55	106	1286	21	370	17	4455	187	240		124	18.4	4.33	10.7	4.94		2.26	1.21		17	10	1.1	38.8	6.2			
Borralan	Syenite	bs818	Thirlwall & Burnard (1990)	59.91	0.366	19.3	2.32	0.079	0.6	3.44	3.57	9.46	0.072	116	2		5	34	157	3314	19.2	65	7.1	2965	47.4	105.4		51.97	8.893	2.347	6.5	3.56		1.195	1.054		7.1			2.8	1.006	3	12.5	
Borralan	Syenite	bs823	Thirlwall & Burnard (1990)	49.32	1.395	17.44	9.08	0.167	2.57	8.55	2.47	8.09	0.469	328	2		10	91	188	2560	113	442	6.3	789	73	173		111									6.3			8		11	17.7	
Borralan	Syenite	bs826	Thirlwall & Burnard (1990)	63.44	0.271	19.29	1.97	0.058	0.16	1.78	6.58	6.3	0.023	63	2		4	34	88.3	2177	16	89	5.7	1726	43	87		38									5.7			3.7		2	26	
Borralan	Syenite	bs832	Thirlwall & Burnard (1990)	49.05	1.541	16.93	8.61	0.206	1.27	9.49	3.8	8.19	0.254	317	6		11	88	237	1709	100	729	14.8	1491	97	235	153										14.8			21.9		5	7.9	
Ach'Uaine	Syenite	CCB10	Fowler & Henney (1996)	62.78	0.51	17.05	3.64	0.08	0.78	2.44	5.18	5.2	0.21	43	0	40	1	58	79	2278	24	523	37	2548	197	360	30.3	100	11.3	2.99	7.2	4.28	0.76	2.02	2.14	0.31	37			52				
Ach'Uaine	Syenite	CCB12	Fowler & Henney (1996)	62.44	0.65	15.91	4.22	0.06	1.62	3.21	4.92	4.82	0.32	57	20	26	10	51	70	2944	25	343	23	2772	132	259	25.3	87	11.7	3.1	7.8	4.79	0.85	2.33	2.31	0.33	23			17				
Ach'Uaine	Syenite	CCB13	Fowler & Henney (1996)	63.82	0.64	15.82	4.05	0.07	1.51	3.33	4.7	5.78	0.31	55	19	30	7	37	75	2218	26	331	22	2843	147	268	25.8	88	11.4	3.02	7.79	4.83	0.87	2.38	2.46	0.36	22	7.6	2.3	15.5	4.6		
Ach'Uaine	Monzodiorite	CCB14	Fowler & Henney (1996)	51.34	0.97	13.67	6.71	0.16	5.56	8.23	3.85	4	0.95	98	250	24	74	103	97	2255	25	312	24	2971	183	378	35.6	137	18.5	4.82	11.8	5.33	0.84	2.06	1.72	0.23	24	7.5	1.5	31.6	8.4		
Ach'Uaine	Monzodiorite	CCB15	Fowler & Henney (1996)	52.17	0.97	13.49	6.39	0.15	5.83	8.3	3.68	4.11	0.92	99	253	27	74	95	95	2246	23	305	23	2870	179	370	34.8	134	18.7	4.91	11.8	5.27	0.84	2.06	1.76	0.23	23			29				
Ach'Uaine	Monzodiorite	CCB16	Fowler & Henney (1996)	52.61	1.52	12.73	6.82	0.12	6.59	8.07	3.15	4.83	1.32	106	229	26	63	94	95	2017	27	419	30	3212	170	373	36.2	144	21.2	5.52	14	6.47	1.03	2.39	1.92	0.25	30	11.5	2.2	34.5	9.2		
Ach'Uaine	"Hybrid"	CCB17	Fowler & Henney (1996)	54.8	1	15.6	6.32	0.1	6.17	6.25	4.76	2.89	0.51	99	166	27	101	95	70	1699	18	249	15		73.3	141	15.1	52	7.11	1.99	5.19	3.48	0.63	1.76	1.79	0.25	15			12				
Ach'Uaine	"Hybrid"	CCB18	Fowler & Henney (1996)	58.23	0.75	15.39	5.6	0.15	3.64	5.44	4.87	3.91	0.65	65	112	21	33	110	72	2135	23	360	24	2482	175	343	31.1	112	15	3.78	9.43	4.65	0.79	2.05	1.9	0.27	24			29				
Ach'Uaine	Monzodiorite	CCB1i	Fowler & Henney (1996)	50.62	1.63	12.38	7.21	0.13	7.29	8	2.77	5.06	1.35	116	247	25	76	111	135	2060	32	376	32	3987	191	410	39.1	158	21.5	5.5	14.5	7.13	1.13	2.61	2.17	0.29	32			32				
Ach'Uaine	Monzodiorite	CCB2	Fowler & Henney (1996)	48.56	1.72	12.24	8.58	0.15	8	10.75	3.54	2.84	1.82	128	186	27	43	139	129	2432	31	485	46	1477	202	472	44.8	187	22.5	5.76	15.7	7.86	1.23	2.75	2.18	0.28	46	13.5	3.2	35.7	10.4		
Ach'Uaine	Monzodiorite	CCB3	Fowler & Henney (1996)	50.33	1.04	13.19	6.91	0.15	7.3	8.52	3.59	3.88	1.01	109	279	26	78	101	98	2023	23	303	24	3057	188	392	36.9	145	19.9	5.11	12.5	5.68	0.9	2.12	1.78	0.24	24	8.5	2.1	38.1	10.8		
Ach'Uaine	Syenite	CCB5a	Fowler & Henney (1996)	62.34	0.64	16.25	3.77	0.07	1.53	3.54	4.48	5.99	0.31	52	16	22	8	42	90	2704	27	335	21	3080	139	272	25.8	89	12.2	3.21	8.2	4.93	0.89	2.43	2.48	0.35	21			15				
Ach'Uaine	"Hybrid"	CCB5i	Fowler & Henney (1996)	57.07	0.85	14.33	5.34	0.12	3.98	6.05	3.36	6.09	0.75	69	133	21	32	78	116	2144	22	354	22	3024	153	301	28.8	105	14.4	3.68	9.45	4.87	0.81	2.09	1.97	0.27	22	8.6	1.8	24	5.7		
Ach'Uaine	Granite	CCB6	Fowler & Henney (1996)	69.63	0.31	16.08	2.25	0.05	0.79	1.04	4.65	5.27	0.11	23	6	54	4	47	139	1097	8	209	13	1121	63.7	116	10.7	33	4.16	1.18	2.71	1.67	0.31	0.87	0.92	0.14	13	5.2	1.9	27.6	4.4		
Ach'Uaine	Granite	CCB7	Fowler & Henney (1996)	70.31	0.36	15.51	1.69	0.02	0.68	1.02	4.13	5.61	0.12	20	6	47	2	27	122	832	10	241	7	979	65.7	103	10.5	32	4.28	1.15	2.88	1.8	0.33	0.86	0.87	0.13	7			25				
Ach'Uaine	Granite	CCB8	Fowler & Henney (1996)	70.66	0.36	15.44	1.8	0.02	0.66	1.35	5.07	4.11	0.09	20	9	73	2	51	101	757	4	205	6	856	49.4	85	8.4	26	3.29	0.82	2.07	1.15	0.2	0.5	0.47	0.07	6	5.6	1.6	23.6	4.8		
Ach'Uaine	Granite	CCB9	Fowler & Henney (1996)	70.62	0.38	15.57	1.9	0.02	0.69	1.44	5.01	4.09	0.11	23	7	49	2	52	100	820	6	213	5	862	57.8	90	9.5	29	3.77	0.97	2.36	1.22	0.21	0.57	0.5	0.07	5			22				
Cluanie	Granite	CL1	Fowler et al. (2008)	50.92	1.096	11.17	8.405	0.161	12.32	8.589	2.026	2.673	0.642	146	658		456	124	92	927.8	31.75	194.2	18	964.3	77.6	148	17.1	60	9.33	2.34	8.24	4.85		1.71	1.89	0.342	18			5				5
Cluanie	Granite	CL3	Fowler et al. (2008)	63.63	0.58	15.59	3.54	0.06	2.09	3.58	4.86	2.29	0.19	60	55		24	52	37	686.7	20.13	194.3	6	656.5	15	22.6	3.3	12.9	2.06	0.536	1.688	1.38		0.575	0.554	0.113	6			0				9
Cluanie	Granite	CL4	Fowler et al. (2008)	69.12	0.305	16.03	2.31	0.067	0.604	2.55	6.073	2.679	0.088	31	30		0	47	54	900.8	21.43	200.7	6	796.5	24.4	36.8	5.32	19	3.4	0.826	2.76	2.28		1.015	1.24	0.255	6			1				23
Cluanie	Granite	CL5	Fowler et al. (2008)	68.82	0.323	15.29	2.27	0.048	1.123	2.115	5.464	2.892	0.078		40.11					884.4	18.27	138.1		1811	26.1	40.8	5.69	49.6	4.62	0.889	3.72	2.7		1.32	0.874	0.204								
Cluanie	Granite	CL6	Fowler et al. (2008)	67.86	0.335	16.08	2.152	0.061	0.61	2.005	4.82	4.745	0.067	26	21		1	47	109	784.9	23.4	163.8	8	2001	23.9	39.4	5.33	20.8	3.66	0.912	2.752	2.57		0.995	1.38	0.257	8			1				31
Cluanie	Granite	CL7	Fowler et al. (2008)	68.58	0.29	15.92	2.052	0.06	0.577	2.414	5.744	2.887	0.061		13.36					835.1	19.98	167.1		953.4	23.8	38.5	5.56	0	4.52	0.859	3.616	2.98		1.44	1.26	0.276								
Cluanie	Granite	CL9	Fowler et al. (2008)	70.61	0.219	15.92	1.552	0.042	0.369	1.727	5.978	3.128	0.018	20	25		0	38	65	857.5	18.55	132.3	4	1067	12.6	20.1	3.29	14.3	2.42	0.568	2.04	1.75		0.765	0.942	0.195	4			0.5				26

Table SA4 Continued

Locality	Rock type	Sample	Source	SiO2	TiO2	Al2O3	FeO	MnO	MgO	CaO	Na2O	K2O	P2O5	V	Cr	Co	Ni	Zn	Rb	Sr	Y	Zr	Nb	Ba	La	Ce	Pr	Nd	Sm	Eu	Gd	Dy	Ho	Er	Yb	Lu	Nb	Hf	Ta	Th	U	Sc	Pb
Ratagain	Monzodiorite	**drr206**	Fowler et al. (2008)	50.3	0.76	7.53	8.36	0.14	14.98	11.13	1.81	1.72	0.4	125			290	36	45	3650	18	109	7	1312	70.3	154	18.3	76.3	12.6	3.26	7.19	4		1.41	1.17	0.14	7	2.7	0.5	5	1.1		3
Ratagain	Monzodiorite	**drr207**	Fowler et al. (2008)	45.28	2.15	16.97	11.42	0.14	6.16	6.86	3.48	3.54	1.65	275			32	103	77	3325	31	113	13	3452	159	345	40.1	162	23.5	6.24	13	6.9		2.44	1.84	0.18	13	2.9	0.6	3.1	0.7		8
Ratagain	Monzodiorite	**drr213**	Fowler et al. (2008)	50.42	1.13	11.77	8.17	0.13	9.6	7.63	3.02	3.42	0.8	150			179	47	69	9400	27	160	14	2178	109	233	27.4	115	18.7	4.98	10.9	5.83		2.1	1.68	0.23	14	3.9	0.6	7.3	1.4		5
Glen Dessarry	Pegmatite	**GD13**	Fowler (1988)	64.98	0.06	19.95	0.63	0	0.11	2.13	7.51	3.73	0.19	7	5		2		83	2530	14	2	2	1373	52.1	96.3	9.8	39.5	6.09	1.28	4.12	2.42		0.97	0.83	0.12	2			6.4	0.6		
Glen Dessarry	Syenite	**GD18**	Fowler (1988)	52.88	1.31	14.24	9.46	0.17	5	7.1	3.82	4.5	0.67	206	91		39		114	1957	40	277	32	1918													32			19.6	4.8		
Glen Dessarry	Syenite	**GD19**	Fowler (1988)	53.02	1.28	14.05	9.37	0.18	5.04	6.99	3.8	4.56	0.66	206	86		38		117	2039	41	289	32	1911													32			17.7	5		
Glen Dessarry	Syenite	**GD20**	Fowler (1988)	53.76	1.26	13.94	9.06	0.17	4.72	6.75	3.76	4.83	0.62	190	85		38		131	2015	37	281	28	1795													28			15.9	4.95		
Glen Dessarry	Syenite	**GD22**	Fowler (1988)	58.27	1	13.4	7.56	0.18	4.11	6.39	2.48	4.9	0.66	178	74		38		81	2525	54	76	21	2559	82.4	150	17.8	82.3	14.4	3.25	11.7	8.88		4.4	3.84	0.54	21	2.7	0.88	6.6	2.7		
Glen Dessarry	Syenite	**GD27**	Fowler (1988)	56.7	0.9	15.36	6.99	0.15	3.26	5.14	3.71	5.81	0.62	155	78		40		93	2628	37	153	14	3993	100	180	19.6	84.1	12.9	4.06	9.35	6.32		3.14	3.08	0.46	14			8.4	1.9		
Glen Dessarry	Syenite	**GD28**	Fowler (1988)	57.24	0.86	15.34	6.62	0.2	2.99	4.77	3.05	7.28	0.56	147	69		34		120	2494	34	133	14	3562	95.4	173	18	75.7	11.4	3.97	8.38	5.72		2.91	2.84	0.42	14			9	1.5		
Glen Dessarry	Syenite	**GD29**	Fowler (1988)	56.88	0.86	15.19	6.84	0.15	3.07	4.79	3.08	7.32	0.58	146	67		31		121	2415	31	126	12	3492													12			9.2	1.7		
Glen Dessarry	Syenite	**GD30**	Fowler (1988)	59.25	0.62	16.28	5.37	0.08	1.75	3.74	4.27	6.47	0.41	100	24		16		99	6097	27	36	11	3915													11			6.1	1.15		
Glen Dessarry	Syenite	**GD31**	Fowler (1988)	53.32	1.18	14.05	9.42	0.16	4.56	6.99	3.49	4.62	0.7	208	77		35		82	2626	39	186	34	2179	96	168	18.2	79.2	12.7	3.41	9.57	6.54		3.28	3.06	0.45	34			36.4	5.55		
Glen Dessarry	Pegmatite	**GD32**	Fowler (1988)	72.21	0.04	15.76	0.55	0	0	1.65	5.96	3.31	0.07	2	2		2		78	726	13	28	3	630	8.46	23.9	1.95	8.24	2.06	0.51	1.83	1.65		0.96	0.99	0.15	3			2.9	0.7		
Glen Dessarry	Syenite	**GD33**	Fowler (1988)	60.64	0.63	17.13	4.44	0.07	0.81	2.19	4.52	7.69	0.23	82	2		7		136	4303	28	55	24	3551													24			8.3	1.45		
Glen Dessarry	Pegmatite	**GD34**	Fowler (1988)	67.29	0.02	19.51	0.2	0	0	1.9	9.35	1.01	0.07	2	2		2		17	3318	6	2	2	257	3.97	7.26	0.83	3.67	0.88	0.41	0.95	1.01		0.54	0.47	0.07	2			0.8	0.3		
Glen Dessarry	Pegmatite	**GD35**	Fowler (1988)	68.43	0.07	17.49	1.13	0.01	0.05	2.04	6.78	2.76	0.1	5	2		2		56	1038	34	25	8	651	32.5	60.3	6.51	28.2	5.45	1.19	4.96	4.75		2.59	2.31	0.32	8			4.8	0.7		
Glen Dessarry	Syenite	**GD42**	Fowler (1988)	51.63	1.32	12.7	10.27	0.19	5.88	8.23	3.36	4.3	0.68	238	119		48		106	1779	42	345	26	1832													26			17.7	4.45		
Glen Dessarry	Syenite	**GD43**	Fowler (1988)	49.1	1.38	13.47	12.13	0.21	6.11	9.33	2.95	2.25	0.81	259	150		59		76	2648	76	159	44	2142	83.2	162	20.5	101	19.1	3.53	16.2	13.1		6.61	5.48	0.76	44			28.8	6.35		
Glen Dessarry	Syenite	**GD44**	Fowler (1988)	52.6	1.15	14.81	9.55	0.16	3.97	5.58	4.02	4.81	0.91	196	53		38		95	7393	29	79	14	5315	81.6	145	16.9	75.4	11.4	3.62	8.38	5.2		2.38	2.04	0.29	14			7.2	2.15		
Glen Dessarry	Syenite	**GD45**	Fowler (1988)	51.8	1.23	14.48	10.16	0.17	4.2	5.96	3.98	4.71	0.97	206	59		40		96	7078	35	32	17	4800													17			9.6	2.6		
Glen Dessarry	Syenite	**GD46**	Fowler (1988)	53.77	1.25	14.2	8.75	0.17	4.64	6.48	3.96	5	0.62	188	81		36		133	1923	37	252	27	1717	88	136		39	14	3.5		5.7			2.8	0.45	27			17.6	4.85		
Glen Dessarry	"Pyroxenite"	**GD48**	Fowler (1988)	39.8	2.39	5.52	17.75	0.28	11.43	16.99	0.85	1.75	2.12	391	127		117		67	646	53	153	10	1819	130	246	29.2	136	21.3	5.38	16.4	10.4		4.81	3.93	0.58	10			6.5	2.3		
Glen Dessarry	"Pyroxenite"	**GD49**	Fowler (1988)	49.93	0.77	3.91	9.51	0.21	12.47	21.58	1.31	0.24	0.46	190	121		66		5	419	33	187	4	118	44.4	90.2	11.8	58.4	10.7	2.82	8.55	6.1		2.87	2.62	0.41	4			5.8	1.3		
Glen Dessarry	Syenite	**GD52**	Fowler (1988)	54.29	1.08	15.58	7.89	0.13	3.96	6.85	3.87	4.44	0.6	147	55		23		103	2467	41	385	32	2320	99.9	163	17.3	71.7	11	2.87	8.5	6.38		3.4	3.25	0.48	32			14.8	4		
Helmsdale	Diorite	**HG159As**	Fowler et al.(2008)	54.12	0.851	13.01	5.099	0.167	3.943	7.408	2.456	6.819	0.347	95	140		115	74	254	944.4	36.58	366.8	22	1851	190	375	41.1	136	19.7	4.48	11.68	6.89		2.195	1.61	0.288	22			45			69
Helmsdale	Granite	**IHG310**	Fowler et al.(2008)	73.35	0.281	14.45	1.401	0.022	0.372	0.313	4.656	5.134	0.002		18.71					332.1	10.51	153.4		1012	32.9	71.7	7.6	22	3.2	0.732	2.536	1.49		0.735	0.582	0.139							
Helmsdale	Granite	**IHG317**	Fowler et al.(2008)	72.37	0.289	14.89	1.466	0.033	0.59	1.141	4.924	4.495	0.009	15	22		4	33	185	676.7	11.98	158.2	9	1309	47.7	76.3	8.42	26.6	3.62	0.918	2.272	1.58		0.605	0.58	0.117	9			9			46
Helmsdale	Granite	**IHG337**	Fowler et al.(2008)	72.26	0.302	14.97	1.342	0.024	0.504	1.001	4.957	4.567	0.0		21.86					536.6	13.03	167.6		1290	46.4	77.8	9.04	29.4	4.04	0.949	2.92	1.71		0.8	0.556	0.134							
Helmsdale	Granite	**IHG807**	Fowler et al.(2008)	72.74	0.294	14.95	1.208	0.022	0.43	0.521	4.904	4.928	0		21.17					493	11.55	167.2		1259	52	73.3	8.47	25.4	3.41	0.819	2.56	1.46		0.655	0.453	0.112							
Helmsdale	Granite	**IHG837**	Fowler et al.(2008)	72.3	0.314	15.08	1.503	0.027	0.591	0.648	4.881	4.827	0.011	30	25		2	31	154	514.2	11.63	175	8	1253	60.3	88.5	9.62	30.3	3.86	0.986	2.344	1.5		0.545	0.473	0.102	8			18			30
Rogart	"Appinite"	**LPR**	Fowler et al. (2001)	49.05	1.23	11.56	7.02	0.12	8.67	9.11	2.87	3.68	1.06	141	423		91	118	133	1846	28	253	25	1950	88.9	209		108	17.2	4.2	11.6	6.02		2.39	1.85		25	9.33	0.72	14.9	4.7		
Ach'Uaine	Monzodiorite	**LYD1**	Fowler & Henney (1996)	46.62	1.53	10.98	7.38	0.14	8.6	10.9	2.98	4.16	2.93	95	180	27	116	104	105	1964	31	398	30	3686	187	425	41.1	174	24.7	6.33	17	7.6	1.18	2.64	2	0.26	30	10.5	1.9	30.5	9		
Loch Ailsh	Syenite	**m92x**		66.84	0.29	17.55	1.92	0.03	0.2	0.45	5.9	6.36	0.03		5		2	30	71	2180	11	213	5.8	1847	31	64	6.8	27	4.5	1.21	3.1	1.99		0.79	0.66	0.09	5.8	2.25	0.33	3.45	0.93		24
Glen Dessarry	Syenite	**MJ001**	Fowler (1992)	59.8	0.69	17.63	4.82	0.1	1.34	2.93	4.59	6.65	0.36	82	9		10		106	4164	32	222	27	3383	98.1	193	20.7	87.5	13	3.56	9.32	5.77		2.69	2.45	0.36	27			12	2.31		
Glen Dessarry	Syenite	**MJ002**	Fowler (1992)	60.23	0.69	17.83	4.57	0.09	1.32	2.73	5.14	6.36	0.31	81	6		11		119	4198	31	159	24	3434	98.5	186	20	82.9	12.4	3.42	8.56	5.28		2.46	2.23	0.33	24			11.3	2.03		
Glen Dessarry	Syenite	**MJ003**	Fowler (1992)	61.28	0.6	17.73	4.03	0.1	0.99	2.96	5.59	6	0.26	80	2		6		81	5530	31	67	15	4198													15			6.2	1.18		
Glen Dessarry	Syenite	**MJ005**	Fowler (1992)	61.14	0.61	17.68	4.09	0.08	0.93	2.7	5.85	6.27	0.25	81	15		6		97	5281	27	66	15	4093	87	151	17	73.2	11.2	3.37	7.79	4.81		2.24	1.84	0.26	15			6.3	1.27		
Glen Dessarry	Syenite	**MJ006**	Fowler (1992)	61.99	0.48	18.35	3.21	0.06	0.62	2.05	5.88	6.4	0.2	63	2		3		101	5933	22	46	12	4330	63.2	114	12.8	53.7	8.21	2.75	5.76	3.63		1.69	1.46	0.21	12			4.9	1.31		
Glen Dessarry	Syenite	**MJ008**	Fowler (1992)	60.78	0.61	17.55	4.18	0.08	1.02	2.77	5.39	6.22	0.3	78	2		6		98	5718	27	64	15	4417													15			7	1.26		
Glen Dessarry	Syenite	**MJ009**	Fowler (1992)	61.28	0.7	17.38	4.26	0.09	1.08	2.73	5.41	6.05	0.29	88	2		7		120	4308	29	82	20	4083	82.1	166	18.1	77.1	11.8	3.36	8.38	5.31		2.45	2.12	0.31	20			7.4	1.68		
Glen Dessarry	Syenite	**MJ010**	Fowler (1992)	60.75	0.66	17.39	4.64	0.08	1.01	2.95	5.25	6.36	0.31	79	2		7		125	4930	27	104	20	3676													20			10	1.85		
Glen Dessarry	Syenite	**MJ011**	Fowler (1992)	60.08	0.59	16.63	4.58	0.1	1.44	3.34	5.06	6.46	0.42	97	9		12		115	5054	34	121	18	5524													18			11.3	2.6		
Glen Dessarry	Syenite	**MJ012**	Fowler (1992)	51.82	1.25	12	10.13	0.2	5.84	8.98	3.65	4.2	1.11	209	118		73		105	4686	51	161	11	4690													11			9.8	1.89		
Glen Dessarry	Syenite	**MJ013**	Fowler (1992)	53.54	1.33	14.5	9.27	0.17	5.12	6.92	3.76	4.61	0.67	200	87		42		117	1933	42	308	28	1933	86	180			13	3.8		6.6		2.3			28			18	4.98		
Glen Dessarry	Syenite	**MJ015**	Fowler (1992)	57.28	0.87	16.14	6.31	0.14	3.02	4.75	3.58	6.9	0.61	130	56		33		110	2933	31	160	11	3264													11			9.3	2.04		
Glen Dessarry	Syenite	**MJ016**	Fowler (1992)	59.31	0.91	17.54	5.82	0.1	1.24	4.02	6.01	4.44	0.31	107	2		7		69	4887	27	88	15	3347													15			6.6	0.9		
Glen Dessarry	Syenite	**MJ020**	Fowler (1992)	51.82	1.29	14.12	10.2	0.21	5.25	7.98	3.06	4.81	0.81	227	78		44		109	2948	41	197	21	2599													21			16.2	2.95		
Glen Dessarry	Syenite	**MJ024**	Fowler (1992)	61.56	0.57	17.7	3.74	0.07	0.93	2.87	5.49	5.97	0.24						77	5373	29	54	14	4293													14			5.9	1.08		
Glen Dessarry	Syenite	**MJ026**	Fowler (1992)	56.96	0.88	18.74	6.24	0.09	1.49	3.91	4.96	4.99	0.38	132	4		10		83	6279	31	71	10	5585													10			6.9	1.22		
Glen Dessarry	Syenite	**MJ027**	Fowler (1992)	61.24	0.62	17.78	4.24	0.08	1.03	2.71	4.86	6.25	0.27	86	2		7		79	5465	25	60	15	5451													15			7.3	1.06		
Glen Dessarry	Syenite	**MJ029**	Fowler (1992)	57.98	0.9	16.22	6.54	0.11	2.82	4.42	4.12	5.87	0.49	109	43		22		161	1694	40	401	35	1557	92	215			11	3.1		5.7			3.1		35			34	9.57		
Loch Borralan	Syenite	**ms382**	Thompson & Fowler (1986)	63.08	0.29	18.69	2.53	0.04	0.2	1.56	6.57	5.41	0.03		1		1	33	88	3134	29	240	4.9	2529	47	67	8.7	39	7.2	2.16	5.9	3.96		2.09	2.18	0.34	4.9	2.51	0.54	3.76	1.18		32
Loch Loyal	Syenite	**ms390**	Thompson & Fowler (1986)	63.76	0.48	16.6	3.23	0.06	1.55	2.03	6.04	5.35	0.35		3		10	58	87	1661	58	474	19	4968	293	389	37.5	167	21.7	5.29	12.9	5.8		2.32	1.54	0.22	19	10	1.77	53	5.46		
Ratagain	Syenite	**ms405**	Thompson & Fowler (1986)	61.49	0.63	17.13	3.57	0.05	2.16	2.65	6.62	4.79	0.35		26		20	51	62	2073	17	464	15	2606	108	211	24.2	91	12.1	2.98	7.2	4.07		2.05	1.1	0.16	15	8.15	1.29	13.3	1.81		24
Ratagain	Diorite	**ms415**	Thompson & Fowler (1986)	56.07	0.91	15.43	6.28	0.12	3.54	7.05	4.92	4.72	0.9		10		12	82	97	3205	28	476	20	3092	175	312	33	127	17.8	4.5	11.2	5.61		2.75	2.53	0.23	20	8.9	1.22	20.6	4.17		28
Ratagain	Granite	**ms434**	Thompson & Fowler (1986)	69.05	0.36	15.2	2.04	0.04	1.33	1.31	5.36	4.76	0.22		12		9	36	76	1667	10	238	11.5	2437	82	145	14.4	52	6.6	1.8	3.9	2.15			0.71	0.1	11.5	4.97	0.94	15.2	1.83		24
Rogart	Tonalite	**NJS1**	Soper (1963)	65.84	0.6	15.4	3.67	0.18	2.7	3.22	4.41	2.97	0.24																															
Rogart	Tonalite	**NJS2**	Soper (1963)	66.54	0.57	15.98	3.1	0.02	2.19	2.62	4.82	3.58	0.23																															

Table SA5 XRF data for representative lamprophyres of the Northern Highlands Minette Suite

Locality	Rock type	Sample	Source	SiO2	TiO2	Al2O3	FeO	MnO	MgO	CaO	Na2O	K2O	P2O5	Mg#	V	Cr	Ni	Zn	Rb	Sr	Y	Zr	Nb	Ba	La	Ce	Pr	Nd	Sm	Eu	Gd	Dy	Ho	Yb	Lu	Nb	Th
Northern Highlands	Lamprophyre	**DO 93/6**	Canning et al. (1996)	51.91	1.39	12.65	7.3	0.1	6.4	9.07	2.81	5.41	2.43	72.33	126	401	140	97	87.1	1751	18.4	341	28.4	3109	170											28.4	
Northern Highlands	Lamprophyre	**DO 93/7**	Canning et al. (1996)	51.4	1.41	12.07	7.64	0.11	7.56	8.33	2.48	5.24	2.49	74.68	138	612	200	75	51	1610	35.9	205	38.3	10021	173.6	398.7	43.3	147.1	19.7	4.5	10.9	4.7	1.29	1.15	0.16	38.3	39
Northern Highlands	Lamprophyre	**GA 93/1**	Canning et al. (1996)	53.62	1.04	12.79	7.12	0.11	8.2	7.73	3.14	3.58	1.03	77.44	108	378	250	83	69.5	1648	27.8	261	14.8	2194	138.5	305.4	33.7	118.6	17.5	4	10.4	4.8	1.48	1.29	0.18	14.8	11
Northern Highlands	Lamprophyre	**DO 93/1**	Canning et al. (1996)	50.83	1.4	12.14	7.6	0.11	7.14	8.14	2.55	5.61	2.43	73.69	138	427	159	103	85	5433	21.9	395	28	4241	178.7	410	48.7	152.3	20.1	4.5	11	4.6	1.18	1.09	0.16	28	2
Northern Highlands	Lamprophyre	**DO 93/3**	Canning et al. (1996)	51.43	0.55	10	8.54	0.13	14.76	7.72	1.49	3.99	0.47	83.75	130	322	127	97	88.2	2294	21.6	377	30	3331	160											30	12
Northern Highlands	Lamprophyre	**PJH 208**	Canning et al. (1996)	45.6	0.81	10.28	5.94	0.14	7.09	10.03	1.19	4.93	1.53	54.41	95	445	150	82	101	2881	31	424	17	14150	208	417	na	216	32.6							17	38
Northern Highlands	Lamprophyre	**PHR 29**	Canning et al. (1996)	46.18	0.8	9.77	6.05	0.17	7.06	10.51	1	5.03	1.73	53.85	86	423	123	71	103	4276	30	319	16	12671	192	449	na	226	33.6							16	36

Table SB1 RbSr isotope analyses and recalculated values for the Ratagain Complex

Sample Name	Sr (ppm)	2 sigma%	Rb (ppm)	2sigma %	$^{87}Sr/^{86}Sr$	% Std Error	λ	$^{87}Rb/^{86}Sr$	$^{87}Sr/^{86}Sri$	T (Ma)
AL013	589.4	1.174	54.68	0.44	0.707413	0.0014	1.42E-11	0.268554	0.705787	4.25E+08
AL059	7014.1	9.016	57.72	0.35	0.706021	0.0011	1.42E-11	0.023818	0.705787	4.25E+08
AL063	1612.8	1.986	50.91	0.39	0.706068	0.0011	1.42E-11	0.091365	0.705515	4.25E+08
AL074	2844.4	3.365	53.47	0.38	0.706516	0.0013	1.42E-11	0.054412	0.706187	4.25E+08
AL092	1980.2	3.217	53.39	0.38	0.706231	0.0011	1.42E-11	0.078039	0.705759	4.25E+08

λ after Steiger & Jäger (1977)

Table SB2 SmNd isotope analyses and recalculated values for the Ratagain Complex

Sample Name	Nd (ppm)	Sm (ppm)	$^{143}Nd/^{144}Nd$	% Std Error	λ	$^{147}Sm/^{144}Nd$	$^{143}Nd/^{144}Ndi$	Ƭ (Ma)	CHUR $^{147}Sm/^{144}Nd$	CHUR $^{143}Nd/^{144}Nd$	Ƭ CHUR	εNd (Ƭ)
AL013	23.196 (+/-0.007)	2.879 (+/-0.001)	0.511618	0.0007	6.54E-12	0.075019	0.511409	4.25E+08	0.1967	0.512638	0.512091	-13.3
AL059	203.189(+/-0.15)	35.925(+/-0.02)	0.511782	0.0007	6.54E-12	0.106870	0.511485	4.25E+08	0.1967	0.512638	0.512091	-11.8
AL063	41.539(+/-0.004)	5.958(+/-0.001)	0.511651	0.001	6.54E-12	0.086694	0.511410	4.25E+08	0.1967	0.512638	0.512091	-13.3
AL074	87.564(+/-0.024)	13.588(+/-0.002)	0.511679	0.0007	6.54E-12	0.093795	0.511418	4.25E+08	0.1967	0.512638	0.512091	-13.1
AL092	49.372(+/-0.004)	7.232(+/-0.001)	0.511658	0.0007	6.54E-12	0.088537	0.511420	4.25E+08	0.1967	0.512638	0.512091	-13.1

λ after Lugmair & Marti (1978)

CHUR values after Jacobsen & Wasserburg (1980)

Table SC1 SEM Standards

Spectrum	SiO2	TiO2	Al2O3	FeO	MnO	MgO	CaO	K2O	Na2O	Cl
MAC std: Albite	**Location:**									
rec. values	71.22		18.42						10.29	
Spectra_Albite1_1	68.69		20.05						11.27	
Spectra_Albite1_2	68.54		20.34						11.12	
Spectra_Albite1_3	68.78		20.03						11.19	
Spectra_Albite2_1	68.65		20.10						11.25	
Spectra_Albite2_2	68.62		20.14						11.24	
Spectra_Albite2_3	68.38		20.48						11.14	
Spectra_Albite3_1	69.19		20.13						10.67	
Spectra_Albite3_2	68.64		20.15						11.22	
Spectra_Albite3_3	68.71		20.05						11.24	
Spectra_Albite4_1	68.72		19.99						11.29	
Spectra_Albite4_2	68.76		20.08						11.16	
Spectra_Albite4_3	68.76		20.09						11.15	
Spectra_Albite5_1	68.38		20.51						11.11	
Spectra_Albite5_2	68.67		20.06						11.27	
Spectra_Albite5_3	68.58		20.12						11.31	
Mean	68.67		20.15						11.18	
std. dev (1σ)	0.19		0.16						0.15	
RSD	0.28		0.79						1.37	
Accuracy	-3.58		9.41						8.60	
MAC std: Diopside	**Location:**									
rec. values	52.70	0.29	1.00	3.27		16.10	25.27		0.17	
Spectra_Diop1_1	53.83	0.30	1.09	3.00		16.36	25.27		0.15	
Spectra_Diop1_2	53.64	0.33	1.17	3.09		16.60	25.02		0.14	
Spectra_Diop1_3	53.79	0.34	0.97	3.16		16.41	25.19		0.15	
Spectra_Diop2_1	53.75	0.34	1.04	3.08		16.43	25.23		0.13	
Spectra_Diop2_2	53.90	0.29	1.04	3.05		16.35	25.24		0.13	
Spectra_Diop2_3	53.53	0.38	1.22	3.08		16.60	25.04		0.14	
Spectra_Diop3_1	53.79	0.33	0.91	3.10		16.34	25.41		0.13	
Spectra_Diop3_2	53.86	0.31	0.92	3.19		16.31	25.29		0.13	
Spectra_Diop3_3	53.78	0.34	1.03	3.10		16.48	25.17		0.10	
Spectra_Diop4_1	53.52	0.31	1.04	3.14		16.68	25.18		0.14	
Spectra_Diop4_2	53.65	0.34	0.98	3.12		16.62	25.14		0.15	
Spectra_Diop4_3	53.49	0.33	1.17	3.07		16.61	25.18		0.15	
Spectra_Diop5_1	53.93	0.29	0.92	3.07		16.30	25.37		0.13	
Spectra_Diop5_2	53.80	0.33	0.92	3.08		16.44	25.29		0.15	
Spectra_Diop5_3	53.72	0.28	1.09	3.17		16.36	25.27		0.11	
Mean	53.73	0.32	1.03	3.10		16.46	25.22		0.14	
std. dev (1σ)	0.14	0.03	0.10	0.05		0.13	0.11		0.02	
RSD	0.25	7.78	9.80	1.58		0.79	0.42		11.12	
Accuracy	1.96	11.09	3.29	-5.22		2.23	-0.20		-20.53	

Table SC1 Continued

MAC std: Hornblende	**Location:**									
rec. values	44.35	0.98	12.05	16.73	0.34	11.76	10.98	0.60	1.92	0.29
Spectra_Horn1_1	43.85	1.05	12.17	17.87	0.32	11.03	10.90	0.59	1.92	0.31
Spectra_Horn1_2	43.93	1.04	12.15	17.63	0.39	11.11	10.89	0.58	1.94	0.33
Spectra_Horn1_3	44.34	0.94	12.08	17.22	0.35	11.46	10.91	0.57	1.86	0.28
Spectra_Horn2_1	44.05	0.96	12.21	17.56	0.38	11.13	10.85	0.57	2.03	0.27
Spectra_Horn2_2	44.02	1.04	12.38	17.57	0.37	10.82	10.92	0.59	1.99	0.30
Spectra_Horn2_3	44.25	1.06	12.10	17.29	0.33	11.28	10.89	0.56	1.97	0.28
Spectra_Horn3_1	43.69	1.11	12.20	17.79	0.29	11.04	10.92	0.64	1.98	0.34
Spectra_Horn3_2	44.05	1.00	12.07	17.65	0.31	11.17	10.91	0.58	1.93	0.31
Spectra_Horn3_3	44.37	1.01	11.92	17.35	0.32	11.37	10.94	0.54	1.90	0.28
Spectra_Horn4_1	44.03	0.95	12.14	17.63	0.26	11.12	10.97	0.59	1.99	0.32
Spectra_Horn4_2	44.49	0.99	11.97	17.34	0.30	11.52	10.78	0.46	1.88	0.27
Spectra_Horn4_3	44.10	0.98	12.19	17.48	0.33	11.22	10.86	0.58	1.97	0.29
Spectra_Horn5_1	44.07	0.98	12.25	17.58	0.35	11.12	10.79	0.53	2.02	0.30
Spectra_Horn5_2	43.78	1.10	12.23	17.70	0.34	11.02	10.95	0.62	1.95	0.32
Spectra_Horn5_3	43.76	1.07	12.31	17.70	0.36	10.95	10.96	0.58	1.98	0.32
Mean	44.05	1.02	12.16	17.56	0.33	11.16	10.90	0.57	1.95	0.30
std. dev (1σ)	0.23	0.05	0.12	0.19	0.03	0.19	0.06	0.04	0.05	0.02
RSD	0.53	5.20	0.99	1.07	10.52	1.70	0.53	7.15	2.49	7.34
Accuracy	-0.67	3.97	0.90	4.97	-2.14	-5.12	-0.78	-5.12	1.72	3.63
MAC std: Orthoclase	**Location:**									
rec. values	63.84		19.7					12.46	3.07	
Spectra_ortho1_1	65.51		19.35					12.09	3.05	
Spectra_ortho1_2	65.40		19.45					11.98	3.18	
Spectra_ortho1_3	65.37		19.53					12.01	3.10	
Spectra_Ortho2_1	65.29		19.58					11.98	3.15	
Spectra_Ortho2_2	65.47		19.07					12.51	2.95	
Spectra_Ortho2_3	65.33		19.53					12.00	3.14	
Spectra_Ortho3_1	65.47		19.52					11.85	3.16	
Spectra_Ortho3_2	65.53		19.13					12.29	3.05	
Spectra_Ortho3_3	65.35		19.60					11.82	3.23	
Spectra_Ortho4_1	65.55		19.30					12.08	3.07	
Spectra_Ortho4_2	65.54		19.28					12.11	3.07	
Spectra_Ortho4_3	65.33		19.56					11.99	3.13	
Spectra_Ortho5_1	65.48		19.36					12.08	3.08	
Spectra_Ortho5_2	65.50		19.38					12.21	2.91	
Spectra_Ortho5_3	65.43		19.89					11.22	3.46	
Mean	65.44		19.43					12.01	3.12	
std. dev (1σ)	0.09		0.20					0.28	0.13	
RSD	0.13		1.04					2.32	4.08	
Accuracy	2.50		-1.35					-3.58	1.48	

Table SC2 SEM data for sample AL013

No	Spectrum	Mineral	SiO2	TiO2	Al2O3	FeO	MnO	MgO	CaO	K2O	Na2O	P2O5	S	Ba	F
1	Spectra_SOI1_1	Orthoclase	64.70		18.75					15.61	0.95				
2	Spectra_SOI1_2	Orthoclase	64.42		18.91					15.75	0.92				
3	Spectra_SOI1_3	Orthoclase	64.45		18.83					15.98	0.73				
4	Spectra_SOI1_4	Plagioclase	67.04		21.18				1.36		10.42				
5	Spectra_SOI1_5	Plagioclase	67.54		20.84				1.06		10.56				
6	Spectra_SOI1_6	Magnetite				100.00									
7	Spectra_SOI2_1	Orthoclase	64.60		18.78					15.72	0.91				
8	Spectra_SOI2_2	Quartz	100.00												
9	Spectra_SOI2_3	Plagioclase	64.71		23.60					2.92	8.78				
10	Spectra_SOI2_4	Quartz	100.00												
11	Spectra_SOI2_5	Orthoclase	64.47		18.95					15.72	0.86				
12	Spectra_SOI2_6	Ankerite?	1.02			26.25	1.05	19.92	51.76						
13	Spectra_SOI2_7	Orthoclase	64.50		18.89					15.88	0.73				
14	Spectra_SOI2_8	Plagioclase	67.24		21.12				1.17		10.47				
15	Spectra_SOI3_1	Orthoclase	64.60		18.87					15.50	1.03				
16	Spectra_SOI3_2	Orthoclase	64.57		18.90					15.64	0.88				
17	Spectra_SOI3_3	Orthoclase	64.52		18.87					15.68	0.93				
18	Spectra_SOI3_4	Plagioclase	67.24		21.10				1.12		10.54				
19	Spectra_SOI3_5	Ankerite?	0.45			22.05	2.19	23.34	51.97						
20	Spectra_SOI3_6	Plagioclase	67.88		20.58				0.71		10.83				
21	Spectra_SOI3_7	Orthoclase	64.50		18.73					16.02	0.75				
22	Spectra_SOI4_1	Plagioclase	67.10		21.14				1.33		10.44				
23	Spectra_SOI4_2	Orthoclase	64.48		18.87					15.84	0.81				
24	Spectra_SOI4_3	Ankerite?	0.25			18.02	1.61	25.80	54.33						
25	Spectra_SOI4_4	Orthoclase	64.50		18.98					15.55	0.98				
26	Spectra_SOI4_5	Plagioclase	68.68		20.13						11.19				
27	Spectra_SOI4_6	Plagioclase	65.79		21.83				2.38		9.99				
28	Spectra_SOI4_7	Orthoclase	64.50		18.86					15.74	0.90				
29	Spectra_SOI5_1	Plagioclase	66.99		21.25				1.37		10.39				
30	Spectra_SOI5_2	Plagioclase	67.18		21.13				1.32		10.37				
31	Spectra_SOI5_3	Orthoclase	64.37		19.02					15.75	0.86				
32	Spectra_SOI5_4	Orthoclase	64.36		18.81					16.44	0.39				
33	Spectra_SOI5_5	Plagioclase	68.51		20.37						11.12				
34	Spectra_SOI5_6	Orthoclase	64.47		18.86					15.92	0.76				
35	Spectra_SOI5_7	Plagioclase	67.41		20.95				1.02		10.62				
36	Spectra_SOI6_1	Orthoclase	64.55		18.91					15.74	0.80				
37	Spectra_SOI6_2	Ankerite?	0.27			14.20	4.72	27.87	52.94						
38	Spectra_SOI6_3	Dolomite?	0.28			5.71	1.31	35.04	57.66						
39	Spectra_SOI6_4	Orthoclase	64.57		18.88					15.69	0.86				
40	Spectra_SOI6_5	Orthoclase	63.89		18.67					17.16	0.28				
41	Spectra_SOI6_6	Orthoclase	64.36		18.78					16.40	0.46				
42	Spectra_SOI6_7	Pyrite				55.99							44.01		
43	Spectra_SOI7_1	Plagioclase	68.72		20.08						11.20				
44	Spectra_SOI7_2	Plagioclase	67.67		20.92				0.48	0.42	10.51				
45	Spectra_SOI7_3	Plagioclase	67.58		20.82				0.68	0.26	10.65				
46	Spectra_SOI7_4	Orthoclase	64.49		18.82					16.09	0.60				
47	Spectra_SOI7_5	Orthoclase	64.63		18.83					15.55	0.99				

Table SC3 SEM data for sample AL059

No	Spectrum	Mineral	SiO2	TiO2	Al2O3	FeO	MnO	MgO	CaO	K2O	Na2O	P2O5	S	Ba	F
1	Spectra_SOI1_1	Amphibole	49.29	1.26	6.28	15.22	0.59	13.80	11.20	0.66	1.70				
2	Spectra_SOI1_2	Orthoclase	64.89		19.19					14.16	1.76				
3	Spectra_SOI1_3	Plagioclase	67.20		21.26				1.21		10.33				
4	Spectra_SOI1_4	Plagioclase	66.71		21.57				1.52		10.19				
5	Spectra_SOI1_5	Plagioclase	66.63		21.68				1.58		10.10				
6	Spectra_SOI1_6	Orthoclase	64.59		19.06					15.05	1.30				
7	Spectra_SOI1_7	Orthoclase	64.61		19.06					15.19	1.15				
8	Spectra_SOI1_8	Orthoclase	64.72		19.25					14.57	1.46				
9	Spectra_SOI2_1	Amphibole	52.88		3.84	13.92	0.74	15.50	11.61	0.35	1.15				
10	Spectra_SOI2_2	Amphibole	51.67		4.86	14.86	0.66	14.56	11.59	0.55	1.24				
11	Spectra_SOI2_3	Amphibole	52.52		4.08	14.17	0.67	15.26	11.82	0.37	1.11				
12	Spectra_SOI2_4	Plagioclase	66.77		21.56				1.47		10.19				
13	Spectra_SOI2_5	Orthoclase	64.75		19.29					14.46	1.49				
14	Spectra_SOI2_6	Plagioclase	66.51		21.76				1.66		10.07				
15	Spectra_SOI2_7	Orthoclase	64.59		19.04					15.04	1.32				
16	Spectra_SOI2_8	Orthoclase	64.40		19.12					15.52	0.96				
17	Spectra_SOI2_9	Orthoclase	64.28		19.13					15.81	0.78				
18	Spectra_SOI2_10	Plagioclase	66.73		21.52				1.60		10.15				
19	Spectra_SOI3_1	Biotite	38.67	3.28	14.36	19.53	0.69	13.59		9.88					
20	Spectra_SOI3_2	Biotite	39.06	3.12	14.14	19.72	0.56	13.41		9.99					
21	Spectra_SOI3_3	Orthoclase	63.85		19.17					14.80	1.17			1.01	
22	Spectra_SOI3_4	Orthoclase	64.16		19.26					14.12	1.72			0.75	
23	Spectra_SOI3_5	Orthoclase	63.64		19.47					14.06	1.54			1.29	
24	Spectra_SOI3_6	Plagioclase	65.64		22.13				2.32	0.39	9.52				
25	Spectra_SOI3_8	Plagioclase	64.75		22.90				2.98		9.37				
26	Spectra_SOI4_1	Titanite	30.73	37.80	1.23	2.66			27.58						
27	Spectra_SOI4_2	Pyroxene	53.54			9.39	0.66	12.80	23.60						
28	Spectra_SOI4_3	Amphibole	51.10	0.58	5.20	14.89	0.62	14.21	11.41	0.66	1.32				
29	Spectra_SOI4_4	Orthoclase	64.60		19.35					14.76	1.29				
30	Spectra_SOI4_5	Orthoclase	64.77		19.35					14.11	1.77				
31	Spectra_SOI4_6	Pyroxene	53.43			9.63	0.78	12.90	23.26						
32	Spectra_SOI4_7	Pyroxene	53.29			9.84	0.59	12.33	23.94						
33	Spectra_SOI4_8	Plagioclase	67.15		21.18				1.27		10.40				
34	Spectra_SOI4_9	Plagioclase	66.29		21.94				1.73		10.04				
35	Spectra_SOI5_1	Biotite	39.25	2.95	14.54	19.23		14.22		9.70	0.12				
36	Spectra_SOI5_2	Biotite	39.25	2.99	14.48	19.23		14.24		9.73	0.08				
37	Spectra_SOI5_3	Apatite							54.99			42.10			2.91
38	Spectra_SOI5_4	Orthoclase	63.25		19.76					13.49	1.74			1.76	
39	Spectra_SOI5_5	Orthoclase	64.10		19.17					14.07	1.49			1.17	
40	Spectra_SOI5_6	Plagioclase	65.68		22.14				2.17	0.24	9.76				
41	Spectra_SOI5_7	Orthoclase	63.20		19.61					13.40	1.66			2.13	
42	Spectra_SOI5_8	Plagioclase	64.49		23.05				3.05	0.37	9.03				
43	Spectra_SOI5_9	Biotite	39.43	3.31	14.44	19.90		13.16		9.75					
44	Spectra_SOI5_10	Plagioclase	65.27		22.47				2.50	0.24	9.53				
45	Spectra_SOI6_1	Biotite	38.82	4.23	14.16	19.48		13.08		10.09	0.15				
46	Spectra_SOI6_2	Biotite	38.90	3.04	14.45	19.60		13.80		10.09	0.13				
47	Spectra_SOI6_3	Plagioclase	64.01		23.50				3.42	0.20	8.87				
48	Spectra_SOI6_4	Orthoclase	63.38		19.60					14.45	1.15			1.42	
49	Spectra_SOI6_5	Orthoclase	63.25		19.88					13.10	1.82			1.96	
50	Spectra_SOI6_6	Plagioclase	66.12		22.06				1.90		9.91				
51	Spectra_SOI6_7	Biotite	38.91	3.68	14.54	20.43		12.88		9.56					
52	Spectra_SOI6_8	Orthoclase	63.01		19.68					13.79	1.42			2.11	
53	Spectra_SOI6_9	Plagioclase	64.87		22.84				2.85	0.22	9.21				
54	Spectra_SOI7_1	Biotite	38.56	4.06	14.36	20.32		12.56		10.15					
55	Spectra_SOI7_2	Biotite	38.84	3.30	14.55	20.00		13.24		10.07					
56	Spectra_SOI7_3	Biotite	38.65	4.75	14.23	19.82		12.62		9.94					
57	Spectra_SOI7_4	Biotite	38.97	3.77	14.40	19.64		13.09		10.13					
58	Spectra_SOI7_5	Orthoclase	63.13		19.67					13.65	1.60			1.95	
59	Spectra_SOI7_6	Orthoclase	63.51		19.80					12.94	2.05			1.71	
60	Spectra_SOI7_7	Plagioclase	65.27		22.48				2.51	0.32	9.42				
61	Spectra_SOI7_8	Orthoclase	62.93		19.47					13.82	1.58			2.20	
62	Spectra_SOI7_9	Plagioclase	65.52		22.37				2.30	0.28	9.53				
63	Spectra_SOI8_1	Pyroxene	53.57		0.90	9.21	0.59	12.75	22.35		0.63				
64	Spectra_SOI8_2	Pyroxene	53.17		0.78	9.74	0.81	12.62	22.29		0.60				
65	Spectra_SOI8_3	Pyroxene	53.02		0.77	9.37	0.73	13.22	21.95		0.95				
66	Spectra_SOI8_4	Orthoclase	64.98		19.54					13.28	2.19				
67	Spectra_SOI8_5	Orthoclase	64.85		19.57					13.66	1.92				
68	Spectra_SOI8_6	Orthoclase	64.98		19.32					13.62	2.08				
69	Spectra_SOI8_9	Plagioclase	66.68		21.49				1.49	0.22	10.12				
70	Spectra_SOI8_10	Plagioclase	65.92		22.08				2.02	0.25	9.73				
71	Spectra_SOI9_1	Biotite	39.17	3.84	14.00	20.28		12.92		9.80					
72	Spectra_SOI9_2	Orthoclase	63.79		19.35					14.08	1.64			1.14	
73	Spectra_SOI9_3	Biotite	39.46	3.12	14.50	18.90		14.07		9.76	0.19				
74	Spectra_SOI9_4	Amphibole	50.77		5.51	15.42	0.70	14.01	11.71	0.57	1.32				
75	Spectra_SOI9_5	Biotite	39.39	3.12	14.22	19.25		14.09		9.81	0.13				
76	Spectra_SOI9_6	Orthoclase	63.16		19.31					15.15	0.91			1.48	
77	Spectra_SOI9_7	Plagioclase	65.99		21.95				1.97	0.34	9.76				
78	Spectra_SOI9_8	Orthoclase	64.03		19.38					13.87	1.57			1.16	
79	Spectra_SOI9_9	Plagioclase	65.67		22.34				2.28		9.71				

Table SC4 SEM data for sample AL063

No	Spectrum	Mineral	SiO2	TiO2	Al2O3	FeO	MnO	MgO	CaO	K2O	Na2O	P2O5	S	Ba	F
1	Spectra_SOI1_1	Biotite	39.11	2.90	14.90	18.31		14.39		10.30	0.10				
2	Spectra_SOI1_2	Plagioclase	65.52		22.20				2.35	0.22	9.72				
3	Spectra_SOI1_3	Orthoclase	64.52		18.99					15.55	0.93				
4	Spectra_SOI1_4	Biotite	40.66	2.16	13.84	17.51		15.51		10.33					
5	Spectra_SOI1_5	Biotite	40.87	2.17	13.76	17.41		15.53		10.26					
6	Spectra_SOI1_6	Orthoclase	64.63		19.03					14.91	1.44				
7	Spectra_SOI1_7	Quartz	100.00												
8	Spectra_SOI1_8	Biotite	40.23	2.52	13.65	18.44		14.75		10.41					
9	Spectra_SOI1_9	Biotite	40.36	2.05	13.90	17.73		15.82		10.14					
10	Spectra_SOI1_10	Orthoclase	64.57		18.96					15.30	1.17				
11	Spectra_SOI1_11	Plagioclase	66.18		21.66				1.85	0.27	10.04				
12	Spectra_SOI2_1	Amphibole	48.98	0.80	6.20	16.02	0.64	13.49	11.41	0.74	1.71				
13	Spectra_SOI2_2	Amphibole	50.89	0.81	4.93	14.52	0.70	14.68	11.29	0.51	1.66				
14	Spectra_SOI2_3	Orthoclase	64.66		19.09					14.77	1.48				
15	Spectra_SOI2_4	Plagioclase	66.41		21.68				1.72		10.19				
16	Spectra_SOI2_5	Orthoclase	64.62		19.10					14.99	1.29				
17	Spectra_SOI2_6	Orthoclase	64.84		18.92					14.80	1.44				
18	Spectra_SOI2_7	Amphibole	50.95		5.67	15.06		14.05	11.93	0.67	1.66				
19	Spectra_SOI2_8	Amphibole	48.89	0.79	6.33	15.95	0.75	13.50	11.30	0.74	1.75				
20	Spectra_SOI2_9	Orthoclase	64.67		19.04					14.90	1.39				
21	Spectra_SOI2_10	Plagioclase	65.53		22.30				2.49		9.68				
22	Spectra_SOI3_1	Plagioclase	66.57		21.57				1.71		10.15				
23	Spectra_SOI3_2	Orthoclase	64.63		19.06					15.18	1.14				
24	Spectra_SOI3_3	Biotite	40.19	2.37	13.71	18.02		15.19		10.52					
25	Spectra_SOI3_4	Biotite	40.59	2.39	13.73	17.89		15.07		10.33					
26	Spectra_SOI3_5	Biotite	40.51	2.59	13.69	17.25		15.33		10.63					
27	Spectra_SOI3_6	Biotite	40.49	2.07	13.66	17.35		15.79		10.63					
28	Spectra_SOI3_7	Biotite	40.48	2.26	13.60	17.61		15.60		10.45					
29	Spectra_SOI3_8	Orthoclase	64.44		19.18					15.18	1.20				
30	Spectra_SOI3_9	Plagioclase	66.66		21.51				1.68		10.15				
31	Spectra_SOI4_1	Biotite	39.92	2.38	13.79	17.48		15.09	1.84	9.49					
32	Spectra_SOI4_2	Biotite	40.35	2.33	13.64	18.09		15.23		10.36					
33	Spectra_SOI4_3	Orthoclase	64.76		18.98					14.53	1.72				
34	Spectra_SOI4_4	Orthoclase	66.11		19.39					9.57	4.93				
35	Spectra_SOI4_5	Plagioclase	67.18		19.77					4.60	8.46				
36	Spectra_SOI4_6	Plagioclase	66.63		21.57				1.69		10.11				
37	Spectra_SOI4_7	Orthoclase	66.75		20.01					7.25	5.99				
38	Spectra_SOI5_1	Biotite	40.24	2.31	13.66	18.03		15.25		10.51					
39	Spectra_SOI5_2	Biotite	40.91	2.13	13.68	16.55		16.14		10.59					
40	Spectra_SOI5_3	Biotite	40.25	2.28	13.61	18.22		15.22		10.41					
41	Spectra_SOI5_4	Orthoclase	64.82		19.00					14.48	1.71				
42	Spectra_SOI5_5	Orthoclase	64.81		19.06					14.44	1.69				
43	Spectra_SOI5_6	Amphibole	49.45	0.95	6.15	15.77		13.81	11.26	0.75	1.87				
44	Spectra_SOI5_7	Orthoclase	64.51		18.95					15.59	0.96				
45	Spectra_SOI5_8	Plagioclase	66.60		21.64				1.76		10.00				
46	Spectra_SOI5_9	Plagioclase	66.91		21.42				1.45		10.23				
47	Spectra_SOI6_1	Orthoclase	64.12		19.52					15.28	1.08				
48	Spectra_SOI6_2	Plagioclase	66.46		21.69				1.76		10.09				
49	Spectra_SOI6_3	Orthoclase	64.75		19.04					14.59	1.62				
50	Spectra_SOI6_4	Orthoclase	64.59		19.30					14.55	1.56				
51	Spectra_SOI6_5	Biotite	40.37	2.30	13.62	18.05		15.28		10.38					
52	Spectra_SOI6_6	Biotite	40.64	2.21	13.55	17.60		15.54		10.46					
53	Spectra_SOI6_7	Orthoclase	64.75		19.07					14.64	1.54				
54	Spectra_SOI6_8	Plagioclase	65.40		22.46				2.67		9.47				
55	Spectra_SOI6_9	Plagioclase	66.61		21.46				1.67		10.26				

Table SC5 SEM data for sample AL074

No	Spectrum	Mineral	SiO2	TiO2	Al2O3	FeO	MnO	MgO	CaO	K2O	Na2O	P2O5	S	Ba	F
1	Spectra_SOI1_1	Plagioclase	64.17		23.43				3.14	0.43	8.83				
2	Spectra_SOI1_2	Plagioclase	63.68		23.54				3.70	0.19	8.90				
3	Spectra_SOI1_3	Plagioclase	63.07		23.93				4.20	0.20	8.60				
4	Spectra_SOI1_4	Biotite	38.86	3.64	14.92	18.37		14.21		10.01					
5	Spectra_SOI1_5	Amphibole	46.88	2.19	8.54	14.57		13.32	11.64	0.81	2.05				
6	Spectra_SOI1_6	Amphibole	45.33	1.49	9.99	16.78		11.90	11.71	1.06	1.74				
7	Spectra_SOI1_7	Biotite	37.29	2.32	16.52	20.60		15.73		7.54					
8	Spectra_SOI2_1	Plagioclase	63.21		23.83				3.98	0.35	8.63				
9	Spectra_SOI2_2	Plagioclase	64.90		22.74				2.87		9.50				
10	Spectra_SOI2_3	Amphibole	43.21	2.79	11.12	16.19		11.63	11.64	1.01	2.42				
11	Spectra_SOI2_4	Amphibole	46.49	2.10	8.72	15.27		13.08	11.73	0.88	1.74				
12	Spectra_SOI2_5	Biotite	39.19	3.56	15.01	17.40		14.41		9.86	0.56				
13	Spectra_SOI2_6	Amphibole	45.73	2.30	9.23	15.20		12.83	11.58	0.97	2.16				
14	Spectra_SOI2_7	Amphibole	48.47	1.80	7.43	13.88		14.20	11.88	0.67	1.67				
15	Spectra_SOI2_8	Biotite	40.49	2.55	14.72	18.29		15.01		8.94					
16	Spectra_SOI3_1	Plagioclase	63.48		23.84				4.01		8.67				
17	Spectra_SOI3_2	Plagioclase	63.60		23.81				3.91		8.69				
18	Spectra_SOI3_3	Plagioclase	64.83		22.91				2.90		9.35				
19	Spectra_SOI3_4	Biotite	39.21	3.12	14.86	17.97		14.70		10.14					
20	Spectra_SOI3_5	Biotite	39.29	3.46	14.69	18.06		14.47		10.02					
21	Spectra_SOI3_6	Amphibole	51.65	0.87	5.30	12.71		15.66	12.01	0.45	1.34				
22	Spectra_SOI3_7	Biotite	39.33	3.50	14.86	17.94		14.40		9.97					
23	Spectra_SOI3_8	Amphibole	45.14	2.35	9.80	15.50		12.56	11.59	0.99	2.08				
24	Spectra_SOI3_9	Biotite	39.30	2.97	14.77	17.94		14.83		10.18					
25	Spectra_SOI4_1	Biotite	39.18	3.89	14.47	17.86		14.45		10.14					
26	Spectra_SOI4_2	Amphibole	47.42	1.85	7.74	14.54		13.73	12.19	0.77	1.76				
27	Spectra_SOI4_3	Amphibole	45.45	2.12	9.51	15.70		12.65	11.80	0.94	1.83				
28	Spectra_SOI4_4	Biotite	39.14	2.92	14.81	18.10		14.86		10.17					
29	Spectra_SOI4_5	Amphibole	48.08	1.80	7.58	14.46		13.84	11.66	0.74	1.84				
30	Spectra_SOI4_6	Plagioclase	63.22		24.22				4.49	0.30	7.77				
31	Spectra_SOI4_7	Plagioclase	64.23		23.19				3.34	0.28	8.95				
32	Spectra_SOI5_1	Plagioclase	64.85		22.88				2.96		9.31				
33	Spectra_SOI5_2	Plagioclase	63.41		23.89				3.94		8.77				
34	Spectra_SOI5_3	Plagioclase	64.82		22.86				3.01		9.31				
35	Spectra_SOI5_4	Biotite	39.06	3.22	15.01	18.03		14.66		10.03					
36	Spectra_SOI5_5	Biotite	39.12	3.35	14.82	18.00		14.59		10.11					
37	Spectra_SOI5_6	Biotite	39.20	2.95	14.88	17.91		14.94		10.12					
38	Spectra_SOI5_7	Biotite	39.54	2.79	14.98	17.57		14.90		10.21					
39	Spectra_SOI6_1	Biotite	39.13	3.21	14.75	18.61		14.12		10.19					
40	Spectra_SOI6_2	Plagioclase	62.45		24.50				4.85		8.20				
41	Spectra_SOI6_3	Amphibole	46.25	2.06	9.22	14.66		13.16	11.90	0.84	1.91				
42	Spectra_SOI6_4	Biotite	38.94	2.93	15.02	18.33		14.82		9.97					
43	Spectra_SOI6_5	Amphibole	46.54	1.86	8.74	15.70		12.74	11.80	0.90	1.72				

Table SC6 SEM data for sample AL092

No	Spectrum	Mineral	SiO2	TiO2	Al2O3	FeO	MnO	MgO	CaO	K2O	Na2O	P2O5	S	Ba	F
1	Spectra_SOI1_1	Biotite	39.45	3.95	14.02	18.14		14.22		10.22					
2	Spectra_SOI1_2	Biotite	39.61	3.75	14.03	18.15		14.44		10.03					
3	Spectra_SOI1_3	Plagioclase	63.77		24.16				2.41	0.84	8.83				
4	Spectra_SOI1_4	Amphibole	50.64	1.22	5.64	13.63		15.15	11.45	0.64	1.63				
5	Spectra_SOI1_5	Biotite	39.35	4.01	13.93	18.59		13.96		10.16					
6	Spectra_SOI1_6	Biotite	39.21	4.01	13.94	19.07		13.91		9.86					
7	Spectra_SOI1_7	Plagioclase	64.57		22.99				2.88	0.37	9.20				
8	Spectra_SOI1_8	Orthoclase	39.40	4.05	13.93	18.51		13.90		10.20					
9	Spectra_SOI1_9	Amphibole	51.27	0.92	5.27	13.63		15.41	11.41	0.49	1.60				
10	Spectra_SOI1_10	Amphibole	52.64	0.62	4.37	12.82		16.17	11.66	0.45	1.27				
11	Spectra_SOI2_1	Amphibole	50.82	1.00	5.45	13.83		15.20	11.59	0.54	1.55				
12	Spectra_SOI2_2	Biotite	39.19	4.48	13.95	18.78		13.48		10.12					
13	Spectra_SOI2_3	Biotite	39.35	4.34	13.94	18.57		13.62		10.18					
14	Spectra_SOI2_4	Biotite	39.35	3.53	13.97	19.21		13.75		10.20					
15	Spectra_SOI2_5	Amphibole	50.98	1.08	5.51	13.60		15.29	11.53	0.51	1.51				
16	Spectra_SOI2_6	Orthoclase	64.41		19.83					14.23	1.54				
17	Spectra_SOI2_7	Plagioclase	64.55		23.20				3.16		9.09				
18	Spectra_SOI2_8	Plagioclase	66.43		21.84				1.69		10.04				
19	Spectra_SOI2_9	Orthoclase	64.61		19.77					13.87	1.75				
20	Spectra_SOI2_10	Plagioclase	67.61		21.13				0.55		10.71				
21	Spectra_SOI3_1	Amphibole	54.47		3.53	11.49		17.05	12.19	0.28	1.00				
22	Spectra_SOI3_2	Orthoclase	64.31		19.31					15.31	1.06				
23	Spectra_SOI3_3	Biotite	39.73	3.39	14.12	18.46		14.74		9.56					
24	Spectra_SOI3_4	Plagioclase	66.09		22.06				2.07		9.78				
25	Spectra_SOI3_5	Orthoclase	64.58		19.28					14.93	1.21				
26	Spectra_SOI3_6	Biotite	39.69	3.59	13.98	17.62		14.78		10.35					
27	Spectra_SOI3_7	Orthoclase	64.31		19.47					15.28	0.94				
28	Spectra_SOI3_8	Plagioclase	66.48		21.71				1.71		10.10				
29	Spectra_SOI3_9	Biotite	39.78	2.96	14.09	18.14		14.82		10.20					
30	Spectra_SOI3_10	Orthoclase	64.65		19.20					14.70	1.45				
31	Spectra_SOI4_1	Amphibole?	56.19		2.17	11.39		17.59	12.12		0.54				
32	Spectra_SOI4_2	Biotite	39.74	3.43	14.14	17.80		14.67		10.23					
33	Spectra_SOI4_3	Plagioclase	65.31		22.55				2.54		9.60				
34	Spectra_SOI4_4	Orthoclase	64.28		19.29					15.56	0.87				
35	Spectra_SOI4_5	Biotite	39.95	3.10	14.07	17.57		15.05		10.26					
36	Spectra_SOI4_6	Orthoclase	64.39		19.32					15.20	1.10				
37	Spectra_SOI4_7	Plagioclase	66.33		21.85				1.80		10.02				
38	Spectra_SOI4_8	Amphibole	50.55	1.12	5.75	13.88		15.01	11.46	0.59	1.63				
39	Spectra_SOI4_9	Plagioclase	65.85		22.12				2.20		9.84				
40	Spectra_SOI4_10	Orthoclase	64.25		19.40					15.41	0.94				
41	Spectra_SOI4_11	Amphibole	51.63	0.81	5.12	13.29		15.50	11.80	0.53	1.31				
42	Spectra_SOI5_1	Biotite	40.25	3.63	14.12	17.68		14.41		9.91					
43	Spectra_SOI5_2	Amphibole	54.19		3.62	12.21		16.75	11.75	0.29	1.18				
44	Spectra_SOI5_3	Amphibole	52.79		4.53	13.18		15.93	11.95	0.41	1.22				
45	Spectra_SOI5_4	Orthoclase	64.31		19.29					15.44	0.96				
46	Spectra_SOI5_5	Plagioclase	65.49		22.38				2.33		9.80				
47	Spectra_SOI5_6	Orthoclase	64.37		19.28					15.35	1.00				
48	Spectra_SOI5_7	Amphibole	55.34		3.07	11.97		16.76	12.21		0.65				
49	Spectra_SOI5_8	Plagioclase	66.09		22.00				2.10		9.81				
50	Spectra_SOI5_9	Plagioclase	66.39		21.73				1.80		10.08				
51	Spectra_SOI5_10	Amphibole	53.55		3.88	12.37		16.78	11.88	0.34	1.21				
52	Spectra_SOI5_11	Orthoclase	64.38		19.38					15.14	1.10				
53	Spectra_SOI5_12	Plagioclase	66.42		21.68				1.79		10.11				
54	Spectra_SOI6_1	Biotite	39.55	3.62	14.10	17.99		14.35		10.39					
55	Spectra_SOI6_2	Orthoclase	64.43		19.27					15.27	1.03				
56	Spectra_SOI6_3	Plagioclase	65.16		22.65				2.60		9.60				
57	Spectra_SOI6_4	Plagioclase	64.97		22.70				2.86		9.47				
58	Spectra_SOI6_5	Biotite	40.05	3.03	14.16	17.59		14.91		10.26					
59	Spectra_SOI6_6	Orthoclase	64.25		19.33					15.43	1.00				
60	Spectra_SOI6_7	Plagioclase	66.03		22.06				2.10		9.81				
61	Spectra_SOI6_8	Orthoclase	64.40		19.27					15.30	1.02				
62	Spectra_SOI6_9	Amphibole	52.60	0.70	4.69	12.45		16.05	11.73	0.46	1.33				
63	Spectra_SOI6_10	Biotite	39.66	3.86	13.95	17.73		14.54		10.26					
64	Spectra_SOI6_11	Biotite	39.89	3.02	14.20	17.88		14.95		10.06					
65	Spectra_SOI6_12	Amphibole	53.77		4.11	13.09		16.10	11.97		0.95				

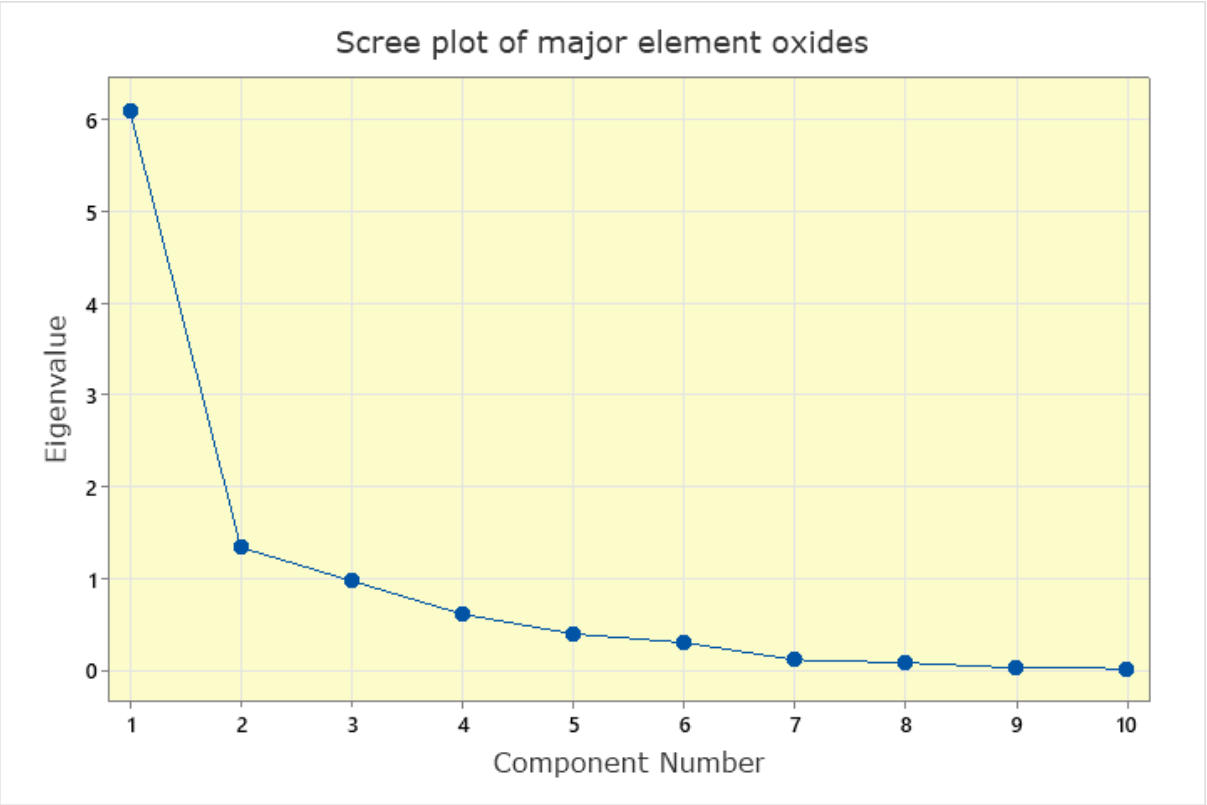
Table SD1 Crystal-liquid separation models for the Ratagain Complex

		SiO2	Al2O3	FeO	MnO	MgO	CaO	Na2O	K2O
AL92 - AL59	Daughter	63.67	18.33	2.77	0.06	0.91	2.27	5.17	6.83
Monzonite to monzonite	Parent	59.29	15.04	5.99	0.09	5.72	5.1	4.54	4.24
42% amp/plag/pyx	Calculated	60.27	14.44	6.92	0.07	4.58	4.99	4.64	4.02
Sum of weighted residuals 2.48	Difference	-0.39	0.3	-0.93	0.03	1.14	0.11	-0.1	0.22
AL92 - AL63	Daughter	65.82	16.12	2.7	0	1.84	2.7	4.66	6.16
Monzonite to qtz-monzonite	Parent	59.29	15.04	5.99	0.09	5.72	5.1	4.54	4.24
42% amp/plag/biot	Calculated	61.7	13.68	6.72	0	4.97	4.54	4.48	3.75
Sum of weighted residuals 3.05	Difference	-0.97	0.68	-0.73	0.09	0.75	0.56	0.06	0.49
AL59 - AL13	Daughter	73.02	14.94	0.83	0.06	0.22	0.99	5.3	4.67
Monzonite to granite	Parent	63.67	18.33	2.77	0	0.91	2.27	5.17	6.83
84% Kspar/plag/amp	Calculated	63.71	18.67	2.84	0.06	1.01	1.94	5.07	6.74
Sum of weighted residuals 0.17	Difference	-0.02	-0.17	-0.07	0.06	-0.1	0.33	0.1	0.09
AL59 - AL73	Daughter	73.15	13.05	2.78	0.04	0.87	0.77	2.2	7.15
Monzonite to granite	Parent	63.67	18.33	2.77	0.06	0.91	2.27	5.17	6.83
88% Kspar/plag/amp	Calculated	63.65	18.83	2.84	0.01	1.01	1.93	5.02	6.71
Sum of weighted residuals 0.23	Difference	0.01	-0.25	-0.07	0.06	-0.1	0.34	0.15	0.12
AL63 - AL13	Daughter	73.02	14.94	0.83	0.02	0.22	0.99	5.3	4.67
Qtz-monzonite to granite	Parent	65.82	16.12	2.7	0	1.84	2.7	4.66	6.16
52% Kspar/plag/amp	Calculated	66.03	16.7	3.3	0.01	1.15	1.9	4.75	6.12
Sum of weighted residuals 1.57	Difference	-0.09	-0.29	-0.59	-0.01	0.69	0.8	-0.09	0.04
AL63 - AL73	Daughter	73.15	13.05	2.78	0.04	0.87	0.77	2.2	7.15
Qtz-monzonite to granite	Parent	65.82	16.12	2.7	0	1.84	2.7	4.66	6.16
63% Kspar/plag/amp	Calculated	65.95	17.12	3.3	0.02	1.14	1.85	4.56	6.02
Sum of weighted residuals 1.84	Difference	-0.05	-0.5	-0.59	-0.02	0.7	0.84	0.1	0.14

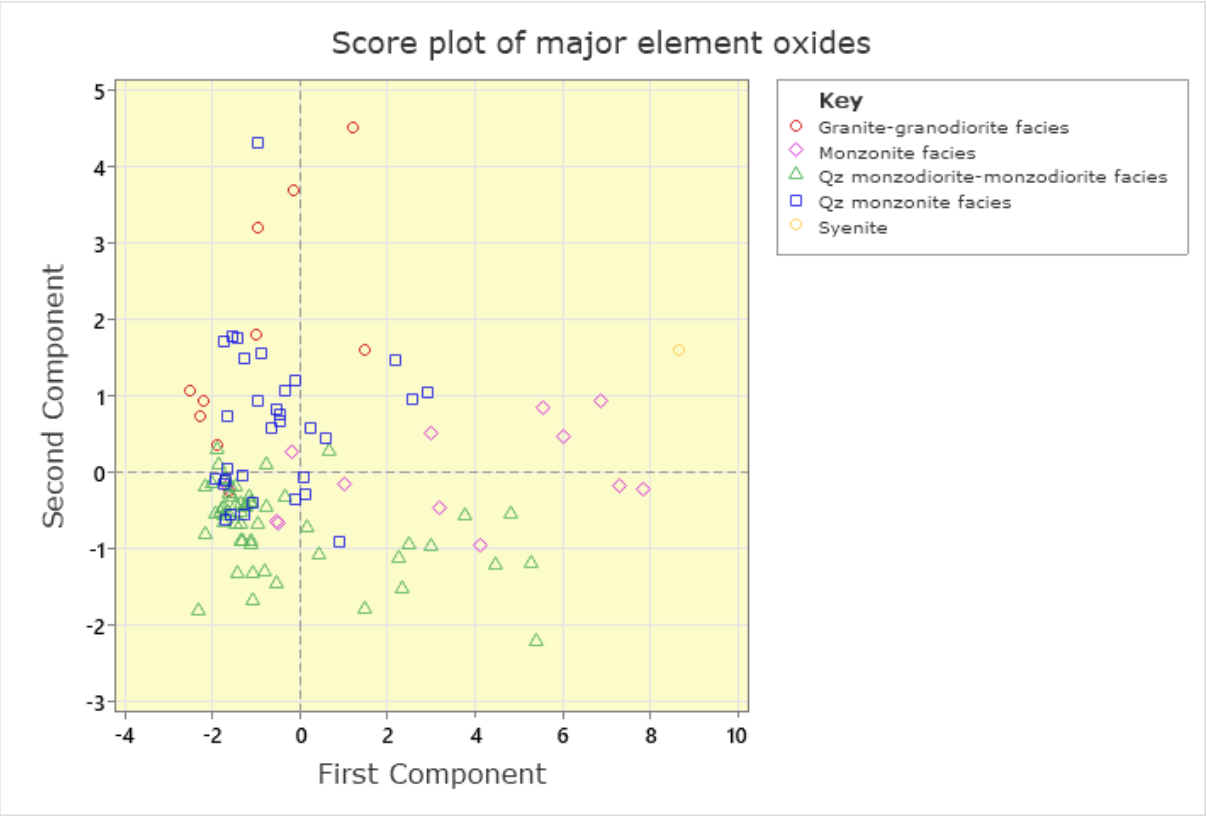
Table SD2 PCA results for the Ratagain Complex

Principal component	PC1	PC2	PC3	PC4	PC5	PC6	PC7	PC8	PC9	PC10
Eigenvalue	6.0864	1.3424	0.9792	0.6172	0.4018	0.3079	0.1199	0.0885	0.032	0.0249
Proportion in total variance	0.609	0.134	0.098	0.062	0.04	0.031	0.012	0.009	0.003	0.002
Cumulative proportion	0.609	0.743	0.841	0.903	0.943	0.973	0.985	0.994	0.998	1
Eigenvector (loading)										
SiO2	-0.357	0.27	-0.245	0.204	-0.127	-0.235	-0.116	-0.041	-0.162	-0.765
TiO2	0.362	-0.024	0.168	-0.169	-0.049	-0.627	0.478	0.028	-0.428	-0.059
Al2O3	-0.267	-0.429	0.537	0.005	0.157	0.04	0.344	0.165	0.378	-0.376
Fe2O3	0.291	0.007	0.043	0.746	0.58	-0.111	-0.055	-0.073	-0.002	0.002
MnO	0.292	-0.26	0.125	0.478	-0.759	0.028	-0.103	0.102	0.064	-0.026
MgO	0.378	-0.097	-0.098	-0.203	0.179	0.167	-0.29	0.745	-0.134	-0.282
CaO	0.367	-0.15	-0.06	-0.108	0.033	0.584	0.219	-0.483	-0.257	-0.371
Na2O	-0.296	-0.53	0.217	-0.018	0.082	-0.078	-0.468	-0.149	-0.568	0.086
K2O	-0.012	0.602	0.708	0.036	-0.059	0.234	-0.119	0.061	-0.245	0.004
P2O5	0.366	0.016	0.212	-0.3	0.031	-0.327	-0.511	-0.374	0.421	-0.21

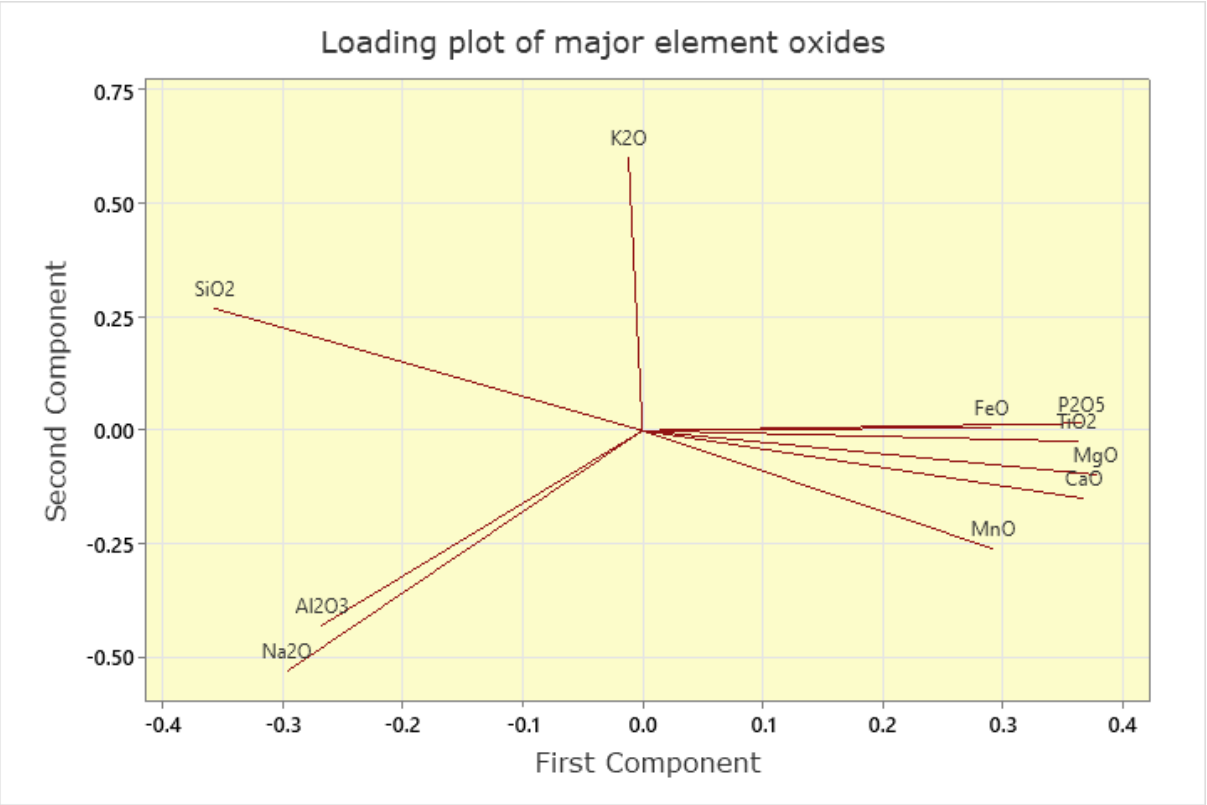
PCA scree plot for samples from the Ratagain Complex



PCA score plot for samples from the Ratagain Complex



PCA loading plot for samples from the Ratagain Complex



APPENDIX 3

Supplementary materials for Chapter 4

Full reading list

AdvanceHE. 2019. *Equality in Higher Education: Staff Statistical Report 2019*. Available from: https://www.advance-he.ac.uk/knowledge-hub/equality-higher-education-statistical-report-2019.

AdvanceHE. 2019. *Equality in Higher Education: Students Statistical Statistical Report 2019*. Available from: https://www.advance-he.ac.uk/knowledge-hub/equality-higher-education-statistical-report-2019.

Ali, H. 2021. Call for a robust anti-racism plan for the geosciences. *Change.org*. Available from: https://www.change.org/p/geoscientists-call-for-a-robust-anti-racism-plan-for-the-geosciences

Allen-Ramdial, S.A.A. & Campbell, A.G. 2014. Reimagining the pipeline: Advancing STEM diversity, persistence, and success. *BioScience*, **64**(7), 612–618. Available from: https://doi.org/10.1093/biosci/biu076

Anadu, J., Ali, H. & Jackson, C. 2020. Ten steps to protect BIPOC scholars in the field. *Eos*, **101**, 30– 31. Available from: https://doi.org/10.1029/2020EO150525

Bernard, R.E. & Cooperdock, E.H.G. 2018. No progress on diversity in 40 years. *Nature Geoscience*, **11**, 292– 295. Available from: https://doi.org/10.1038/s41561-018-0116-6

Boliver, V. 2015. Why are British ethnic minorities less likely to be offered places at highly selective universities? In: Alexander CA, J (ed.) *Aiming Higher: Race, Inequality and Diversity in the Academy* (pp. 15–18). London: Runnymede Trust.

Bracken, L. & Mawdsley, E. 2004. 'Muddy glee': Rounding out the picture of women and physical geography fieldwork. *Area*, **36**(3), 280– 286. Available from: https://doi.org/10.1111/j.0004-0894.2004.00225.x

Cranfield Trust (2020, Jan 24). Cranfield Trust and Black2Nature: Celebrations for Birdgirl [Blog post]. Available from: https://www.cranfieldtrust.org/articles/33-cranfield-trust-and-black2nature-celebrations-for-birdgirl

Crenshaw, K. 1989. Demarginalizing the Intersection of Race and Sex: A Black Feminist Critique of Antidiscrimination Doctrine, Feminist Theory and Antiracist Politics. *University of Chicago Legal Forum*, **1989**(1), 139-167.Available from: http://chicagounbound.uchicago.edu/uclf/vol1989/iss1/8

Datta, R.K. 2018. Rethinking environmental science education from indigenous knowledge perspectives: an experience with a Dene First Nation community. *Environmental Education Research*, **24**(1), 50–66. Available from: https://doi.org/10.1080/13504622.2016.1219980

DEFRA 2019. *Landscapes Review*. Available from: https://assets.publishing.service.gov.uk/government/uploads/system/uploads/attachment_data/file/833726/landscapes-review-final-report.pdf

Drayton, R., 2000. *Nature's Government: Science, Imperial Britain, and the "Improvement" of the World*. London: Yale University Press.

Di Capua, G., Peppoloni, S. & Bobrowsky, P.T. 2017. The Cape Town statement on geoethics. *Annals of Geophysics*, **60**, 1– 6. Available from: https://doi.org/10.4401/ag-7553

Dutt, K., 2021. Addressing racism through ownership: *Nature Geoscience*, **14**, 58–58. Available from: https://doi/10.1038/s41561-021-00688-2.

Dutt, K. 2020. Race and racism in the geosciences. *Nature Geoscience*, **13**, 2– 3. https://doi.org/10.1038/s41561-019-0519-z

Dutt, K. 2019. Promoting racial diversity in geoscience through transparency. *Eos*, **100**. Available from: https://doi.org/10.1029/2019EO136977

Esri UK (2021, February 23), Scholarships for Black and mixed Black heritage students [Blog post]. Available from: https://storymaps.arcgis.com/stories/040fb424ceb247d28ea4736133d07c44.

European Commission. 2017. *Analysis and comparative review of equality data collection practices in the European Union: Data collection in the field of ethnicity*. Available from: https://data.europa.eu/doi/10.2838/447194

Fazackerley, A. (2019, September 12). "Look at how white the academy is": why BAME students aren't doing PhDs. *The Guardian*. Available from: https://www.theguardian.com/education/2019/sep/12/look-at-how-white-the-academy-is-why-bame-students-arent-doing-phds?CMP=Share_iOSApp_Other.

Fernando, B., & Antell, G. 2020. *Recommendations for improving racial equality, diversity, and inclusion in the Department of Earth Sciences, University of Oxford*. Available from: https://www.earth.ox.ac.uk/wp-content/uploads/2020/06/BAME-EDI-Report.pdf

Gewin, V. 2020. The time tax put on scientists of colour. Nature, **583**, 479–481 Nature 583, 479-481. Available from: https://doi.org/10.1038/d41586-020-01920-6

Giles, S., Bond, A., Britton, B., Ford, H., Greene, S., Grieve, S., Jackson, C., Lengger, S., Littler, K., & Pancost, R., 2020. Open letter concerning CDT and DTP student recruitment across the UK [Open letter] Available from: https://docs.google.com/document/d/1EInAKFl7px2DxYv-sAZxVOyTjkm-AE29CzFFnjxw6hg/edit.

Giles, S., Jackson, C., & Stephen, N. 2020. Barriers to fieldwork in undergraduate geoscience degrees. *Nature Reviews Earth & Environment*, **1**, 77–78. Available from: https://doi.org/10.1038/s43017-020-0022-5.

Gill, J.C., 2017, Geology and the Sustainable Development Goals. *Episodes*, **40**(1), 70–76, Available from: https://doi/10.18814/epiiugs/2017/v40i1/017010

Gillborn, B.D. 2005. Education policy as an act of white supremacy: Whiteness, critical race theory and education reform. *Journal of Education Policy*, **20**(4), 485–505, Available from: https://doi.org/10.1080/02680930500132346

Gillborn, D., Warmington, P. & Demack, S., 2018, QuantCrit: education, policy, 'Big Data' and principles for a critical race theory of statistics. *Race Ethnicity and Education*, **21**(2),158–179, Available from: https://doi.org/10.1080/13613324.2017.1377417

Goldberg, E. (2019, December 23). Earth Science Has a Whiteness Problem. *The New York Times*. Available from: https://www.nytimes.com/2019/12/23/science/earth-science-diversity-education.html

Gormally, A. 2019. The role of sustainability in HE and the GEES disciplines; recommendations for future practice. *Journal of Geography in Higher Education*, **43**(4),599–608. Available from: https://doi.org/10.1080/03098265.2019.1660627

GOV.UK, 2018. *Population of England and Wales*. Available from: https://www.ethnicity-facts-figures.service.gov.uk/uk-population-by-ethnicity/national-and-regional-populations/population-of-england-and-wales/latest

GOV.UK, 2018. *Regional ethnic diversity*. Available from: https://www.ethnicity-facts-figures.service.gov.uk/uk-population-by-ethnicity/national-and-regional-populations/regional-ethnic-diversity/latest

Guertin, L. (2019, December 8). Want to be more inclusive? Stop making geology conferences about the beer. [Blog post]. *AGU Blogosphere*. Available from: https://blogs.agu.org/geoedtrek/2019/12/08/inclusive-agu-conferences/

Hide, L. (2020, August 26). *Working to Decolonise the Sedgwick Museum: Geoscience in Context Seminar Series* [YouTube]. Available from: https://www.youtube.com/watch?v=yE1tGPhufKQ

Higher Education Statistics Authority. 2019. *Higher Education Staff Data*. Available from: https://www.hesa.ac.uk/data-and-analysis/staff.

Higher Education Statistics Authority. 2019. *Personal Characteristics by Subject of Study*. Available from: https://www.hesa.ac.uk/data-and-analysis/students/what-study/characteristics.

Higher Education Statistics Authority. 2021. *Publications archive*. Available from: https://www.hesa.ac.uk/data-and-analysis/publications.

Inge, S. (2020, June 11). Scale of Oxford's 'white bias' laid bare by internal report. *Research Professional News*. Available from: https://www.researchprofessionalnews.com/rr-he-student-trends-2020-6-scale-of-oxford-s-white-bias-laid-bare-by-internal-report/

Laland, K.N., 2020. Racism in academia, and why the 'little things' matter. *Nature*, **584**, 653–654. Available from: https://doi.org/10.1038/d41586-020-02471-6

Lawrence, A. (2020, October 19). Six simple steps to make fieldwork more accessible and inclusive [Blog post]. *Geoscience for the Future*. Available from: https://geoscienceforthefuture.com/six-simple-steps-to-make-fieldwork-more-accessible-and-inclusive/

Leading Routes. 2019. *The Broken Pipeline*. Available from: https://leadingroutes.org/mdocs-posts/the-broken-pipeline-barriers-to-black-students-accessing-research-council-funding.

Marín-Spiotta, E., Barnes, R.T., Berhe, A.A., Hastings, M.G., Mattheis, A., Schneider, B., & Williams, B.M. 2020. Hostile climates are barriers to diversifying the geosciences. *Advances in Geosciences*, **53**, 117–127. Available from: https://doi.org/10.5194/adgeo-53-117-2020

Mora, G., 2013. The need for geologists in sustainable development. *GSA Today*, **23**(12), 36–37. Available from: https://doi.org/10.1130/GSATG185GW.1

National Union of Students, and Universities UK, 2019. *Black, Asian and Minority Ethnic Student Attainment at Universities: #Closing the Gap*. Available from: https://www.universitiesuk.ac.uk/sites/default/files/field/downloads/2021-07/bame-student-attainment.pdf

Office for National Statistics. 2020. *Child poverty and education outcomes by ethnicity*. Available from: https://www.ons.gov.uk/economy/nationalaccounts/uksectoraccounts/compendium/economicreview/february2020/childpovertyandeducationoutcomesbyethnicity#child-poverty-and-ethnicity

Office for National Statistics. 2018. *Regional Ethnic Diversity*. Available from: https://www.ethnicity-facts-figures.service.gov.uk/uk-population-by-ethnicity/national-and-regional-populations/regional-ethnic-diversity/latest

Office for National Statistics. 2011. *Population of England and Wales*. Available from: https://www.ethnicity-facts-figures.service.gov.uk/uk-population-by-ethnicity/national-and-regional-populations/population-of-england-and-wales/latest

Oregon State University (n.d.) *Increasing Diversity in Earth Sciences scheme (IDES).* Available from: https://ides.science.oregonstate.edu/

Peters, M.A. 2015. Why is My Curriculum White? *Educational Philosophy and Theory*, **47**(7), 641-646. Available from: https://doi.org/10.1080/00131857.2015.1037227

Pickrell, J. (2020, March 11). Scientists push against barriers to diversity in the field sciences. *Science*, **374**. Available from: https://doi.org/10.1126/science.caredit.abb6887

Pilkington, A. 2013. The interacting dynamics of institutional racism in higher education. *Race Ethnicity and Education*, **16**(2), 225–245. Available from: https://doi.org/10.1080/13613324.2011.646255

Quardokus Fisher, K., Kaufman, E., Calagna, O., Myles, L.T., Brinkworth, C., Simmons, D.R. & Dixon, P.G. 2019. Developing scientists as champions of diversity to transform the geosciences. *Journal of Geoscience Education*, **67**(4),459–471. Available from: https://doi.org/10.1080/10899995.2019.1618692

Reano, D. 2020. Using Indigenous Research Frameworks in the Multiple Contexts of Research, Teaching, Mentoring, and Leading. *The Qualitative Report*, **25**(11), 3902-3926. Available from: https://doi.org/10.46743/2160-3715/2020.4317

Sevilla, E. (2020, July 22) *Addressing inequalities in the Volcanic and Magmatic Studies Group Community: A series of virtual discussion meetings- Panel 1* [YouTube]. Available from: https://www.youtube.com/watch?v=tjulJcVndqY

Stafford, R.A. 1984. Geological Surveys, Mineral Discoveries, and British Expansion, 1835–71. *The Journal of Imperial and Commonwealth History*, **12**(3), 5–32. Available from: https://doi.org/10.1080/03086538408582669.

Stevenson, J., O'Mahony, J., Khan, O., Ghaffar, F. & Stiell, B. 2019. *Understanding and overcoming the challenges of targeting students from under-represented and disadvantaged ethnic backgrounds: Report to the Office for Students*. Available from: https://www.officeforstudents.org.uk/media/d21cb263-526d-401c-bc74-299c748e9ecd/ethnicity-targeting-research-report.pdf

Stewart, I.S., & Gill, J.C. 2017. Social geology — integrating sustainability concepts into Earth sciences. *Proceedings of the Geologists' Association*, **128**(2),165–172, Available from: https://doi.org/10.1016/j.pgeola.2017.01.002

The Diversity Practice, 2020. *AboutStellarHE*. Available from: https://www.stellarhe.com/about

UK Research and Innovation. 2020. *Diversity Results for UKRI funding data 2014/15 to 2018-19*. Available from: https://www.ukri.org/files/about/ukri-diversity-report/

Wahlquist, C. & Allam, L. (2020, August 4). Rio Tinto blew up Juukan Gorge rock shelters "to access higher volumes of high-grade ore". *The Guardian*. Available from: https://www.theguardian.com/australia-news/2020/aug/04/rio-tinto-blew-up-juukan-gorge-rock-shelters-to-access-higher-volumes-of-high-grade-ore

White Rose DTP, 2020. *WRDTP/Stuart Hall Foundation Awards*. Available from: https://wrdtp.ac.uk/studentships/wrdtp-stuart-hall-foundation-awards/